Development of an enzymatic assay on biochip measuring DNA double strand breaks repair capacity : biological validation and applications

Xavier Tatin

THÈSE

Pour obtenir le grade de

DOCTEUR DE L'UNIVERSITE GRENOBLE ALPES

Spécialité : **Biotechnologie, instrumentation, signal et imagerie pour la biologie, la médecine et l'environnement**

Arrêté ministériel : 25 mai 2016

Présentée par

Xavier TATIN

Thèse dirigée par **Jean BRETON, MCU, Université Grenoble Alpes**, et codirigée par **Sylvie SAUVAIGO, CSO, LXRepair SAS**

préparée au sein du **Laboratoire Systèmes Moléculaires et nanoMatériaux pour l'Energie et la Santé**
dans **l'École Doctorale Ingénierie pour la Santé, la Cognition et l'Environnement**

Développement d'un test de mesure de réparation des cassures double-brin de l'ADN sur biopuce : validations biologiques et applications

Thèse soutenue publiquement le **9 juillet 2021**,

devant le jury composé de :

Monsieur Marc AUDEBERT
Directeur de recherche, INRAE, Toulouse, Rapporteur
Madame Emmanuelle LAURENCEAU
Maître de conférences, Institut des Nanotechnologies de Lyon, Rapportrice
Monsieur Pierre RAY
Professeur, Université Grenoble Alpes, Président
Monsieur Christophe DENOYELLE
Maître de conférences, Université de Caen Normandie, Examinateur
Madame Patricia KANNOUCHE
Directrice de recherche, CNRS, Villejuif, Examinatrice
Madame Laurence LAFANECHERE
Directrice de recherche, CNRS, Grenoble, Examinatrice
Monsieur Jean BRETON
Maître de conférences, Université Grenoble Alpes, Directeur de thèse
Madame Sylvie SAUVAIGO
Présidente, LXRepair SAS, Grenoble, Co-directrice de thèse

REMERCIEMENTS

Avant toute chose, je tiens à remercier sincèrement le Dr. Emmanuelle LAURENCEAU et le Dr. Marc AUDEBERT pour avoir accepté d'évaluer ce travail de thèse. Mes remerciements vont également aux autres membres du jury, le Dr. Christophe DENOYELLE, le Dr. Patricia KANNOUCHE, le Dr. Laurence LAFANECHÈRE ainsi que le Pr. Pierre RAY, pour l'intérêt qu'ils ont porté à ce travail.

À mon directeur de thèse Jean BRETON et ma co-directrice Sylvie SAUVAIGO, qui m'ont permis de travailler pendant ces trois années avec LXRepair et le CIBEST : merci !

Jean, un grand merci pour ta bienveillance, ta disponibilité, tes conseils et ton soutien, notamment pour tes (nombreuses) corrections et commentaires précis et rigoureux. Je te souhaite une belle continuation au sein du CIBEST et à l'UGA !

Sylvie, merci pour ta disponibilité et ton regard éclairé sur la réparation de l'ADN et la technologie des puces. Merci pour ton optimisme et tes incitations à chercher au-delà des a priori quand les choses ne marchaient pas comme prévu. J'ai eu l'occasion de voir grandir l'aventure LXRepair et je lui souhaite un bel avenir.

J'adresse un énorme merci collectif à toute l'équipe CIBEST qui a rythmé ces trois années par sa bonne humeur et sa bienveillance. Je me souviendrai des discussions et des bons moments en salle café, dans les bureaux, les labos et à l'extérieur. Merci notamment à Sylvain pour ton aide dans tous les domaines et pour ta participation à l'ambiance collective, que tu as su égayer d'une manière particulièrement créative. À Dadou, un grand merci pour tes réponses et tes coups de mains en salle de culture, ainsi que pour les nombreuses discussions au labo entre deux incubations. Merci pour ta patience malgré toutes les misères que j'ai pu te faire subir avec mes complices (tu connais les noms) !

Merci également à Marie CARRIÈRE pour tes conseils sur les marquages 53BP1 et les analyses statistiques, ainsi que pour les discussions sur des thèmes plus agronomes ! Merci aussi à Jean-Luc RAVANAT pour ton aide et pour les bons moments en salle café. Et à Thierry DOUKI, merci pour tes conseils scientifiques et pour les discussions moins sérieuses. Je ferai toujours attention à mettre de la crème solaire !

Merci également à tous les autres membres du CIBEST et du secrétariat pour leur aide et pour tous les bons souvenirs que je garderai de ces trois années. Merci notamment à Pascale DELANGLE pour avoir pris le temps de m'aider ou répondre à mes questions quand j'en avais besoin.

J'ai une pensée particulière pour les autres doctorants de l'équipe, Antonia, Fanny, Jérémy, Laura, Nour, Marie, Anna… merci pour votre soutien et pour tous ces bons moments au C5 et en-dehors ! À Antonia et Marie, ainsi qu'à Pawel et Auriane, bon courage pour la suite/fin de vos thèses ! Merci aussi aux post-docs, stagiaires et autres non-permanents (Micka, Leslie, Caro, Éline, Fanny L., Taïna, Ana… et tous ceux que j'oublie) pour les conseils et les sourires !

Je n'oublie bien sûr pas l'autre moitié de ces trois années, j'ai cité la team LXRepair ! Je vous adresse mes chaleureux remerciements pour m'avoir accompagné et soutenu tout au long de ce projet.

Déjà, je remercie Sarah, pour… tout. Pour la planification du travail de labo, pour les astuces de paillasse aussi bien que pour l'administratif, mais aussi et surtout pour le soutien de tous les jours et pour les

discussions sur tout et n'importe quoi ! Un énorme merci aussi à toi, Giovanna, pour toute l'aide et le soutien que tu as pu m'apporter, aussi bien sur des détails que sur l'interprétation des résultats. Merci pour les anecdotes et les discussions animées autour d'un café, sur fond de gestuelle appuyée et d'envolées sonores ! J'adresse également mes remerciements à Bertrand, notamment pour tous ces échanges divers et variés et autres discussions en tous genres (longue vie à Jack White !). Enfin, aux *terrible twins*, Marta et Rajat, merci pour votre soutien et pour les bons moments passés ensemble ! Bon courage pour la suite, mais je vous fais confiance pour vous en tirer brillamment !

Merci enfin à tous les autres membres de la team, présent ou passés ! Thierry, Robin, et tous les nombreux stagiaires… Je vous adresse à tous de sincères remerciements pour m'avoir accompagné au long de mon projet.

Mes remerciements vont également à l'ANRT, ainsi qu'à LXRepair et au CEA pour avoir financé et/ou hébergé mon travail de thèse. Merci à Alexandra E., pour son aide dans mes recherches.

A mes colocs et amis : Nico, Julia, Marie, Cédric, Charlène… Merci de m'avoir apporté tous ces bons souvenirs et de m'avoir si souvent redonné le sourire quand mes cellules me l'avaient enlevé ! Régisse, merci pour rien. Big up à Manu et toute la team BJ (Raph, Antoine, Samy…), à mes agros préférés (notamment Llaume et Boubou) et à tous les autres que je ne peux pas citer ici mais qui se reconnaîtront. Votre amitié m'a fait chaud au cœur, ne changez pas !

Enfin, j'envoie d'énormes remerciements à ma famille, notamment mes parents, mes frères et sœur et surtout à So, pour toute la motivation, l'amour et l'attention que vous m'avez apportés au cours de ces trois années. Merci pour vos encouragements et vos pensées qui m'ont tant aidé à avancer.

CONTENTS

ABBREVIATIONS

(6-4) PP	(6-4) photoproduct
53BP1	p53-binding protein 1
8-oxodG	8-oxo-7,8-dihydro-2'-deoxyguanosine
8-oxoG	8-oxo-7,8-dihydroguanine
911 complex	RAD9-RAD1-HUS1 complex
AbaS	Abasic site
a-EJ	Alternative (backup) non-homologous end joining
AFU	Arbitrary fluorescence units
alt-NHEJ	Alternative (backup) non-homologous end joining
ANOVA	Analysis of variance
AP site	Apurinic/apyrimidinic site
APE1	AP endonuclease 1
APTX	Aprataxin
ATCC	American Type Culture Collection
ATM	Ataxia telangiectasia mutated kinase
ATP	Adenosine triphosphate
ATR	Ataxia telangiectasia and RAD3-related
AU	Arbitrary units
BARD1	BRCA1-associated RING domain protein 1
BCL-2	B-cell lymphoma 2 protein
BER	Base excision repair
BIR	Break-induced replication
BLM	Bloom syndrome helicase
BRCA1/2	Breast cancer susceptibility proteins 1 or 2
BSA	Bovine serum albumin
CDK	Cyclin-dependent kinase
CDP	Cyclobutane pyrimidine dimer
CHK1/2	Checkpoint kinases 1/2
CisP	Cisplatin
c-NHEJ	Canonical (classical) non-homologous end joining
CPK	Creatine phosphokinase
CRISPR	Clustered regulatory interspaced short palindromic repeat
CSA/B	Cockayne syndrome WD repeat proteins A and B
CtIP	C-terminal-binding protein-interacting protein
Cy3/5	Cyanine 3 or 5
DAPI	4′,6-diamidino-2-phenylindole
DDR	DNA damage response
DMEM	Dulbecco's modified Eagle's medium
DMSO	Dimethyl sulfoxide
DNA	Deoxyribonucleic acid
DNA-PK	DNA-dependent protein kinase
DNA-PKcs	DNA-PK, catalytic subunit
Dox	Doxorubicin
D-PBS	Dulbecco's phosphate-buffered saline
DR	Direct reversal
dRp	Deoxyribose phosphate
DSB	Double-strand break
DSBR	Double strand break repair
dsDNA	Double-stranded DNA
DTT	Dithiothreitol
EDTA	Ethylenediaminetetraacetic acid
ERCC1	Excision repair cross-complementation group 1
ETAA1	Ewing's tumor-associated antigen 1
EtBr	Ethidium bromide
EXO1	Exonuclease 1
FA	Fanconi anemia

FBS	Fetal bovine serum
FEN1	Flap endonuclease 1
FI	Fluorescence intensity
Fpg	Formamidopyrimidine DNA glycosylase
GG-NER	Global genome NER
HCR	Host cell reactivation
HEPES	4-(2-hydroxyethyl)-1-piperazineethanesulfonic acid
HMGN1	High mobility group nucleosome-binding domain-containing protein 1
HR	Homologous recombination
HRP	Horseradish peroxidase
hSSB1	Human ssDNA binding protein 1
IC10	Inhibitory concentration of 10 percent
IC50	Half maximal inhibitory concentration
ICL	Inter-strand crosslink
ICLR	Inter-strand crosslink repair
IDL	Insertion-deletion loop
IF	Immunofluorescence
IR	Ionizing radiation
MDC1	Mediator of DNA damage checkpoint 1
MDM2	Mouse double minute 2 homolog
MEM	Eagle's minimal essential medium
MGMT	O^6-methylguanine-DNA methyltransferase
MMEJ	Microhomology-mediated end joining
MMR	Mismatch repair
MRE11	Meiotic recombination 11 protein
mTOR	Mammalian target of rapamycin
MTT	3-(4,5-dimethylthiazol-2-yl)-2,5-diphenyltetrazolium bromide
NADP+	Nicotinamide adenine dinucleotide phosphate
NBS1	Nijmegen breakage syndrome protein 1
NE	Nuclear extracts
NER	Nucleotide excision repair
NF-κB	nuclear factor-κB
NHEJ	Non-homologous end joining
nt	Nucleotide
OGG1	8-oxoguanine glycosylase 1
PAR	Poly (ADP-ribose)
PARP	Poly(ADP-ribose) polymerase
PARPi	PARP inhibitor
PAXX	Paralog of XRCC4 and XLF
PC	Phosphocreatine
PCR	Polymerase chain reaction
PFGE	Pulse-field gel electrophoresis
PI3K	Phosphatidylinositol 3 kinase
PIDD	p53-inducible protein with a death domain
PIKK	PI3K-related protein kinase
PK	Proteinase K
PNKP	Polynucleotide kinase/phosphatase
POL	DNA polymerase
PTEN	Phosphatase and tensin homolog
PTIP	PAX transactivation activation domain-interacting protein
RE	Restriction enzyme
RIF1	RAP1-interacting factor 1
RNA	Ribonucleic acid
RNF8	RING finger protein 8
ROS	Reactive oxygen species
RPA	Replication protein A
SCID	Severe combined immunodeficiencies
SD	Standard deviation

SD-MMEJ	Synthesis-dependent MMEJ
SDS	Sodium dodecyl sulfate
SDSA	Synthesis-dependent strand annealing
SSA	Single-strand annealing
SSB	Single-strand break
SSBR	Single-strand break repair
ssDNA	Single-stranded DNA
SUMO	Small ubiquitin-like modifier
TALEN	Transcription activator-like effector nucleases
TBE	Tris/Borate/EDTA
TBS	Tris-buffered saline
TC-NER	Transcription-couped NER
TdT	Terminal deoxynucleotidyl transferase
TLS	Translesion synthesis
TOP1	DNA topoisomerase I
TOPBP1	Topoisomerase 2-binding protein 1
UDG	Uracil-DNA glycosylase
UV	Ultraviolet
UVSP7	Ubiquitin-specific-processing protease 7
UVSSA	UV-stimulated scaffold protein A
XAB2	XPA-binding protein 2
XLF	XRCC4-like factor
XP	Xeroderma pigmentosum
XRCC4	X-ray repair cross-complementing protein 4
γH2AX	Ser139-phopshorylated H2A histone X

LIST OF FIGURES

LIST OF TABLES

FOREWORD

The life of a DNA molecule is far from being quiet. Cells are under constant threat from exogenous and endogenous factors that modify DNA bases, cleave nucleotides, bind them or break DNA strands. In humans, such processes are not necessarily anormal; they can be part of cellular processes as essential as DNA replication. In other cases, however, these alterations are caused by biological threats or following exposure to chemical or physical agents such as ultraviolet (UV) light or ionizing radiation (IR). These agents are termed genotoxic and cause a large panel of DNA lesions. Cells have developed protective mechanisms that allow the recognition and repair of DNA damage, thereby preventing the alteration of genetic information and its potential transmission to daughter cells. These complex systems are evolutionarily conserved and their failure can lead to dramatic cellular consequences. Indeed, unrepaired DNA lesions can result in mutations or genomic translocations, which participates in the deregulation of cellular activities and can trigger cell death, premature aging or diseases such as neurodegenerative disorders and cancers.

In this context, we studied the most deleterious kind of DNA lesion, DNA double-strand breaks (DSB), which are characterized by a complete rupture of the DNA molecule. Unplanned DSBs are generated directly by genotoxic agents or when several single-strand breaks are induced close to each other, through the action of IR or clastogenic compounds. Unrepaired DSBs are associated with the acquisition and progression of a cancerous phenotype, and alterations DSB repair (DSBR) are commonly found in tumors. On the other hand, preventing cancer cells to repair these lesions can lead them to activate programmed cell death mechanisms. Thus, anticancer therapies are commonly based on a genotoxic agent that induces lesions and more recent developments also introduce repair inhibitors in order to saturate cancer cells with DNA lesions, resulting in tumor resorption. Hence, DSBR processes represent major clinical targets for anticancer therapies. However, current methods do not always succeed in identifying DSBR deficiencies and the effect of DSBR inhibitors is still incompletely described, thereby reducing positive therapeutic outcome. There is a strong need for methods that could improve the efficiency of anticancer treatments and reduce their toxicity in normal cells. Besides, DSBR mechanisms are still incompletely understood, which limits the global comprehension of DNA repair processes.

In this study, we present a novel multiplexed, functional DSBR assay on biochip that measures enzymatic activities from several DSBR pathways in protein extracts. We describe its use on different cellular models and compare it to another DSBR method based on agarose gel electrophoresis. We measured baseline repair activities as well as following exposure to various genotoxic and/or DSBR-inhibiting treatments. In parallel, we quantified DSB formation and tracked the expression and activity of several DSBR factors. A better understanding of DSBR mechanisms finds direct application in mechanistic

research, but also in the development of novel DSBR inhibitors and in the optimization of current anticancer treatments.

This project was conducted within the framework of a cooperation between the CIBEST team from the SyMMES laboratory (UMR 5819 CEA-CNRS-UGA) and biotechnology company LXRepair.

- CIBEST (Chemistry-Biology Interface for environment, health and Toxicology, formerly LAN/SCIB) has an expertise in biology and chemistry for the study of DNA damage, toxicology and health. The team investigates novel biomarkers, drugs or imaging tools to better characterize the cellular and molecular effects of various chemical or physical agents and nanomaterials.
- LXRepair is a CEA spin-off founded in 2013 by Sylvie Sauvaigo. The company designs and manufactures multiplexed DNA repair assays on biochip. These patented methods expose modified DNA substrates to cell extracts and measure several DNA repair activities simultaneously to provide a specific enzymatic repair signature.

This manuscript is divided into five chapters; we first provide the reader with important notions regarding the cellular response to DNA damage, the mechanisms of DNA repair and the methods that allow the measurement of DSBR activities in human cells. Secondly, we detail the materials and methods that were used to achieve the study's objectives. Thirdly, we detail the results that were obtained; these results are discussed in the fourth and fifth chapter, which respectively interpret our data based on current scientific literature and present prospects for the optimization and use of our DSBR assay.

PUBLICATIONS

A review article was produced in the course of this Ph. D. project and is upon final validation for publication in *Mutation Research – Reviews in Mutation Research*. In addition, a research article is being prepared to present the development of the Next-SPOT assay, for which a patent is also intended.

CHAPTER 1 – BIBLIOGRAPHIC CONTEXT

1. Overview of DNA damage

DNA is the physical support of genetic information and the vector of its transmission along subsequent generations of cells. Genetic alterations can occur under the action of a large panel of agents. We define as DNA lesion (or DNA damage) any abnormal chemical modification of the structure of the DNA molecule. It differs from mutations, that consist in the replacement of standard base pairs by others. DNA damage can be caused by endogenous factors, that are naturally found within the cell. These factors include for instance hydrolysis, DNA alkylation and reactive oxygen species (ROS) produced as a result of normal metabolic processes (Berquist and Wilson, 2012; Gates, 2009; Soll *et al.*, 2017). Up to 10^5 endogenous lesions are thought to form per cell and per day (Hoeijmakers, 2009)… and there are about 10^{13} cells in an average human (Bianconi *et al.*, 2013). Besides, exogenous factors induce additional DNA damage; as an illustration, a day of bright sunlight exposure can induce up to 10^5 photoproducts in each skin keratinocyte (Hoeijmakers, 2009).

Cells have developed complex response mechanisms that prevent the accumulation of such damage, which could otherwise result in mutations hampering cellular activities and induce cell death, cancer and senescence. For instance, mutations that appear at critical sequences in DNA can lead to the inactivation of tumor suppressor genes and the activation of oncogenes, which, in turn, participates in the initiation and progression of cancer. The outcome depends on repair complexity, which is determined by the type of damage. Some lesions, such as 8-oxo-7,8-dihydroguanine (8-oxoG), are mostly mutagenic, while others like strand breaks have a cytotoxic or cytostatic impact (Akbari and Krokan, 2008).

Specific repair pathways are mobilized depending on the kind of DNA damage. An overview of DNA damaging agents, resulting lesions and associated repair mechanism is provided in figure 1. In the next sections, we detail the spectrum of known DNA lesions and show the characteristics of DNA double-strand breaks. Some lesions will only be briefly reviewed, for they have a lower interest in the context of this project. The reader is oriented toward the literature we provide for more details.

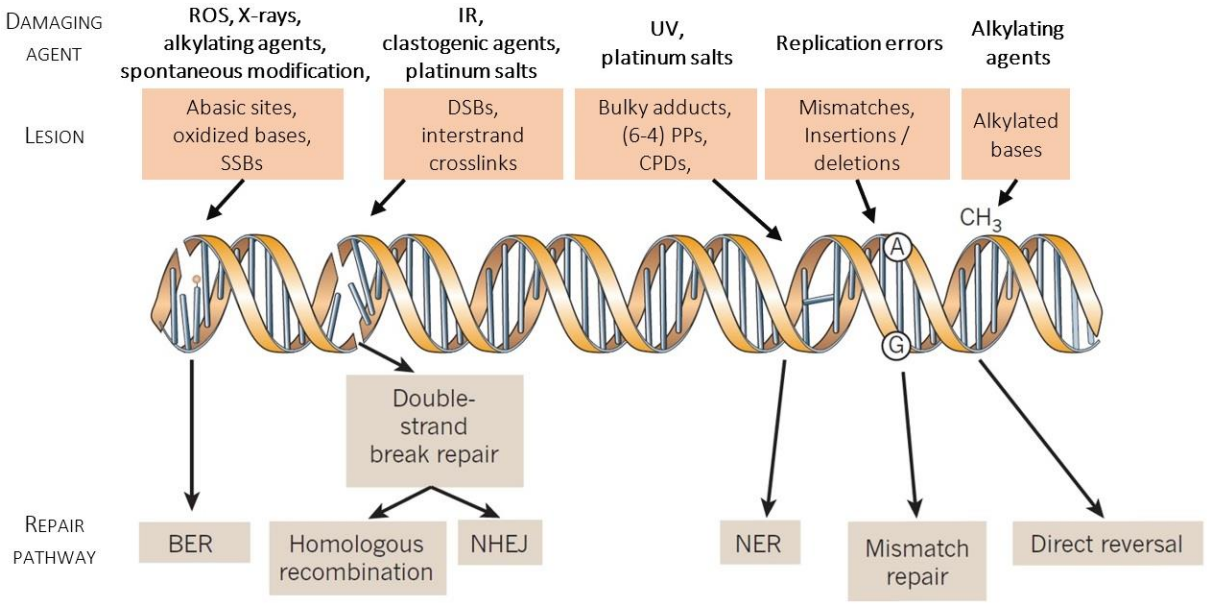

Figure 1. Overview of the most common DNA lesions and associated DNA repair pathways.
Adapted from Lord and Ashworth (Lord and Ashworth, 2012). BER: base excision repair; CPDs: cyclobutane pyrimidine dimers; NER: nucleotide excision repair; NHEJ: non-homologous end joining; PPs: photoproducts; SSBs: single-strand breaks.

1.1. Mismatches and replication errors

DNA mismatches occur when two non-complementary nucleobases are aligned in duplex DNA. Such lesions result from replication errors, for instance when the proofreading activity of DNA polymerases is deficient (Barbari and Shcherbakova, 2017). Mispairings that induce a small distortion of the DNA double helix are more likely to be tolerated by the polymerase active site (Kunz *et al.*, 2009)

They were also shown occur during heteroduplex formation, after spontaneous deamination or following exposure to agents such as mutagenic chemicals or ionizing radiation (which relates to any subatomic particle or electromagnetic wave that possesses enough energy to liberate electrons from atoms) (Cannan and Pederson, 2016; Goodman *et al.*, 1993; Kunz *et al.*, 2009; Wildenberg and Meselson, 1975). Though non-mutagenic mismatches are described in homologous recombination intermediates, most mismatches are mutagenic lesions that induce mutations if left unrepaired (Kunz *et al.*, 2009). Notably, uracil is a common mutagenic lesion in DNA caused by cytosine deamination and misincorporation during replication (Lindahl, 1982)

1.2. Abasic sites

Abasic sites, also termed apurinic or apyrimidinic site (AbaS or AP sites), are caused by the hydrolysis of the N-glycosidic bond between a DNA nucleobase and the sugar backbone of the DNA molecule, revealing a reactive hydroxyl group (figure 2). AbaS are among the most common DNA lesions in human cells, with up to 18,000 events per cell and per day in humans (Friedberg *et al.*, 2006).

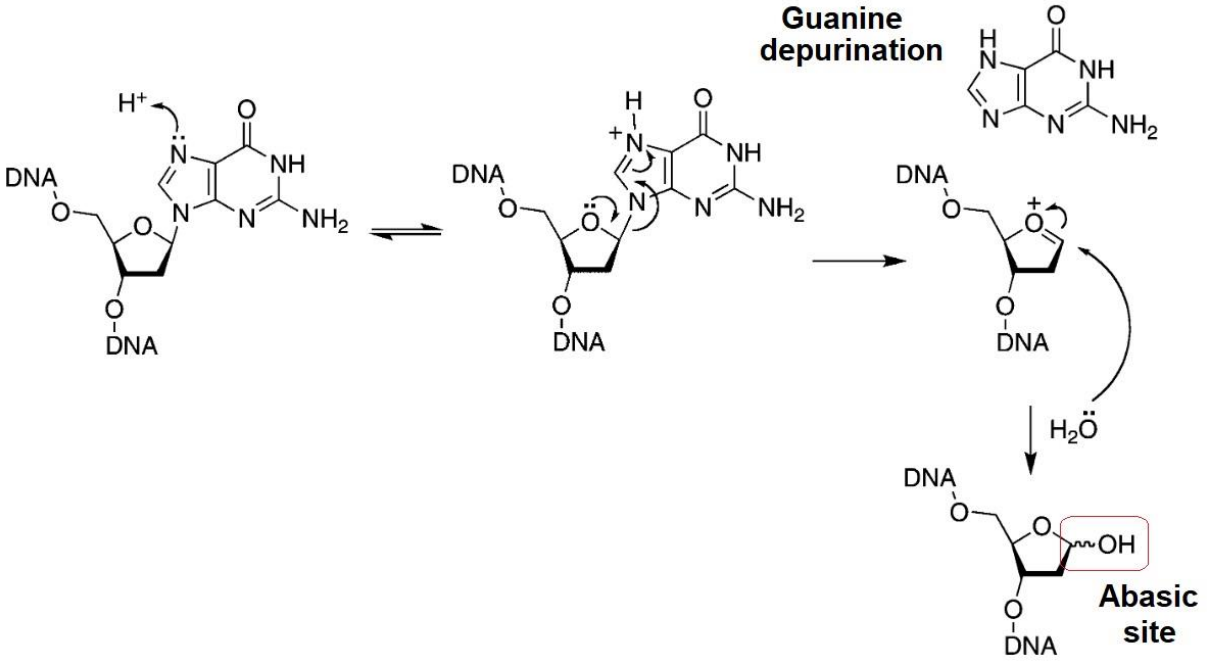

Figure 2. Example of abasic site formation: loss of a guanine base. Adapted from K.S. Gates (Gates, 2009).

The hydrolysis reaction can occur spontaneously, with faster kinetics in puric bases (Gates, 2009). Abasic sites are also known to form under the effect of ROS and alkylating agents (Greenberg, 2014; Kow and Dare, 2000). In addition, DNA repair can generate abasic sites as repair intermediates. This if notably the case in base excision repair (BER), during which the removal of the damaged base by DNA glycosylases converts the lesion to an abasic site (Admiraal and O'Brien, 2015; Friedberg *et al.*, 2006; Krokan *et al.*, 1997). These processes will be detailed further in the manuscript.

1.3. Oxidative DNA damage

ROS is collective term that describes hydrogen radicals such as superoxide ($O_2^{\bullet -}$) and hydroxyl ($HO^{\bullet}$), as well as nonradical oxidizing agents like hydrogen peroxide (H_2O_2). They are found at steady but low levels in human cells, where they are produced as natural byproducts of the aerobic oxygen metabolism and represent a full part of normal cell physiology (Bayr, 2005). Aside from metabolic oxygen reduction, ROS are produced by specific enzymes like peroxidases or NADPH oxidases, but also as part of lipid metabolism in peroxisomes. ROS mediate various cellular mechanisms, such as mitochondrial electron transport, redox metabolism, signal transduction, gene expression and they are known to play a role in reaction to pathogens (Paiva and Bozza, 2014). Additionally, exogenous factors such as UV light, IR and

environmental pollutants also generated ROS, either directly or following their metabolization within the cells (Krumova and Cosa, 2016). Cellular levels of ROS are regulated by the activity of a number of reducing agents like superoxide dismutase and other ROS scavengers that prevent their accumulation (Krumova and Cosa, 2016). In this section, we detail some of the deleterious impacts of ROS on DNA.

8-oxo-7,8-dihydro-guanine

Among DNA nucleobases, guanine has the lowest redox potential, which makes it the most vulnerable to oxidation (Neeley and Essigmann, 2006). The most common ROS-induced oxidation lesion is 8-oxo-7,8-dihydroguanine (8-oxoG), and its associated deoxyribonucleoside, 8-oxo-7,8-dihydro-2'-deoxyguanosine (8-oxodG), is a routine marker of oxidation stress in cells (Cadet, 2003). In eukaryotic nuclear DNA, it is estimated that several 8-oxoG bases form per 10^6 guanine bases, which corresponds to thousands of lesions per cell (ESCODD *et al.*, 2005; Swenberg *et al.*, 2011).

Various mechanisms of formation have been described, notably under the action of superoxide and hydroxyl radicals and as a result of one-electron reactions (Hall *et al.*, 1996; Neeley and Essigmann, 2006). Under replication, 8-oxoG was found to form stable hydrogen bonds with other DNA bases than cytosine, especially with adenine (figure 3). These 8-oxoG:A mispairs can lead G:C to T:A transversion mutations to incorporate into the genome.

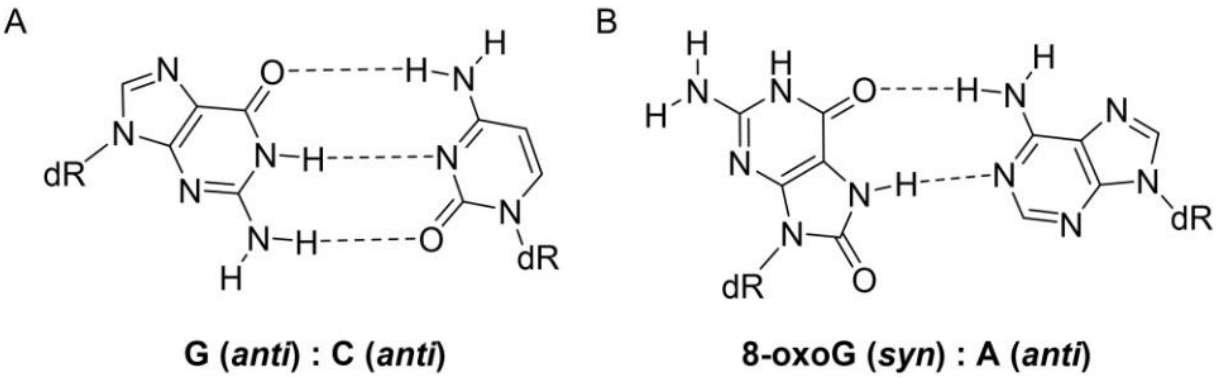

Figure 3. 8-oxoG results in base mispairing.
(A) *Guanine normally pairs with cytosine, while 8-oxoG may adopt a syn conformation about its glycosidic bond and form a stable 8-oxoG:A base pair following DNA replication* ***(B)****. After another round of replication, a T:A base pair is formed instead of the original G:C. Adapted from Banda* et al. *(Banda* et al.*, 2017).*

Cytosine and thymine glycols

The C5-C6 double bond in pyrimidines is targeted by free radicals to generate intermediate glycol bases (figure 4), which can undergo additional modifications but are stable in double-stranded DNA (Breen and Murphy, 1995; Tremblay and Wagner, 2007; Tremblay *et al.*, 1999).

Pyrimidine glycols are formed as a result of a Fenton reaction based on the reduction of H_2O_2 by transition state metal ions, and following exposure to ionizing radiation or UV light (Cooke *et al.*, 2003; Tremblay *et al.*, 1999). They can lead to base transitions, which are the most frequent kind of base substitution (Wang *et al.*, 1998).

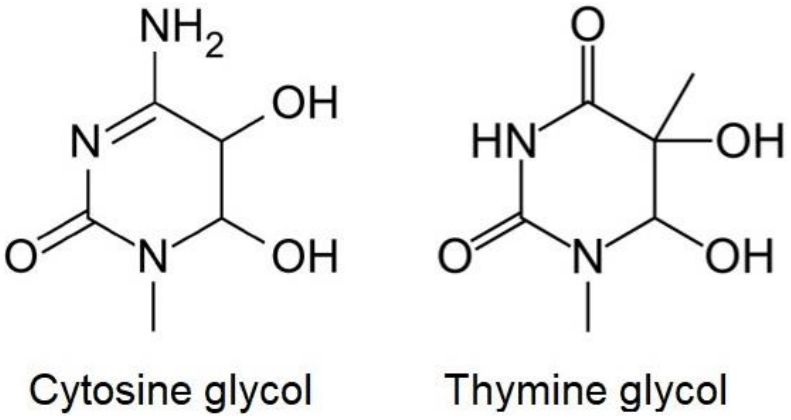

Figure 4. Structure of thymine and cytosine glycol.

1.4. Photoproducts

DNA absorption peaks at 260 nm and covers UVC radiation (190-290 nm) and a proportion of UVB (290-320 nm), but not UVA (320-400 nm). The highest-energy radiation, UVC, is absorbed by atmospheric ozone at high altitude, thus this radiation has little direct effect. UVB photons, however, were shown to be directly absorbed by nucleobases within skin cells, causing photo-induced reactions to occur (Douki and Cadet, 2003). UVB photons cause a cycloaddition reaction between the C5-C6 double bonds in pyrimidine bases, resulting in the formation of cyclobutane pyrimidine dimers (CPDs) within a few picoseconds (Schreier *et al.*, 2007), as depicted in figure 5. UVA photons can lead to CPD formation through an indirect energy transfer following the excitation of exogenous chromophores such as aromatic ketones (Ridley *et al.*, 2009). Although interstrand photoproducts have been described, CPDs form predominantly between adjacent bases *in vivo* (Cadet *et al.*, 2012).

(6-4) photoproducts ((6-4) PPs) are another common UV-induced DNA lesion. They are based on a Paternò-Büchi reaction that involves a cycloaddition at the C5-C6 double bond of one base and the C4 carbonyl group of the second. The reaction resulting in (6-4) PP formation causing a more important torsion of the DNA molecule and makes these lesions highly mutagenic, but they are efficiently removed by repair systems (Cadet *et al.*, 2012). In contrast, CPDs represent the vast majority (about 80%) of mutagenic events induced by UV irradiation (You *et al.*, 2001), mostly through the induction of T-C transversions and CC-TT tandem mutations.

The generation of oxidation products such as 8-oxodG following exposure to UVB was found to be much lower than the formation of CPDs and (6-4) PPs (Cadet *et al.*, 2012). Exposure to a range of radiations as in direct sunlight can lead to combined effects, such the UVA-mediated conversion of UVB-induced (6-4) PPs into their Dewar valence isomers, a third class of pyrimidine dimer photoproducts (figure 5).

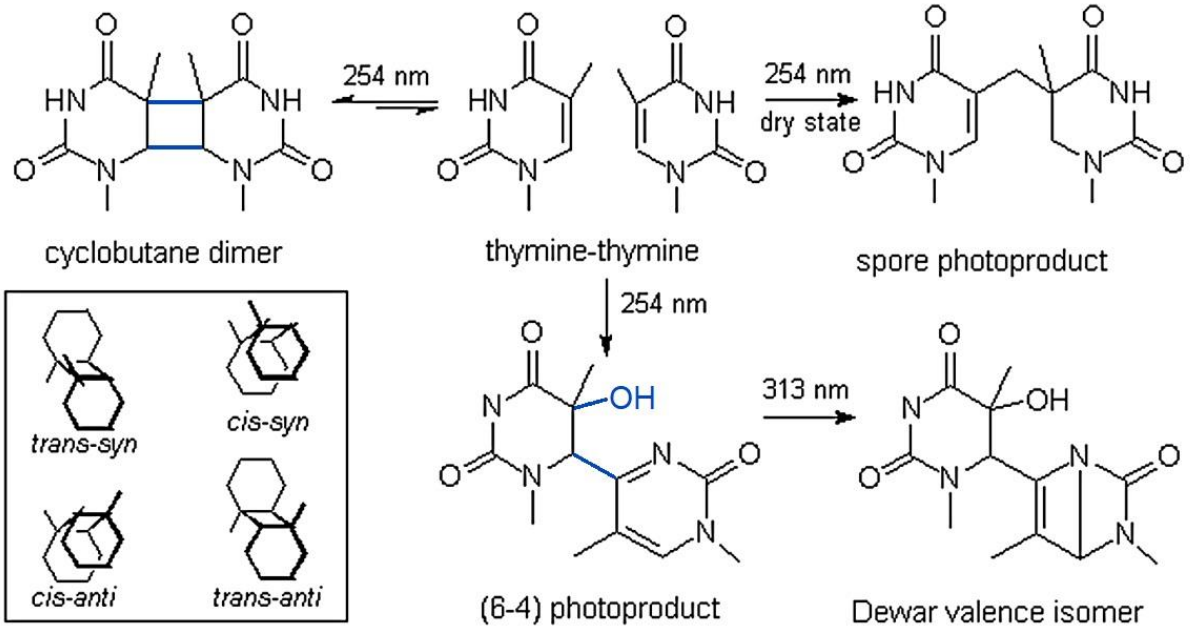

Figure 5. Generation of CPD and (6-4) PPs following exposure to UV light.
UV-induced covalent bonds in both molecules are indicated in blue. Adapted from Douki et al. *(Douki* et al.*, 2000).*

1.5. Alkylation lesions and bulky adducts

DNA alkylation describes the addition of an alkyl group on DNA bases. The most common reaction involves methyl radicals covalently binding nitrogen or oxygen atoms in puric nucleobases to form N7- or O^6-Me-guanine (figure 6), as well as N3-Me-adenine. When alkylated sites are not involved in base pairing, as for N7-Me-guanine, alkylation was not found to have significant biological consequences (Boysen *et al.*, 2009). On the contrary, alkylation at sites that are involved in Watson-Crick base pairing was shown to be highly mutagenic and high levels of O^6-Me-guanine are found in cancerous cells (Lord and Ashworth, 2012).

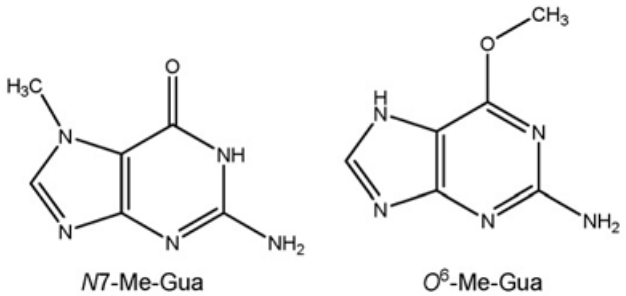

Figure 6. Examples of guanosine methylation (Boysen et al.*, 2009)*

Alkylation events are also observed following the oxidation of fatty acids by ROS in lipid peroxidation. Indeed, this process results in the formation of reactive compounds such as malondialdehyde and 4-hydroxy-2-nonenal, which participate in the formation of DNA adducts, defined as the covalent bonding of a molecule to a nucleophilic DNA site. Ethenobases depicted in figure 7 are an example of peroxidation-induced lesions (Avendaño and Menéndez, 2015; Tudek *et al.*, 2017; Winczura *et al.*, 2012).

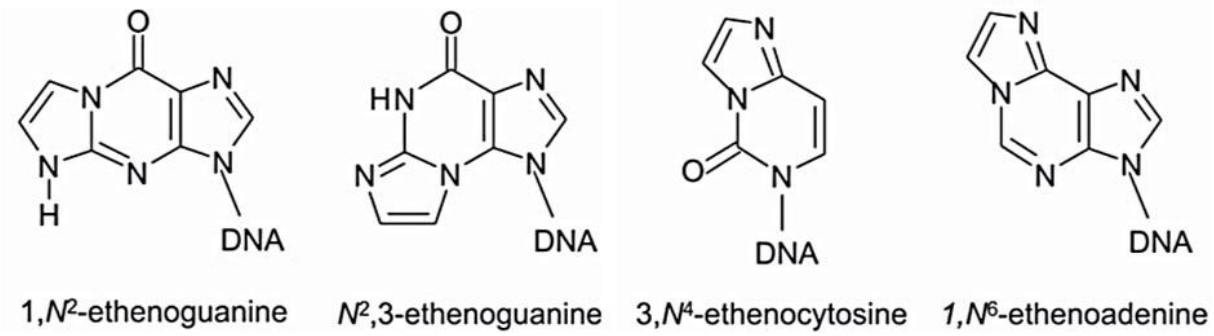

Figure 7. Examples of DNA adducts resulting from lipid peroxidation.
Original figure by Winczura et al. *(Winczura* et al.*, 2012).*

DNA adducts form either directly or after metabolic activation to DNA-reactive intermediates. Adduct formation can occur in numerous sites in DNA, with a specificity that depends on the reactive species and on the reactivity of the DNA sites toward the electrophilic molecules. The ring nitrogens such as N3 and N7 in guanine and adenine are the most nucleophilic sites and represent first class targets for adduct formation, but exocyclic oxygen sites usually form more mutagenic lesions (La and Swenberg, 1996). The carcinogenic effect originates from the chemical alteration of DNA, which upon DNA replication results in the conversion of repairable lesions to heritable mutations.

For instance, DNA adducts derived from bulky aromatic carcinogens appear to induce mutations by causing conformational changes in DNA. As an illustration, DNA adducts formed at the C8 position of guanine residues by 2-Acetylaminofluorene were shown to induce frameshift mutations in DNA and to be highly carcinogenic (Burnouf *et al.*, 1990). Another illustration is provided by benzopyrene-7,8-diol-9,10-epoxide a metabolite of polycyclic aromatic hydrocarbon benzo[a]pyrene, which was shown to form bulky adducts with several nucleobases and induce carcinogenesis (Melendez-Colon *et al.*, 1999).

1.6. DNA crosslinks

The activity of various anticancer agents is based on the formation of specific kinds of DNA adducts in cancer cells. Most notably, platinum salts are known to covalently bind DNA bases. Cisplatin (CisP) and its derivatives carboplatin and oxaliplatin are among the most common DNA-targeted agents used in

cancer therapy. Upon hydrolysis, their substitution-active groups form strong covalent Pt(II)-N bonds with guanine and adenine nucleobases. They can bind one or several bases, located on the same strand or on opposite strands of the DNA molecule, resulting in the formation of single-base adducts, intra-strand crosslinks and inter-strand crosslinks (ICLs) (Alderden *et al.*, 2006), as depicted in figure 8. It was shown that interstrand crosslinks are more unstable than the other forms of adducts, into which they tend to be converted (Malinge *et al.*, 1999). These adducts induce structural DNA changes, notably a strong distortion of the DNA molecule (Lopez-Martinez *et al.*, 2016; Malinge *et al.*, 1999), which results in the inhibition of vital cellular functions such as gene expression and DNA replication.

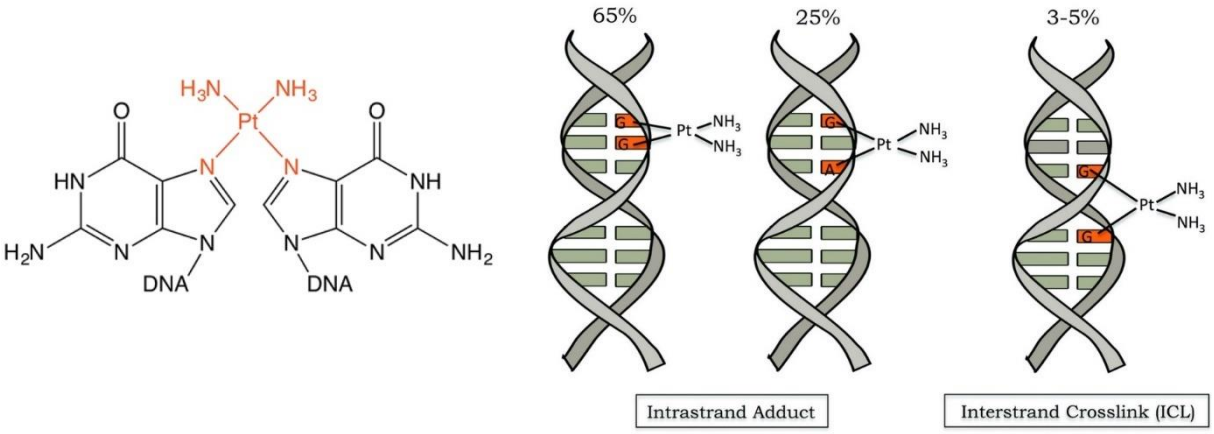

Figure 8. Cisplatin-induced formation of intra- and inter-strand crosslinks.
Adapted from (Lopez-Martinez et al.*, 2016; Rocha* et al.*, 2018).*

Endogenous crosslinking agents are also described, including for instance nitrous acid (Kirchner *et al.*, 1992) and aldehydes such as formaldehyde and malondialdehyde (Huang and Hopkins, 1993; Niedernhofer *et al.*, 2003). These compounds are usually found under conditions of oxidative stress. Endogenous levels of ICLs are low (Williams *et al.*, 2013).

Most adducts and DNA crosslinks lead to strand breakage, either spontaneously or during the repair or DNA replication process, whereas others break DNA through direct interaction.

1.7. Single-strand breaks

DNA breaks are characterized by the rupture of the sugar backbone of the DNA strand. As for other lesions, strand breakage occurs under the action of both endogenous and exogenous mechanisms.

For instance, SSBs are formed by ionizing radiation under the action of high-energy particles and radiolysis radicals. IR is known to split water molecules near DNA, creating hydrogen and hydroxyl free radicals. Besides the generating abasic sites and oxidized bases, these radicals can directly attack the 2-deoxyribose sugar backbone and result in SSB formation, with phosphate- or phosphoglycolate-bearing ends (Pogozelski and Tullius, 1998). The ionizing radiation dose-response relationship for SSB formation has been found to be linear over a wide range (Krisch *et al.*, 1991). Other agents, such as anticancer

drug bleomycin, generate highly reactive oxygen species that induce DNA breaks between 3'-4' bonds in deoxyribose (Brandt and Gerriets, 2021).

Alternatively, SSBs can arise indirectly following the enzymatic cleavage of the phosphodiester backbone, for instance in the process of DNA repair during which specific endonucleases such as APE1 generate single-stranded DNA (ssDNA) intermediates, as we will show in subsequent sections. Another example of endogenous damage is provided by enzymes such as DNA topoisomerase I (TOP1), which generate transient SSBs as part of their normal catalytic cycle to relax DNA torsion (Wang, 2002). In cases such as the proximity of other DNA lesions, the religation activity of TOP1 can be aborted, leading to the appearance of a SSB (Pouliot *et al.*, 1999). In mammalian cells, more than 5.10^4 SSBs per day are estimated to form in each cell, which corresponds to approximately one SSB per 10^5 bp (Tice and Setlow, 1985).

Most toxic agents that introduce SSBs (oxidizing and alkylating agents, ionizing radiation) also generate a range of other DNA damage such as base lesions, but some of them also form DSBs (Friedberg *et al.*, 2006).

1.8. Double-strand breaks

1.8.1. Formation

DSBs are known to occur under the action of a large panel of agents and cellular mechanisms.

Firstly, DSBs formation and their subsequent repair are required in a programmed, site-specific manner as part of several physiologically and developmentally important processes. For instance, V(D)J recombination relies on controlled DSB formation to randomly assemble immunoglobulin antigen and T-cell receptor genes. DSBs also form during immunoglobulin class switch recombination (Aplan, 2006) and chromosome segregation in human meiosis is based on DSB-induced recombination at defined hotspots of programmed DSBs (Lam and Keeney, 2015).

In addition, DSBs can occur in an unprogrammed manner, which will be the focus of our study. Here, we briefly describe the most common sources of unscheduled DNA DSBs, including:

- Replication stress and transcription anomalies
- IR, radiomimetic compounds and other clastogens
- Endonucleases
- Repair-induced DSBs

Endogenous DSBs are estimated to occur at a relatively low level. The most common source of DSB in the absence of exogenous agents is replication anomaly (Mehta and Haber, 2014), such as:

- An unusual DNA conformation or chromatin structure, for instance if the replication fork meets nicked DNA
- The collision of replication machinery with transcription proteins or other DNA-binding factors.

Figure 9 illustrates DSB formation following replication fork arrest. Aside from replication-related DSB formation, DNA breakage is known to occur following the formation of R-loops, which form when nascent RNA elongation outpaces the action of topoisomerases, resulting in the reannealing of a portion of the nascent RNA to reanneal to its DNA complement. R-loops are processed into DSBs by endogenous endonucleases such as XPG (*xeroderma pigmentosum* type G), but also when encountered by replication forks (Sollier and Cimprich, 2015).

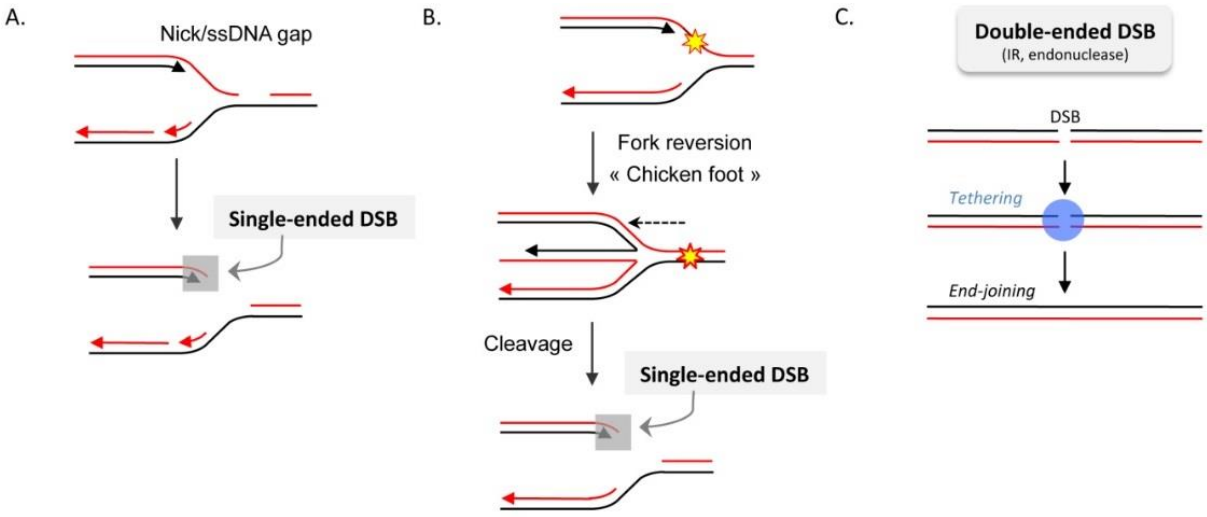

Figure 9. Formation of single- or double-ended DSBs.
A. *ssDNA gaps or DNA nicks can block replication forks (arrows) and lead to single-ended DSBs (grey square).* ***B.*** *Blocking DNA lesions (yellow star) such as pyrimidine dimers, abasic sites and inter-strand crosslinks can lead to replication fork stalling, which can cause replication fork regression. This process partially displaces nascent strands, allowing their annealing. The newly synthesized lagging strand may serve as a template to further extend the leading strand, which forms a "chicken foot" intermediate analogous to a Holliday Junction. The cleavage of this cruciform structure by resolvases results in a single-ended DSB.* ***C.*** *Double-ended DSB form under the action of exogenous factors (IR, clastogens) or endonucleases. Tethering close double ended DSBs reduces genomic instability. This process does not occur on single-ended DSBs. Adapted from So* et al. *(So* et al.*, 2017).*

Alternatively, DSBs form when SSBs are generated close to each other. For instance, high doses of irradiation can generate nicks are in complementary DNA strands within one helical turn, resulting in DSB formation. However, this phenomenon occurs with a lower probability than SSBs, and it is estimated that IR-induced DSBs form at a ratio of 1 DSB for 10 SSBs (Roots *et al.*, 1985). For their part, Vilenchik

and Knudson report that about 1% of single-strand lesions are converted to endogenous DSBs per human cell, which corresponds to approximately 50 DSBs per cell cycle or one DSB per 6.10^7 bp (Vilenchik and Knudson, 2003). The proportion of DSBs to SSBs is known to vary depending on the DNA-damaging agent (Cannan and Pederson, 2016), as well as the configuration of the lesion. For instance, IR generates clusters of "dirty" single and double strand DNA breaks (figure 10) with complex, less processable ends bearing chemical groups such as phosphoglycolates while endonucleases usually generate "clean" 3' hydroxyl- and 5' phosphate ends (Winters *et al.*, 1992).

Such endonucleases are found in several DSBR mechanisms (as detailed in subsequent sections), but they also found a particular significance in biochemistry. Meganucleases, chimeric zinc finger nucleases, transcription activator-like effector nucleases (TALENs) and RNA-guided Cas9 nucleases became routine tools for experimental DSB induction.

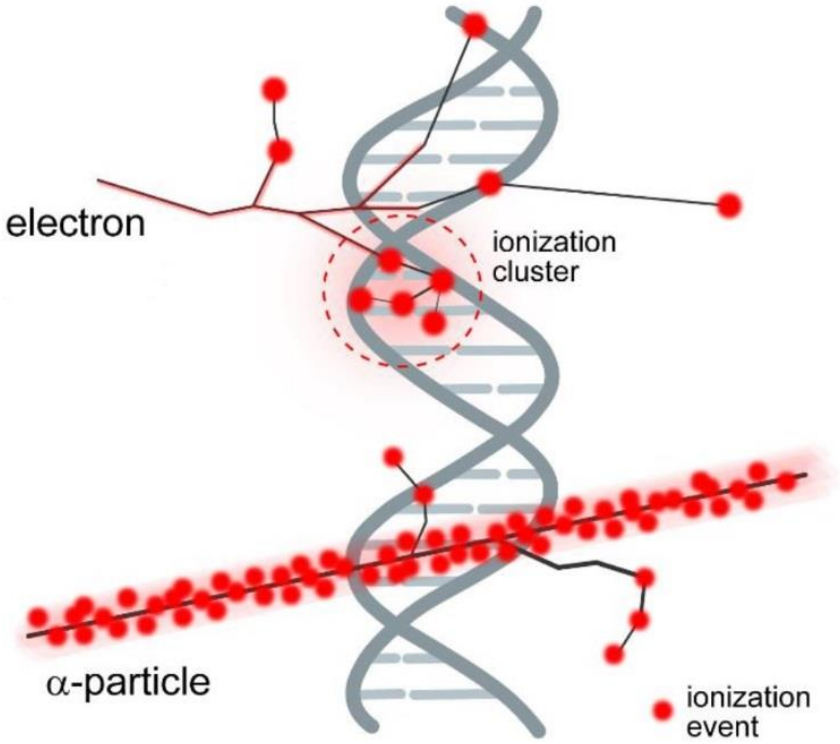

Figure 10. Ionizing radiation generates DNA lesions grouped along the particle track or withing ionization clusters. *DSBs are formed directly when ionization events simultaneously break both DNA strands, but also indirectly through the generation of free radicals in other molecules such as water. Complex ionization clusters can be formed due to increased indirect effects in the vicinity of the DNA helix. Adapted from Iliakis and colleagues (Iliakis* et al.*, 2019).*

1.8.2. Biological consequences

Though much less frequent as lesions like oxidative damage to DNA bases, DNA DSBs are believed to be much more important biologically than are SSBs, due to their very high cytotoxicity.

The genotoxic effect of DSBs is illustrated by a panel of inherited defects in DSBR processes that were found to be associated with various human diseases, including immunodeficiencies (for instance severe

combined immunodeficiencies, SCID), increased cancer susceptibility and specific syndromes such as Ataxia telangiectasia (McKinnon, 2012). Another clear illustration is found in germline mutations in breast cancer susceptibility proteins 1 and 2 (BRCA1/2), that are required for one of the main DSBR pathways. The deficiency of these proteins results in increased levels of unrepaired DSBs, which causes aneuploidy and extensive chromosomal rearrangements such as translocations (Hoppe *et al.*, 2018; Moynahan and Jasin, 2010).

Although other also result in increased genomic instability, a wealth of literature established that DSBs are major inductors of genomic aberrations, including chromosome rearrangements and repeat copy number instability, mostly through impaired replication and mitotic aberrations. Notably, broken chromosomes do not evenly partition between daughter cells during mitosis (Dasika *et al.*, 1999). In addition, DSBs can result in partially re-replicated DNA, which can also participate in genome instability (Alexander and Orr-Weaver, 2016). Chromosomal aberrations simultaneously impact many genes, causing extensive cellular malfunctions and potentially leading to cell death (van Gent *et al.*, 2001).

They were found to participate in senescence, oncogenic transformation and the proliferation of aberrant cells (figure 11). Nevertheless, such extensive alterations can also be important drivers of evolution.

Interestingly, oncogenic chromosomal translocations were found in peripheral blood cells from healthy individuals, which suggests that chromosomal translocations alone are not the only factor inducing malignant transformation, and that mutations act as a complement for the initiation of a frank malignancy (Aplan, 2006).

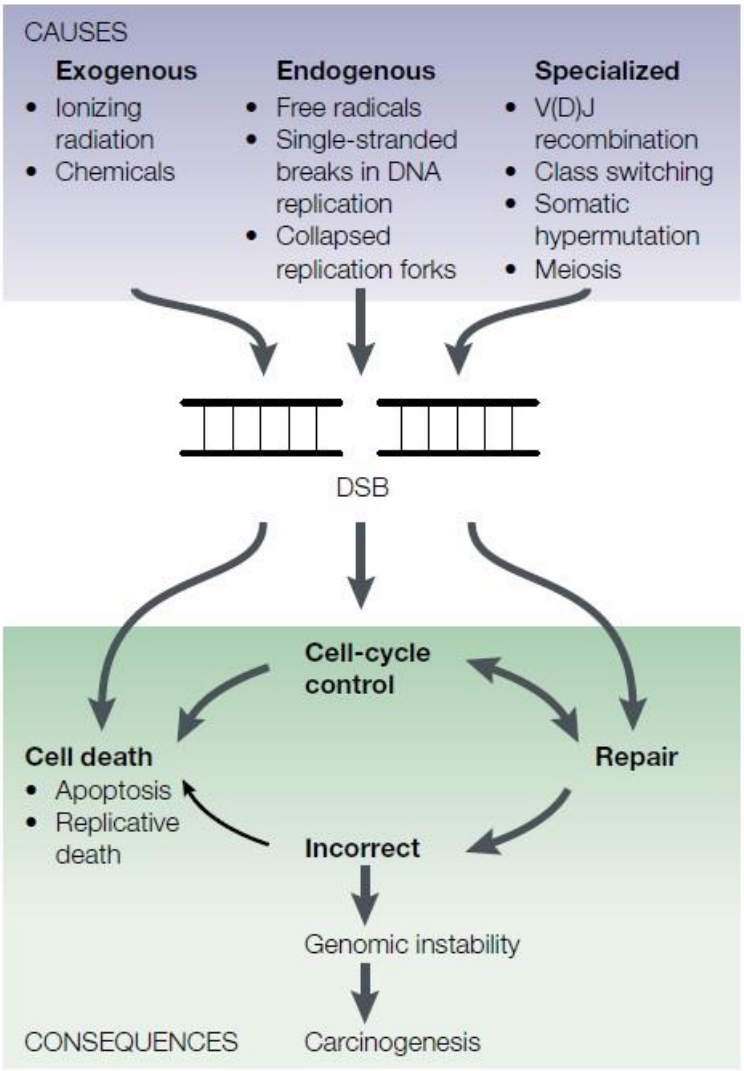

Figure 11. Summary of the causes and consequences of DSB formation in human cells (van Gent et al.*, 2001).*

2. DNA damage response

Eukaryotic cells have developed complex response systems in response to DNA damage, which constitute the DNA damage response (DDR). They allow the detection of the lesions, the recruitment of factors, the completion of DNA repair activities and the arrest of cell proliferation, thereby preventing harmful cellular consequences and the transmission of damaged DNA to daughter cells. In this section, we describe the mechanisms that trigger DNA repair or orient the cell toward other responses. As we will show, DNA repair is not the only option in the DDR. For instance, high levels of damage can lead the cell to suicide for the greater good in complex organisms.

The DDR is made of an orchestrated interaction between different cellular pathways that mobilize a plethora of collaborating or competing factors, altogether resulting in a cellular response. These factors are usually regrouped into three main categories (Zhou and Elledge, 2000):

- Damage sensors, which are the primer identifiers of cellular anomalies
- Transducers and mediators, which are activated by damage sensors and orient the cellular response by mobilizing repair factors and other actors of the DDR
- Effectors which carry out the functional part of the DDR, including DNA repair activities, apoptosis and the regulation of gene expression.

It must be pointed that this classification varies between studies. Some proteins have overlapping roles and some authors classify them into different categories depending on the focus of their work.

The DDR is regulated in time and space, primarily through reversible post-translational modifications of existing proteins (Oberle and Blattner, 2010). This allows a quick response to cellular anomalies without the need of *de novo* protein synthesis. Additionally, this process limits energy expenses by reducing the risk of transcribing damaged DNA, which may result in non-functional response proteins.

These post-translational modifications include phosphorylation, ubiquitination, small ubiquitin-like modifier (SUMO)-ylation, poly(ADP-ribose) (PAR)-ylation, methylation and acetylation (Oberle and Blattner, 2010; Polo and Jackson, 2011). The reversion of the biochemical modifications allows their regulation, thereby modulating the intensity of the response. Notably, this process allows the dissociation of repair factors and the re-initiation of normal cellular activities if DNA damage is repaired.

Ubiquitination is mostly known for leading to the degradation of targeted proteins into proteasomes, but it is also involved in DDR signaling. Several DDR proteins, such as BRCA1, RING finger protein 8 (RNF8) and mouse double minute 2 homolog (MDM2) are ubiquitin ligases that influence the activity of other DNA damage response proteins. Protein ubiquitination was shown to be modulated by additional SUMOylation-based regulation, as illustrated by the increased ligase activity of the BRCA1/BARD1

(BRCA1-associated RING domain protein 1) heterodimer following its SUMOylation (Morris *et al.*, 2009). Just as for dephosphorylation, deubiquitination, deSUMOylation and dePARylation are major regulations that tune the DDR (Kassab and Yu, 2019; Liu *et al.*, 2016; Polo and Jackson, 2011).

In addition, non-coding RNAs such as micro RNAs (miR-18a, miR-100, miR-622, etc.) and long non-coding RNAs (such as CCND1) were shown to regulate multiple aspects of the DDR. These factors were shown to indirectly modulate the expression of regulatory proteins such as p53 (Gioia *et al.*, 2019; Liu *et al.*, 2016; Meryet-Figuière *et al.*, 2016) or to directly influence the expression and activity of DDR components. For instance, miR-622 was shown to directly impact the regulation of DSBR pathways, resulting in potential clinical applications (Vigneron *et al.*, 2020).

It must be noted that the DDR is energetically demanding. Phosphorylation, ubiquitination and SUMOylation are ATP-consuming.

2.1. Damage detection and signal transduction

The DDR can be activated by cellular anomalies including but not limited to DNA damage. For instance, replication stress also stimulates DDR factors (Ciccia and Elledge, 2010). Sensors such as Ataxia telangiectasia mutated kinase (ATM), DNA-dependent protein kinase (DNA-PK), ATR (Ataxia telangiectasia and RAD3-related) and poly(ADP-ribose) polymerases (PARP) are key players in the detection of these anomalies and the activation of transducers.

2.1.1.The ATM and DNA-PK pathways

The heterotrimeric meiotic recombination 11 (MRE11)/RAD50/Nijmegen breakage syndrome protein 1 (NBS1) complex (MRN complex) is one of the first factors to directly bind to DSBs (D'Amours and Jackson, 2002). It was shown to gather at DSBs and activate various proteins in a process called primary recruitment, including ATM, a major transducer of the response to DNA DSBs (figure 12). Human ssDNA binding protein 1 (hSSB1) also directly binds ssDNA ends and is thought mediate the recruitment of the MRN complex at DSBs (Croft *et al.*, 2019; Richard *et al.*, 2008).

In its inactive form, ATM forms dimers complexed with histone acetyl transferases MOF and Tip60, and ATM phosphorylation is maintained at a low level as a result of PP5 and PPA2 phosphatase activity (Thompson, 2012). ATM is activated by the MRN complex in a RAD50-mediated manner (Lee and Paull, 2007). Chromatin relaxation upon DSB formation may also be a key event for ATM activation (Thompson, 2012) as well as phosphatase and tensin homolog (PTEN) (Zhang *et al.*, 2016). ATM activation is thought to be promoted by phosphatase PP5, since PP5 depletion was shown to reduce DSB-induced ATM activity (Ali *et al.*, 2004). However, the exact interaction between these proteins in still unclear. Once activated, ATM phosphorylates itself as well as a number of signal transducers and

repair proteins that will be detailed further, including p53-binding protein 1 (53BP1), the MRN complex, replication protein A (RPA) and histones such as H2AX.

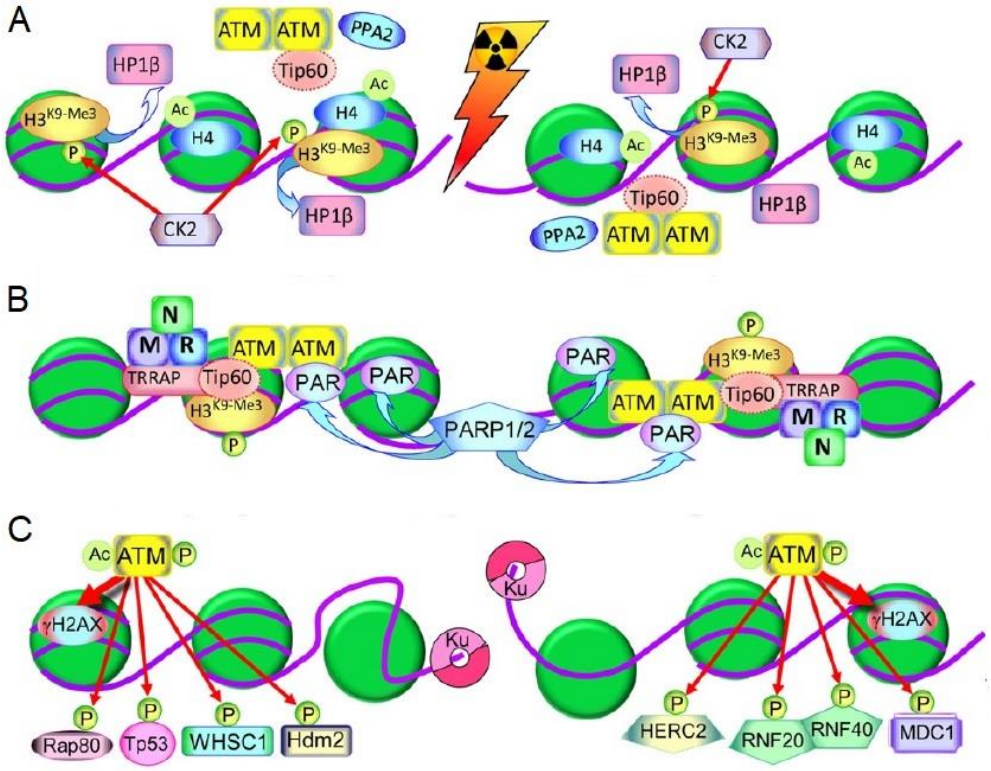

*Figure 12. Mobilization of DDR sensors, transducers, mediators and effectors following IR-induced DSB formation. Damage sensors (MRN complex, KU heterodimer, PARPs) participate in the activation of ATM, which in turn phosphorylate additional mediators and effectors of the DDR. **A.** Dimeric ATM is not activated right upon DSB formation **B.** The MRN complex is mobilized at the DSB and participates in the recruitment of ATM. PARP1 and PARP2 sense an interruption in the DNA molecule and initiate the PARylation of various DDR and DNA repair factors, including histones, ATM and PARPs themselves. **C.** The Ku heterodimer assembles at free DNA ends. Activated ATM phosphorylates its numerous substrates, that participate directly in the repair process or mobilize additional factors. In spite of extensive research, the exact sequence of events is not known and it is likely that several processes occur simultaneously. Adapted from Thompson and coworkers (Thompson, 2012).*

DNA-PK is a holoenzyme composed of a regulatory heterodimer of approximately 70- and 80-kDa (KU70 and KU80) and a 460 kDa catalytic subunit (DNA-PKcs). DNA-PK is a serine/threonine protein kinase from the phosphatidylinositol 3 kinase (PI3K)-related protein kinase (PIKK) family, and it is involved in the initiation and modulation of a large panel of repair activities (Davidson *et al.*, 2013)

The KU heterodimer sensor was shown to bind free DNA ends when they become available, and it participates in the recruitment of DNA-PKcs, which plays a dual role in DDR signaling as well as in DSBR through canonical nonhomologous end joining detailed further. Like ATM, DNA-PKcs autophosphorylates and also phosphorylates key factors of the cellular response like histone H2AX, RPA, Artemis and X-ray repair cross-complementing protein 4 (XRCC4). This results in the decondensation of the chromatin at the damaged site, which facilitates the initiation of the DDR and the recruitment of

subsequent factors on the damaged DNA (Lu *et al.*, 2019). ATM and DNA-PKcs have partly overlapping roles, but also have specific substrates (Burma and Chen, 2004).

2.1.2.The ATR pathway

ATR is activated in response to a larger range of DNA damage than ATM and DNA-PK. It was also shown to be mobilized in response to DNA SSBs as well as replicative stress, in an RPA-dependent manner. RPA binds ssDNA and interacts with ATRIP for the recruitment of ATR. The resulting RPA-ATRIP-ATR complex interacts with the RAD9-RAD1-HUS1 complex (911 complex) in a process mediated by Rad17 and RFC2-5, which allows the phosphorylation of RAD9 and the activation ATR following its association with DNA topoisomerase 2-binding protein 1 (TOPBP1) (figure 13). Besides, TopBP1 is also an ATR substrate, resulting in a positive retroaction and enhanced ATR activity. RPA also interacts independently with two other sensors, Ewing's tumor-associated antigen 1 (ETAA1) and hSSB1, to recruit ATR-ATRIP and activate ATR (Croft *et al.*, 2019; Haahr *et al.*, 2016).

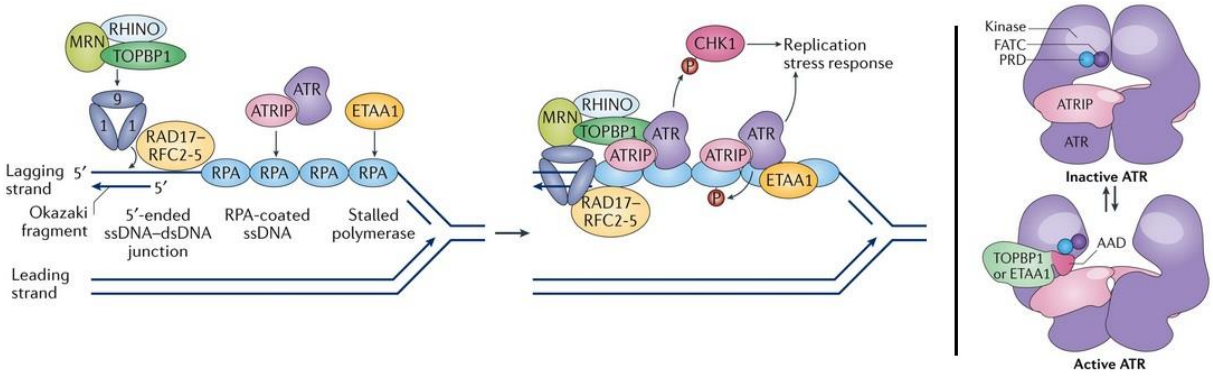

Figure 13. Mechanism of ATR activation.
A conformational change is thought to occur upon binding of the AAD domain of TOPBP1 or ETAA1 to the ATR-ATRIP complex induces a conformational change in ATR, which increases its catalytic activity (Saldivar et al.*, 2017).*

Due to its ability to bind ssDNA, RPA is also included among damage sensors by some authors, together with the MRN complex (Feng *et al.*, 2016).

2.1.3.PARPs

Finally, PARP enzymes are a family of glycosyltransferases with at least 17 members (Vyas *et al.*, 2014), among which PARP1 and PARP2 are most relevant in this study. These enzymes catalyze the formation of poly(ADP-ribose) chains onto various proteins in an NAD^+-dependent manner. PARPs are sensitive SSB and DSB sensors that are mobilized in the very initial steps of the DDR (figure 12). The recognition of interruptions in the DNA molecule is achieved through zinc fingers that mediate the activation of the protein. Once activated, PARP initiate PARylation on themselves and other substrates, including histones H1 and H2B, thereby facilitating chromatin remodeling. Similarly, PARP family members stimulate ALC1 helicase and the recruitment of the NuRD chromatin-remodeling complex, thus

increasing nucleosome destabilization. ATM ribosylation may also contribute to its activation. PARP1 and 2 have been suggested to modulate the binding of KU to DNA ends (Wang *et al.*, 2006).

2.1.4.Signal transduction

The communication of the DNA damage signal from sensors to DDR mediators is referred to as transduction. This process is mainly achieved through phosphorylation cascades and ubiquitination. These mechanisms are carried out by class IV PIKKs, a subset of the PI3K family of serine/threonine kinases composed of ATM, ATR, DNA-PK and mammalian target of rapamycin (mTOR). These proteins phosphorylate a large number of targets, including themselves; autophosphorylation represents a critical step for their activation, notably for DNA-PKcs. Contradicting reports are found regarding the importance of the autophosphorylation of ATM and ATR (Blackford and Jackson, 2017).

2.2. Mediators of the DDR

DDR mediators allow the recruitment of additional proteins, either directly or through the recruitment of scaffold proteins which act as landing platforms for the mobilization of a large panel of agents.

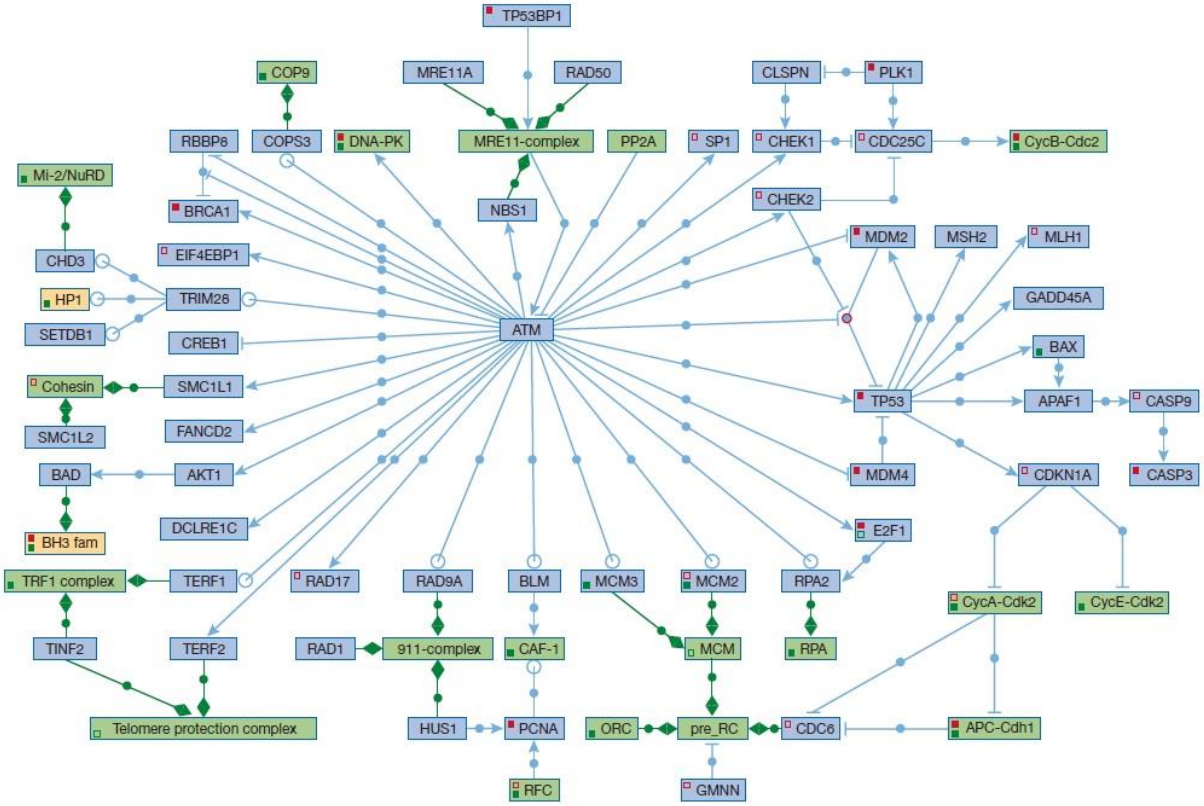

Figure 14. Overview of the pathways controlled by ATM (Lavin et al.*, 2006).*
Single proteins are indicated in blue, protein families in yellow and protein complexes in green. Blue lines represent regulatory relations (arrows for activation, blocked lines for inhibition and an open circle for unclear regulation) and green arrows underlie containment relations. Red and green dots indicate additional interactions that are not represented.

Figure 14 represents a subset of ATM substrates, thereby illustrating the importance of this transducer DSB-induced DDR. In a large-scale proteomic study, Matsuoka and coworkers found more than 900 regulated phosphorylation sites recognized by ATM in a total of more than 700 proteins (Matsuoka *et al.*, 2007). Listing all mediators of the DDR is far beyond the scope of this manuscript, but we will discuss some of the most relevant substates of the response transducers.

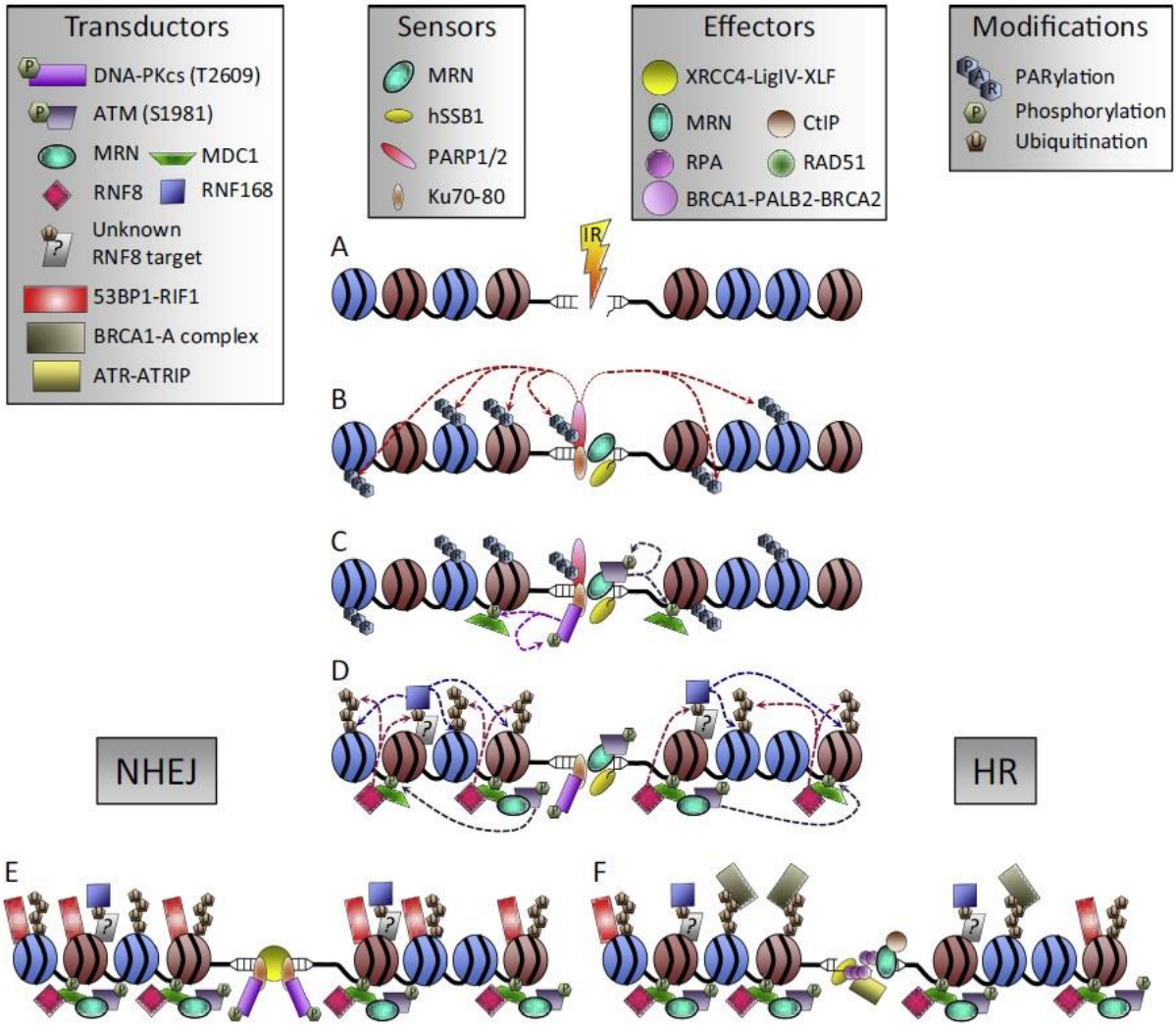

Figure 15. Mediation of the DNA damage signal from DNA sensors to the effectors.
Figure by Vignard and coworkers (Vignard et al., 2013).

A common target of ATM, ATR and DNA-PK is H2AX, a histone variant of the H2A family, which is phosphorylated at serine 139 upon DSB formation. Phosphorylation of H2AX is one of the most rapid cellular responses following breakage and it causes a chromatin remodeling that plays a major role in the recruitment of damage-signaling or repair factors to the site of DNA damage (Polo and Jackson, 2011). γH2AX interacts with the mediator of DNA damage checkpoint 1 (MDC1), which is another ATM target, in a process mediated by the MRN complex. MDC1 amplifies the MRN-ATM interaction, thereby further extending H2AX phosphorylation at the DSB. In addition, it serves as a docking platform for

numerous effector proteins E3 ubiquitin ligases RNF8 and RNF168, that target H2AX in a concerted, ATM-dependent manner (Vignard *et al.*, 2013). This was shown to play a critical role in the recruitment of downstream regulators of the DSB response such as 53BP1 and BRCA1 (Mattiroli *et al.*, 2012), as depicted in figure 15.

The various processes leading to the recruitment of response factors result in their quick and intense mobilization at damaged sites. γH2AX was shown to cover up to several megabase pairs around the DSBs, forming discrete structures called foci. These foci appear within seconds following the generation of a DSB, making γH2AX the most widely used indicator of DSB induction (Kopp *et al.*, 2019; Sharma *et al.*, 2012). Interestingly, DNA-PKcs-mediated H2AX phosphorylation is less extensive and less dense than that induced by ATM, which is to be related with different subsequent processes (Savic *et al.*, 2009).

53BP1 accumulation at the DSB is the result of a complex mixture of phosphorylation, ubiquitination and methylation processes (Lou *et al.*, 2020) and plays a critical role in mediation of the DDR (figure 15 and figure 16).

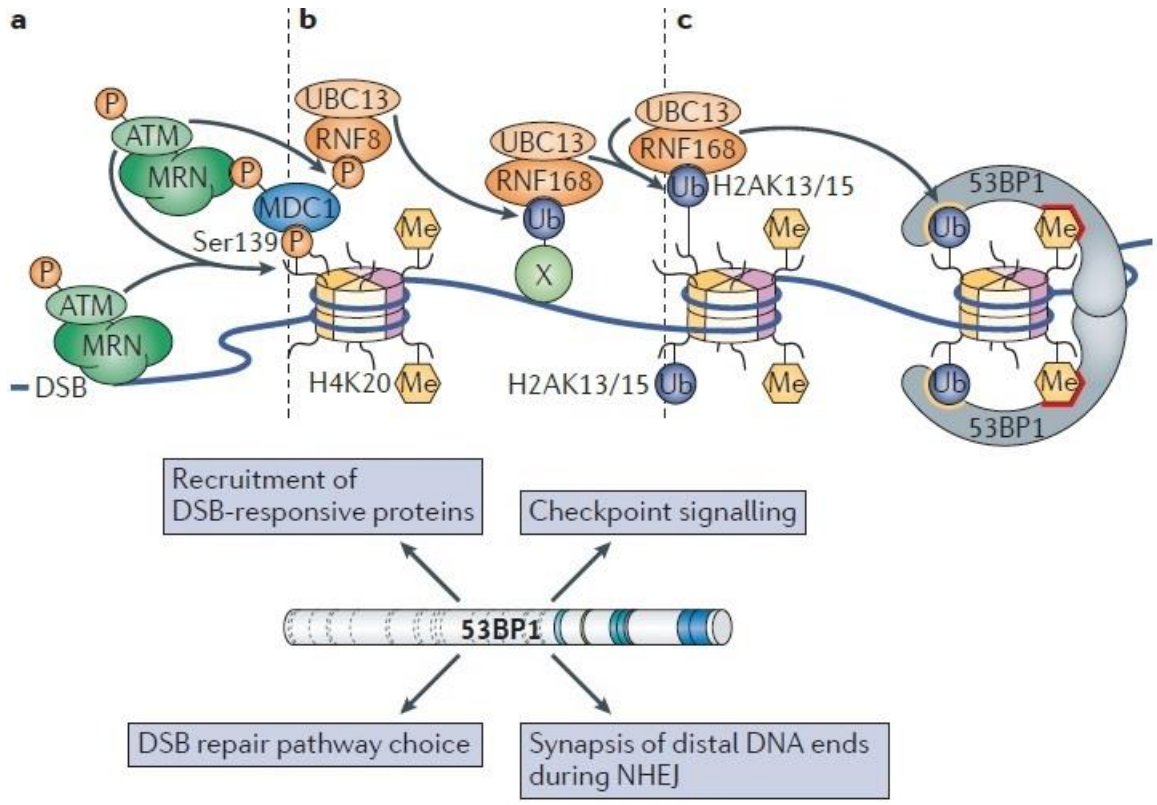

Figure 16. Recruitment of 53BP1 dimers in an ATM-dependent manner, and main biological functions of 53BP1. Based on figures by S. Panier and S.J. Boulton (Panier and Boulton, 2014).

Firstly, 53BP1 foci are scaffolds for DSB-responsive factors such as RAP1-interacting factor 1 (RIF1) and PAX transactivation activation domain-interacting protein (PTIP). Secondly, 53BP1 is commonly recognized as a determining factor in DSB repair pathway choice. Indeed, it promotes non-homologous

end joining by mediating the mobilization of NHEJ effectors and opposing DSB end cleavage (Chapman *et al.*, 2013). Finally, 53BP1 binds p53 and promotes checkpoint signaling by stimulating the ATM-dependent phosphorylation of Checkpoint kinase 2, p53 and BRCA1. A direct interaction between 53BP1 and the MRN complex (and potentially PTIP) also increases ATM activity (Panier and Boulton, 2014).

2.3. DDR effectors and cellular responses

Effectors carry out the functional part of the DDR, thereby participating in the observed cellular response. There are hundreds of DDR effectors and we detail only a few significant actors, including DNA repair effectors (which are described further), as well as checkpoint kinases, p53, CDC25a, p21, p38, CDK2 and B-cell lymphoma 2 protein (BCL-2) (Liu *et al.*, 2016). Here, we briefly describe the main cellular responses in which DDR effectors participate.

2.3.1. Cell cycle arrest

In normal cells, cell-cycle progression depends upon cyclin and cyclin-dependent kinases (CDK), which can be blocked in case anomalies are detected. Cell cycle checkpoints prevent cells bearing DNA damage from initiating DNA replication (G1-S phase checkpoint) or completing it (intra-S phase checkpoint). Damaged cells can also be arrested before starting mitosis (G2-M checkpoint) (Dasika *et al.*, 1999). The activation of these checkpoints is regulated mainly by two major proteins, checkpoint kinases 1 and 2 (CHK1 and CHK2). An overview of cell cycle arrest processes is presented in figure 17.

The G1/S checkpoint is controlled by ATM in a p53-independent manner through CHK2 and CDC25A, but also in a p53/MDM2-mediated fashion (Falck *et al.*, 2001; Maya, 2001). ATM-CHK2 signaling is rather specific to the response to DSBs (Smith *et al.*, 2010; Zhang and Hunter, 2014). Thr68 phosphorylation by ATM is a perquisite for CHK2 activation, but other CHK2 phosphorylations also play a role (Lavin *et al.*, 2006). Once activated, CHK2 inhibits the complexes formed by cyclin A/E and CDK2 and stimulates downstream upregulation of DNA repair machinery in a p53-dependent manner, which blocks the cells in late G1 phase or in S phase.

CHK1 activation is ATR-dependent and plays a critical role in triggering DNA repair and the replication checkpoint. Indeed, activated CHK1 directly stimulates the phosphorylation of WEE1, and it phosphorylates CDC25A and CDC25C, leading to their inactivation. Disabling these phosphatases increases the level of CDK1 phosphorylation, leading to checkpoint 2 activation and G2-phase arrest (Ding *et al.*, 2020). The S-phase checkpoint is also directly or indirectly regulated by C-terminal-binding protein-interacting protein (CtIP), NBS1, BRCA1 and Fanconi anemia group D2 protein (FANCD2)

(D'Amours and Jackson, 2002; You and Bailis, 2010). CDC25 phosphatases can also be inhibited upon ATM activation, resulting in S/G2 arrest.

CHK1 also plays a role in the activation of the G2/M checkpoint. Activation of CHK1 blocks cells in G2 phase, allowing DNA to repair or cell death to occur if DNA damage is irreversible and CHK1 inactivation is required for the cells to initiate mitosis (Meuth, 2010).

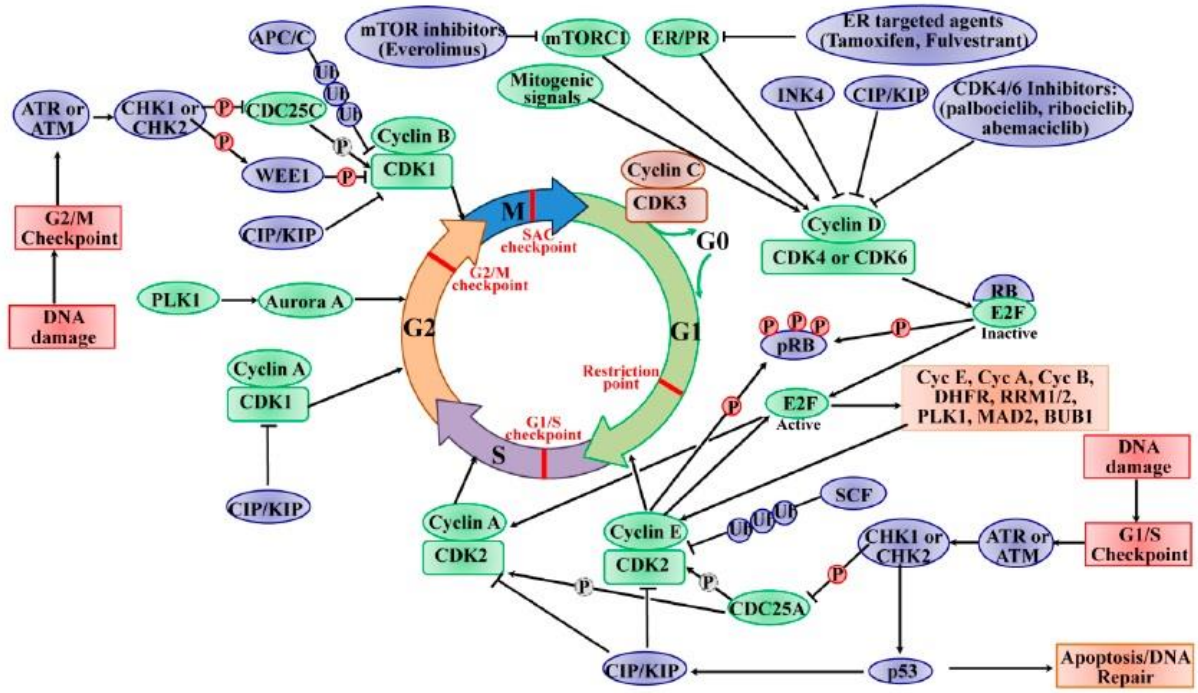

Figure 17. Progression of the cell cycle and its regulation by the CDKs and checkpoints in response to cellular stress (Ding et al.*, 2020).*

Both CHK1 and CHK2 pathways are mediated by p53. This protein is a well-known tumor suppressor which is often found to be mutated in human cancers (van Gent *et al.*, 2001). It is also a direct target substrate for ATM and ATR-induced phosphorylation. Additionally, p53 is regulated through ubiquitination, as illustrated by MDM2 activity and its downregulation by ATM and ATR (Cheng *et al.*, 2009; Shinozaki *et al.*, 2003). p53 is involved in a wide range of cellular mechanisms that we will briefly cover, including programmed cell death, DNA repair and autophagy. Its mutation in cancer cells also drives their metabolic reprogramming (Liu *et al.*, 2019).

ATM was shown to finely tune cell death by activating the nuclear transcription factor-κB (NF-κB), which favors the expression of anti-apoptotic factors. On the contrary, ATM-dependent phosphorylation of PIDD (p53-inducible protein with a death domain) triggers cell death in response to genotoxic stress (Shiloh and Ziv, 2013).

2.3.2.Apoptosis

If DNA repair is not successfully completed or if stress signals are not alleviated during cell-cycle arrest, cells can engage into apoptosis, a form of programmed cellular death that prevents the accumulation of genomic irregularities and the uncontrolled proliferation of aberrant cells (Koniaras *et al.*, 2001; Shiloh and Ziv, 2013).

There are two distinct, pathways to apoptosis in mammalian cells: the intrinsic pathway, activated by cellular stress and regulated by BCL-2, and the so-called death receptor (or extrinsic) pathway, which is activated by tumor necrosis factor receptors bearing an intracellular death domain (Aubrey *et al.*, 2018).

The intrinsic pathway upregulates certain BCL-2 family members, the BH3-only proteins, which inhibit pro-survival BCL-2 proteins, and activate the cell death effectors BCL-2-associated protein X (BAX) and BCL-2 homologues antagonist/killer (BAK). These factors cause extensive mitochondrial outer membrane permeabilization, resulting in mitochondrial to discharge into the cytosol, allowing the assembly of apoptotic factors like cytochrome C, procaspase-9 and its activator APAF-1. Finally, this complex cleaves executioner caspases 3, 6 and 7 into their active form, which dismantle numerous cellular substrates (especially factors of cellular integrity), leading to cytoskeleton collapse, nuclear envelope disassembly and genomic DNA fragmentation (Aubrey *et al.*, 2018; Green, 2005).

Even though some reports indicate the activation of the extrinsic apoptosis pathway under the action of cytotoxic drugs and γ-radiation (Friesen *et al.*, 1996) , this pathway is not the main source of DNA damage-induced apoptosis and we will not detail it further.

2.3.3.Senescence

Checkpoint activation is often considered a transient phenomenon after which cell proliferation restarts unless apoptosis occurs. However, DNA damage can also result in a permanent cell-cycle arrest, as observed in senescent cells. Senescence refers to this irreversible condition in which damaged cells survive but are unable to proliferate. Besides persistent DNA damage, senescence can also be caused by the aberrant activation of proliferative pathways, as seen for instance upon the expression of oncogenes (d'Adda di Fagagna, 2008).

Typically, senescent cells are blocked in G1 phase and present functional and morphological singularities (Cho *et al.*, 2004). Various pathways leading to senescence have been described in recent years, some of which appear to be independent of the DDR (Mijit *et al.*, 2020). However, the most extensively studied pathway involves p53 and p21. The exact mechanisms through which cells engage into senescence rather than apoptosis are still unclear, but it seems that a stable stimulus favors slow p53 activation by DDR kinases, which leads to its stabilization and to p53-mediated transcription of CDK inhibitor p21,

resulting in a stable cell-cycle arrest. On the opposite, transient stimuli tend to induce a transient cell cycle arrest, resulting in DNA repair or apoptotic response (d'Adda di Fagagna, 2008; Mijit *et al.*, 2020).

Once activated by p53, p21 modulate various cellular activities through the inactivation of CDK4/6 and the recruitment of the E2F4 repression complex, thereby disrupting the balance of retinoblastoma protein phosphorylation and inducing G1 arrest (Benson *et al.*, 2014). Notably, p21 opposes apoptosis by inhibiting apoptotic factors, and p21 inactivation in senescent cells initiates the caspase activation cascade (Yosef *et al.*, 2017).

The cellular microenvironment also seems to play a role in the induction of p53-mediated senescence. For instance, an inflammatory environment was shown to be necessary for the stabilization of the senescence induced by BRAF overexpression in fibroblasts (Kuilman *et al.*, 2008).

Senescence results in a lower rate of cell renewal and has a major role in aging. In addition, senescent cells are thought to impact their tissue microenvironment through an increased secretion of inflammatory cytokines, thereby impact normal tissue functioning (Mijit *et al.*, 2020). However, senescence induction eliminates early neoplastic cells from the proliferative pool, making this process a potent cellular response to oncogenesis.

2.3.4.Nuclear recruitment of DNA repair factors

As illustrated by Dahal *et al.*, mitochondrial DNA is also affected by DNA lesions and repair pathways have been shown to operate in mitochondria (Dahal *et al.*, 2018). However, these processes will not be discussed in this manuscript, since nuclear DNA represents the most important proportion of human DNA and is also the most valuable for a cell to transfer its genetic information. Upon DNA damage, extensive protein relocations have been described (figure 18), including that of DNA repair factors relocating from the cytoplasm to the nucleus (Tembe and Henderson, 2007). Among other relocating factors, the epidermal growth factor (EGFR) directly phosphorylates substrates like ATM and DNA-PK within the nucleus, thereby stimulating and modulating the DDR (Liccardi *et al.*, 2011; Toulany, 2019). Numerous DNA repair proteins are known to harbor nuclear localization signal sequences facilitating their import to the nucleus and co-importation has also been suggested to explain the simultaneous relocation of several repair factors (Knudsen *et al.*, 2009).

This relocation is thought to occurs within minutes following the detection of DNA damage, but the exact mechanisms through which it is carried out remain unclear (Friis and Solov'yov, 2018; Gildemeister *et al.*, 2009), in spite of the ever-growing description of the activities these factors operate once inside the nucleus. This response is faster than the transcription and translation of the associated genes, which, in addition, may also be damaged by the lesions. Hence, the relocalization of DNA repair protein is a key step in the DDR, which, as for posttranslational modifications, saves the cells both energy and time.

In addition, the localization of DNA repair activities was also shown to vary in the nucleus and the nuclear position of DNA lesions is thought to impact DNA repair pathway choice (Kalousi and Soutoglou, 2016; Marnef and Legube, 2017; Oza *et al.*, 2009).

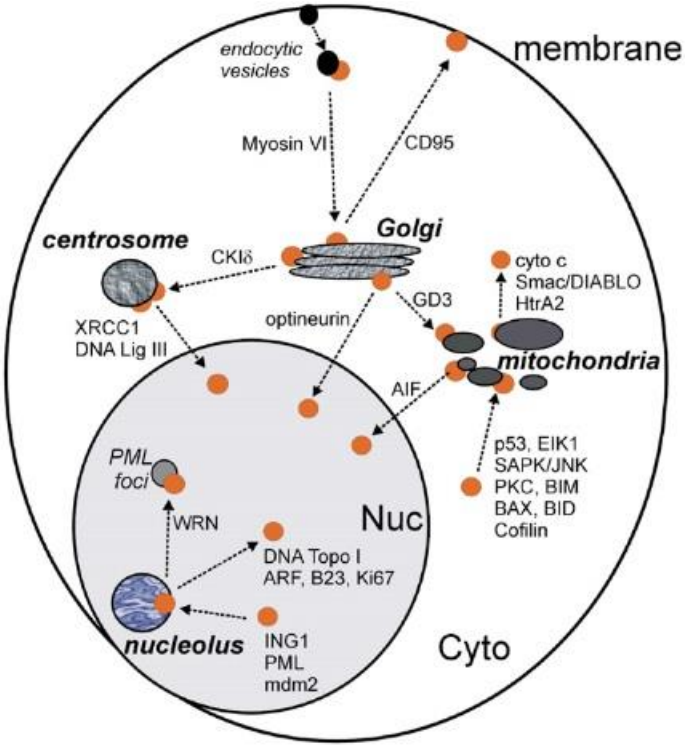

Figure 18. Damage-induced protein relocations (Tembe and Henderson, 2007).

3. Double-strand break repair

DSBs differ from other DNA lesions in that both DNA strands are damaged. Hence, the complementary DNA strand cannot be used as a template for repair. Consequently, DSBs can be potent inducers of mutations and chromosomal aberrations. In humans, at least four main DSBR pathways have been identified so far: homologous recombination (HR), canonical non-homologous end joining (c-NHEJ), alternative non-homologous end joining (alt-NHEJ) and single-strand annealing (SSA). They mobilize a large panel of repair proteins, some of which have already been presented due to their role in the DDR. These pathways all restore the physical integrity of the DNA molecule, but do not systematically restore the genetic information, which has important implications from a cellular point of view.

3.1. Homologous recombination repair

Figure 19 represents the two dominant DSBR mechanisms in humans, HR and c-NHEJ. HR is a mechanism shared with few alterations among higher eukaryotes and it is generally considered the optimal option to process DNA DSBs. This pathway is based on the use of another DNA molecule - either a sister

chromatid or a homologous chromosome - as a repair template, mostly in S- and G2-phase where this material is available (Wright *et al.*, 2018).

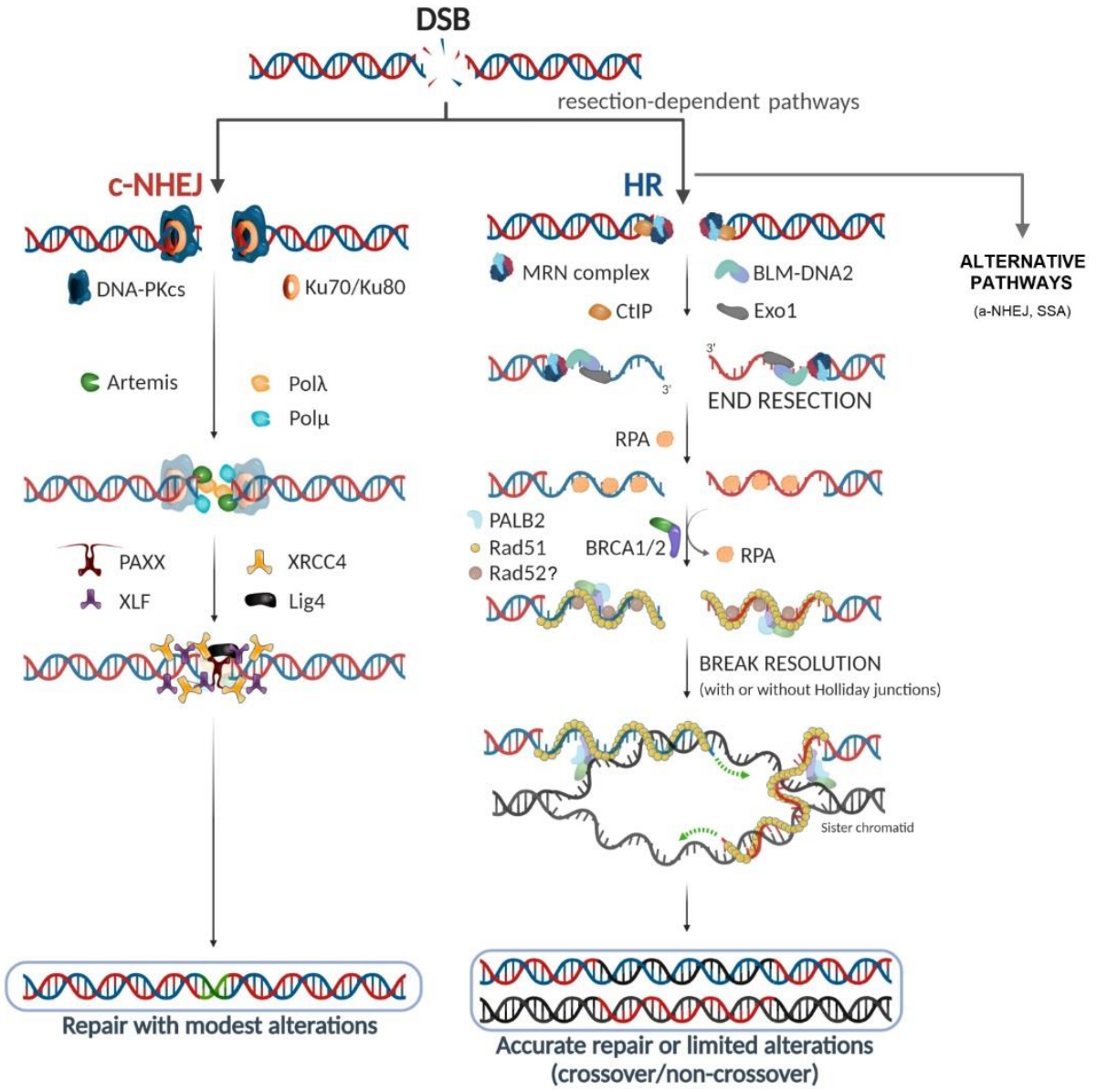

Figure 19. Synthetic representation of the HR and c-NHEJ pathways.
As opposed to c-NHEJ, HR is characterized by long range end resection, allowing the formation of the RAD51 nucleofilament that invades the template DNA molecule. Only the double Holliday junction mechanism is represented in this figure. c-NHEJ mobilizes fewer actors and achieves repair with faster kinetics, at the cost of modest sequence alterations. See sections 3.1 and 3.2 for details. (Tatin et al.*) - under reviewing.*

HR is characterized by an extensive 5' to 3' end resection at the vicinity of the break, forming 3'-OH ssDNA overhangs. This process is dependent on the MRN complex and has been shown to initiate events of the DDR (Williams *et al.*, 2010). The activity of the MRN complex is supervised by CtIP, which stimulates the transition from detecting DNA damage to resecting DNA strands (You and Bailis, 2010;

Makharashvili *et al.*, 2014). Exonuclease 1 (EXO1), endonuclease DNA2 and the Bloom syndrome helicase (BLM) then take over long range resection (Mimitou and Symington, 2011; Nimonkar *et al.*, 2011; Paudyal *et al.*, 2017), while ssDNA coating by the RPA complex lowers the reactivity of the newly formed overhangs with other ssDNA ends and challenges the formation of the RAD51 nucleofilament (Liu *et al.*, 2010). The stabilized RPA-coated ends are targeted by other mediators and recombinases, including breast cancer type 2 susceptibility protein (BRCA2), PALB2 and RAD51 paralogs. These proteins cooperate with BRCA1 and BARD1 to remove RPA, thereby facilitating the recruitment of RAD51, which forms a nucleofilament and enables strand invasion (Liu *et al.*, 2010; Sung *et al.*, 2003; Feng and Jasin, 2017). BRCA1 also polyubiquitinylates CtIP, which stimulates end resection; this interaction is promoted by the CDK-dependent phosphorylation of CtIP in S/G2 phase (Yu and Chen, 2004; Yu *et al.*, 2006). RAD52 has been implicated in yeast but seems to play a secondary role in mammalian HR (Hanamshet *et al.*, 2016).

HR is characterized by an important "search for homology", in which the RAD51 nucleofilament plays a critical role (Haber, 2018). During this process, homologous donor sequences are sought after to pair with the broken DNA ends. If an appropriate template is found (usually a sister chromatid), HR enters into a "synaptic" phase, characterized by the formation of a displacement loop (D-loop) and the displacement of DNA strand from the broken double helix and those of the donor (figure 19 and figure 20). In the postsynaptic phase, the resolution of the extended synaptic structures results in the exchange of DNA fragments and the restoration of DNA integrity in both the repaired and donor chromatid.

Three processes have been described (figure 20). Globally speaking, the repair option mostly depends on the interaction between DNA ends and the formation of a displacement loop and Holliday junctions (McVey *et al.*, 2016; Wright *et al.*, 2018; Li *et al.*, 2019a; Sebesta and Krejci, 2016).

The extended D-loop can be displaced by a helicase and undergo synthesis-dependent strand annealing (SDSA), resulting in non-crossover products. For single-ended DSBs (as seen following after the collapse of replication forks), break-induced replication (BIR) is engaged, which establishes a replication fork-like structure resulting in the donor sequence being copied until the end of the chromosome. Hence, non-crossover repair products are also formed. D-loop dismantling may involve RTEL and FANCM. "DSBR", in the post-synaptic context, refers to the subpathway that implies the formation of a double Holliday junction, in a process that may involve RAD52. This structure is resolved by proteins such as SLX1/SLX4, GEN1, MLH1 and EXO1. BLM has also been involved in the formation of a hemicatenane resulting from convergence of the double Holliday junction, which forms non-crossover products (Sebesta and Krejci, 2016). In figure 19, HR is illustrated with a double Holliday junction process.

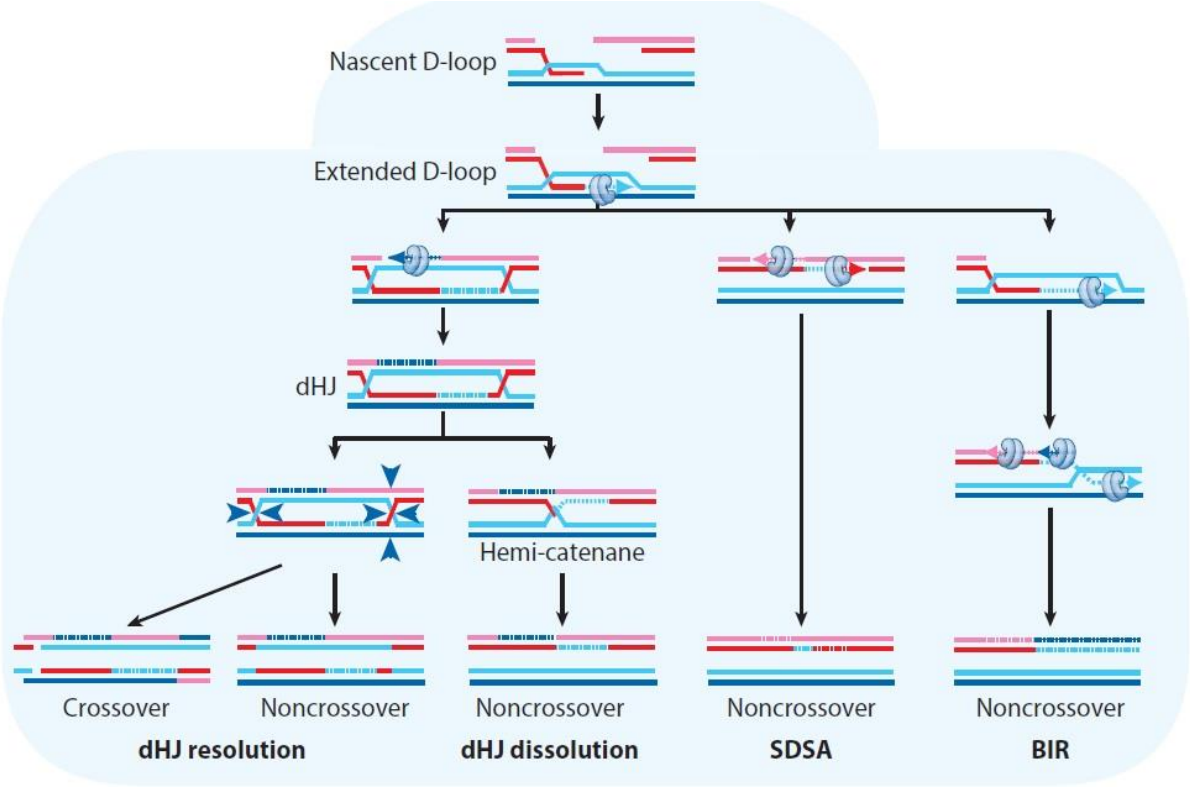

Figure 20. Post-synapsis mechanisms for the completion of HR.
Adapted from McVey et al. *(McVey* et al.*, 2016)*

HR is globally considered a highly conservative mechanism, even though some reports pointed out HR-related crossing-overs or mutagenesis (McVey *et al.*, 2016). However, it is a complex process that involves a large diversity of actors, resulting in relatively slow kinetics (approximately one to a few hours) (Vignard *et al.*, 2013; Kochan *et al.*, 2017), and its limited occurrence in the cell cycle calls for other mechanisms that challenge HR's limitations.

3.2. Classical non-homologous end joining

c-NHEJ, also referred to as "dominant" NHEJ, is the main competitor of HR; it is active all along the cell cycle, and is considered the default DSB repair pathway in human cells (Mladenov *et al.*, 2016). c-NHEJ is initiated by DNA-PK. DSB sites are detected by the KU70-KU80 dimer, which binds DNA end and participates in the recruitment of repair effectors (figure 19). KU has been shown to interact with CtIP to initiate end resection and stimulate the excision of damaged nucleotides at the DSB site. However, it seems that KU prevents long range resection by blocking DNA ends (Mimitou and Symington, 2010). Furthermore, it has a higher affinity for blunt or short ssDNA ends than for long ssDNA overhangs, hence engages less likely than HR effectors on the latter substrates. KU is involved in the recruitment of the DNA-PK catalytic subunit, which after both ATM-dependent and auto-phosphorylation mobilizes various repair proteins such as Artemis, terminal deoxynucleotidyl transferase (TdT), POLμ and POLλ, which carry out final DNA end processing and fill in the small gaps contained in aligned duplexes.

Polynucleotide kinase (PNK) has been shown to allow the processing of unligatable termini such as 5'-OH and 3'-phosphate ends induced by IR (Koch *et al.*, 2004). XRCC4 then initiates the final ligation steps in cooperation with the XRCC4-like factor (XLF) and their paralog (PAXX), by interacting with KU and DNA-PKcs to bring DNA end together and recruit ligase 4 to complete the ligation.

As opposed to HR, c-NHEJ operates in an almost template-independent manner, since less than 4 bp microhomologies are required to initiate repair (Pannunzio *et al.*, 2017). However, this limited reliance on homology increases the pathway's mutagenic potential, together with initial end processing which can also generate repair-induced mutations. However, depending on the configuration of the DSB, this pathway can repair the DSB without altering the initial nucleotide sequence (van Heemst *et al.*, 2004).

Besides, the operating sequence of c-NHEJ is less complicated and more reactive than HR, thereby allowing faster repair (half-time of 10 to 20 minutes) (Scully *et al.*, 2019; Vignard *et al.*, 2013; Iliakis *et al.*, 2004). Its ability to ligate non-complementary ends also provides a higher flexibility, making c-NHEJ a very efficient tool to reduce genomic instability.

Besides the HR/c-NHEJ paradigm, biological models with knockout or knockdown key proteins (such as RAD51 or DNA-PKcs) displayed unexpected repair activities, leading to the investigation of "backup" repair pathways relying on alternative sets of enzymes. These backup pathways, SSA and alt-NHEJ, are usually distinguished by their respective requirement for long or short repeat sequences (microhomologies). Nevertheless, we will see that the exact mechanisms behind these pathways are still poorly understood and several sub-pathways have been proposed. Some authors even avoid the presumption of independent pathways and do not distinguish between them (Kelso *et al.*, 2019).

3.3. Alternative non-homologous end joining

alt-NHEJ, also referred to as "backup" NHEJ or microhomology-mediated end joining (MMEJ) is one of the alternative processes that explain the repair capacity observed following inhibition of HR and NHEJ. It must be specified that the terminology varies among authors and alt-NHEJ is sometimes defined genetically by all the end joining pathways active in the absence of c-NHEJ, whereas microhomology-mediated end joining is defined by the molecular mechanism. Alt-NHEJ activity was first believed to be limited to cases of c-NHEJ deficiency, but it was later shown to be operating regardless of c-NHEJ status (Sfeir and Symington, 2015; Truong *et al.*, 2013). In this manuscript, we refer to the mechanism depicted in this section with the terms "MMEJ", "alt-NHEJ" and "a-EJ" in an equivalent manner.

a-NHEJ shares similarities with c-NHEJ in that the DNA ends are juxtaposed without using a homologous template as a guide. A prominent characteristic of a-NHEJ is its reliance on short microhomologies on each side of the DSB (Mladenov *et al.*, 2016; Black *et al.*, 2016; Chang *et al.*, 2017), though MMEJ is

sometimes classified only as a subset of a-NHEJ (Seol *et al.*, 2018). In spite of lasting uncertainties regarding the exact mechanistic details of alt-NHEJ repair, key players have been identified (figure 21).

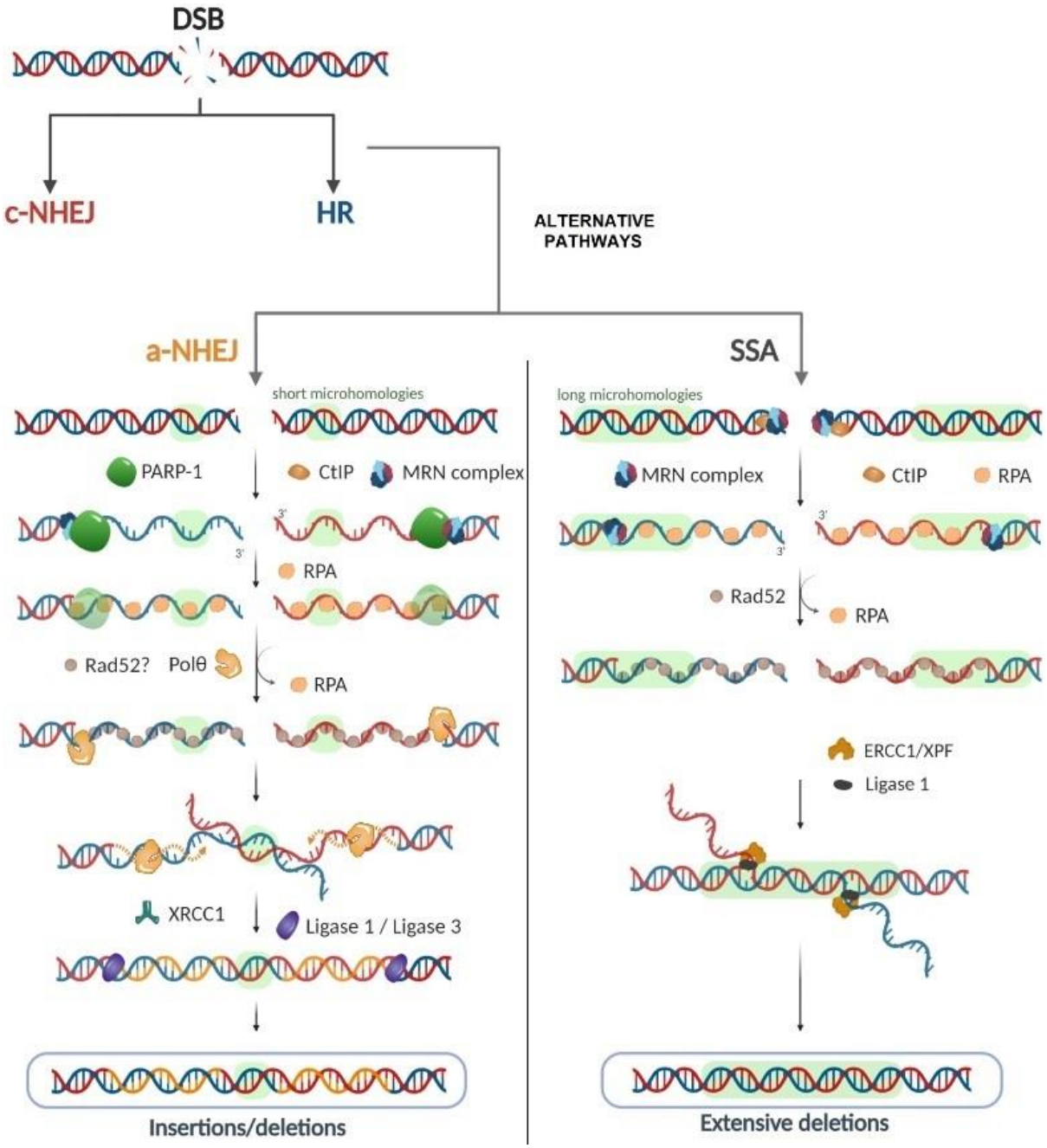

Figure 21. Synthetic representation of alternative DSB repair pathways.
a-NHEJ and SSA both depend on the initiation of DSB end resection, mobilizing proteins involved in early steps of HR. However, they require a lesser degree of homology and result in alterations of the original DNA sequence due to error-prone polymerase activities (a-NHEJ) or extensive ssDNA trimming (SSA). See sections 3.3 and 3.4 for details. (Tatin et al.*) - under reviewing.*

PARP1 is a typical repair protein involved in this pathway (Audebert *et al.*, 2004); it has been suggested to act as an antagonist of KU and thus to oppose the initiation of c-NHEJ (Wang *et al.*, 2006; Paddock *et*

al., 2011). Its activity may be enhanced by histone H1 (Rosidi et al., 2008). PARP1 targets include DNA ligase 3, POLβ, and scaffolding proteins such as XRCC1 (Isabelle *et al.*, 2010). It also participates in the recruitment of the MRN complex, especially at staled replication forks (Bryant *et al.*, 2009), where it promotes resection.

As a matter of fact, a-NHEJ depends on the initiation of DSB ends resection, which helps reveal microhomologies, allowing DSB alignment by pairing base of ssDNA ends; such a resection mobilizes the same proteins as for HR (MRN complex, CtIP) (Rass *et al.*, 2009; Badie *et al.*, 2015). However, *in vitro* studies have also shown that a-NHEJ can operate a direct ligation of complementary DNA ends as well as blunt or non-ligatable termini (Audebert *et al.*, 2006, 2008). PNK has been shown to play a role in this process, as in c-NHEJ.

PARP1 is also involved in the recruitment of polymerase θ (Mateos-Gomez *et al.*, 2015), which fills-in the flanking ssDNA regions. It also promotes DNA synapsis (Audebert *et al.*, 2004), stabilizes paired intermediates and opposes long-range resection (which may result in HR taking over the repair process).

The extension of ssDNA tails by POLθ has been shown to occur in both a template-dependent and independent fashion, causing the appearance of insertion mutations, as well as small deletions (Black *et al.*, 2016; Brambati *et al.*, 2020). The interaction of XRCC1 and ligase 3 results in the final end joining (Audebert *et al.*, 2004; Sharma *et al.*, 2015a), with a possible involvement of ligase 1 (Liang *et al.*, 2008; Lu *et al.*, 2016; Mladenov *et al.*, 2016; Paul *et al.*, 2013). It is worth mentioning that several actors of a-NHEJ are also involved in other repair pathways such as HR (MRN, RAD52, CtIP), NER (ligase 1) or BER (PARP1, XRCC1, ligase 1 and 3). RPA has been reported to oppose a-NHEJ in yeast, which may indicate a role in the promotion of the much safer HR pathway (Deng *et al.*, 2014).

a-NHEJ is an error-prone pathway that considerably modifies the sequence of the original DNA molecule. Even though it can serve normal processes such as V(D)J recombination, a-NHEJ seems to favor DSBs joining on different chromosomes, thus increasing the risk of genomic rearrangements and cellular transformation (Chiruvella *et al.*, 2013; Ceccaldi *et al.*, 2015; Kent *et al.*, 2015). a-NHEJ mutagenicity was first attributed to incorrect c-NHEJ, until further investigations revealed that was the result of this alternative mechanism.

This pathway is active throughout the cell cycle, but predominantly in G2 rather than in G1 phase due to lower resection in the latter (Huertas, 2010). Importantly, the synthesis of a sister chromatid is not a perquisite for end resection. Thus, alternative repair pathways can be initiated before the S-phase while HR is not active (Bhargava *et al.*, 2016).

However, a-NHEJ is not fully understood and it remains the object of recurrent debate. Some reports clearly differentiate between MMEJ and alt-NHEJ, and even associate MMEJ with a slow component of

DSB repair in G0/G1 phase that involves c-NHEJ factors but not alt-NHEJ, in a "resection-dependent c-NHEJ" mechanism that is distinct from the resection process in HR (Biehs *et al.*, 2017). Other authors separate two alt-NHEJ pathways based on their dependence on microhomology and their recruitment of LIG1 or LIG3 (Decottignies, 2013).

3.4. Single-strand annealing

SSA is sometimes characterized as a sub-pathway of HR due to its reliance on HR-related machinery and its dependence on homology. Typically, SSA is engaged when extensive homology exists between sequences at either side of the DSB (usually more than 20 to 50 bp in mammals) (Chang *et al.*, 2017; Kelso *et al.*, 2019). SSA starts with the same resection pattern as HR with the participation of proteins such as the MRN complex, CtIP and RPA, which also reveal microhomologies (Aparicio *et al.*, 2014). However, unlike HR where resected ends serve as a landing base for DNA polymerases and recombinases, SSA is characterized by the annealing of the two homologous DNA tails after RPA removal in a process that involves RAD52 (Stark *et al.*, 2004). Excision repair cross-complementation group 1 (ERCC1) complexed with *xeroderma pigmentosum* Group F-complementing protein (XPF) carry out the trimming of single-stranded flaps, while ligase 1 operates the final ligation of annealed DNA ends. This annealing results in major deletions on each side of the break (figure 21), with up to several hundred base-pairs long lost during SSA repair (Mladenov *et al.*, 2016).

SSA is thought to require longer end resection than alt-NHEJ, since extensive resection increases the probability of revealing long stretches of homologies. However, the exact required length of this resection is still a matter of debate (Bhargava *et al.*, 2016).

While both SSA and alt-NHEJ both anneal repeat sequences near the DSB, they were shown to be distinct on several levels. Firstly, RAD52 mediates the synapsis of the annealing intermediate in SSA, while it does not seem to be required in mammalian alt-NHEJ (Bennardo *et al.*, 2008; Guirouilh-Barbat *et al.*, 2004). Importantly, SSA is a RAD51-independent pathway that does not require the presence of a sister chromatid. However, it is initiated by DSB end resection, which mostly occur in the S and G2 phases of the cell cycle (Bhargava *et al.*, 2016; You *et al.*, 2009). Both RAD52 and POLθ are synthetic lethal targets for cells deficient in BRCA1 and BRCA2 (Ceccaldi *et al.*, 2015; Lok and Powell, 2012).

3.5. Balancing DSB repair: pathway choice and interactions

DSBR is regulated at the cellular level by:

- The cell cycle phase (figure 22). The activity of repair factors is mediated by CDKs and a pathway like HR is only active when a template is available in S/G2 phase. DSB end resection is specifically

activated in S and G2 phases, in part due to the CDK-dependent phosphorylation of CtIP (Chen *et al.*, 2008; Huertas and Jackson, 2009; Sartori *et al.*, 2007).

- The configuration of the break. For instance, KU preferentially binds blunt or short ssDNA ends.
- The interaction between DSBR factors (figure 23).

The interaction between DSBR proteins is complex and characterized by a duality between competition and cooperation. As an illustration, 53BP1 is a key DSBR actor that promotes c-NHEJ and MMEJ while opposing the mobilization of DSB end resection factors (Escribano-Díaz *et al.*, 2013; Xiong *et al.*, 2015; Spies *et al.*, 2019), while the PARP1-mediated inhibition of KU limits c-NHEJ and favors alt-NHEJ. For its part, BRCA1 competes with 53BP1 and promotes the resection-dependent initiation of HR (Bunting *et al.*, 2010; Symington, 2014). Importantly, the loss of 53BP1 in BRCA1-deficient cells partially restores HR activity (Bouwman *et al.*, 2010; Bunting *et al.*, 2010), while the inactivation of RAD51 or BRCA2 (and thus HR) increases SSA activity (Mladenov *et al.*, 2016).

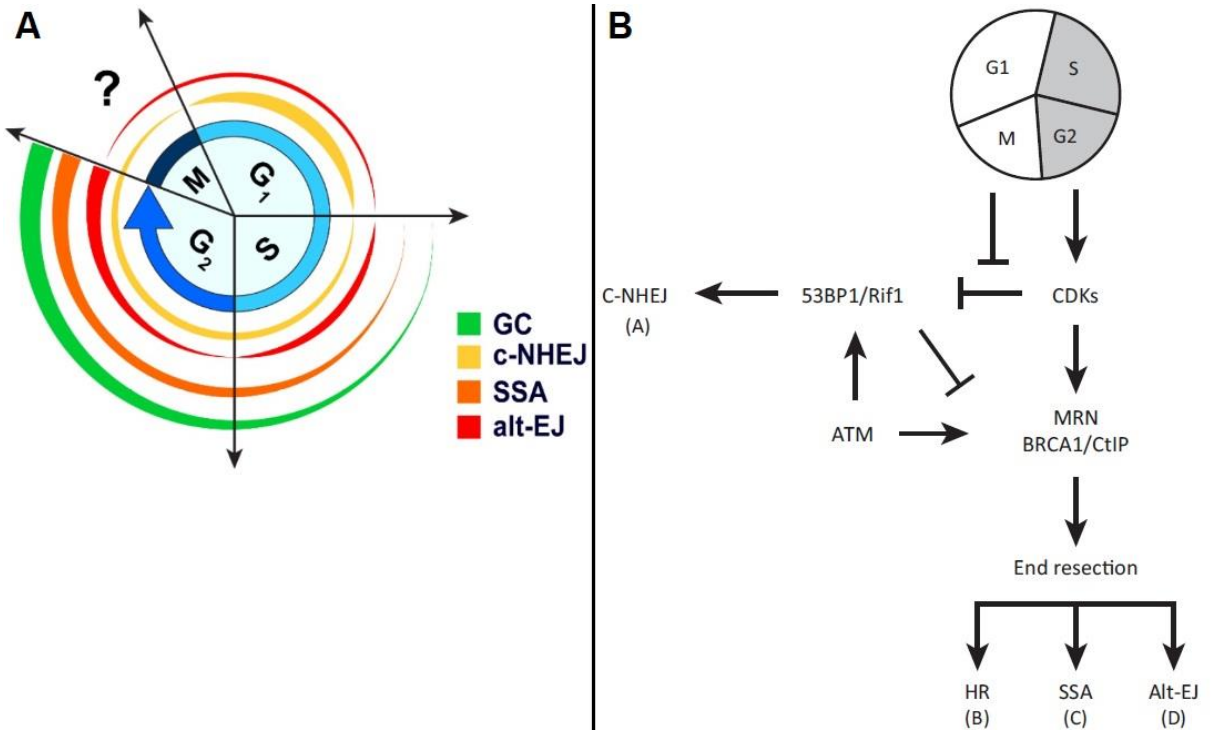

Figure 22. Influence of the cell cycle on DSBR activities and its molecular origin.
A. *The activities of each repair pathway vary along the cell cycle. c-NHEJ is active regardless of cell-cycle phase but operates most of DSBR in G1. The homologous recombination-based pathway (here referred to as gene conversion, GC) operates only in S and G2 phase, where backup pathways also peak due to the increased probability of end resection (Iliakis* et al.*, 2019).*
B. *Simplified overview of the regulation of repair pathway choice by CDKs (Ceccaldi* et al.*, 2016).*

On the other hand, factors like the MRN complex have an overlapping role in different repair pathways. Hence, repair proteins can intervene in case the initial chosen pathway is inefficient in repairing the DSB. For instance, repair can thus be switched to c-NHEJ if only a few nucleotides have been resected (which can still allow KU to operate), or otherwise be shunted to alt-NHEJ (Mladenov *et al.*, 2016).

BLM offers another illustration of the duality of DSBR. Indeed, it has been shown to repress alt-NHEJ in an epistatic fashion with 53BP1 and RIF1. Conversely, BLM can favor alt-NHEJ when 53BP1 and RIF1 are deficient (Grabarz *et al.*, 2013; Gravel *et al.*, 2008).

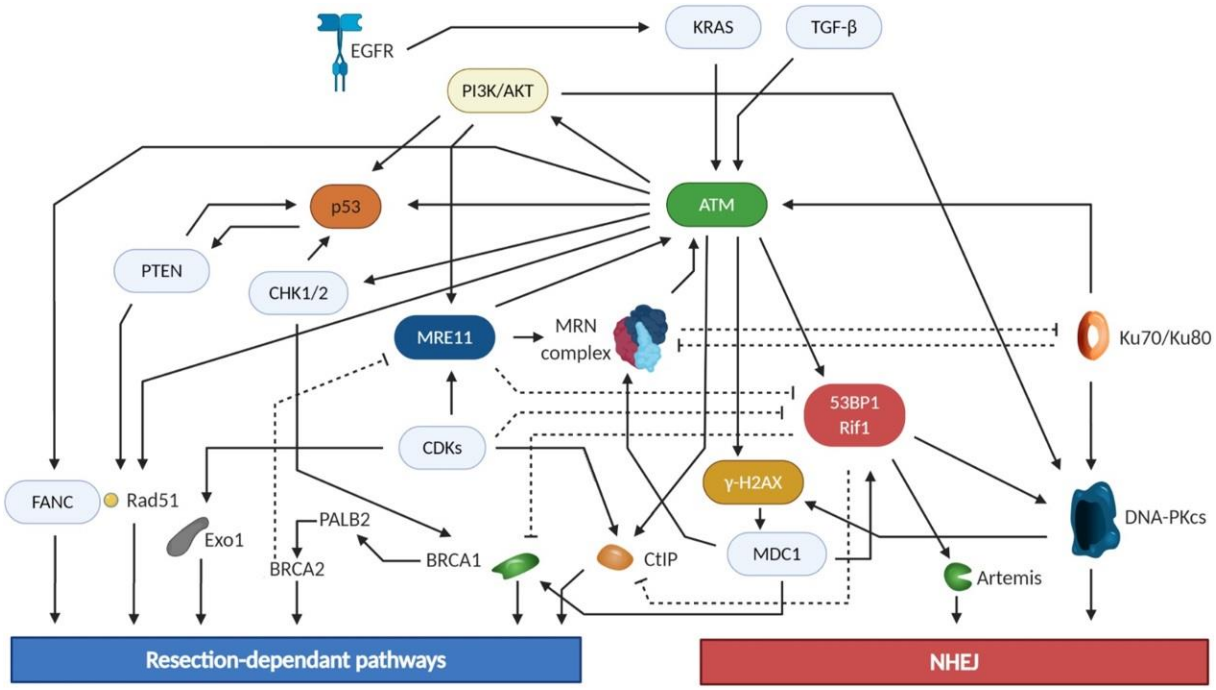

Figure 23. Schematic overview of the interactions between DSBR proteins (Tatin et al.*) - under reviewing.*

Table 1 summarizes the main features of the described DSBR pathways. The exact mechanisms of DSBR and its regulation are still the object of passionate debate. For instance, the alternative- versus classical-NHEJ model is still incompletely understood. Numerous alt-NHEJ pathways have been described, including a synthesis-dependent MMEJ (Yu and McVey, 2010) and a BLM-dependent pathway (Grabarz *et al.*, 2013; So *et al.*, 2004). It seems that pieces are still missing to the DNA repair puzzle. Contradicting results have been obtained regarding the key proteins involved in DSBR, the kinetics of their accumulation and the interactions between them, and much remains to be explored (Kochan *et al.*, 2017).

Table 1. Global characteristics of DSBR pathways.
Ranges are proposed based on available literature. nt: nucleotide.

	HR	c-NHEJ	a-NHEJ	SSA
Fidelity	Very high	Correct (no alteration to 1-4 nt deletions)	Short insertions or deletions	Large deletions
Homology requirement	Extensive (sister chromatid)	None to 4-6 nt microhomologies	< 20 bp microhomologies	Up to 50 bp microhomologies
Cell-cycle phase	S and G2	All along the cell cycle	G1, S and G2	S and G2
Kinetics	Slow (several hours)	Fast (tens of minutes)	Quite slow *in vivo* (several hours)	Variable

As previously mentioned, DSBs can originate from the conversion of other DNA lesions, notably upon DNA replication. Hence, DSBR pathways are also part of a bigger DNA repair picture, and we need to present the processes that repair non-DSB damage and thereby prevent the formation of more harmful lesions. Some of these mechanisms were also investigated during this PhD project.

4. Repair of non-DSB lesions

4.1. Base excision repair

BER ensures the correction of the most abundant DNA damage in cells: oxidized bases, abasic sites, alkylated bases and SSBs. These lesions, as opposed to bulky DNA adducts or ICLs, do not introduce major distortions of the DNA molecule. DNA damage is identified and processed by a specific family of enzymes, DNA N-glycosylases, which are critical BER factors. Three other types of enzymes are required for the completion of BER: an AP endonuclease or DNA lyase, a DNA polymerase, and a DNA ligase (Robertson *et al.*, 2009). The overall BER process is summarized in figure 24.

4.1.1. Detection and removal of damaged nucleobases by DNA N-glycosylases

DNA N-glycosylases catalyze the cleavage of the N-glycosidic bond between DNA nucleobases and the sugar backbone, thereby removing damaged bases and creating an AP site. These enzymes have appeared through convergent evolution in living cells and are spread across six structural superfamilies. At least 11 different DNA N-glycosylases have been identified in mammals (Krokan and Bjoras, 2013) and a subset of them is presented in table 2. Their detailed mechanism of action is beyond the scope of this manuscript, but DNA N-glycosylases share interesting features.

Table 2. Common mammalian DNA N-glycosylases (Beard et al.*, 2019).*

Enzyme	Abbreviation	General substrates
Monofunctional[a]		
Methyl-CpG-binding domain protein 4	MBD4	T and U paired with G
MutY homolog	MYH	A paired with 8-oxoG
N-Methylpurine-DNA glycosylase	MPG, AAG	3-AlkylA
Thymine-DNA glycosylase	TDG	T and U paired with G
Uracil-DNA glycosylase	UDG	U
Bifunctional[a]		
8-Oxoguanine glycosylase 1	OGG1	8-OxoG paired with C
Endonuclease III homolog 1	NTH1	Oxidized bases
Nei-like DNA glycosylase	NEIL (1, 2, and 3)	Oxidized bases

[a]These labels refer to the number of enzymatic activities: monofunctional, glycosylase activity only; bifunctional, glycosylase and lyase activities.

Firstly, these enzymes have a high affinity towards specific substrates and their activity results in the formation of an AP site. For instance, 8-oxoguanine glycosylase 1 (OGG1), one of the most studied glycosylases, processes two oxidation products including 8-oxoG paired with a cytosine. Uracil-DNA glycosylase (UNG, also named UDG) on the other hand, detects and cleaves uracil incorporated into DNA (Krokan *et al.*, 1997). Secondly, most DNA N-glycosylases induce a conformational change in the

minor groove and extrude the substrate base from the DNA double helix, stabilize into their active site and activate the glycosidic bond for cleavage. Finally, several of these enzymes have a specific catalytic cycle referred to as “burst kinetics”, with a slow product release phase that protects the enzyme-bound DNA repair intermediate from cellular signaling systems that detect DNA damage. This process prevents the lesion under repair to be confused an unprocessed lesion (Beard *et al.*, 2019).

As shown in table 2, DNA glycosylases are divided into two categories:

- Monofunctional DNA glycosylases cleave the N-glycosylic bond and leave an abasic site.
- Bifunctional DNA glycosylases have an additional lyase activity and cleave the sugar backbone of the DNA molecule (Krokan *et al.*, 1997).

4.1.2.Strand incision

If the damaged based was processed by a monofunctional DNA N-glycosylase, the resulting abasic site is recognized by an AP endonuclease, which cleaves the phosphodiester backbone 5’ to the abasic site, resulting in the formation of a SSB with a 3’-OH and a 5’-deoxyribose phosphate (dRp) end. In humans, this reaction is mainly carried out by AP endonuclease 1 (APE1), a member of the ExoIII family that was found to mediate more than 95% of AP site incisions in human cell extracts *in vitro* (Wilson and Barsky, 2001).

Alternatively, bifunctional N-glycosylases can carry out the hydrolysis of the phosphodiester backbone following the cleavage of the damaged base. Different mechanisms are described, that result in different end configurations (notably 3’-blocked ends) which can require enzymatic conversion into processable ends (Hegde *et al.*, 2008a; McCullough *et al.*, 2001; McNeill *et al.*, 2020; Robertson *et al.*, 2009). Among others, APE1, polynucleotide kinase/phosphatase (PNKP) and aprataxin (APTX) are involved in trimming the blocking residues and generating 5’ phosphate and 3’-hydroxyl ends (Beard *et al.*, 2019). This configuration enables the recruitment and activity of subsequent BER factors that act in two interconnected sub-pathways, the short patch and long-patch BER, which are named based on the extent of DNA resynthesis (figure 24).

4.1.3.Repair completion through short-patch BER

Short-patch BER is characterized by the replacement of one single nucleotide. Polymerase β (POLβ) operates DNA resynthesis on the 3’-OH end, resulting in the addition of the appropriate nucleotide (based on the complementary DNA strand). In addition, it can trim inappropriate DNA termini, such as the 5’-dRp end generated by an APE1-mediated base cleavage. The removal of the blocking dRp allows DNA ligation. Ligase 1 and 3 have been proposed to mediated the ligation step, but ligase 3 is the most commonly cited factor; their participation is thought to be more important in the nucleus and

mitochondria, respectively (Beard *et al.*, 2019; Krokan and Bjoras, 2013; McNeill *et al.*, 2020; Robertson *et al.*, 2009).

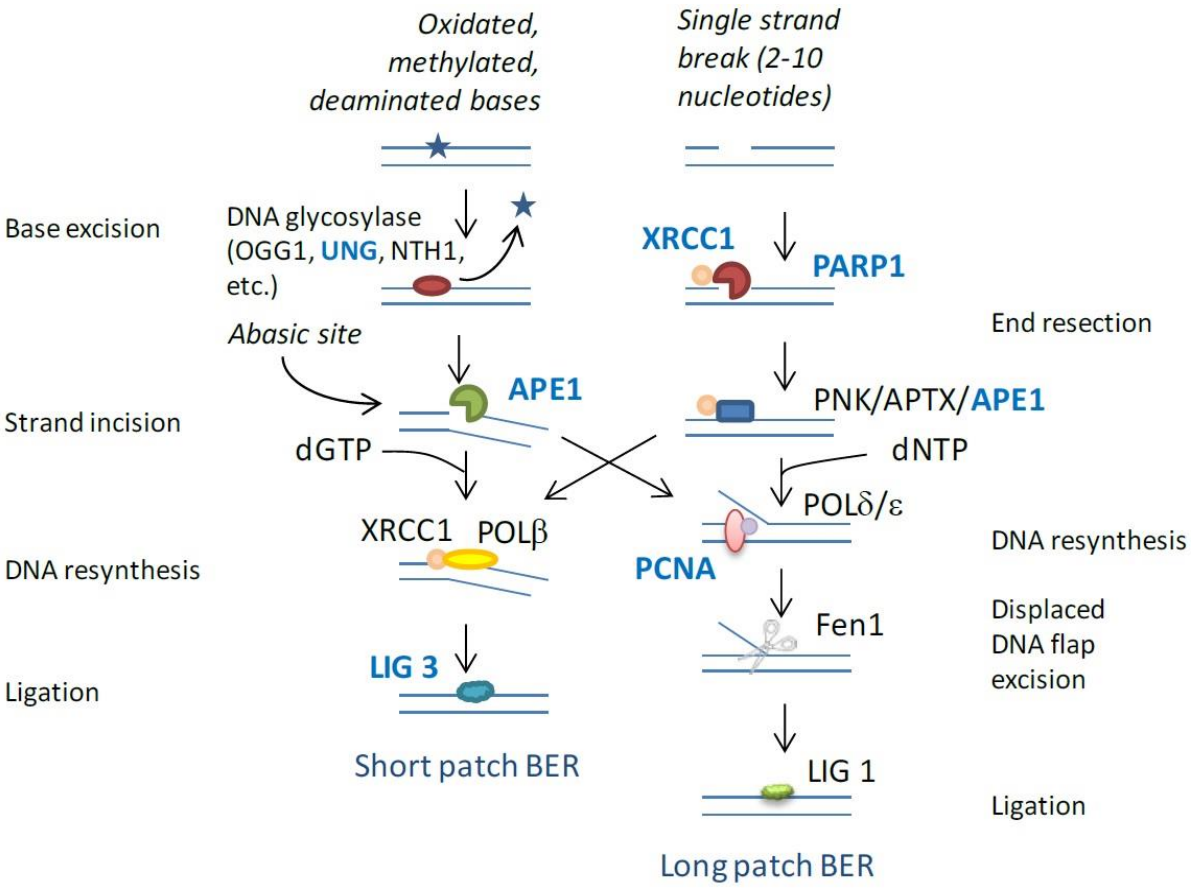

Figure 24. Schematic representation of short and long-patch BER. Original figure by Biola-Clier et al. *(Biola-Clier* et al.*, 2017).*

4.1.1.Repair completion through long-patch BER

The second BER pathway replaces a longer DNA portion (2 to 10 nucleotides) by recruiting additional DNA polymerases, POLδ and ε. This process also mobilizes RFC and PCNA and flap endonuclease 1 (FEN1). DNA polymerases operate the displacement of the SSB-bearing strand and DNA resynthesis; the resulting 5'-flap is removed by FEN1.

The identification of the exact long-patch factors is still debated, but the current consensus is that important interconnections exist between both pathways. For instance, POLβ and FEN1 were shown to cooperate during long-patch BER (Liu *et al.*, 2005). POLλ has also been involved as a FEN1 partner (Lebedeva *et al.*, 2005), though its role in DNA repair is still imprecise.

In addition, POLβ was suggested to be more active in non-proliferating cells, while proliferating cells had higher long-patch BER activity and may rely more extensively on POLδ and ε (Akbari *et al.*, 2009). Although ligase 1 was long thought to be the major long-patch ligase (Prigent *et al.*, 1994), both ligase

1 and 3 have since been involved in the final ligation step, as detailed by Krokan *et al*. (Krokan and Bjoras, 2013).

Short-patch BER is thought to be the dominant BER pathway, representing 75 to 90% of BER-mediated repair events (Nilsen and Krokan, 2001), but contradicting studies found similar activities in both pathways, as illustrated by Hou *et al.* using cell extracts *in vitro* (Hou *et al.*, 2007).

Overall, BER is influenced by various factors, including the type of lesion, which drives the recruitment of DNA N-glycosylate expression and hence the configuration of the transient SSB; in addition, the activity of key BER factors varies during the cell cycle. For instance, NEIL1 is expressed at a higher level in S phase suggesting that NEIL1 may preferentially mediate replicative damage in a POLδ-ϵ dependent manner (Hegde *et al.*, 2008b).

4.1.1.Role of PARP in BER

Since BER introduces transient SSBs in DNA, SSB repair (SSBR) and BER are closely related. Some studies include SSBs as a subset of the lesions processed *via* BER, while others consider BER as a sub-pathway of SSBR (Caldecott, 2008).

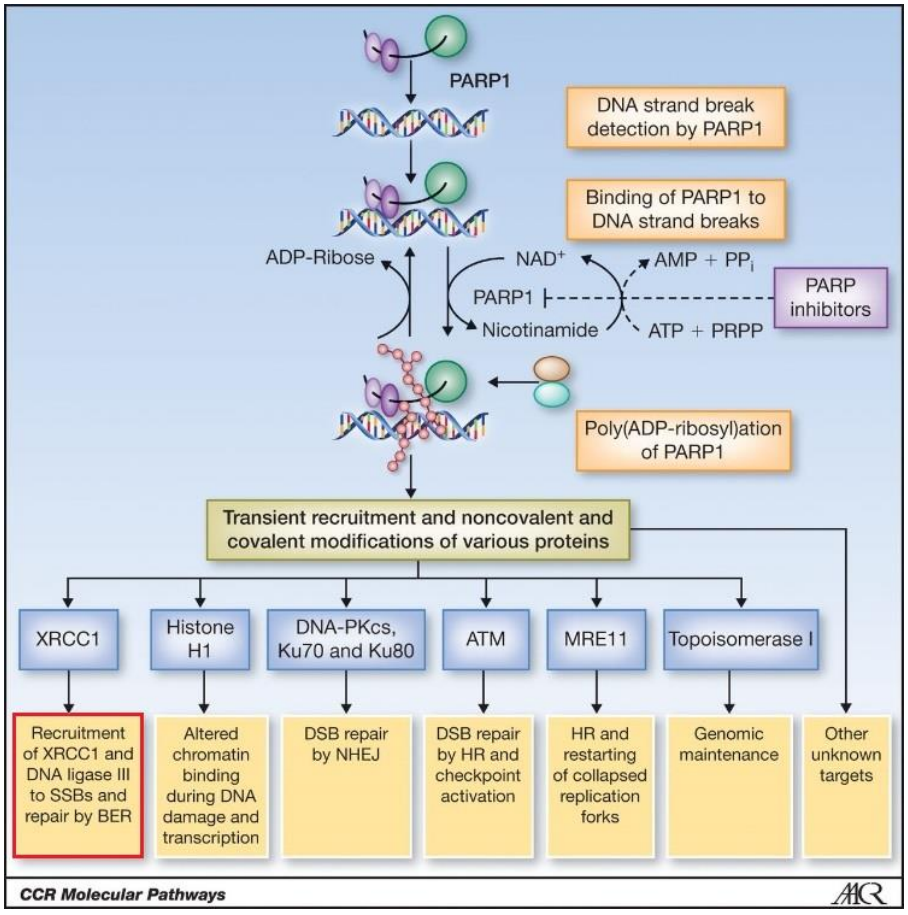

Figure 25. Role of PARP1 in BER among other biological functions. Adapted from Do and Chen (Do and Chen, 2013).

Among its diverse other functions, numerous studies investigated the role of PARP in BER-mediated SSBR (figure 25). PARP1 dimers are known to bind SSBs and prevent their conversion to more harmful lesions such as DSBs (Althaus *et al.*, 1999). However, contradictory results are found regarding the direct recruitment of BER proteins following the identification of a damage site. For instance, PARP1 depletion does not always result in reduced BER activity, as detailed by Woodhouse and Dianov (Woodhouse and Dianov, 2008). Intriguing reports showed that active PARP1 could even decrease BER kinetics (Allinson *et al.*, 2003; Orta *et al.*, 2014; Strom *et al.*, 2011).

Extensive PARylation of PARP1 and other DNA repair proteins was shown indirectly mediate the mobilization of the BER machinery in an iterative process composed of a PARP1-mediated SSB protection phase and BER-mediated repair phase following PARP1 removal (Dianov and Hübscher, 2013). In this model, PARP1 is still a critical factor of the repair response to DNA SSBs, in accordance to previous studies (Caldecott, 2008), but its presence is fine-tuned at the initiation of the BER mechanism. It seems that PARP1 mediation is strongly dependent on lesion type, as additional investigations support that the repair of repair of induced DNA lesions is achieved both by PARP1-dependent and PARP1-independent BER sub-pathways. PARP1 would thus be required for the repair of purine base damage but dispensable for the elimination of the pyrimidine base lesions (Reynolds *et al.*, 2015) or for the repair of small base lesions (Strom *et al.*, 2011).

Hence, the definition of the different pathways is a complex matter. It can be mentioned that DNA glycosylases NEIL1 and NEIL3 were found to target ICLs and bulky adducts (Mullins *et al.*, 2019), thereby expanding the potential scope of BER, which may overlap with nucleotide excision repair (NER), described below.

4.2. Nucleotide excision repair

NER processes a wide range of DNA helix-distorting lesions, such as photoproducts and bulky DNA adducts (Kusakabe *et al.*, 2019; Reed, 1998; Spencer *et al.*, 2008).

As its name suggests, NER is based on the cleavage of damaged nucleotides and *de novo* DNA synthesis. Indeed, NER is characterized by a dual incision mechanism over a longer length than in BER (24 to 32 nucleotides), resulting in the formation of a damage-containing oligonucleotide (Song *et al.*, 2017). NER has a highly versatile process and it recognizes the wider spectrum of lesions among DNA repair pathways. It removes lesions from the entire genome, although with uneven efficiency. For instance, the excision of lesions such as UVC-induced CPDs was found to be rapid on the transcribed strands of active genes than from the coding strands, which lead to the identification of a specific subpathway, transcription-couped NER (TC-NER). Alternatively, the “mainstream” NER pathway repair is termed

global genome NER (GG-NER) (Spivak, 2015). Both pathways differ in their initial recognition of DNA lesions. An overview of NER is provided in in figure 26.

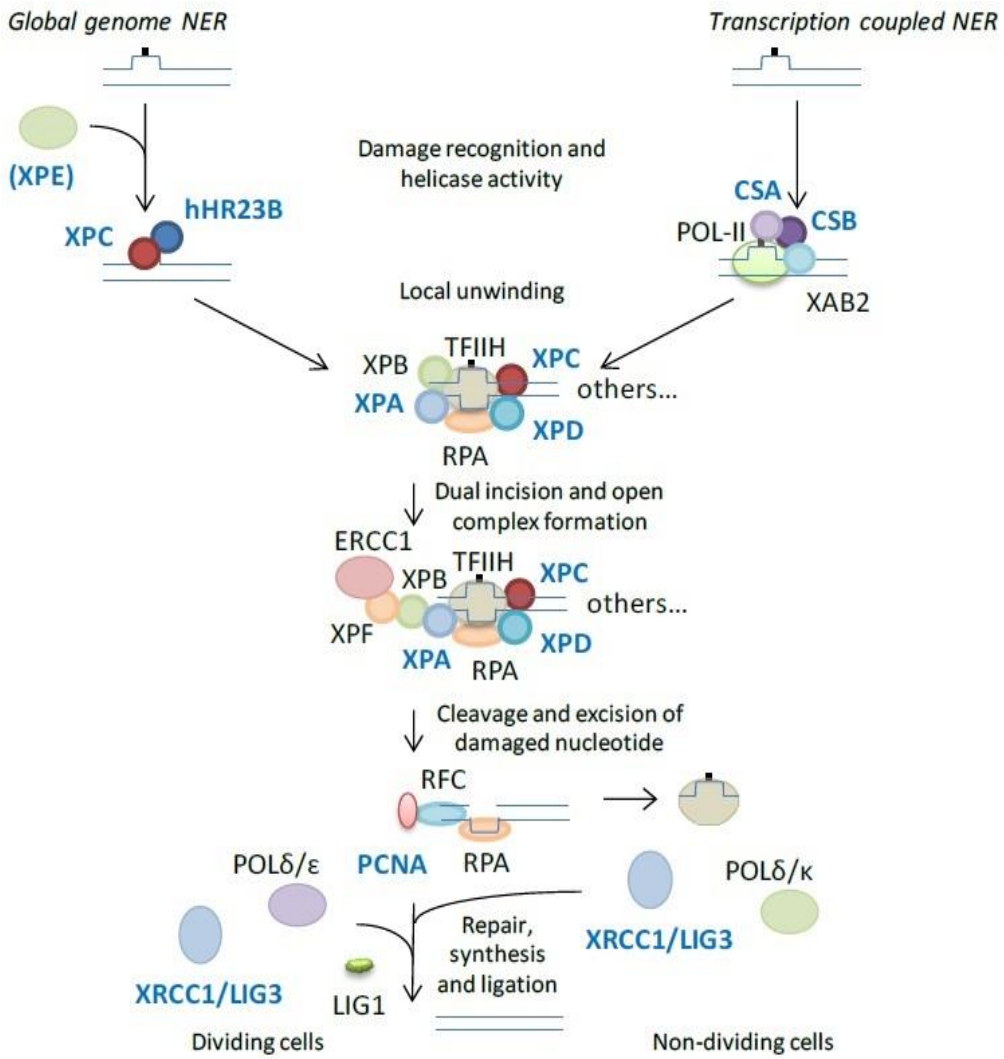

Figure 26. Schematic representation of GG- and TC-NER.
DNA damage is indicated by a black dot. Adapted from Biola-Clier et al. *(Biola-Clier* et al.*, 2017).*

4.2.1. Initiation of transcription-coupled NER

Human RNA polymerases are not known to bypass helix-distorting DNA adducts. RNA polymerase blockage at damaged sites during gene transcription results in the initiation of TC-NER; the interruption of transcript elongation seems to be the initiating factor, in a process that is still incompletely understood. Cockayne syndrome WD repeat proteins A and B (CSA and CSB, also referred to as ERCC8 and 6) are recruited by stalled RNA Pol II and mediate the assembly of TC-NER machinery (Fousteri *et al.*, 2006), including XPA-binding protein 2 (XAB2), UV-stimulated scaffold protein A (UVSSA), ubiquitin-specific-processing protease 7 (USP7) and high mobility group nucleosome-binding domain-containing

protein 1 (HMGN1), which participate in the subsequent recruitment of TFIIH. UVSSA and USP7 are key regulators of the activity of CSB, that they stabilize through deubiquitylation (Schwertman *et al.*, 2012; Zhang *et al.*, 2012). The interaction between core TC-NER factors also backtracks, displaces or degrades the RNA polymerase (which covers about 35 nucleotides), thereby allowing subsequent repair factors to access the lesion (Marteijn *et al.*, 2014; Tornaletti *et al.*, 1999).

4.2.2.Completion of NER

The two NER pathways share common features following the recruitment of TFIIH. This complex possesses two ATPase/helicase subunits, XPB and XPD (Schaeffer *et al.*, 1993, 1994), which unwind the DNA and form a bubble of about 20-30 nucleotides. Other TFIIH subunits are required for the completion of NER by stimulating XPB and XPD and ensuring the recruitment of key NER proteins (Singh *et al.*, 2015). XPD and XPB are involved in the correct verification of the presence of a DNA lesion, in cooperation with the XPA complex which detects altered nucleotide structures in ssDNA (Camenisch *et al.*, 2006).

RPA binds the undamaged ssDNA, thereby protecting it from degradation by endonucleases. It also coordinates the mobilization of additional NER factors. Notably, RPA interacts with XPA in the recruitment of XPG and the XPF-ERCC1 endonuclease. XPG and XPF-ERCC1 respectively incise the damaged strand in 3' and 5' to the lesion (Schärer, 2013). This role is supported by the fact that RPA binds ssDNA at approximately 30 nucleotides, which roughly corresponds to the size of the oligomer excised in NER (Fan and Pavletich, 2012). It was shown that the 3' incision operated by XPG is only triggered after the 5' incision by ERCC1-XPF (Staresincic *et al.*, 2009). Hence, DNA incision by ERCC1-XPF generates a free 3'hydroxyl group that can directly be used by the repair factors to initiate repair synthesis, while the XPG-induced, which cannot directly be used for DNA polymerization, only comes second, thereby limiting the exposure of the DNA nick and reducing the risk of DNA degradation at the 5' end. The lesion-containing oligonucleotide is then released with TFIIH and is eventually degraded.

XPG is also involved in the mobilization of PCNA and RFC, which participate in the recruitment of DNA resynthesis factors in interaction with RPA and induce the displacement of the XPF/ERCC1 complex. To our knowledge, some uncertainties remain regarding the DNA polymerases involved in NER for DNA resynthesis. As detailed by O.D. Schärer, at least three DNA polymerases are involved: POLδ and ε, as well as the error-prone translesion synthesis polymerase POLκ, each functioning with distinct interaction partners (Schärer, 2013). Since POLε is more active in dividing cells, it can be assumed that polymerase choice is influenced by cell cycle progression (Lehmann, 2011; Ogi *et al.*, 2010). Additionally, polymerase η could be involved in specific NER subpathways (Sassa *et al.*, 2019; Zheng *et al.*, 2003). The final step of NER, the religation of the cleaved DNA strand, also depends on cellular proliferation. It is

mainly carried out by the DNA ligase IIIa-XRCC1 complex in non-dividing cells, but also involves the replicative DNA ligase I-FEN1 complex in dividing cells (Moser *et al.*, 2007).

4.3. ICL repair

Inter-strand crosslinks (see section 1.5) are formed by endogenous agents like aldehydes or exogenous molecules such as cisplatin, which block DNA and RNA polymerases, hence hampering vital cellular processes. ICL repair (ICLR) is deficient in a rare genetic disorder, Fanconi Anemia (FA).

ICLR regroups features from both NER and DSBR, since these lesions resemble bulky adducts but both DNA strands have to be repaired.

ICLs are predominantly problematic during DNA replication, recombination and RNA transcription. Here, we present the mechanism of ICLR in a replicating cell. Other ICLR processes occur outside replication (Williams *et al.*, 2013), but they are not as well understood and their presentation is beyond the scope of our study. The complexity of such mechanisms is illustrated by Kato et al., who identified MMR proteins as alternative ICL repair factors in non-dividing cells (Kato *et al.*, 2017).

During replication, ICL-induced fork stalling is detected by the complex made of FA complementation group M protein (FANCM) and FA core complex associated protein 24, which is associated with FANCM-interacting histone fold proteins 1 and 2 and has a high affinity for branched DNA structures (Ciccia *et al.*, 2007; Yan *et al.*, 2010) (figure 27). Together with FAAP20 and P100 and FANC- proteins A, B, C, E, F, G, L and M, these factors constitute a central ICLR complex termed “FA core complex”. The assembly of the FA core complex and the monoubiquitylation of the FANCD2-FANCI are key steps for the continuation of the ICLR process (Kim *et al.*, 2008). This ubiquitination is carried out by FANCL and UBE2T (Machida *et al.*, 2006). The FANCM-FAAP24 complex also mediates the recruitment of RPA at the replication fork (Huang *et al.*, 2010).

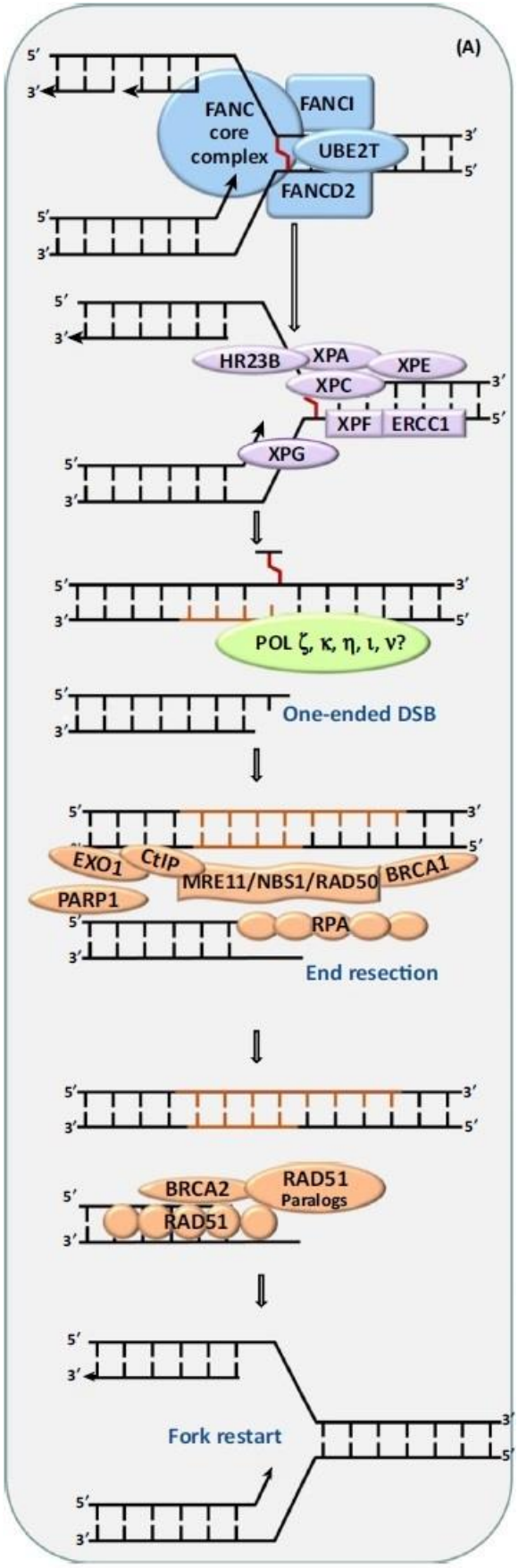

Other factors have also been suggested to play a role in the detection of ICLs and the initiation of the FA pathway, such as MutS homologues (MSH) (Huang *et al.*, 2011b).

The next set of events involves endonucleases such as XPF-ERCC1, SLX1-SLX4 or XPG, that cleave the stalled replication fork. Alternatively, human Mus81 was shown to operate in ICLR (Nomura *et al.*, 2007). DNA polymerases are then involved in DNA resynthesis following the removal of the damaged nucleotides. POLζ, κ, η and ν have been proposed to play a role in this step, in a process mediated by Rev1 (Roy and Schärer, 2016). These translesion DNA polymerases can replicate beyond DNA lesions, as described in the next section. To our knowledge, the identity of ICLR polymerases and the modalities of their recruitment is still debated.

Figure 27. Global scheme of ICLR in replicating cells (Nikolova et al.*, 2017).*

The following steps mobilize some HR factors to repair the DSB intermediate, based on the availability of a homologous template. It was shown that BRCA1, BRCA2 and Rad51 deficiency increases sensitivity to crosslinking agents (Bhattacharyya *et al.*, 2000; Kraakman-van der Zwet *et al.*, 2002; Moynahan *et al.*, 2001); BRCA1 is thought to have a specific action in ICLR, in which it may participate in upstream assembly of the repair machinery independently of its role in HR (Bunting *et al.*, 2012).

Hence, ICLR requires the interplay between repair factors implicated in other DNA repair pathways, including NER, HR and c-NHEJ. This further highlights the complexity of DNA repair systems and the extent of their interconnection.

4.4. Tolerance to DNA lesions: translesion synthesis

Translesion synthesis (TLS), is not a proper DNA repair pathway but rather a DNA damage tolerance mechanism. It is characterized by a replacement of common DNA polymerases found in DNA replication and repair (such as POLδ) by a special polymerase that possesses the ability to overpass DNA lesions such as ICLs or pyrimidine dimers (figure 28). The active site of TLS polymerases is less stringent toward the configuration of the DNA template, allowing them to incorporate nucleotides opposite DNA lesions (Shilkin *et al.*, 2020; Waters *et al.*, 2009). It has been proposed that POLη, κ and ι operate the incorporation of nucleotides opposite the lesion while POLζ carries out DNA synthesis beyond the damaged site (Shilkin *et al.*, 2020).

TLS is an inaccurate process due to the tolerance of the polymerases' active site towards the DNA template. Besides, TLS polymerases have little to no exonucleolytic proofreading activity. Hence, while replicative polymerases incorporate one incorrect nucleotide for every 10^6 to 10^8 replicated nucleotides, TLS polymerases have error rates around one error for every 10 to 10^4 nucleotides when replicating undamaged DNA (Makarova and Burgers, 2015; Shilkin *et al.*, 2020; Waters *et al.*, 2009).

This much lower average fidelity is somewhat contrasted by the capacity of TLS polymerases to incorporate the correct base opposite specific DNA lesions. For instance, POLη operates an accurate replication across photoproducts (Masutani *et al.*, 1999).

One of the main mediators of TLS is PCNA, that allows polymerase switching upon RAD6/RAD18-mediated ubiquitination. Rev1 is also required to assist translesion polymerization (Chang and Cimprich, 2009; Powers and Washington, 2018).

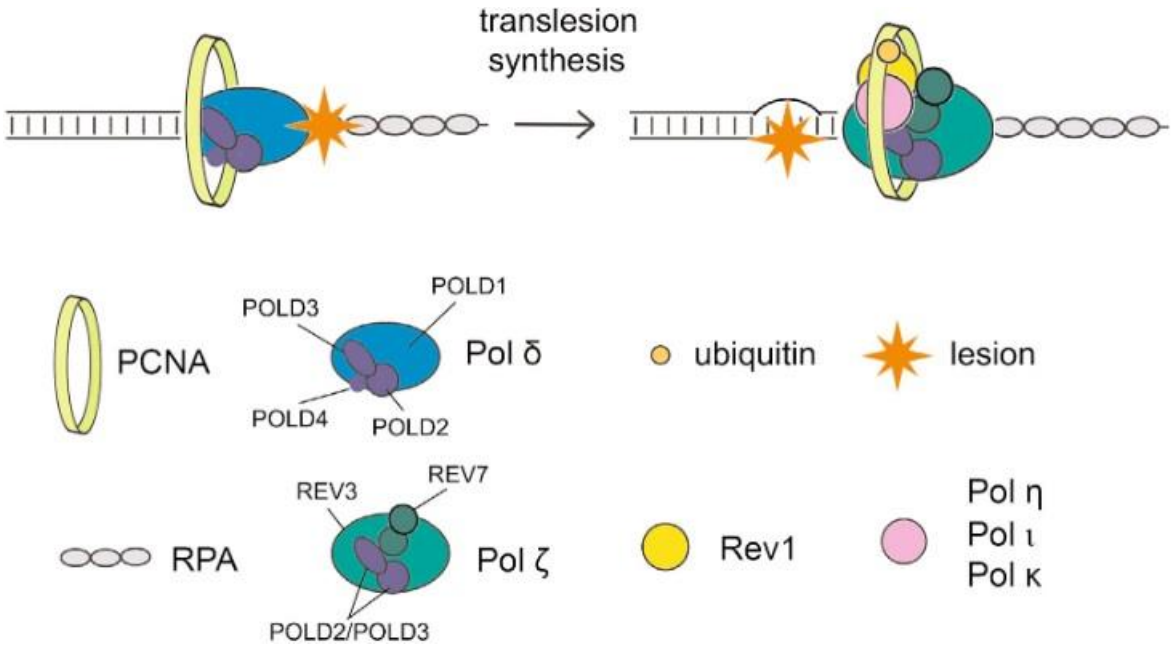

Figure 28. Representation of translesion DNA synthesis (Shilkin et al.*, 2020).*
PCNA ubiquitination initiates the assembly of the translesome and the replacement of a "standard" DNA polymerase (here POLδ) by TLS polymerases. The exact mechanisms of the interaction between the different TLS polymerases (POLη, κ and ι) are not shown.

In conclusion, the activity of TLS proteins and their access to replication forks are tightly controlled. TLS allows the cells to carry on with replication instead of waiting for repair. Although this may lead to mutations, it can be deemed preferable to a complete arrest DNA replication, which can potentially lead to cell death in case of ineffective or slow repair. The connection is tight between TLS and repair pathways, as shown by the participation in TLS factors in the processing of lesions such as ICLs (Haynes *et al.*, 2015; Roy and Schärer, 2016) or DSBs (Ma *et al.*, 2013), and the mechanisms through with these processes are controlled require further investigation.

4.5. Oher DNA repair mechanisms

Additional DNA repair mechanisms have been extensively studied. Direct reversal (DR) efficiently removes methyl groups from damaged bases and mismatch repair (MMR) processes mismatched bases as well as insertion-deletion loops (IDLs). These processes mobilize key DNA repair factors such as O^6-methylguanine-DNA methyltransferase (MGMT, involved in DR) or proteins such as EXO1, POLδ and LIG1 (MMR), that are also mobilized in DSBR pathways. A brief overview of these mechanisms is given in appendix 1.

5. DSBR: a need for further investigation

5.1. DSBR and disease

Deficiencies in DSBR pathways result in an altered DDR, increased rates of mutation and genomic aberrations, usually resulting in elevated cancer predisposition. In addition, such defects can impair the immune system by altering the repair of programmed DSBs during V(D)J and class switch recombination, leading to SCIDs. Finally, some of these disorders are also characterized by anomalies such as growth retardation and microcephaly, which highlights the role of correct DSBR in embryonic development, growth and aging. Table 3 briefly describes the most common disorders associated with impaired DSBR activities. The reader is oriented towards more detailed papers for additional information (McKinnon and Caldecott, 2007; O'Driscoll, 2012; Thompson and Schild, 2002).

Table 3. Most common human diseases related with DSBR.

Disease	Protein deficiency	Altered pathway	Biological Consequences	Estimated prevalence
Familial breast and ovarian cancer	BRCA1, BRCA2, RAD51	HR	Increased risk of breast and ovarian cancer, higher rate of chromosomal translocation, altered DDR	15-20% of breast cancers, 20-25% of ovarian cancers (USA) (Meaney-Delman and Bellcross, 2013)
Fanconi anemia	RAD51C/FANCO, FANCD1/BRCA2, PALB2, SLX4 (and others)	ICLR, HR	Bone marrow failure, development of acute myeloid leukemia and solid tumors (head and neck)	1 in 360,000 live births (Mamrak *et al.*, 2017)
NHEJ-deficient SCIDs	Lig4, Artemis, Cernunnos/XLF, DNA-PKcs	c-NHEJ	SCID, due to altered synthesis of immunoglobins and T-cell receptors. Potentially, developmental anomalies such as microcephaly and growth delay.	< 1 in 240,000 live births (Huang, 2005)
Nijmegen breakage syndrome and NBS-like disorder	RAD50, NBS1 (MRN complex)	HR	Altered DDR. Combined immunodeficiency, and increased risk of lymphoma. Growth retardation and microcephaly.	Approx. 1:100,000 worldwide (Varon *et al.*, 1993)
Bloom syndrome	BLM helicase	HR	Impaired growth, immunodeficiency and sunlight sensitivity, fertility defects, increased risk of cancer.	Approx. 300 individuals worldwide in 2019 (Flanagan and Cunniff, 1993)

The initiating event, such as a genotoxic insult, results in the irreversible modification of the genetic information which is inherited by daughter cells. Most somatic mutations do not individually have dramatic consequence, but extensive translocations as well as mutations in tumor suppressor genes or in key DDR and DNA repair factors can favor the pursuit of oncogenic transformation. For instance, mutation in the *TP53* gene can favor apoptotic bypass and cellular proliferation. The weakening of

cellular safeguards and cellular checkpoints increases the risk of uncontrolled multiplication of damaged cells that accumulate novel mutations (Ciccia and Elledge, 2010).

This stage corresponds to the pre-cancerous phase. An increase in proliferation rate is associated with additional cellular deregulations due to the cumulation of mutations, resulting in a clinically detectable tumor. This tumor evolves in size and complexity over time. It interacts with its environment through complex mechanisms that highjack other cellular mechanism (for example, angiogenesis allows solid tumors to be nurtured) and escape the immune system.

DSBR is a critical factor in the appearance and evolution of cancers. The progress in tumor sequencing underlined the dual role of DSBR in tumor suppression (reduction of the genomic instability) and oncogenic transformation (imprecise repair and increased mutagenesis) (Mladenov *et al.*, 2016).

Conversely, the most common anticancer treatments, radiotherapy and chemotherapy, are based on DNA damaging agents that aim at saturating cancer cells with damage, thereby resulting in cell death. Hence, downregulating DSBR in these cells is also a critical therapeutic lever (Aparicio *et al.*, 2014).

5.2. Development of repair inhibitors

The last two decades saw a sharp increase in the development of novel DNA repair inhibitors. Here, we focus on DSBR, but articles expertly describe the relevance of other DDR inhibitors for various clinical indications (Brown *et al.*, 2017; Cleary *et al.*, 2020).

A case-of-study on this topic is PARP inhibition (figure 29). PARP inhibitors such as olaparib are indicated for the treatment of ovarian and breast cancers; they trigger synthetic lethality in *BRCA*-mutated, HR-deficient tumors by inducing a critical increase in genomic instability due to an enhanced dependency upon mutagenic mechanisms. In addition, PARP1 inactivation impacts alt-NHEJ (Audebert *et al.*, 2004; Howard *et al.*, 2015; Mansour *et al.*, 2013; Wang *et al.*, 2006), thereby increasing the amount of unrepaired DNA.

Hence, potent and specific inhibitors have a high potential as anticancer agents in combination with "classical" DNA damaging treatments. The characterization of DSBR activities has major clinical implications for the correct identification of responsive patients, as will be developed in the "discussion" chapter. In addition, it may serve the identification of sensitive individuals, that may develop adverse effect due to low DSBR capacity. Finally, we showed that DSBR pathways are still incompletely understood, and new tools could help better describe and comprehend these complex mechanisms.

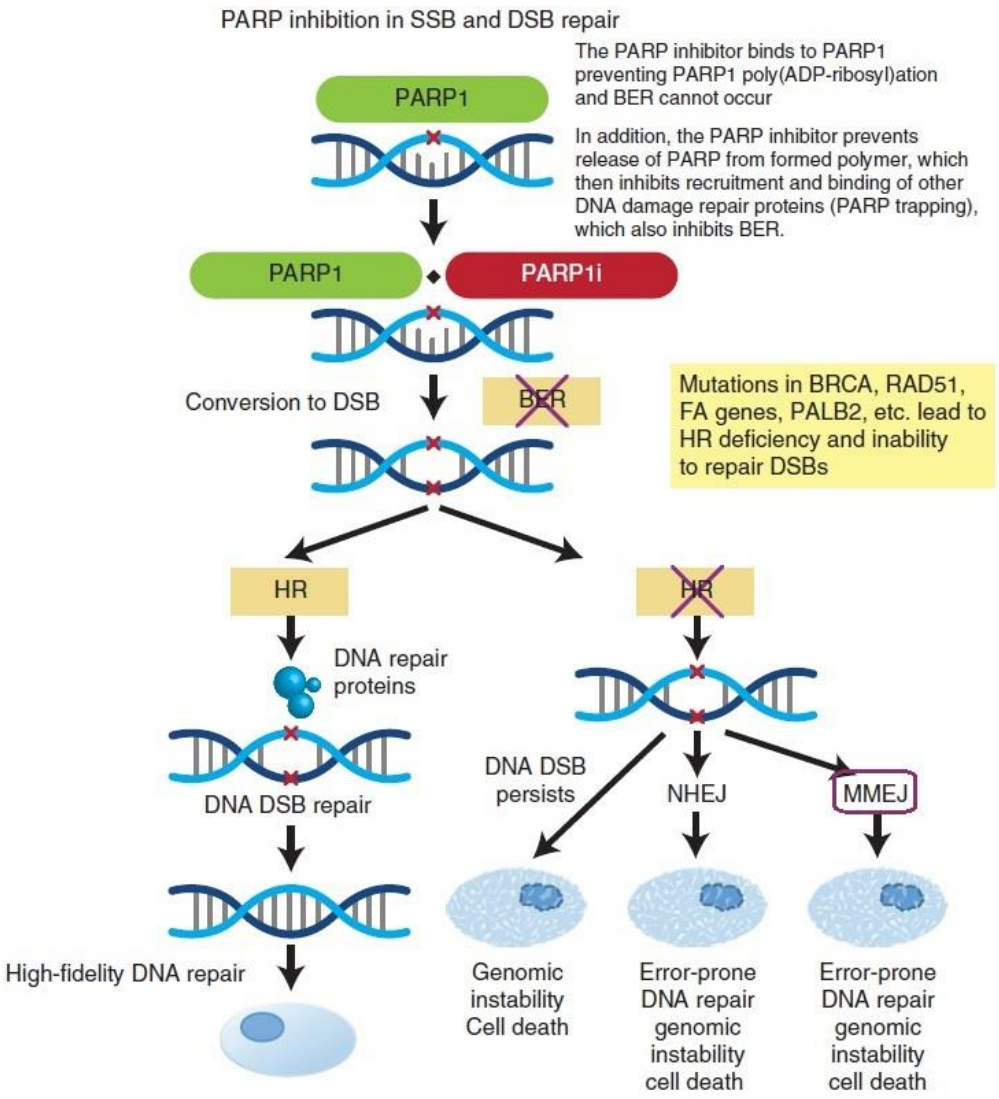

Figure 29. Consequences of PARP inhibition on DNA repair outcome.
PARP inhibition favors the persistence of SSBs due to the inactivation of BER and leads to their conversion to DSBs upon replication. In HR-deficient cells, DSBR is carried out by more mutagenic pathways, resulting in excessively high levels of genomic instability. In the absence of repair, persistent DSBs increase genomic instability and cell death. Adapted from G.E. Konecny and R.S. Kristeleit (Konecny and Kristeleit, 2016).

6. Measuring DSB repair capacity: current methods

6.1. From "omics" to functional assays

The first biomarkers of reduced DSBR proficiency in humans were mutations in genes such as BRCA1/2, ATM and RAD51, that result in increased genomic instability and are associated with high cancer susceptibility (Foulkes and Shuen, 2013). As presented in the previous sections, such mutations lower the overall DSBR capacity and increase the dependency upon error-prone repair pathways. The identification of such mutations by sequencing allows the personalized management of their carriers. This approach is "non-functional": the structure of the gene is investigated, not the activity of DDR or repair proteins themselves (figure 30). Other genomic methods like genomic scar assays, investigate fingerprints of DSBR defects (for instance gross chromosomal rearrangements), regardless of which pathway component is inoperant. These approaches rely on methods such as array-based comparative genomic hybridization to identify mutational signatures so as to characterize DSBR deficiencies (Hoppe *et al.*, 2018). For instance, HR deficiencies can be identified through the large-scale chromosomal breaks they leave in a genomic profile (Manié *et al.*, 2016). Nevertheless, these genomic signatures may only reflect past events, since reversion mechanisms or secondary mutations sometimes occur, as illustrated by tumors with mutant BRCA (Sakai *et al.*, 2008; Dhillon *et al.*, 2011). Such processes do not erase the genomic signature of the HR deficiency, but the tumor restored at least some extent of HR repair capacity. However, some degree of additional information may be accessed by quantifying epigenetic changes such as hypermethylation events (Staaf *et al.*, 2019).

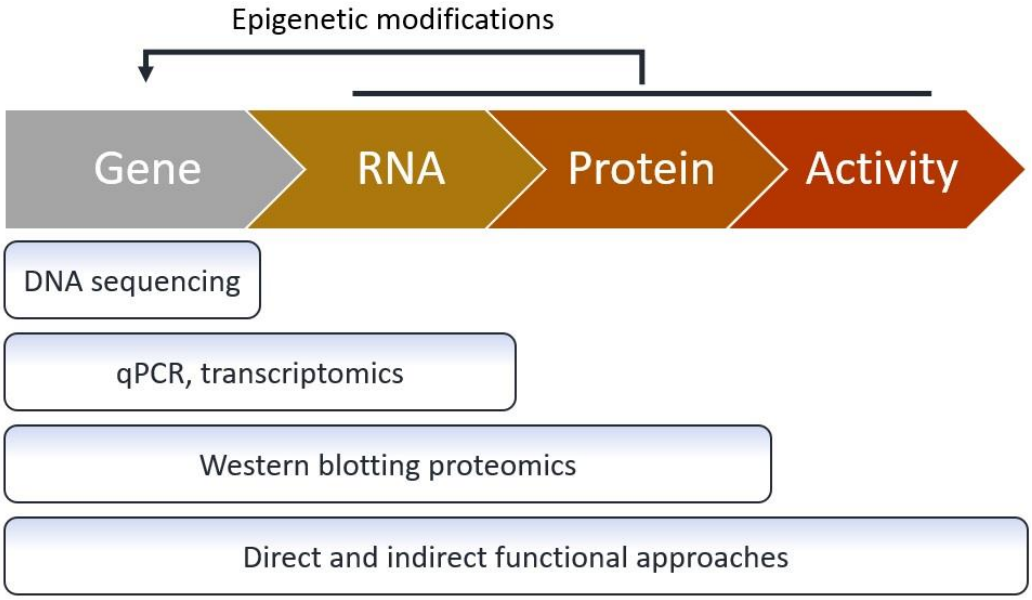

Figure 30. From gene to activity: the different layers of DNA repair and the information provided by the main approaches.
Adapted from C. George (George, 2017).

Transcriptomics and proteomics can complement this data: the lack of a mRNA or protein is likely to result in the inactivity of the associated pathway. However, backup mechanism may allow for DSB processing (Mladenov *et al.*, 2016) and their activity may not be visible by measuring RNA or protein levels due to the post-translational regulation of the DDR and repair activities, thus repair may be inefficient even in the presence of the appropriate DSBR effectors (Hoppe *et al.*, 2018).

Alternatively, "functional" methods quantify DSBR capacity and provide a downstream picture of repair processes that can shed a new light on the repair processes at stake. In short, these assays characterize the ability to carry out the repair activity instead of informing on the status of individual DSBR factors. They are divided in two categories that we detail in the next sections: indirect approaches induce damage and measure DSB levels, while direct methods use artificial models of DSB, the repair of which is tracked in cell extracts or in live cells.

6.2. Indirect functional methods

Indirect techniques rely on the formation of DSBs in live cells before measuring the DSB levels and their variation over time. The estimation of DSBR capacity is based on the comparison between different cell populations (treated and untreated, deficient and proficient, etc.).

6.2.1. Physical methods: quantification of DNA fragmentation

The first methods measuring DSBR capacity appeared in the 1970s. These physical techniques are based on the assessment of DNA size and/or chromosome breakage. They all rely on the physical separation of damaged DNA from unfragmented DNA (Iliakis *et al.*, 1991a, 1991b; Bryant, 2012).

The first methods measuring DSBs were low-speed neutral sucrose gradient sedimentation and neutral elution assays (Bradley and Kohn, 1979; Hutchinson, 1989). They were improved in the 1980s by pulse-field gel electrophoresis (PFGE), which relies on alternating electric fields to make DNA migrate in different directions. This increases the separation of the different DNA fragments, thereby overcoming the inability of classical gel electrophoresis to separate DNA pieces longer than 50 kbp (Schwartz *et al.*, 1983). By extension, the term PFGE includes several alternative techniques based on the original PFGE assay, including AFIGE or CHEF, but they are not detailed here.

PFGE became a gold-standard method of reference for the identification of pathogens in bacterial epidemiology (Sharma-Kuinkel *et al.*, 2014), but also brought a major contribution to the comprehension of genome alterations and DSBR (Iliakis *et al.*, 2012; Joshi and Grant, 2014; Windhofer *et al.*, 2007). Figure 31 illustrates the use of the method for the estimation of DSBR capacity.

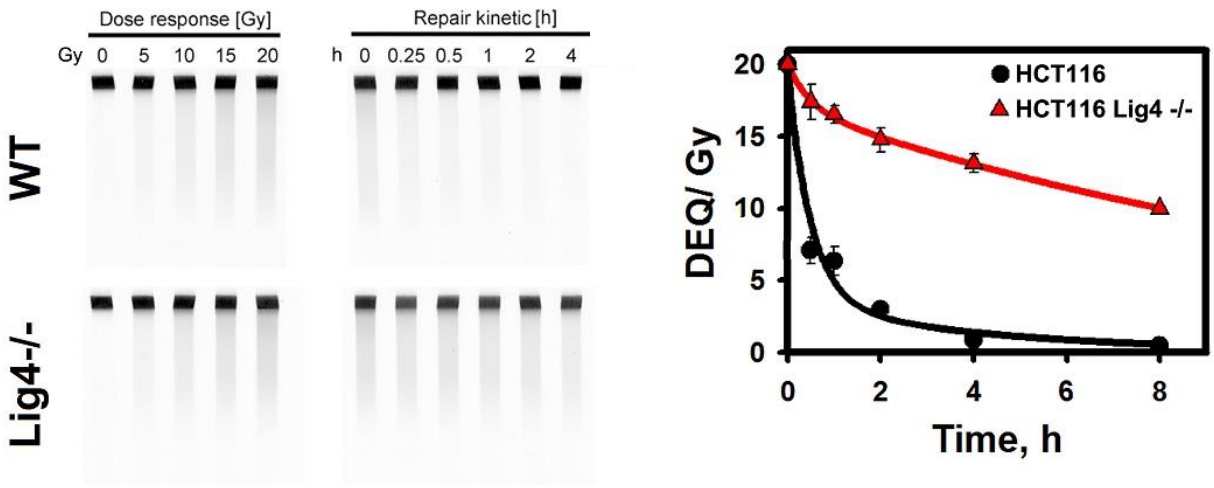

Figure 31. PFGE allows the quantification of DSB levels.
IR-induced DSBs result in smears on PFGE gels; upon DSBR, the intensity of these smears is reduced, and comparing the kinetics of this decreased in different cell populations allows the estimation of their DSBR capacity. Here, residual damage (equivalent dose (DEQ), in Gy) is higher in Lig4-deficient HCT116 cells compared to control, revealing a low DSBR capacity. Figure by G. Iliakis and S. Magin, in (Tatin et al.*) - under reviewing.*

Although PFGE studies any kind of biological material and can be adapted to various experimental settings (Lopez-Canovas *et al.*, 2019), it is a labor-demanding technique with long migration times (usually more than 24 hours), which is why it tends to be replaced by more rapid, simpler and more specific methods with a higher throughput (Vignard *et al.*, 2013). In addition, PFGE requires high doses of IR or other genotoxic agents to detect DSBs, which may not be biologically relevant since cell may engage into apoptosis rather than DNA repair (Antonelli *et al.*, 2015; Deckbar *et al.*, 2007). Structures such as replication forks can also make the analysis difficult due to atypical migration patterns (El-Awady *et al.*, 2003; Vignard *et al.*, 2013). Finally, non-DSB damage can be converted into DSBs, resulting in the overestimation of DSB levels (Iliakis *et al.*, 1991c; Gustafsson *et al.*, 2015).

6.2.2.The comet assay

Single-cell gel electrophoresis, also referred to as the comet assay, addresses some of the limitations of PFGE. This physical approach is generally used to measure the level of DNA damage but it can be used to estimate repair capacities, by tracking the kinetics of damage increase and reduction. It is based on regular agarose gel electrophoresis, but in individual cells. It was set up in 1984 and measures DNA fragmentation (including both SSBs and DSBs) but protocols based on lesion-specific enzymes such as formamidopyrimidine DNA glycosylase (*Fpg*) can also quantify the level of oxidative damage (Azqueta *et al.*, 2013). In brief, cells are embedded in low-melting point agarose and spread on microscope slides. A lysis step permeabilizes the nuclear membrane and fragmented DNA migrates outside the nucleus upon electrophoresis, forming a comet-shape pattern after DNA staining. The length and DNA content of the comet tail increases with the level of DNA fragmentation, while undamaged cells retain most of the DNA in the nucleus (comet “head”). Hence, the comparison of DNA content found in comet tails

over time in damaged and undamaged cells allows the estimation of repair capacity (Valdiglesias *et al.*, 2011), as represented in figure 32.

Advantages of the comet assay

This assay is among the most common techniques for the investigation of DNA damage. It is indeed flexible, simple and inexpensive (Glei *et al.*, 2016). The equipment it requires (standard electrophoresis accessories, epifluorescence microscope) is common and affordable. Finally, it can study various tissues and cellular models (although soft tissues are known to require the elaboration of specific protocols) with only small amounts of biological material needed (Olive and Banáth, 2006) and was used for the investigation of a large panel of physical and chemical DNA damaging agents (Afanasieva and Sivolob, 2018; Sauvaigo *et al.*, 1998). In addition, this assay analyses individual cells, which is useful in removing outliers (e.g., experimental artefacts) and in comparing potential subpopulations within the same sample.

Limitations of the comet assay

On the other hand, the comet assay is not very specific to DSBs. Indeed, it measures DSBs and SSBs, but also DNA adducts, AP sites and alkali labile sites that can be converted to strand breaks (Ostling and Johanson, 1984; Calini *et al.*, 2002; Speit and Rothfuss, 2012; Collins, 2014; Azqueta *et al.*, 2019). Two protocols have been developed, in neutral or alkaline conditions. The neutral comet assay is performed under non-denaturing conditions, which is considered to increase selectivity to DSBs (Olive *et al.*, 1991; Olive, 2009; Afanasieva and Sivolob, 2018). However, it was shown that this protocol still reveals some extent of SSBs due to the SSB-induced relaxation of DNA supercoiling (Afanasieva and Sivolob, 2018; Dmitrieva and Burg, 2007; Collins *et al.*, 2008; Collins and Azqueta, 2014). Improvements such as the two-tailed comet assay were presented more recently allowing a better differentiation between the two kinds of lesions (Cortés-Gutiérrez *et al.*, 2014, 2017), which is more appropriate to estimate DSBR capacity.

Since the results are impacted by the conversion of non-DSB lesions to DSBs, sample preparation steps (cell dissociation and pre-treatment) may need to be adapted to prevent the introduction of artificial DNA damage and skew the analysis (Rojas *et al.*, 2014).

In addition, the comet assay does not provide quantitative results. As for PFGE, DNA lesions are not individualized, and no information is obtained regarding the size of the DNA fragments or the number of DSBs induced by a given dose of genotoxic agent.

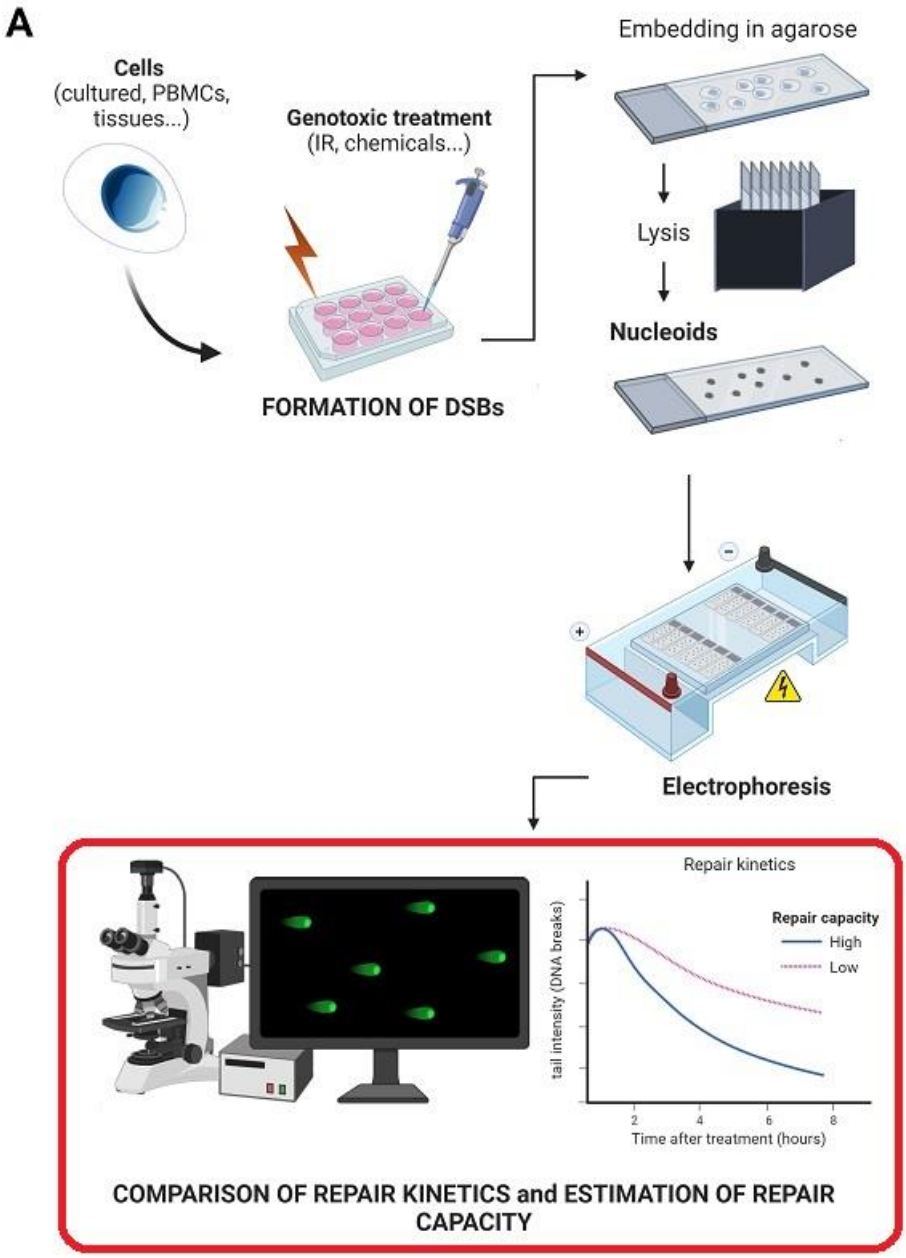

Figure 32.Determination of repair capacity with the comet assay.
A. *Principle of the comet assay. Cells are embedded in agarose, lysed and electrophoresis is performed. Repair capacity is estimated based on the comparison of strand breakage over time, measured by the size of the comets.* ***B.*** *Comets in human fibroblasts. Left: undamaged control, right: extensive DNA damage after exposure to 400 µM hydrogen peroxide. (Tatin* et al.*) - under reviewing.*

Finally, one of the main limitations of this method is its low reproducibility, which mostly originates from low standardization (Moller, 2006; Gagné, 2014). The protocols vary between users and laboratories, and no standards allow the comparison of the results. Parameters such as lysis duration, pH and migration time are among the frequently reported sources of variability (Moller, 2006; Ersson *et al.*, 2013; Enciso *et al.*, 2018). This variability is also problematic when measuring DNA repair activities in a large number of samples, since the actual variability inherent in the samples can be shaded by high inter-experimental variations (Trzeciak *et al.*, 2008). Nevertheless, recent standardization efforts must be noted, with general guidelines aiming at improving the reproducibility of the comet assay (Møller *et al.*, 2020a).

6.2.3.Immunofluorescence approaches

As previously detailed, a number of DNA repair factors, ranging from sensors to effectors, are mobilized at DNA lesions. The immunofluorescent (IF) approach relies on specific antibodies to stain the focal accumulations (foci) of proteins recruited at DSBs. Hence, these lesions are directly visualized, which allows a tracking of their rate of formation and disappearance, thereby providing an estimation of DSBR capacity (figure 33).

The most common DSB marker used in immunofluorescent assays is γH2AX (Kopp *et al.*, 2019; Sharma *et al.*, 2012), the H2AX variant phosphorylated at Ser139 upon DSB formation (see section 2.2). It was first described in 1998 by Rogakou *et al.*, who initially isolated γH2AX using two-dimensional gel electrophoresis (Rogakou *et al.*, 1998). A few years later, anti-γH2AX antibodies were used (Rogakou *et al.*, 1999). Various protocols have been described based on western blotting, ELISA, fluorescence microscopy and flow cytometry, the latter two approaches being the most common presently (Matsuzaki *et al.*, 2010; Kopp *et al.*, 2019)

This method is very sensitive and each DSB induces the formation of a γH2AX focus (Rothkamm and Lobrich, 2003). Conversely, DSBR is correlated to γH2AX dephosphorylation (Chowdhury *et al.*, 2005), which is confirmed by the comparison with PFGE (Löbrich *et al.*, 2010). γH2AX typically form in less than one minute after the formation of a DSB, peak after 30 minutes and progressively decrease over a few hours (Kinner *et al.*, 2008; Mah *et al.*, 2010; Sak and Stuschke, 2010).

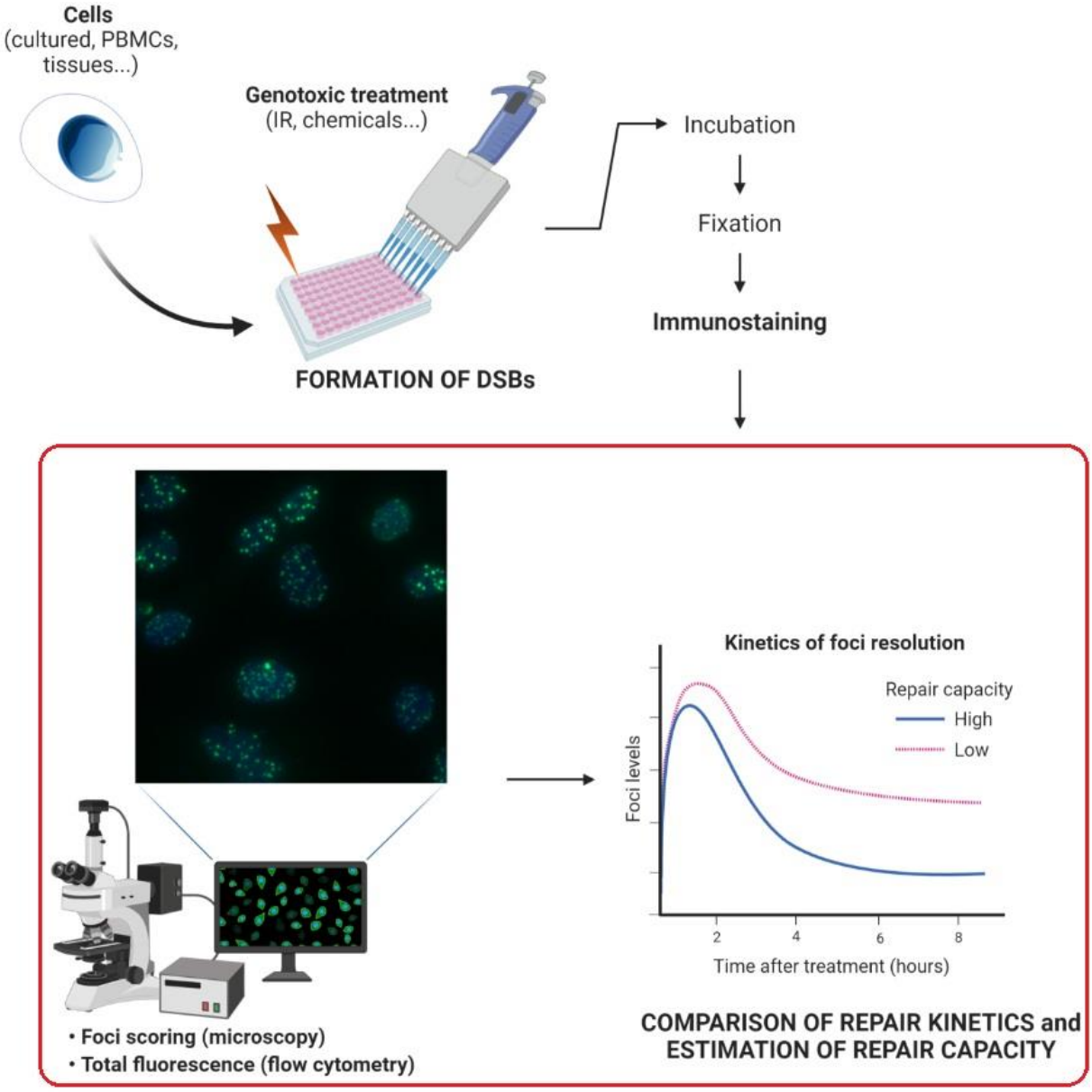

Figure 33. Estimation of DSBR capacity using an immunofluorescence approach.
DSBR-associated proteins are stained using specific antibodies, allowing the detection and counting of DSBs and the estimation of DSBR capacity. Focus: 53BP1 staining in M059J cells exposed to 8 nM doxorubicin for 48 hours. (Tatin et al.*) - under reviewing.*

We presented how other factors accumulate at DSBs, which can also be used as an alternative to γH2AX. 53BP1 is another common DSB marker, as well as ATM, RAD51 and BRCA1 (Sharma *et al.*, 2012). These factors are not recruited with the same kinetics, which is mostly explained by their role as DSBR mediators or effectors. For instance, fast kinetics are reported for ATM, γH2AX and 53BP1 foci formation, while HR factors RAD51 form foci in hours (Polo and Jackson, 2011; Sharma *et al.*, 2012; Sak and Stuschke, 2010).

Advantages of immunofluorescence

The sensitivity of IF assays is one of their main advantages. As opposed to physical assays, low doses of IR (as low as 1 mGy) or chemicals can be used to track DSBR capacity (Rothkamm and Lobrich, 2003; Bhogal *et al.*, 2009; Redon *et al.*, 2010), which is often more biologically relevant than high dose exposure (Rothkamm and Lobrich, 2003). At high doses of genotoxic agent (notably IR), the induction of multiple DSBs close to each other may result in underestimated foci counts if foci are overlap (Nikitaki *et al.*, 2016).

Sample preparation steps are usually less numerous than for the physical methods described above, which reduces the risk of converting lesions to DSBs (Rothkamm and Lobrich, 2003; Kinner *et al.*, 2008). They can be used on a large range of biological materials (Redon *et al.*, 2011), including cell extracts, tissue lysates, cells and tissues (Bonner *et al.*, 2008). In addition, simplified protocols have been developed, for instance for a rapid analysis of blood samples (Heylmann and Kaina, 2016). Additionally, the use of fusion proteins rather than antibodies can inform on DSBR in live cells (Karanam *et al.*, 2012), though artefacts may be induced (Mehta and Haber, 2014).

Fluorescence microscopy offers the possibility to characterize DSBR in single cells and allows tridimensional measurements, for instance to detail foci formation along the track of a particle (Hagiwara *et al.*, 2019; Jezkova *et al.*, 2018; Muggiolu *et al.*, 2017). This approach also enables the investigation of repair activities in genomic regions different levels of DNA condensation or transcription levels (Goodarzi *et al.*, 2008).

Another advantage of IF methods is their potential for automation. Important efforts have been developed during the last decade (Turner *et al.*, 2011), and a number of studies are now based on 96 well-plates or higher-throughput formats, for high-content analysis (Kopp *et al.*, 2019; Lin *et al.*, 2016; Hajjar *et al.*, 2017; Hershman *et al.*, 2017; Hopp *et al.*, 2017). Among other assays, imaging flow cytometry is worth citing due to its combination of the advantages of flow cytometry and fluorescence microscopy (Durdik *et al.*, 2015; Parris *et al.*, 2015; Zhao *et al.*, 2017; Lee *et al.*, 2019), with sufficient hindsight to critically assess the quality of generated data (Pischel *et al.*, 2018).

Limitations of IF methods

DSBR capacity can be measured regardless of cell cycle phase (Solovjeva et al., 2017), but γH2AX levels vary along the cell cycle, with an increase in S-phase and during mitosis, especially under conditions of replicative stress (MacPhail *et al.*, 2003; McManus and Hendzel, 2005; Popp *et al.*, 2017; Tu *et al.*, 2013a; Ward and Chen, 2001). Synchronizing cells has also been reported to generate γH2AX foci (Goodarzi and Jeggo, 2012), together with markers that allow the identification of replicating cells, such as 5-ethynyl-2'-deoxyuridine (EdU), (Fujii *et al.*, 2013; Zhao *et al.*, 2013). Hence, additional precautions may

be required when measuring γH2AX foci and data analysis is not necessarily straightforward. 53BP1 foci have been reported to be less retained than γH2AX at ssDNA regions formed in replicating cells (Goodarzi and Jeggo, 2012). They overlap with γH2AX foci but with different kinetics (Anderson *et al.*, 2001b; Noon and Goodarzi, 2011), and are also found in heterochromatin (Noon *et al.*, 2010). Hence, 53BP1 can serve as an alternative marker of DSBs and it is commonly tracked in addition to γH2AX (Holton *et al.*, 2017; Popp *et al.*, 2017; Shah *et al.*, 2016).

In addition, the one-to-one correlation between the generation of a DSB and the formation of a γH2AX foci found in early studies (Rothkamm and Lobrich, 2003; Sedelnikova *et al.*, 2002), has not been confirmed in all cell types (Han *et al.*, 2006; Belyaev, 2010) due to variations in the endogenous foci levels or because of insufficient standardization across laboratories (Chua and Rothkamm, 2013).

It has been reported that DSBR kinetics measured by physical methods differ from IF results (Goodarzi *et al.*, 2008; Han *et al.*, 2006; Kinner *et al.*, 2008; Weingeist *et al.*, 2013), which suggests that foci remain after the physical repair of the breaks. Residual foci are found in contradictory studies (Leatherbarrow *et al.*, 2006; Löbrich *et al.*, 2010; Mah *et al.*, 2010) and it is not sure whether they are associated with slow repair or with other cellular mechanisms (Siddiqui *et al.*, 2015; Ricoul *et al.*, 2019). Thus, if one DNA DSB results in the formation of a focus, the opposite is still debated.

Multiplexing

All DSBR factors cannot be efficiently tracked for the identification of DSBs, since some proteins do not aggregate as foci, are expressed in too small amounts or are mobilized only in certain cell cycle phases (Nakamura *et al.*, 2010; Polo and Jackson, 2011; Sharma *et al.*, 2012). To our knowledge, staining sensors such as PARP1 or KU did not produce much results due to transient mobilization and excessive abundance (Vignard *et al.*, 2013).

However, some proteins can provide it valuable information regarding the modalities of DSBR. Notably, it can inform on the pathway that operates repair, which is a highly valuable piece of information to complement overall DSBR capacity (Kakarougkas and Jeggo, 2014; Marrero *et al.*, 2016; Nikitaki *et al.*, 2016; Spies *et al.*, 2019). For instance, tracking RAD51 and phosphorylated DNA-PKcs in parallel can allow an estimation of the relative contribution of HR and c-NHEJ in the repair process (Pauty *et al.*, 2016).

In sum, γH2AX and 53BP1 are the most commonly used markers of DSB formation, while RAD51, phosphorylated DNA-PKcs, BRCA1/2, RPA, CtIP and the MRN complex are usually stained to gain additional insight on repair processes.

Alternatively, other approaches directly quantify the cellular repair of an artificial DNA substrate instead of tracking the levels of DSBs in live cells after exposure to damaging agents.

6.3. Direct functional methods

6.3.1. Reporter assays

These methods DSBR capacity by tracking the expression of a reporter gene which is usually inserted inside the cells by transfection. DSBs can be induced by several means, including TALENs, precise clustered regulatory interspaced short palindromic repeat (CRISPR)/Cas-based RNA-guided nucleases or meganucleases such as I-SceI (Aparicio *et al.*, 2014). DSBs can be induced directly inside the cells, or prior to transfection as in host cell reactivation assays (HCR). Considering that DSBs completely prevent the transcription of the reporter, DSBR is required for the restoration of its expression.

These assays became popular based on pioneering work in the late 1990s and early 2000s (Akyüz *et al.*, 2002; Pierce *et al.*, 1999). Since then, a diversity of methods appeared, based on various reporter cassettes and different detection techniques. The most commonly used reporter genes code fluorescent proteins such as GFP, allowing the quantification of DSBR activities based on the level of fluorescence measured by flow cytometry or fluorescence microscopy (figure 34). Alternatively, PCR and qPCR to measure DSB rejoining.

Using specific expression cassettes, these assays can decline DSBR capacity into the repair capacity through different pathways. Some assays are commercially available, among which a commonly found system measuring HR proficiency (Zhang *et al.*, 2017; Liang *et al.*, 2018). Other assays characterize c-NHEJ, SSA and alt-NHEJ subpathways either independently of simultaneously (Slebos and Taylor, 2001; Rahal *et al.*, 2010; Sears and Turchi, 2012; Bindra *et al.*, 2013; Deniz *et al.*, 2016; Nagel *et al.*, 2017; Lacoste *et al.*, 2017; Gomez-Cabello *et al.*, 2013; Kostyrko and Mermod, 2016).

Strengths and limitations

Once transfected, plasmids were shown to be integrated into functional nucleosomal structures that can undergo histone modifications upon the induction of DNA damage (Mladenova *et al.*, 2009), which provides a better overview of in vivo DSBR capacity than cell-free assays (see next section). Some studies relied on the induction of genomic damage rather than using transfected plasmids (Gravells *et al.*, 2015; Miyaoka *et al.*, 2016; Roidos *et al.*, 2020). Although these methods are labor-demanding, they provide the most detailed information regarding the mechanistic modalities of DSBR among all techniques reviewed in this chapter (Roidos *et al.*, 2020; Ahrabi *et al.*, 2016; Du *et al.*, 2018).

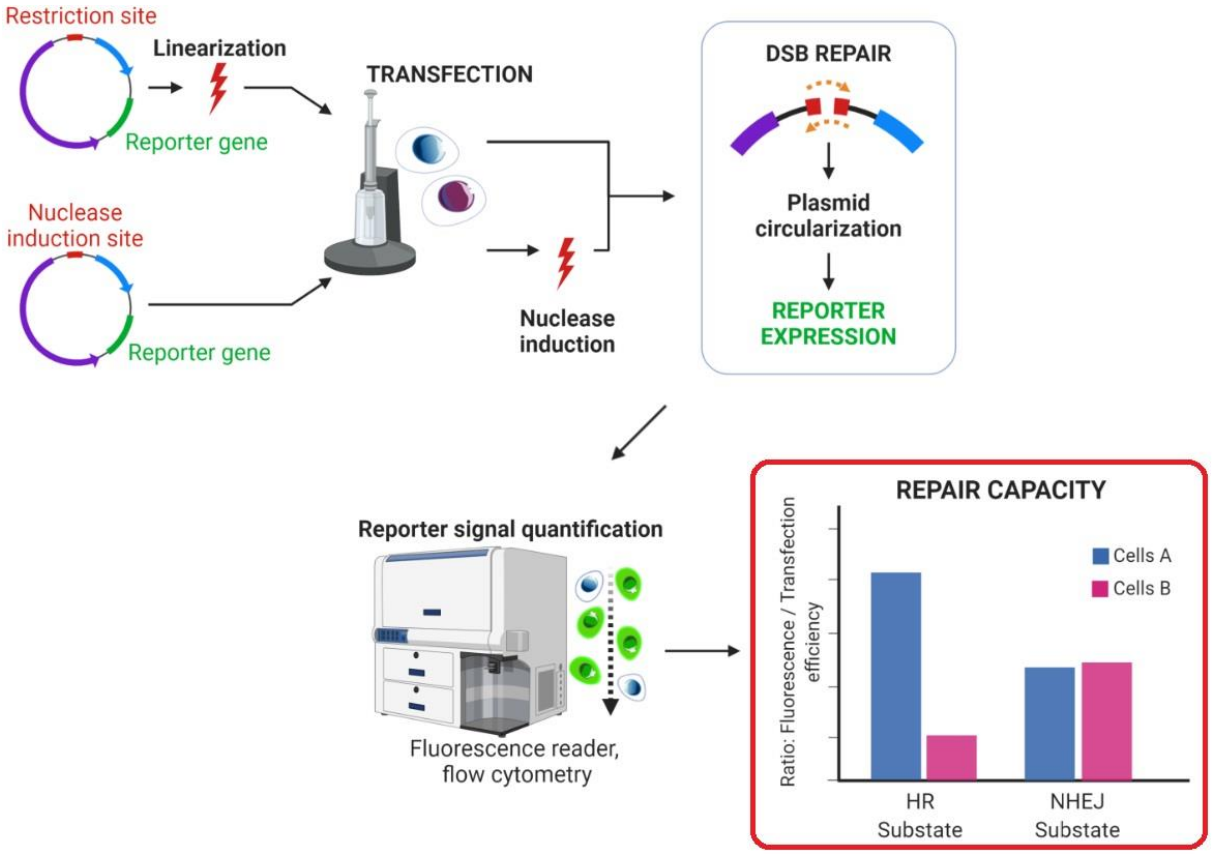

Figure 34. Simplified principle of reporter-based assays.
Plasmid substrates contain a specific DSB lesion that is induced prior or after transfection into live cells. Cellular machinery operates DSB repair, resulting in the expression of the reporter gene. Measuring expression levels allows the estimation of DSBR capacity. Custom constructs orient repair toward specific pathways, such as HR and c-NHEJ. (Tatin et al.*) - under reviewing.*

In addition, high-throughput reporter-based assays have become more common in recent years. Miniaturized formats have been developed for easily cultured material such as cancer cell lines (Goglia *et al.*, 2015; López-Saavedra *et al.*, 2016).

Recently, an alternative non-invasive method was proposed by Chien et al., who quantified DSB repair activities directly in culture medium and blood samples, allowing several measurements to be performed on the same cells or individuals (Chien *et al.*, 2020).

However, some limitations are also to be mentioned for reporter-based assays. Most of these methods can only study transfectable cells, which can be an issue for the direct investigation of biopsy samples and other non-cultured material. An interesting study used transgenic mice carrying an integrated recombination fluorescent reporter, which allowed the direct investigation of HR *in vivo* (Sukup-Jackson *et al.*, 2014). Though this study offers interesting prospects, it remains unapplicable in humans.

The induction of DSB by endonucleases restricts the generated DSB ends to specific configurations. As detailed previously, genotoxic compounds and IR often result in complex lesions. Only HCR assays offer an opportunity to insert specific DSB structures prior to transfection (Nagel *et al.*, 2014).

6.3.2.Cell-free assays

Finally, cell-free assays are based on damaged artificial DNA templates for the *in vitro* investigation of DSBR capacity in cellular extracts or tissue lysates. Repair proteins contained in the extracts can operate the repair of the DSB, thereby providing a direct estimation of DSBR capacity.

Various DNA templates are used, that undergo treatment with restriction enzymes (REs), chemical compounds or ionizing radiation to induce damage. DSB repair restores plasmid circularity and/or results in linear plasmid oligomers. Repair products are then usually separated using agarose gel electrophoresis (Pfeiffer *et al.*, 2014) and revealed using Southern blotting, autoradiography (if a radio-labelled DNA was used), or – more commonly – fluorescent intercalants (Pastwa *et al.*, 2009).

PCR can also be useful, especially for the detection and interpretation of complex repair events. For instance, those that involve the processing of incompatible ends can be associated with lower NHEJ activity and make repaired products harder to detect (Budman and Chu, 2006; Ma and Lieber, 2006). In the end, DSBR capacity is estimated based on the ratio between the amount of rejoined products and that of initial DNA substrates (figure 35).

Advantages and limitations

Cell-free assays mainly describe c-NHEJ activity, but HR and SSA have also been investigated (Kucherlapati *et al.*, 1985; Carroll, 1996; Dahal *et al.*, 2018). At least eleven different assays have be reported, that are based on different types of extracts or DNA substrates (Pfeiffer *et al.*, 2014). They were used for the analysis of clinical samples, including blood and tumor biopsies (Bau *et al.*, 2007; Diggle *et al.*, 2003).

This approach is simpler the historical methods such as PFGE, no damage induction is required on the biological material, only a protein extraction is needed. As for reporter assays, the DSB model is not randomly generated. On the contrary, it is formed at a defined location on the DNA template, with a known configuration. Additionally, baseline repair activities can be assessed in detail, which is much less true using indirect methods.

Depending on the extraction protocol, these assays can investigate specific cellular compartments, such as the nucleus, cytoplasm or mitochondria (Dahal *et al.*, 2018; Daza *et al.*, 1996; Cheong *et al.*, 1998).

If needed, the sequence of the repair joints can be determined, which allows the mechanistic investigation of DSBR. Although it adds additional steps to the study, it is much more sensitive than gel electrophoresis and provides extensive information.

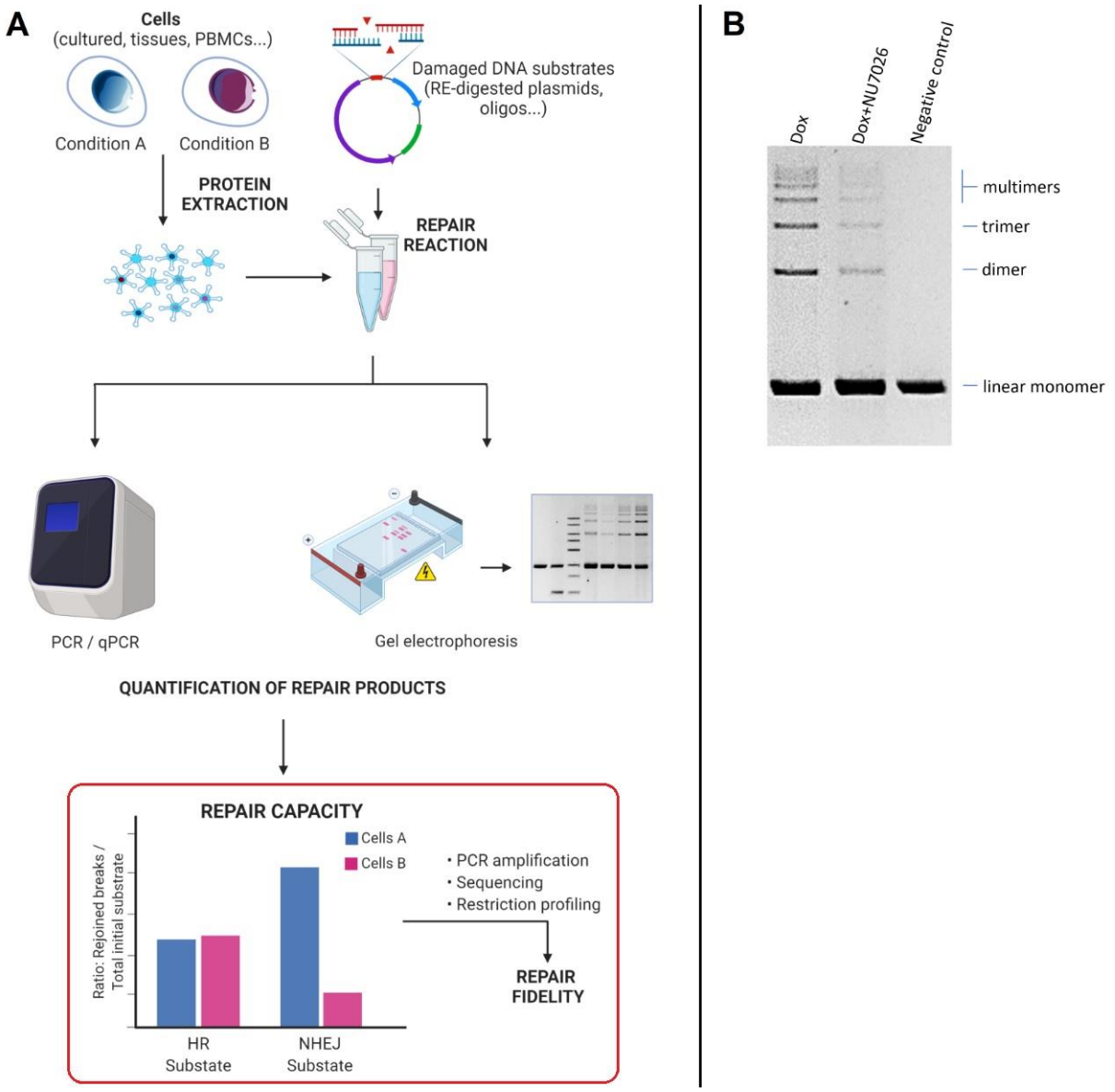

Figure 35. General principle of cell-free assays.
A. Simplified principle of cell-free assays, here with HR- and c-NHEJ-specific substrates. B. Simple cell-free NHEJ assay using a 3kb AflIII*-digested pBlueScript plasmid as a substrate for ligation by HeLa nuclear extracts from doxorubicin-treated cells (Dox) or following repair inhibition by DNA-PKcs inhibitor NU7026. Repair activities result in the formation of plasmid oligomers revealed by agarose gel electrophoresis. (Tatin* et al.*) - under reviewing.*

Although authors also questioned the correlation between DSB repair in plasmids compared to genomic DNA (Joshi and Grant, 2014), studies comparing both activities showed that both methods play complementary roles for the description of DSBR (Cheong *et al.*, 1998).

Cell-free assays considerably increased the global understanding of DSBR (Perrault *et al.*, 2004; Kumar *et al.*, 2010; Ghoshal *et al.*, 2017) and their high flexibility allows them to assess DSBR capacity based on different DNA substrates. Hence, they have the potential to measure different repair activities simultaneously rather than focusing on a single pathway, thereby providing a systemic estimation of DSBR capacity.

Nevertheless, to our knowledge, no assay currently describes HR, SSA and NHEJ simultaneously. In addition, current methods have a limited throughput due to the multiplication of experimental steps such as the purification of repair products, and little automation or miniaturization effort is reported in the literature. A notable exception is the assay on microchip developed by the Duez team, based on Experion™ automated electrophoresis systems (Charles *et al.*, 2012, 2014). This method provided quality results than a regular c-NHEJ assay in a much shorter amount of time.

6.4. Current development prospects

LXRepair and the CIBEST team developed two multiplexed assays on biochip for the investigation of BER and NER activities (Millau *et al.*, 2008a; Forestier *et al.*, 2012; Sauvaigo *et al.*, 2016). In this study, we describe Next-SPOT, a novel enzymatic cell-free assay for the investigation of DSBR. As we detail in the next chapter, this assay combines several measurements to characterize different DSBR activities based on the incubation of cell extracts with two different plasmids printed on a biochip.

OBJECTIVES

In this introductive chapter, we highlighted the complexity of the DDR and DSBR system, as well as their importance for maintenance of normal cellular function and the prevention -or the induction- of human diseases. A better understanding of these mechanisms would have direct applications in the clinic or in research. However, all methods currently in use have limitations regarding damage specificity, throughput or required biological material.

The assay developed by LXRepair, Next-SPOT, aims at characterizing double-strand break repair activities in any kind of biological material, based on the use of protein extracts to determine enzymatic repair signatures. The main goal of this study is to optimize the assay and to test its ability to detect variations in the activity of DSBR processes.

To this intent, we used three human cancer cell lines (HeLa, M059J and M059K) and compared repair activities using Next-SPOT and a reference cell-free method based on gel electrophoresis, as detailed in the following chapters. Cellular DSBR activity was measured at the basal level and following treatment by a known DSB inducer, the anticancer compound doxorubicin, which is expected to activate DDR mechanisms.

In addition, we used various repair inhibitors involved in the main DSBR pathways (HR, c-NHEJ and alt-NHEJ) and measured their impact on cellular repair activities, with or without a combined exposure to doxorubicin.

This project aims at:

- Setting up optimal assay conditions for the novel Next-SPOT technique
- Providing details of the mechanisms at stake on the chip
- Validating Next-SPOT's ability to detect alterations in specific repair pathways
- Comparing the assay to other techniques that measure DSBR

The following chapter present the details of experimental procedures, including the description of the two DSBR assays that we relied on in this study. We also describe the different models that were tested and the molecules that induced DSBs and inhibited repair activities.

CHAPTER 2 – MATERIALS AND METHODS

1. Chemicals

1.1. Doxorubicin

Doxorubicin (Dox, also referred to as Adriamycin®, Doxil® or Myocet®) is an antibiotic derived from *Streptomyces peucetius*. It belongs to the anthracycline family and has been widely used as chemotherapeutic agent since the 1960s due to its genotoxic properties. It has been shown to intercalate DNA by creating hydrogen bonds with stacked DNA base pair (figure 36), to inhibit DNA and RNA polymerases and to prevent sister chromatid exchange (Meredith and Dass, 2016; Johnson-Arbor and Dubey, 2020), leading to various adverse effects in the cells.

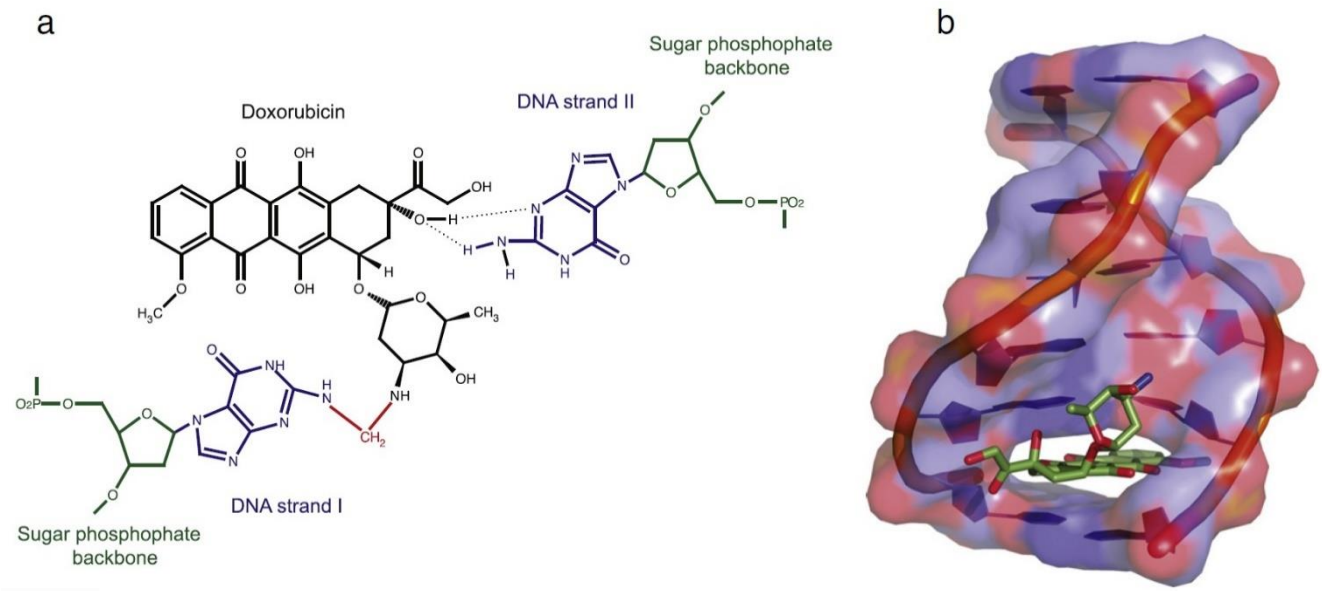

Figure 36. Interaction between doxorubicin and DNA.
a. Doxorubicin forms hydrogen and covalent bonds with DNA bases, especially guanine. Various cellular species increase covalent bonding (here cellular formaldehyde, carbon in red), thereby forming DNA adducts.
b. Doxorubicin intercalation into DNA; flanking base pairs are pushed apart and the sugar moiety intercalates into the minor groove. Original figure by Yang and coworkers *(Yang* et al.*, 2014)*

Firstly, doxorubicin intercalation has been shown to affect topoisomerase II activity. This enzyme is involved in regulating chromosome condensation, decondensation and segregation and it plays a crucial role in maintaining DNA topology. During replication, topoisomerase II disentangles dsDNA by cleaving its phosphodiester backbone, thereby generating a transient enzyme-bridged DSB that allows the relaxation of helical tension; the DSB is then religated (figure 37). DNA-intercalated doxorubicin binds topoisomerase II and stabilizes its cleavage complex, resulting in the formation of permanent DNA double-strand breaks (Zhu *et al.*, 2016; Baxter-Holland and Dass, 2018). Dox-induced DNA breaks were shown to be repaired predominantly by HR and NER to due to their high activity in replicating cells (Spencer *et al.*, 2008).

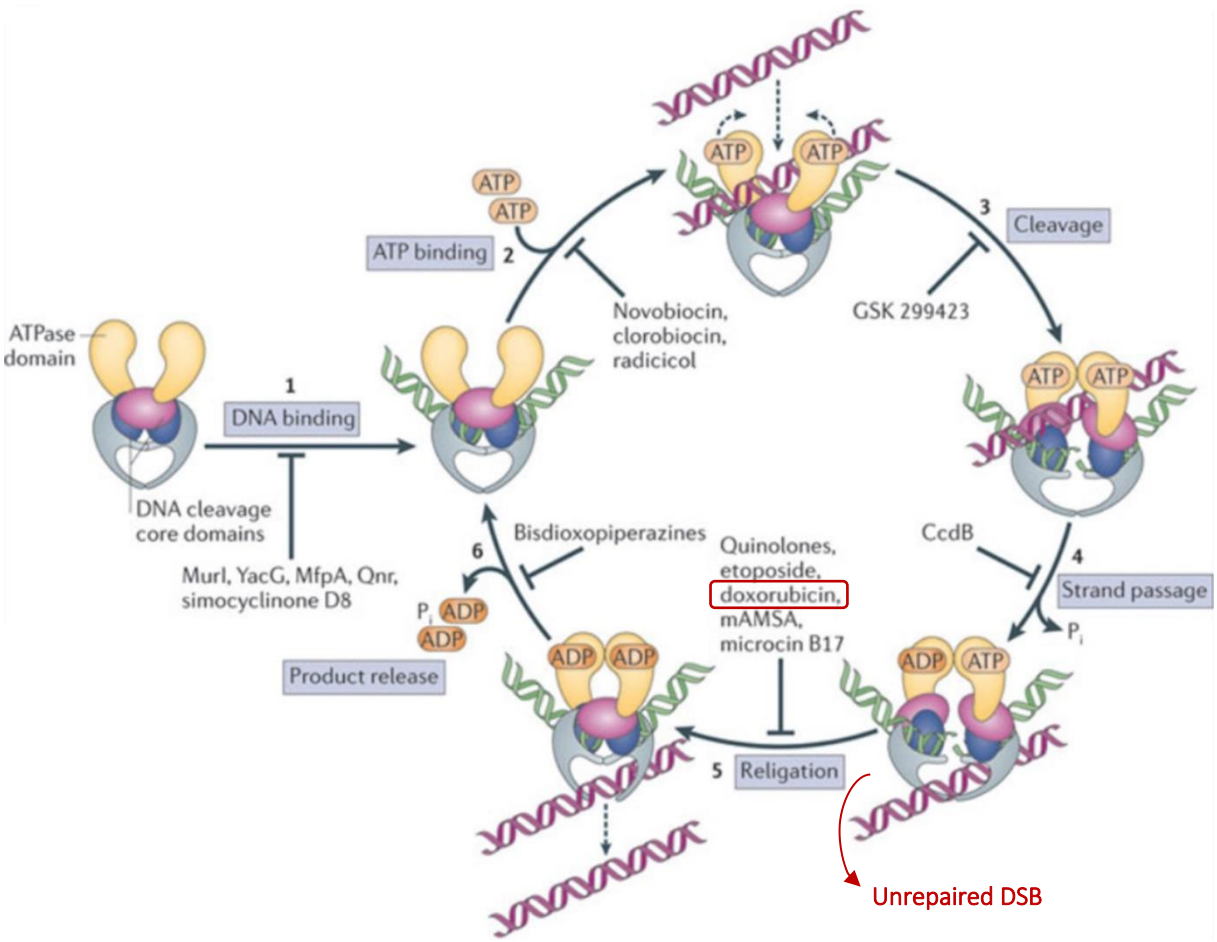

Figure 37. Generation of DSBs following doxorubicin-mediated topoisomerase II inhibition.
Doxorubicin inhibits the DNA religation step of topoisomerase II's catalytic cycle, thereby stabilizing the cleavage complex and generating permanent DSBs. Adapted from Mehta and collaborators (Mehta et al.*, 2018).*

Besides doxorubicin intercalation in DNA, the inhibition of DNA and RNA polymerases induces a cell-cycle arrest, thereby blocking cell proliferation. However, the extent to which polymerase inhibition represents a significant part of doxorubicin effect is a long-lasting debate, especially at *in vivo* therapeutic doses (Aubel-Sadron and Londos-Gagliardi, 1984).

Early hypotheses suggested that quinone groups in doxorubicin may accept electrons, initiating a redox cycling process in the presence of NADH dehydrogenase, resulting the generation of reactive oxygen species such as hydrogen peroxide (Goodman and Hochstein, 1977; Mizutani *et al.*, 2005). Oxidative damage is thought to induce the hyperactivation of caspase-3 and PARP1, leading to metabolic failure and apoptosis (Tacar *et al.*, 2013). Free radicals have also been involved in lipid peroxidation, inducing further damage to cellular membranes (Mizutani *et al.*, 2005; Tacar *et al.*, 2013), though the impact of such processes at clinical doses is still discussed (Meredith and Dass, 2016).

Finally, it is clear that doxorubicin activates various mechanisms leading to apoptotic cell death, at least *via* the mobilization of the AMP-activated protein kinase (AMPK), BCL-2, BAX and p53 (Tacar *et al.*, 2013; Meredith and Dass, 2016; Shabalala *et al.*, 2017).

These various mechanisms of action have been used extensively to induce cancer cell death and inhibit tumor growth as part of antitumor therapies, and doxorubicin is a common treatment in leukemias, lymphomas, sarcomas, breast/lung cancers, neuroblastoma and germ-cell malignancies (Pendleton *et al.*, 2014), in spite of its high toxicity to normal cells (cardiotoxicity is particularly documented, as for many anthracyclines).

1.2. RAD51 inhibitor B02

RAD51 is the primary targets to disrupt HR (Trenner and Sartori, 2019), which is of considerable interest to our study. B02 (3-(Phenylmethyl)-2-[(1E)-2-(3-pyridinyl)ethenyl]-4(3H)-quinazolinone) is a small molecule identified in 2011 as part of a high-throughput screening of the NIH Small Molecule Repository by Huang and coworkers, who revealed its inhibitory effect on human RAD51 recombinase (Huang *et al.*, 2011a). They showed that B02 specifically binds to RAD51 and inhibits both its DNA strand exchange activity and branch migration activity, by inhibiting D-loop formation and by preventing the formation of the RAD51 nucleofilament as well as its binding to dsDNA (Huang *et al.*, 2011a, 2012). B02 was then shown to block RAD51 foci formation and inhibit HR in several cell lines, and it was found to increase their sensitivity to various genotoxics (Huang and Mazin, 2014; Huang *et al.*, 2012). Though the exact mechanism of inhibition is unclear, this compound was shown to dock to several putative sites in a homology model of human RAD51, including the ATPase domain (Ward *et al.*, 2017), as shown in figure 38.

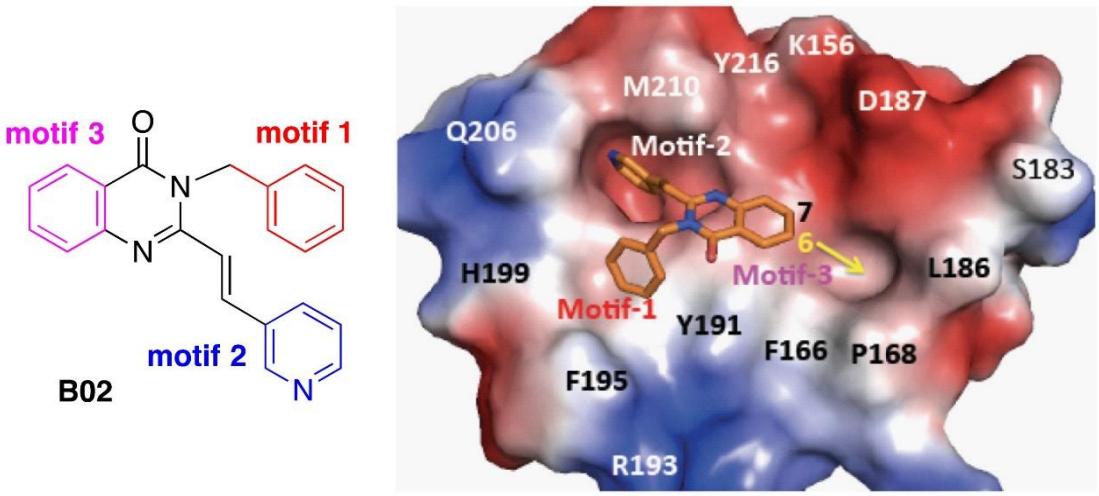

Figure 38. B02 fixation at the ATPase domain of a homology model of human RAD51. Original figure by Ward and coworkers (Ward et al.*, 2017).*

1.3. DNA-PK inhibitor NU7026

NU7026 (2-(morpholin-4-yl)-benzo-[h]chomen-4-one, also referred to as LY293646, figure 39) is a small molecule developed as part of a research program looking for potent and selective DNA-PK inhibitors amenable to eventual clinical evaluation. In the absence of a suitable crystal structure of DNA-PK in the 2000s, template molecules were used as core pharmacophores for inhibitor design and for the investigation of structure-activity relationships (SARs) (Hollick *et al.*, 2003).

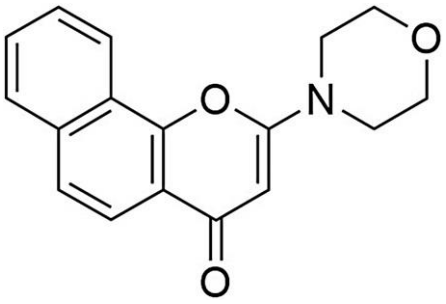

Figure 39. Structure of DNA-PKcs inhibitor NU7026.

NU7026 inhibits phosphoinositide 3-kinase (*in vitro* IC_{50} = 13 µM) and various PI3K-related kinases such as ATM and ATR (IC_{50} > 100 µM), but it is most selective for DNA-PK (IC_{50} = 0.23 µM), especially compared to other small molecules such as Wortmannin (Nutley *et al.*, 2005). NU7026 blocks DNA-PK phosphorylation by competitive inhibition with ATP (Veuger *et al.*, 2003; Davidson *et al.*, 2013; Harnor *et al.*, 2017), thereby blocking the subsequent activation of key enzymes involved in DNA repair. An illustration of DNA-PK inhibition is provided in appendix 2. This drug potentiates various chemotherapeutic agents including doxorubicin and etoposide (Willmore *et al.*, 2004).

1.4. PARP inhibitor olaparib

Olaparib (4-[[3-[4-(cyclopropanecarbonyl) piperazine-1-carbonyl]-4-fluorophenyl] methyl] -2H-phthalazin-1-one, also referred to as AZD2281, KU0059436 or Lynparza™, figure 40) is a PARP inhibitor approved by the US Food and Drug Administration and the European Medicines Agency. It has a dual mechanism of action: firstly, it selectively blocks the PARylation activity of PARP1 and PARP2 by binding to their catalytic domain, thereby preventing PARP-dependent signaling in repair mechanisms such as BER and a-NHEJ (Bryant *et al.*, 2005).

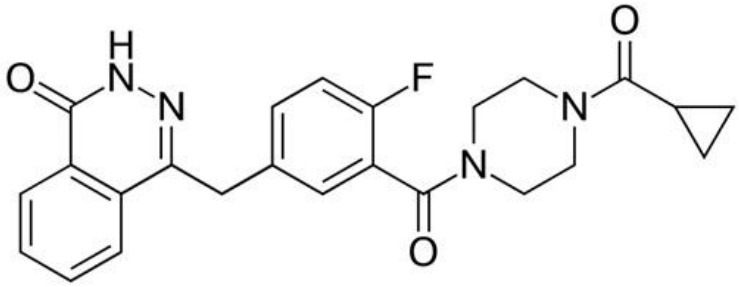

Figure 40. Structure of PARP inhibitor olaparib.

Secondly, olaparib prevents the dissociation of PARP-DNA complexes. Trapped PARP form replication and repair obstacles, resulting in the formation of DSBs in replicating cells (Bochum *et al.*, 2018). Such lesions usually mobilize HR for effective repair in normal cells, but they are processed by more mutagenic pathways or can be left unrepaired in HR-deficient cells, conducing to synthetic lethality due to increased genomic instability, as depicted in figure 29.

Hence, olaparib is indicated for a number of applications, including breast and ovarian cancer with deficient HR factors such as BRCA proteins. It is also used as a potentiating agent for platinum salt chemotherapy (Bochum *et al.*, 2018) or in combination with topoisomerase inhibitors such as doxorubicin (Del Conte *et al.*, 2014).

1.5. Chemicals and solubilization

Genotoxic chemicals and DNA repair inhibitors are listed in table 4. The molecules cited were solubilized in dimethyl sulfoxide (DMSO).

Stock solutions were stored at +4°C or -20°C according to the supplier's instructions.

Table 4. Details of the chemicals used for cellular treatments

Molecule	Effect	CAS Number	Supplier	Reference	Stock concentration
B02	RAD51 inhibitor	1290541-46-6	Sigma-Aldrich, USA	SML0364	15 mM
NU7026	DNA-PK inhibitor	154447-35-5	Sigma-Aldrich, USA	N1537	15 mM
Olaparib	PARP inhibitor	763113-22-0	Cayman Chemicals, USA	10621	15 mM
Doxorubicin	Genotoxic (topoisomerase inhibitor)	25316-40-9	Sigma-Aldrich, USA	44583	10 mM

2. Cell culture, treatments and cytotoxicity assays

Three cellular models were selected, with characteristics in line with the project's objectives (table 5).

The first model used for routine applications is the HeLa cell line. This epithelial cell line was established in 1951 from a metastatic cervix carcinoma in a 31-year-old female patient. It is worth mentioning that it is the first human cell line ever to proliferate for more than a few days (Masters, 2002). These cells have been extensively used for research purposes and it is described by a large spectrum of scientific literature. In our case, HeLa cells have proven to be a valuable material for technical optimizations, due to their fast growth and convenient use in cell culture.

M059J and M059K cells were isolated from the same tumor in a 33-year-old male affected with an untreated malignant glioblastoma. These glial cell lines differ in their genotypic characteristics: M059J

cells have a frameshift mutation in the *PRKDC* gene coding for the catalytic subunit of DNA-PK, resulting in an inactive truncated protein and a c-NHEJ deficiency (Anderson *et al.*, 2001a). On the contrary, M059K cell do not have this particular mutation. Hence, these two models have been extensively used for comparative analyses of DSB repair activities.

Table 5. Main characteristics of the cellular models used in this study.
Source: Catalogue of somatic mutations in cancer, https://cancer.sanger.ac.uk

CELL LINE	ORIGIN	CANCER	TYPE	MUTATION OF INTEREST	CONSEQUENCES	OTHER MUTATIONS
HeLa	Cervix	Adenocarcinoma	Epithelial	-	-	CDK9, EGFR, MAP3K19, LRRK1
M059J	Brain	Glioblastoma	Glial	*PRKDC* 4048delA	DNA-PKcs deficiency (c-NHEJ)	FANCA, PTEN, RAD54B, RB1, TP53
M059K	Brain	Glioblastoma	Glial	-	Comparison to M059J cells	Data not specified

All cell lines are adherent and were cultured in monolayer in 25, 75 or 175 cm² Falcon® Tissue Culture Treated flasks, Petri dishes and 6 to 96-well plates (respectively 353109/136/112/003/072, Corning Inc., USA). Additional information regarding cell culture is provided in appendix 3 and appendix 4.

2.1. Cell culture

2.1.1. Cell freezing and thawing

Upon reception of a new cell line, vials were stored in liquid nitrogen before amplification. Cell thawing procedure was based on the supplier's instructions or on the following protocol: vial content was quickly thawed at 37°C and immediately diluted in 9 volumes of complete culture medium before a 3 minute-500 g centrifugation in order to remove residual cryopreservation medium. Cells were then plated in complete growth medium into 25 or 75 cm² flasks. Medium was renewed the following day, after they adhered to the bottom of the flasks and initiated their proliferation.

Cell freezing was achieved using the following procedure: flasks or dishes were rinsed with D-PBS and cells were detached using 0.05% Trypsin-EDTA (25300-062, Gibco, USA). Trypsin was then blocked by adding a minimum of 4 volumes of complete culture medium, and cells were pelleted by a 5-minute, 500 g centrifugation. After automated counting (Countess, Invitrogen, USA), the supernatant was discarded and the pellet resuspended at the desired concentration into 2 mL cryotubes in a cryopreservation medium made of 90% decomplemented fetal bovine serum (FBS; A3160801, Gibco, USA) and 10% DMSO (D2650, Sigma-Aldrich, MO, USA). Cryotubes were quickly stored at -80°C for 24 hours before being transferred into liquid nitrogen for long-term storage.

2.1.2.HeLa cell line

HeLa cells (CCL-2™, ATCC®, VA, USA) were originally purchased from the American Type Culture Collection by the Laboratoire Des Lésions Des Acides Nucléiques; cells were cultured in Opti-MEM™ (31985-047, Gibco, USA) completed with 10% heat-inactivated FBS (20 minutes at 56°C), 1% non-essential amino acids solution (11140-035, Gibco), 1% 200 mM L-Glutamine solution (25030-024, Gibco, USA) and 1% penicillin-streptomycin solution (5,000 units/mL et 5 000 µg/mL respectively; 15070-063, Gibco, USA). Cells were passaged twice a week by a 1-to-20 (first day of the week) or 1-to-10 ratio (fifth day). After rinsing with D-PBS (14190-094, Gibco, USA), cells were detached with 0.05% Trypsin-EDTA (25300-062, Gibco, USA) for 2 minutes at 37°C under 5% CO_2 and diluted to the required subculture ratio in complete medium after centrifugation (5 minutes, 500 g). Flasks were incubated at 37°C under 5% CO_2.

2.1.3.M059J and M059K cell lines

M059J (CRL-2366™, ATCC®, VA, USA) and M059K (CRL-2365™, VA, USA) cells were purchased from the ATCC and cultured in DMEM+GlutaMAX™ (31966-021, Gibco, USA) completed with 10% heat-inactivated FBS, 1% non-essential amino acids solution and 1% penicillin-streptomycin solution. M059J cells were passaged twice a week by a 1-to-4 (first day of the week) or 1-to-3 ratio (fifth day). M059K cells were subcultured by a 1-to-5 or 1-to-4 ratio.

After rinsing with D-PBS, cells were detached in 0.05% Trypsin-EDTA for 5 minutes at 37°C under 5% CO_2 and diluted to the required subculture ratio in complete medium after centrifugation (5 minutes, 1,500 g). Flasks were incubated at 37°C under 5% CO_2.

2.1.4.Prevention of *Mycoplasma* contamination

Mycoplasma contamination was systematically investigated during the preparation of stock vials; routine controls were also conducted when thawing new batches of cells. Cultures were tested by microscopic examination following staining of cellular DNA with DAPI. Additional PCR tests were occasionally run for double-checking. No contamination was ever detected during the course of the project.

2.2. Cytotoxicity assays

Tetrazolium dye MTT (3-(4,5-dimethylthiazol-2-yl)-2,5-diphenyltetrazolium bromide) assay is a common colorimetric biochemistry method used to assess cellular viability. It relies on the reduction of MTT salt by mitochondrial NAD(P)H-dependent oxidoreductase enzymes into insoluble formazan, which precipitates in aqueous solutions into deep purple crystals. Upon medium removal and solubilization in DMSO, spectrophotometric quantification of the solution's absorbance reflects cell viability.

MTT (M5655, Sigma-Aldrich, USA) was diluted to 5 mg/mL into D-PBS (14190-094, Gibco, USA) and aliquots were stored away from light at -20°C. Upon testing, MTT solution was added to a final concentration of 0.5 mg/mL on culture plates containing proliferating cells and left incubating for 2 hours at 37°C under 5% CO_2. Plates were then centrifugated at 200 g for 5 minutes before rinsing wells with 200 µL D-PBS. Following removal of remaining liquids, 100 µL DMSO was added to each well and plates were shaken at 700 rpm for 1 minute before spectrophotometric readout at 560 nm.

Initial setting-up experiments were run in order to adjust the initial seeding population. Cell suspensions were serially diluted in complete culture medium and seeded into 96-well plates with 1.10^2 to 8.10^4 cells per well. Cell growth was assessed daily for 96 hours using the MTT assay. The optimal initial seeding was determined as the maximal cell concentration allowing exponential growth after 96 hours without reaching plateau phase. Plates were also visually checked in order to verify that full confluency was not reached.

The MTT assay was then used to assess the cytotoxicity of the chemicals listed in table 4. Cells were seeded in 96-well plates in 90 µL of culture medium and left into the incubator for 24 hours (37°C, 5% CO_2) in order to initiate cell growth. Chemicals were serially diluted into the appropriate solvent and transferred into complete culture medium. 10 µL were added onto the plates to a final concentration ranging from 3 nM to 150 µM, in 0.5% DMSO. Cell viability was tracked immediately after exposure to the chemicals in order to check the absence of interference with culture medium; similarly, viability was measured 24 hours and 48 hours following exposure in order to conclude on the molecules' toxicity. Results were analyzed using GraphPad Prism, v. 8.4.2; growth-inhibiting concentrations of 10%, 50% and 80% of the cell population were extracted (IC_{10}, IC_{50} and IC_{80}, respectively) based on non-linear regression with variable slope. When required, bottom and top constraints were set to 0 and 100% viability, respectively

Due to variations in toxicity depending on the growth support (96-well plates, Petri dishes or culture flasks), additional setup experiments were run in order to adjust reference concentrations (see the "Results" chapter for details). Cells were plated in 6-well plates, treated and detached after the desired amount of time. Cellular suspensions were then counted automatically (Countess, Invitrogen, USA) to check the actual cell viability in supports larger than 96-well plates.

2.3. *In cellulo* treatments

Two types of treatments were performed within the course of this project. "*In cellulo*" treatments refer to the addition of the compounds of interest in cultured cells during their proliferation, while "*in vitro*" treatments (described in the Next-SPOT section) were used in experiments based on cell extracts and refer to the addition of the inhibitors in the reaction mix, with the extracts.

For cellular treatments, cells were plated in 100 mm tissue culture-treated Petri dishes (353003, Corning, USA) and left into the incubator for 24 hours to allow the initiation of cell proliferation. Initial cellular seeding was calculated to ensure 80 to 90% confluency at the end of the treatment. Cells were treated with the chemicals diluted into complete growth medium to the desired concentration in 0.3% DMSO. Doxorubicin was added at IC_{10} in order to induce a genotoxic stress without impairing cell growth. DNA repair inhibitors were added to their IC_{50}, either alone or in combination with doxorubicin, to ensure sufficient repair inhibition. Due to the mechanism of action of doxorubicin, it was deemed more relevant to allow at least one doubling time (and thus ensure a cycle of DNA replication) before collecting the cells. Hence, treatment time was set to 48 hours, after which cells were detached using trypsin-EDTA, counted automatically and frozen in FBS-DMSO at -80°C. The counting step, combined with a visual examination of the dishes, allowed for a verification of treatment efficiency. After another 24 hours, cells were either thawed for protein extraction or stored in liquid nitrogen. Preliminary tests were run to assess the impact of DMSO at a concentration of 0.3% on cell viability and repair activities; no effect of DMSO was found (data not presented) and this condition was used as a reference for treated cells.

2.4. Immunofluorescence analyses

Cells were seeded in black clear-bottom 96 plates (655090, Greiner Bio-One GmbH, Austria), with the same surface density as for treatments in dishes. Cultures were treated after 24 hours and put back in the incubator for 24 to 48 hours. Additional tests were run by replacing treatment solutions by fresh culture medium after 48 hours to allow for the investigation of damage repair activities. Etoposide was used as a positive control based on routine experiments run by specialized team members; this drug is a topoisomerase II inhibitor which has been shown to induce SSBs and DSBs at low concentrations (Meresse *et al.*, 2004; Baldwin and Osheroff, 2005).

Cells were fixed at 24, 48 or 72 hours by carefully adding 1 volume of 8% formaldehyde solution to each well to a final concentration of 4%. Plates were incubated at room temperature for 30 minutes and rinsed three times with PBS before immediate protein staining or short-term storage at 4°C.

Cells were permeabilized for 15 minutes with PBS solution containing 3% bovine serum albumin (BSA, A2153, Sigma-Aldrich, USA) and 0.2% Triton X-100 before blocking non-specific sites for 15 minutes with PBS-3% BSA. Anti-53BP1 primary antibody (PAB12506, Abnova Corporation, Taiwan) was diluted to 1:1,000 in a PBS solution containing 3% BSA and 0.02% sodium azide and incubated with the cells for 1 hour (30 µL per well) before three 5-minute rinses with PBS.

30 µL of anti-rabbit secondary antibody (λ_{ex} 504 nm, λ_{em} 521 nm; Atto 488, Sigma-Aldrich, USA) diluted to 1:2,000 in PBS-3% BSA were added to each well and incubated for 1 hour away from light, before

rinsing the plates three times for 15 minutes with PBS-0.2% Triton. After quickly rinsing the plates three times with PBS, nuclei were stained by adding 100 µL of Hoechst 33342 (λ_{ex} 346 nm, λ_{em} 460 nm; B2261, Sigma-Aldrich, USA) diluted in PBS to a final concentration of 0.3 µg/mL. Hoechst specifically binds AT-rich regions of double-stranded DNA, hence revealing the nuclei, allowing the exclusion of irrelevant staining artefacts outside the cells as opposed to actual 53BP1 foci within the nuclei. After incubating for 20 minutes away from light, 100 µL of PBS-50% glycerol was dispensed in each well to prevent excessive evaporation from occurring during long-term storage at 4°C.

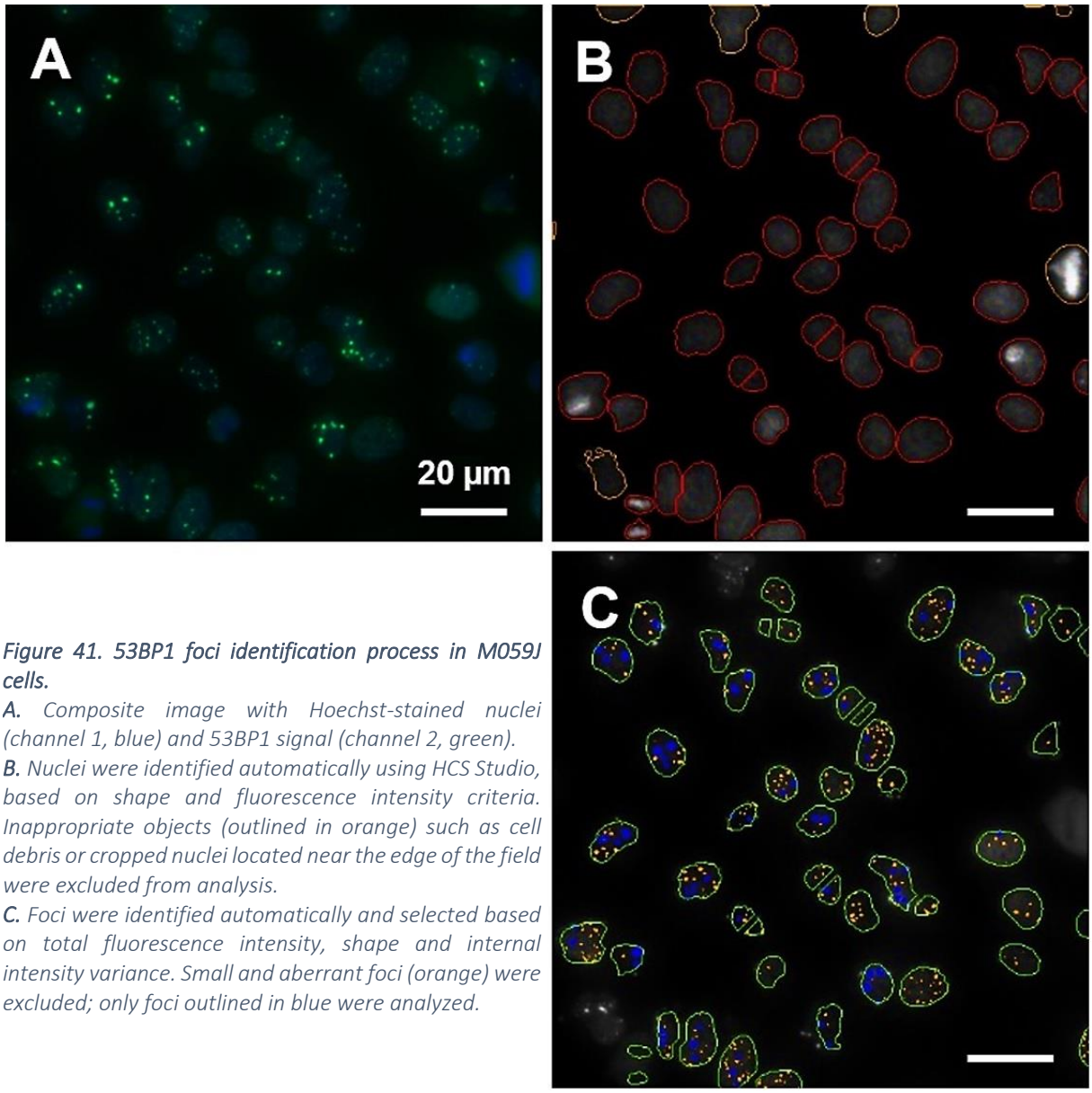

Figure 41. 53BP1 foci identification process in M059J cells.
A. Composite image with Hoechst-stained nuclei (channel 1, blue) and 53BP1 signal (channel 2, green).
B. Nuclei were identified automatically using HCS Studio, based on shape and fluorescence intensity criteria. Inappropriate objects (outlined in orange) such as cell debris or cropped nuclei located near the edge of the field were excluded from analysis.
C. Foci were identified automatically and selected based on total fluorescence intensity, shape and internal intensity variance. Small and aberrant foci (orange) were excluded; only foci outlined in blue were analyzed.

53BP1 foci were counted using an automated high-content screening platform (CellInsight CX5, ThermoFisher Scientific, USA). Images of at least 500 cells per well were acquired at 20x magnification using the 386 nm excitation laser on the first channel to capture Hoechst staining and the 485 nm one on the second channel to identify 53BP1 signal. Nuclear foci were identified and counted using Thermo Scientific HCS Studio Cellomics Scan 6.5.0 (figure 41). Assay parameters such as foci size and intensity

thresholds were set based on visual observation. This means that for each cell line, preliminary calibrations were made to adjust the automatic foci count to the visual estimation made by two different users.

Exported parameters included total foci fluorescence and foci area per cell, as well as the average foci number per cell. We mostly analyzed this last parameter. Assay calibrations were run prior to the analysis of treated cells in order to ensure that the number of automatically analyzed foci matched manual estimations by the observer.

3. Protein extraction

3.1. Nuclear protein extracts (NE)

Cells were thawed and quickly transferred into Eppendorf® tubes before centrifugation (500 g, 5 minutes at 4°C). Unless otherwise stated, all further processing steps were conducted at 4°C with cold reagents. Samples were rinsed with 1X PBS, centrifuged and incubated on ice for 20 minutes in hypotonic buffer A to achieve cytoplasmic membrane lysis (see table 6). Cells were then vortexed for 30 seconds and lysis efficiency was controlled under the microscope after Trypan blue staining. Due to lower lysis rates for HeLa cells, Triton-X 100 concentration was increased for this cell line. Intact nuclei were pelleted by centrifugation at 2,300 g, resuspended in hypertonic buffer B (see table 6) and incubated on ice for 20 minutes to achieve nuclear membrane lysis. This step was completed by two cycles of freezing in liquid nitrogen for 30 seconds and thawing 4°C for 2 minutes. After a final centrifugation step at 16,000 g for 10 minutes, proteins of interest isolated in the supernatant were aliquoted, snap-frozen into liquid nitrogen and stored at -80°C. 2 µL samples were diluted by a 1:160 ratio in protease-free water (W4502, Sigma-Aldrich, USA) for protein quantification. Nuclear debris contained in the pellets were discarded.

Table 6. Composition of lysis buffers A and B for nuclear protein extraction. *Solvent: Milli-Q®-purified H_2O.*

BUFFER A		BUFFER B	
Cytoplasmic membrane lysis		Nuclear membrane lysis	
Reagent	Final concentration	Reagent	Final concentration
HEPES-KOH	10 mM	HEPES-KOH	10 mM
KCl	10 mM	KCl	400 mM
$MgCl_2$	1.5 mM	$MgCl_2$	1.5 mM
DTT	0.5 mM	DTT	0.5 mM
PMSF	103 µM	PMSF	103 µM
Triton X-100	0.03% (HeLa cells) 0.02% (other cell lines)	EDTA-NaOH	0.2 mM
		Glycerol	25 %
		cOmplete™ Protease Inhibitor Cocktail (11836153001, Roche)	0.7X
0.5 to 1.5 mL (0.5 to 5 million cells)		10 µL per million cells	

Additional tests were made to compare nuclear protein extracts with whole cell extracts, using the protocol described in appendix 5.

3.2. Protein quantification: bicinchoninic acid assay

Protein concentration in the cellular extracts was determined using a dedicated kit (UP75860A, Interchim, France), according to the manufacturer's instructions. Briefly, extracts were diluted in 96 well-plates (1:200 to 1:530 dilution of the original extracts); standard solutions were prepared by serially diluting a 2 mg/mL BSA solution (UP36859A, Interchim, France). The supplied MicroBC Assay solutions were mixed according to the manufacturer's instructions and added into sample and standard wells. The assay is based on the protein-dependent reduction of cupric ion Cu(II) to Cu(I) in alkaline medium; bicinchoninic acid specifically chelates Cu^{+} ions to produce a water soluble purple colored complex with a maximal optical absorption at 562 nm. The formation of this complex was accelerated by a 1-hour incubation at 60°C; plates were then cooled down to room temperature before colorimetric measurements on an automated plate reader (SpectraMax® iD3, Molecular Devices, USA). At working concentrations (1-100 µg protein/mL), a direct linear relationship correlates absorbance to protein content in the extracts.

4. Quantification of protein expression

4.1. Experimental procedure

Cell extracts were diluted into protease-free water to a final 20 µg of protein per tube, in 1X Laemmli buffer. After a 10-minute, 90°C heat treatment, samples were loaded on 4–20% precast polyacrylamide gels (4568094 or 4568096, Bio-Rad, USA) and migrated in a buffer containing 25 mM Tris, 192 mM glycine and 0.1% sodium dodecyl sulfate (SDS) for 30 minutes under 90 V and 60 minutes under 120 V.

Gels were then activated using a Stain-Free™-enabled imager (ChemiDoc XRS+, Bio-Rad, USA) to reveal total proteins. Briefly, trihalo compounds contained in the stain-free gels form covalent bonds with tryptophan residues in the proteins and enhance their fluorescence when exposed to UV light, thus allowing protein quantification after a short photoactivation.

Proteins were then transferred onto a nitrocellulose membrane (1704158, Bio-Rad, USA) using the manufacturer's optimized protocol (MIXED MW, Trans-Blot Turbo system, Bio-Rad, USA). Total proteins on the membranes were then revealed to validate the transfer before a 1-hour blocking step at room temperature in 1X Tris-buffered saline (TBS) complemented with 0.5% TWEEN® 20 and 10% dehydrated milk. Primary antibodies (table 7) were diluted to the desired concentration in TBS-0.5% TWEEN® 20-10% milk and incubated overnight at 4°C with the membranes.

Table 7: primary and secondary antibodies used for western blotting

ANTIBODY	REFERENCE	SUPPLIER	ORIGIN	DILUTION
Anti-RAD51	ab88572	Abcam, UK	mouse	1:1,000
Anti-PARP1	9542	Cell Signalling Technologies, USA	rabbit	1:3,000
Anti-DNA-PKcs	ab32566	Abcam, UK	rabbit	1:1,000
Anti-phospho(S2056) DNA-PKcs	ab124918	Abcam, UK	rabbit	1:8,000
Anti-βactin	A2228	Sigma-Aldrich, USA	mouse	1:10,000
Anti-mouse	NA931V	Cytiva Life Sciences, UK	sheep	1:10,000
Anti-rabbit	NA934VS	Cytiva Life Sciences, UK	donkey	1:10,000

Membranes were then agitated at room temperature for one hour, quickly washed three times in TBS-0.5% TWEEN® 20 and rinsed three times for 5 minutes, before being incubated for one hour with a secondary antibody linked to horseradish peroxidase (HRP) and diluted in TBS-0.5% TWEEN® 20-10% milk. Membranes were then rinsed (three times quickly, three times for 5 minutes) and taken to the imager; total proteins were measured to adjust for any variations in protein content due to membrane manipulation. One colorimetric measurement allowed the acquisition of the ladder wells to be merged with chemiluminescent acquisitions. Peroxide reagent and luminol/enhancer solutions (Tris Clarity™ ECL 1705060, Bio-Rad, USA) were then mixed and added for chemiluminescent measurement of the protein of interest.

Membranes were then rinsed three times in TBS-0.5% TWEEN® 20 and bound antibodies were removed by a stripping buffer (25 mM glycine, 1% SDS, pH 2) for 30 minutes at room temperature and washed (three times quickly, three times for 5 minutes) before repeating the blocking step and the incubation with another primary antibody. Up to three proteins were measured on the same membrane, always with increasing intensity of signal to prevent the measurement of any residual signal after stripping.

4.2. Estimation of protein expression

Protein expression was calculated as the ratio between the luminescent signal obtained for the protein of interest and total proteins transferred onto the membrane. Protein loading was also verified based on β-actin staining as an alternative normalization standard in addition to stain-free acquisitions. Since actin provided a strong signal, it was usually stained after other proteins of interest were revealed on the membrane.

The two methods usually provided similar results but variations were sometimes observed, that were attributed to alterations in the membrane surface after 2 cycles of staining-stripping. Thus, protein expression results were normalized based on stain-free measurements. DNA-PKcs phosphorylation was expressed as a ratio between phopsho-Ser2056 signal and total DNA-PKcs. When comparing various treatment conditions, data was normalized to the untreated control.

5. Quantification of PARP activity

PARP activity was measured in nuclear extracts using a ELISA system (4685-096-K, R&D Systems, USA), which tracks the NAD-dependent addition of poly(ADP-ribose). Extracts were diluted in their original buffer to a protein concentration of 1,000 ng/µL. Then, serial dilutions were made in the supplied assay buffer up to 2 ng/µL and 25 µL of diluted extracts were dispensed onto each well of a histone-coated plate. Standard solutions containing a recombinant PARP enzyme were adjusted to contain 1:500 of extracts buffer. An additional 25 µL of reaction mix containing activated DNA and 2 mM NAD was added into each well and the plates were incubated at room temperature for 30 minutes. Following 2 rinses in PBS-0.1% Triton X-100 and 2 rinses in PBS, 1:1000 anti-PAR antibody was added for a 30-minute incubation. After rinsing, 1:1000 anti-mouse IgG-HRP conjugate was dispensed and incubated for 30 minutes. The wells were rinsed again, PeroxyGlow™ solutions were added and the plate was taken to the automated reader (SpectraMax® iD3, Molecular Devices, USA) for chemiluminescent measurement.

Results were expressed in PARP mU/µl based on internal calibration standards. When investigating cellular treatments, data was normalized to the untreated controls.

6. Quantification of excision/synthesis activities on the ExSy-SPOT biochip

6.1. Assay principle

The ExSy-SPOT assay quantifies excision and resynthesis activities from the NER, BER and crosslink repair pathways by tracking the incorporation of fluorescently labelled dNTPs. In brief, plasmids containing specific lesions are immobilized on a chip and incubated with cell extracts. Lesions are first detected by cellular sensors and DNA repair machinery, cleaved (excision) and resulting gaps are filled-in by 5'-3' polymerase activity (synthesis) using the labelled dNTPs present in the reaction mix. Repair efficiency on each damaged plasmid is assessed by fluorescence quantification and by comparing the signal obtained on lesion-containing plasmids to the undamaged control.

6.2. Experimental procedure

6.2.1. Production of damaged plasmids

The assay is based on the 2961 base pairs plasmid pBlueScript II SK (+/-) (detailed in figure 44, section 7). Plasmid production and purification was carried out as described in previous work (George, 2017; Millau, 2006; Millau *et al.*, 2008b). The plasmid was resuspended either in 1X PBS or in nuclease-free water (W4502, Sigma-Aldrich, USA) depending on the intended use.

Purified plasmids were exposed to various physical or chemical treatments in order to generate six different kinds of lesions (table 8). The protocols used for the generation of 8-oxoG, AP sites (AbaS), cytosine/thymine glycols and photoproducts (CDP-64) are described by J.F. Millau (Millau, 2006; Millau *et al.*, 2008b) and the obtention of ethenobases is detailed by C. George (George, 2017). CisP adducts were generated based on an LXRepair procedure by incubating pBlueScript with 30 µM cisplatin. A total of seven plasmids were dispensed on the chip, containing these six different DNA lesions that are commonly repaired by either NER or BER, as detailed in the previous chapter. These protocols were validated before this PhD project by HPLC-MS/MS quantification to ensure sufficient damage levels on the plasmids and guarantee lesion specificity following the different treatments. DNA integrity was checked for each plasmid batch using 0.8% agarose gel electrophoresis, to verify the absence of breakage.

Table 8: Lesion-containing plasmids used for the functionalization of the ExSy-SPOT chip.

NOMENCLATURE	DETAILS	TREATMENT	ORIGIN	REPAIR PATHWAY
Control	Undamaged control plasmid	None	-	-
8-oxoG	Plasmid containing 8-oxoguanine lesions	Riboflavin, UVA	UV radiation, oxidative stress	BER
AbaS	Plasmid with abasic sites	Sodium Citrate (acid pH)	Depurination, hydrolysis	BER
Glycols	Plasmid containing thymine and cytosine diols	$KMnO_4$	Oxidative stress	BER
Etheno	Plasmid containing ethenobases εG, εA and εC	Chloroacetaldehyde	Environmental agents, oxidative damage	BER
CisP	Plasmid containing CisP adducts	Cisplatin	Cross-linking agents	NER
CPD-64	Plasmid containing cyclobutane pyrimidine dimers and (6-4) photoproducts	UVC	UV radiation	NER

6.2.2.Slide functionalization

Damaged and control plasmids in 1X PBS were diluted to 40 µg/mL in a 96 well plate and secondary ½ dilution was realized into the control lesion-free plasmid (40 µg/mL). Hence, total plasmid concentration was constant in both cases, only the amount of lesions varied (100% or 50%). Plasmids were printed on 3D-hydrogel-coated slides (SCHOTT NEXTERION®, Germany) using a specific arrayer (sciFLEXARRAYER S5, Scienion AG, Germany). This instrument relies on a piezoelectric technology allowing the dispensing of very small volumes (usually around 900 pL) without any physical contact with the slide's surface.

14 pads were printed per slide; each pad contains 28 spots consisting of plasmid drops of approximately 230 µm diameter. 4 spots correspond to 100% of undamaged control plasmid (40 µg/µL), and the remaining 24 spots are divided into 6 duplicates of 100% lesion-containing plasmids (6 lesions, two replicate spots per lesion) and 6 duplicates of ½ diluted lesion-containing plasmids (figure 42).

Printing quality was checked by visual control on the instrument's camera and by the use of water sensitive pH paper (3100-0011, Quantifoil Instruments) on control slides. Typically, the presence of dust or aggregates in the instrument or in the plasmid solutions would result in printing offsets that were detected during these control steps.

Printed slides were blocked for 30 minutes in a Na-phosphate bath (0.3 M, pH 8.5, 25°C) and stored at -20°C in sealed bags until use.

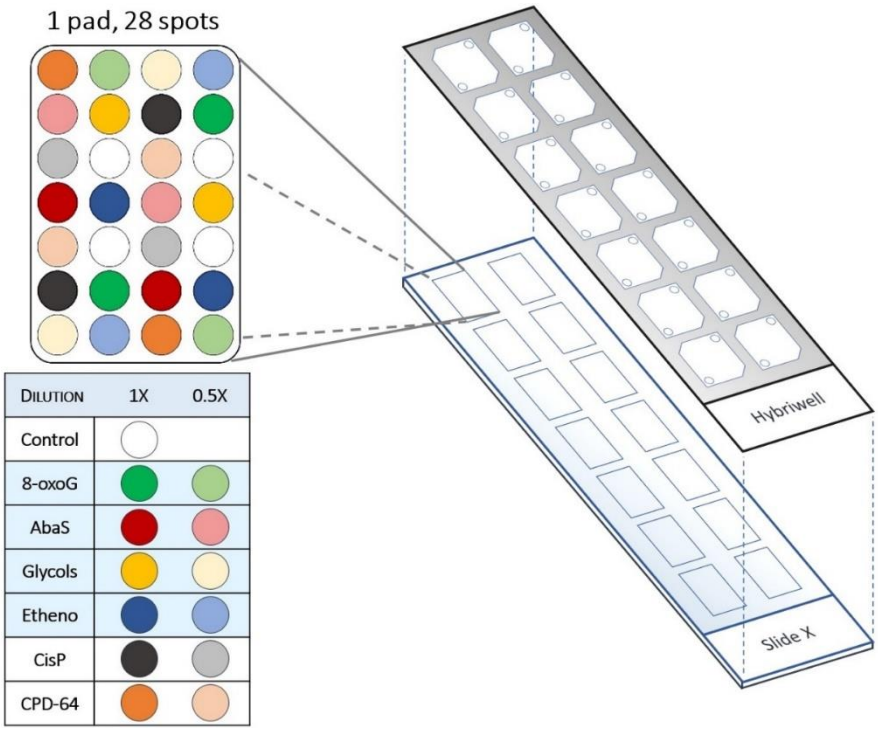

Figure 42. ExSy-SPOT biochip design and assembly. Each slide contains 14 pads with 28 spots of plasmids.

6.2.3. *In vitro* excision/resynthesis reaction

Most assay conditions, including buffer composition, incubation time and temperature, were set by J.F. Millau (Millau, 2006). However, adjustments were made in recent years regarding reagents and storage conditions. A 1.25X ready-to-use reaction buffer was prepared in advance by mixing the following reagents before storage at -20°C for a maximum of 6 months:

- 1.25 mM ATP (GE27-2056-01, Sigma-Aldrich, USA)
- 0.30 µM Cy3-labelled dCTP (GEPA53021, Sigma-Aldrich, USA)
- 1.25X ATG buffer from a 5X solution containing 0.5 mg/mL BSA, 250 µg/mL creatine phosphokinase (CPK; C3755, Sigma-Aldrich, USA), 50 mM phosphocreatine (PC; P7936, Sigma-Aldrich, USA), 2.5 mM DTT, 10 mM EDTA-NaOH, 220 mM HEPES-KOH, 35 mM $MgCl_2$, 1.25 µM dATP, 1.25 µM dGTP, 1.25 µM dTTP (N0446S, New England Biolabs, USA) and 17% glycerol

Upon testing, functionalized slides were thawed at room temperature for 20 minutes and covered with a plastic cover (Hybriwell™ RD481551-M, Grace Bio-Labs, USA) in order to isolate individual reaction chambers for each pad (figure 42).

For each sample, a 30 µL reaction mix was prepared as follows:

- 6 µL of nuclear extracts diluted in the extraction buffer (buffer B) to the desired concentration (typically 0.1 to 0.6 mg/mL in the final 30 µL reaction mix)
- 24 µL of 1.25X ready-to-use reaction buffer

Commercial HeLa extracts (HeLa Nuclear Extracts, IpraCell, Belgium) were used on each slide as a control; they were diluted in an extract buffer containing 20% glycerol, 0.5 mM DTT, 0.2 mM EDTA-NaOH, 20 mM HEPES-KOH, 450 mM KCl. Control HeLa extracts were mixed to the same test reagents as for sample extracts, to a final concentration of 0.2 mg/mL. For each set of experiments, control extracts all originated from the same batch stored at -80°C in single-use aliquots.

Final reagent concentrations upon testing are listed in table 9.

Table 9. Final reagents concentration in the ExSy-SPOT assay

REAGENT	FINAL TEST CONCENTRATION	REAGENT	FINAL TEST CONCENTRATION
ATP	1 mM	$MgCl_2$	7.3 mM
Cy3-dCTP	0.25 µM	dNTPs	0.25 µM
BSA	0.1 mg/mL	KCl	80 mM
Creatine phosphokinase	50 µg/mL	Glycerol	8.4%
Phosphocreatine	10 mM	PMSF	20 µM
DTT	0.6 mM	Protease inhibitors	0.14X
EDTA-NaOH	2.04 mM	Nuclear protein extracts	0.1-0.6 mg/mL
HEPES-KOH	46 mM	-	

Immediately after dispensing the reaction mix in each reaction chamber, slides were covered with an adhesive strip to seal dispensing holes and prevent undesired evaporation during the incubation step. Slides were incubated away from light for 3 hours at 30°C in a humid environment without shaking (PHMP shaker, GrantInstruments Ltd, UK).

The Hybriwell™ cover and the adhesive strip were then removed before rinsing the slides with Milli-Q®-purified water (1 active shaking step followed by two sets of 3 rinses and 3-minute incubation in Milli-Q®-purified water). Remaining water was removed by a 5-minute centrifugation at 800 g in Falcon tube followed by a 20-minute drying step at 37°C. Slides were then taken to the scanner (InnoScan 710 AL, Innopsys, France) for fluorescence readout.

6.2.4.Fluorescence quantification and data analysis

Cy3 signal was measured at 532 nm, 5.0 mW, digital gain 19. This last parameter describes the ability of the scanner's photomultiplier to amplify the signal by increasing the ratio of analog-to-digital units to electrons acquired on the sensor, which determines the apparent pixel brightness at a given exposure. In short, digital gain was adjusted in order to prevent saturation on the DNA spots. Focus was automatically controlled by the scanner, hence allowing adjustments during the slide readout, for instance in the case of an uneven coating of the hydrogel covering the slide's surface. Readout and quantification were performed using Mapix software (Mapix 8.5.0, Innopsys, France).

Each cell extract sample was dispensed in independent duplicate pads on the slide, each comprising two replicate spots (4 for the undamaged control plasmid, see figure 42). Total fluorescence intensity (FI) on each spot was exported in arbitrary fluorescence units (AU) and replicate spots were normalized automatically using a Mapix plugin designed specifically for LXRepair applications. Briefly, data recorded for a same lesion was exported *via* the TransfertGPR software and normalized with the NormalizeIt tool developed by LXRepair. This normalization step centered and standardized data from the couples of experimental duplicates, thus setting a similar mean and standard deviation to all replicates. A recursive, weighted linear regression was run between all combinations of coupled replicates, as detailed by J.F. Millau (Millau, 2006; Millau *et al.*, 2008b). Weighting coefficients corresponded to the reproducibility factors among replicates and varied between 0 and 1; the closer the factor was to 1, the more similar (ideally identical) replicates were. Inversely, a reproducibility factor close to 0 indicated that at least one of the two replicate deposits did not operate properly. Values from each duplicate were then weighted with their reproducibility factor to finalize the normalization step, thereby correcting internal bias among replicates and reducing intra- and inter-pad variability. Normalized data provided by the plugin was automatically compiled into a single text file combined with a PDF summary allowing a rapid evaluation of the analyzed data.

When required (incorrect spot identification, dust on the spot…), manual adjustments were made before exporting data. Further analysis steps were carried out manually on Microsoft Excel Professional 2016 (Microsoft Corporation, USA); FI on the control plasmid was subtracted from that of each lesion plasmid in order to focus on the part of the signal which originates from damage repair. Additional analysis details are provided in section 9 of this chapter.

7. Implementation of the electrophoretic DSBR assay

A protocol was established to study in-vitro end-joining activities in cell extracts, based on the same principle as classical cell-free NHEJ assays (Sharma and Raghavan, 2010). This assay was to be used as a standard method to guide the development of the biochip assay. In short, a DNA plasmid was linearized by an *Afl*III-mediated restriction and incubated with cell extracts. Reaction products were separated by agarose gel electrophoresis and band quantification allowed the estimation of ligation intensity.

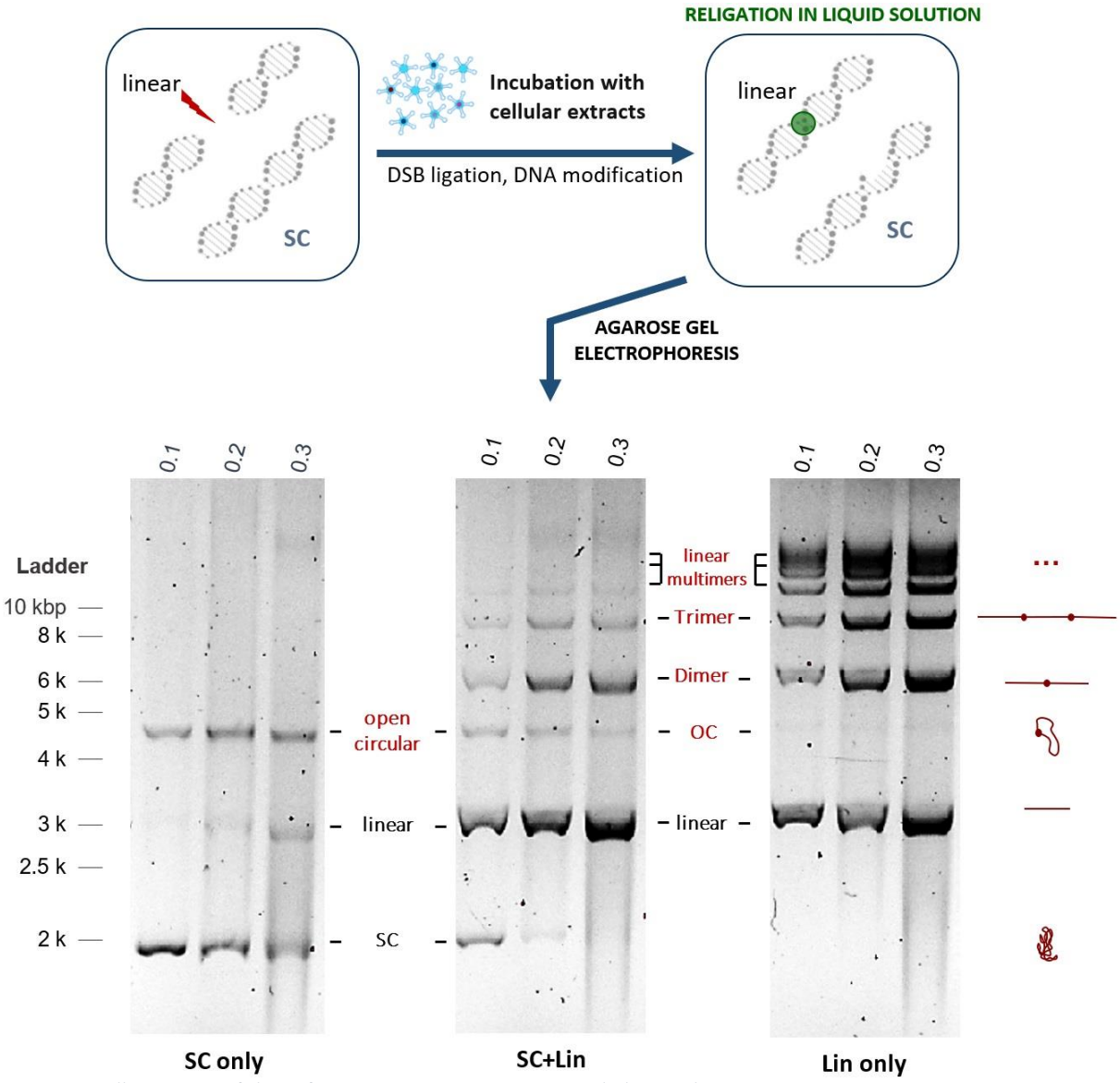

Figure 43. Illustration of the reference c-NHEJ assay using gel electrophoresis.
Plasmid oligomers were generated by HeLa nuclear extracts that carry out the ligation of the substrate DNA. Supercoiled (SC) and/or AflIII*-digested linear pBlueScript plasmids (Lin) were diluted to 5 ng/µL and incubated with HeLa nuclear extracts at concentrations ranging from 0.1 to 0.3 mg/ml. The original SC and Lin plasmids are annotated in black underlined font, while novel DNA species formed after incubation with cell extracts are annotated in red. A schematic illustration of the different DNA species is presented to the right of the gels.*

7.1. Assay principle

More specifically, the electrophoretic assay explores ligation activities from the c-NHEJ pathway by tracking the oligomerization of a pBlueScript plasmid digested by a restriction enzyme. In brief, the digestion mimics a DNA break, and the incubation with DSB repair proteins contained in cell extracts results in the formation of various DNA species corresponding to the recircularized plasmid or oligomers of rejoined linear plasmids. Ligation products are separated using agarose gel electrophoresis (figure 43), and the quantification of each band allows the estimation of DSB rejoining activity in the cell extracts. The assay was originally based on a fluorescent plasmid, but a simplified method has been developed as presented in this section and in the "Results" chapter.

7.2. Production of DNA substrates

The pBlueScript II SK (+/-) plasmid (figure 44) was produced and extracted with the same procedure as for the ExSy-SPOT assay (see section 6.2).

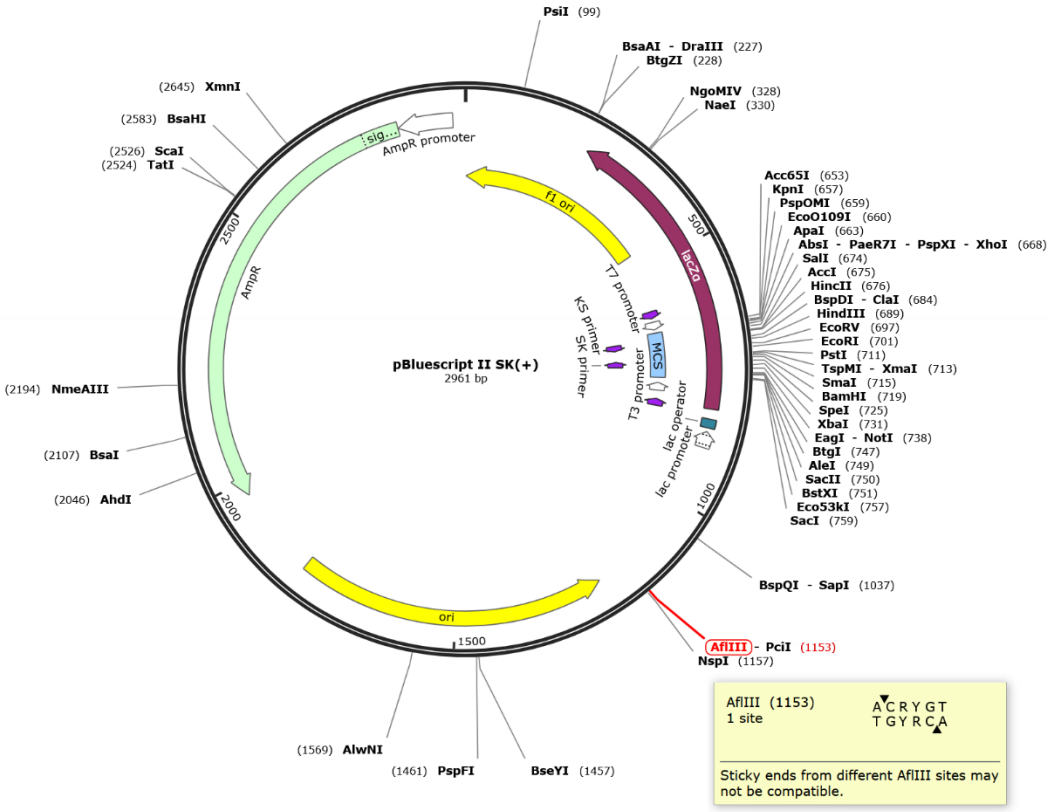

Figure 44. pBlueScript SK (+) plasmid map.
The annotated site is targeted by restriction enzyme AflIII *used for DSB assays.* AflIII *restriction generates a 3 kbp-long linear double-stranded fragment with sticky ends (5' overhangs).* AflIII *target site: R = A or G, Y = C or T; pBlueScript* AflIII *site sequence: ACATGT. Source:* www.snapgene.com.

7.2.1. *Afl*III digestion

pBlueScript plasmid was digested by restriction enzyme *Afl*III (figure 44); the typical 2 mL reaction mix was made of 1556 µL H_2O, 200 µL Buffer 3.1 (B7203, New England Biolabs, USA), 20 µL 100X BSA (9001S, NEB, USA), 200 µL plasmid in H_2O (1 mg/ml) and 24 µL of restriction enzyme *Afl*III (R0541, NEB, USA). Digestion was run for 1 hour at 37°C, after which 1 volume of 2-propanol (I9516, Sigma-Aldrich, USA) and 0.1 volume of sodium acetate 3 N (S2889, Sigma-Aldrich, USA) were added and homogenized before centrifugation for 30 minutes at 16,000 g, 4°C.

Supernatants were discarded and pellets washed with 70% ethanol before a 5-minute centrifugation at 10,000 g, 4°C. Ethanol rinsing and centrifugation steps were repeated once more before discarding removing remaining ethanol and diluting pelleted the digested plasmid in 45 µL of PBS or nuclease-free water depending on subsequent experiments.

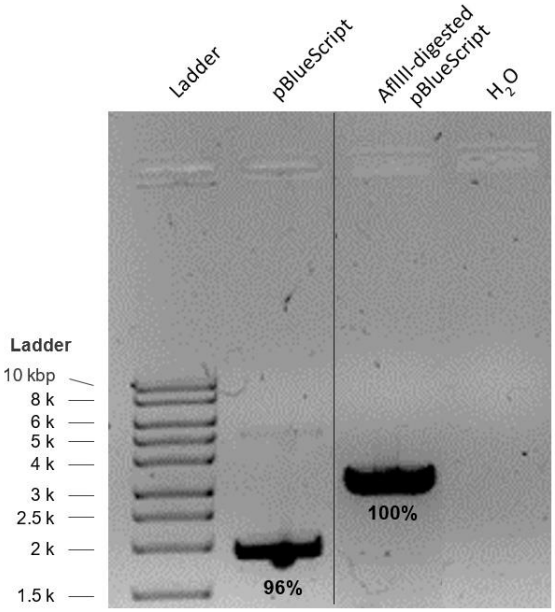

Figure 45. Quality control following plasmid purification and digestion.
Untreated and AflIII-digested pBlueScript plasmids controlled by gel electrophoresis. Values indicate the intensity of each band relative to the total intensity of the lane bands.

Plasmid solutions were set aside for at least 10 minutes at 4°C to allow a better homogenization. DNA concentration and purity were measured by spectrophotometric measurement. DNA content was adjusted to 1,000 ng/µL prior to storage at -80°C. A small aliquot was sampled for rapid control using agarose gel electrophoresis (figure 45).

Briefly, 200 ng of sample plasmids were loaded onto 0.8% agarose gel with 1 µg/mL ethidium bromide (EtBr) and digestion efficiency was controlled by visual observation and band quantification (ImageLab 6.0.1, Bio-Rad, USA). The desired form (supercoiled after plasmid purification, linear after digestion) had to reach at least 85% of the total observed DNA species for the plasmids to be validated. Indeed, other

band forms can correspond to damaged plasmids, and we had to ensure they were kept as low as possible in order to prevent undesired reactions to occur during the repair assays.

7.2.2.Cyanine 3 staining

Undamaged and digested plasmids were labelled using a dedicated kit (Label IT® Cy®3, Mirus Bio, USA), which covalently binds cyanine fluorophores to nucleic acids through reactive alkylating groups. Briefly, kit reagents were used in a single experiment, by preparing six 100 µL reaction mixtures containing nuclease-free water complemented with 10 µg of plasmid in H_2O, 10 µL of 10X labelling buffer and 7.5 µL of Cy3 reagent. Reactions were run away from light for 30 minutes at 37°C before quickly vortexing the tubes to allow covalent bonds to form, and samples were incubated for another 90 minutes at 37°C.

Plasmids were then precipitated by adding 0.1 volume of 5 M NaCl and 2 volumes of cold 100% ethanol before cooling tubes down to -20°C for 30 minutes. After a 30-minute, 16,000 g centrifugation at 4°C, supernatant was discarded and 400 µL of cold 70% ethanol was added in each tube before centrifugating 10 minutes, 16,000 g at 4°C. The 70% ethanol rinsing step and 10-minute centrifugation were repeated once and pellets were resuspended in 40 µL Milli-Q®-purified water. Stained plasmids were quantified using the NanoDrop™ spectrophotometer; labeling density was calculated based on the manufacturer's instructions. Estimates were on average of approximately one label every 200 base pairs. Stained plasmids were controlled on agarose gel in a similar fashion as digested plasmids in the previous section.

7.3. Original assay

7.3.1.Ligation reaction

The reaction buffer contained HEPES (pH 7.8, final test concentration of 20 mM), 10 mM $MgCl_2$, 80 mM KCl, 1 mM ATP, 1 mM DTT and 0.1 mg/mL BSA, diluted into in Milli-Q®-purified water. Tubes were kept at 4°C until incubation with cell extracts. Digested or undamaged plasmids diluted in H_2O were added to a final test concentration of 35 ng/µl, as well as Cy3-labelled plasmids. Whenever possible, all subsequent steps until EtBr bath were conducted away from light. Finally, cellular extracts were added to a final concentration ranging from 0.1 to 0.5 mg/mL. Ligation was then allowed for 15 minutes at room temperature.

Ligation products were then purified by adding 0.1 volume of 5M NaCl and 2 volumes of cold 100% ethanol into each 20 µL reaction tube. Samples were homogenized and cooled down to -20°C for 1 hour before a 30-minute centrifugation at 16,000 g, 4°C. Supernatant was discarded and pellets were washed with cold 70% ethanol before centrifugation at 16,000 g for 10 minutes at 4°C. Supernatant was then

discarded and leftover ethanol was air-dried before dilution of the pellets into 20 µL of Milli-Q®-purified H_2O.

7.3.2.Gel electrophoresis

200 ng of plasmid DNA (as calculated from the initial 35 ng/µL plasmid concentration) were loaded onto an agarose gel prepared with 200 mL 0.5X Tris-borate-EDTA (TBE; T4415, Sigma-Aldrich, USA) with 0.8% agarose and without ethidium bromide. Migration was run for 3 hours at 120 V. End ligation was initially quantified by specifically revealing labelled plasmids (Typhoon 9400, Amersham Biosciences/Cytiva Life Sciences, UK; emission filter 580 nm BP30 Cy3, TAMRA, AlexaFluor 546). The gel was then bathed into a 1 µg/mL EtBr solution (E1510, Sigma-Aldrich, USA) for 1 hour, rinsed with Milli-Q®-purified H_2O and taken to the imager (ChemiDoc XRS+, Bio-Rad, USA) to reveal total DNA.

7.4. Optimization process

Due to technical adjustments on the biochip assay (see section 8), it became necessary to modify assay conditions on our electrophoretic method. More details regarding technical optimizations are provided in the "Results chapter".

Nuclear extract concentration was set at a maximum of 0.2 mg/mL in both methods, since it is the average concentration reached in biopsy extracts for clinical and R&D applications; higher concentrations were used for technical optimization with cancer cell lines, but it was important for us not to set routine extracts concentrations that would not be reachable with all kinds of biological material.

The initial assay was based on a supercoiled and an *Afl*III-digested, cy3-labelled pBlueScript plasmid at a concentration of 35 ng/µL each, while the *Afl*II-digested plasmid was introduced at 2.5 ng/µL in the Next-SPOT biochip assay. Having a different nuclear protein to DNA ratio between the electrophoretic assay and the biochip was not deemed optimal for the comparison between both methods, so plasmid concentration was set to 2.5 ng/µL of each added plasmid, which also reduced the consumption of labelled substrate.

7.5. Modified electrophoretic assay

Since the assay was to provide a better understanding of the reactions occurring on the biochip, tests were made in order to maximize comparability between both methods. The optimization process resulted in a final protocol that is described in this section.

The reaction mix was adjusted based on the optimizations of the biochip; a pre-mix of 625 µg/mL BSA, 125 mM Tris-HCl, 62.5 mM $MgCl_2$, 12.5 mM DTT, 312.5 µg/mL CPK, 62.5 mM PC and 1.6 µM dAdTdG

was prepared in advanced in Milli-Q®-purified H_2O and dispensed in single-use aliquots stored at -20°C. Each 30 µL reaction tube contained the following solutions:

- 18 µL of reaction pre-mix complemented upon testing with ATP and unlabeled dCTP
- 6 µL of 25 ng/µL plasmid suspensions (*Af*lII-digested plasmid only or mixture of damaged and undamaged plasmid)
- 6 µL of cell extracts diluted into their original extraction buffer (buffer B for nuclear extracts)

Final reagent concentrations upon testing are detailed in table 10.

Table 10. Final reagents concentration in the electrophoretic assay

REAGENT	FINAL TEST CONCENTRATION	REAGENT	FINAL TEST CONCENTRATION
ATP	1 mM	$MgCl_2$	10 mM
dCTP	0.25 µM	dNTPs	0.25 µM
BSA	0.1 mg/mL	KCl	80 mM
Creatine phosphokinase	50 µg/mL	Glycerol	5%
Phosphocreatine	10 mM	PMSF	20 µM
DTT	2 mM	Protease inhibitors	0.14X
EDTA-NaOH	40 µM	Plasmid substrates	2.5 ng/µL each, or 5 ng/µL of a single plasmid
HEPES-KOH	2 mM	Nuclear protein extracts	0.1-0.6 mg/mL

Tubes were incubated away from light for 1 hour at 30°C (ThermoBlock, Biometra, Germany) to allow plasmid ligation. Proteinase K (PK; P2308, Sigma-Aldrich, USA) was then added in each tube to a final concentration of 0.5 mg/mL and incubated for 30 minutes at 37°C. Ligation products were then frozen at -20°C for short-term storage or separated immediately using agarose gel electrophoresis.

75 ng of plasmid DNA (corresponding to 16 µL per reaction tube as calculated from the initial plasmid concentration) were loaded onto a 200 mL, 0.5X TBE and 0.8% agarose gel stained with 1 µg/mL ethidium bromide. Migration was run for 3 hours at 120 V, before reading the gel on the imager (ChemiDoc XRS+, Bio-Rad, USA), allowing the identification of plasmid oligomers as presented in figure 43.

The signal intensity of each band was expressed as a ratio to the total intensity measured in the lane; repair efficiency was expressed as the total percentage of ligated plasmid bands, as opposed to remaining non-ligated plasmids (linear or supercoiled plasmids initially introduced in the mix).

8. Enzymatic DSB repair assay on biochip (Next-SPOT)

8.1. Assay principle and working hypotheses

The Next-SPOT assay explores strand invasion, ligation and polymerase activities from several DSB repair pathways by tracking the fixation of a fluorescently labeled pBlueScript plasmid digested by a restriction

enzyme onto a linearized or supercoiled plasmid immobilized on a biochip. It relies on the same general principle as the electrophoretic technique but aims at improving throughput and increase the amount of biological information obtained. The digestion process is the same as for the electrophoretic reference assay, and the incubation with DSB repair proteins contained in cell extracts results in the fixation of labelled plasmid on the plasmid substrates immobilized on the chip. Additionally, the assay measures the incorporation of labelled dNTPs on each substrate plasmid. The general Next-SPOT workflow is described in figure 46. Both the reaction environment (liquid with the reference assay, semi-solid on the biochip) and the revelation method (gel electrophoresis with the reference assay, fluorescence readout on the chip) vary between the two assays.

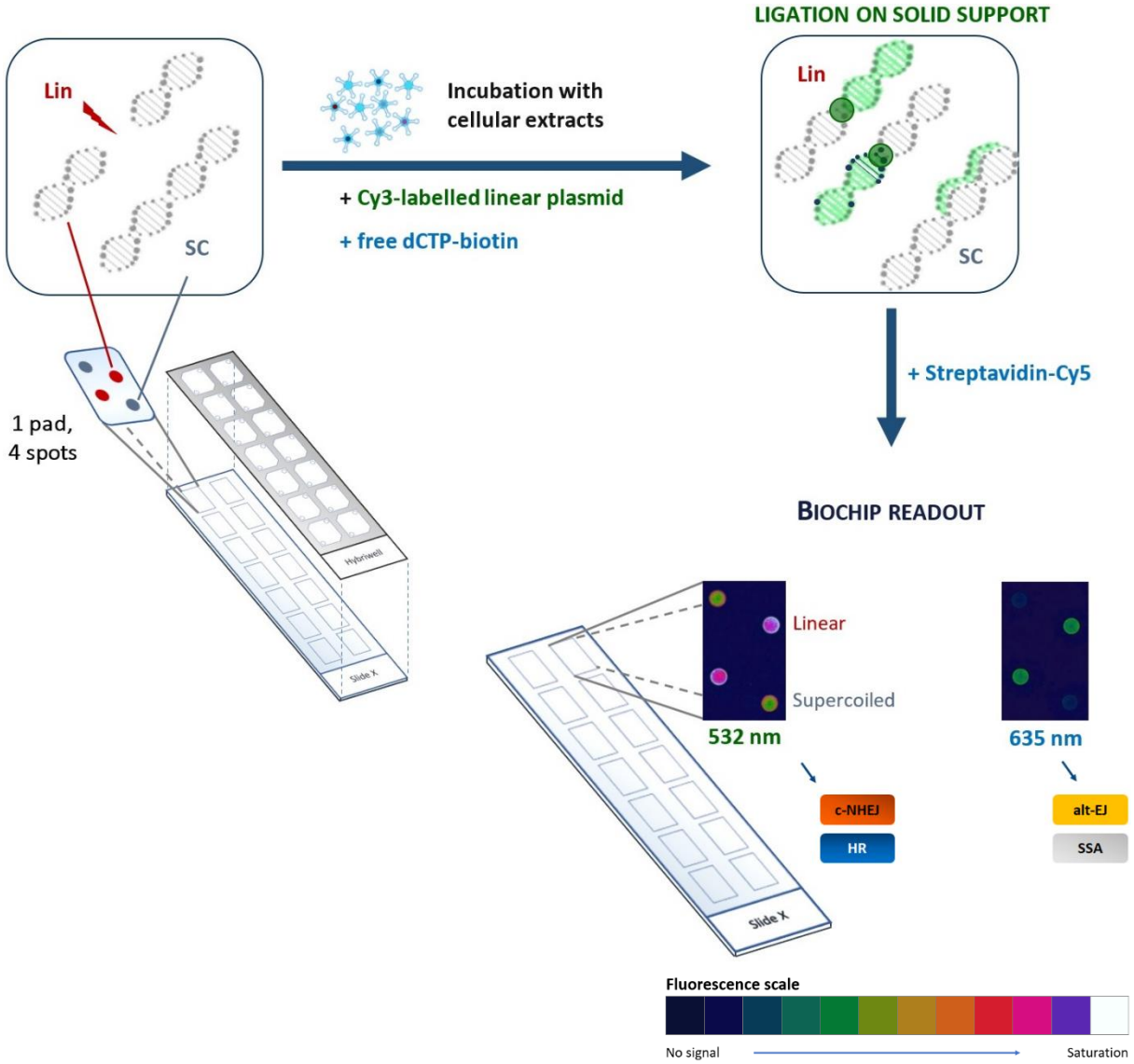

Figure 46. Global overview of the Next-SPOT biochip (14 pads version).
Each slide contains 14 pads with 4 spots of unlabeled plasmids each. Slides are incubated with cell extracts and a mix containing a labelled digested plasmid and biotin-dNTPs; the latter are stained by a streptavidin-cy5 bath. Fluorescence intensity informs i) on the integration of labelled plasmid and ii) on the incorporation of dNTPs on the DNA immobilized on the chip. SC: supercoiled pBlueScript; Lin: AflIII*-digested pBlueScript. Additional information on the hypothesized repair mechanisms is provided in subsequent figures (figure 47 to 51).*

Hence, on each pad, Next-SPOT generates data on four different conditions, depicted in the lower right corner of figure 46:

1. Invasion of the labelled damaged plasmid onto the supercoiled undigested plasmid (cy3, 532 nm)
2. Ligation of the labelled damaged plasmid on the linear, *Afl*III-digested plasmid (cy3, 532 nm)
3. Incorporation of labelled dNTPs on the supercoiled undigested plasmid (cy5, 635 nm)
4. Incorporation of labelled dNTPs on the linear, *Afl*III-digested plasmid (cy5, 635 nm)

Hypotheses were made based on mechanistic literature in order to associate assay measurements to potential DSB repair activities. Using the electrophoretic method, we showed that cell extracts induced an increase in the open circular and linear forms of the original supercoiled plasmid (see figure 43, left panel), which reflects the remodeling and cleavage of the plasmid (Smith-Ravin and Jeggo, 1989). Hence, repair proteins present within the cell extracts can reshape and excise the intact supercoiled pBlueScript plasmid and offer a potential substrate for the initiation of end resection, the ligation of plasmid ends or the incorporation of nucleotides as part of resynthesis activities.

It has been shown that particular structures such as DNA triplexes form in supercoiled DNA when mainly pyrimidine (or purine) bases occupy the major groove of the DNA double helix (Frank-Kamenetskii and Mirkin, 1995). Such structures are involved in the initiation of recombination and they were shown to promote HR, while the loss of supercoiling cancelled the stimulation (Frank-Kamenetskii and Mirkin, 1995; Rooney and Moore, 1995). Some purine/pyrimidine-rich sections of the pBlueScript plasmid (for instance the ones starting at position 1144 or 2791) are good candidates for the formation of DNA triplexes, although no validations were run during this project. In addition, DNA supercoiling is the result of HR mechanisms such as RAD51 and RAD54 activity and it allows homologous DNA pairing in the presence of an ATP-regenerating system (Sigurdsson *et al.*, 2002). Hence, we suggested that the supercoiled plasmid functionalized on the chip may serve as a substrate for HR-like recombination in the presence of the fluorescently labelled linear plasmid. Two possible hypotheses were made based on the literature:

- A first model was proposed based on the investigation of HR intermediates between DNA duplexes (West and Howard-Flanders, 1984; Lopez *et al.*, 1987). Following nucleolytic cleavage on the SC plasmid, DNA nicks could initiate the recruitment of RAD51 and allow a homologous pairing with the fluorescent linearized plasmid (figure 47A). RAD51 would then initiate a strand exchange between the two plasmids.
- An alternative mechanism mobilizes the MRN complex and other resection factors on the 5' tails of the linear plasmid to initiate the formation of 3' overhangs on each side of the *Afl*III

restriction site (figure 47B). The complete homology between the linear and SC plasmids would very likely result in the formation of a displacement loop following the recruitment of RAD51, BRCA1/2 and PALB2 on the single-stranded DNA flaps. This hypothesis is a simplified version of the concatemers studied by Smirnov *et al*. with barcoded DNA (Smirnov *et al.*, 2019).

In the end, these mechanisms result in the integration of the fluorescent linear plasmid onto the SC pBlueScript printed on the chip, thereby producing the observed signal observed at 532 nm. It is worth noting that these processes are not exclusive and are probably taking place at the same time on the chip.

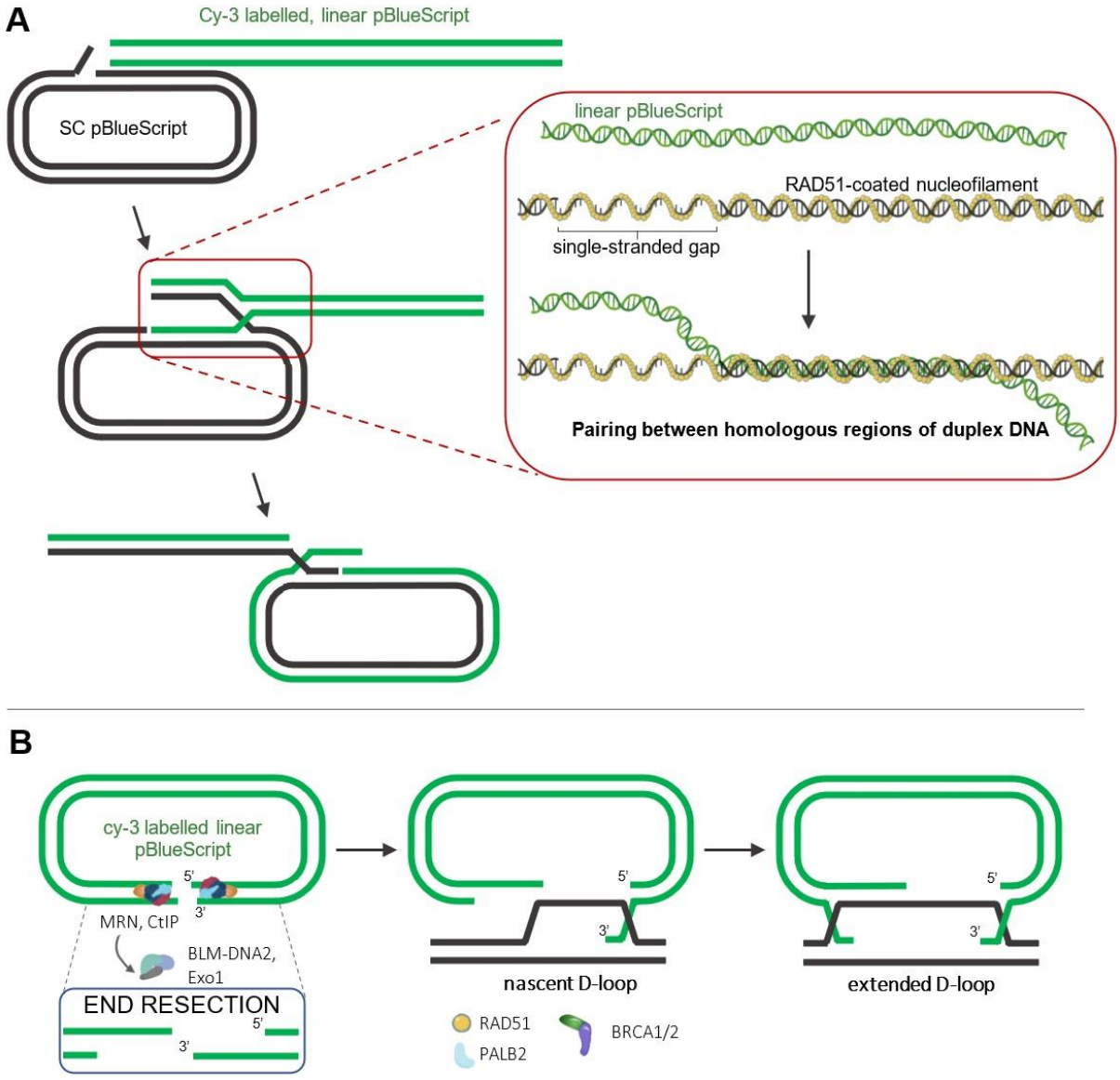

Figure 47. Working Hypothesis on the immobilized SC plasmid for the observation of HR-like processes.
A. *Resection-free hypothesis. Limited cleavage of the supercoiled pBlueScript would allow the formation of single-stranded gaps triggering the recruitment of RAD51 and initiate a pairing with the fluorescent linear plasmid.*
B. *Resection-based hypothesis. The* AflIII *restriction site can be bound by the MRN complex, allowing the initiation of 5' ends resection based on the activity of BLM-DNA2 and EXO1. Strand invasion into the SC plasmid would then be initiated following RAD51 binding on ssDNA tails, in cooperation with HR proteins BRCA1-2 and PALB2, thereby forming a recombination complex with both plasmids.*

Although this assumption remains a working hypothesis, results from LXRepair studies strongly suggest that the incorporation of labelled plasmid on the supercoiled pBlueScript (condition 1) correlates with HR proficiency in the cellular extracts (data not shown).

For its part, the linear, *Afl*III-digested plasmid immobilized on the chip presents cohesive ends with very short 5' overhangs, an ideal substrate for KU and DNA-PKcs to bind DNA ends and initiate c-NHEJ (figure 48).

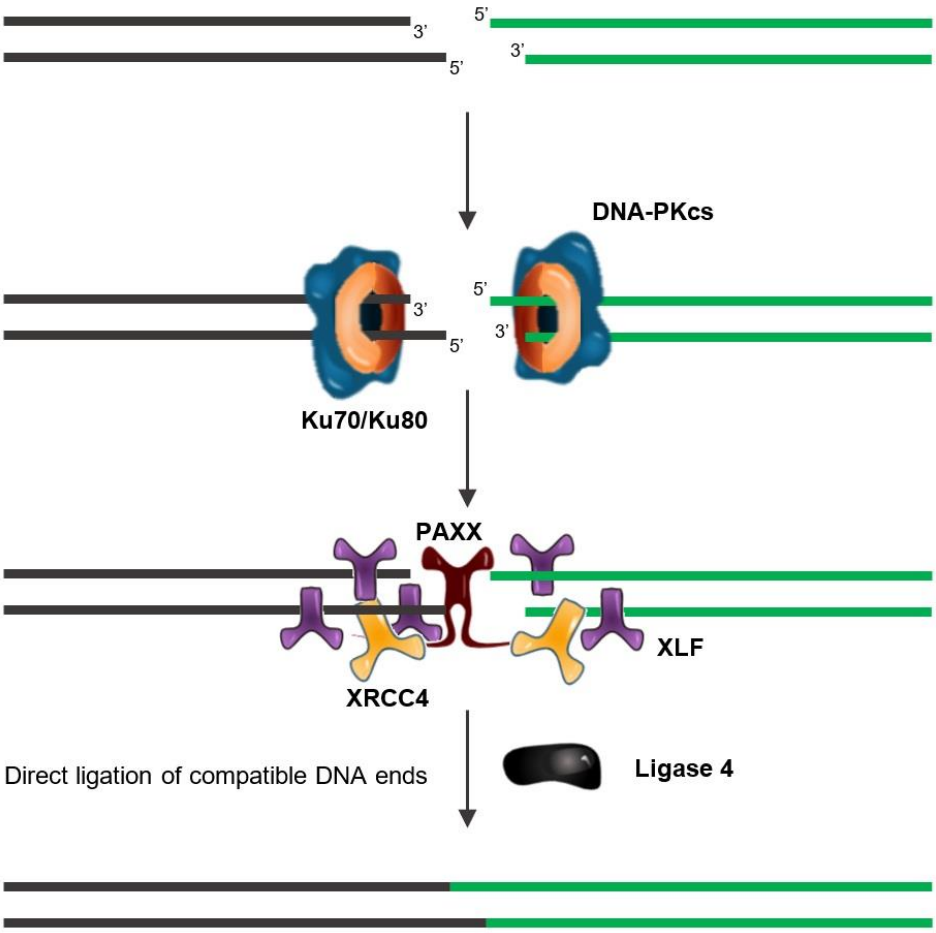

Figure 48. Religation model for the linearized plasmids.
The KU heterodimer binds short 5' overhangs and mobilizes DNA-PKcs for the recruitment of scaffold proteins and ligase 4, which operates the ligation of plasmid ends.

Furthermore, incubation with T4 DNA ligase, which has been used as a model for the last steps of c-NHEJ (Labhart, 1999), resulted in high levels of fluorescent plasmid fixation on the damaged plasmid compared to the supercoiled pBlueScript (figure 49), suggesting that the linear plasmid printed on the chip is an ideal substrate to track NHEJ-like ligation processes.

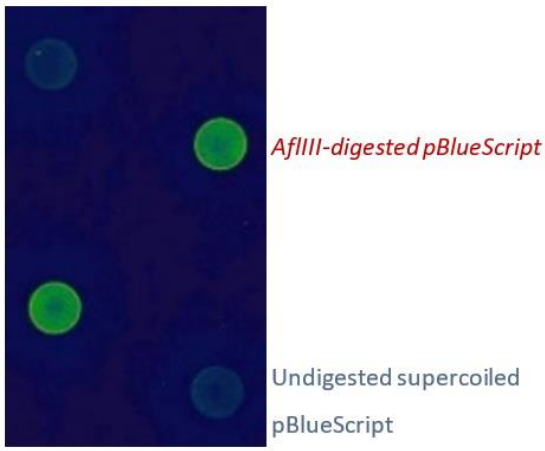

Figure 49. Ligation of labelled AflIII-digested pBlueScript on the functionalized plasmid following incubation with T4 ligase (532 nm).

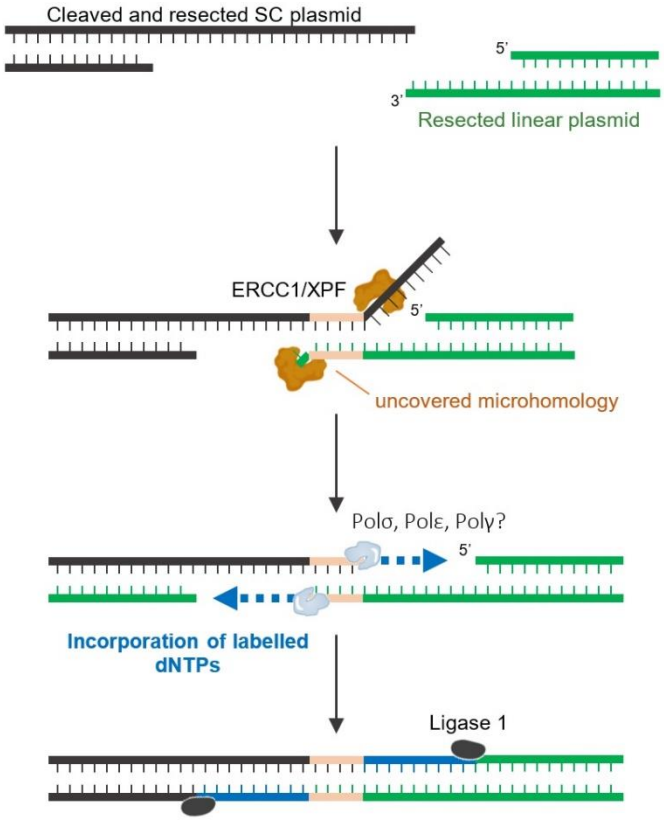

Figure 50. Model of strand annealing on a resected SC plasmid.
Resected DNA ends with unveiled microhomologies represent a substrate for direct annealing by the SSA machinery.

Fluorescence measurement at 635 nm on the undigested plasmid (condition 3) can spot events similar to the DNA pairing and recombination-associated DNA synthesis described by Liu *et al*. (Liu *et al.*, 2011). Following the initiation of HR, repair can be shunted to SSA, which is a faster mechanism that does not rely on strand invasion and D-loop formation, as opposed in the classical HR sub-pathways (Li *et al.*,

2019b); it can also be used as a backup option if the recombination process stalls or if extensive homologies are found within the resected 3' overhangs (Bhargava *et al.*, 2016). In our case, extensive resection is more likely to occur on the supercoiled plasmid in the presence of the nuclear extracts than on the linear one, on which DNA ends are more readily bound to KU. Besides, it is unlikely that a full HR reaction can occur due to the limited reaction time (1.5 hour). Hence, LXRepair correlates *de novo* synthesis on the supercoiled plasmid to the SSA pathway (figure 50).

Finally, the most appropriate candidate to achieve the incorporation of labelled nucleotides on the linearized plasmid is POLθ. This activity would require the initiation of a resection on the substrate plasmid; it is likely that only a limited resection would take place, due to the opposition of c-NHEJ factors such as KU. However, the mobilization of PARP was shown to compete with the activity of KU (Wang *et al.*, 2006) and it is possible that its recruitment would allow the initiation of a limited end resection on the linearized plasmids (figure 51).

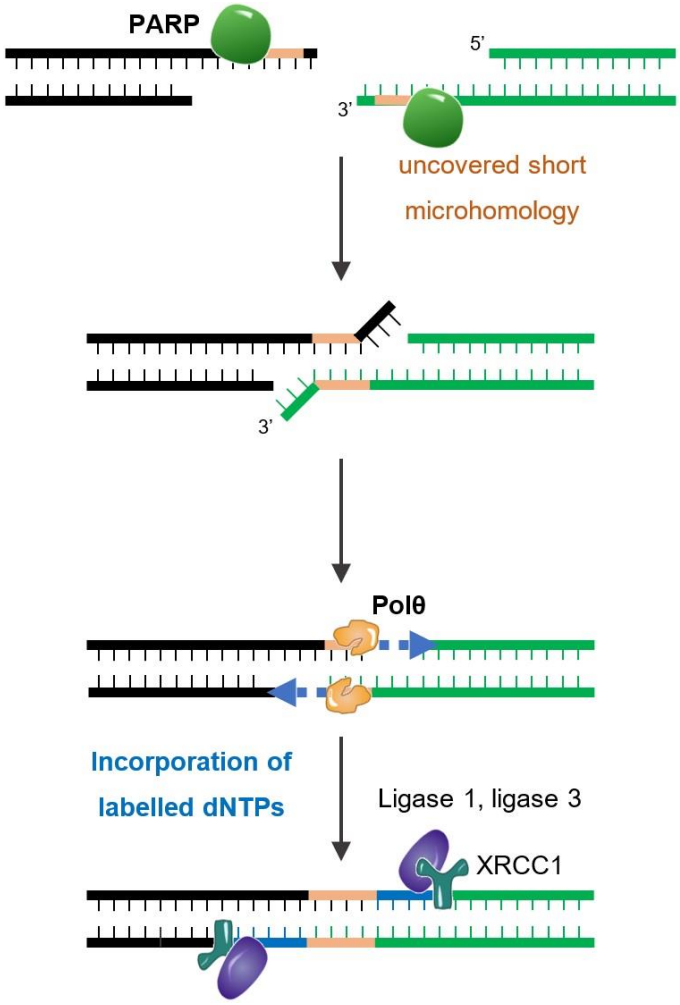

Figure 51. Working hypothesis on the linearized plasmid.
a-EJ proteins are expected to compete with c-NHEJ factors and to operate a certain extent of ligation, especially on resected DSB ends.

As opposed to SSA, a-EJ does not necessarily require an extensive end resection since only short flanking microhomologies need to be uncovered (Bhargava *et al.*, 2016; Mladenov *et al.*, 2016). Hence condition

4 would inform on late alt-NHEJ DNA synthesis; this hypothesis is confirmed by the loss of signal on this condition following the inhibition of key players in alt-EJ, as part of confidential contractual studies. However, Next-SPOT provides no information regarding DNA end synapsis as described in other assays (Audebert *et al.*, 2004).

It must be noted that all repair pathways can potentially occur on each condition on the chip. Notably, the a-NHEJ pathway can initiate on the digested plasmid and thus compete with c-NHEJ. However, our assay is based on the competition between repair factors and some mechanisms are more likely to take over. Based on the literature and on results gathered by LXRepair outside this PhD project (notably using deficient cell lines and specific repair inhibitors), the signals generated on each condition by the Next-SPOT assay were attributed to either HR, c-NHEJ, SSA or a-NHEJ. These hypotheses will be further discussed in the 'Discussion' chapter, based on the results obtained following the exposure to doxorubicin and/or repair inhibitors.

8.2. Assay procedure

8.2.1. Technical optimization

Assay conditions were continuously optimized during the course of the project, and only the final version used to draw biological conclusions is described in the materials and methods. More information regarding the optimization process is provided in the "Results" chapter.

8.2.2.Slide and plasmid production

Plasmids were produced as explained previously (section 6.2.1) before *Afl*III digestion and Cy3 labelling (see section 7.2). Digested and control plasmids in 1X PBS were diluted to 40 µg/mL in a 96 well plate in a similar fashion as for the ExSy-SPOT assay (see section 6.2). Plasmids were printed on 3D-hydrogel-coated slides (SCHOTT NEXTERION®, Germany) using the sciFLEXARRAYER S5 dispenser (Scienion, Germany). In the final Next-SPOT version, 21 pads were printed per slide each containing 4 spots of supercoiled or *Afl*III-digested plasmid, in duplicates (figure 46). Printing process and verifications were identical to the ExSy-SPOT slide production.

8.2.3.Assay procedure

The reaction mix containing 625 µg/mL BSA, 125 mM Tris-HCl, 62.5 mM $MgCl_2$, 12.5 mM DTT, 312.5 µg/mL CPK, 62.5 mM PC and 1.6 µM dAdTdG was prepared in advanced in Milli-Q®-purified H_2O and dispensed in single-use aliquots stored at -20°C.

Upon testing, functionalized slides were thawed at room temperature for 20 minutes and covered with a Hybriwell™ cover. The solution pre-mix was diluted five-fold in nuclease-free H_2O and complemented

with ATP, labelled linearized plasmid and biotin-coupled dCTPs to a final concentration of 1.25 mM, 2.5 ng/µl and 0.31 µM, respectively.

Each 30 µl reaction tube contained the following solutions:

- 24 µl of reaction mix
- 6 µl of cell extracts diluted into their original extraction buffer (buffer B for nuclear extracts)

As for the ExSy-SPOT assay (section 6), commercial HeLa nuclear extracts were used as a standard, allowing technical validation of the reaction mix as well as inter-slide comparisons. Final reagent concentrations upon testing are detailed in table 11.

Table 11. Final reagents concentration for the Next-SPOT assay

REAGENT	FINAL TEST CONCENTRATION	REAGENT	FINAL TEST CONCENTRATION
ATP	1 mM	$MgCl_2$	10 mM
dCTP	0.25 µM	dNTPs	0.25 µM
BSA	0.1 mg/mL	KCl	80 mM
Creatine phosphokinase	50 µg/mL	Glycerol	5%
Phosphocreatine	10 mM	PMSF	20 µM
DTT	2 mM	Protease inhibitors	0.14X
EDTA-NaOH	40 µM	Cy3-labelled *Afl*III-digested plasmid	2 ng/µl
HEPES-KOH	2 mM	Nuclear protein extracts	0.1-0.6 mg/mL

Slides were incubated away from light for 1 hour at 30°C in a humid environment. The Hybriwell™ content was then flushed by vigorous inversions in Milli-Q®-purified water before removing the cover and rinsing the slides in Milli-Q®-purified water (1 active shaking step followed by two sets of 3 rinses and 3-minute incubation in Milli-Q®-purified water). Special care was paid to rinsing steps, in order to i) ensure the correct elimination of unfixed plasmids and nucleotides and ii) remove a maximal amount of background noise. For instance, interactions between the cyanine dyes and the Hybriwell™ glue were observed and thorough rinsing of the slide surface greatly reduced leftover traces on the final images. Remaining water was removed by a 5-minute centrifugation at 800 g in Falcon tube followed by a 20-minute drying step at 37°C. Slides were then taken to the scanner (InnoScan 710 AL, Innopsys, France) for fluorescence readout.

8.2.4.Fluorescence quantification and data analysis

Cy3 signal was measured at 532 nm, 5.0 mW, digital gain 15, while Cy5 signal was acquired at 635 nm, 5.0 mW, digital gain 30. Readout and quantification were controlled using Mapix software (Mapix 8.5.0, Innopsys, France). Total fluorescence intensity (FI) on each spot was exported in arbitrary fluorescence units (AU) and replicate spots. When required (incorrect spot identification, dust on the spot…), manual adjustments were made before exporting data. Further analysis steps were carried out manually on

Microsoft Excel Professional 2016 (Microsoft Corporation, USA). Further analysis details are provided in section 9 of this chapter.

Detection limit was estimated based on the background signal obtained on the slides outside the plasmid spots. On each slide, average background values were extracted and detection limited was calculated as the standard deviation of the background values among all tested slides, multiplied by a factor of 3. Approximately 0.3% of our measurements were below this limit, and never in control cells. These signals were systematically obtained in treated cells with very low repair activities.

8.2.5. Alternative Next-SPOT protocol for "*in vitro*" treatment with repair inhibitors

An alternative approach was used for the treatment with repair inhibitors: rather than treating the cells, only cellular extracts were exposed to the compounds. Inhibitors were diluted into DMSO and nuclease-free H_2O to the desired concentration before incorporation onto nuclear extracts from cells treated with doxorubicin (IC_{10}) or the solvent only (0.3% DMSO). After a 30-minute incubation at room temperature, concentrated assay reagents were added to reach the final test concentrations listed below for a 30 µl reaction volume:

- Diluted inhibitor solution: 400 µM, 3% DMSO
- 0.2 mg/mL nuclear extracts
- 1X reagent assay reagents, as described for the regular assay in the previous section

This final reaction was then dispensed on Hybriwell™-covered slides and the assay run as previously described.

9. Statistical analysis

Experiments were run at least in triplicates, though additional repetitions were sought after in order to increase result robustness. Data was normalized as presented in captions, usually as a ratio to the control condition. In this case, plotted error bars represent standard deviation (SD) adjusted by the ratio between the plotted value and that of the control. ExSy-SPOT and Next-SPOT data were presented either as raw fluorescence values, treated-to-untreated ratio, or as relative pathway contributions. The latter represents the contribution of the values obtained on each assay condition to the sum of all measured signals.

Non-linear regressions of cytotoxicity data were run on Graphpad Prism 9.0.1 (GraphPad Software, Inc., USA). All subsequent statistical analyses were performed using RStudio v.1.4.1103 based on R v.4.0.3

(www.cran.r-project.org). Unless otherwise stated, outliers were not removed from the analysis. Null hypotheses were rejected for a probability (*p*-value) lower than a significance level (α) of 0.05.

We first tested the normal distribution and variance homogeneity of the data using the Shapiro-Wilk and Bartlett tests, respectively. However, samples were often not normally distributed, or small sample size prevented the normality of sample distribution to be assessed in a relevant manner, which prevented a parametric analysis of variance (ANOVA) to be performed. Thus, we used non-parametric tests, which are more appropriate for small populations or if the result of the Shapiro-Wilk test shows that samples are not normally distributed.

Kruskal-Wallis test, a non-parametric equivalent of ANOVA, was performed to test if all studied groups were random samples from the same population or if differences existed between groups. If so, we performed post-hoc analyses in order to identify which ones presented significant differences. In case groups were large enough, pairwise comparisons were run for this purpose using Mann–Whitney–Wilcoxon rank sum tests with Bonferroni correction. Otherwise, we performed pairwise Dunn tests to identify significantly different groups; the standard significance level for this test is a *p*-value equal to α/2.

Unsupervised hierarchical clustering was used to visualize the associations between treatment effects in the different cell lines, using the “pheatmap” and “pvclust” packages. Plotted data corresponded to the base 2 logarithm of the ratio between Next-SPOT data from treated and untreated cells. Clustering was based on two dissimilarity measures:

- Euclidean distance, which regroups profiles with both similar intensity levels and covariation. This classification considers both the co-regulation of repair pathways and intensity level.
- Correlation dissimilarity measure, which regroups profiles with similar covariation independently of their intensity levels. This classification considers only the co-regulation of repair pathways.

pvclust provides two types of p-values, bootstrap probability and approximately unbiased p-value. The latter has superiority in bias over the value calculated by the ordinary bootstrap resampling (Suzuki and Shimodaira, 2006) and clusters with approximately unbiased p-value above 95% were considered significant.

Finally, principal components analysis was performed using the R package "factoextra", based on raw data from the two DSBR methods and 53BP1 foci counting.

CHAPTER 3 – RESULTS

1. Introduction

This chapter details experimental results and provides an overview of the response of the cellular models to various treatments. The overall approach was to expose the cells to doxorubicin in order to generate a genotoxic stress and activate the DNA damage response. Besides this genotoxic stress, some cells were simultaneously exposed to repair inhibitors targeting key players in HR, c-NHEJ or a-NHEJ, with the aim of altering the cellular response to the genotoxic compound. The impact of the inhibitors was investigated with or without activation by doxorubicin; changes in DSBR pathways activity were tracked using two different assays: an electrophoretic NHEJ method and the Next-SPOT assay on biochip; our final objective is to validate Next-SPOT's ability to track the various DSBR repair activities and to offer prospects for further investigations and applications. This chapter covers three main topics.

Firstly, the cytotoxicity of the compounds was assessed in order to determine treatment doses. Once established, immunofluorescent 53BP1 staining was run in order to assess the molecules' genotoxicity and their ability to activate DSB response mechanisms. Further investigations were run to characterize the consequences of the treatments on protein expression and activity levels, as well as on the repair of non-DSB lesions using the ExSy-SPOT approach.

Secondly, a cell-free NHEJ method was optimized to track repair activities in treated and untreated cells, thereby allowing the comparison of basal repair levels and the analysis of the treatments' effect. The assay provided a comparison basis with the biochip method.

Finally, the Next-SPOT assay was used to analyze DSBR activities. These experiments were run following a series of technical optimizations which are also presented. Two protocols were tested on Next-SPOT: analyses were first run on the same extracts as for the electrophoretic assay, ExSy-SPOT and protein expression/activity levels, all based on treated cells. Another protocol was also tested as described in the materials and methods in order to investigate the behavior of the proteins present in the cell extracts: inhibitors were added "*in vitro*" directly in the reaction mix, just prior to the test.

2. Characterization of three cellular models: toxicity, expression/activity of repair factors and excision/resynthesis activity

2.1. Cytotoxicity assays

MTT tests were run in order to assess the toxicity of various genotoxics and repair inhibitors. Generally speaking, a similar behavior was observed on the three cell lines, with a higher sensitivity to RAD51 inhibitor B02 compared to the other repair inhibitors (figure 52A). No striking difference was noted between the different cell lines. The models showed a different level of sensitivity to doxorubicin, with a lower toxicity found in M059K than in M059J and HeLa (figure 52B).

Half maximal inhibitory concentrations (IC_{50}) were calculated for each repair inhibitor; this value corresponds to the compound concentration that inhibits cell proliferation by 50%. Genotoxics and inhibitors were compared based on their IC_{50} and IC_{10} values (figure 53).

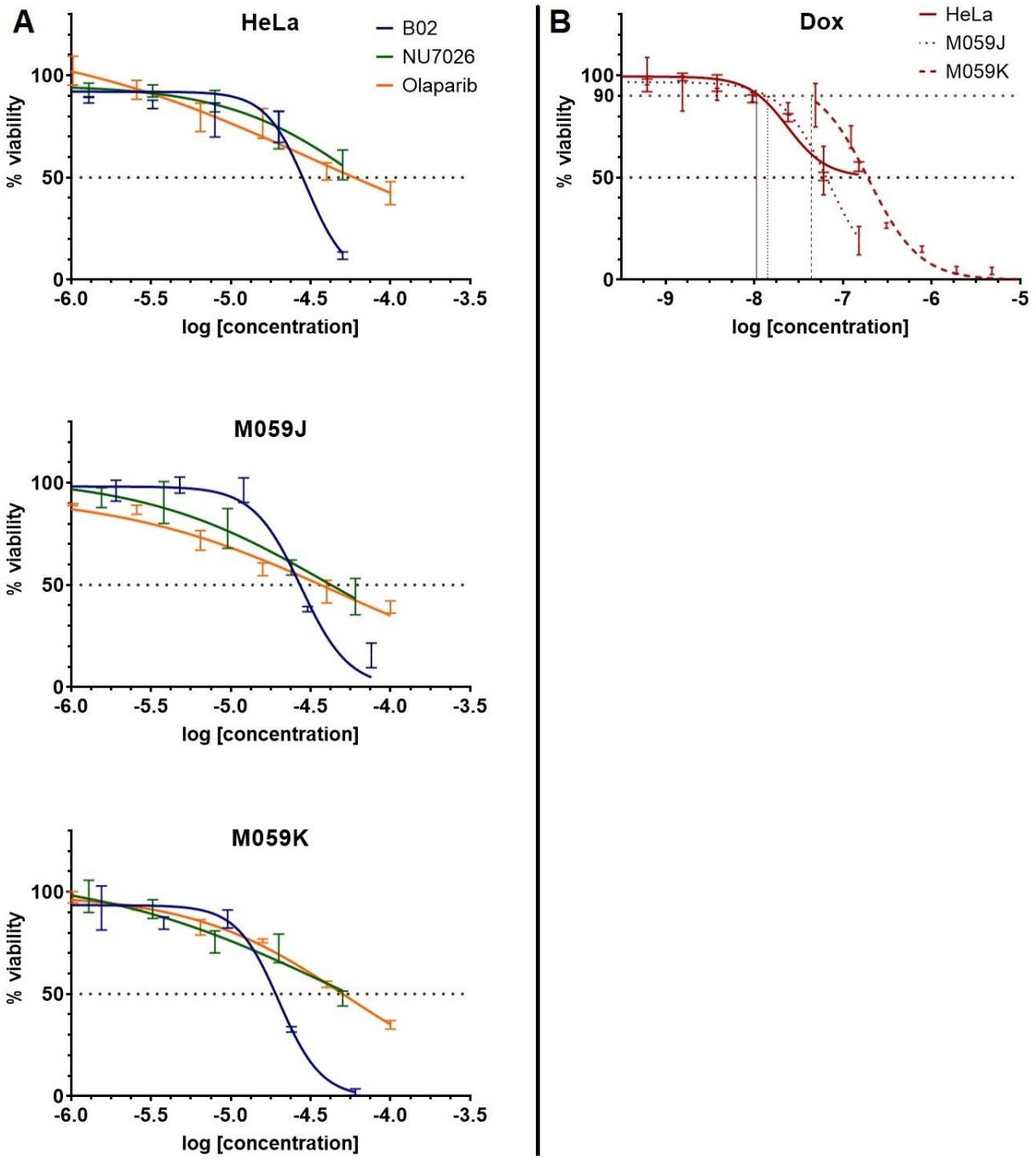

Figure 52. Cytotoxicity of the compounds on the three cellular models, assessed by the MTT assay in 96 well plates.
A. Dose-response curves obtained for each cellular model after exposure to the repair inhibitors for 48 hours.
B. Dose-response curves following a 48-hour treatment with doxorubicin. Decimal logarithm of the IC_{10} value is annotated. Plotted data originates from a single experiment, though tests were repeated at least three times to extract mean IC_{50} and IC_{90} values. Error bars: standard deviation of the technical replicates.

Concentration choice was guided by the need for repair inhibitors to be present at a sufficient concentration to exert their action on the targeted proteins; it was observed in previous studies from both the laboratory and the company that IC_{50} was a good reference value for treatment with repair inhibitors. For their part, genotoxic treatments aimed at triggering the DNA damage response, but it was observed in preliminary tests that going above the IC_{10} could lead to high mortality levels in combined treatments with repair inhibitors (data not shown). Hence, we set this value as a reference for doxorubicin.

An unexpected observation was their higher sensitivity in Petri dishes and culture flasks compared to 96 well plates, especially for repair inhibitors (figure 53). This shift caused high mortality levels (> 80% in cells treated with repair inhibitors combined to doxorubicin), which was first attributed to experimental errors. The persistence of this issue confirmed inappropriate treatment doses, which is thought to result from differential cell proliferation on a small area or to inappropriate seeding concentrations for MTT experiments in 96 well plates. Toxicity was verified by automatic counting of viable treated cells after Trypan blue staining; though more laborious than MTT tests, it provided a reliable confirmation of compound toxicity. Dishes concentrations were set as reference doses for all subsequent experiments, and it was decided to focus on repair inhibitors B02, NU7026 and olaparib only for subsequent characterization steps.

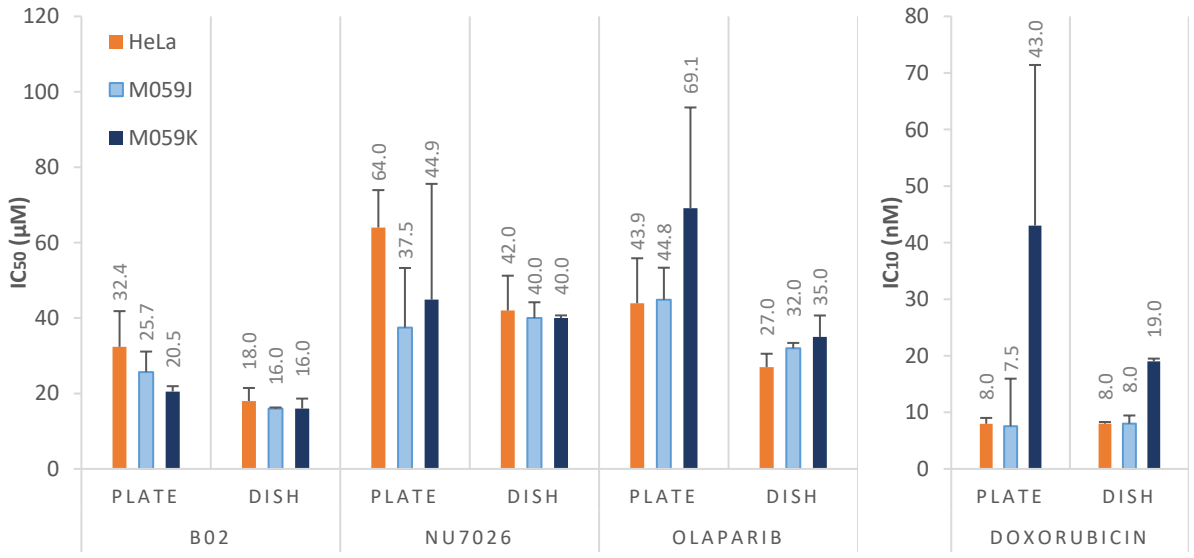

Figure 53. Shift in sensitivity between 96-well culture plates and Petri dishes.
Average values are noted in grey; error bars: standard deviation between n=2 or 3 independent experiments.

Table 12. Reference values for cellular treatments (Petri dishes). Mean ± SD, n=2 or 3.

Cell line	B02 IC_{50}, µM	NU7026 IC_{50}, µM	Olaparib IC_{50}, µM	Doxorubicin IC_{10}, nM
HeLa	18 ± 3.5	42 ± 9.2	27 ± 3.5	8 ± 0.3
M059J	16 ± 0.3	40 ± 4.2	32 ± 1.4	8 ± 1.4
M059K	16 ± 2.6	40 ± 0.7	35 ± 5.7	19 ± 0.5

Sensitivity to the inhibitors was similar between the three models, which had lower IC_{50} values for B02 compared to olaparib and NU7026 (table 12). An interesting feature was only spotted for doxorubicin, for which HeLa and the radiosensitive cell line M059J had a lower IC_{10} than M059K.

2.1. Genotoxicity assay (53BP1)

53BP1 staining revealed different baseline foci levels in the different cell lines and confirmed the genotoxic effect of doxorubicin at the chosen IC_{10} (figure 54 and figure 55).

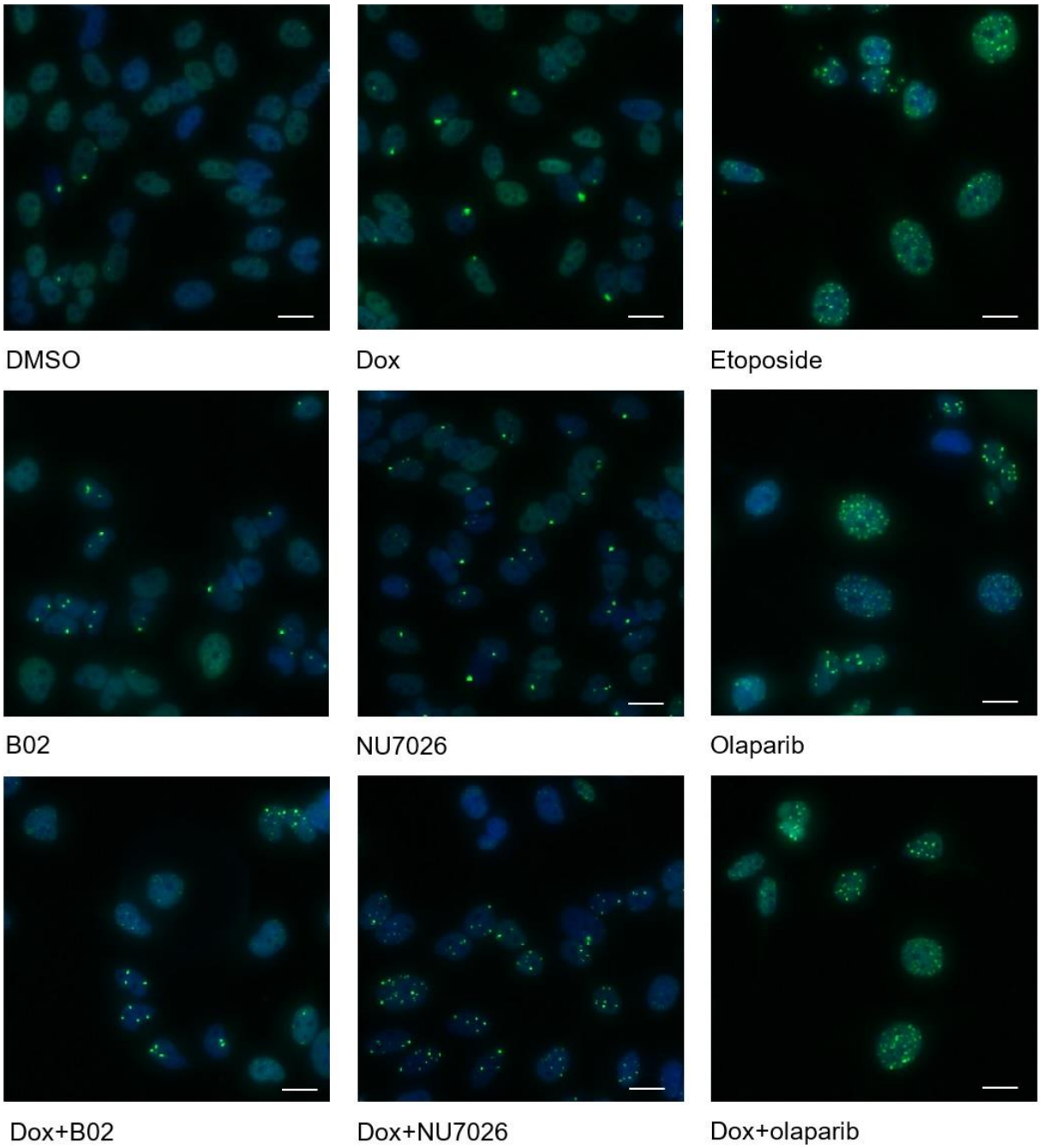

Figure 54. 53BP1 foci in HeLa cells after exposure to doxorubicin and/or DSB repair inhibitors B02, NU7026 and olaparib for 48h.
Positive control: etoposide 0.5 µM. Scale bar: 15 µm.

Mean numbers increased from 0.3 to 0.5 foci per cell in HeLa upon treatment with doxorubicin. In M059J and M059K cells, baseline levels rose from about 3 foci to 11.6 and 7.1 foci per cell, respectively (figure 55). Besides the increase in foci numbers, a change in foci shape was also observed (figure 54), especially after treatment with olaparib and etoposide.

For these treatments, foci were smaller and more numerous, and the number of cells with pan-nuclear staining increased; a striking modification in cell morphology was also noted, with bigger but less numerous cells observed. Foci images in treated M059J and M059K cells are provided in appendix 6.

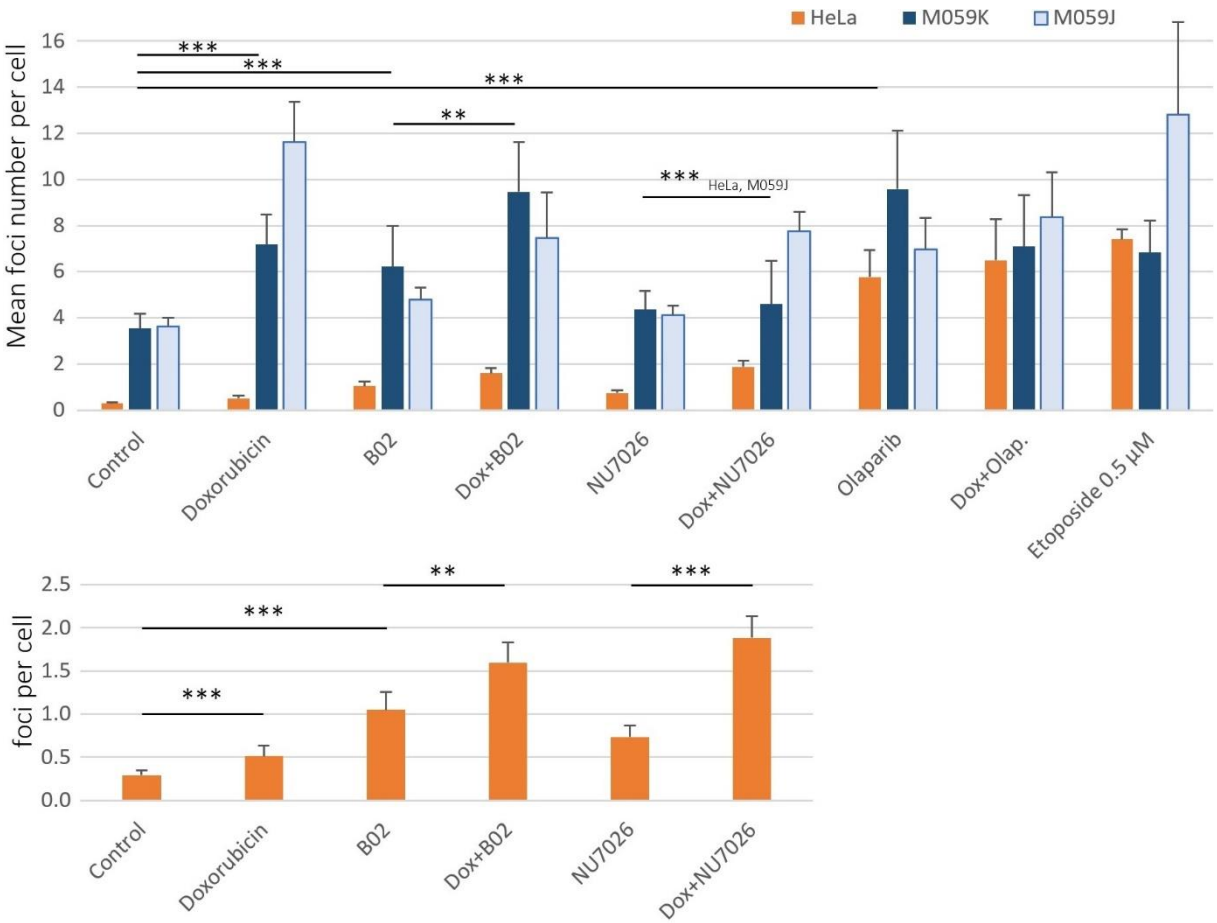

Figure 55. Average 53BP1 foci measured per cell in HeLa, M059K and M059J cell after treatment with doxorubicin and/or DSB repair inhibitors for 48 hours.
A. *Global results for the three cell lines (mean ±SD).* ***B.*** *Focus on HeLa cells exposed to doxorubicin and/or B02 and NU7026.Three independent experiments were performed (n=3). *p<0.05, **p<0.01, ***p<0.001 (Wilcoxon-Mann-Whitney test); only the most relevant pairwise comparisons are annotated; for details, see appendix 6 and appendix 7.*

A clear difference appeared between cellular models, with lower foci levels found in HeLa cells than in M059J and M059K, except after treatment with olaparib and etoposide (figure 55). IC_{10} Doxorubicin treatment led to a modest though significant increase in 53BP1 levels in M059K and HeLa cells ($p<0.01$), thereby validating the chosen IC_{10} treatment dose. Interestingly, a sharp increase was observed in M059J cells, showing a high genotoxic effect this mutated cell line. Exposure to DSB repair inhibitors led

to a significant increase in foci levels in all cell lines, except NU7026, which did not impact M059K cells. Besides, damage was also higher for B02 or NU7026 when combined with doxorubicin (IC_{10}); only NU7026 in M059K did not produce any significant effect. A multitude of very small dots was observed in this cell line, but they were too small to be quantified as foci (appendix 6, M059K).

For its part, olaparib increased foci numbers in all cells, but the combined treatment with doxorubicin did not enhance this effect.

Kinetic measurements revealed a different behavior between M059J and M059K cells, the latter displaying a reduction in foci levels after treatment with doxorubicin and etoposide (figure 56), indicating the initiation of DSBR activities. In M059J, this effect was either not observed or it was shaded by high technical variability. In both cell lines, B02 and NU7026 did not generate notable damage at 24 hours, except in some cases in combination with doxorubicin, while olaparib already induced high foci levels. On average, M059J cells displayed higher foci counts than the wild-type M059K.

Interestingly, no repair was observed in the cells exposed to repair inhibitors after removing treatment solutions; foci levels globally increased or remained stable, suggesting a long-term inhibition of repair proficiency.

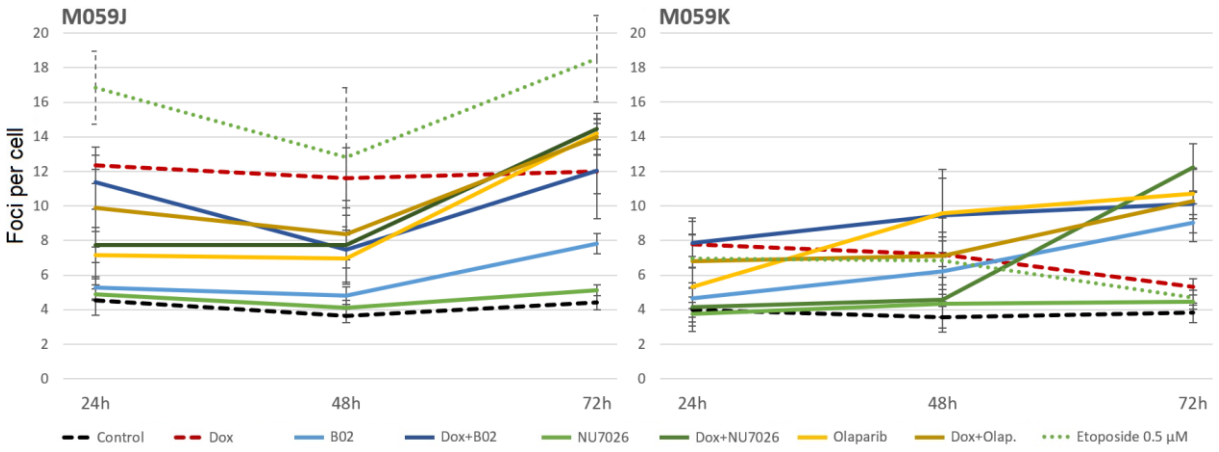

Figure 56. Damage levels and repair kinetics in M059J and M059K cells.
After 48 hours, the genotoxic and repair inhibitors were removed and replaced with fresh medium to allow DNA damage repair. Three experiments were performed (n=3). Error bars: standard deviation.

It can be pointed that NU7026 triggers a late answer in M059K when combined with doxorubicin, which was not observed at 24 or 48 hours only.

The interpretation of this data remains limited due to the absence of information on the cell cycle; cell division may impact foci levels, as will be discussed in the next chapter. However, genotoxicity tests were complemented by data regarding the expression and activity of key DSBR factors.

2.2. Variations in expression and activity of key repair proteins

2.2.1. Basal protein expression

An initial validation step concerned the verification of DNA-PKcs status in M059J cells. When exposed to anti-DNA-PKcs antibodies targeting amino acids 2000-2100 (S2056 phospho-DNA-PKcs) and 4050 (total DNA-PKcs), these cells showed a different western blotting profile than HeLa and M059K (figure 57), thereby validating this cells line's lack of an operational DNA-PKcs. Based on these conclusions, DNA-PKcs expression and phosphorylation were not further investigated in M059J cells.

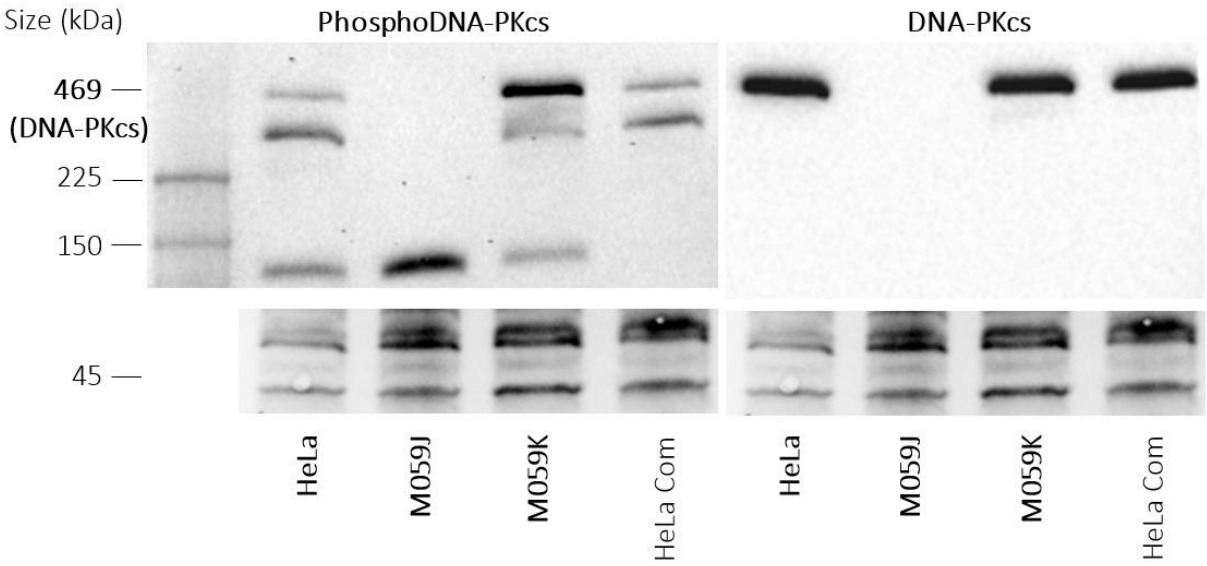

Figure 57. Western blotting of nuclear protein extracts exposed to anti-phosphoS2056-DNA-PKcs or anti-DNA-PKcs. *Commercial HeLa extracts were used as a control. The two heaviest bands obtained for the phosphorylated protein were observed with various relative intensity on a same sample and were attributed to variable denaturation during the sample preparation step; both were quantified. The band at approx. 130 kDa was not known to the manufacturer and was linked to non-specific binding; this band was not included in subsequent quantifications. Protein levels were adjusted for total protein content in each lane, as illustrated by the bands around 45 kDa. Additional information regarding loading control is provided in appendix 8. Images correspond to the same membrane exposed successively to each antibody.*

Basal protein levels were compared between the different cell lines, showing variation in RAD51 and DNA-PKcs levels between HeLa and M059K (figure 57 and figure 58).

Besides, PARP1 cleavage was found to be relatively higher in HeLa than in the glioblastoma models; conversely, DNA-PKcs auto-phosphorylation on Ser2056 was found significantly higher in M059K than on HeLa.

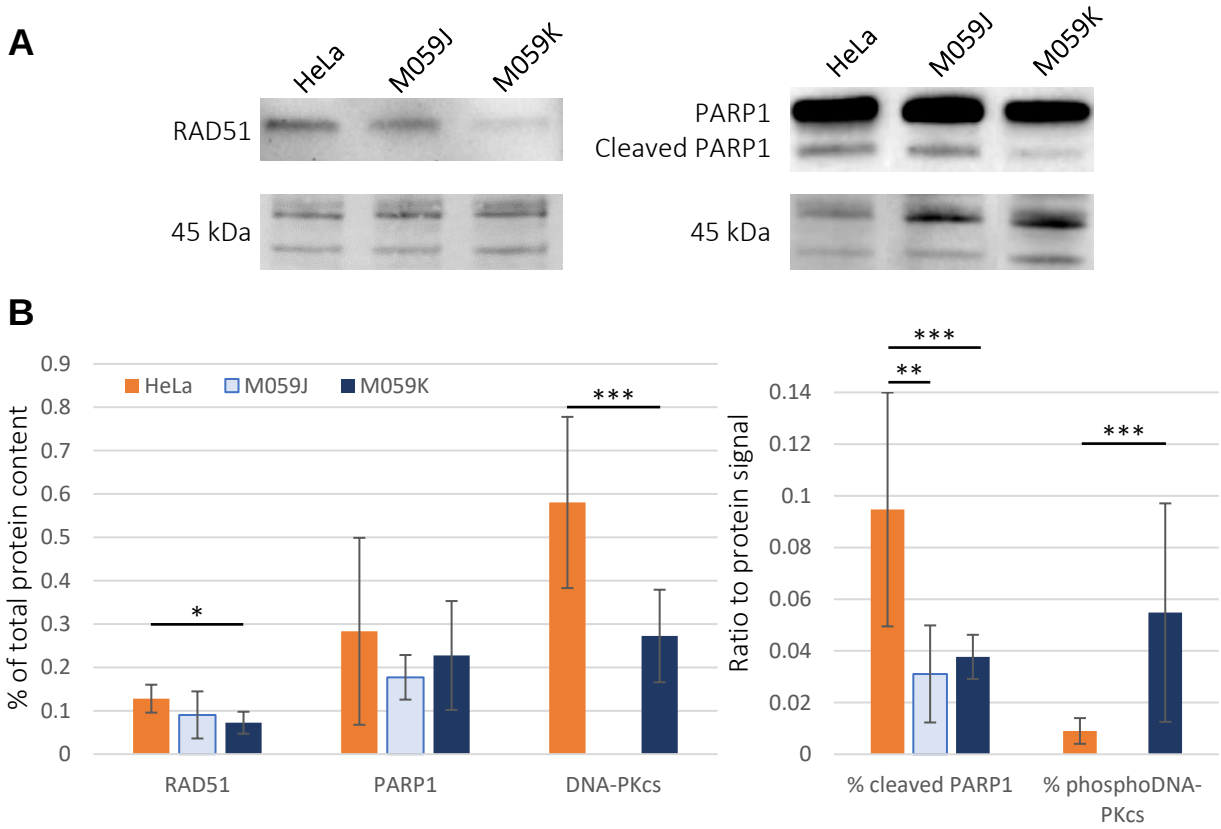

Figure 58. Basal expression levels in the cellular models.
A. *Montage of western blot membranes stained with anti-RAD51 and anti-PARP1 antibodies.* ***B.*** *Protein expression levels in HeLa, M059J and M059K. Proteins were quantified as a ratio to the total protein content in each lane, a subset of which is presented at 45 kDa. PARP cleavage and DNA-PKcs Ser2056 phosphorylation are expressed as a ratio to total PARP1 and native DNA-PKcs signal, respectively. Plotted data represents the mean ± SD of 9 independent experiments (n=9); *p<0.05, **p<0.01, ***p<0.001 (Wilcoxon-Mann-Whitney test).*

In addition to basal expression levels, we assessed the effect of doxorubicin on protein expression levels but it was not found to be significant (Wilcoxon-Mann-Whitney test rank test, $p > 0.05$, data not shown). We then investigated the effect of the different inhibitors, as presented in the following sections.

2.2.2.Expression and activity profiles following RAD51 inhibition

A decrease in RAD51 expression was seen in HeLa cells upon treatment with the inhibitor B02, but no effect was observed in M059 cells (figure 59 and figure 60A). No significant variation was found in PARP1 expression, though it seemed to decrease in M059K. However, an increase in PARP cleavage was seen in HeLa and M059K exposed to B02 either alone or with doxorubicin (figure 59 and figure 60B); on the opposite, no clear effect was seen in M059J regarding PARP cleavage.

B02 decreased PARylation in HeLa and M059K when combined with doxorubicin (figure 60B), which reveals a reduction in PARP1 activity. Little effect was seen in M059J.

RAD51 inhibition decreased DNA-PKcs expression, but this impact was significant in M059K cells only (figure 59 and figure 60C). In addition, this inhibitor caused a sharp increase in DNA-PKcs S2056 phosphorylation. In HeLa, this effect was not dependent on a combined exposure to doxorubicin, but it was in M059K.

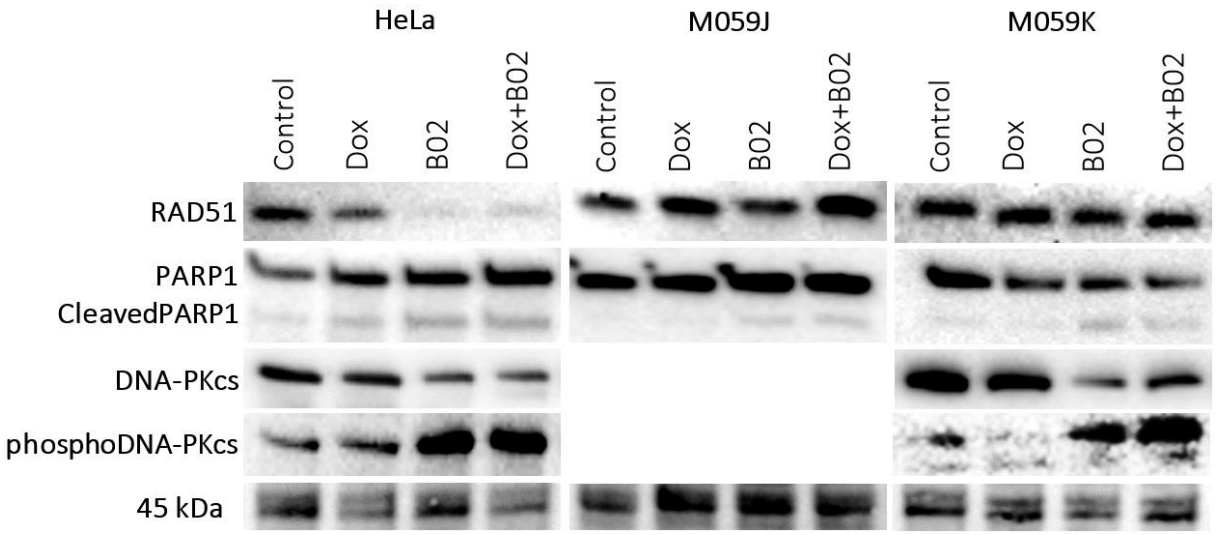

Figure 59. RAD51, PARP1, DNA-PKcs and phosphoS2056-DNA-PKcs detected by Western blotting in HeLa, M059J and M059K cells treated with Dox and/or B02.
The intensity of each band was adjusted to the total protein content of the lane; the bands observed at 45 kDa represent a subset of total protein content.

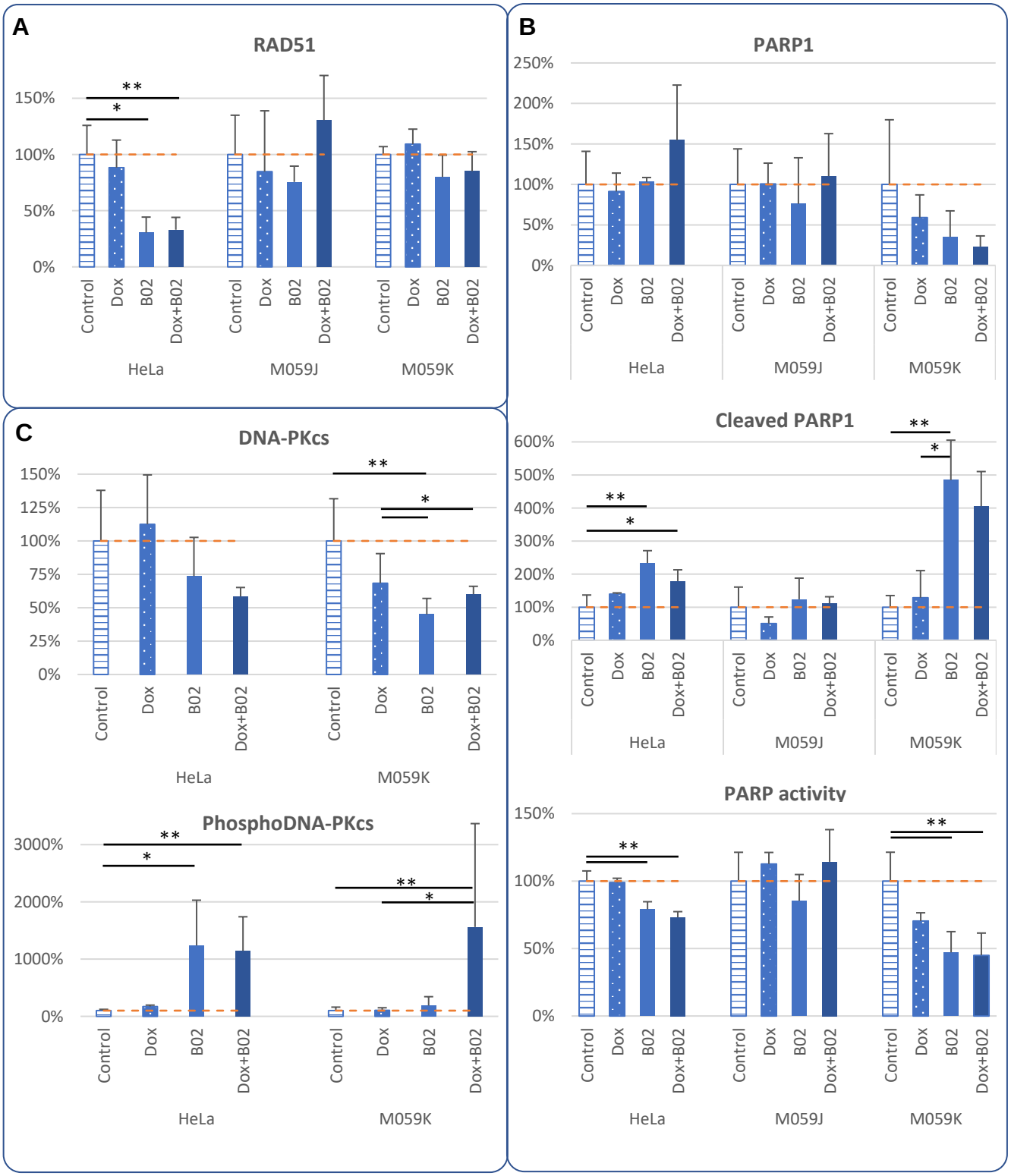

Figure 60. Expression and activity of RAD51, PARP1 and DNA-PKcs following B02-dependent RAD51 inhibition (IC_{50}), combined or not with Dox (IC_{10}).

A. *RAD51 expression measured by Western blotting.* ***B.*** *PARP1 expression and cleavage quantified by Western blotting and PARylation activity measured by the chemiluminescent PARP assay. PARP cleavage was quantified as a ratio to total PARP levels.* ***C.*** *DNA-PKcs expression and proportion of S2056 phosphorylation measured by Western blotting; phosphorylation was calculated as a ratio to total DNA-PKcs. Expression measurements were first normalized to total protein signal in each well; data is presented as a ratio to the control condition (DMSO only). Three independent experiments were performed (n=3). * $p<\alpha/2$, ** $p<0.01$ (non-parametric Dunn test). Error bars: standard deviation.*

1.1.1. Expression and activity profiles following DNA-PKcs inhibition

NU7026 caused a sharp increase in RAD51 levels in HeLa cells treated with doxorubicin; no conclusion was drawn from M059J and K (figure 61 and figure 62A). Just as for RAD51 inhibition, no particular effect was found in PARP1 expression following DNA-PKcs inhibition (figure 61 and figure 62B). However, NU7026 increased PARP1 cleavage in HeLa cells; this effect was not observed in the glioblastoma cells.

The inhibitor also reduced PARP activity by 20% and 50% in HeLa and M059K, respectively, but no significant observation was made in M059J.

DNA-PKcs expression was significantly lowered by the inhibitor in HeLa, especially in Dox-treated cells; it had no effect in M059K (figure 61 and figure 62C). Strikingly, Ser2056 phosphorylation soared in both cell lines following DNA-PKcs inhibition combined to the genotoxic treatment.

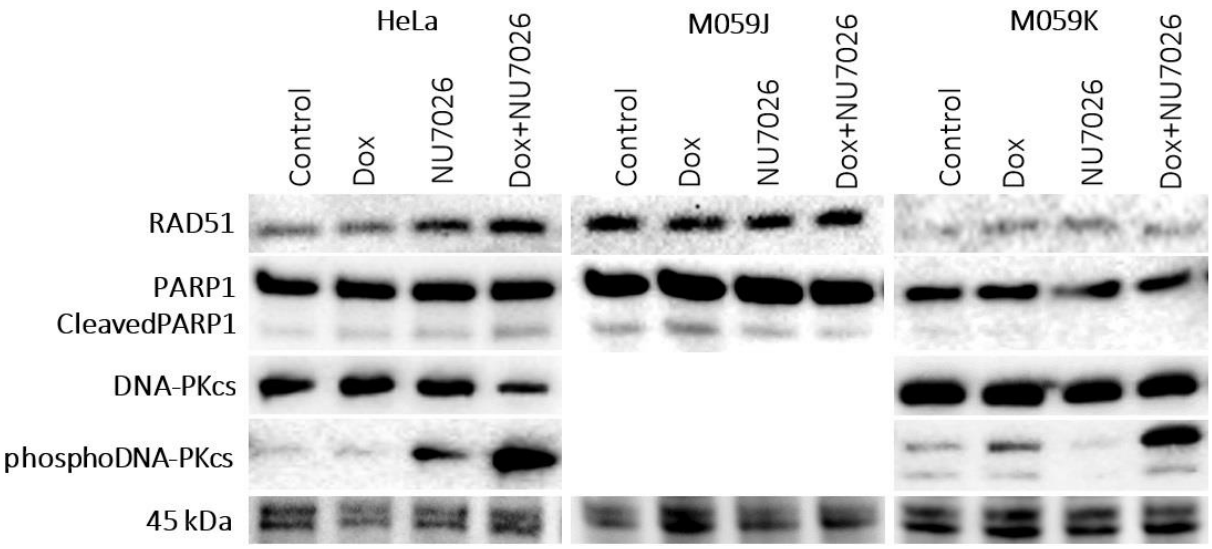

Figure 61. RAD51, PARP1, DNA-PKcs and phosphoS2056-DNA-PKcs detected by Western blotting in HeLa, M059J and M059K cells treated with Dox and/or NU7026.
The intensity of each band was adjusted to the total protein content of the lane; the bands observed at 45 kDa represent a subset of total protein content.

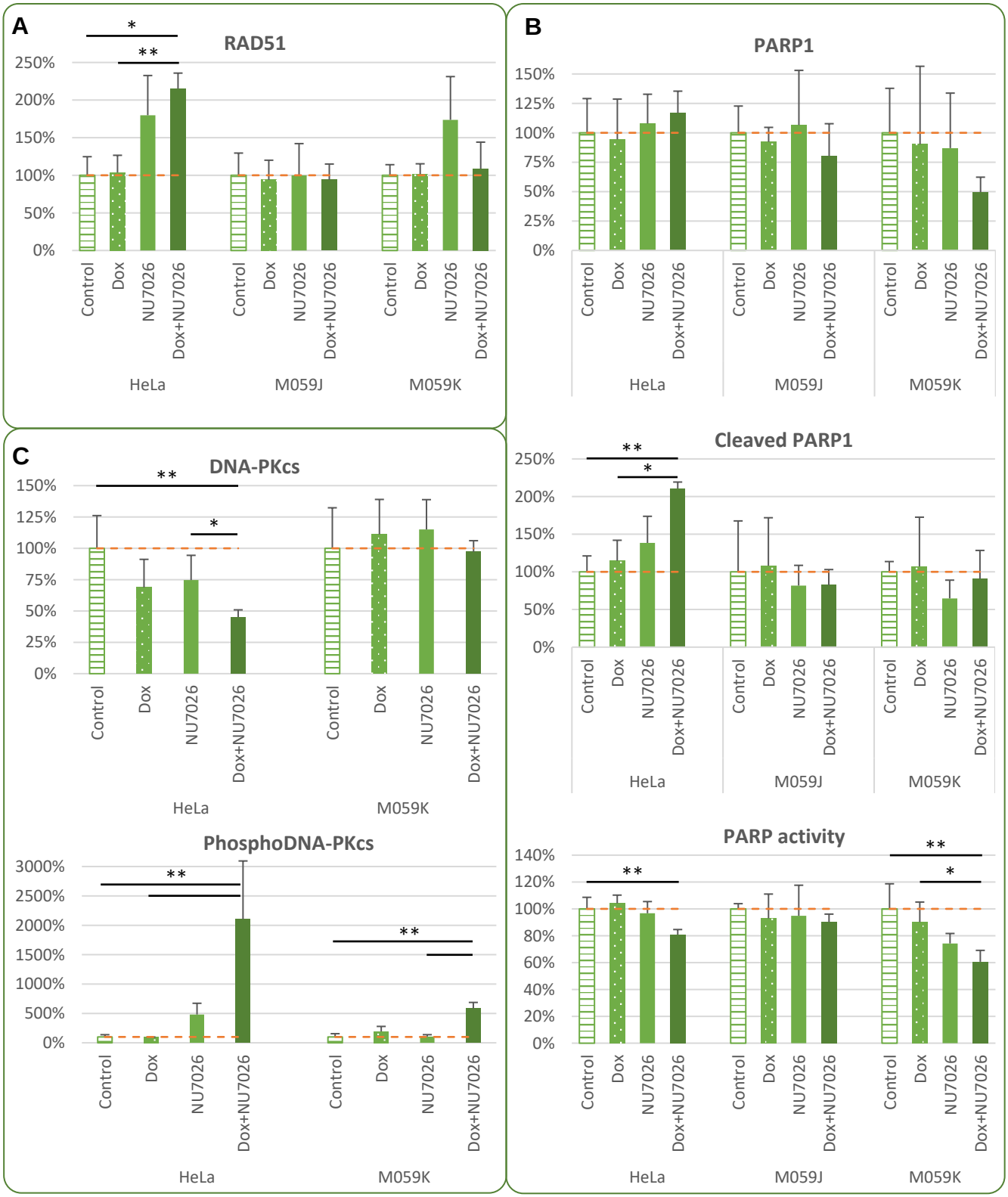

Figure 62. Expression and activity of RAD51, PARP1 and DNA-PKcs following NU7026-dependent DNA-PKcs inhibition (IC_{50}), combined or not with Dox (IC_{10}).

A. *RAD51 expression measured by Western blotting.* ***B.*** *PARP1 expression and cleavage quantified by Western blotting and PARylation activity. PARP cleavage was quantified as a ratio to total PARP levels.* ***C.*** *DNA-PKcs expression and proportion of S2056 phosphorylation measured by Western blotting; phosphorylation was calculated as a ratio to total DNA-PKcs. Expression measurements were first normalized to total protein signal in each well; data is presented as a ratio to the control condition (DMSO only). Three independent experiments were performed (n=3). * $p<\alpha/2$, ** $p<0.01$ (non-parametric Dunn test). Error bars: standard deviation.*

2.2.3.Expression and activity profiles following PARP inhibition

Upon treatment with olaparib, RAD51 levels increased in M059J and K, but not HeLa (figure 63 and figure 64A). No significant variation was found in PARP expression (figure 63 and figure 64B), but its cleavage increased in all cell lines. PARP activity was lowered with olaparib combined with doxorubicin (HeLa) or whenever olaparib was present (M059J and K).

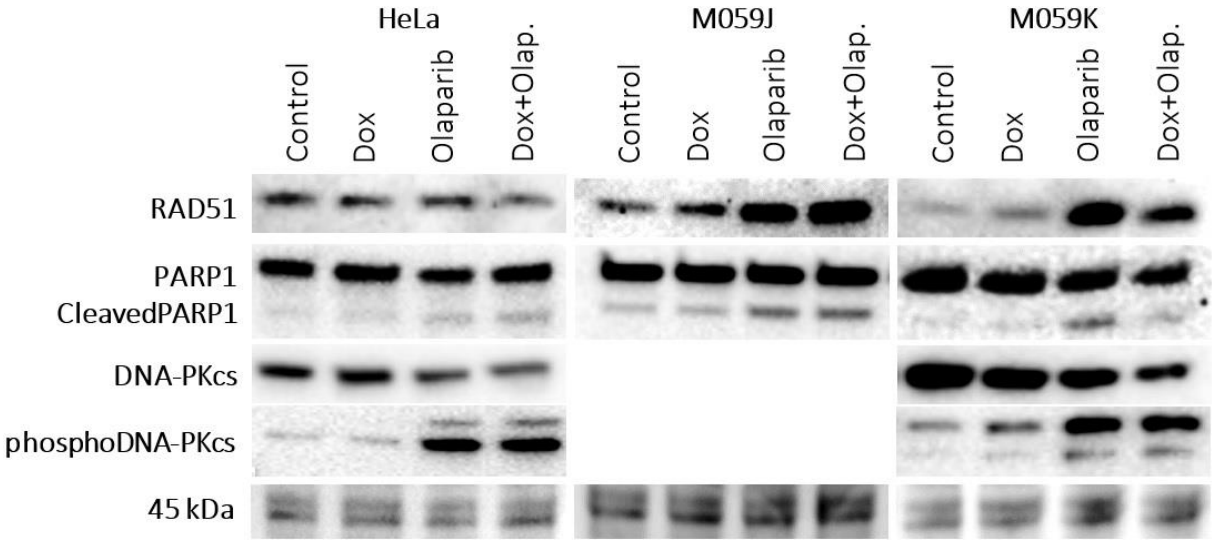

Figure 63. RAD51, PARP1, DNA-PKcs and phosphoS2056-DNA-PKcs detected by Western blotting in HeLa, M059J and M059K cells treated with Dox and/or olaparib.
The intensity of each band was adjusted to the total protein content of the lane; the bands observed at 45 kDa represent a subset of total protein content.

DNA-PKcs expression was only affected in M059K cells, with a clear decrease after olaparib treatment (figure 63 and figure 64C). For its part, S2056 phosphorylation was found significantly higher in HeLa and M059K in the presence of the PARP inhibitor.

The global increase in PARP1 cleavage and Ser2056 DNA-PKcs phosphorylation in the presence of repair inhibitors suggests an important cellular stress and the initiation of a cellular response, as discussed in the next chapter.

In order to gain insight into the response of the cellular models to the different compounds, we then characterized repair activities related to BER and NER.

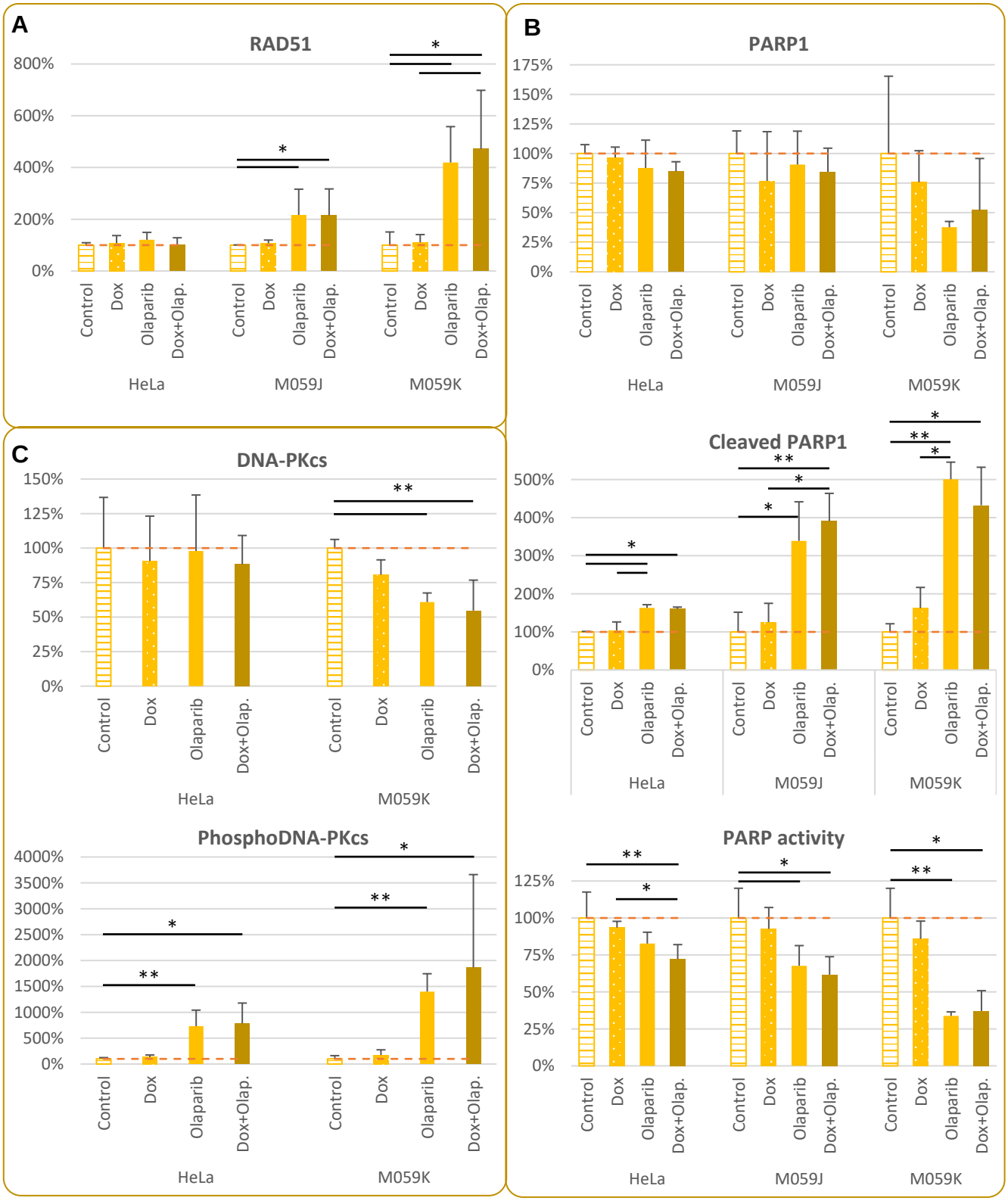

Figure 64. Expression and activity of RAD51, PARP1 and DNA-PKcs following olaparib-dependent PARP inhibition (IC_{50}), combined or not with Dox (IC_{10}).

A. *RAD51 expression measured by Western blotting.* ***B.*** *PARP1 expression and cleavage quantified by Western blotting and PARylation activity. PARP cleavage was quantified as a ratio to total PARP levels.* ***C.*** *DNA-PKcs expression and proportion of S2056 phosphorylation measured by Western blotting; phosphorylation was calculated as a ratio to total DNA-PKcs. Expression measurements were first normalized to total protein signal in each well; data is presented as a ratio to the control condition (DMSO only). Three independent experiments were performed (n=3). * p<α/2, ** p<0.01 (non-parametric Dunn test). Error bars: standard deviation.*

2.3. Excision/resynthesis activity in the cellular models

2.3.1. Basal repair activity

Base or nucleotide excision repair-related activities were investigated using the ExSy-SPOT biochip assay, which measures DNA resynthesis in the final steps of these biological processes (see "Materials and methods"). We found different levels of BER and NER activities in the cellular models, with higher repair intensities in M059K cells compared to M059J and HeLa (figure 65).

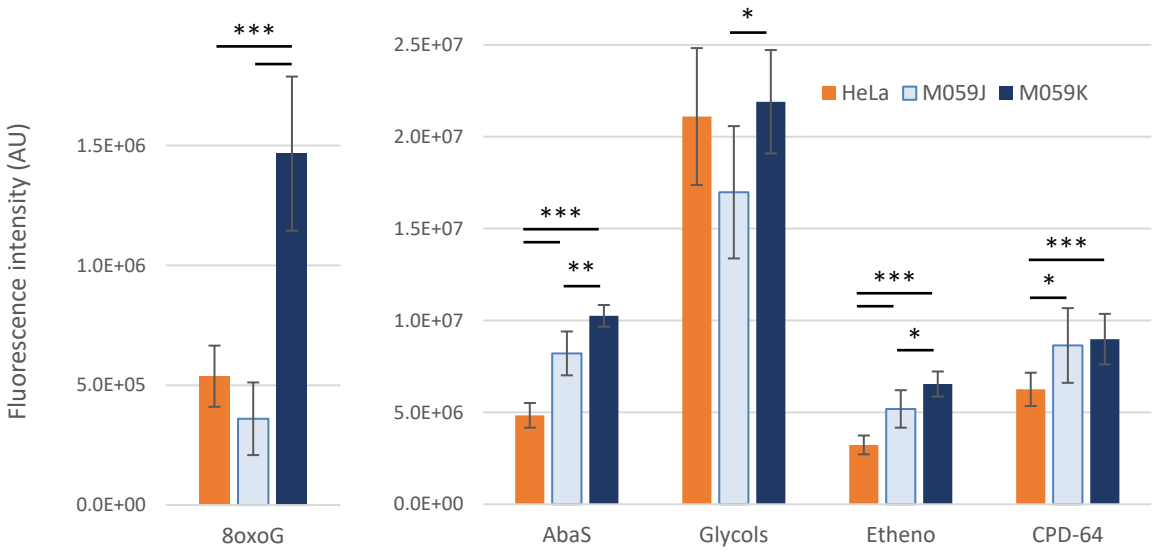

Figure 65. Basal repair activities of the different lesions studied by the ExSy-SPOT assay in nuclear extracts from control HeLa, M059J and M059K cells.

*High fluorescence intensity underscores an elevated repair activity; plotted data represents the mean ± SD of 9 independent experiments (n=9); * p<0.05, ** p<0.01, *** p<0.001 (Wilcoxon-Mann-Whitney test).*

2.3.2. Impact of doxorubicin

When gathering data from all batches of Dox-treated cells, we observed a small stimulating effect in M059J, although it did not reach significance in data from individual sets of experiments (see section 2.3.3). No significant effect was found in M059K or HeLa (figure 66). Repair activities on the plasmid containing CisP lesions were not impacted but doxorubicin (appendix 9).

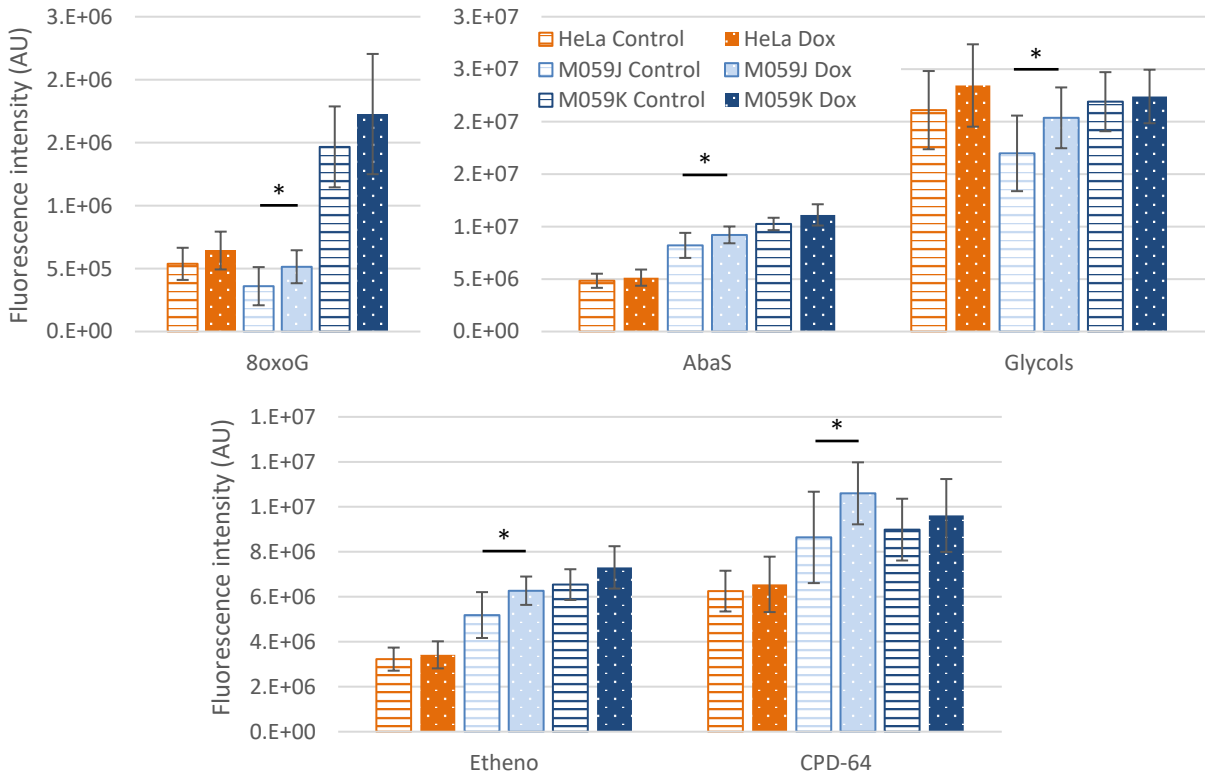

Figure 66. Effect of doxorubicin on BER and NER activities assessed by the ExSy-SPOT assay in biochip.
*Mean ± SD of 9 independent experiments (n=9); * p<0.05 (Wilcoxon-Mann-Whitney test).*

2.3.3.Response to repair inhibitors

Interestingly, we observed significant effects of the DSB repair inhibitors on BER and NER activities measured by the ExSy-SPOT assay. In HeLa cells, B02 induced a decrease in the repair of abasic sites, thymine and cytosine diols, ethenobases and photoproducts (CPDs and (6-4) PPs) whenever the inhibitor was present (figure 67 and figure 68A). No particular effect of doxorubicin was seen.

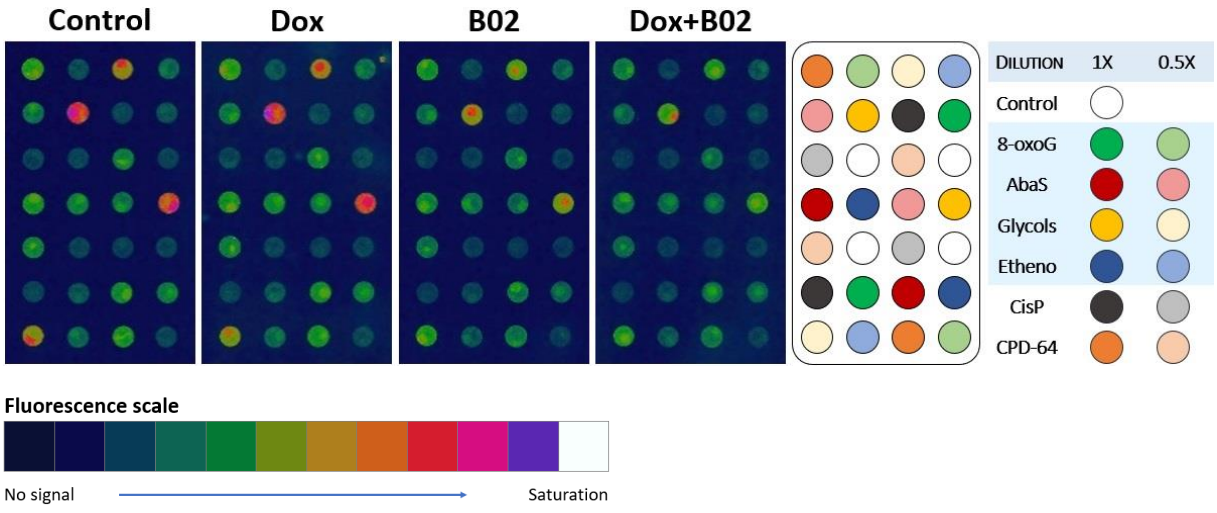

Figure 67. Images of the ExSy-SPOT biochip obtained with nuclear extracts from HeLa cells treated with doxorubicin and/or RAD51 inhibitor B02.

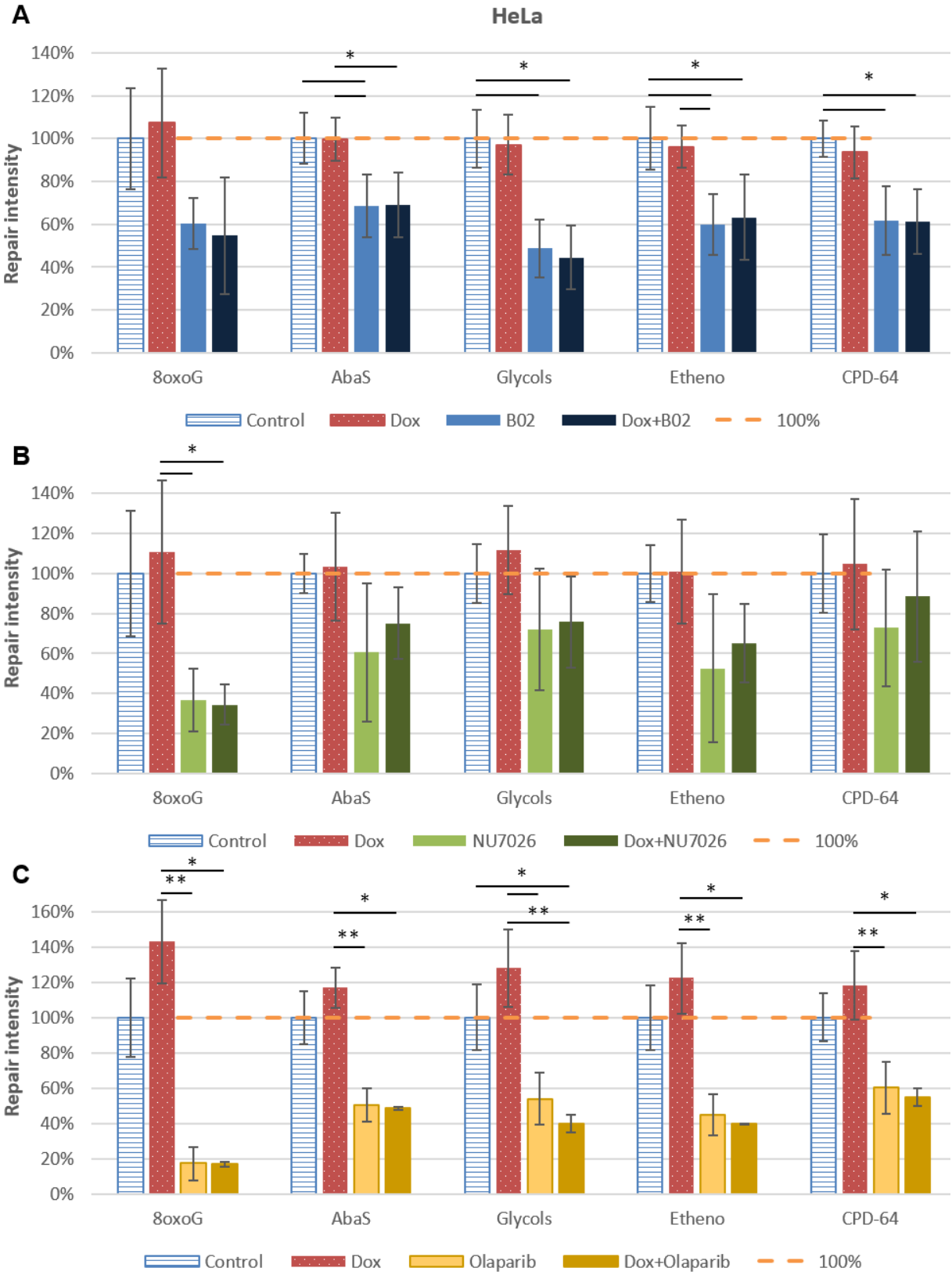

Figure 68. Impact of the treatments on excision/resynthesis activities measured by the ExSy-SPOT assay in nuclear extracts from HeLa cells.

*A. Repair activities after exposure to RAD51 inhibitor B02 B. Repair activities after exposure to DNA-PKcs inhibitor NU7026 C. Repair activities after exposure to PARP inhibitor olaparib. Data is presented as a ratio to the control condition. Three independent experiments were performed (n=3); * p<α/2, ** p<0.01 (non-parametric Dunn test). Error bars: standard deviation.*

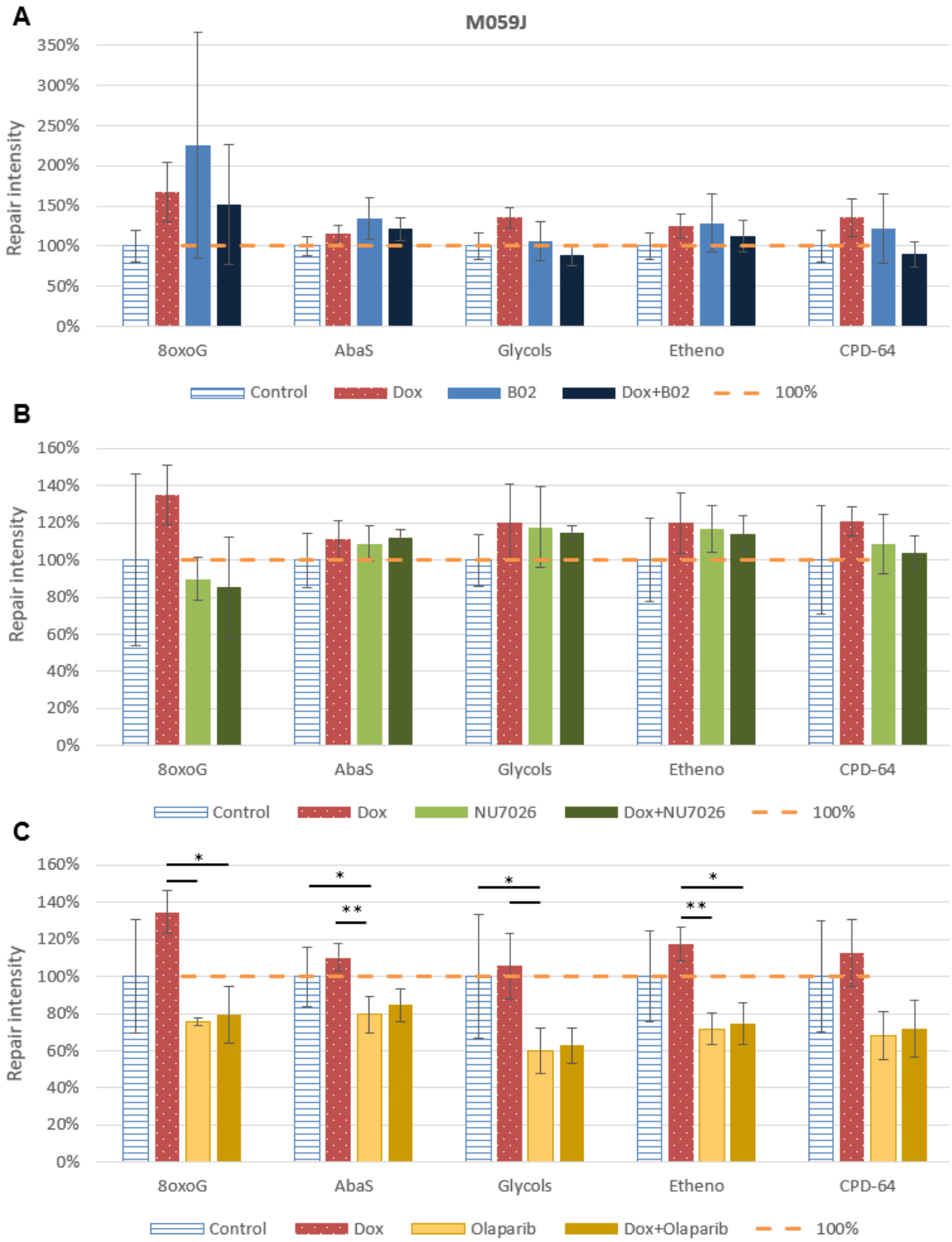

Figure 69. Impact of the treatments on excision/resynthesis activities measured by the ExSy-SPOT assay in nuclear extracts from M059J cells.

A. *Repair activities after exposure to RAD51 inhibitor B02* ***B.*** *Repair activities after exposure to DNA-PKcs inhibitor NU7026* ***C.*** *Repair activities after exposure to PARP inhibitor olaparib. Three independent experiments were performed (n=3); * p<α/2, ** p<0.01 (non-parametric Dunn test). Error bars: standard deviation.*

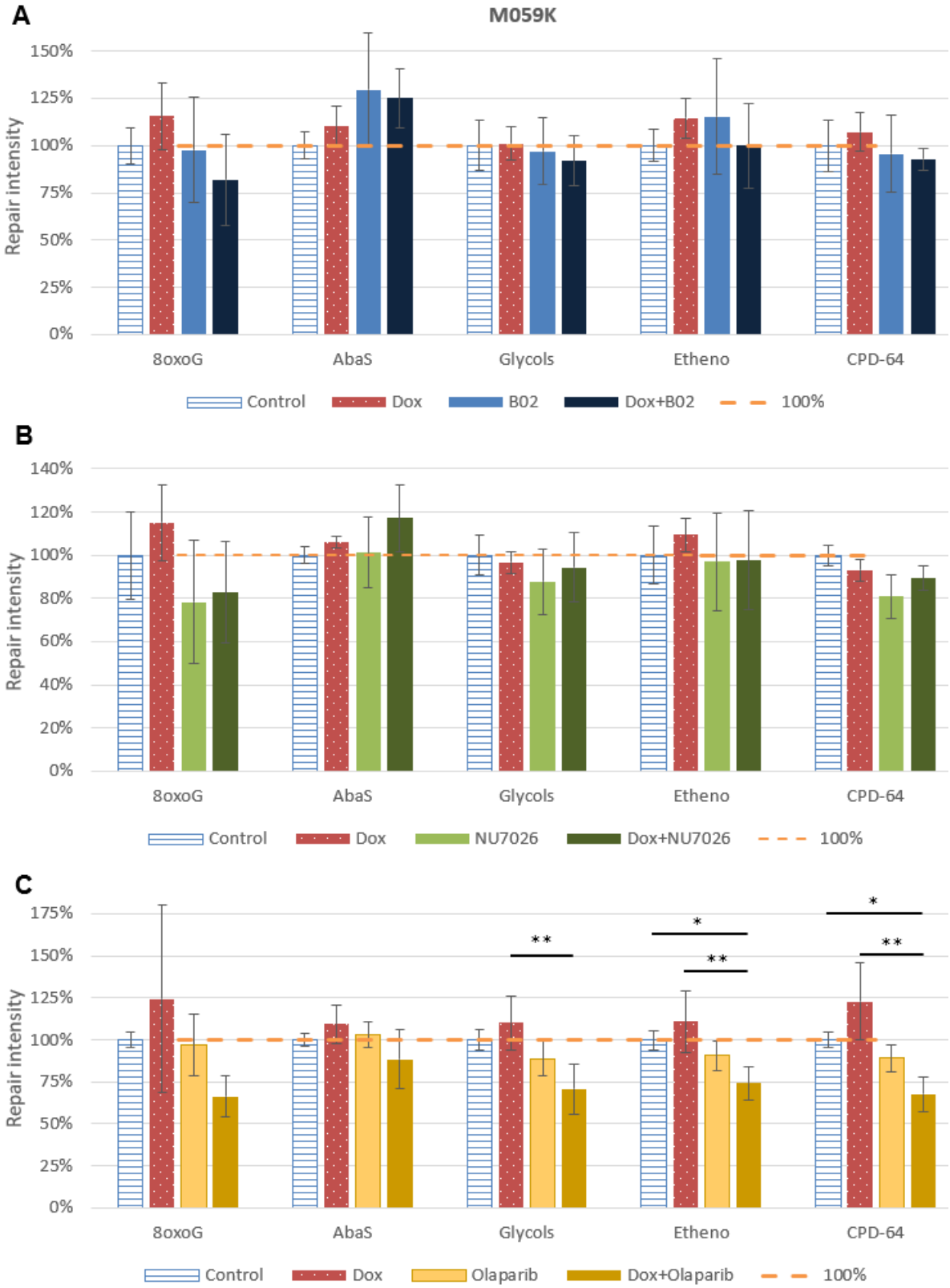

Figure 70. Impact of the treatments on excision/resynthesis activities measured by the ExSy-SPOT assay in nuclear extracts from M059K cells.

A. *Repair activities after exposure to RAD51 inhibitor B02* ***B.*** *Repair activities after exposure to DNA-PKcs inhibitor NU7026* ***C.*** *Repair activities after exposure to PARP inhibitor olaparib. Three independent experiments were performed (n=3); * p<α/2, ** p<0.01 (non-parametric Dunn test). Error bars: standard deviation.*

The same trend was seen for NU7026, though it was only significant for the repair of 8-oxoguanine lesions (figure 68B); experimental variability was often high in cells treated with NU7026 preventing conclusions to be drawn. Finally, olaparib produced the strongest effect, with a strong inhibition of repair activities observed for all cited lesions (figure 68C). Interestingly, this inhibition was especially seen between cells treated with doxorubicin only and cells treated with doxorubicin and olaparib. Except for the repair of glycols, no significant effect was seen between the control and olaparib-treated cells. Hence, olaparib induced a sharp decrease in excision/resynthesis activities associated with BER and NER in the presence of doxorubicin.

The glioblastoma models were less impacted by repair inhibitors than HeLa (figure 69 and figure 70). No effect was seen in M059J cells exposed to B02 and NU7026 (figure 69A and B) but olaparib impacted repair activities (figure 69C), except for the repair of pyrimidine dimers where the decrease was not significant. The effect of doxorubicin in addition to olaparib was not as clear as in HeLa cells; for instance, no significant inhibition appeared between doxorubicin only and dox+olaparib extracts for the repair of AbaS and glycols. Just as for HeLa cells, no significant response was observed for doxorubicin alone compared to the control.

B02 and NU7026 had no clear effect in M059K (figure 70A and B). Once more, olaparib induced a different response, with a clear reduction in the glycols, ethenobases and CPD repair activities (figure 70C). This effect was always dependent upon the presence of doxorubicin, suggesting that the activation of the DDR is a perquisite for the PARP inhibitor to exert its effect.

A significant alteration in the repair of CisP lesions was seen in M059K only, in which RAD51 and PARP inhibition led to a significant decrease in repair activity when combined to doxorubicin (appendix 9). No effect was seen in HeLa and M059J (data not shown).

Figure 71 summarizes the effects of the repair inhibitors across cell lines. A similar clustering was performed using correlation dissimilarity measure, but it did not identify significant groups (not shown). The glioblastoma models are grouped within a significantly isolated cluster (approximately unbiased p-value > 0.95, see appendix 10), while high inhibitory effects of the inhibitors are seen in HeLa cells.

Treatments tend to group together across cell lines: the inhibitory effect of olaparib (alone or combined with doxorubicin) is significantly within a cluster (figure 71 group 1, see also appendix 10). Other trends are seen, including the regrouping of doxorubicin treatments across the different lesions (group 2). Group 3 includes all other treatments, but it can be noted that compounds tend to regroup across lesions (see the regrouping of olaparib treatments, for instance). Overall, it can be pointed that treatments with repair inhibitors alone tend to be grouped close to the treatments with a combination

of inhibitor and doxorubicin, suggesting that the effects of the treatments tend to originate from the inhibitors rather than from doxorubicin.

In addition, M059K and most of all M059J display a small stimulation of repair activities in response to B02 and/or NU7026, while HeLa cells always display reduced excision/resynthesis activities.

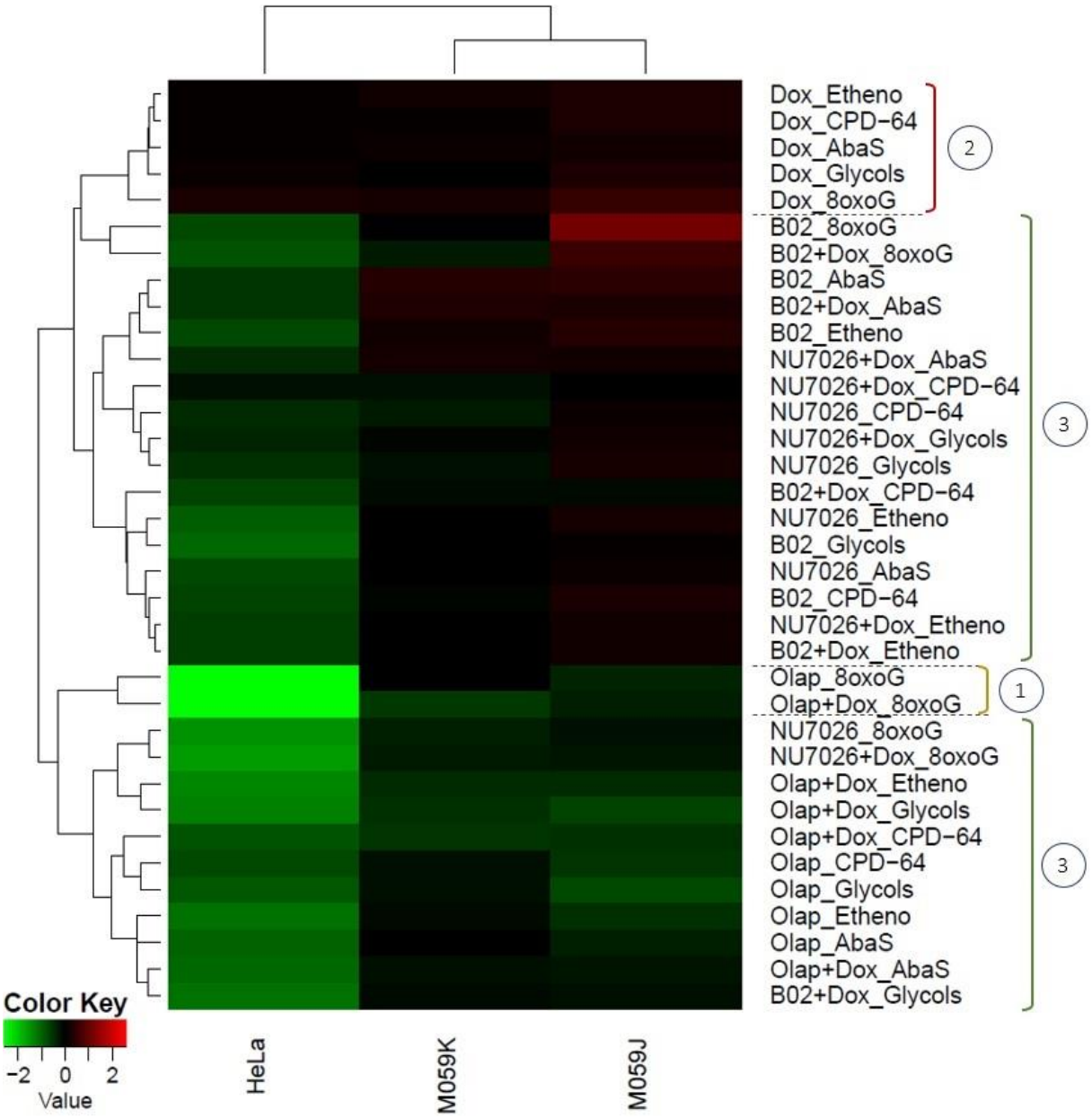

Figure 71. Analysis of the DNA repair response in the cellular models across treatments and lesions.
Heatmap based on the log2-transformed ratios of the fluorescence intensity obtained on each ExSy-SPOT condition between treated and non-treated cells (log2(T/NT)), following the suppression of the signal obtained on the control plasmid. Hierarchical clustering algorithm with Euclidean dissimilarity measure was used to group the three models. In the first dimension, cell lines were clustered by similarity of the intensity and covariation of their response profile across treatments. In the second dimension, treatments were clustered by similarity of their response across the cell lines. Positive values in the log2 scale (in red) indicate a stimulation of repair activities compared to control cells. Negative values in green indicate an inhibition. Values around zero (in black) indicate no detected effect of the treatment. Indicated groups (1-4) are detailed in text.

In conclusion, ExSy-SPOT results revealed an effect of olaparib on BER and NER. Off-target effects were hypothesized for B02 and, to a lesser extent, NU7026. We then assessed the effect of these compounds on DSBR capacity.

Box 1. Main ExSy-SPOT results:

- ✓ On average, M059K cells have higher repair activities than M059J and HeLa.
- ✓ Doxorubicin significantly stimulates excision/resynthesis in M059J cells only.
- ✓ HeLa cells are characterized by the reduction of some excision/resynthesis activities by B02 and NU7026, which is not seen in glioblastoma models.
- ✓ Olaparib reduces excision/resynthesis activities in all cell lines.

3. Measurement of DSBR activity with the reference assay

DSBR activities were first assessed by the electrophoretic method to be compared with the biochip alternative under validation. In this section, we describe the optimization process aimed at adapting the electrophoretic assay conditions to the ones set by the needs of the biochip, and we then present the main biological results obtained in the cells treated with doxorubicin and the inhibitors.

3.1. Assay optimization

As presented in the materials and methods, adjustments were made to the original protocol in order to maximize the comparability with the biochip assay, to increase the signal of interest and reduce experimental variability. Adjusted parameters are indicated in **bold**.

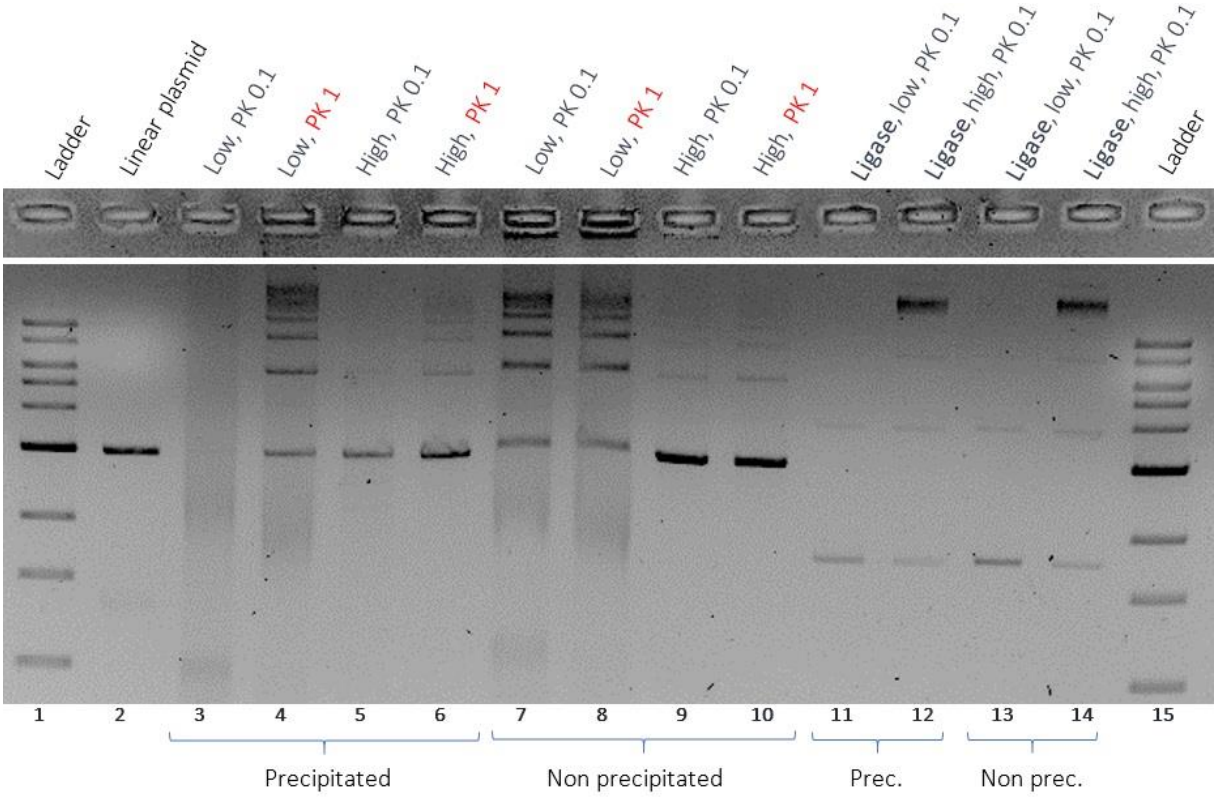

Figure 72. Effect of precipitation, plasmid concentration and proteinase K treatment on ligation efficiency.
Linear pBlueScript plasmid was diluted to final concentration of 2.5 (low) or 25 ng/µl (high) and exposed to 0.3 mg/ml HeLa nuclear extracts for 60 minutes at 30°C. Control: T4 ligase. Ligation products were treated with 0.1 or 1 mg/ml proteinase K and either frozen directly or precipitated as described in the original protocol. Samples were then loaded onto an agarose gel stained with EtBr (50 ng of plasmid per well).

DNA trapping was at times observed in the wells, due to nuclear proteins and genomic DNA present in the extracts, which can prevent plasmids to correctly penetrate the agarose (figure 72, lanes 4, 7, 8). The **DNA precipitation** step from the original protocol limited this issue but it also increased experimental variability, with the risk of losing samples as seen in figure 72 (lane 3, loss of plasmid DNA resulting from incorrect recovery of the ligated products).

Hence, this step was removed in all subsequent analyses. A treatment with proteinase K was added after the end joining reaction in order to reduce DNA trapping.

Interestingly, higher ligation yields were obtained with cell extracts when lowering the **plasmid concentration**, but it was usually not the case for the ligase control. Smears appeared at low plasmid concentration and were slightly reduced when increasing **proteinase K concentration**; little effect of proteinase K concentration was seen in end-joining activities.

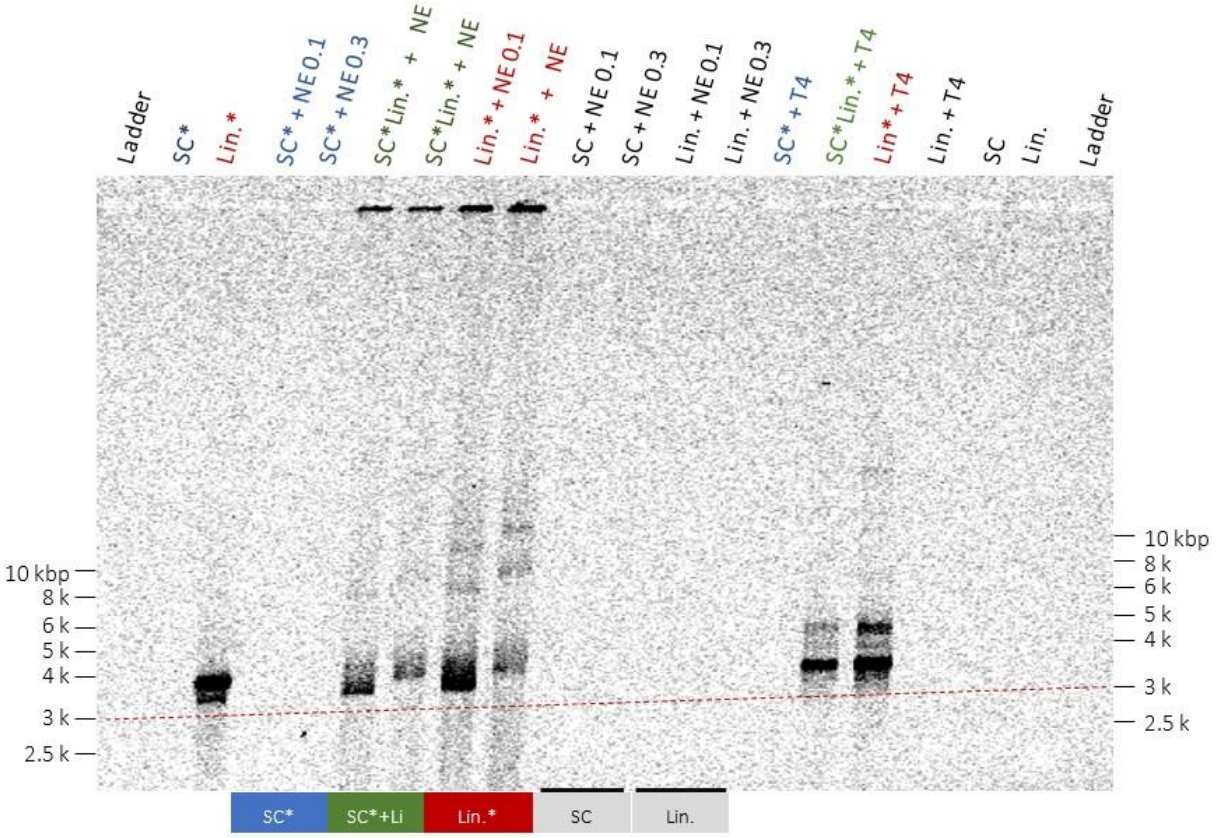

Figure 73. Cy3 readout of an electrophoretic NHEJ assay exposing a supercoiled (SC) and/or linear (Lin) pBlueScript plasmid to HeLa nuclear extracts (0.1 or 0.3 mg protein/ml).
Ligation products were not precipitated and were incubated with 0.5 mg/ml proteinase K. Asterisks indicate biotin-bound SC or cy3-labelled Lin, either alone (2x 2.5 ng/µl; blue and red, respectively) or mixed together (2.5 ng/µl each, green). Control: T4 ligase. Red line: 3 kbp marker.

Various **combinations of plasmids** and **labels** were also tested in order to select the more relevant mix to analyze with extracts from treated cells (figure 73). Though ligation bands could be specifically observed at 532 nm, it quickly appeared that their low intensity prevented a precise estimation of the compounds' biological effect in treated cells. Despite proteinase K treatment, DNA trapping still occurred in some wells.

Incubation with cy5-labelled streptavidin was expected to allow the identification of specific bands relative to the biotin-bound supercoiled plasmid, thereby providing mechanistic insights into its remodeling in the presence of nuclear proteins. However, results were mostly disappointing, since we

observed an imprecise staining of the targeted bands as well as a massive background noise in the absence of the biotin-bound plasmid (appendix 11), in areas devoid of EtBr-stained DNA (figure 74). Besides, the lanes with labelled plasmids (especially the cy3-labelled linear one) displayed lower amounts of total DNA and lower end joining activity than with the unlabeled plasmids (figure 74).

Additional experiments were not run to test other production batches of labeled plasmids; indeed, gel readouts and EtBr bath resulted in important gel manipulation, thereby increasing the risk of technical mistakes and reducing the quality of the agarose surface by the end of the experiment. It was decided to use unlabeled plasmids and to directly add EtBr in the agarose gel instead of multiplying processing steps.

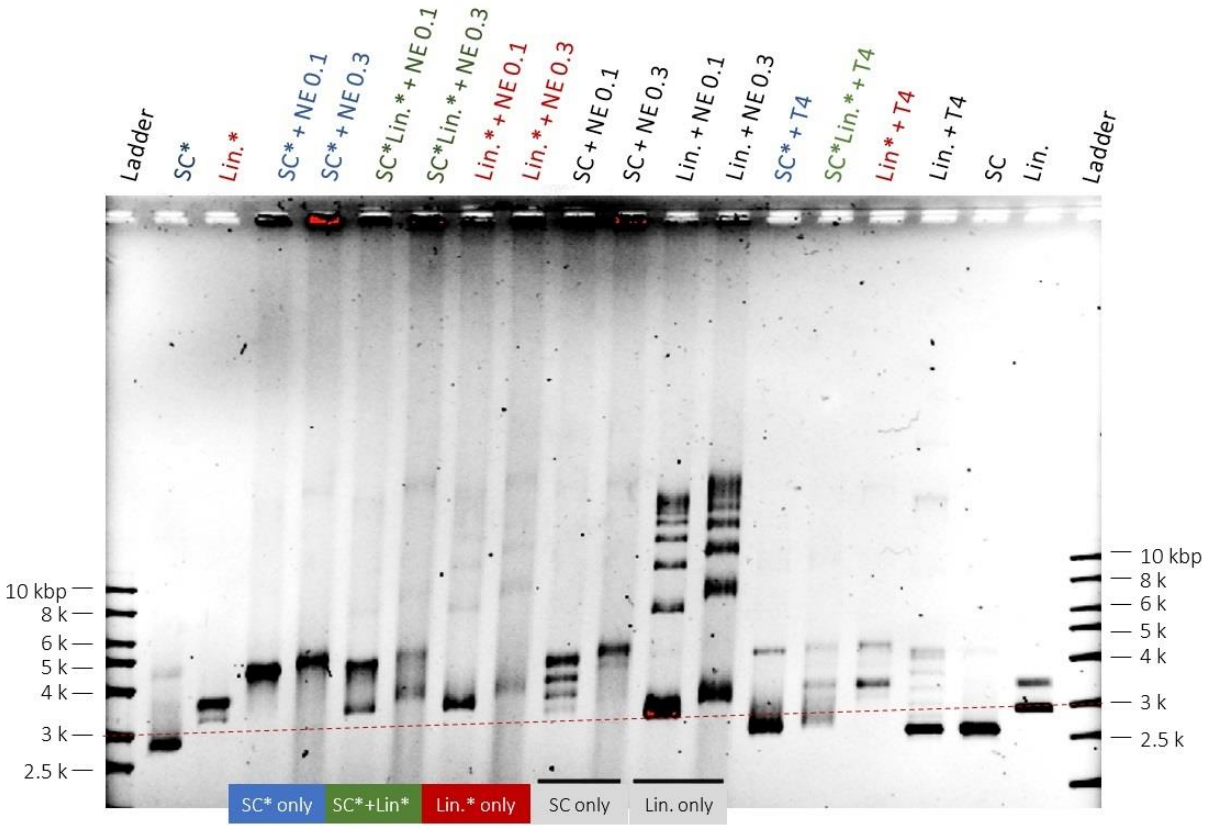

Figure 74. EtBr staining of an electrophoretic NHEJ assay exposing a supercoiled (SC) and/or linear (Lin) pBlueScript plasmid to HeLa nuclear extracts (0.1 or 0.3 mg protein/ml).
Ligation products were not precipitated and were incubated with 0.5 mg/ml proteinase K. Asterisks indicate biotin-bound SC or cy3-labelled Lin, either alone (2x 2.5 ng/µl; blue and red, respectively) or mixed together (2.5 ng/µl each, green). Control: T4 ligase. Red line: 3 kbp marker.

It is worth noting that a shift in band position is observed between the two concentrations of nuclear extracts. This observation was not systematic and it is thought to originate from an increase in DNA trapping at higher extract concentrations, thus delaying the migration of the bands.

Other changes include the modification of incubation time and temperature, as well as the composition of the reaction mix, that were set in line with the biochip method. Though it was deemed valuable for the comparison with the biochip to add both the supercoiled and the linear plasmid in the reaction mix, only limited information was extracted in the end. Hence, the last experiments were limited to the study of the ligation of the linear plasmid. In the next section, we only focus on this condition.

3.2. Characterization of c-NHEJ activity with the reference repair assay

This assay informs on the ligation activities operated by the canonical non-homologous end joining pathway (see "Materials and methods"). These activities varied among cellular models, with a lower average response in M059K extracts compared to HeLa (figure 75). Surprisingly, M059J did show a relatively high repair activity, even slightly above M059K, though not significantly.

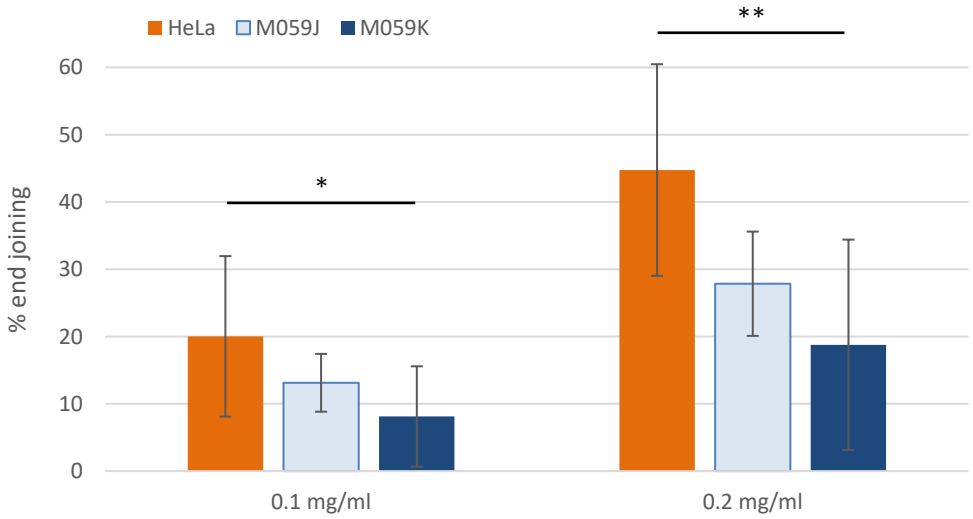

Figure 75. End joining of the linear AflIII-digested pBlueScript by nuclear extracts from control HeLa, M059J and M059K cells.

*Values correspond to the total intensity of the rejoined oligomers (mean ± SD of 9 independent experiments (n=9)); * p<0.05, ** p<0.01, (Wilcoxon-Mann-Whitney test).*

Ligation intensity increased with extract concentration in a similar fashion for all cell lines. In order to simplify data visualization, only the conditions with 0.2 mg/ml NE are represented in subsequent figures. This choice was guided by the fact that a higher concentration of nuclear extracts resulted in more intense bands for repair products, which better illustrates our data. Dose-response curves are shown in appendix 12. It is worth precising that the samples' response varied between culture batches (for instance between 5% to 38% total EJ with 0.1 mg/ml HeLa extracts). Thus, data was then normalized to the control to ease the visualization of the treatment effects. An example of gel is provided in appendix 13.

Doxorubicin treatment did not stimulate end-joining activities: no significant effect was seen in the ligation of the linear plasmid (figure 76). The trend was rather a decrease in repair activity upon treatment with doxorubicin.

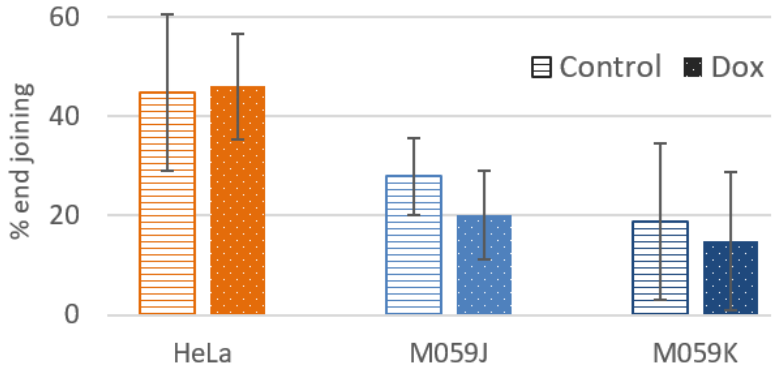

Figure 76. Mean end joining of the linear AflIII-digested pBlueScript by nuclear extracts from HeLa, M059J and M059K cells treated with doxorubicin.
Values correspond to the total intensity of the rejoined oligomers (mean ± SD of 9 independent experiments (n=9); Wilcoxon-Mann-Whitney test).

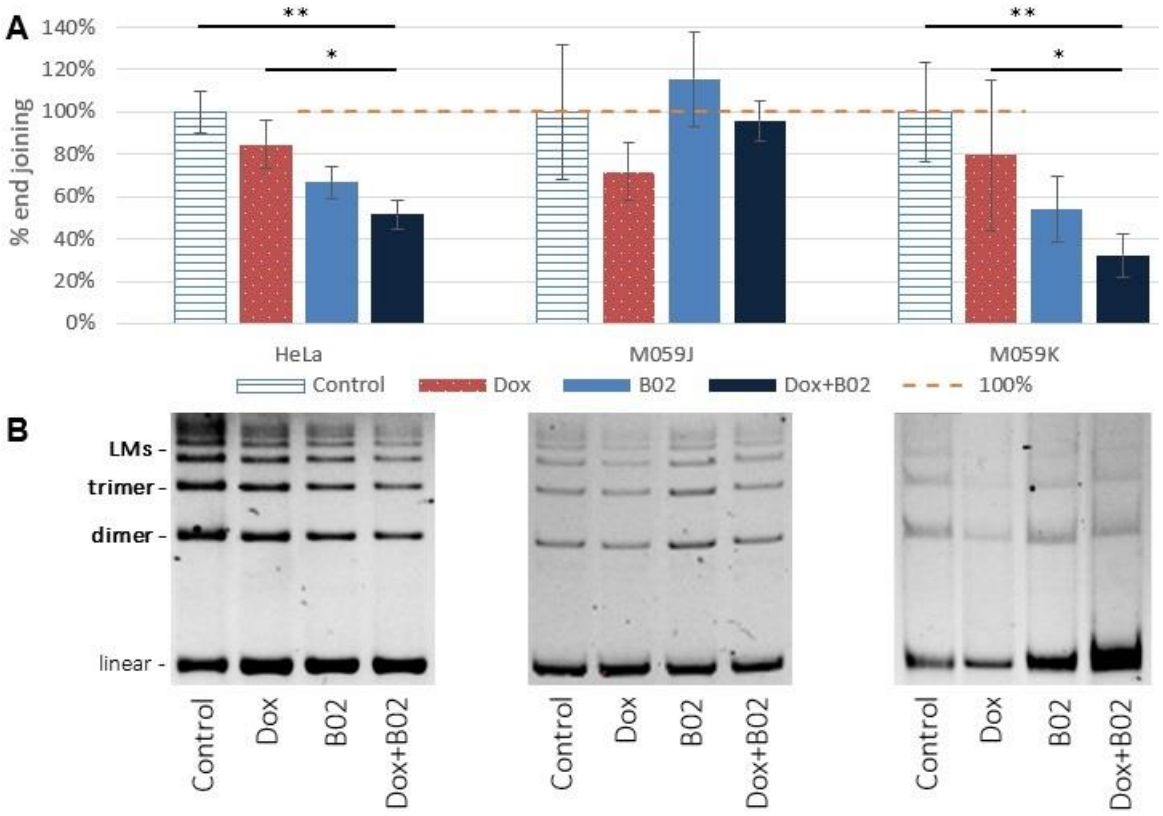

Figure 77. End joining activity in nuclear extracts from cells exposed to Dox and/or RAD51 inhibitor B02.
A. *Total end joining quantified in ligation bands (dimers, trimers, LMs), normalized to the untreated controls (mean±SD). Three independent experiments were performed (n=3); * p<α/2, ** p<0.01 (non-parametric Dunn test).*
B. *Montages of agarose gel electrophoresis results corresponding to each set of experiments. LMs: linear multimers.*

RAD51 inhibition led to a decrease in DSB end joining in HeLa and M059K cells (figure 77). This effect was significant only when doxorubicin was present. In M059J, B02 did not produce any particular effect.

Blocking DNA-PKcs with NU7026 led to a significant stimulation of DNA end joining in HeLa; surprisingly, the same effect was also seen in the deficient cell line M059J (figure 78). Remarkably, this action was suppressed when doxorubicin was combined to the inhibitor. No conclusion was drawn in M059K due to high experimental variability.

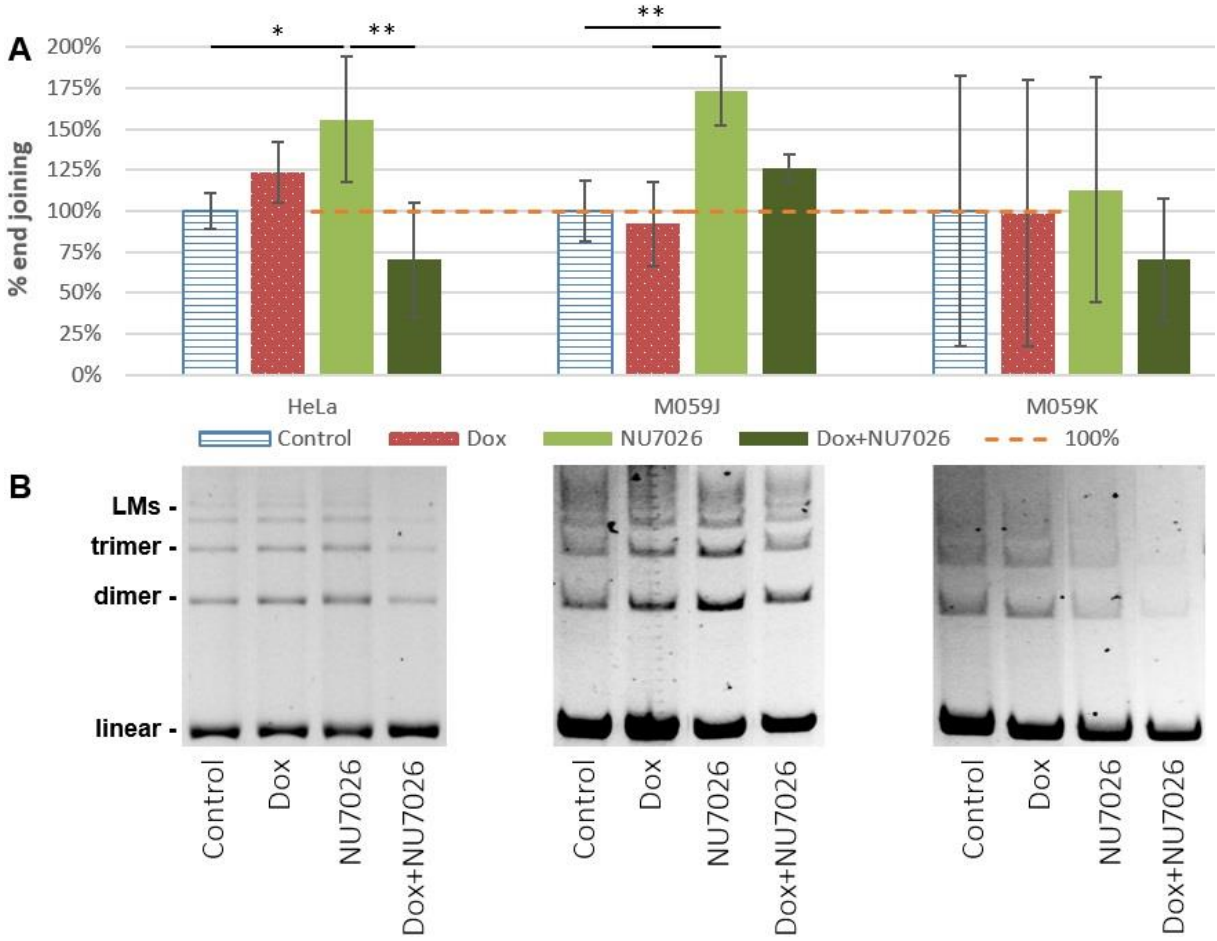

Figure 78. End joining activity in nuclear extracts from cells exposed to Dox and/or DNA-PKcs inhibitor NU7026. ***A.*** *Total end joining activity quantified in ligation bands, normalized to the untreated controls (mean±SD). Three independent experiments were performed (n=3); * p<α/2, ** p<0.01 (non-parametric Dunn test).* ***B.*** *Montages of agarose gel electrophoresis results corresponding to each set of experiments. LMs: linear multimers.*

Finally, olaparib significantly reduced end joining in M059K only, in which this impact did not depend on the combined addition of doxorubicin (figure 79).

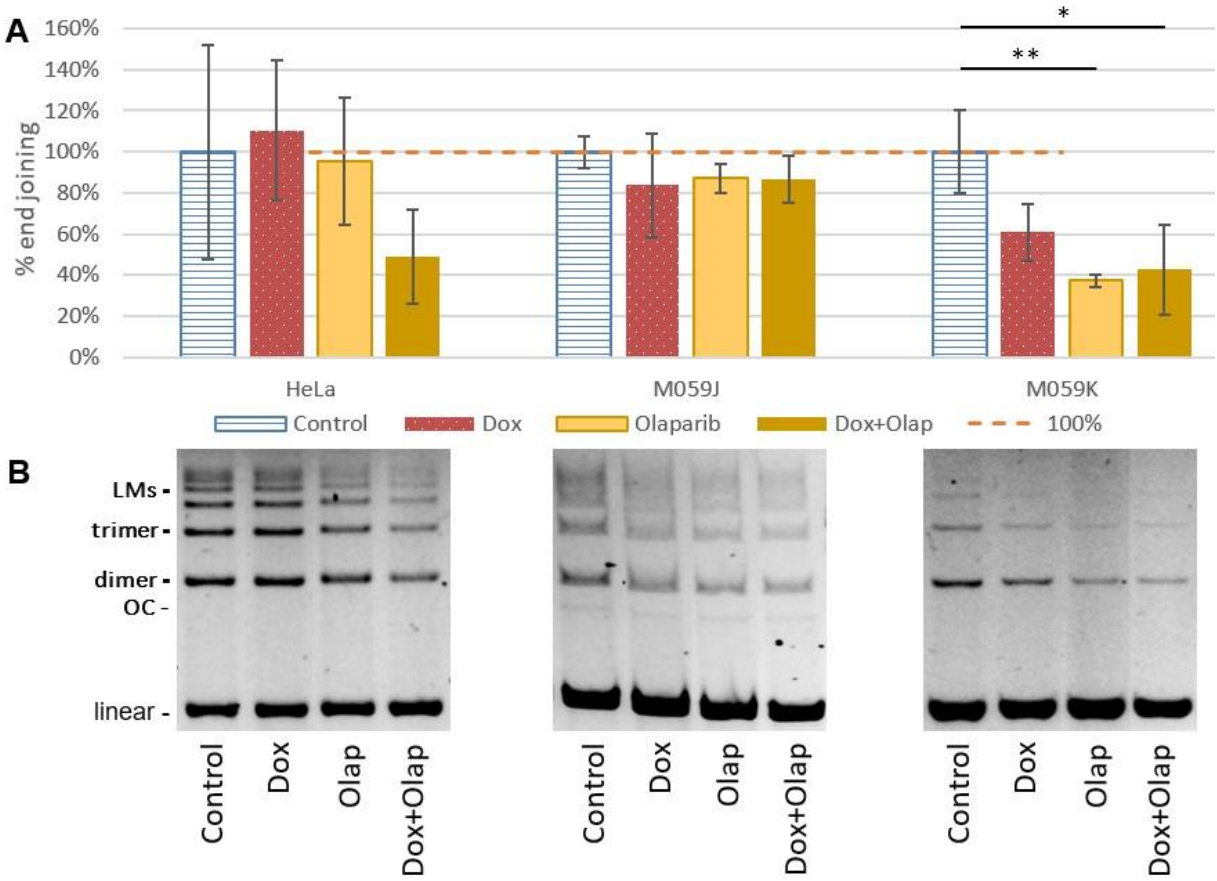

Figure 79. End joining activity in nuclear extracts from cells exposed to Dox and/or PARP inhibitor olaparib. ***A.*** *Total end joining activity quantified in ligation bands, normalized to the untreated controls (mean±SD). Three independent experiments were performed (n=3); * p<α/2, ** p<0.01 (non-parametric Dunn test).* ***B.*** *Montages of agarose gel electrophoresis results corresponding to each set of experiments. LMs: linear multimers; OC: open circular.*

3.3. Comparison of repair activities in the glioblastoma cell lines

In order to better visualize the relative effect of the treatments in M059K and in the mutated cell line M059J, we calculated the ratio between end-joining activities in both cell lines (figure 80).

Regardless of extract concentration, the mutated cell line M059J showed 1.5 to 9-fold higher end-joining activities than M059K, showing very clearly that it is fully proficient to achieve the late ligation steps of NHEJ. This point will be further discussed in the next chapter.

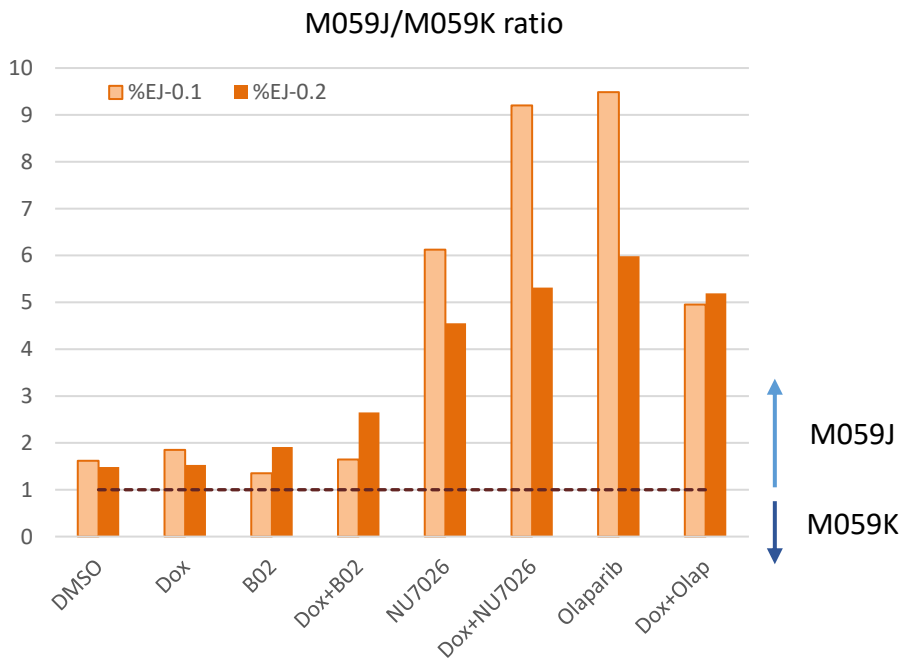

Figure 80. Ratio between end joining activities in M059J and M059K measured by the electrophoretic NHEJ assay.
Mean of at least 3 independent experiments, with 0.1 or 0.2 mg/ml nuclear extracts. Values above 1 indicate a higher activity in M059J compared to M059K.

These results were then used as a reference for the comparison with Next-SPOT assay on biochip, described in the next section.

Box 2. Main results obtained with the reference DSBR assay:

- ✓ NHEJ activities are higher in HeLa than in M059K. M059J cells operate DSB religation to equivalent rates as M059K.
- ✓ Repair activities are positively correlated with the concentration of nuclear protein extracts.
- ✓ Doxorubicin alone does not modify religation activities.
- ✓ All inhibitors have an effect on DSB religation, but they do not impact all cell lines.
- ✓ The effect of repair inhibitors is modulated by doxorubicin.

4. Measurement of DSBR on biochip with Next-SPOT assay

4.1. Assay optimization

A large panel of modifications were made on the biochip DSBR assay during the course of this project in order to stabilize signal before running biological validations. Issues were faced with the initial protocol based on polyacrylamide slides, including non-reproducible response and background issues; more robust results were obtained with a different supplier (SCHOTT Nexterion AG, Germany). Additional information is given in appendix 14.

A direct protocol was set up by LXRepair in the last year of the project, based on labelled dNTPs instead of biotin-bound dCTP that need to be revealed by an incubation with cy5-streptavidin. Though this optimization further simplified the assay, it was observed that atmospheric ozone levels could strongly reduce cyanine fluorescence, especially on cy5-labelled dCTPs (figure 81). Hence, the indirect protocol using streptavidin-bound dCTPs was chosen for all of the experiments presented in the following sections. Ozone levels were cautiously traced and no experiment was run above 30 µg/m^3 (0.015 pmm).

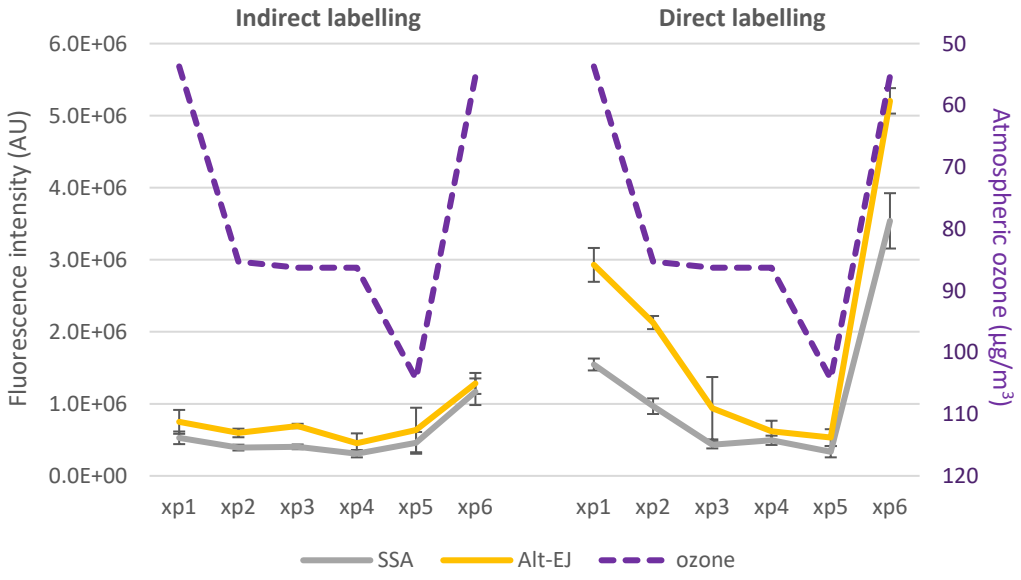

Figure 81. Impact of ozone levels on cy5 fluorescence at 635 nm (alternative pathways), using biotin-dCTPs (indirect labelling) or cy5-dCTPs. Atmospheric ozone levels are represented in inversed scale to ease visualization.

4.2. Biological results following cellular treatments

4.2.1.Comparison of basal repair activities

Just as for the electrophoretic method, fluorescence intensity increased with the concentration of nuclear extracts (figure 82). HR and c-NHEJ showed the same difference in basal repair activities as observed for c-NHEJ using the electrophoretic assay: HeLa cells displayed higher repair activities than the glioblastoma models. Cy5 readout at 635 nm produced a much lower signal (notice the difference in scale) and a different pattern was found in M059K, which produced a higher SSA response than HeLa cells.

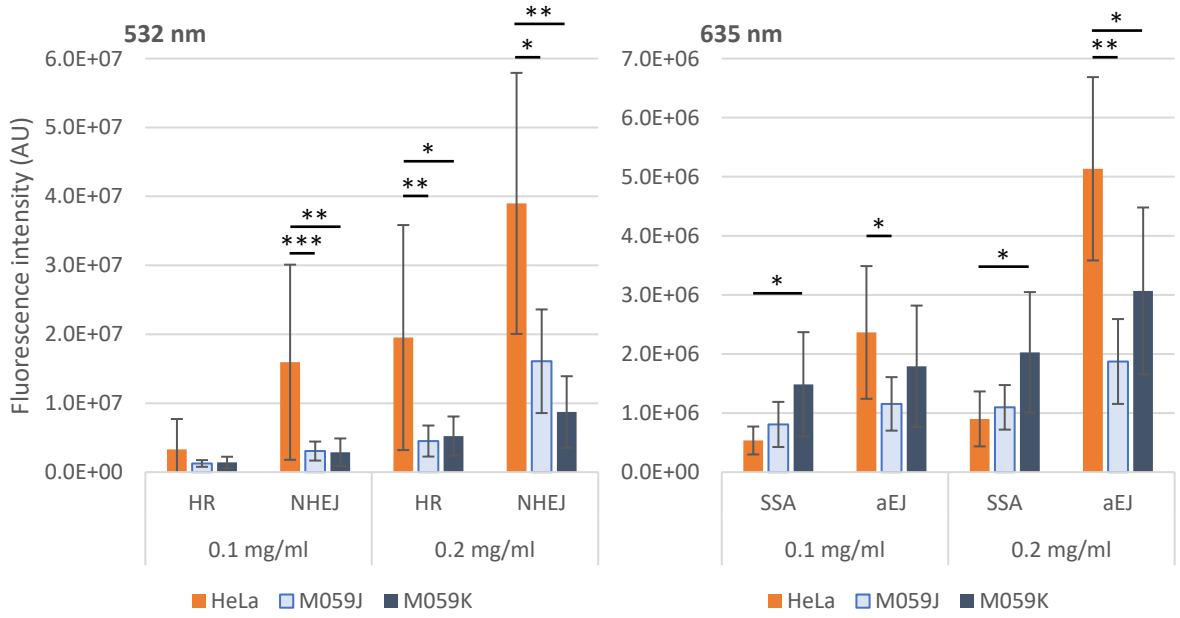

Figure 82. Basal repair activities measured by the next-SPOT assay in control HeLa, M059J and M059K cells. Nuclear extracts were added at 0.1 and 0.2 mg/ml.

*Fluorescence of the cy3 (HR, NHEJ) and cy5 (SSA, aEJ) was acquired at 532 nm and 635 nm, respectively. The reader's attention is drawn to the difference in numeric scale between both graphs. High fluorescence intensity underscores an elevated repair activity; plotted data represents the mean ± SD of 9 independent experiments (n=9); * p<0.05, ** p<0.01, *** p<0.001 (Wilcoxon-Mann-Whitney test).*

4.2.2.Effect of doxorubicin

Next-SPOT results did not show a significant impact of doxorubicin on the cellular response, as presented with 0.2 mg/ml NE in figure 83. Similar results were obtained at 0.1 mg/ml (data not shown). As for the electrophoretic method, variability was observed depending on the treatment batch, as seen in the high standard deviation values.

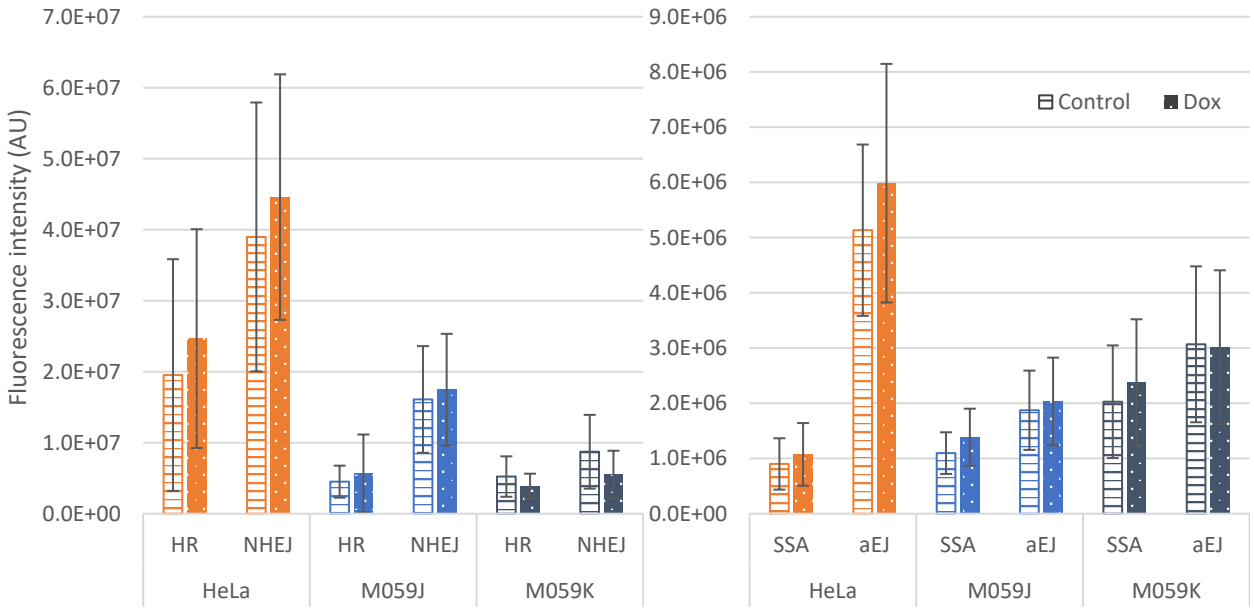

Figure 83. Comparison of nuclear extracts from control (striped bars) and Dox-treated cells (dotted bars) analyzed at 0.2 mg/ml with the Next-SPOT assay.

Plotted data represents the mean ± SD of 9 independent experiments (n=9) on HeLa (orange), M059J (light blue) and M059K cells (dark blue). Comparison with the control: Wilcoxon-Mann-Whitney test.

4.2.3. Effect of repair inhibitors alone or combined with doxorubicin

Besides the effect of doxorubicin, Next-SPOT results show that repair inhibitors impact different pathways, as illustrated by figure 84 and detailed in the next sections. These experiments allowed the estimation of the impact of the genotoxic on the inhibitors' activity.

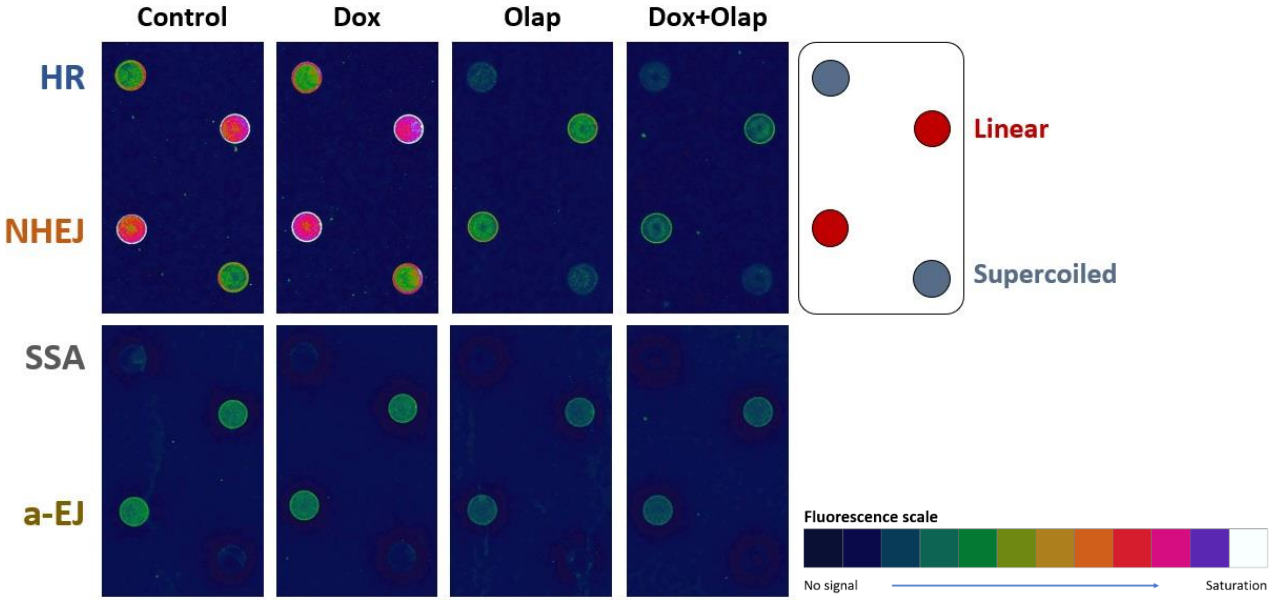

Figure 84. Images of the Next-SPOT biochip obtained with nuclear extracts from HeLa cells treated with doxorubicin and/or PARP inhibitor olaparib.

Inhibition of RAD51

No significant effect was seen in HeLa following exposure to B02, though a global trend suggested a decrease in all DSBR activities, especially for the combined treatment with doxorubicin (figure 85).

M059J provided similar results, but a significant inhibition of a-NHEJ was seen in cells exposed to both B02 and Dox. In M059K, HR and NHEJ dropped in the presence of B02, but the inhibitor had no striking action on alternative repair pathways.

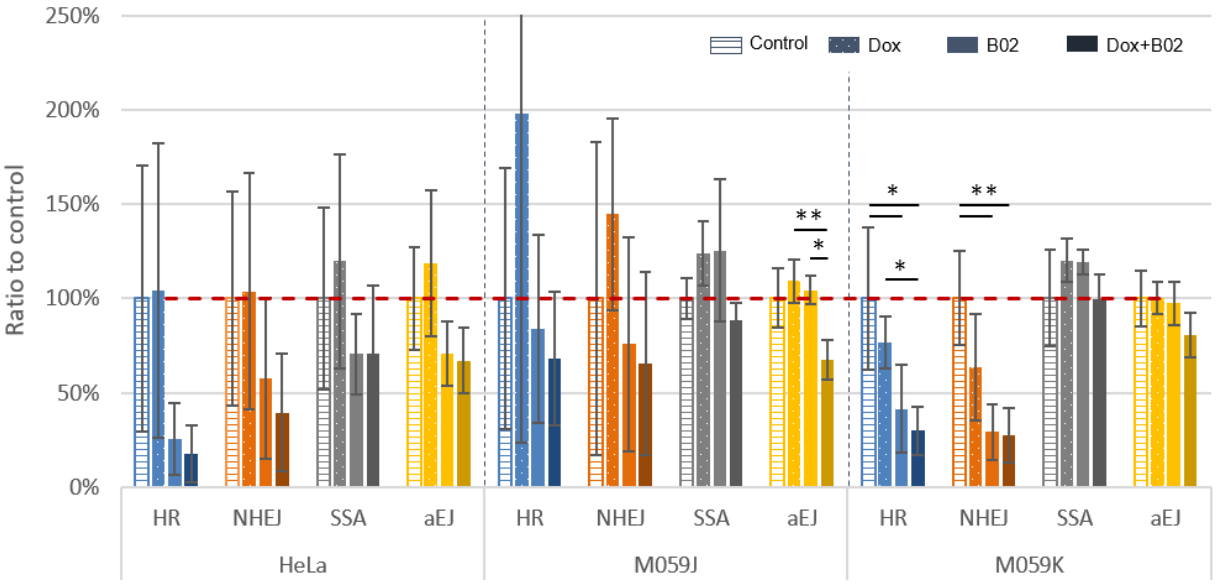

Figure 85. Effect of RAD51 inhibitor B02 on the repair activities assessed by the Next-SPOT assay.
*Plotted data represents the fluorescence obtained with 0.2 mg/ml NE, normalized to the untreated control (mean ± SD). Patterns indicate the different treatment conditions (control, doxorubicin alone, inhibitor alone or inhibitor combined to doxorubicin), while colors (blue, orange, grey and yellow) represent the signal attributed to HR, NHEJ, SSA and alt-NHEJ, respectively. Three independent experiments were performed (n=3); * p<α/2, ** p<0.01 (non-parametric Dunn test).*

Inhibition of DNA-PKcs

No effect of NU7026 was seen in HeLa and M059J, though the inhibitor alone seemed to stimulate HR and NHEJ activity (figure 86). On the contrary, a decrease in NHEJ repair was seen in M059K cells treated with both NU7026 and Dox, and a non-significant trend was seen in HR. Interestingly, DNA-PKcs inhibition caused an effect quite similar to RAD51 inhibition in M059K.

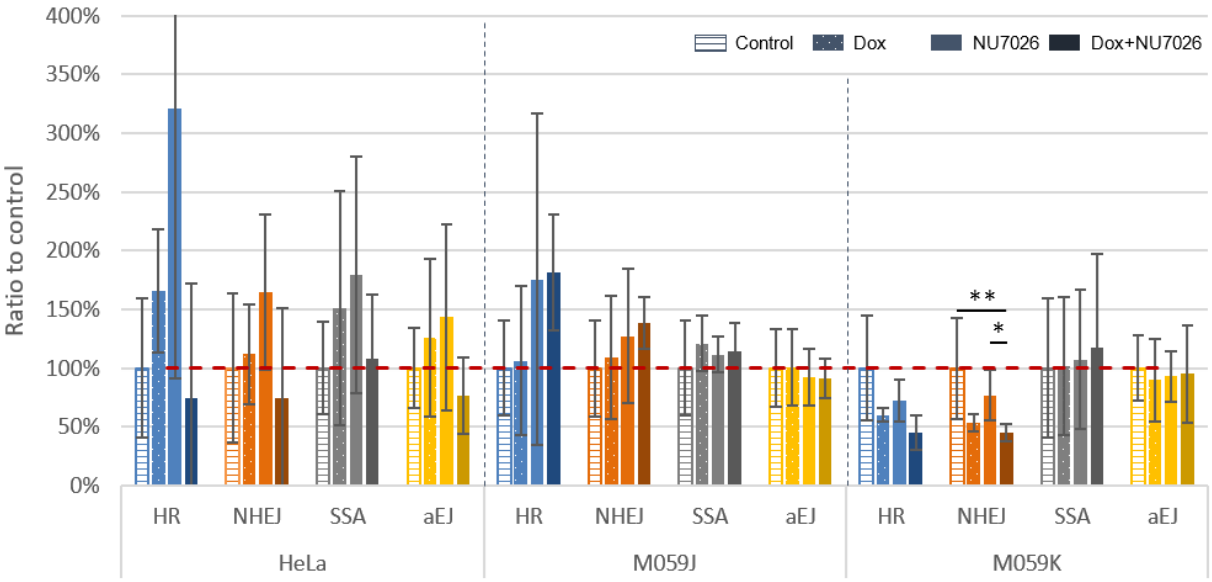

Figure 86. Effect of DNA-PKcs inhibitor NU7026 on the repair activities assessed by the Next-SPOT assay.
*Plotted data represents the fluorescence obtained with 0.2 mg/ml NE, normalized to the untreated control (mean ± SD). Three independent experiments were performed (n=3); * p<α/2, ** p<0.01 (non-parametric Dunn test).*

Inhibition of PARP

A significant inhibition of alternative end-joining activities was found in M059K cells exposed to olaparib, but only combined with Dox. This decrease was not statistically significant in M059J and HeLa (figure 87). Interestingly, an inhibition of c-NHEJ was also seen in M059K and HeLa. HR was altered in HeLa only, but the trend was the same in all cell lines.

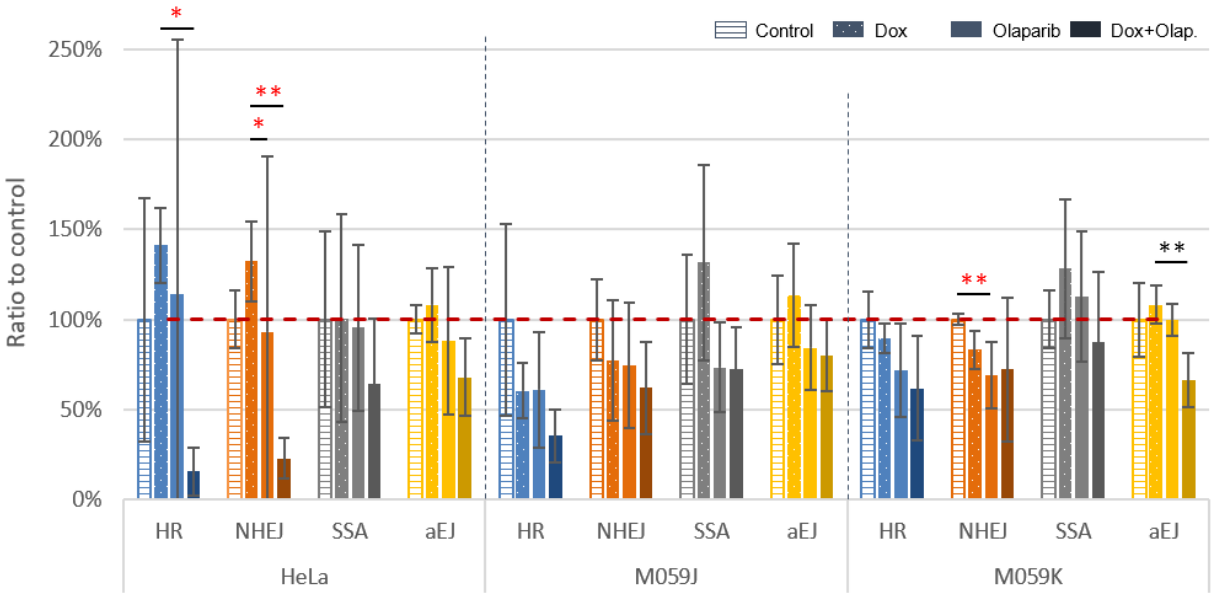

Figure 87. Effect of PARP inhibitor olaparib on the repair activities assessed by the Next-SPOT assay.
*Plotted data represents the fluorescence obtained with 0.2 mg/ml NE, normalized to the untreated control (mean ± SD). Three independent experiments were performed (n=3); red asterisks indicate that outliers were removed from analysis, as detailed in appendix 15. * p<α/2, ** p<0.01 (non-parametric Dunn test).*

According to our results, it can be hypothesized that all repair activities were impacted by the inhibitors due to a global reduction of DSBR, as a response to high cellular stress. An alternative representation of the results was considered for a similar effect on all pathways not to be accounted for.

4.2.4.Summary of treatment effects

Figure 88 regroups the effect of the different treatments across cell lines. Most clusters were not significantly separated (approximately unbiased p-values < 95%, see appendix 16), but some interesting trends are seen.

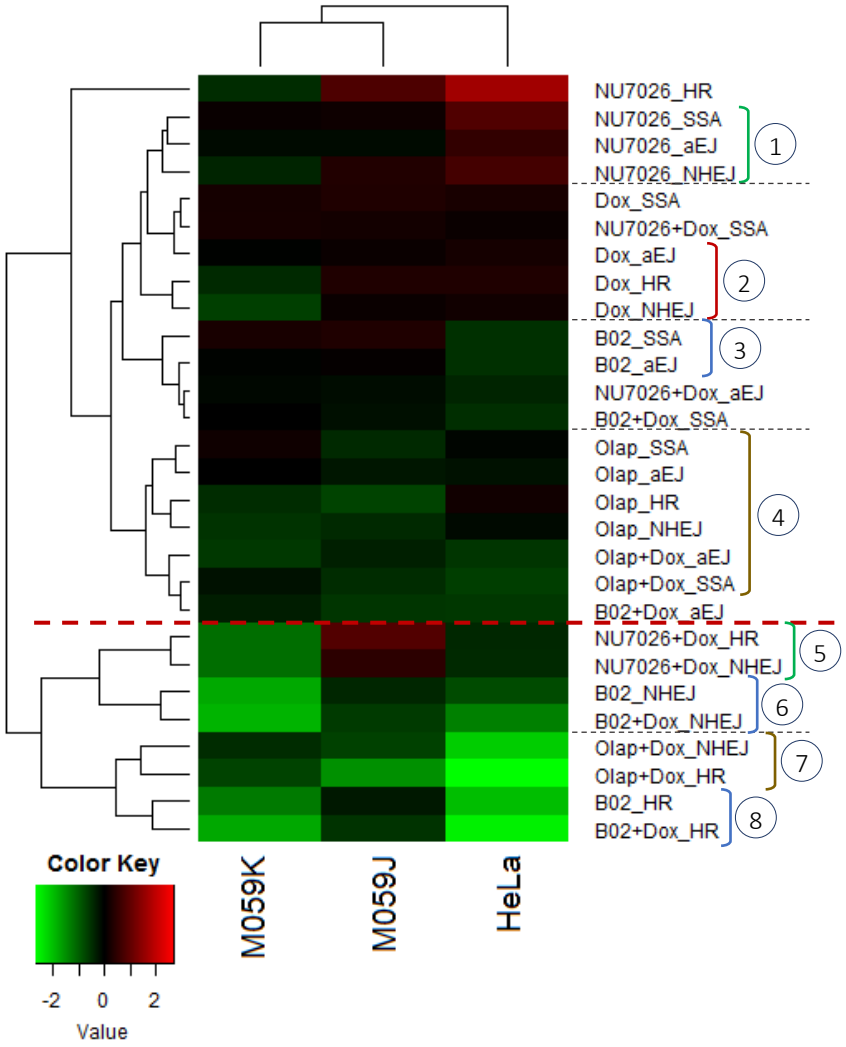

Figure 88. Analysis of the DNA repair response in the cellular models across treatments and repair pathways.
Heatmap based on the log2-transformed ratios of the fluorescence intensity obtained on each Next-SPOT condition between treated and non-treated cell lines (log2(T/NT)). Hierarchical clustering algorithm with Euclidean dissimilarity measure was used to group the three models. In the first dimension, cell lines were clustered by similarity of the intensity and covariation of their DSBR response profile across treatments. In the second dimension, treatments were clustered by similarity of their response across the cell lines. Positive values in the log2 scale are shaded in red and indicate a stimulation of repair activities compared to control cells whereas negative values are colored in green and indicate an inhibition. Values around zero (in black) indicate no detected effect of the treatment. Indicated groups (1-8) are detailed in text.

Firstly, glioblastoma cell lines tended to group together but in a non-significant fashion (approximately unbiased p-value < 95 %). Correlation distance did not provide significant results (see appendix 17). This observation is to be paralleled with ExSy-SPOT data in which glioblastoma cell lines had a similar global response.

General trends can be seen in the clustering across treatment effects: NU7026 alone impacts HeLa and glioblastoma cells in a different fashion, and its effect on HR is isolated from its impact on other pathways (group 1). Olaparib alone impacts all pathways in a similar manner, and the combined treatment with doxorubicin led to effects on a-EJ and SSA that were included in the same group (group 4). Combined 'NU7026+doxorubicin' and 'olaparib+doxorubicin' treatments appear to affect HR and NHEJ differently from the treatment with the inhibitors alone (groups 1 & 5 and 7 & 4, respectively), while this is not observed for B02, which seems to have a different effect on NHEJ, HR and alternative pathways (groups 6, 8 and 3, respectively). Overall, it suggests that the effect of NU7026 and olaparib is more impacted by doxorubicin than the effect of B02 on HR and NHEJ, and that an activation of repair proteins by the genotoxic stress induced by doxorubicin can make them more sensitive to repair inhibition.

An interesting observation concerns the cluster regrouping the dominant pathways (HR and NHEJ) following treatment with the three inhibitors combined with doxorubicin (groups 5 to 8), which highlights their strong effect on repair activities as well as the exception of 'NU7026+doxorubicin' treatment in the DNA-PKcs-deficient M059J cell line. Finally, this representation also underlines the limited action of doxorubicin alone, with small, non-significant effects on repair activities (group 2).

4.2.5. Relative contributions

This representation underlines the much higher basal contribution of alternative pathways in M059K compared to M059J and HeLa (figure 89 to figure 91).

Overall, this representation allows the identification of specific effects that can be missed when looking at each signal individually. For instance, when all repair activities tend to be reduced, it clearly shows if some pathways are more affected compared to others. However, conclusions are delicate since a reduction in one pathway mechanically results in the increase of the relative contribution of the others.

Inhibition of RAD51

As can be expected, the participation of HR in total fluorescence decreased in HeLa and M059K cells treated with B02. While raw data showed a non-significant reduction in both HR and NHEJ in HeLa (figure 85), relative contributions highlight a significant decrease in HR only, while the contribution of NHEJ was not reduced (figure 89). In parallel, the relative contribution of SSA increased. In M059K, the

contribution of c-NHEJ was also significantly reduced by B02 while that of alt-NHEJ increased. These effects were most pronounced in cells which received the combined treatment with Dox.

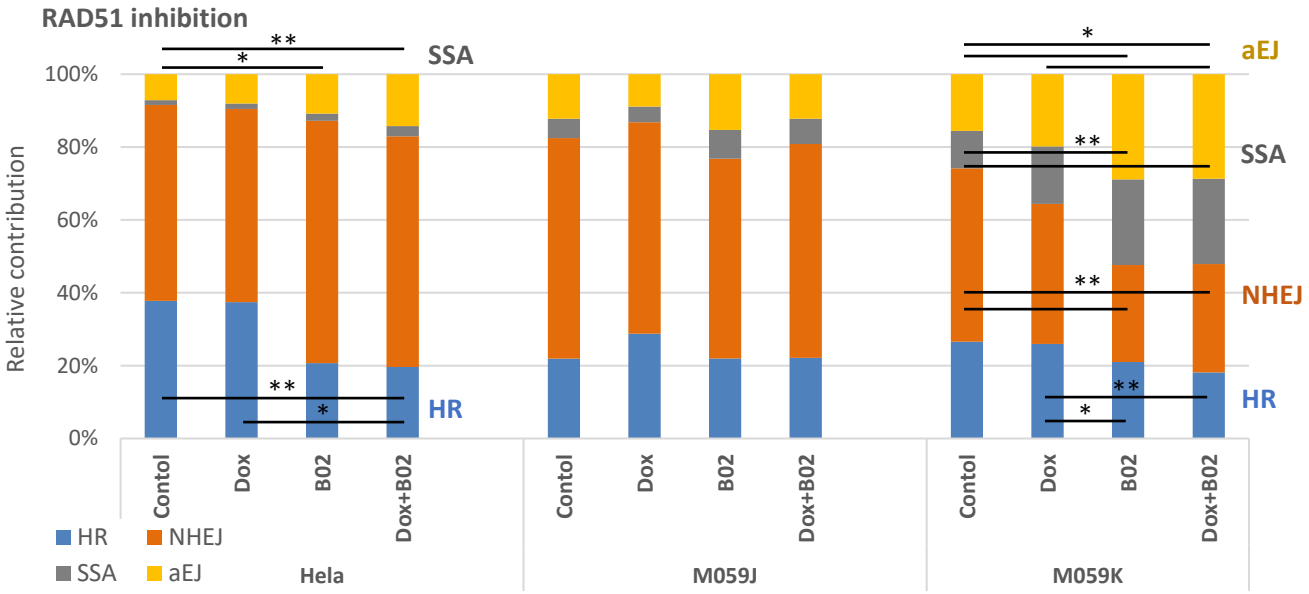

Figure 89. Relative pathways contribution to the total fluorescence in cells treated with Dox and/or B02.
*Mean ± SD of three independent Next-SPOT experiments with 0.2 mg/ml NE (n=3); * p<α/2, ** p<0.01 (non-parametric Dunn test).*

Inhibition of DNA-PKcs

High variability was observed in relative pathway contributions following DNA-PKcs inhibition, and the only significant observation was an increase in the proportion of HR in HeLa upon treatment with NU7026 alone (figure 90). A concomitant decrease was seen in NHEJ but it was not significant. However, the increase in HR was suppressed when doxorubicin was combined to NU7026 and no inhibition of NHEJ was found compared to control cells.

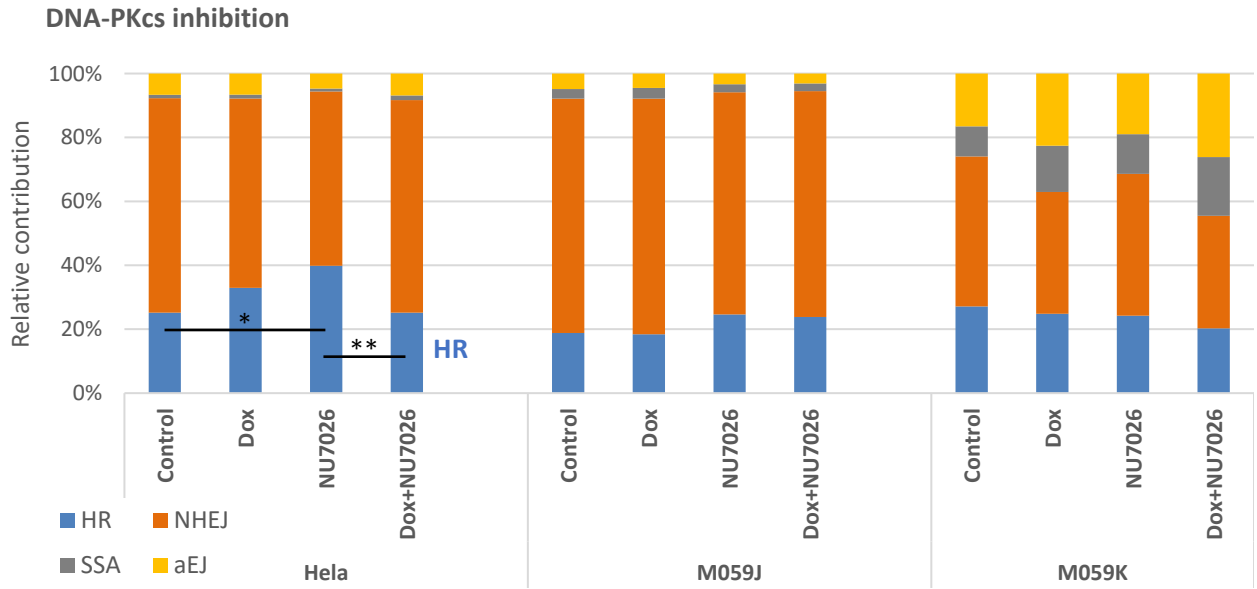

Figure 90. Relative pathways contribution to the total fluorescence in cells treated with Dox and/or NU7026.
*Mean ± SD of three independent Next-SPOT experiments with 0.2 mg/ml NE (n=3); * p<α/2, ** p<0.01 (non-parametric Dunn test).*

Inhibition of PARP

Surprisingly, PARP inhibition increased the relative contribution of a-NHEJ to the total repair signal in HeLa (figure 91). That was paralleled to HR decrease (not significant). The participation of c-NHEJ was reduced in HeLa and enhanced in M059K.

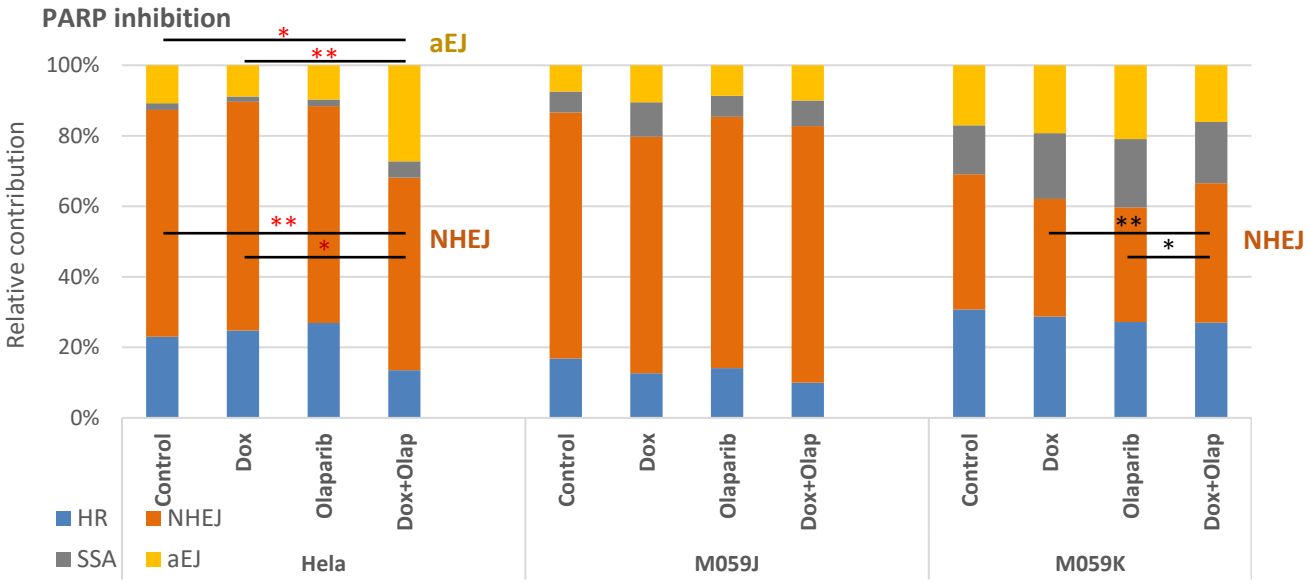

Figure 91. Relative pathways contribution to the total fluorescence in cells treated with Dox and/or olaparib.
*Mean ± SD of three independent Next-SPOT experiments with 0.2 mg/ml NE (n=3); * p<α/2, ** p<0.01 (non-parametric Dunn test). Red asterisks indicate that outliers were removed from analysis, as detailed in appendix 15.*

4.2.6. Global summary

Table 13 regroups the most striking observations for the reader to compare Next-SPOT data with other results presented in this chapter.

Table 13. Summary of Next-SPOT results compared to the reference assay and 53BP1 foci counts following treatment with repair inhibitors.
Significant stimulations and inhibitions are indicated in red and blue, respectively. Brackets specify if the effect was observed only in control or doxorubicin-treated cells. Data originates from the experiments detailed in the "Results" chapter.

		HeLa			M059J			M059K		
		B02	NU7026	Olaparib	B02	NU7026	Olaparib	B02	NU7026	Olaparib
Next-SPOT (raw data)	HR			(Dox)						
	NHEJ			(Dox)					(Dox)	(Ctl)
	SSA									
	a-EJ				(Dox)					(Dox)
Next-SPOT (relative contribution)	HR	(Dox)	(Ctl)					(Dox)		
	NHEJ			(Dox)						(Dox)
	SSA									
	a-EJ			(Dox)						
Reference assay		(Dox)	(Ctl)			(Ctl)		(Dox)		
53BP1 foci						(Dox)				

4.3. Effect of repair inhibitors following *in vitro* treatment of the nuclear extracts

As a complement to cellular treatments, an alternative protocol was tested on cells treated with doxorubicin only, with inhibitors added *in vitro* in the Next-SPOT reaction mix. This protocol aimed at preventing the potential observation of mechanisms associated with the DDR such as the triggering of apoptosis, by observing direct inhibitions resulting from a direct interaction between drugs and repair proteins within the extracts.

The first question that arose was the choice of the treatment dose. Setup experiments compared a range of concentrations, from 20 to 400 µM (appendix 18). High doses required the final DMSO concentration to be set at 3%, which impacted fluorescence levels. It was observed that low doses of inhibitors only produced limited effects, hence the dose for *in vitro* treatments was set at 400 µM, 3% DMSO. Similar conclusions were drawn in M059J and M059K (data not shown).

In HeLa, *in vitro* treatment with B02 only produced a small inhibition of alt-NHEJ in cells treated with doxorubicin (figure 92). No particular observation was made on HR. Interestingly, DNA-PKcs inhibitor NU7026 caused a sharp increase in fluorescence intensity for HR and c-NHEJ, but caused an inhibition of alt-NHEJ. Olaparib did not produce a significant effect in HeLa; the only significant observation (decrease in c-NHEJ) was based on the effect of doxorubicin.

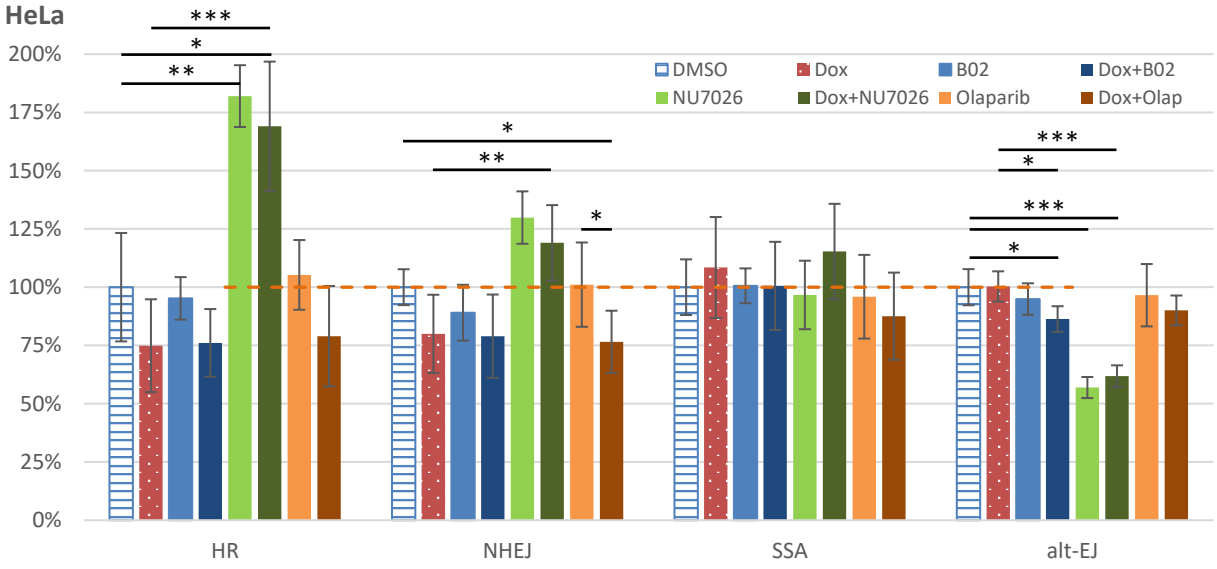

Figure 92. Variation in repair activities assessed by the Next-SPOT assay following in vitro treatment with DSB repair inhibitors in NEs from HeLa cells exposed to doxorubicin.

*Data was normalized to the untreated control. Mean ± SD of three independent experiments (n=3). * p<α/2, ** p<0.01, *** p<0.001 (non-parametric Dunn test).*

A pronounced inhibitory effect of doxorubicin was seen on HR and c-NHEJ in M059J (figure 93). This effect was not seen in cellular treatments (figure 83), and thus seems to originate from the different

experimental procedure. The action of the inhibitors was shaded by that of Dox, and no clear effect could be seen.

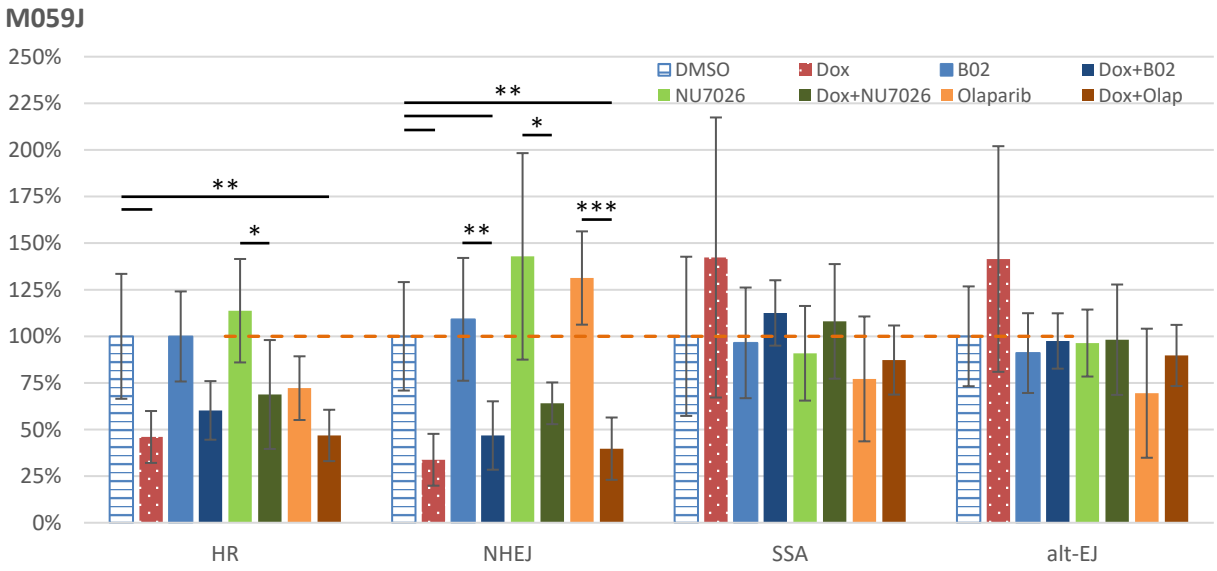

Figure 93. Variation in repair activities assessed by the Next-SPOT assay following in vitro treatment with DSB repair inhibitors in NEs from M059J cells exposed to doxorubicin.
*Data was normalized to the untreated control. Mean ± SD of three independent experiments (n=3). * p<α/2, ** p<0.01, *** p<0.001 (non-parametric Dunn test).*

A similar effect of doxorubicin was found in M059K (figure 94). No clear action of RAD51 inhibition was seen, but NU7026 led to a significant increase in HR. The same trend was observed in NHEJ but it was not significant. PARP inhibition caused a decrease in SSA in control cells, but not in cells treated with Dox.

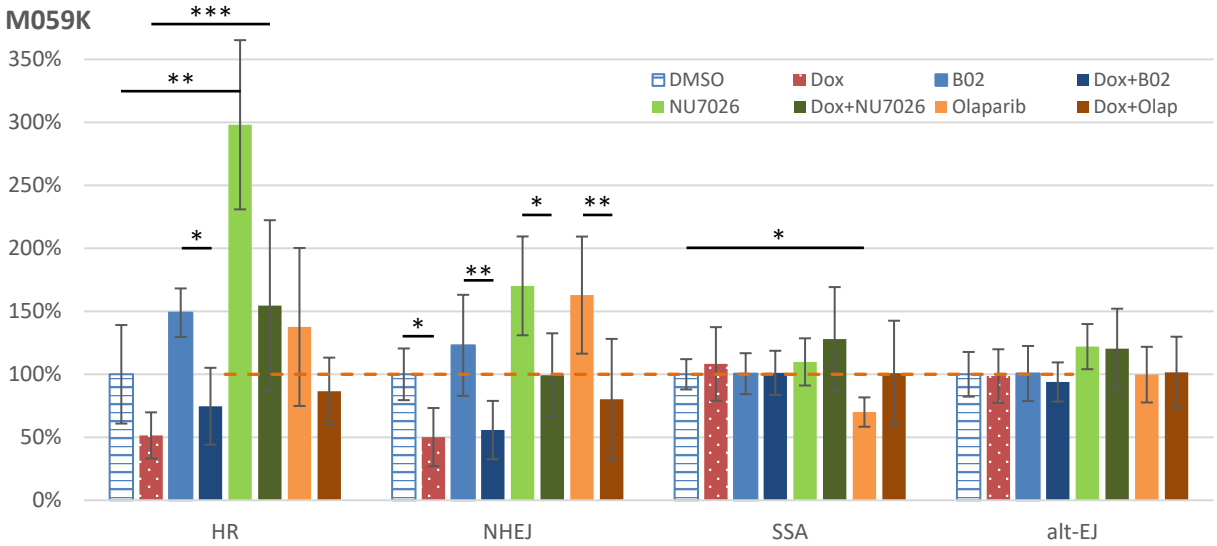

Figure 94. Variation in repair activities assessed by the Next-SPOT assay following in vitro treatment with DSB repair inhibitors in NEs from M059K cells exposed to doxorubicin.
*Data was normalized to the untreated control. Mean ± SD of three independent experiments (n=3). * p<α/2, ** p<0.01, *** p<0.001 (non-parametric Dunn test).*

4.4. Comparison of repair activities in M059J and M059K

The comparative representation of repair activities emphasized the higher (or similar) HR and c-NHEJ repair activities in M059J cells (figure 95A); the NHEJ results correlate with the response seen in the electrophoretic assay, though with a less pronounced amplitude. More specifically, the relative signal obtained in M059J particularly increased in HR and NHEJ following DNA-PKcs inhibition. PARP inhibition also increased the relative NHEJ activity in the mutated cells. Cy5 readouts, which inform on alternative activities, were always higher in M059K, except following olaparib treatment in Dox-treated cells.

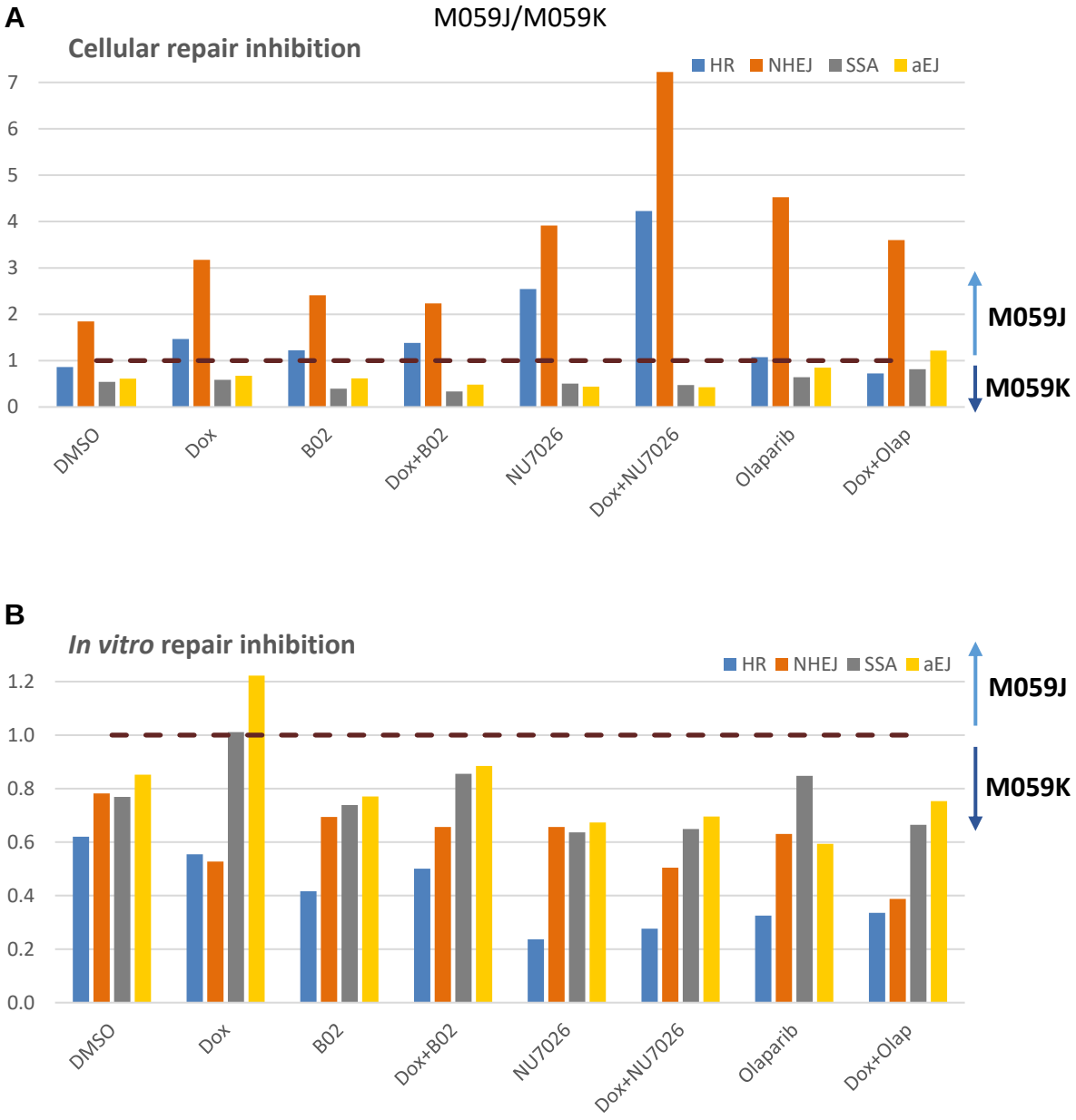

Figure 95. Ratio between repair activities in M059J and M059K measured by the Next-SPOT assay following cellular or in vitro *repair inhibition.*
A. *Cellular treatments with DNA repair inhibitors were added in the culture medium together with Dox.* ***B.*** In vitro *treatments with inhibitors added in the nuclear extracts. Mean of at least 3 independent experiments, with 0.2 mg/ml nuclear extracts. Values above 1 indicate a higher activity in M059J compared to M059K.*

Interestingly, the profile was completely different with the *in vitro* protocol; most DSBR activities shifted to M059K, in which a clearly higher signal was obtained for HR in the presence of the DNA-PKcs and PARP inhibitors (figure 95B). NHEJ was also higher in the wild-type cells following PARP inhibition in Dox-treated cells.

5. Comparison of DNA-PKcs-deficient and NU7026-treated cells

In this section, we present a focus on a subset of our repair assays for the reader to compare the response of cells treated with DNA-PKcs inhibitor NU7026 and that of DNA-PKcs deficient M059J cells (figure 96). When comparing M059J cells to M059K cells exposed to NU7026, either alone or combined to Dox, we could not identify striking similitudes in repair activities. Experimental variability was too high to allow conclusions to be drawn. M059K cells treated with the inhibitor also had clearly different relative contributions from control M059J cells (figure 96B). Our general conclusion is that the inactivation of DNA-PKcs by NU7026 in M059K cells did not produce an M059J-like behavior. In HeLa, no assertions could be made due to high standard deviation between replicate experiments.

The comparison of the ratios between NHEJ and HR signals highlighted the strong effect of NHEJ alone in HeLa, but no other conclusion was made (appendix 19). Data from the *in vitro* Next-SPOT assay is presented in appendix 20 and appendix 21.

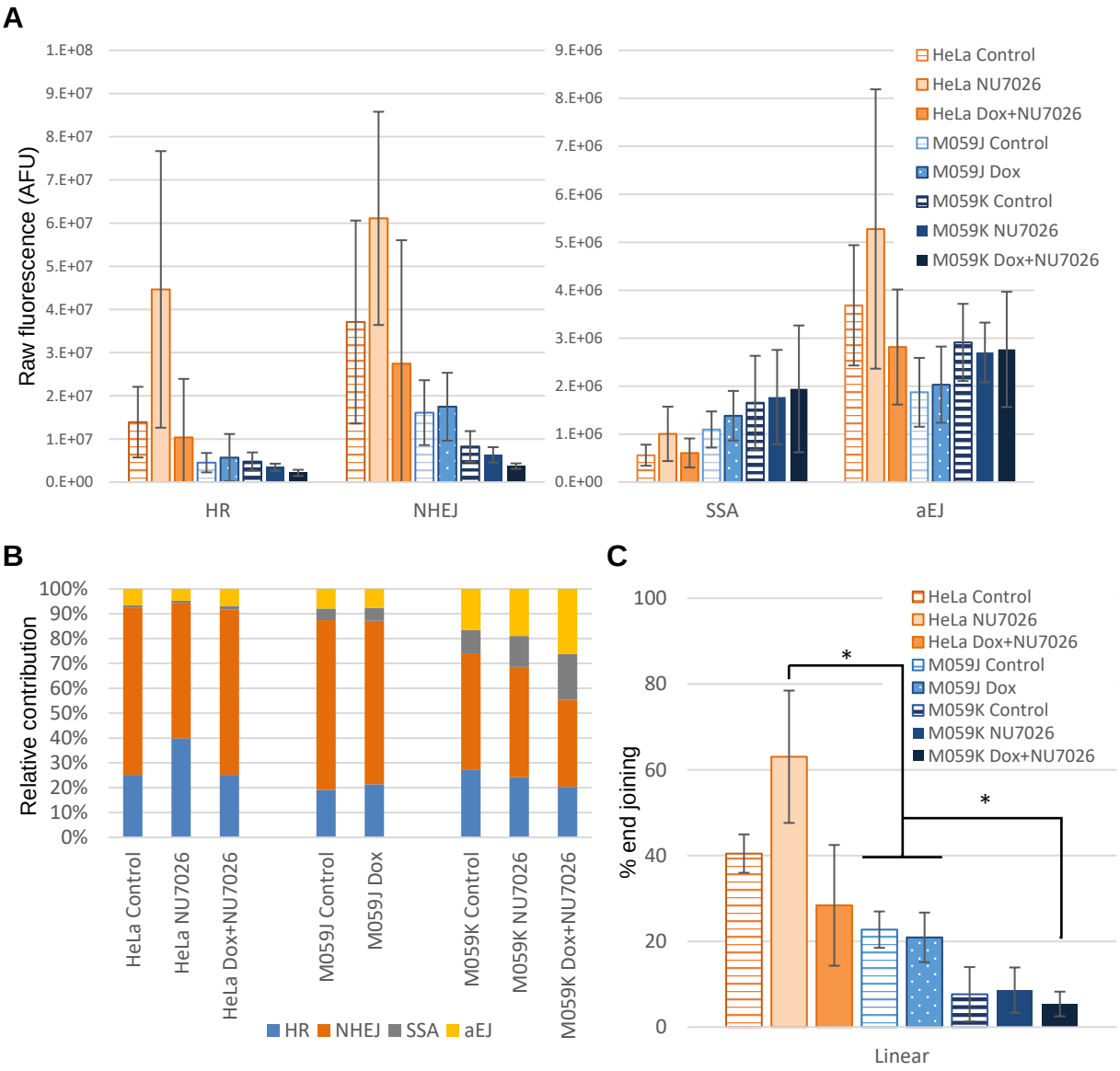

Figure 96. Comparison of DSBR response in HeLa and M059K cells treated with NU7026 and untreated M059J cells. ***A.*** *Raw Next-SPOT data.* ***B.*** *Relative pathway contribution following cellular treatment.* ***C.*** *End-joining activities measured by the electrophoretic approach. Data originates from the same sets of experiments as described previously.*

Box 3. Main results obtained with the Next-SPOT assay:

- ✓ Repair activities are positively correlated with the concentration of nuclear protein extracts.
- ✓ Basal HR, c-NHEJ and alt-NHEJ activities are higher in HeLa than in glioblastoma cells. On the contrary, SSA is higher in M059K than HeLa.
- ✓ Basal repair activities in M059J cells do not significantly differ from that of M059K cells.
- ✓ Repair activities are unchanged following treatment with doxorubicin alone.
- ✓ All repair inhibitors have an effect on DSB religation, but they do not impact all cell lines.
- ✓ The effect of repair inhibitors varies across pathways and it is modulated by doxorubicin.
- ✓ Relative pathway contributions bring additional data that complete raw fluorescence values.
- ✓ The "*in vitro*" protocol leads to different conclusions compared to the standard Next-SPOT assay.

CHAPTER 4 – DISCUSSION

1. Methods: comparison of the two DSBR assays

We used two different DSBR methods for the investigation of the effect of doxorubicin and repair inhibitors; in this section we discuss technical aspects regarding the information obtained, the experimental workload and the variability of these methods.

1.1. Information obtained

The two techniques rely on the same original substrate, the pBlueScript plasmid, either in a supercoiled or linearized form. The main differences between both methods lie in the environment of the plasmids (liquid solution for the reference assay, solid support for Next-SPOT) and in the quantification of repair activities (electrophoresis for the reference assay, fluorescence readout for Next-SPOT). Once printed on Next-SPOT slides, plasmids go through the 3D-coating and physically bind the surface *via* covalent amine bonds before unbound DNA is rinsed off the slides. This is expected to modify steric hindrance and thus reshape the interaction between DNA and repair proteins.

As previously described, the supercoiled plasmid was initially added in the reaction mix of the electrophoretic assay, in addition to the linearized plasmid, which was expected to provide clues on the potential mechanisms that could occur on the "HR" condition on the biochip. Nevertheless, little information was obtained from this condition and it was not systematically investigated in subsequent experiments. Hence, data provided by our electrophoretic assay was limited to c-NHEJ, while we show that the biochip is able to describe more conditions simultaneously. Next-SPOT measurements are associated with either HR, c-NHEJ and backup repair pathways (alt-NHEJ and SSA) in a single well, which considerably simplifies the comparison of the different signals for the exact same sample and brings additional information.

This feature allows the comparison of the relative contribution of each signal to the total fluorescence measured on the chip. Such a representation can complement raw data, since some effects of the treatments were not observed when looking at raw fluorescence results. These possibilities could not be accessed by the electrophoretic method, which only measured a single pathway, c-NHEJ. In the next chapter, we suggest potential optimizations that could further improve the description of the different mechanisms analyzed on the chip.

We found the same basal c-NHEJ activities across the different cell lines with Next-SPOT and with the reference assay, and we observed the same increase in repair activity when augmenting protein extract concentration. In addition, we saw that cellular treatments with doxorubicin and repair inhibitors had either the same effect or that it followed a close trend with both methods, as illustrated in figure 97.

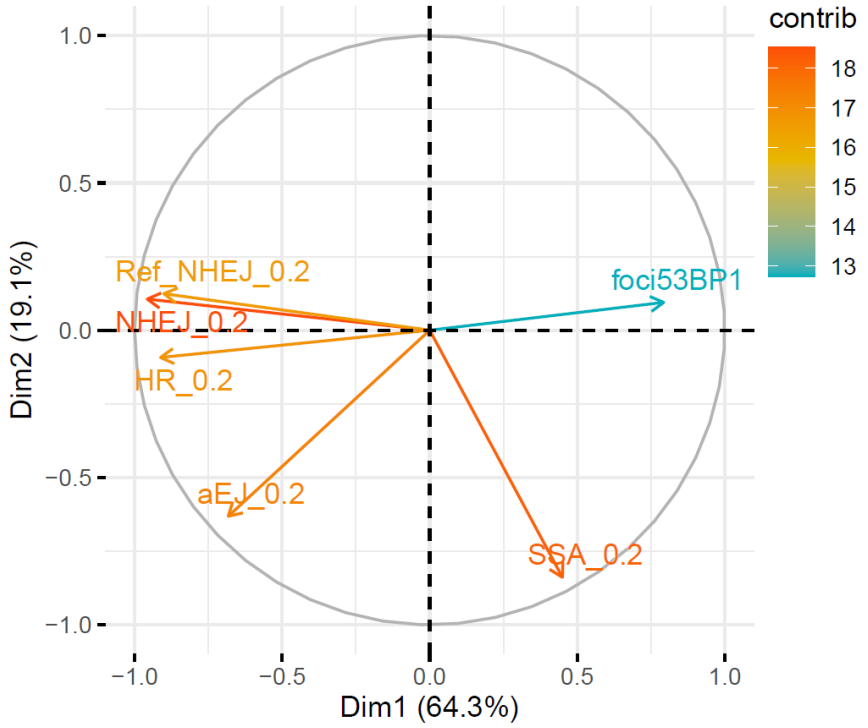

Figure 97. Principal components analysis of data from the electrophoretic reference assay (Ref_NHEJ), the Next-SPOT assay on biochip and 53BP1 foci counting.
Raw data were gathered from all previously described experiments in HeLa, M059J and M059K cells exposed to doxorubicin and/or repair inhibitors. For DSBR experiments, extracts were introduced at a concentration of 0.2 mg protein/ml. The color scale represents cos² values, with a higher value indicating a larger contribution of the component to the total distance.

Data obtained within this project show that HR and c-NHEJ usually follow the same trend on the chip. However, it must be pointed that it is not systematically observed by LXRepair: opposite variations have been seen in other tests performed by the company. The two conditions are thus independent from each other, although data from this study usually show a decrease in both repair activities.

Interestingly, the response of alternative pathways was usually found to differ from the variation of HR and c-NHEJ. From a technical point of view, these pathways are measured through a different parameter: alternative repair intensity is based on the quantification of the incorporation of labelled nucleotides, while HR and NHEJ activities are estimated based on the fixation of the fluorescent linear plasmid. But most of all, these pathways are regulated through different biological mechanisms than the dominant DSBR pathways. More specifically, SSA is usually strongly repressed in humans (Bhargava *et al.*, 2016; Mladenov *et al.*, 2016) and it is thus relevant to find a different response for this pathway. It can be noted that variations in 53BP1 foci levels are directly opposed to HR and NHEJ levels; typically, the number of foci increases when repair activities decrease, which is in line with our expectations. Conversely, alt-NHEJ and SSA signals are less clearly correlated to 53BP1 foci levels, which underlines the complex activity of backup pathways and questions the information obtained from the incorporation of nucleotides on the chip. More insight into the interpretation of biological results will be provided in section 2 of this chapter.

1.2. Experimental workload

The two methods do not require the same amount of time per sample (throughput). In this domain, Next-SPOT achieves a clear improvement. Raw data produced by the biochip were available within a maximum of two hours after the end of the incubation, while the electrophoretic method required at least one full gel had to be cast and run for 3 hours before analyzing one set of samples. Besides, two plasmids were tracked simultaneously (and in replicates) in one pad on the biochip, while adding the supercoiled plasmid besides the linear one doubled the number of lanes used on a gel, thus multiplying the overall experimental time by two if several gels had to be run.

Next-SPOT required **specific preparation steps** (plasmid labelling, slide preparation and quality control), but reagents were shown to be stable for several months, so these steps were regrouped into production batches which did not represent a high experimental burden per sample.

Overall, the **Next-SPOT assay reduced "wet lab" experiment time** three-fold. The multiplication of the gels with the electrophoretic method also requires samples to be run on different gels, thus increasing experimental variability among the measurements. Besides, adding new conditions on the chip, such as other plasmids with different lesions, would not increase the length of each individual experiment, while it would considerably extend the reference NHEJ assay.

Analysis time was similar in both methods; each analysis software allowed a semi-automated quantification, but adjustments were required in both cases to adjust background and control the identification of the bands or fluorescent spots. However, the Next-SPOT has much higher optimization prospects: the development of an automated plugin such as the one used for the ExSy-SPOT assay is completely doable and would considerably reduce analysis time.

Next-SPOT's multiplexing also results in a **lower consumption of biological material**. For instance, studying the ligation of two different plasmids can be done simultaneously on the biochip with less than 10 µg of cell extracts, while it requires separate reactions mixtures to be prepared when using the electrophoretic method.

1.3. Assay precision

The initial version of both assays produced highly variable results. Due to numerous modifications brought to the assays in the first half of the project, no stable versions of the protocols were to be tested and this variability was not investigated. Even in the final part of the project, during which most of our data was generated, we set up analytical validations of the Next-SPOT assay that were only partly completed, and no dedicated study was performed on the reference assay.

For the Next-SPOT assay, we estimated the closeness of agreement between independent Next-SPOT based on data from 27 repeat experiments performed in similar conditions: identical experimental procedure, similar environment and laboratory equipment, same operator; the same batch of commercial HeLa aliquots was used for each experiment. However, tests were performed on different batches of slides and spread on three months instead of being run in a row as planned initially. We calculated the coefficient of variation (CV) for each of the four conditions tracked by the Next-SPOT assay and found that relative pathway contributions provided more repeatable values (table 14). Indeed, it can be noted that raw data are more likely to be influenced by variations in fluorescence from one slide to another, due to slight variations in the coating quality, the laser power and autofocus parameters on the scanner. Since the resulting shift in fluorescence intensity affects all measured signals, analyzing the relative contribution of each condition to the sum of all signals removes this variability.

Table 14. Coefficient of variation of repair activity measured in commercial HeLa extracts by the Next-SPOT assay

CV	HR	c-NHEJ	SSA	alt-NHEJ
Raw fluorescence intensity	34%	17%	62%	36%
Relative contribution	22%	**6%**	48%	29%

Only the relative contribution of c-NHEJ provided a coefficient of variation below 10%. The religation of the linearized plasmid in c-NHEJ may mobilize fewer factors than for other repair pathways and it could therefore be less impacted by slight variations in the experimental environment. Most specifically, we observed that monitoring temperature, relative humidity and ozone levels was critical during the production of the slides and during the experiment. Even though these parameters were surveyed and experiments were planned based on the lab environment, some recent improvements such as the installation of an ozone filter could not benefit to the data presented here.

1.4. Comparative summary

Table 15. Global comparison of the two DSBR methods

Parameter	Reference electrophoretic assay	Next-SPOT
Multiplexing	No (c-NHEJ)	**Yes** (HR, c-NHEJ, SSA, alt-NHEJ)
Relative pathway contributions	No	**Yes**
Average throughput (samples per day, in duplicates)	2.7	**9.1**
Flexibility	Limited	**High** (additional conditions easily tested)
Potential for automation	Very limited	**Yes** (analysis steps)
Batch productions	No	**Yes**
Consumption of biological material	Quite low	**Very low**
Equipment required	**Basic and inexpensive**	User: quite basic (slide scanner) Manufacturer: very specific (ultra-low volume dispensing system)
Toxic waste	DNA dyes and contaminated buffers	**Small amounts of toxic waste**

The next step in the validation of the assay is the estimation repeatability and reproducibility. A preliminary study showed similar features as for the presented variability data (results not shown).

Overall, Next-SPOT provided more data than the electrophoretic method in a lesser amount of time and with a lower technical burden. It requires dedicated equipment but allows batches of identical slides to be prepared in advance. Table 15 summarizes the main characteristics of the two methods.

1.5. Comparison to alternative methods

There is presently no optimal approach to assess DSBR. As presented in our introduction, all methods are based on different markers and thus provide different information. Next-SPOT is a direct approach that can describe several mechanisms simultaneously. On the contrary, most indirect methods only describe global repair activities.

However, the biochip does not inform on the fidelity of repair mechanisms, as opposed to some cell-free assays or reporter assays that can allow the recovery of product's sequence after break resolution. However, it is also complex to access this information when using PFGE, the comet assay or IF, since induced damage occurs randomly. Nevertheless, IF assays easily compare repair activities at the sub-cellular level, for instance in euchromatin or heterochromatin regions. Cell-free methods like ours can mainly analyze different compartments depending on the extraction protocol (whole cell, cytoplasmic or nuclear extracts). Cell extracts have also been used with an in vitro comet assay (Azqueta *et al.*, 2019), but to our knowledge it has never been used to study DSBR.

Just like other DSBR methods, the biochip assay has a full potential to provide kinetics of DSBR activities. In our study, we only performed tests following 48 hours of treatment, but comparing repair activities at different times points would be valuable data to collect, especially in parallel with other measurements described in the "Prospects" chapter. A valuable characteristic of our system is its capacity to analyze undamaged cells. Indirect repair assays require a genotoxic stress to be triggered for repair foci to form, while the biochip and the other direct approaches can estimate repair activities at the basal level in cells that did not receive any particular treatment. This kind of information is valuable when studying the effect of a drug independently of a synergetic DNA-damaging treatment.

We show that Next-SPOT has a very good potential for multiplexing, as opposed to physical methods such as PFGE and the comet assay. IF techniques that track several proteins simultaneously can provide clues regarding the activity of DSBR pathways, but such markers remain indirect and validation with numerous markers is often required to ensure that the observed pathway is fully active. Besides, debate is still ongoing regarding persistent γ-H2AX foci and foci formation resulting from non-DSB lesions (Antonelli *et al.*, 2015; Ricoul *et al.*, 2019; Rothkamm *et al.*, 2015; Siddiqui *et al.*, 2015; Valdiglesias *et al.*, 2013). Cell-free assays and reporter methods track various pathways through the custom design of

the DNA substrates with specific end configurations. However, direct methods also require sample preparation steps such as protein extraction or plasmid transfection that can alter the original cellular response to an undetermined extent.

Next-SPOT and other cell-free assays can virtually analyze any cell type or tissue since they only require protein extraction (potentially preceded by tissue dissociation). This is not the case of reporter assays, that rely on transfection or transduction of the DNA substrate, which prevents them from being used in non-cultured cells.

It is a difficult task to compare the assay on biochip to other DSBR methods; Next-SPOT is a novel method and available data is too limited to allow a direct comparison of the biological results we obtained with that of another approach. From the technical point of view, the limited sample preparation steps and the use of artificial DNA substrates makes NEXT-SPOT a good candidate for standardization, but similar comments are found regarding other cell-free assays (Pastwa *et al.*, 2009), reporter-based methods (Valdiglesias *et al.*, 2011) and most of all immunofluorescent approaches, which are currently considered the gold standard for DSBR studies, with a high reproducibility and easy implementation. Only the comet assay is known to produce different results across different laboratories, in spite of recent standardization efforts (Møller *et al.*, 2020b).

Aside from a fluorescence scanner, the biochip assay requires little equipment and can be performed in a cost-efficient manner. Only the preparation of the slides requires a high-precision dispenser, but this step can be outsourced to LXRepair or other specialized manufacturer that produce tailored materials. This equipment may be more expensive than the one used in classical cell-free methods, but we experienced a clear economy of experiment time with the Next-SPOT assay, which considerably balances this drawback. LXRepair developed semi-automatic procedures that allow “medium-throughput” analyses. The assay is not yet comparable to high-throughput screening immunofluorescent platforms (Garty *et al.*, 2016; Lee *et al.*, 2019), but promising miniaturization work is ongoing to further extend its performance. Besides, even though such platforms considerably lower the cost per sample in population studies, few labs can afford their implementation.

Finally, our experience shows that methods may provide different results, but this does not mean that any assay is necessarily wrong: DSBR activities are tracked via different markers and reflect different information (Deniz *et al.*, 2016). We clearly observe the absence of scientific consensus regarding the exact mechanisms of DSBR, and any approach suffers internal limitations that can result in analysis bias and inappropriate conclusions. Hence, combining several methods is an appropriate way to validate critical biological conclusion, as shown by numerous examples (Cai *et al.*, 2020; Liang *et al.*, 2018; McKay *et al.*, 2019; Schrank *et al.*, 2018; Yang and Wang, 2017). For instance, Cai et al. used IF to estimate DSB

end resection and hypothesize pathway activities, and they confirmed alterations in HR and c-NHEJ activity with *in cellulo* reporter assay (Cai *et al.*, 2020).

Nevertheless, all studies cannot afford to perform labor-intensive experiments. As opposed to detailed mechanistic studies, large-scale population studies are more likely to suffer low biological material availability and demand to select the most appropriate method. Hence, the most suitable set of analyses is dictated by the study's requirement, depending on the application of the DSBR assay.

In the next section, we discuss the biological information that was obtained from these assays and from complementary analyses. More specifically, we detail the impact of doxorubicin treatment in the different cell lines and the effect of repair inhibitors, either alone or in combination with this genotoxic agent.

2. Biological results

2.1. IC_{10} doxorubicin treatment induces limited cellular effects

Doxorubicin is known to induce various cellular effects, including genotoxic, oxidative and energetic stress (Goodman and Hochstein, 1977; Mizutani *et al.*, 2005; Gratia *et al.*, 2012). Doxorubicin-dependent activation of p53 and induction of cell-cycle arrest are clear signs of its disruption of normal cellular processes, and the mobilization of repair regulators such as ATM and ATR support the activation of repair mechanisms following doxorubicin-induced damage (Attardi *et al.*, 2004; Spencer *et al.*, 2008; Forrest *et al.*, 2012; Cruet-Hennequart *et al.*, 2012).

We observed a clear increase in **53BP1 foci levels** in cells treated with doxorubicin (especially M059J and M059K), which confirms that this compound generates DSBs at the IC_{10}, and it can thus be expected to initiate the DDR and the recruitment of repair proteins at the DSBs. Early studies showed that the higher sensitivity observed in M059J cells was due to a DSBR defect rather than increased initial damage levels (Allalunis-Turner *et al.*, 1995), and we found residual foci levels after 24 hours or more to be much higher in M059J, in line with reduced repair activities. Other studies have found a similar effect in HeLa (Nair *et al.*, 2015; Patne *et al.*, 2017). Even though 53BP1 foci formation is less documented in M059J and K cells, it is known that doxorubicin induces DNA damage in these models (Friesen *et al.*, 2008). The formation of DNA damage activates DNA damage sensors such as the MRN complex, 53BP1 and γ-H2AX, thereby initiating chromatin relaxation, post-translational modifications of repair proteins and cell cycle checkpoint activation (Ziv *et al.*, 2006; Oberle and Blattner, 2010; El-Awady *et al.*, 2016). It can be noted that in case of a cycle arrest, DNA repair activities can be lowered, as discussed in subsequent sections.

However, we did not find any significant effect of doxorubicin exposure on the **expression of RAD51**, **PARP1** or **DNA-PKcs**. Doxorubicin was previously shown to reduce overall protein expression and to stimulate that of proteins involved in DSBR, such as Rad51 (Alagpulinsa *et al.*, 2014; Halim *et al.*, 2018; Xu *et al.*, 2019). Friesen *et al*. found an increase in apoptotic signals in DNA-$PK^{-/-}$ cells (M059J) exposed to doxorubicin, including PARP cleavage and caspase-3/8 activation; they did not see this effect in M059K (Friesen *et al.*, 2008). It must be observed that these works are based on high doxorubicin treatment doses (from 160 nM to more than 1 µM), a more than 10-fold higher setting than for our IC_{10} tests. Many studies use acute doxorubicin exposure to trigger a sharp cellular response, just as for high exposure of IR (Attardi *et al.*, 2004; Escobar *et al.*, 2015). Given our experimental setup (low intensity genotoxic stress and strong DSBR inhibition at the IC_{50}), higher amounts of genotoxics were expected to result in excessive cell mortality, as proven by preliminary tests with IC_{20} doxorubicin treatment (data not presented). Excessive mortality introduces experimental artefacts, since apoptotic and necrotic cells do not sustain DNA repair activities; beyond a certain dose of genotoxic agents, the DDR is oriented

towards cell cycle stop and apoptosis rather than DNA repair (Nikoletopoulou *et al.*, 2013; Wang, 2001). Regarding repair inhibitors, the IC_{50} dose was set based on previous results from LXRepair and the CIBEST team suggesting poor inhibition efficiency at low concentrations.

Our results are in line with other studies that relied on lower doxorubicin doses, though in different models. For instance, Alikarami and colleagues saw no effect of doxorubicin on DNA-PKcs expression with a treatment setting quite similar to ours on leukemia cells (Alikarami *et al.*, 2017).

The fact that we observed a doxorubicin-induced genotoxic stress (53BP1 foci) but no significant change in some repair protein levels may be explained by the post-translational regulation of the DDR, in response to stress signals and by protein-protein interactions (Oberle and Blattner, 2010). A low dose of doxorubicin may only modify the recruitment of DSBR actors based on protein phosphorylation or ubiquitination, without completely disrupting the balance of synthetized DSBR proteins. Hence, we looked into protein activity to find a potential effect that would not have been observed by studying expression levels.

We first studied **PARP activity**, since it is involved in the detection of DNA damage, recruitment of DNA repair factors, and regulation of biochemical activities. We focused on PARP-1, for which structure, mechanism of action and biological function are best described among PARP family members. Besides, it is the main PARylation factor in response to DNA damage (Pascal, 2018; Wang *et al.*, 2019). We saw that doxorubicin only poorly affected PARylation activity in all three models, suggesting no PARP-mediated activation of the DDR. Most reports show an increase in PARP activity and expression following doxorubicin exposure (Pacher *et al.*, 2002; Bartha *et al.*, 2011; Wozniak *et al.*, 2013; Wang *et al.*, 2014; Shin *et al.*, 2015) but available data is contradictory (Bowman *et al.*, 2001; Wang *et al.*, 2012; Alagpulinsa *et al.*, 2014). Low dose treatments are rarely reported; studies usually rely on doxorubicin concentrations above 1 µM.

Another capital protein involved in the detection DNA damage and in the recruitment of repair factors, DNA-PK, was investigated as a complement to PARP activity measurements. We chose to study the **phosphorylation of DNA-PKcs** using specific antibodies. Several phosphorylation sites are known in DNA-PKcs, including Ser2056 and Thr2609. Ser2056 is an attested autophosphorylation site *in vivo* (Nagasawa *et al.*, 2017), which has already been used as an indicator of DNA-PKcs activity (Alikarami *et al.*, 2017; Ciszewski *et al.*, 2014; Lafont *et al.*, 2018; Lu *et al.*, 2019; Sowd *et al.*, 2014) and the decrease of phosphorylation is associated to a reduction in various DNA-PKcs activities (Mohiuddin and Kang, 2019). Thus, the absence of Ser2056 phosphorylation that we observed in cells treated with doxorubicin further comforted the lack of a clear stimulation of the DDR at the selected dose.

This absence of stimulation was also seen in DNA repair assays, indicating that repair systems are not particularly activated. We only observed a small increase in repair activities with the ExSy-SPOT test in M059J cells. This effect can be due to the formation of DNA adducts and crosslinks that were shown to be processed by NER (Spencer *et al.*, 2008; Bret *et al.*, 2013); doxorubicin-induced oxidative stress can also lead to the stimulation of BER (Mizutani *et al.*, 2005; Saha *et al.*, 2010; Zhu *et al.*, 2016).

Clearly, the treatment with doxorubicin alone did not result in increased DSBR activities. Such an observation is difficult to interpret and little literature was found on this topic. Doxorubicin has been shown to reduce the repair of IR-induced DSBs (Bonner and Lawrence, 1990), but no other reports were found. It has been shown that high expression of DNA-PKcs can avert the effects of doxorubicin due to increased repair activities (Hansen *et al.*, 2003; Shen *et al.*, 1998; Srivastava and Raghavan, 2015; Sun *et al.*, 2017), but we did not draw the same conclusions since we observed that i) M059J cells with truncated DNA-PKcs did not show particularly high DSBR activities in the presence of doxorubicin and ii) HeLa cells had higher DNA-PKcs levels than M059K but had an increased sensitivity to doxorubicin.

Besides our interrogations regarding treatment doses, it could be that the cellular models are already in a state of replicative or oncogene-induced stress, which overshadows the effect of doxorubicin. However, notable effects of this agent were found upon treatment with repair inhibitors.

2.2. Doxorubicin emphasizes the effect of repair inhibitors

Preliminary tests showed a decrease in the inhibitors' IC_{50} when an IC_{10} dose of doxorubicin was added (data not shown), suggesting that doxorubicin emphasizes the effect of repair inhibitors.

In the absence of doxorubicin, we saw that the three inhibitors that we used globally stimulated 53BP1 foci formation, which is associated with increased genotoxic stress due to the high treatment dose. Cancer cell lines are characterized by an activated replicative and oncogenic stress and a high genomic instability (Yao and Wei, 2014), thus it is not surprising that blocking DSBR proteins results in an increase in DNA damage. Even in the absence of DNA lesions, foci can also be induced by an arrest of the cell cycle resulting from blocked DSB repair factors (Soutoglou and Misteli, 2008; Tu *et al.*, 2013b).

Interestingly, doxorubicin enhanced this effect after 48 hours of treatment in cells exposed to B02, which suggests an increase in genotoxic and/or replicative stress. We described the same effect in M059J and HeLa cells exposed to NU7026; in M059K, doxorubicin induced the delayed answer to DNA-PKcs inhibition after 72 hours of treatment, but the absence of effect at 48 hours was puzzling since the inhibition of c-NHEJ was expected to increase the level of unrepaired DSBs. Only olaparib did not show any particular effect when combined with doxorubicin, maybe due to redundancy in the generated

lesions: olaparib indirectly causes replication forks to collapse resulting in DSBs and replication stress, a mechanism shared with doxorubicin (Bochum *et al.*, 2018; Spencer *et al.*, 2008); IC_{50} olaparib treatment alone results in high foci levels, that are not significantly impacted by the additional IC_{10} doxorubicin treatment.

Strikingly, NU7026 had a clear effect on the **expression and/or activity** of RAD51, DNA-PKcs S2056 and PARP in HeLa and M059K only when cells were treated with doxorubicin. To a lesser extent, doxorubicin also emphasized the impact of RAD51 and olaparib treatments. In a similar way, the sharpest effects in BER/NER activities were seen between 'Dox' and 'Dox + repair inhibitor' treatments, in all cell lines. These results suggest that the treatment with doxorubicin makes cells more sensitive to repair inhibition. It also shows that the inhibitors impact other activities than DSBR only, as discussed in section 2.5.

Most interestingly, DSBR repair assays showed that the effect of repair inhibitors was modulated by doxorubicin. As demonstrated by the **electrophoretic method**, only the combination of doxorubicin and B02 (not B02 or doxorubicin alone) produced significant inhibitions; a quite similar observation was made with olaparib, especially in HeLa cells. Doxorubicin also modulated the response observed in the presence of NU7026: the inhibitor alone stimulated repair activities, but not when combined with doxorubicin.

Finally, out of eight significant variations noted on the raw **Next-SPOT** data, seven originated from a combined 'Dox + inhibitor' treatment. This cumulative effect is documented for RAD51, DNA-PK and PARP inhibitors that potentiate the antiproliferative action of the DNA damaging agent (Alagpulinsa *et al.*, 2014; Ciszewski *et al.*, 2014; Alikarami *et al.*, 2017; Willoughby *et al.*, 2019; Perez *et al.*, 2020). Our hypothesis is that doxorubicin induces a faint stimulation of DDR proteins and this effect becomes apparent mainly upon strong DNA repair inhibition.

2.3. Information obtained from the different methods: the HeLa example

In this section, we discuss the contribution of Next-SPOT to the understanding of DSBR activities based on HeLa results.

Next-SPOT's raw fluorescence intensity results allowed the comparison of basal repair activities, showing that HeLa cells have higher repair levels than glioblastoma cell lines, except for SSA. The results completed data from the **electrophoretic method**, which drew a similar conclusion on c-NHEJ only.

Basal levels of 53BP1 foci were low, suggesting that these high activities do not originate from high levels of endogenous damage. **Next-SPOT's relative pathway contributions** implied that basal repair activities were mainly operated by c-NHEJ and HR.

Upon treatment with doxorubicin and RAD51 inhibitor B02, the comparison of **treated-to-control ratios** simplified the visualization of the inhibitor's effect. The electrophoretic assay found a decrease in c-NHEJ while no significant effect was seen on Next-SPOT data. However, the **relative contribution** of HR dropped after the treatment while that of SSA was enhanced, thus suggesting the initiation of strand annealing following HR abortion. This is supported both by the requirement of resected ends for SSA and by the strong opposition of HR factors such as RAD51 to the annealing option (Bhargava *et al.*, 2016). Hence, relative pathway contributions shed a different light on some trends that were not significant when looking a raw fluorescence intensity; both measurements provide different information and both are thought to be valuable in the identification of specific enzymatic repair signatures.

The decrease in **RAD51 protein levels** and the **increase in phosphorylated DNA-PKcs** comforted our conclusions by suggesting a reduction of HR and activation of DNA-PKcs. However, we will see that protein levels and activities sometimes provided confusing data compared with DSBR assays.

2.4. Comparison of M059J and M059K: these models display deregulated DSBR activities

2.4.1. DNA-PKcs deficiency impacts cytotoxicity and genotoxicity

We saw that M059J cells are more sensitive to doxorubicin than M059K (lower IC_{10}), which is in agreement with various reports that study topoisomerase inhibition (Guo *et al.*, 2011; Kopa *et al.*, 2020) and other DSB-inducing treatments (Allalunis-Turner *et al.*, 1993; Lees-Miller *et al.*, 1995; Wang *et al.*, 1996).

We observed a similar cytotoxic effect of NU7026 in both cell lines (IC_{50} around 40 µM), which contradicts most studies that investigate DNA-PKcs inhibition in these glioblastoma models: the inhibitor alone is usually reported to impact M059K but not the mutant M059J. For instance, Guo and coworkers observed a decrease in colony formation in M059K cells treated with DNA-PKcs inhibitor NU7441 but not in M059J (Guo *et al.*, 2011). The combined treatment with topoisomerase poisons is usually shown to increase toxicity in M059K, but not in M059J (Hisatomi *et al.*, 2011; Kopa *et al.*, 2020; Liu *et al.*, 2015; Tavecchio *et al.*, 2012), and this observation can be extended to many *PRKDC*$^{-/-}$ cells, which do not express DNA-PKcs (Willoughby *et al.*, 2019). We performed preliminary tests that partly comforted this observation, with a 2-fold decrease in the IC_{50} of NU7026 when combined to doxorubicin in M059K, while the reduction was about 1.2-fold in M059J.

Interestingly, we found that 53BP1 foci formation followed a similar pattern following RAD51 and PARP inhibition in all cell lines, but not after DNA-PKcs inhibition. The abrogation of 53BP1 foci formation in M059K cells exposed to NU7026 was a surprising observation, since we expected damage to occur. This result inspires two comments: firstly, glioblastoma cell lines are known to be particularly resistant to anticancer treatments and DNA repair inhibitors (Atkins *et al.*, 2015; Erasimus *et al.*, 2016; Nagel *et al.*,

2017; Ohgaki and Kleihues, 2005). Secondly, other reports support our observation: Stiff *et al*. observed normal 53BP1 foci formation in M059J but it was abrogated in DNA-PKcs-proficient cells exposed to a DNA-PKcs inhibitor (Stiff et al., 2004). Among possible explanations, NU7026 could inhibit an upstream kinase such as ATM without resulting in additional genotoxic stress (Fok *et al.*, 2019). Alternatively, Reindl *et al*. found that 53BP1 is strongly repressed at the DSB site following the engagement in homologous recombination repair (Reindl *et al.*, 2017). Hence, the low levels of 53BP1 mobilization could signify an intense mobilization of HR factors as a result to the inhibition of c-NHEJ. However, other mechanisms than HR activity are necessarily involved, otherwise the absence of c-NHEJ in M059J cells should conduct to a systematic exclusion of 53BP1. An interesting observation is the fact that the treatment with DNA-PKcs inhibitor NU7026 in M059K cells is the only one that does not lead to an increase in 53BP1 foci and also the only one that induces a significant effect on the Next-SPOT biochip: NU7026 has no impact in M059J and HeLa, while it reduces the NHEJ signal in M059K. Additional experiments, such as kinetic measurements of both 53BP1 foci and repair activities, are required to interpret this observation.

53BP1 has other interactions with factors such as RIF1 and BLM that have variable relationships with HR (Buonomo *et al.*, 2009; Chapman *et al.*, 2013; Gupta *et al.*, 2014); notably, 53BP1 has been shown to mobilize at stalled replication forks and participate in their recovery in a RIF1-dependent manner. This mobilization could explain the formation of 53BP1 foci in M059J cells, and it also supports the sharp increase in foci levels following PARP inhibition in all cell lines, due to an important replication stress.

Finally, doxorubicin alone induced significantly more foci in M059J than when combined with repair inhibitors, which was not seen in other cell lines. No explanation was found to this observation, since M059J is expected to rely extensively on mechanisms such as HR and MMEJ as an alternative to c-NHEJ (DiBiase *et al.*, 2000; Iliakis *et al.*, 2004; Patel *et al.*, 2011; Zhang *et al.*, 2020). Tracking additional DSBR proteins such as γH2AX, RAD51, RPA and RIF1 would be a considerable addition to the elucidation of the mechanisms at stake in this model.

2.4.2.M059J cells operate higher rates of c-NHEJ

A striking result that we obtained with both DSBR assays is the high level of c-NHEJ ligation operated by M059J cells. In addition, DNA repair inhibition globally produced little cellular response in this cell line, which is not commonly found in the literature and calls for further discussion. Many studies rely on M059J's deficiency to assess repair via c-NHEJ, but our results suggest that this cell line has complex repair mechanisms and that special care is required before drawing conclusions in this model.

High levels of c-NHEJ suggest that an inactive DNA-PKcs does not prevent the completion of the ligation process. Possibly, the mobilization of ligation factors such as XRCC4-XLF, PAXX and ligase 4 could result

in the high ligation intensity observed at the basal level in M059J and in other models treated with NU7026. Balmus *et al*. found that XRCC4 and ligase 4, but not DNA-PKcs, mediate a form of toxic NHEJ which operates aberrant chromosome fusions *in cellulo* (Balmus *et al.*, 2019).

In addition, some studies showed that M059J cells, despite lacking an operational DNA-PKcs, retain some V(D)J activity, with a similar expression of signal joints as for M059K (Belenkov *et al.*, 2002).

Cancer cell lines are characterized by a large panel of genomic aberrations, mutations in key regulators of cellular proliferation and epigenetic alterations that result in an increased capacity to sustain selective pressure (Mladenov *et al.*, 2016; Yao and Wei, 2014). M059J cells lack one of the main actors of the dominant repair pathway in normal cells, but they have developed a particular set of skills enabling them to escape cellular safeguards and survive in spite of their high instability. Besides, studies have found a synthetic lethality of both ATM and DNA-PKcs defects (Riabinska *et al.*, 2013) and the fact that M059J cells proliferate with both low ATM level and deficient DNA-PKcs supports the deregulation of their repair activities and their reliance on alternative mechanisms. However, very limited data is available regarding the backup process through which DSBR can alternatively be carried out in M059J. Kang et al. showed that PARP inhibition could promote alt-NHEJ in cells deficient for c-NHEJ (Kang and Yan, 2018), showing that the regulation of DSBR activities in NHEJ mutants is still incompletely described. Besides, Neal and Meek observed no differences in end joining activity in cells that do not express DNA-PKcs compared to cells with inactivated DNA-PKcs, in spite of phenotypic differences (Neal and Meek, 2019). This suggests that DNA-PKcs holds non-catalytic roles, in line with our observation that NU7026-mediated inhibition in M059K does not confer a M059J-like behavior.

2.4.3. Alternative repair processes are involved in both cell lines upon treatment with repair inhibitors

Interestingly, Next-SPOT results showed a higher basal contribution of alternative pathways in M059K compared to M059J and HeLa, which was surprising due to the absence of known DSBR anomaly in M059K cells. The effect of repair inhibitors raised additional questions regarding the regulation of DSBR in the glioblastoma models.

PARP inhibition suggests complex backup mechanisms besides HR in M059J

As opposed to the other two cell lines, the DNA-PKcs mutant showed significant responses in protein expression and activity only after PARP inhibition. This included an increase in RAD51 expression and PARP cleavage, as well as a reduction in PARP activity; potentially, this could indicate a response to the inhibition of a-NHEJ, the increase in cellular stress and a potential shift to HR. Patel et al. reported that BRCA1 knockdown sensitized M059J cells with reconstituted DNA-PKcs to PARP inhibition, but not the

original M059J cells (Patel *et al.*, 2011), which shows that these cells can shift between repair pathways in order to maintain DSBR and it further supports the reliance of M059J on backup mechanisms.

HR activity may be reduced in M059J. Indeed, this cell lines has low ATM levels (Neal and Meek, 2019; Peng *et al.*, 2005), which can impact initiation of HR (Bakr *et al.*, 2015; Golding *et al.*, 2004; Jin and Oh, 2019). Bee *et al*. showed a reduced recruitment of HR factors in M059J, suggesting reduced HR capacity (Bee *et al.*, 2013). This would explain why we did not find any effect of RAD51 and NU7026 on PARP1 cleavage and activity, while olaparib did have an effect. However, DSBR assays revealed no effect of the inhibitors (only B02 slightly reduced aEJ). Hence, it seems that i) additional mechanisms are involved which are not characterized by our assay, and/or ii) the treatment with repair inhibitors affects the regulation of DNA repair in this cell line.

PARP inhibition alters the participation of HR and c-NHEJ in M059K

In M059K cells, the increase in RAD51 expression and the reduction in DNA-PKcs expression were seen following PARP inhibition, which could reflect a mobilization of HR and a reduction of c-NHEJ as a response to the replication stress induced by olaparib. The increase in DNA-PKcs S2056 phosphorylation can be interpreted as an increase in the detection of DNA damage by DNA-PK and it may also underly a competition with HR (Cui *et al.*, 2005; Javvadi *et al.*, 2012; Davis *et al.*, 2014). Still, DSB end ligation as measured by the reference electrophoresis assay collapsed, which highlights a decrease in c-NHEJ. The Next-SPOT assay did not provide any additional information to this assay; only the inhibition of alt-NHEJ was confirmed. The relative contribution of c-NHEJ to the total response increased following PARP inhibition in doxorubicin-treated M059K. Hence, we find two apparently contradictory pieces of information: c-NHEJ is reduced upon treatment with doxorubicin and olaparib, but its relative contribution increases. HR was expected to be the dominant pathway involved following this treatment in M059K, but its completion depends on cell cycle phase and it may not be excluded that DNA-PK mobilizes DNA ends following a takeover of KU in the competition with PARP (Paddock *et al.*, 2011; Wang *et al.*, 2006). This hypothesis is supported by the fact that PARP1 was shown to influence the balance between HR and c-NHEJ in the favor of recombination-based repair (Caracciolo *et al.*, 2019; Du *et al.*, 2016), which could result in an enhanced participation of c-NHEJ.

RAD51 inhibition also impacts c-NHEJ but may stimulate backup pathways

RAD51 inhibition did not alter protein expression and activity levels in M059J and it did not impact end ligation activities with the reference electrophoretic assay, but it resulted in an inhibition of the repair mechanism associated with a-NHEJ on the biochip method. In M059K, RAD51 inhibition shared similitudes with PARP inhibition, with a decrease in DNA-PKcs expression and an increase in S2056 phosphorylation and PARP cleavage. The electrophoretic method revealed a sharp decrease in c-NHEJ

activity. Hence, no shift from HR to c-NHEJ occurred; to our knowledge, M059K cells are not known to rely particularly on HR and it is puzzling to observe such a collapse of repair activities in the presence of B02. The Next-SPOT assay confirmed this observation on HR and c-NHEJ but no particular effect was seen on alternative pathways. However, an increase in their relative contribution was seen, as opposed to HR and c-NHEJ for which it dropped. Our hypothesis is that repair activities are sustained by a-EJ and/or SSA following RAD51 inhibition rather than being shifted to c-NHEJ, which is in line with the conclusion of other studies in different cells (So *et al.*, 2019). It is worth noting that the synthesis of a sister chromatid is not required for end resection (Bhargava *et al.*, 2016), thus this shift could occur in any cell-cycle phase.

NU7026 does not clearly inactivate DNA-PKcs and c-NHEJ

NU7026-mediated DNA-PKcs inhibition was not complete, since DNA-PKcs Ser2056 phosphorylation was activated by the inhibitor, in contradiction with usual reports based on ATP-competitive DNA-PKcs inhibitors (Alikarami *et al.*, 2017; Ciszewski *et al.*, 2014; Liu *et al.*, 2015; Okazawa *et al.*, 2013; Tavecchio *et al.*, 2012; Timme *et al.*, 2018; Yang *et al.*, 2016). In addition, NU7026 produced highly variable results in DSBR assays. For instance, Next-SPOT revealed a clear effect of the inhibitor only in M059K cells, while end-joining efficiency was not reduced in HeLa. In this cell line, effects were only seen in protein expression levels. NU7026 is reported to inhibit other PIKKs or structurally related PI3Ks (Fok *et al.*, 2019), which may partly explain our results. However, further investigation is needed to understand the lack of phosphorylation of DNA-PKcs.

2.4.4. The mobilization of repair factors from other pathways may explain c-NHEJ results

The DSBR assays used in this study are based on protein activities that mimic the actual processes at stake *in vivo*, and it is also possible that other factors than c-NHEJ proteins are mobilized in the ligation process. For instance, Lig4 is the main actor involved in DSB end-joining, but Lig1 and Lig3 which take part in other pathways -such as alt-NHEJ, NER and BER (Kaminski *et al.*, 2018; Paul *et al.*, 2013)- may be mobilized if c-NHEJ is deficient. For instance, Lig3 is able to ligate undamaged DSB ends (Conlin *et al.*, 2017) such as the ones formed following *Afl*III digestion. Hence, other factors than typical c-NHEJ proteins may be involved in the rejoining of *Afl*III-induced DSBs in our assays, which would explain the deregulation of NHEJ in M059J cells and the high signal obtained at the basal level in DSBR assays. Some suggestions are made in the next chapter to gain additional insight into this matter.

2.4.5. Different regulations of the DDR are reported in M059J and M059K cells

Finally, a common feature shared by our cellular models is their disruption of cell cycle checkpoints. M059J and K are reported to G1/S checkpoint-deficient (Bee *et al.*, 2013; Holgersson *et al.*, 2005), as well as HeLa cells, due to HPV E6 inactivation of p53 (Hwang *et al.*, 1996; Scheffner *et al.*, 1990). M059K

cells are also G2/M checkpoint-deficient, as opposed to M059J (Bee *et al.*, 2013; Holgersson *et al.*, 2005). This observation partly explains the slower proliferation that we observed for M059J and it also impacts the cellular response to repair inhibitors since the activation of damage checkpoints considerably alters repair activities. As an illustration, early studies showed that M059J cells did not recover from replication arrest while it was the case in M059K and HeLa, suggesting that DNA-PKcs signaling favors repair activities and cell survival (Guan, 2000). Thus, the differences we observed in M059J cells also result from a different regulation of the DDR, not only from the role of DNA-PKcs in the completion of c-NHEJ activity *per se*. More generally, cancer cells display strong deregulations of their repair activities, and our results highlight this perturbation by individualizing specific repair signatures in cells such as M059J.

2.5. Repair inhibitors impact other processes than DSBR

We showed that DNA repair inhibition not only affected DNA repair processes such as HR and c-NHEJ, but we also observed inhibitions in other pathways. Hence, we wondered if the latter were a consequence of the inhibition of the target proteins or if they should be considered as off-target effects.

2.5.1. PARP cleavage and apoptosis

We observed that the levels of native, full-length PARP were not significantly impacted by the treatments. On the other hand, a reduction of PARP activity and an increase in PARP cleavage were seen in HeLa and M059K cells treated with both doxorubicin and repair inhibitors. Such a cleavage usually indicates the induction of apoptotic cell death; it has been shown to be operated by caspases 3 and 7 in vivo, and results in the formation of i) a 89 kDa fragment with reduced enzymatic activity, that does not recognize DNA damage and ii) a 24 kDa fragment containing the DNA-binding domain (Soldani and Scovassi, 2002), which irreversibly binds DNA ends and inhibits repair activities (D'Amours *et al.*, 2001; Soldani and Scovassi, 2002). In line with our data, reports indicate an increase in PARP cleavage following a genotoxic insult combined with RAD51 depletion (Aubry *et al.*, 2020), DNA-PKcs inhibition (Tichy *et al.*, 2014) and olaparib-induced PARP inhibition (Park *et al.*, 2018). Since full length PARP was not significantly affected, it is possible that the increase in PARP cleavage reflects an early induction of apoptotic signals or that a small subset of the cells was engaged into apoptosis. However, the induction of apoptosis is generally associated with a disengagement from DNA repair (Roos and Kaina, 2013) and it could strongly affect our interpretation of repair activities. Further investigation is thus required to determine the extent of apoptotic stress in the treated cells and its potential impact on DSBR activities.

2.5.2.Base and nucleotide excision repair

In HeLa, **RAD51 inhibition** decreased all excision/resynthesis activities studied by the ExSy-SPOT assay. It has been suggested that BER (at least the long patch pathway) is mainly acting in proliferating cells (Mjelle *et al.*, 2015) and it is not excluded that cell-cycle progression is blocked following the inactivation of RAD51. In parallel, PARP activity also decreased, but whether the inhibition of excision/resynthesis activities is due to the role of PARP enzymes in BER (Lavrik, 2020; Noël *et al.*, 2006), to an upstream regulation of the DDR or from a combination of both remains to be established.

BER was not affected in M059K in spite of the reduction of PARP activity, suggesting different regulation mechanisms between M059K and HeLa. In line with other reports, we showed that RAD51 expression is high in HeLa (Chen *et al.*, 2017; Choi *et al.*, 2017) and it is reduced more drastically than in other cell lines, suggesting that HeLa cells are strongly affected by B02. RAD51 inhibition in HeLa cells was shown to induce aberrant replication dynamics, with increased ATR/Chk1-mediated replication stress signaling (Krajewska *et al.*, 2015). We also observed a decrease in NER activities such as the repair of CPD lesions; HR factors were shown to supplement NER (Ma *et al.*, 2013) but RAD51 is not a prerequisite in the completion of these pathways to our knowledge. This supports a strong reliance on HR in HeLa, in which RAD51 inhibition would greatly increase cellular stress and affect all repair activities. In glioblastoma cells, the absence of effect on BER may be due to their previously mentioned resistance mechanisms. In any case, our results show that differential regulations are at stake in the three cellular models. In a similar fashion, only M059K cells presented a decrease in the repair of CisP adducts following PARP inhibition. Such a reduction of platinum DNA-adduct repair capacity has already been described (Olaussen *et al.*, 2013), but we could not explain why it only affected M059K cells.

NU7026 only impacted BER in HeLa, more specifically the repair of 8oxoG. As mentioned earlier, NU7026 may inhibit other proteins than DNA-PKcs, including regulators of the DDR, which could indirectly affect excision/resynthesis activities. An *et al.* showed that DNA-PKcs silencing decreased OGG1 expression in HeLa cells (An *et al.*, 2005), which suggests that the reduction in 8oxoG repair results from an indirect impact of DNA-PKcs inhibition rather than from an non-specific effect of NU7026. It has been mentioned as a consequence of the loss of DNA-PKcs-mediated phosphorylation and has been shown to affect the repair of additional lesions (Powley *et al.*, 2009). No such report was found regarding the glioblastoma models, in which this inhibitor had no effect on excision/resynthesis signals.

We showed that **PARP inhibition** directly affected the repair of 8oxoG, abaS, glycols and etheno, consistent with the role of PARP1 in the regulation and the completion of BER. Besides, an effect was also seen in the repair of CPD-64 photoproducts, in line with previous reports of PARP1's activity in the removal of bulky adducts through NER (Ray Chaudhuri and Nussenzweig, 2017; Robu *et al.*, 2013).

PARP1 and PARP2 also regulate Rad51 assembly and stabilize replication forks that encounter repair intermediates (Ronson *et al.*, 2018). Hence, disruption of PARP activities not only reduces BER activities, but it also leads to the destabilization of RAD51 at damaged replication forks and to uncontrolled end resection, thereby causing DNA damage during replication. As for DSBR, studies show that olaparib can reduce DNA damage repair activity by blocking the cell cycle in G2 phase in a p53-dependent manner (Jelinic and Levine, 2014).

Our conclusions are in line with the global reduction of DSBR activity in cells treated with doxorubicin and the inhibitors. Such a decrease suggests an overall reduction in DNA repair capacity, as observed in cells undergoing intense stress.

2.5.3. Treated cells are thought to experience high replication stress

We did not observe a similar increase in foci numbers in cells treated with B02 or NU7026 and cells treated with PARPi, and we correlate these results with differences in replication stress.

A change from occasional large foci to numerous small nuclear foci after the generation of DSBs is described in the literature (Stiff *et al.*, 2004), particularly in S phase cells after replication blockage and replication fork collapse (Feng *et al.*, 2015; Harrigan *et al.*, 2011; Her *et al.*, 2018; Lukas *et al.*, 2011a). 53BP1 plays an important role in protecting replication forks and in the modulation of cell cycle progression (Her *et al.*, 2018; Wang *et al.*, 2002). Hence, our hypothesis is that olaparib causes extensive replication fork stalling, resulting in a strong replication stress that blocks a high proportion of cells in early S phase.

B02 and NU7026 treatment resulted in lower levels of 53BP1 foci in HeLa and/or M059K, which would indicate a milder replication stress allowing a subset of cells to progress until the next G1 phase. However, the reason why such a mild stress would result in PARP cleavage and in the abrogation of DSBR capacity remains unclear. Some reports suggest that levels of damage that trigger apoptosis may not result in a particular alteration of the immunofluorescent profile (Torudd *et al.*, 2005). Additional tests are required to draw more robust conclusions, as detailed in the next chapter.

2.6. Comparison of cellular and "*in vitro*" treatments

Interestingly, the investigation of *in vitro* addition of repair inhibitors in cell extracts rather than in live cells provided completely different results whether comparing raw data or relative pathway contributions, as illustrated in table 16.

The high concentration of inhibitors that we used for *in vitro* treatments led to a very high inhibitor-to-target protein ratio, which favored direct drug-protein interactions, and it is very unlikely that our

compounds failed to exert their inhibitory effect. On the contrary, off-target inhibitions could have been expected to occur and to result in the inhibition of all signals on the chip, which was not observed.

Our results show that the inhibition of DSBR proteins during the experiment (*in vitro* inhibition, in cell extracts) does not systematically inhibit the processes measured on the chip, suggesting that an orchestrated cellular response is required for the inhibitor to have an observable effect. For instance, B02 had much less significant effects when incubated with nuclear extracts *in vitro*, suggesting that blocking RAD51 on the chip does not prevent repair reactions to occur. On the contrary, blocking this protein within the cells leads to an inactivation of HR that considerably modifies the balance in pathway activities.

Table 16. Variation of the relative pathway contributions obtained with cellular or in vitro treatment with repair inhibitors.

Significant stimulations and inhibitions are indicated in red and blue, respectively. Brackets specify if the effect was observed only in control or doxorubicin-treated cells; when unspecified, a significant effect was observed in both cell populations. Data originates from Next-SPOT experiments detailed in the "Results" chapter and in appendix 20.

In cellulo	Dox				B02				NU7026				Olaparib			
	HR	NHEJ	SSA	a-EJ	HR	NHEJ	SSA	a-EJ	HR	NHEJ	SSA	a-EJ	HR	NHEJ	SSA	a-EJ
HeLa	-	-	-	-	(Dox)	-		-	(Ctl)	-	-	-	-	(Dox)	-	(Dox)
M059J	-	-	-	-	-	-	-	-	-	-	-	-	-	-	-	-
M059K	-	-	-	-	(Dox)				-	-	-	-	-	(Dox)	-	-
In vitro	**Dox**				**B02**				**NU7026**				**Olaparib**			
	HR	c-NHEJ	SSA	a-EJ	HR	c-NHEJ	SSA	a-EJ	HR	c-NHEJ	SSA	a-EJ	HR	c-NHEJ	SSA	a-EJ
HeLa	-	-	-	-	-	-	-	-		-			-	-	-	-
M059J	-				-	-	-	-	-	-	-	(Dox)	-	-	-	-
M059K	-				-	-	-	-		-	(Ctl)		-	-	(Ctrl)	-

It also seems to participate in the appearance of a cellular stress that impacts processes such as cell cycle progression, thereby further impacting repair activities. In a similar fashion, PARP inhibition *in vitro* does not appear to significantly impact repair processes, which can be attributed to a lack of trapping on DNA and a reduction of PARP signaling inhibition. A notable observation is that inhibitors added *in vitro* spend less than two hours in contact with nuclear extracts, which may not be sufficient for a full alteration of DDR activities. Additionally, activation of the DDR was often required in cells to observe a significant effect of the inhibitors; the inhibitors did not exert the same effects *in vitro,* even in extracts from cells exposed to doxorubicin. *In cellulo* treatments affect reaction cascades that allow the modulation of the cellular response, while *in vitro* inhibitions mainly act through direct interactions, with an immediate effect on the measured repair activities.

Although further investigation is required, our results suggest that the direct inhibition of the targeted proteins represent only a small part of the total cellular response. Most of the final effects observed in

cells seem to result from the modification of the balance between repair activities and the activation of non-DSBR process rather than from the direct effect of blocking a single step of a repair pathway. Most importantly, cultured cells may activate cell cycle checkpoints and be retained in a given phase, while this effect is less likely to be seen with *in vitro* treatments since cells experience lower levels of stress. The results suggest that PARP and RAD51 are not direct players in the biochemical mechanisms at stake in the reaction that occurs *in vitro* on the chip, although their inhibition resulted in strong biological effects in live cells.

A notable exception is the effect of NU7026, which was more pronounced following *in vitro* treatment. This result suggests that DNA-PKcs inhibition leads to rapid effects that are counterbalanced *in cellulo*. DNA-PKcs is involved in a large panel of cellular activities, including the direct recruitment of repair proteins. Considering that c-NHEJ is a rapid process, we propose that a high concentration of NU7026 favors end resection and the mobilization of HR factors such as RAD51 at the DSB ends, in a process that could also oppose alt-NHEJ and SSA. Alternatively, the inhibition of other kinases due to the high concentration of NU7026 may deactivate other effectors of the ligation. Indeed, this molecule is an ATP-like molecule that may block other active sites than that of DNA-PKcs. But then, the reason why other repair mechanisms are not further affected remains unknown. Little effect is found in NU7026-treated M059J extracts, which contradicts this hypothesis. We looked for documented off-target effects and found that high doses of NU7026 reduce CHK1 phosphorylation and ATR activity and may also inhibit ATM (Bischoff *et al.*, 2020; DeLoughery *et al.*, 2015), while direct off-target effects are not clearly described for B02 (Alagpulinsa *et al.*, 2014) and olaparib (Antolin *et al.*, 2020).

Overall, we conclude that this *in vitro* protocol provided less straightforward data that the cellular treatments with the inhibitors. However, it raised interesting questions that could disserve further investigation. Optimizations could allow more understandable results to be obtained and we suggest reducing concentrations of DMSO and inhibitors in the *in vitro* assay to better conclude on the mechanisms at stake on the chip.

CHAPTER 5 – PROSPECTS

Our study illustrates the complexity of DNA repair systems and we showed that some results deserve further investigation for us to conclude on the mechanisms that are described.

1. Improvement prospects

1.1. Alternative treatment procedures

Treating our cellular models with an IC_{10} dose of doxorubicin alone did not particularly activate DSBR pathways. It is not excluded that this observation was due to the choice of the DNA damaging compound, and we considered using other agents; IR or other radiomimetic molecules are currently used in the clinic and damage DNA through different mechanisms than doxorubicin. We investigated another clastogenic agent, bleomycin, which is used for the treatment of head and neck cancer, testicular carcinoma and Hodgkin's lymphoma (Brandt and Gerriets, 2021). However, it had a much lower cytotoxic effect than doxorubicin (data not shown) and we did not lead further investigations. Another possibility would have been to use higher doxorubicin exposure and compare the effect of acute and long exposure (48 hours), and to combine both treatments to lower amounts of repair inhibitors (IC_{20}). This would probably allow the induction of a stress that would originate from the genotoxic of doxorubicin rather that from the inhibitors, as we suspect in this study. However, such tests remained only to the preliminary step (1 replicate) and were not presented here. Alternatively, all cell lines can be tested to the same dose of genotoxic and/or inhibitors, as done in many studies referenced in the previous chapter. This approach simplifies treatments but it ignores the specific response of each cell line. In our case, NU7026 had a similar toxicity in the DNA-PKcs-deficient cell line M059J as in the other models, so we preferred to use the IC_{50}. Another approach that was considered for doxorubicin was to set treatment dose according to the observed genotoxic effect rather than on cytotoxicity. Indeed, the latter can originate from various mechanisms, including secondary metabolites and oxidative stress. Considering our focus on DSB formation, setting the dose according to the increase of damaged-induced foci is an interesting alternative that is still uncommon in the literature.

1.2. Further investigation of DSBR activities

We showed that our repair inhibitors provided complex results and using additional molecules inhibiting the same targets or other actors of the same pathways would be a valuable complement to our study.

Additional inhibitions

For instance, DNA-PKcs inhibitors has a similar mechanism of action as NU7026 but is sometimes reported to be more efficient; for instance, Yang *et al*. observed a greater reduction in S2056 phosphorylation of DNA-PKcs (Yang *et al.*, 2016) and measuring repair activities with this compound

could shed a new light on our data. Besides, debate is still ongoing regarding the exact role of the different phosphorylation clusters of DNA-PKcs, and it seems appropriate to investigate T2609 besides S2056 to validate our estimation of DNA-PKcs activity. Otherwise, dedicated assays as presented by Lafont *et al*. could validate or refute our observations (Lafont *et al.*, 2018).

SCR7, for its part, is a Lig4 inhibitor that potentiates the effect of doxorubicin on HeLa cells (Kumar *et al.*, 2017) and could be valuable in order to block the ligation step of c-NHEJ, which could for instance help understand the origin of high ligation activities in M059J cells. In a similar fashion, inhibiting upstream (MRN complex, ATM) or downstream (XRCC4, POLθ) factors would considerably refine our data and provide insights into the mechanisms measured by Next-SPOT. More specifically, the recent identification of a novel POLθ inhibitor offers interesting perspectives for the investigation of the balance between aEJ, SSA and HR on the chip (Zhou *et al.*, 2020). Additionally, we showed that PARP inhibition induced strong cellular effects, which may originate from PARP trapping on besides the inhibition of the catalytic activity. Hence, the investigation of PARP inhibitors with different inhibitory and PARP trapping potency would help discriminate between these two distinct effects. Molecules such as talazoparib are reported to have a much higher trapping potency as olaparib for a similar inhibitory activity (Min and Im, 2020).

Nevertheless, all proteins do not have known inhibitors and small molecules may have undesirable effects. Immunodepleting cell extracts is a straightforward *in vitro* option (Audebert *et al.*, 2004, 2006) that would complement current results with repair inhibitors and help identify the role main DSBR proteins such as KU, RAD51 or XRCC4 in the signals obtained from the Next-SPOT assay. As an alternative, interrupting protein expression with siRNAs or using genome editing tools can be considered to address these issues.

Complementary methods

Aside from PARP and DNA-PKcs, we did not identify *in vitro* assays that directly measure protein activity, which was a valuable information to assess the effect of our treatments. Nevertheless, we suggest immunofluorescence as an indirect approach to assess the recruitment of other factors at the DSBs; alternatively, measuring phosphorylation levels by western blotting as we did for DNA-PKcs would provide additional information. We focused our IF study on 53BP1 for it is reported to be slightly more specific for DSBs as γ-H2AX (Goodarzi and Jeggo, 2012). Nevertheless, co-staining with an anti-γ-H2AX antibody would have allowed i) to validate identified foci as indicators of DSBs, ii) a better description of replication stress, since γ-H2AX is also found at ssDNA regions (Rothkamm *et al.*, 2015) and iii) a more neutral analysis as with 53BP1, that orients repair towards c-NHEJ. In addition, tracking foci formation of upstream (RIF1, DNA-PK, MRN complex) or downstream (RAD51, RAD52, XRCC4, BRCA1) factors

would provide clues regarding repair pathway choice and would refine other results such as expression levels. RAD51 foci formation is used as an indicator of HR-mediated repair proficiency by the D'Andrea lab (Hill et al., 2018) and it can identify major HR deficiencies (Naipal *et al.*, 2014). The comparison with HR signal obtained with Next-SPOT would provide a better understanding of the effect of DSBR inhibitors. Direct staining of repair proteins on the chip will also be experimented in order to investigate the mobilization of repair factors *in vitro*. Another option is to use reporter-based assays to complement Next-SPOT data. As opposed to IF approaches, such methods inform on the religation of specific DNA sequences, which would provide details on the exact repair activities operated by the models we used.

In addition, a better understanding of the cellular response to repair inhibition could be gained from more detailed timelapse experiments. Repair activities were only measured 48 hours following treatment, but the evolution of the balance between repair activities all along the treatment represents an interesting piece of information, especially if combined with 53BP1, RAD51 and DNA-PK foci staining.

As presented, we set up an alternative DSBR method with repair inhibitors added *in vitro*. Our data shows that further optimizations are required using a range of concentration of DMSO and inhibitors. As part of the validation process, it is also required to assess protein activities in extracts incubated with inhibitors (for instance PARP activity after incubation with olaparib), in order to validate treatments before drawing conclusions on the cellular response. Notably, it is not sure whether repair inhibitors have an immediate effect and kinetic studies are required to determine the appropriate treatment setting. This protocol may not be adapted to all kinds of repair inhibitors, since *in vitro* inhibition requires a direct interaction with the target enzyme, which can for instance be prevented if the protein is trapped within a complex. Additionally, activation of the DDR may be required for the inhibitor to have a biological effect. However, the interest of the *in vitro* treatment lies in a simplified evaluation of numerous inhibitors while requiring a much lower cell culture workload than cellular treatments, which could be highly beneficial for screening purposes.

1.3. Cell cycle and cellular stress

Most of all, information regarding the evolution of the cell cycle in the different cell lines after each treatment would be a major addition to our data. Indeed, our models have different checkpoint deficiencies and tracking the progression of the cell cycle would provide clues regarding pathway activities, for instance if a restoration of G1/M blockage is seen. Besides, comparing the extent of G2/S blockage would inform on the extent of the replication stress. Such tests could be performed by measuring DNA content in flow cytometry or by assessing EdU uptake or cyclin expression in immunofluorescence. In addition, it was shown that the transmission of DNA damage can result in weak points in sister cells, causing a strong mobilization of 53BP1 in the subsequent G1 phase and resulting

in the formation of intense foci called “nuclear bodies” (Lukas *et al.*, 2011a; Spies *et al.*, 2019). Information on cell cycle progression would help conclude on the nature of the foci we observed, for instance in HeLa cells treated with doxorubicin.

Our results call for further investigation of the mechanisms triggered by the inhibitors, including the extent of apoptotic stress. Measuring caspase expression or annexin V levels would be an appropriate way to verify the extent of apoptosis stress and to adjust treatment doses as a result. Additionally, we found that repair inhibitors inhibited excision/resynthesis activities on plasmids carrying lesions processed by BER or NER and an analysis of oxidative stress levels (for instance using dihydrorhodamine 123) in treated cells would further document the biological effects of the inhibitors that we used.

2. Modelling biological processes

2.1. Biological models

We studied three cellular models of different origin, with specific genotypic and phenotypic characteristics. Nevertheless, other cell lines have a good potential for the investigation of DSB repair. Other candidates include breast cell lines HCC1937 (BRCA1-mutated) and MCF-7 (wild-type), as well as the BRCA2-deficient Capan-1 which originates from pancreatic tissue. These models are extensively used for to study the biological impact of HR deficiency and they are expected to provide valuable information regarding the balance between DSBR activities upon treatment with repair inhibitors.

M059J and M059K cells were established from a heterogenous tumor and we show that they present dissimilarities and that treatment of M059K cells with NU7026 does not simply confer a M059J-like behavior. Some authors complemented M059J cells with a wild-type copy of the *PRKDC* gene (Hoppe *et al.*, 2000) and it would be interesting to test c-NHEJ activity in such models or in KO M059K cells. In general, the generation of KO cell lines would be an alternative solution to the use of deficient cells that have developed complex survival mechanisms. KO cells can provide radically different results from cells treated with repair inhibitors (Ma *et al.*, 2012) and they consequently represent valuable models for the description of DSBR activities.

Our work was based on cell lines that represent a convenient kind of biological material: they proliferate rapidly, do not differentiate or senesce and they are described by previous literature, making them valuable model for preliminary experiments. Cancer cell lines are known to harbor extensive genomic aberrations and to possess deregulated activities that impact their phenotype, which is also the case in most tumors. However, additional studies using primary cells would provide a better representation of cellular responses in normal cells, which can be valuable in some applications discussed in subsequent

sections. Cells isolated from patients with known DSBR characteristics can be expected to be used as a validation material to test a subset of repair inhibitors and genotoxics on the chip.

2.2. Simulation of DSBs

The use of *Afl*III for the generation of the DSB only roughly mimics the lesions formed in vivo by DNA-damaging agents such as IR or radiomimetic molecules (Pastwa *et al.*, 2003). However, this artificial model of lesion is high reproducible and sequence-specific, whereas other DNA-damaging agents can generate random lesion on the plasmid, hence considerably enhancing assay variability.

Besides, we currently study a single kind of DNA ends (4-nucleotide, 5' cohesive ends). This configuration represents a potential substrate for various pathways, including alt-NHEJ (Audebert *et al.*, 2004). However, since the configuration of the break influences repair outcome, we may favor the recruitment of specific factors and thus introduce a bias in the estimation of pathway activities. Hence, a tempting improvement of our biochip is the addition of other kinds of lesions, using different restriction enzymes as illustrated in figure 98. For instance, using digested plasmids with long ssDNA ends would allow the validation of resection-based mechanisms by limiting the recruitment of c-NHEJ factors at the lesion. This can be combined to the use of other plasmids in order to challenge the current biochip setting based on fully homologous plasmids. A change in homology is likely to impact the recruitment of HR factors as well as the unveiling of microhomologies following plasmid resection. Hence, we would gain insights on the mechanisms currently attributed to each signal measured on the chip and considerably refine the final analysis. A few experiments have been performed using a linearized pGlow-TOPO plasmid, but too few tests have been performed so far to draw conclusions. In addition, lower repair yields can be expected from blunt ends and this substrate has not been tested yet.

Tailored end configurations could also be used to measure end processing activities. For instance, Lig4 was shown to directly bind DSB ends with helix-distorting 8-oxoG lesions or mispairs, and to guide end-processing choices (Conlin *et al.*, 2017). Measuring the ligation of a labelled linear plasmid onto a damaged oligonucleotide printed on the chip could thus indirectly inform on c-NHEJ-dependent end processing. Besides, we focused on the incorporation of labelled dCTPs, but the addition of other labelled deoxyribonucleoside triphosphates could add partial information regarding the length and fidelity of repair activities.

terminus configurations	ends	mechanism
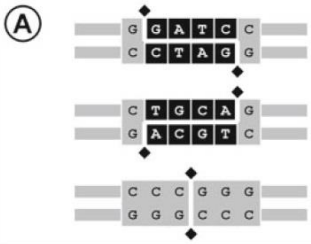	5'-coh. 3'-coh. blunt	accurate ligation
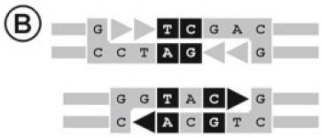	5'/5' 3'/3'	accurate NHEJ: overlap of anti-parallel ends
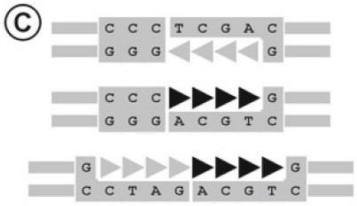	bl/5' bl/3' 5'/3'	accurate NHEJ: fill-in of abutting ends
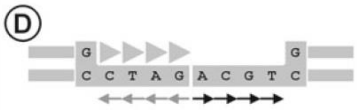	any	inaccurate NHEJ: blunting of 5' or 3' ends in any configuration
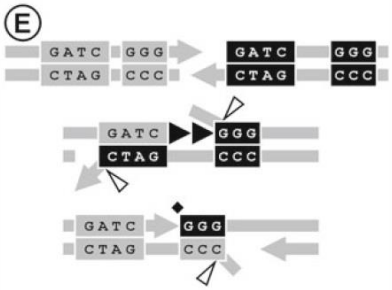	any	inaccurate NHEJ: μhom-SSA μhom priming μhom ligation

Figure 98. Candidates of end configurations to be added on the biochip. Various DSB termini are induced by different restriction enzymes, leading to the mobilization of different repair mechanisms.
Complementary base pairs are indicated by white letters on black ground. Adapted from Pfeiffer and coworkers (Pfeiffer et al., 2014).

3. Applications

In conclusion, this section reviews a set of current research questions and clinical needs in the field of DSBR, and we show how functional assays like Next-SPOT represent valuable tools to address these questions.

3.1. Mechanistic studies

Functional tests have direct application in mechanistic studies, to i) describe the interactions between DSBR factors, ii) participate in the identification of novel players in DSBR, iii) investigate the kinetics and sub-cellular location of DSBR and iv) describe the regulation of DSBR across different individuals, tissues or cell types. Next-SPOT does not yet provide the same degree of information as other cell-free assays, that can for instance recover the sequence of rejoined DSBs to describe the fidelity of the repair process. However, it can be used to evaluate DSBR capacity in response to the inactivation of DSBR proteins, thereby informing on the interaction between repair factors. It can be a good complement to immunofluorescent results, which are commonly used to track the phosphorylation of DSBR and DDR factors (Kurashige *et al.*, 2016), the localization of repair activities (Cowell *et al.*, 2007) and protein-protein interactions (Li *et al.*, 2011). Further developments on our biochip could be most useful to quickly compare the activity of DSBR proteins on a large panel of DNA substrates.

3.2. Biomonitoring, toxicology and identification of vulnerable populations

A broad spectrum of environmental, occupational and lifestyle factors are known or suspected to increase DSB formation and impact repair activities. Nevertheless, the effects of factors such as environmental pollutants or long-term drug intake are still incompletely described. Functional DSBR assays would be useful in environmental and pharmacological toxicology to better apprehend the biological processes triggered by such exposures, to evaluate the risk of disease and provide health agencies with the information required for the establishment of sanitary guidelines in exposed populations. In this context, our Next-SPOT assay is an appropriate alternative to various functional assays**.** The comet assay identified genotoxic compounds, tracked lesion levels and investigated intra- and inter-individual variations in repair capacity, but mostly in BER and NER (Azqueta *et al.*, 2019; Collins *et al.*, 2014; Grover *et al.*, 2003; Nikolova *et al.*, 2017); the biochip approach may be an appropriate alternative to focus analyses on DSBR, since comet results suffers low specificity for these lesions and are limited by high variability (Banath *et al.*, 1998; Trzeciak *et al.*, 2008). Next-SPOT could participate in the identification of specific repair signatures in aging populations, thereby complementing other studies that established an inverse correlation between age and DSBR proficiency in blood lymphocytes (Garm *et al.*, 2013); such information can for instance underlie an increased vulnerability to toxic agents.

γ-H2AX staining was used to identify genotoxic compounds (Khoury *et al.*, 2020; Kopp *et al.*, 2019) and it could serve as a biodosimetric tool to assess accidental radiation exposure (Chua and Rothkamm, 2013). Our biochip could reinforce this data by evaluating relative pathway contributions in reaction to such exposures.

In addition, numerous studies in molecular epidemiology investigate the association between genetic polymorphisms and disease risk; for instance, Wang *et al.* review the impact of various DNA repair polymorphisms (e.g. Arg399Gln in *XRCC1*) on the risk of head and neck cancer and the relationship with drinking or smoking status (Rossner *et al.*, 2015; Wang *et al.*, 2013), but functional assays describing DSB repair capacity could be valuable tools to link such polymorphisms to their phenotypic consequence. In this regard, it still seems that high-throughput IF methods have a most promising potential than Next-SPOT to perform rapid screenings in numerous individuals (Heylmann and Kaina, 2016; Nelson *et al.*, 2017).

3.3. Novel biomarkers in oncology

DNA repair anomalies acquired by cancer cells throughout their evolution can result in increased reliance on backup repair processes that can be targeted to trigger cell death following exposure to DNA damaging agents such as Dox, CisP or IR. Predictive biomarkers such as *MGMT* silencing (Butler *et al.*, 2020) or *BRCA*1/2 status (Hoppe *et al.*, 2018) are related to DNA repair activities and help determine an appropriate therapeutic option (temozolomide and olaparib, respectively). However, particular repair profiles are not systematically identified by genotyping approaches, due to complex survival mechanisms and to the incomplete understanding of DNA repair systems (Abad *et al.*, 2020). Functional assays, on the other hand, measure downstream activities that reflect a series of upstream events, and they are thereby likely to provide highly valuable clues as a complement to current routine methods (Hoppe *et al.*, 2018). In addition, dramatic pathway deficiencies are not systematically found in cancer cells while imbalanced repair activities and altered DDR are almost systematic (Cao *et al.*, 2009; Heyer *et al.*, 2010). Thus, Next-SPOT finds direct applications in the discovery of novel predictive biomarkers, which address two clinical goals: i) to determine if a given patient is eligible for a specific treatment (for instance with DSBR modulators) and ii) to limit toxicities caused by these treatments in normal cells (Begg *et al.*, 2011; Gavande *et al.*, 2016). Such biomarkers would be useful in the most common anticancer therapies, including chemotherapy, radiotherapy and treatments with DNA repair modulators.

3.3.1. Identification of responsive tumors

Our assay on biochip provides clues regarding the balance between different repair pathways, which is likely to be more helpful than assessing global DSBR capacity. Indeed, information such as repair

pathway choice would refine mutation-based stratifications and could thus be used to determine tailored treatment options (Hill *et al.*, 2018). For example, identifying cancer cells with reduced HR activity would help identify platinum salts-responsive individuals (Garutti *et al.*, 2019). Multiplexed reporter assays show a good potential in using repair activities for the prediction of tumor responsiveness and identify the dependence upon specific repair mechanisms (Deniz *et al.*, 2016; Nagel *et al.*, 2017). However, such tests were performed in tumor-derived cell types, PBLs and xenograft models which represent demanding sets of material. On the other hand, cell-free approaches can measure repair activities in biopsies, thereby allowing a more direct tumor stratification. To our knowledge, no assay has been described yet to achieve such analyses with sufficient throughput and sensitivity, two issues that are currently being addressed by the optimization of Next-SPOT. The use of IF techniques is reported both on biopsies and surrogate cells but their description of functional, pathway-specific activities remains incomplete (Asakawa *et al.*, 2010; Willers *et al.*, 2015). Surrogate tissues such as blood lymphocytes can produce conflicting results (Willers *et al.*, 2015) additional methods may be required to complement current data.

As an illustration of current clinical needs, resistance to PARPi in HR-deficient tumors represents a case-study. Synthetic lethality induced by PARP inhibition can be hindered by *de novo* resistance mechanisms in a subset of tumors (Trenner and Sartori, 2019; Wurster *et al.*, 2016; D'Andrea, 2018), and extensive research investigates potential biomarkers compatible with real-time decision-making (Vigneron *et al.*, 2020). Functional data regarding tumoral DSBR activities would help determine the most appropriate combination of synthetically lethal treatments (Lord and Ashworth, 2017). RAD51 foci scoring has proven its interest for the identification of HR deficiencies in breast cancer biopsies (Naipal *et al.*, 2014). It was also reckoned to be more relevant than other techniques to stratify tumor biopsies in a study using IF, reporter methods and a radial chromosome assay (Wurster *et al.*, 2016). Nevertheless, the high variability in foci scoring across different studies still reduces the standardization of this method (Hoppe *et al.*, 2018), and it would be most interesting to compare RAD51 staining to Next-SPOT results on the same samples to prove our biochip's potential as an alternative method.

3.3.2. Limitation of treatment-induced toxicities

Anticancer therapies are known to cause a large panel of short- to long-term adverse effects, which can be irreversible; these effects are influenced by the kind of therapeutic agent and by individual sensitivity to the treatment (Barnett *et al.*, 2009; Berkey, 2010; Griggs, 1998; Nurgali *et al.*, 2018; Soussain *et al.*, 2009). Variations in DSBR capacity in healthy and cancerous cells have been show to impact the risk of treatment failure and the occurrence of side effects, especially in radiotherapy (Chistiakov *et al.*, 2008;

Gavande *et al.*, 2016; Sakata *et al.*, 2007). Hence, anticipating a patient's response to the therapy while optimizing anti-tumor effects would be a major step forward in the reduction of negative outcomes. Currently, most functional assays that aim at assessing radiosensitivity are IF methods, due to short the response time, high sensitivity (which enables the analysis of biologically relevant doses of genotoxic agents) and high throughput of this approach (Borràs *et al.*, 2015; Chua and Rothkamm, 2013; Ivashkevich *et al.*, 2012; Rothkamm *et al.*, 2015; Rübe *et al.*, 2008). Even though a poor predictive value was found in past *in vitro* studies (Olive *et al.*, 2008; Werbrouck, 2009; Werbrouck *et al.*, 2011), more recent reports correlate patient radiosensitivity with residual γ-H2AX and the rate of foci loss in PBLs (Herschtal *et al.*, 2018; van Oorschot *et al.*, 2016; Sharma *et al.*, 2015b) and encouraging studies show an improvement in the prediction of IR induced acute toxicities (Pouliliou *et al.*, 2015). Phosphorylated ATM is also investigated as a complement to IF assays that track DSBR actors (Berthel *et al.*, 2019a; Pereira *et al.*, 2018; Vogin *et al.*, 2018).

It may be noted that analyzing several individual factors at a time, even in a high-throughput setting, may only partially reflect the global endpoint activity that results from their interaction. Some recent studies started investigating regulators of DSBR besides repair effectors themselves (Cai *et al.*, 2020). Alternatively, LXRepair is currently involved in several clinical studies that look for correlations in DSBR signatures and treatment outcome; the exact biochemical mechanisms occurring on the chip are still unknown, but we showed that variations in fluorescent signals can reflect deregulations in DSBR capacity. These signals make up a unique DSBR signature and its comparison of across numerous patients provides promising results for the identification of specific patient groups (data not shown).

The development and optimization of functional assays face important clinical constraints: assay calibration is a long process that requires scarcely available biopsies (Hoppe *et al.*, 2018; Lambin *et al.*, 2013). As an alternative, organotypic and primary cultures produced encouraging results in the last few years (Hill *et al.*, 2018) but further efforts are necessary for functional methods to reach their full potential as predictive assays (Berthel *et al.*, 2019b).

3.4. Drug development

In the last 20 years, molecules that influence DNA repair have received growing interest, especially for the development of anticancer treatments, and numerous modulators of DSBR are placed on the market or under evaluation in clinical trials (Biau *et al.*, 2019; Brown *et al.*, 2017; Gavande *et al.*, 2016; Hu *et al.*, 2021; Mehta *et al.*, 2021), but aside from direct clinical applications, functional DSBR assay also have direct applications in biomolecular screening. Screening compounds libraries can refine the activities of compounds that impact DSBR but it can also unveil novel effects in molecules that were not identified as modulators of repair processes (Goglia *et al.*, 2015; Tay *et al.*, 2020; Yu *et al.*, 2015). Secondly,

functional assays can help guide the optimization of identified hits by providing criteria to compare their effects on cellular activities. Finally, a better understanding of the drug's mode of action is highly valuable for an improved therapeutic outcome; anticipating adverse effects is also a critical issue to prevent additional costs and reduce the risk of failure in clinical trials (Fogel, 2018; Mohs and Greig, 2017).

Various examples illustrate the potential of functional DSBR assay in the identification and development of novel therapeutic options, using immunofluorescence (Dertinger *et al.*, 2019; Surovtseva *et al.*, 2016), the comet assay (Tay *et al.*, 2020; Weingeist *et al.*, 2013), cell-free approaches (Ray *et al.*, 2020) or reporter methods (Goglia *et al.*, 2015). The advantages of Next-SPOT (multiplexing, diversity of the biological materials, satisfying throughput) could be beneficial to the biomolecular screening of active molecules performed by academic laboratories or companies as part preclinical studies.

CONCLUSION

All along this research project, we adapted two DSBR assays to measure repair activities at the basal level and in response to genotoxic stress.

First of all, assay setting-up is a critical step that determines subsequent biological results; the development of the chip was performed in parallel to biological tests and additional analyses such as cell-cycle tracking are still required. Hence, our data does not confirm or refute the initial working hypotheses that were elaborated based on the literature and previous results from LXRepair, regarding the description of pathway activities. However, we show that the c-NHEJ results on the biochip are in line with our reference assay and that Next-SPOT provides additional data with a much higher throughput.

We found a deregulation in repair activities in our cellular models, as illustrated by M059J cells that operate DSB end ligation through c-NHEJ in spite of their reportedly lower DSBR activity. Our models represent a preliminary evaluation of Next-SPOT's ability to track various repair activities and other cell lines or biological materials are to be tested to further understand our results. KO and/or primary cells represent interesting candidates to this end.

Interestingly, we did not observe any significant Dox-induced stimulation of DSBR activities, apart from an increase in 53BP1 foci levels. This contrasts both with the literature and with previous studies performed in our laboratory, that found DDR response to be activated even at low doses of genotoxic agents (George, 2017). However, doxorubicin emphasized the effect of repair inhibitors; a modification of our treatment setting and the analysis of other DSB-inducing agents could provide additional clues.

The general paradigm assumes that DSB formation activates repair pathways and that high levels of damage trigger cell-cycle arrest or even apoptotic cell death. We suspect such mechanisms to be triggered by the inhibitors, leading to an overall decrease in DSBR capacity. Most notably, the inhibition of one pathway (HR for instance) did not result in a clear stimulation of competing mechanisms (in this case, c-NHEJ). However, interesting observations were made when looking into relative pathway contributions. These results emphasize the complexity of the DDR and DSBR processes; cells are highly reactive systems and repair inhibition triggered a set of cellular responses that affected overall pathway activities. Enzymatic signatures reflect a series of upstream events and their interpretation is not straightforward. We hypothesized potential explanations in regard to the scientific literature, but additional tests are needed to better understand the variations we observed. Development is still ongoing and complementary analyses (IF, cell cycle progression, reporter assays) would help explain our data.

It must be noted that all signals did not evolve in a similar fashion across repair pathway and cell lines, which underlines the potential of the biochip approach to describe DSBR activities. Next-SPOT is a multiplexed repair assay, that brings additional data to current cell-free methods and complements other functional tools that usually track a limited number of markers. This method allows us to access numerous pieces of information using less than 10 µg of protein extracts and a publication is planned to describe this novel DSBR technique measuring DSBR activities. However, the assay faces internal limitations, such as a high sensitivity to environmental factors; technical progress is ongoing to reduce experimental variability. Additional tests are required to ascertain the putative mechanisms at stake on each condition, and it can also be argued that the design based on plasmids may not fully reflect the processes that occur in genomic DNA (Cheong, 1996; Lukas *et al.*, 2011b). However, the most direct application of the assay is the estimation of enzymatic activities and their variation across different cells or patients; in this scope, the assay is fully amenable to compare enzymatic signatures regardless of the exact accordance to chromatin-based processes.

The field of DNA repair is an ever-changing landscape, and we showed that it is still only partly understood. Contradictory reports found in the literature are likely to underlie undescribed mechanism and subtle shades in the interaction between repair factors and DDR regulators. Our results are another illustration of the complexity of DSBR systems.

We presented the diversity of prospects that could help improve our study; among them, priorities are the correlation of repair activities with cell cycle phase as well as the investigation of the mobilization of DSBR factors on the chip and through immunofluorescent staining in cultured cells. Application to PBMCs and other cell types (biopsies) could not be performed, but promising results were obtained as part of contractual studies by LXRepair. This encourages further validations for the identification of radiosensitive patients and tumors, thereby providing clinicians with tools to select of the most potent and less toxic treatment options. Alternatively, the assay could be used for as a screening tool for the investigation of current or novel DNA repair modulators.

We sincerely hope that this study will make its contribution to the field of DNA repair and bring an additional tool for the improvement of anticancer therapies.

REFERENCES

- Abad, E., Graifer, D., and Lyakhovich, A. (2020). DNA damage response and resistance of cancer stem cells. Cancer Lett. 474, 106–117.
- Admiraal, S.J., and O'Brien, P.J. (2015). Base excision repair enzymes protect abasic sites in duplex DNA from interstrand cross-links. Biochemistry 54, 1849–1857.
- Afanasieva, K., and Sivolob, A. (2018). Physical principles and new applications of comet assay. Biophys. Chem. 238, 1–7.
- Ahmad, A., Nay, S.L., and O'Connor, T.R. (2015). Direct Reversal Repair in Mammalian Cells. In Advances in DNA Repair, C.C. Chen, ed. (InTech), p.
- Ahrabi, S., Sarkar, S., Pfister, S.X., Pirovano, G., Higgins, G.S., Porter, A.C.G., and Humphrey, T.C. (2016). A role for human homologous recombination factors in suppressing microhomology-mediated end joining. Nucleic Acids Res. 44, 5743–5757.
- Akbari, M., and Krokan, H.E. (2008). Cytotoxicity and mutagenicity of endogenous DNA base lesions as potential cause of human aging. Mech. Ageing Dev. 129, 353–365.
- Akbari, M., Peña-Diaz, J., Andersen, S., Liabakk, N.-B., Otterlei, M., and Krokan, H.E. (2009). Extracts of proliferating and non-proliferating human cells display different base excision pathways and repair fidelity. DNA Repair 8, 834–843.
- Akyüz, N., Boehden, G.S., Susse, S., Rimek, A., Preuss, U., Scheidtmann, K.-H., and Wiesmuller, L. (2002). DNA Substrate Dependence of p53-Mediated Regulation of Double-Strand Break Repair. Mol. Cell. Biol. 22, 6306–6317.
- Alagpulinsa, D.A., Ayyadevara, S., and Shmookler Reis, R.J. (2014). A Small-Molecule Inhibitor of RAD51 Reduces Homologous Recombination and Sensitizes Multiple Myeloma Cells to Doxorubicin. Front. Oncol. 4, 289.
- Alderden, R.A., Hall, M.D., and Hambley, T.W. (2006). The Discovery and Development of Cisplatin. J. Chem. Educ. 83, 728.
- Alexander, J.L., and Orr-Weaver, T.L. (2016). Replication fork instability and the consequences of fork collisions from rereplication. Genes Dev. 30, 2241–2252.
- Ali, A., Zhang, J., Bao, S., Liu, I., Otterness, D., Dean, N.M., Abraham, R.T., and Wang, X.-F. (2004). Requirement of protein phosphatase 5 in DNA-damage-induced ATM activation. Genes Dev. 18, 249–254.
- Alikarami, F., Safa, M., Faranoush, M., Hayat, P., and Kazemi, A. (2017). Inhibition of DNA-PK enhances chemosensitivity of B-cell precursor acute lymphoblastic leukemia cells to doxorubicin. Biomed. Pharmacother. 94, 1077–1093.
- Allalunis-Turner, M.J., Barron, G.M., Day, R.S., Dobler, K.D., and Mirzayans, R. (1993). Isolation of two cell lines from a human malignant glioma specimen differing in sensitivity to radiation and chemotherapeutic drugs. Radiat. Res. 134, 349–354.
- Allalunis-Turner, M.J., Zia, P.K., Barron, G.M., Mirzayans, R., and Day, R.S. (1995). Radiation-induced DNA damage and repair in cells of a radiosensitive human malignant glioma cell line. Radiat. Res. 144, 288–293.
- Allinson, S.L., Dianova, I.I., and Dianov, G.L. (2003). Poly(ADP-ribose) polymerase in base excision repair: always engaged, but not essential for DNA damage processing. Acta Biochim. Pol. 50, 169–179.
- Althaus, F.R., Kleczowska, H.E., Malanga, M., Müntener, C.R., Pleschke, J.M., Ebner, M., and Auer, B. (1999). Poly ADP-ribosylation: A DNA break signal mechanism. Mol. Cell. Biochem. 193, 5–11.

- An, J., Xu, Q.-Z., Sui, J.-L., Bai, B., and Zhou, P.-K. (2005). Silencing of DNA-PKcs alters the transcriptional profile of certain signal transduction genes related to proliferation and differentiation in HeLa cells. Int. J. Mol. Med. 16, 455–462.
- Anderson, C.W., Dunn, J.J., Freimuth, P.I., Galloway, A.M., and Joan Allalunis-Turner, M. (2001a). Frameshift Mutation in PRKDC, the Gene for DNA-PKcs, in the DNA Repair-Defective, Human, Glioma-Derived Cell Line M059J. Radiat. Res. 156, 2–9.
- Anderson, L., Henderson, C., and Adachi, Y. (2001b). Phosphorylation and Rapid Relocalization of 53BP1 to Nuclear Foci upon DNA Damage. Mol. Cell. Biol. 21, 1719–1729.
- Antolin, A.A., Ameratunga, M., Banerji, U., Clarke, P.A., Workman, P., and Al-Lazikani, B. (2020). The kinase polypharmacology landscape of clinical PARP inhibitors. Sci. Rep. 10, 2585.
- Antonelli, F., Campa, A., Esposito, G., Giardullo, P., Belli, M., Dini, V., Meschini, S., Simone, G., Sorrentino, E., Gerardi, S., et al. (2015). Induction and Repair of DNA DSB as Revealed by H2AX Phosphorylation Foci in Human Fibroblasts Exposed to Low- and High-LET Radiation: Relationship with Early and Delayed Reproductive Cell Death. Radiat. Res. 183, 417–431.
- Aparicio, T., Baer, R., and Gautier, J. (2014). DNA double-strand break repair pathway choice and cancer. DNA Repair 19, 169–175.
- Aplan, P.D. (2006). Causes of oncogenic chromosomal translocation. Trends Genet. 22, 46–55.
- Asakawa, H., Koizumi, H., Koike, A., Takahashi, M., Wu, W., Iwase, H., Fukuda, M., and Ohta, T. (2010). Prediction of breast cancer sensitivity to neoadjuvant chemotherapy based on status of DNA damage repair proteins. Breast Cancer Res. 12, R17.
- Atkins, R.J., Ng, W., Stylli, S.S., Hovens, C.M., and Kaye, A.H. (2015). Repair mechanisms help glioblastoma resist treatment. J. Clin. Neurosci. 22, 14–20.
- Attardi, L.D., de Vries, A., and Jacks, T. (2004). Activation of the p53-dependent G1 checkpoint response in mouse embryo fibroblasts depends on the specific DNA damage inducer. Oncogene 23, 973–980.
- Aubel-Sadron, G., and Londos-Gagliardi, D. (1984). Daunorubicin and doxorubicin, anthracycline antibiotics, a physicochemical and biological review. Biochimie 66, 333–352.
- Aubrey, B.J., Kelly, G.L., Janic, A., Herold, M.J., and Strasser, A. (2018). How does p53 induce apoptosis and how does this relate to p53-mediated tumour suppression? Cell Death Differ. 25, 104–113.
- Aubry, A., Pearson, J.D., Huang, K., Livne-bar, I., Ahmad, M., Jagadeesan, M., Khetan, V., Ketela, T., Brown, K.R., Yu, T., et al. (2020). Functional genomics identifies new synergistic therapies for retinoblastoma. Oncogene 39, 5338–5357.
- Audebert, M., Salles, B., and Calsou, P. (2004). Involvement of Poly(ADP-ribose) Polymerase-1 and XRCC1/DNA Ligase III in an Alternative Route for DNA Double-strand Breaks Rejoining. J. Biol. Chem. 279, 55117–55126.
- Audebert, M., Salles, B., Weinfeld, M., and Calsou, P. (2006). Involvement of Polynucleotide Kinase in a Poly(ADP-ribose) Polymerase-1-dependent DNA Double-strand Breaks Rejoining Pathway. J. Mol. Biol. 356, 257–265.
- Audebert, M., Salles, B., and Calsou, P. (2008). Effect of double-strand break DNA sequence on the PARP-1 NHEJ pathway. Biochem. Biophys. Res. Commun. 369, 982–988.
- Avendaño, C., and Menéndez, J.C. (2015). Anticancer Drugs Acting via Radical Species. In Medicinal Chemistry of Anticancer Drugs, (Elsevier), pp. 133–195.
- Azqueta, A., Arbillaga, L., Lopez de Cerain, A., and Collins, A. (2013). Enhancing the sensitivity of the comet assay as a genotoxicity test, by combining it with bacterial repair enzyme FPG. Mutagenesis 28, 271–277.
- Azqueta, A., Langie, S.A.S., Boutet-Robinet, E., Duthie, S., Ladeira, C., Møller, P., Collins, A.R., and Godschalk, R.W.L. (2019). DNA repair as a human biomonitoring tool: Comet assay approaches. Mutat. Res. Mutat. Res. 781, 71–87.

- Badie, S., Carlos, A.R., Folio, C., Okamoto, K., Bouwman, P., Jonkers, J., and Tarsounas, M. (2015). BRCA 1 and Ct IP promote alternative non-homologous end-joining at uncapped telomeres. EMBO J. 34, 410–424.
- Bakr, A., Oing, C., Köcher, S., Borgmann, K., Dornreiter, I., Petersen, C., Dikomey, E., and Mansour, W.Y. (2015). Involvement of ATM in homologous recombination after end resection and RAD51 nucleofilament formation. Nucleic Acids Res. 43, 3154–3166.
- Baldwin, E.L., and Osheroff, N. (2005). Etoposide, topoisomerase II and cancer. Curr. Med. Chem. Anti-Cancer Agents 5, 363–372.
- Balmus, G., Pilger, D., Coates, J., Demir, M., Sczaniecka-Clift, M., Barros, A.C., Woods, M., Fu, B., Yang, F., Chen, E., et al. (2019). ATM orchestrates the DNA-damage response to counter toxic non-homologous end-joining at broken replication forks. Nat. Commun. 10, 87.
- Banath, P., Fushiki, M., and Olive, P.L. (1998). Rejoining of DNA single- and double-strand breaks in human white blood cells exposed to ionizing radiation. Int. J. Radiat. Biol. 73, 649–660.
- Banda, D.M., Nuñez, N.N., Burnside, M.A., Bradshaw, K.M., and David, S.S. (2017). Repair of 8-oxoG:A mismatches by the MUTYH glycosylase: Mechanism, metals and medicine. Free Radic. Biol. Med. 107, 202–215.
- Barbari, S.R., and Shcherbakova, P.V. (2017). Replicative DNA polymerase defects in human cancers: Consequences, mechanisms, and implications for therapy. DNA Repair 56, 16–25.
- Barnett, G.C., West, C.M.L., Dunning, A.M., Elliott, R.M., Coles, C.E., Pharoah, P.D.P., and Burnet, N.G. (2009). Normal tissue reactions to radiotherapy: towards tailoring treatment dose by genotype. Nat. Rev. Cancer 9, 134–142.
- Bartha, E., Solti, I., Szabo, A., Olah, G., Magyar, K., Szabados, E., Kalai, T., Hideg, K., Toth, K., Gero, D., et al. (2011). Regulation of kinase cascade activation and heat shock protein expression by poly(ADP-ribose) polymerase inhibition in doxorubicin-induced heart failure. J. Cardiovasc. Pharmacol. 58, 380–391.
- Bau, D.-T., Mau, Y.-C., Ding, S., Wu, P.-E., and Shen, C.-Y. (2007). DNA double-strand break repair capacity and risk of breast cancer. Carcinogenesis 28, 1726–1730.
- Baxter-Holland, M., and Dass, C.R. (2018). Doxorubicin, mesenchymal stem cell toxicity and antitumour activity: implications for clinical use. J. Pharm. Pharmacol. 70, 320–327.
- Bayr, H. (2005). Reactive oxygen species. Crit. Care Med. 33, S498–S501.
- Beard, W.A., Horton, J.K., Prasad, R., and Wilson, S.H. (2019). Eukaryotic Base Excision Repair: New Approaches Shine Light on Mechanism. Annu. Rev. Biochem. 88, 137–162.
- Bee, L., Fabris, S., Cherubini, R., Mognato, M., and Celotti, L. (2013). The Efficiency of Homologous Recombination and Non-Homologous End Joining Systems in Repairing Double-Strand Breaks during Cell Cycle Progression. PLoS ONE 8, e69061.
- Begg, A.C., Stewart, F.A., and Vens, C. (2011). Strategies to improve radiotherapy with targeted drugs. Nat. Rev. Cancer 11, 239–253.
- Belenkov, A.I., Paiement, J.-P., Panasci, L.C., Monia, B.P., and Chow, T.Y.K. (2002). An antisense oligonucleotide targeted to human Ku86 messenger RNA sensitizes M059K malignant glioma cells to ionizing radiation, bleomycin, and etoposide but not DNA cross-linking agents. Cancer Res. 62, 5888–5896.
- Belyaev, I.Y. (2010). Radiation-induced DNA repair foci: Spatio-temporal aspects of formation, application for assessment of radiosensitivity and biological dosimetry. Mutat. Res. Mutat. Res. 704, 132–141.
- Bennardo, N., Cheng, A., Huang, N., and Stark, J.M. (2008). Alternative-NHEJ Is a Mechanistically Distinct Pathway of Mammalian Chromosome Break Repair. PLoS Genet. 4, e1000110.

- Benson, E.K., Mungamuri, S.K., Attie, O., Kracikova, M., Sachidanandam, R., Manfredi, J.J., and Aaronson, S.A. (2014). p53-dependent gene repression through p21 is mediated by recruitment of E2F4 repression complexes. Oncogene 33, 3959–3969.
- Berkey, F.J. (2010). Managing the adverse effects of radiation therapy. Am. Fam. Physician 82, 381–388, 394.
- Berquist, B.R., and Wilson, D.M. (2012). Pathways for repairing and tolerating the spectrum of oxidative DNA lesions. Cancer Lett. 327, 61–72.
- Berthel, E., Ferlazzo, M.L., Devic, C., Bourguignon, M., and Foray, N. (2019a). What Does the History of Research on the Repair of DNA Double-Strand Breaks Tell Us?—A Comprehensive Review of Human Radiosensitivity. Int. J. Mol. Sci. 20, 5339.
- Berthel, E., Foray, N., and Ferlazzo, M.L. (2019b). The Nucleoshuttling of the ATM Protein: A Unified Model to Describe the Individual Response to High- and Low-Dose of Radiation? Cancers 11, 905.
- Bhargava, R., Onyango, D.O., and Stark, J.M. (2016). Regulation of Single-Strand Annealing and its Role in Genome Maintenance. Trends Genet. 32, 566–575.
- Bhattacharyya, A., Ear, U.S., Koller, B.H., Weichselbaum, R.R., and Bishop, D.K. (2000). The Breast Cancer Susceptibility Gene BRCA1 Is Required for Subnuclear Assembly of Rad51 and Survival following Treatment with the DNA Cross-linking Agent Cisplatin. J. Biol. Chem. 275, 23899–23903.
- Bhogal, N., Jalali, F., and Bristow, R.G. (2009). Microscopic imaging of DNA repair foci in irradiated normal tissues. Int. J. Radiat. Biol. 85, 732–746.
- Bianconi, E., Piovesan, A., Facchin, F., Beraudi, A., Casadei, R., Frabetti, F., Vitale, L., Pelleri, M.C., Tassani, S., Piva, F., et al. (2013). An estimation of the number of cells in the human body. Ann. Hum. Biol. 40, 463–471.
- Biau, J., Chautard, E., Verrelle, P., and Dutreix, M. (2019). Altering DNA Repair to Improve Radiation Therapy: Specific and Multiple Pathway Targeting. Front. Oncol. 9, 1009.
- Biehs, R., Steinlage, M., Barton, O., Juhász, S., Künzel, J., Spies, J., Shibata, A., Jeggo, P.A., and Löbrich, M. (2017). DNA Double-Strand Break Resection Occurs during Non-homologous End Joining in G1 but Is Distinct from Resection during Homologous Recombination. Mol. Cell 65, 671-684.e5.
- Bindra, R.S., Goglia, A.G., Jasin, M., and Powell, S.N. (2013). Development of an assay to measure mutagenic non-homologous end-joining repair activity in mammalian cells. Nucleic Acids Res. 41, e115–e115.
- Biola-Clier, M., Beal, D., Caillat, S., Libert, S., Armand, L., Herlin-Boime, N., Sauvaigo, S., Douki, T., and Carriere, M. (2017). Comparison of the DNA damage response in BEAS-2B and A549 cells exposed to titanium dioxide nanoparticles. Mutagenesis 32, 161–172.
- Bischoff, N., Wimberger, S., Maresca, M., and Brakebusch, C. (2020). Improving Precise CRISPR Genome Editing by Small Molecules: Is there a Magic Potion? Cells 9, 1318.
- Black, S., Kashkina, E., Kent, T., and Pomerantz, R. (2016). DNA Polymerase θ: A Unique Multifunctional End-Joining Machine. Genes 7, 67.
- Blackford, A.N., and Jackson, S.P. (2017). ATM, ATR, and DNA-PK: The Trinity at the Heart of the DNA Damage Response. Mol. Cell 66, 801–817.
- Bochum, S., Berger, S., and Martens, U.M. (2018). Olaparib. In Small Molecules in Oncology, U.M. Martens, ed. (Cham: Springer International Publishing), pp. 217–233.
- Bonner, J.A., and Lawrence, T.S. (1990). Doxorubicin Decreases the Repair of Radiation-induced DNA Damage. Int. J. Radiat. Biol. 57, 55–64.
- Bonner, W.M., Redon, C.E., Dickey, J.S., Nakamura, A.J., Sedelnikova, O.A., Solier, S., and Pommier, Y. (2008). γH2AX and cancer. Nat. Rev. Cancer 8, 957–967.

- Borràs, M., Armengol, G., De Cabo, M., Barquinero, J.-F., and Barrios, L. (2015). Comparison of methods to quantify histone H2AX phosphorylation and its usefulness for prediction of radiosensitivity. Int. J. Radiat. Biol. 91, 915–924.
- Bouwman, P., Aly, A., Escandell, J.M., Pieterse, M., Bartkova, J., van der Gulden, H., Hiddingh, S., Thanasoula, M., Kulkarni, A., Yang, Q., et al. (2010). 53BP1 loss rescues BRCA1 deficiency and is associated with triple-negative and BRCA-mutated breast cancers. Nat. Struct. Mol. Biol. 17, 688–695.
- Bowman, K.J., Newell, D.R., Calvert, A.H., and Curtin, N.J. (2001). Differential effects of the poly (ADP-ribose) polymerase (PARP) inhibitor NU1025 on topoisomerase I and II inhibitor cytotoxicity in L1210 cells in vitro. Br. J. Cancer 84, 106–112.
- Boysen, G., Pachkowski, B.F., Nakamura, J., and Swenberg, J.A. (2009). The formation and biological significance of N7-guanine adducts. Mutat. Res. 678, 76–94.
- Bradley, M.O., and Kohn, K.W. (1979). X-ray induced DNA double strand break production and repair in mammalian cells as measured by neutral filter elution. Nucleic Acids Res. 7, 793–804.
- Brambati, A., Barry, R.M., and Sfeir, A. (2020). DNA polymerase theta (Polθ) – an error-prone polymerase necessary for genome stability. Curr. Opin. Genet. Dev. 60, 119–126.
- Brandt, J.P., and Gerriets, V. (2021). Bleomycin. In StatPearls [Internet], (Treasure Island (FL): StatPearls Publishing), p.
- Breen, A.P., and Murphy, J.A. (1995). Reactions of oxyl radicals with DNA. Free Radic. Biol. Med. 18, 1033–1077.
- Bret, C., Klein, B., and Moreaux, J. (2013). Nucleotide excision DNA repair pathway as a therapeutic target in patients with high-risk diffuse large B cell lymphoma. Cell Cycle Georget. Tex 12, 1811–1812.
- Brown, J.S., O'Carrigan, B., Jackson, S.P., and Yap, T.A. (2017). Targeting DNA Repair in Cancer: Beyond PARP Inhibitors. Cancer Discov. 7, 20–37.
- Bryant, H.E. (2012). DNA Double-Strand Break Damage and Repair Assessed by Pulsed-Field Gel Electrophoresis. In DNA Repair Protocols, L. Bjergbæk, ed. (Totowa, NJ: Humana Press), pp. 315–321.
- Bryant, H.E., Schultz, N., Thomas, H.D., Parker, K.M., Flower, D., Lopez, E., Kyle, S., Meuth, M., Curtin, N.J., and Helleday, T. (2005). Specific killing of BRCA2-deficient tumours with inhibitors of poly(ADP-ribose) polymerase. Nature 434, 913–917.
- Bryant, H.E., Petermann, E., Schultz, N., Jemth, A.-S., Loseva, O., Issaeva, N., Johansson, F., Fernandez, S., McGlynn, P., and Helleday, T. (2009). PARP is activated at stalled forks to mediate Mre11-dependent replication restart and recombination. EMBO J. 28, 2601–2615.
- Budman, J., and Chu, G. (2006). Assays for Nonhomologous End Joining in Extracts. In Methods in Enzymology, (Elsevier), pp. 430–444.
- Bunting, S.F., Callén, E., Wong, N., Chen, H.-T., Polato, F., Gunn, A., Bothmer, A., Feldhahn, N., Fernandez-Capetillo, O., Cao, L., et al. (2010). 53BP1 Inhibits Homologous Recombination in Brca1-Deficient Cells by Blocking Resection of DNA Breaks. Cell 141, 243–254.
- Bunting, S.F., Callén, E., Kozak, M.L., Kim, J.M., Wong, N., López-Contreras, A.J., Ludwig, T., Baer, R., Faryabi, R.B., Malhowski, A., et al. (2012). BRCA1 Functions Independently of Homologous Recombination in DNA Interstrand Crosslink Repair. Mol. Cell 46, 125–135.
- Buonomo, S.B.C., Wu, Y., Ferguson, D., and de Lange, T. (2009). Mammalian Rif1 contributes to replication stress survival and homology-directed repair. J. Cell Biol. 187, 385–398.
- Burma, S., and Chen, D.J. (2004). Role of DNA–PK in the cellular response to DNA double-strand breaks. DNA Repair 3, 909–918.
- Burnouf, D., Koehl, P., and Fuchs, R.P. (1990). Position of a single acetylaminofluorene adduct within a mutational hot spot is critical for the related mutagenic event. Basic Life Sci. 52, 277–287.

- Butler, M., Pongor, L., Su, Y.-T., Xi, L., Raffeld, M., Quezado, M., Trepel, J., Aldape, K., Pommier, Y., and Wu, J. (2020). MGMT Status as a Clinical Biomarker in Glioblastoma. Trends Cancer 6, 380–391.
- Cadet, J. (2003). Oxidative damage to DNA: formation, measurement and biochemical features. Mutat. Res. Mol. Mech. Mutagen. 531, 5–23.
- Cadet, J., Mouret, S., Ravanat, J.-L., and Douki, T. (2012). Photoinduced Damage to Cellular DNA: Direct and Photosensitized Reactions†. Photochem. Photobiol. 88, 1048–1065.
- Cai, M.-Y., Dunn, C.E., Chen, W., Kochupurakkal, B.S., Nguyen, H., Moreau, L.A., Shapiro, G.I., Parmar, K., Kozono, D., and D'Andrea, A.D. (2020). Cooperation of the ATM and Fanconi Anemia/BRCA Pathways in Double-Strand Break End Resection. Cell Rep. 30, 2402-2415.e5.
- Caldecott, K.W. (2008). Single-strand break repair and genetic disease. Nat. Rev. Genet. 9, 619–631.
- Calini, V., Urani, C., and Camatini, M. (2002). Comet assay evaluation of DNA single- and double-strand breaks induction and repair in C3H10T1/2 cells. Cell Biol. Toxicol. 18, 369–379.
- Camenisch, U., Dip, R., Schumacher, S.B., Schuler, B., and Naegeli, H. (2006). Recognition of helical kinks by xeroderma pigmentosum group A protein triggers DNA excision repair. Nat. Struct. Mol. Biol. 13, 278–284.
- Cannan, W.J., and Pederson, D.S. (2016). Mechanisms and Consequences of Double-Strand DNA Break Formation in Chromatin. J. Cell. Physiol. 231, 3–14.
- Cao, L., Xu, X., Bunting, S.F., Liu, J., Wang, R.-H., Cao, L.L., Wu, J.J., Peng, T.-N., Chen, J., Nussenzweig, A., et al. (2009). A Selective Requirement for 53BP1 in the Biological Response to Genomic Instability Induced by Brca1 Deficiency. Mol. Cell 35, 534–541.
- Caracciolo, D., Montesano, M., Tagliaferri, P., and Tassone, P. (2019). Alternative non-homologous end joining repair: a master regulator of genomic instability in cancer. Precis. Cancer Med. 2, 8–8.
- Carroll, D. (1996). Homologous Genetic Recombination in Xenopus: Mechanism and Implications for Gene Manipulation. In Progress in Nucleic Acid Research and Molecular Biology, (Elsevier), pp. 101–125.
- Ceccaldi, R., Liu, J.C., Amunugama, R., Hajdu, I., Primack, B., Petalcorin, M.I.R., O'Connor, K.W., Konstantinopoulos, P.A., Elledge, S.J., Boulton, S.J., et al. (2015). Homologous-recombination-deficient tumours are dependent on Polθ-mediated repair. Nature 518, 258–262.
- Ceccaldi, R., Rondinelli, B., and D'Andrea, A.D. (2016). Repair Pathway Choices and Consequences at the Double-Strand Break. Trends Cell Biol. 26, 52–64.
- Chang, D.J., and Cimprich, K.A. (2009). DNA damage tolerance: when it's OK to make mistakes. Nat. Chem. Biol. 5, 82–90.
- Chang, H.H.Y., Pannunzio, N.R., Adachi, N., and Lieber, M.R. (2017). Non-homologous DNA end joining and alternative pathways to double-strand break repair. Nat. Rev. Mol. Cell Biol. 18, 495–506.
- Chapman, J.R., Barral, P., Vannier, J.-B., Borel, V., Steger, M., Tomas-Loba, A., Sartori, A.A., Adams, I.R., Batista, F.D., and Boulton, S.J. (2013). RIF1 Is Essential for 53BP1-Dependent Nonhomologous End Joining and Suppression of DNA Double-Strand Break Resection. Mol. Cell 49, 858–871.
- Charles, C., Ouedraogo, M., Belayew, A., and Duez, P. (2012). On-chip microelectrophoresis for the study of in vitro nonhomologous end-joining DNA double-strand break repair. Anal. Biochem. 425, 76–79.
- Charles, C., Nachtergael, A., Ouedraogo, M., Belayew, A., and Duez, P. (2014). Effects of chemopreventive natural products on non-homologous end-joining DNA double-strand break repair. Mutat. Res. Toxicol. Environ. Mutagen. 768, 33–41.
- Chatterjee, N., and Walker, G.C. (2017). Mechanisms of DNA damage, repair, and mutagenesis: DNA Damage and Repair. Environ. Mol. Mutagen. 58, 235–263.

- Chen, L., Nievera, C.J., Lee, A.Y.-L., and Wu, X. (2008). Cell Cycle-dependent Complex Formation of BRCA1·CtIP·MRN Is Important for DNA Double-strand Break Repair. J. Biol. Chem. 283, 7713–7720.
- Chen, Q., Cai, D., Li, M., and Wu, X. (2017). The homologous recombination protein RAD51 is a promising therapeutic target for cervical carcinoma. Oncol. Rep. 38, 767–774.
- Cheng, Q., Chen, L., Li, Z., Lane, W.S., and Chen, J. (2009). ATM activates p53 by regulating MDM2 oligomerization and E3 processivity. EMBO J. 28, 3857–3867.
- Cheong, N. (1996). In vitro rejoining of double-strand breaks in cellular DNA by factors present in extracts of HeLa cells. Int. J. Radiat. Biol. 69, 665–677.
- Cheong, N., Perrault, A.R., and Iliakis, G. (1998). In vitro rejoining of DNA double strand breaks: a comparison of genomic-DNA with plasmid-DNA-based assays. Int. J. Radiat. Biol. 73, 481–493.
- Chien, J.C.-Y., Tabet, E., Pinkham, K., da Hora, C.C., Chang, J.C.-Y., Lin, S., Badr, C.E., and Lai, C.P.-K. (2020). A multiplexed bioluminescent reporter for sensitive and non-invasive tracking of DNA double strand break repair dynamics in vitro and in vivo. Nucleic Acids Res. 48, e100–e100.
- Chiruvella, K.K., Liang, Z., and Wilson, T.E. (2013). Repair of Double-Strand Breaks by End Joining. Cold Spring Harb. Perspect. Biol. 5, a012757–a012757.
- Chistiakov, D.A., Voronova, N.V., and Chistiakov, P.A. (2008). Genetic variations in DNA repair genes, radiosensitivity to cancer and susceptibility to acute tissue reactions in radiotherapy-treated cancer patients. Acta Oncol. 47, 809–824.
- Cho, K.A., Ryu, S.J., Oh, Y.S., Park, J.H., Lee, J.W., Kim, H.-P., Kim, K.T., Jang, I.S., and Park, S.C. (2004). Morphological Adjustment of Senescent Cells by Modulating Caveolin-1 Status. J. Biol. Chem. 279, 42270–42278.
- Choi, E.-H., Yoon, S., Hahn, Y., and Kim, K.P. (2017). Cellular Dynamics of Rad51 and Rad54 in Response to Postreplicative Stress and DNA Damage in HeLa Cells. Mol. Cells 40, 143–150.
- Chowdhury, D., Keogh, M.-C., Ishii, H., Peterson, C.L., Buratowski, S., and Lieberman, J. (2005). γ-H2AX Dephosphorylation by Protein Phosphatase 2A Facilitates DNA Double-Strand Break Repair. Mol. Cell 20, 801–809.
- Chua, M.L.K., and Rothkamm, K. (2013). Biomarkers of Radiation Exposure: Can They Predict Normal Tissue Radiosensitivity? Clin. Oncol. 25, 610–616.
- Ciccia, A., and Elledge, S.J. (2010). The DNA Damage Response: Making It Safe to Play with Knives. Mol. Cell 40, 179–204.
- Ciccia, A., Ling, C., Coulthard, R., Yan, Z., Xue, Y., Meetei, A.R., Laghmani, E.H., Joenje, H., McDonald, N., de Winter, J.P., et al. (2007). Identification of FAAP24, a Fanconi Anemia Core Complex Protein that Interacts with FANCM. Mol. Cell 25, 331–343.
- Ciszewski, W.M., Tavecchio, M., Dastych, J., and Curtin, N.J. (2014). DNA-PK inhibition by NU7441 sensitizes breast cancer cells to ionizing radiation and doxorubicin. Breast Cancer Res. Treat. 143, 47–55.
- Clapham, K.M., Rennison, T., Jones, G., Craven, F., Bardos, J., Golding, B.T., Griffin, R.J., Haggerty, K., Hardcastle, I.R., Thommes, P., et al. (2012). Potent enantioselective inhibition of DNA-dependent protein kinase (DNA-PK) by atropisomeric chromenone derivatives. Org. Biomol. Chem. 10, 6747.
- Cleary, J.M., Aguirre, A.J., Shapiro, G.I., and D'Andrea, A.D. (2020). Biomarker-Guided Development of DNA Repair Inhibitors. Mol. Cell 78, 1070–1085.
- Collins, A.R. (2014). Measuring oxidative damage to DNA and its repair with the comet assay. Biochim. Biophys. Acta BBA - Gen. Subj. 1840, 794–800.
- Collins, A.R., and Azqueta, A. (2014). Methods for Measuring DNA Repair: Introduction and Cellular Repair. In Genotoxicity and DNA Repair, L.M. Sierra, and I. Gaivão, eds. (New York, NY: Springer New York), pp. 365–376.

- Collins, A., Koppen, G., Valdiglesias, V., Dusinska, M., Kruszewski, M., Møller, P., Rojas, E., Dhawan, A., Benzie, I., Coskun, E., et al. (2014). The comet assay as a tool for human biomonitoring studies: The ComNet Project. Mutat. Res. Mutat. Res. 759, 27–39.
- Collins, A.R., Oscoz, A.A., Brunborg, G., Gaivao, I., Giovannelli, L., Kruszewski, M., Smith, C.C., and Stetina, R. (2008). The comet assay: topical issues. Mutagenesis 23, 143–151.
- Conlin, M.P., Reid, D.A., Small, G.W., Chang, H.H., Watanabe, G., Lieber, M.R., Ramsden, D.A., and Rothenberg, E. (2017). DNA Ligase IV Guides End-Processing Choice during Nonhomologous End Joining. Cell Rep. 20, 2810–2819.
- Cooke, M.S., Evans, M.D., Dizdaroglu, M., and Lunec, J. (2003). Oxidative DNA damage: mechanisms, mutation, and disease. FASEB J. 17, 1195–1214.
- Cortés-Gutiérrez, E.I., López-Fernández, C., Fernández, J.L., Dávila-Rodríguez, M.I., Johnston, S.D., and Gosálvez, J. (2014). Interpreting sperm DNA damage in a diverse range of mammalian sperm by means of the two-tailed comet assay. Front. Genet. 5.
- Cortés-Gutiérrez, E.I., Fernández, J.L., Dávila-Rodríguez, M.I., López-Fernández, C., and Gosálvez, J. (2017). Two-Tailed Comet Assay (2T-Comet): Simultaneous Detection of DNA Single and Double Strand Breaks. In Histochemistry of Single Molecules, C. Pellicciari, and M. Biggiogera, eds. (New York, NY: Springer New York), pp. 285–293.
- Cowell, I.G., Sunter, N.J., Singh, P.B., Austin, C.A., Durkacz, B.W., and Tilby, M.J. (2007). γH2AX Foci Form Preferentially in Euchromatin after Ionising-Radiation. PLoS ONE 2, e1057.
- Croft, L.V., Bolderson, E., Adams, M.N., El-Kamand, S., Kariawasam, R., Cubeddu, L., Gamsjaeger, R., and Richard, D.J. (2019). Human single-stranded DNA binding protein 1 (hSSB1, OBFC2B), a critical component of the DNA damage response. Semin. Cell Dev. Biol. 86, 121–128.
- Cruet-Hennequart, S., Prendergast, Á.M., Shaw, G., Barry, F.P., and Carty, M.P. (2012). Doxorubicin induces the DNA damage response in cultured human mesenchymal stem cells. Int. J. Hematol. 96, 649–656.
- Cui, X., Yu, Y., Gupta, S., Cho, Y.-M., Lees-Miller, S.P., and Meek, K. (2005). Autophosphorylation of DNA-Dependent Protein Kinase Regulates DNA End Processing and May Also Alter Double-Strand Break Repair Pathway Choice. Mol. Cell. Biol. 25, 10842–10852.
- Dahal, S., Dubey, S., and Raghavan, S.C. (2018). Homologous recombination-mediated repair of DNA double-strand breaks operates in mammalian mitochondria. Cell. Mol. Life Sci. 75, 1641–1655.
- D'Amours, D., and Jackson, S.P. (2002). The MRE11 complex: at the crossroads of DNA repair and checkpoint signalling. Nat. Rev. Mol. Cell Biol. 3, 317–327.
- D'Amours, D., Sallmann, F.R., Dixit, V.M., and Poirier, G.G. (2001). Gain-of-function of poly(ADP-ribose) polymerase-1 upon cleavage by apoptotic proteases: implications for apoptosis. J. Cell Sci. 114, 3771–3778.
- D'Andrea, A.D. (2018). Mechanisms of PARP inhibitor sensitivity and resistance. DNA Repair 71, 172–176.
- Dasika, G.K., Lin, S.-C.J., Zhao, S., Sung, P., Tomkinson, A., and Lee, E.Y.-H.P. (1999). DNA damage-induced cell cycle checkpoints and DNA strand break repair in development and tumorigenesis. Oncogene 18, 7883–7899.
- Davidson, D., Amrein, L., Panasci, L., and Aloyz, R. (2013). Small Molecules, Inhibitors of DNA-PK, Targeting DNA Repair, and Beyond. Front. Pharmacol. 4.
- Davis, A.J., Lee, K.-J., and Chen, D.J. (2013). The N-terminal Region of the DNA-dependent Protein Kinase Catalytic Subunit Is Required for Its DNA Double-stranded Break-mediated Activation. J. Biol. Chem. 288, 7037–7046.
- Davis, A.J., Chi, L., So, S., Lee, K.-J., Mori, E., Fattah, K., Yang, J., and Chen, D.J. (2014). BRCA1 modulates the autophosphorylation status of DNA-PKcs in S phase of the cell cycle. Nucleic Acids Res. 42, 11487–11501.

- Daza, P., Reichenberger, S., Göttlich, B., Hagmann, M., Feldmann, E., and Pfeiffer, P. (1996). Mechanisms of Nonhomologous DNA End-Joining in Frogs, Mice and Men. Biol. Chem. Hoppe. Seyler 377, 775–786.
- Deckbar, D., Birraux, J., Krempler, A., Tchouandong, L., Beucher, A., Walker, S., Stiff, T., Jeggo, P., and Löbrich, M. (2007). Chromosome breakage after G2 checkpoint release. J. Cell Biol. 176, 749–755.
- Decottignies, A. (2013). Alternative end-joining mechanisms: a historical perspective. Front. Genet. 4.
- Del Conte, G., Sessa, C., von Moos, R., Viganò, L., Digena, T., Locatelli, A., Gallerani, E., Fasolo, A., Tessari, A., Cathomas, R., et al. (2014). Phase I study of olaparib in combination with liposomal doxorubicin in patients with advanced solid tumours. Br. J. Cancer 111, 651–659.
- DeLoughery, Z., Luczak, M.W., Ortega-Atienza, S., and Zhitkovich, A. (2015). DNA Double-Strand Breaks by Cr(VI) Are Targeted to Euchromatin and Cause ATR-Dependent Phosphorylation of Histone H2AX and Its Ubiquitination. Toxicol. Sci. 143, 54–63.
- Deng, S.K., Gibb, B., de Almeida, M.J., Greene, E.C., and Symington, L.S. (2014). RPA antagonizes microhomology-mediated repair of DNA double-strand breaks. Nat. Struct. Mol. Biol. 21, 405–412.
- Deniz, M., Kaufmann, J., Stahl, A., Gundelach, T., Janni, W., Hoffmann, I., Keimling, M., Hampp, S., Ihle, M., and Wiesmüller, L. (2016). In vitro model for DNA double-strand break repair analysis in breast cancer reveals cell type–specific associations with age and prognosis. FASEB J. 30, 3786–3799.
- Dertinger, S.D., Kraynak, A.R., Wheeldon, R.P., Bernacki, D.T., Bryce, S.M., Hall, N., Bemis, J.C., Galloway, S.M., Escobar, P.A., and Johnson, G.E. (2019). Predictions of genotoxic potential, mode of action, molecular targets, and potency via a tiered multiflow® assay data analysis strategy. Environ. Mol. Mutagen. 60, 513–533.
- Dhillon, K.K., Swisher, E.M., and Taniguchi, T. (2011). Secondary mutations of BRCA1/2 and drug resistance. Cancer Sci. 102, 663–669.
- Dianov, G.L., and Hübscher, U. (2013). Mammalian Base Excision Repair: the Forgotten Archangel. Nucleic Acids Res. 41, 3483–3490.
- DiBiase, S.J., Zeng, Z.C., Chen, R., Hyslop, T., Curran, W.J., and Iliakis, G. (2000). DNA-dependent protein kinase stimulates an independently active, nonhomologous, end-joining apparatus. Cancer Res. 60, 1245–1253.
- Diggle, C.P., Bentley, J., and Kiltie, A. (2003). Development of a rapid, small-scale DNA repair assay for use on clinical samples. Nucleic Acids Res. 31, 83e–883.
- Ding, L., Cao, J., Lin, W., Chen, H., Xiong, X., Ao, H., Yu, M., Lin, J., and Cui, Q. (2020). The Roles of Cyclin-Dependent Kinases in Cell-Cycle Progression and Therapeutic Strategies in Human Breast Cancer. Int. J. Mol. Sci. 21, 1960.
- Dmitrieva, N.I., and Burg, M.B. (2007). Osmotic Stress and DNA Damage. In Methods in Enzymology, (Elsevier), pp. 241–252.
- Do, K., and Chen, A.P. (2013). Molecular pathways: targeting PARP in cancer treatment. Clin. Cancer Res. Off. J. Am. Assoc. Cancer Res. 19, 977–984.
- Douki, T., and Cadet, J. (2003). Formation of the spore photoproduct and other dimeric lesions between adjacent pyrimidines in UVC-irradiated dry DNA. Photochem. Photobiol. Sci. 2, 433.
- Douki, T., Court, M., and Cadet, J. (2000). Electrospray–mass spectrometry characterization and measurement of far-UV-induced thymine photoproducts. J. Photochem. Photobiol. B 54, 145–154.
- Du, J., Yin, N., Xie, T., Zheng, Y., Xia, N., Shang, J., Chen, F., Zhang, H., Yu, J., and Liu, F. (2018). Quantitative assessment of HR and NHEJ activities via CRISPR/Cas9-induced oligodeoxynucleotide-mediated DSB repair. DNA Repair 70, 67–71.

- Du, W., Amarachintha, S., Wilson, A.F., and Pang, Q. (2016). Hyper-active non-homologous end joining selects for synthetic lethality resistant and pathological Fanconi anemia hematopoietic stem and progenitor cells. Sci. Rep. 6, 22167.
- Durdik, M., Kosik, P., Gursky, J., Vokalova, L., Markova, E., and Belyaev, I. (2015). Imaging flow cytometry as a sensitive tool to detect low-dose-induced DNA damage by analyzing 53BP1 and γH2AX foci in human lymphocytes: Imaging Flow Cytometry for DNA Damage Analysis. Cytometry A 87, 1070–1078.
- El-Awady, R.A., Dikomey, E., and Dahm-Daphi, J. (2003). Radiosensitivity of human tumour cells is correlated with the induction but not with the repair of DNA double-strand breaks. Br. J. Cancer 89, 593–601.
- El-Awady, R.A., Semreen, M.H., Saber-Ayad, M.M., Cyprian, F., Menon, V., and Al-Tel, T.H. (2016). Modulation of DNA damage response and induction of apoptosis mediates synergism between doxorubicin and a new imidazopyridine derivative in breast and lung cancer cells. DNA Repair 37, 1–11.
- Enciso, J.M., Gutzkow, K.B., Brunborg, G., Olsen, A.-K., López de Cerain, A., and Azqueta, A. (2018). Standardisation of the in vitro comet assay: influence of lysis time and lysis solution composition on the detection of DNA damage induced by X-rays. Mutagenesis 33, 25–30.
- Erasimus, H., Gobin, M., Niclou, S., and Van Dyck, E. (2016). DNA repair mechanisms and their clinical impact in glioblastoma. Mutat. Res. Mutat. Res. 769, 19–35.
- Ersson, C., Moller, P., Forchhammer, L., Loft, S., Azqueta, A., Godschalk, R.W.L., van Schooten, F.-J., Jones, G.D.D., Higgins, J.A., Cooke, M.S., et al. (2013). An ECVAG inter-laboratory validation study of the comet assay: inter-laboratory and intra-laboratory variations of DNA strand breaks and FPG-sensitive sites in human mononuclear cells. Mutagenesis 28, 279–286.
- Escobar, D., Hepp, M.I., Farkas, C., Campos, T., Sodir, N.M., Morales, M., Álvarez, C.I., Swigart, L., Evan, G.I., Gutiérrez, J.L., et al. (2015). Sall2 is required for proapoptotic Noxa expression and genotoxic stress-induced apoptosis by doxorubicin. Cell Death Dis. 6, e1816.
- ESCODD, (European Standards Committee on Oxidative DNA Damage), Gedik, C.M., and Collins, A. (2005). Establishing the background level of base oxidation in human lymphocyte DNA: results of an interlaboratory validation study. FASEB J. 19, 82–84.
- Escribano-Díaz, C., Orthwein, A., Fradet-Turcotte, A., Xing, M., Young, J.T.F., Tkáč, J., Cook, M.A., Rosebrock, A.P., Munro, M., Canny, M.D., et al. (2013). A Cell Cycle-Dependent Regulatory Circuit Composed of 53BP1-RIF1 and BRCA1-CtIP Controls DNA Repair Pathway Choice. Mol. Cell 49, 872–883.
- d'Adda di Fagagna, F. (2008). Living on a break: cellular senescence as a DNA-damage response. Nat. Rev. Cancer 8, 512–522.
- Falck, J., Mailand, N., Syljuåsen, R.G., Bartek, J., and Lukas, J. (2001). The ATM–Chk2–Cdc25A checkpoint pathway guards against radioresistant DNA synthesis. Nature 410, 842–847.
- Fan, J., and Pavletich, N.P. (2012). Structure and conformational change of a replication protein A heterotrimer bound to ssDNA. Genes Dev. 26, 2337–2347.
- Feng, W., and Jasin, M. (2017). Homologous Recombination and Replication Fork Protection: BRCA2 and More! Cold Spring Harb. Symp. Quant. Biol. 82, 329–338.
- Feng, L., Li, N., Li, Y., Wang, J., Gao, M., Wang, W., and Chen, J. (2015). Cell cycle-dependent inhibition of 53BP1 signaling by BRCA1. Cell Discov. 1, 15019.
- Feng, Y.-L., Xiang, J.-F., Kong, N., Cai, X.-J., and Xie, A.-Y. (2016). Buried territories: heterochromatic response to DNA double-strand breaks. Acta Biochim. Biophys. Sin. 48, 594–602.
- Flanagan, M., and Cunniff, C.M. (1993). Bloom Syndrome. In GeneReviews®, M.P. Adam, H.H. Ardinger, R.A. Pagon, S.E. Wallace, L.J. Bean, G. Mirzaa, and A. Amemiya, eds. (Seattle (WA): University of Washington, Seattle), p. last updated 2019.

- Fogel, D.B. (2018). Factors associated with clinical trials that fail and opportunities for improving the likelihood of success: A review. Contemp. Clin. Trials Commun. 11, 156–164.
- Fok, J.H.L., Ramos-Montoya, A., Vazquez-Chantada, M., Wijnhoven, P.W.G., Follia, V., James, N., Farrington, P.M., Karmokar, A., Willis, S.E., Cairns, J., et al. (2019). AZD7648 is a potent and selective DNA-PK inhibitor that enhances radiation, chemotherapy and olaparib activity. Nat. Commun. 10, 5065.
- Forestier, A., Sarrazy, F., Caillat, S., Vandenbrouck, Y., and Sauvaigo, S. (2012). Functional DNA Repair Signature of Cancer Cell Lines Exposed to a Set of Cytotoxic Anticancer Drugs Using a Multiplexed Enzymatic Repair Assay on Biochip. PLoS ONE 7, e51754.
- Forrest, R.A., Swift, L.P., Rephaeli, A., Nudelman, A., Kimura, K.-I., Phillips, D.R., and Cutts, S.M. (2012). Activation of DNA damage response pathways as a consequence of anthracycline-DNA adduct formation. Biochem. Pharmacol. 83, 1602–1612.
- Foulkes, W.D., and Shuen, A.Y. (2013). In Brief: BRCA1 and BRCA2. J. Pathol. 230, 347–349.
- Fousteri, M., Vermeulen, W., van Zeeland, A.A., and Mullenders, L.H.F. (2006). Cockayne syndrome A and B proteins differentially regulate recruitment of chromatin remodeling and repair factors to stalled RNA polymerase II in vivo. Mol. Cell 23, 471–482.
- Frank-Kamenetskii, M.D., and Mirkin, S.M. (1995). Triplex DNA Structures. Annu. Rev. Biochem. 64, 65–95.
- Friedberg, E.C., Walker, G.C., Siede, W., Wood, R.D., Schultz, R.A., and Ellenberger, T. (2006). DNA Repair and Mutagenesis (Washington, DC, USA: ASM Press).
- Friesen, C., Herr, I., Krammer, P.H., and Debatin, K.M. (1996). Involvement of the CD95 (APO-1/FAS) receptor/ligand system in drug-induced apoptosis in leukemia cells. Nat. Med. 2, 574–577.
- Friesen, C., Uhl, M., Pannicke, U., Schwarz, K., Miltner, E., and Debatin, K.-M. (2008). DNA-Ligase IV and DNA-Protein Kinase Play a Critical Role in Deficient Caspases Activation in Apoptosis-resistant Cancer Cells by Using Doxorubicin. Mol. Biol. Cell 19, 3283–3289.
- Friis, I., and Solov'yov, I.A. (2018). Activation of the DNA-repair mechanism through NBS1 and MRE11 diffusion. PLOS Comput. Biol. 14, e1006362.
- Fujii, Y., Genet, M.D., Roybal, E.J., Kubota, N., Okayasu, R., Miyagawa, K., Fujimori, A., and Kato, T.A. (2013). Comparison of the bromodeoxyuridine-mediated sensitization effects between low-LET and high-LET ionizing radiation on DNA double-strand breaks. Oncol. Rep. 29, 2133–2139.
- Gagné, F. (2014). Genotoxicity. In Biochemical Ecotoxicology, (Elsevier), pp. 171–196.
- Garm, C., Moreno-Villanueva, M., Bürkle, A., Petersen, I., Bohr, V.A., Christensen, K., and Stevnsner, T. (2013). Age and gender effects on DNA strand break repair in peripheral blood mononuclear cells. Aging Cell 12, 58–66.
- Garty, G., Turner, H.C., Salerno, A., Bertucci, A., Zhang, J., Chen, Y., Dutta, A., Sharma, P., Bian, D., Taveras, M., et al. (2016). THE DECADE OF THE RABiT (2005–15). Radiat. Prot. Dosimetry 172, 201–206.
- Garutti, M., Pelizzari, G., Bartoletti, M., Malfatti, M.C., Gerratana, L., Tell, G., and Puglisi, F. (2019). Platinum Salts in Patients with Breast Cancer: A Focus on Predictive Factors. Int. J. Mol. Sci. 20, 3390.
- Gates, K.S. (2009). An overview of chemical processes that damage cellular DNA: spontaneous hydrolysis, alkylation, and reactions with radicals. Chem. Res. Toxicol. 22, 1747–1760.
- Gavande, N.S., VanderVere-Carozza, P.S., Hinshaw, H.D., Jalal, S.I., Sears, C.R., Pawelczak, K.S., and Turchi, J.J. (2016). DNA repair targeted therapy: The past or future of cancer treatment? Pharmacol. Ther. 160, 65–83.
- van Gent, D.C., Hoeijmakers, J.H.J., and Kanaar, R. (2001). Chromosomal stability and the DNA double-stranded break connection. Nat. Rev. Genet. 2, 196–206.

- George, C. (2017). Mise au point et utilisation d'un test de mesure d'activités enzymatiques de réparation de l'ADN in vitro sur biopuces pour l'identification de marqueurs d'expositions à des agents génotoxiques de l'environnement. phdthesis. Université Grenoble Alpes.
- Ghoshal, N., Sharma, S., Banerjee, A., Kurkalang, S., Raghavan, S.C., and Chatterjee, A. (2017). Influence of reduced glutathione on end-joining of DNA double-strand breaks: Cytogenetical and molecular approach. Mutat. Res. Mol. Mech. Mutagen. 795, 1–9.
- Gildemeister, O.S., Sage, J.M., and Knight, K.L. (2009). Cellular Redistribution of Rad51 in Response to DNA Damage. J. Biol. Chem. 284, 31945–31952.
- Gioia, U., Francia, S., Cabrini, M., Brambillasca, S., Michelini, F., Jones-Weinert, C.W., and d'Adda di Fagagna, F. (2019). Pharmacological boost of DNA damage response and repair by enhanced biogenesis of DNA damage response RNAs. Sci. Rep. 9, 6460.
- Glei, M., Schneider, T., and Schlörmann, W. (2016). Comet assay: an essential tool in toxicological research. Arch. Toxicol. 90, 2315–2336.
- Goglia, A.G., Delsite, R., Luz, A.N., Shahbazian, D., Salem, A.F., Sundaram, R.K., Chiaravalli, J., Hendrikx, P.J., Wilshire, J.A., Jasin, M., et al. (2015). Identification of Novel Radiosensitizers in a High-Throughput, Cell-Based Screen for DSB Repair Inhibitors. Mol. Cancer Ther. 14, 326–342.
- Golding, S.E., Rosenberg, E., Khalil, A., McEwen, A., Holmes, M., Neill, S., Povirk, L.F., and Valerie, K. (2004). Double Strand Break Repair by Homologous Recombination Is Regulated by Cell Cycle-independent Signaling via ATM in Human Glioma Cells. J. Biol. Chem. 279, 15402–15410.
- Gomez-Cabello, D., Jimeno, S., Fernández-Ávila, M.J., and Huertas, P. (2013). New Tools to Study DNA Double-Strand Break Repair Pathway Choice. PLoS ONE 8, e77206.
- Goodarzi, A.A., and Jeggo, P.A. (2012). Irradiation induced foci (IRIF) as a biomarker for radiosensitivity. Mutat. Res. Mol. Mech. Mutagen. 736, 39–47.
- Goodarzi, A.A., Noon, A.T., Deckbar, D., Ziv, Y., Shiloh, Y., Löbrich, M., and Jeggo, P.A. (2008). ATM Signaling Facilitates Repair of DNA Double-Strand Breaks Associated with Heterochromatin. Mol. Cell 31, 167–177.
- Goodman, J., and Hochstein, P. (1977). Generation of free radicals and lipid peroxidation by redox cycling of adriamycin and daunomycin. Biochem. Biophys. Res. Commun. 77, 797–803.
- Goodman, M.F., Creighton, S., Bloom, L.B., and Petruska, J. (1993). Biochemical basis of DNA replication fidelity. Crit. Rev. Biochem. Mol. Biol. 28, 83–126.
- Grabarz, A., Guirouilh-Barbat, J., Barascu, A., Pennarun, G., Genet, D., Rass, E., Germann, S.M., Bertrand, P., Hickson, I.D., and Lopez, B.S. (2013). A Role for BLM in Double-Strand Break Repair Pathway Choice: Prevention of CtIP/Mre11-Mediated Alternative Nonhomologous End-Joining. Cell Rep. 5, 21–28.
- Gratia, S., Kay, L., Potenza, L., Seffouh, A., Novel-Chaté, V., Schnebelen, C., Sestili, P., Schlattner, U., and Tokarska-Schlattner, M. (2012). Inhibition of AMPK signalling by doxorubicin: at the crossroads of the cardiac responses to energetic, oxidative, and genotoxic stress. Cardiovasc. Res. 95, 290–299.
- Gravel, S., Chapman, J.R., Magill, C., and Jackson, S.P. (2008). DNA helicases Sgs1 and BLM promote DNA double-strand break resection. Genes Dev. 22, 2767–2772.
- Gravells, P., Ahrabi, S., Vangala, R.K., Tomita, K., Brash, J.T., Brustle, L.A., Chung, C., Hong, J.M., Kaloudi, A., Humphrey, T.C., et al. (2015). Use of the HPRT gene to study nuclease-induced DNA double-strand break repair. Hum. Mol. Genet. 24, 7097–7110.
- Green, D.R. (2005). Apoptotic pathways: ten minutes to dead. Cell 121, 671–674.
- Greenberg, M.M. (2014). Abasic and Oxidized Abasic Site Reactivity in DNA: Enzyme Inhibition, Cross-Linking, and Nucleosome Catalyzed Reactions. Acc. Chem. Res. 47, 646–655.
- Griggs, J.J. (1998). Reducing the toxicity of anticancer therapy: new strategies. Leuk. Res. 22, S27–S33.

- Grover, P., Danadevi, K., Mahboob, M., Rozati, R., Banu, B.S., and Rahman, M.F. (2003). Evaluation of genetic damage in workers employed in pesticide production utilizing the Comet assay. Mutagenesis 18, 201–205.
- Guan, J. (2000). The catalytic subunit DNA-dependent protein kinase (DNA-PKcs) facilitates recovery from radiation-induced inhibition of DNA replication. Nucleic Acids Res. 28, 1183–1192.
- Guirouilh-Barbat, J., Huck, S., Bertrand, P., Pirzio, L., Desmaze, C., Sabatier, L., and Lopez, B.S. (2004). Impact of the KU80 Pathway on NHEJ-Induced Genome Rearrangements in Mammalian Cells. Mol. Cell 14, 611–623.
- Guo, L., Liu, X., Jiang, Y., Nishikawa, K., and Plunkett, W. (2011). DNA-Dependent Protein Kinase and Ataxia Telangiectasia Mutated (ATM) Promote Cell Survival in Response to NK314, a Topoisomerase IIα Inhibitor. Mol. Pharmacol. 80, 321–327.
- Gupta, A., Hunt, C.R., Chakraborty, S., Pandita, R.K., Yordy, J., Ramnarain, D.B., Horikoshi, N., and Pandita, T.K. (2014). Role of 53BP1 in the Regulation of DNA Double-Strand Break Repair Pathway Choice. Radiat. Res. 181, 1–8.
- Gustafsson, A.-S., Hartman, T., and Stenerlöw, B. (2015). Formation and repair of clustered damaged DNA sites in high LET irradiated cells. Int. J. Radiat. Biol. 91, 820–826.
- Haahr, P., Hoffmann, S., Tollenaere, M.A.X., Ho, T., Toledo, L.I., Mann, M., Bekker-Jensen, S., Räschle, M., and Mailand, N. (2016). Activation of the ATR kinase by the RPA-binding protein ETAA1. Nat. Cell Biol. 18, 1196–1207.
- Haber, J.E. (2018). DNA Repair: The Search for Homology. BioEssays 40, 1700229.
- Hagiwara, Y., Oike, T., Niimi, A., Yamauchi, M., Sato, H., Limsirichaikul, S., Held, K.D., Nakano, T., and Shibata, A. (2019). Clustered DNA double-strand break formation and the repair pathway following heavy-ion irradiation. J. Radiat. Res. (Tokyo) 60, 69–79.
- Hajjar, D., Kremb, S., Sioud, S., Emwas, A.-H., Voolstra, C.R., and Ravasi, T. (2017). Anti-cancer agents in Saudi Arabian herbals revealed by automated high-content imaging. PLOS ONE 12, e0177316.
- Halim, V.A., García-Santisteban, I., Warmerdam, D.O., van den Broek, B., Heck, A.J.R., Mohammed, S., and Medema, R.H. (2018). Doxorubicin-induced DNA Damage Causes Extensive Ubiquitination of Ribosomal Proteins Associated with a Decrease in Protein Translation*. Mol. Cell. Proteomics 17, 2297–2308.
- Hall, D.B., Holmlin, R.E., and Barton, J.K. (1996). Oxidative DNA damage through long-range electron transfer. Nature 382, 731–735.
- Han, J., Hendzel, M.J., and Allalunis-Turner, J. (2006). Quantitative Analysis Reveals Asynchronous and more than DSB-Associated Histone H2AX Phosphorylation after Exposure to Ionizing Radiation. Radiat. Res. 165, 283–292.
- Hanamshet, K., Mazina, O., and Mazin, A. (2016). Reappearance from Obscurity: Mammalian Rad52 in Homologous Recombination. Genes 7, 63.
- Hansen, L.T., Lundin, C., Helleday, T., Poulsen, H.S., Sørensen, C.S., Petersen, L.N., and Spang-Thomsen, M. (2003). DNA repair rate and etoposide (VP16) resistance of tumor cell subpopulations derived from a single human small cell lung cancer. Lung Cancer Amst. Neth. 40, 157–164.
- Harnor, S.J., Brennan, A., and Cano, C. (2017). Targeting DNA-Dependent Protein Kinase for Cancer Therapy. ChemMedChem 12, 895–900.
- Harrigan, J.A., Belotserkovskaya, R., Coates, J., Dimitrova, D.S., Polo, S.E., Bradshaw, C.R., Fraser, P., and Jackson, S.P. (2011). Replication stress induces 53BP1-containing OPT domains in G1 cells. J. Cell Biol. 193, 97–108.
- Haynes, B., Saadat, N., Myung, B., and Shekhar, M.P.V. (2015). Crosstalk between translesion synthesis, Fanconi anemia network, and homologous recombination repair pathways in interstrand DNA crosslink repair and development of chemoresistance. Mutat. Res. Mutat. Res. 763, 258–266.

- van Heemst, D., Brugmans, L., Verkaik, N.S., and van Gent, D.C. (2004). End-joining of blunt DNA double-strand breaks in mammalian fibroblasts is precise and requires DNA-PK and XRCC4. DNA Repair 3, 43–50.
- Hegde, M.L., Hazra, T.K., and Mitra, S. (2008a). Early steps in the DNA base excision/single-strand interruption repair pathway in mammalian cells. Cell Res. 18, 27–47.
- Hegde, M.L., Theriot, C.A., Das, A., Hegde, P.M., Guo, Z., Gary, R.K., Hazra, T.K., Shen, B., and Mitra, S. (2008b). Physical and functional interaction between human oxidized base-specific DNA glycosylase NEIL1 and flap endonuclease 1. J. Biol. Chem. 283, 27028–27037.
- Her, J., Ray, C., Altshuler, J., Zheng, H., and Bunting, S.F. (2018). 53BP1 Mediates ATR-Chk1 Signaling and Protects Replication Forks under Conditions of Replication Stress. Mol. Cell. Biol. 38.
- Herschtal, A., Martin, R.F., Leong, T., Lobachevsky, P., and Martin, O.A. (2018). A Bayesian Approach for Prediction of Patient Radiosensitivity. Int. J. Radiat. Oncol. 102, 627–634.
- Hershman, J.M., France, B., Hon, K., and Damoiseaux, R. (2017). Direct quantification of gamma H2AX by cell-based high throughput screening for evaluation of genotoxicity of pesticides in a human thyroid cell lines: Pesticides Cause DNA DSB in Human Thyroid Cells. Environ. Mol. Mutagen. 58, 522–528.
- Heyer, W.-D., Ehmsen, K.T., and Liu, J. (2010). Regulation of Homologous Recombination in Eukaryotes. Annu. Rev. Genet. 44, 113–139.
- Heylmann, D., and Kaina, B. (2016). The γH2AX DNA damage assay from a drop of blood. Sci. Rep. 6.
- Hill, S.J., Decker, B., Roberts, E.A., Horowitz, N.S., Muto, M.G., Worley, M.J., Feltmate, C.M., Nucci, M.R., Swisher, E.M., Nguyen, H., et al. (2018). Prediction of DNA Repair Inhibitor Response in Short-Term Patient-Derived Ovarian Cancer Organoids. Cancer Discov. 8, 1404–1421.
- Hisatomi, T., Sueoka-Aragane, N., Sato, A., Tomimasu, R., Ide, M., Kurimasa, A., Okamoto, K., Kimura, S., and Sueoka, E. (2011). NK314 potentiates antitumor activity with adult T-cell leukemia-lymphoma cells by inhibition of dual targets on topoisomerase II and DNA-dependent protein kinase. Blood 117, 3575–3584.
- Hoeijmakers, J.H.J. (2009). DNA Damage, Aging, and Cancer. N. Engl. J. Med. 361, 1475–1485.
- Holgersson, Å., Heiden, T., Castro, J., Edgren, M.R., Lewensohn, R., and Meijer, A.E. (2005). Different G2/M accumulation in M059J and M059K cells after exposure to DNA double-strand break–inducing agents. Int. J. Radiat. Oncol. 61, 915–921.
- Hollick, J.J., Golding, B.T., Hardcastle, I.R., Martin, N., Richardson, C., Rigoreau, L.J.M., Smith, G.C.M., and Griffin, R.J. (2003). 2,6-Disubstituted pyran-4-one and thiopyran-4-one inhibitors of DNA-Dependent protein kinase (DNA-PK). Bioorg. Med. Chem. Lett. 13, 3083–3086.
- Hollick, J.J., Rigoreau, L.J.M., Cano-Soumillac, C., Cockcroft, X., Curtin, N.J., Frigerio, M., Golding, B.T., Guiard, S., Hardcastle, I.R., Hickson, I., et al. (2007). Pyranone, Thiopyranone, and Pyridone Inhibitors of Phosphatidylinositol 3-Kinase Related Kinases. Structure–Activity Relationships for DNA-Dependent Protein Kinase Inhibition, and Identification of the First Potent and Selective Inhibitor of the Ataxia Telangiectasia Mutated Kinase. J. Med. Chem. 50, 1958–1972.
- Holton, N.W., Andrews, J.F., and Gassman, N.R. (2017). Application of Laser Micro-irradiation for Examination of Single and Double Strand Break Repair in Mammalian Cells. J. Vis. Exp.
- Hopp, N., Hagen, J., Aggeler, B., and Kalyuzhny, A.E. (2017). Automated High-Content Screening of γ-H2AX Expression in HeLa Cells. In Signal Transduction Immunohistochemistry, A.E. Kalyuzhny, ed. (New York, NY: Springer New York), pp. 273–283.
- Hoppe, B.S., Jensen, R.B., and Kirchgessner, C.U. (2000). Complementation of the Radiosensitive M059J Cell Line. Radiat. Res. 153, 125–130.
- Hoppe, M.M., Sundar, R., Tan, D.S.P., and Jeyasekharan, A.D. (2018). Biomarkers for Homologous Recombination Deficiency in Cancer. JNCI J. Natl. Cancer Inst.

- Hou, E.W., Prasad, R., Asagoshi, K., Masaoka, A., and Wilson, S.H. (2007). Comparative assessment of plasmid and oligonucleotide DNA substrates in measurement of in vitro base excision repair activity. Nucleic Acids Res. 35, e112–e112.
- Howard, S.M., Yanez, D.A., and Stark, J.M. (2015). DNA Damage Response Factors from Diverse Pathways, Including DNA Crosslink Repair, Mediate Alternative End Joining. PLOS Genet. 11, e1004943.
- Hu, S., Hui, Z., Lirussi, F., Garrido, C., Ye, X.-Y., and Xie, T. (2021). Small molecule DNA-PK inhibitors as potential cancer therapy: a patent review (2010–present). Expert Opin. Ther. Pat. 1–18.
- Huang, H. (2005). Newborn screening for severe combined immunodeficiency (SCID): a review. Front. Biosci. 10, 1024.
- Huang, F., and Mazin, A.V. (2014). A Small Molecule Inhibitor of Human RAD51 Potentiates Breast Cancer Cell Killing by Therapeutic Agents in Mouse Xenografts. PLoS ONE 9, e100993.
- Huang, H., and Hopkins, P.B. (1993). DNA interstrand cross-linking by formaldehyde: nucleotide sequence preference and covalent structure of the predominant cross-link formed in synthetic oligonucleotides. J. Am. Chem. Soc. 115, 9402–9408.
- Huang, F., Motlekar, N.A., Burgwin, C.M., Napper, A.D., Diamond, S.L., and Mazin, A.V. (2011a). Identification of Specific Inhibitors of Human RAD51 Recombinase Using High-Throughput Screening. ACS Chem. Biol. 6, 628–635.
- Huang, F., Mazina, O.M., Zentner, I.J., Cocklin, S., and Mazin, A.V. (2012). Inhibition of Homologous Recombination in Human Cells by Targeting RAD51 Recombinase. J. Med. Chem. 55, 3011–3020.
- Huang, M., Kim, J.M., Shiotani, B., Yang, K., Zou, L., and D'Andrea, A.D. (2010). The FANCM/FAAP24 complex is required for the DNA interstrand crosslink-induced checkpoint response. Mol. Cell 39, 259–268.
- Huang, M., Kennedy, R., Ali, A.M., Moreau, L.A., Meetei, A.R., D'Andrea, A.D., and Chen, C.C. (2011b). Human MutS and FANCM complexes function as redundant DNA damage sensors in the Fanconi Anemia pathway. DNA Repair 10, 1203–1212.
- Huertas, P., and Jackson, S.P. (2009). Human CtIP Mediates Cell Cycle Control of DNA End Resection and Double Strand Break Repair. J. Biol. Chem. 284, 9558–9565.
- Hutchinson, F. (1989). On the Measurement of DNA Double-Strand Breaks by Neutral Elution. Radiat. Res. 120, 182.
- Hwang, E.S., Naeger, L.K., and DiMaio, D. (1996). Activation of the endogenous p53 growth inhibitory pathway in HeLa cervical carcinoma cells by expression of the bovine papillomavirus E2 gene. Oncogene 12, 795–803.
- Iliakis, G., Blöcher, D., Metzger, L., and Pantelias, G. (1991a). Comparison of DNA Double-strand Break Rejoining as Measured by Pulsed Field Gel Electrophoresis, Neutral Sucrose Gradient Centrifugation and Non-unwinding Filter Elution in Irradiated Plateau-phase CHO Cells. Int. J. Radiat. Biol. 59, 927–939.
- Iliakis, G., Metzger, L., Okayasu, R., Pantelias, G., and Cicilioni, O. (1991b). Measurement of DNA Double Strand Breaks in Mammalian Cells: Comparison Between Pulsed Field Gel Electrophoresis and Non-Unwinding Filter Elution. In The Early Effects of Radiation on DNA, E.M. Fielden, and P. O'Neill, eds. (Berlin, Heidelberg: Springer Berlin Heidelberg), pp. 55–69.
- Iliakis, G., Wang, H., Perrault, A.R., Boecker, W., Rosidi, B., Windhofer, F., Wu, W., Guan, J., Terzoudi, G., and Pantelias, G. (2004). Mechanisms of DNA double strand break repair and chromosome aberration formation. Cytogenet. Genome Res. 104, 14–20.
- Iliakis, G., Mladenov, E., and Cheong, N. (2012). In Vitro Rejoining of Double Strand Breaks in Genomic DNA. In DNA Repair Protocols, L. Bjergbæk, ed. (Totowa, NJ: Humana Press), pp. 471–484.
- Iliakis, G., Mladenov, E., and Mladenova, V. (2019). Necessities in the Processing of DNA Double Strand Breaks and Their Effects on Genomic Instability and Cancer. Cancers 11, 1671.

- Iliakis, G.E., Metzger, L., Denko, N., and Stamato, T.D. (1991c). Detection of DNA Double-strand Breaks in Synchronous Cultures of CHO Cells by Means of Asymmetric Field Inversion Gel Electrophoresis. Int. J. Radiat. Biol. 59, 321–341.
- Isabelle, M., Moreel, X., Gagné, J.-P., Rouleau, M., Ethier, C., Gagné, P., Hendzel, M.J., and Poirier, G.G. (2010). Investigation of PARP-1, PARP-2, and PARG interactomes by affinity-purification mass spectrometry. Proteome Sci. 8, 22.
- Ivashkevich, A., Redon, C.E., Nakamura, A.J., Martin, R.F., and Martin, O.A. (2012). Use of the γ-H2AX assay to monitor DNA damage and repair in translational cancer research. Cancer Lett. 327, 123–133.
- Javvadi, P., Makino, H., Das, A.K., Lin, Y.-F., Chen, D.J., Chen, B.P., and Nirodi, C.S. (2012). Threonine 2609 phosphorylation of the DNA-dependent protein kinase is a critical prerequisite for epidermal growth factor receptor-mediated radiation resistance. Mol. Cancer Res. MCR 10, 1359–1368.
- Jelinic, P., and Levine, D.A. (2014). New Insights into PARP Inhibitors' Effect on Cell Cycle and Homology-Directed DNA Damage Repair. Mol. Cancer Ther. 13, 1645–1654.
- Jezkova, L., Zadneprianetc, M., Kulikova, E., Smirnova, E., Bulanova, T., Depes, D., Falkova, I., Boreyko, A., Krasavin, E., Davidkova, M., et al. (2018). Particles with similar LET values generate DNA breaks of different complexity and reparability: a high-resolution microscopy analysis of γH2AX/53BP1 foci. Nanoscale 10, 1162–1179.
- Jin, M.H., and Oh, D.-Y. (2019). ATM in DNA repair in cancer. Pharmacol. Ther. 203, 107391.
- Jiricny, J. (2006). The multifaceted mismatch-repair system. Nat. Rev. Mol. Cell Biol. 7, 335–346.
- Johnson-Arbor, K., and Dubey, R. (2020). Doxorubicin. In StatPearls, (Treasure Island (FL): StatPearls Publishing), p.
- Joshi, N., and Grant, S.G. (2014). Pulsed-Field Gel Electrophoresis Analysis of Multicellular DNA Double-Strand Break Damage and Repair. In Molecular Toxicology Protocols, P. Keohavong, and S.G. Grant, eds. (Totowa, NJ: Humana Press), pp. 193–202.
- Kakarougkas, A., and Jeggo, P.A. (2014). DNA DSB repair pathway choice: an orchestrated handover mechanism. Br. J. Radiol. 87, 20130685.
- Kalousi, A., and Soutoglou, E. (2016). Nuclear compartmentalization of DNA repair. Curr. Opin. Genet. Dev. 37, 148–157.
- Kaminski, A.M., Tumbale, P.P., Schellenberg, M.J., Williams, R.S., Williams, J.G., Kunkel, T.A., Pedersen, L.C., and Bebenek, K. (2018). Structures of DNA-bound human ligase IV catalytic core reveal insights into substrate binding and catalysis. Nat. Commun. 9, 2642.
- Kang, Y.-J., and Yan, C.T. (2018). Regulation of DNA repair in the absence of classical non-homologous end joining. DNA Repair 68, 34–40.
- Karanam, K., Kafri, R., Loewer, A., and Lahav, G. (2012). Quantitative Live Cell Imaging Reveals a Gradual Shift between DNA Repair Mechanisms and a Maximal Use of HR in Mid S Phase. Mol. Cell 47, 320–329.
- Kassab, M.A., and Yu, X. (2019). The role of dePARylation in DNA damage repair and cancer suppression. DNA Repair 76, 20–29.
- Kato, N., Kawasoe, Y., Williams, H., Coates, E., Roy, U., Shi, Y., Beese, L.S., Schärer, O.D., Yan, H., Gottesman, M.E., et al. (2017). Sensing and Processing of DNA Interstrand Crosslinks by the Mismatch Repair Pathway. Cell Rep. 21, 1375–1385.
- Kelso, A.A., Lopezcolorado, F.W., Bhargava, R., and Stark, J.M. (2019). Distinct roles of RAD52 and POLQ in chromosomal break repair and replication stress response. PLOS Genet. 15, e1008319.
- Kent, T., Chandramouly, G., McDevitt, S.M., Ozdemir, A.Y., and Pomerantz, R.T. (2015). Mechanism of microhomology-mediated end-joining promoted by human DNA polymerase θ. Nat. Struct. Mol. Biol. 22, 230–237.

- Khoury, L., Zalko, D., and Audebert, M. (2020). Evaluation of the genotoxic potential of apoptosis inducers with the γH2AX assay in human cells. Mutat. Res. Toxicol. Environ. Mutagen. 852, 503165.
- Kim, J.M., Kee, Y., Gurtan, A., and D'Andrea, A.D. (2008). Cell cycle–dependent chromatin loading of the Fanconi anemia core complex by FANCM/FAAP24. Blood 111, 5215–5222.
- Kinner, A., Wu, W., Staudt, C., and Iliakis, G. (2008). Gamma-H2AX in recognition and signaling of DNA double-strand breaks in the context of chromatin. Nucleic Acids Res. 36, 5678–5694.
- Kirchner, J.J., Sigurdsson, S.T., and Hopkins, P.B. (1992). Interstrand cross-linking of duplex DNA by nitrous acid: covalent structure of the dG-to-dG cross-link at the sequence 5'-CG. J. Am. Chem. Soc. 114, 4021–4027.
- Knudsen, N.Ø., Andersen, S.D., Lützen, A., Nielsen, F.C., and Rasmussen, L.J. (2009). Nuclear translocation contributes to regulation of DNA excision repair activities. DNA Repair 8, 682–689.
- Koch, C.A., Agyei, R., Galicia, S., Metalnikov, P., O'Donnell, P., Starostine, A., Weinfeld, M., and Durocher, D. (2004). Xrcc4 physically links DNA end processing by polynucleotide kinase to DNA ligation by DNA ligase IV. EMBO J. 23, 3874–3885.
- Kochan, J.A., Desclos, E.C.B., Bosch, R., Meister, L., Vriend, L.E.M., van Attikum, H., and Krawczyk, P.M. (2017). Meta-analysis of DNA double-strand break response kinetics. Nucleic Acids Res. 45, 12625–12637.
- Konecny, G.E., and Kristeleit, R.S. (2016). PARP inhibitors for BRCA1/2-mutated and sporadic ovarian cancer: current practice and future directions. Br. J. Cancer 115, 1157–1173.
- Koniaras, K., Cuddihy, A.R., Christopoulos, H., Hogg, A., and O'Connell, M.J. (2001). Inhibition of Chk1-dependent G2 DNA damage checkpoint radiosensitizes p53 mutant human cells. Oncogene 20, 7453–7463.
- Kopa, P., Macieja, A., Gulbas, I., Pastwa, E., and Poplawski, T. (2020). Inhibition of DNA-PK potentiates the synergistic effect of NK314 and etoposide combination on human glioblastoma cells. Mol. Biol. Rep. 47, 67–76.
- Kopp, B., Khoury, L., and Audebert, M. (2019). Validation of the γH2AX biomarker for genotoxicity assessment: a review. Arch. Toxicol. 93, 2103–2114.
- Kostyrko, K., and Mermod, N. (2016). Assays for DNA double-strand break repair by microhomology-based end-joining repair mechanisms. Nucleic Acids Res. 44, e56–e56.
- Kow, Y.W., and Dare, A. (2000). Detection of Abasic Sites and Oxidative DNA Base Damage Using an ELISA-like Assay. Methods 22, 164–169.
- Kraakman-van der Zwet, M., Overkamp, W.J.I., van Lange, R.E.E., Essers, J., van Duijn-Goedhart, A., Wiggers, I., Swaminathan, S., van Buul, P.P.W., Errami, A., Tan, R.T.L., et al. (2002). Brca2 (XRCC11) Deficiency Results in Radioresistant DNA Synthesis and a Higher Frequency of Spontaneous Deletions. Mol. Cell. Biol. 22, 669–679.
- Krajewska, M., Fehrmann, R.S.N., Schoonen, P.M., Labib, S., de Vries, E.G.E., Franke, L., and van Vugt, M.A.T.M. (2015). ATR inhibition preferentially targets homologous recombination-deficient tumor cells. Oncogene 34, 3474–3481.
- Krisch, R.E., Flick, M.B., and Trumbore, C.N. (1991). Radiation Chemical Mechanisms of Single- and Double-Strand Break Formation in Irradiated SV40 DNA. Radiat. Res. 126, 251.
- Krokan, H.E., and Bjoras, M. (2013). Base Excision Repair. Cold Spring Harb. Perspect. Biol. 5, a012583–a012583.
- Krokan, H.E., Standal, R., and Slupphaug, G. (1997). DNA glycosylases in the base excision repair of DNA. Biochem. J. 325 (Pt 1), 1–16.
- Krumova, K., and Cosa, G. (2016). Chapter 1. Overview of Reactive Oxygen Species. In Comprehensive Series in Photochemical & Photobiological Sciences, S. Nonell, and C. Flors, eds. (Cambridge: Royal Society of Chemistry), pp. 1–21.

- Kucherlapati, R.S., Spencer, J., and Moore, P.D. (1985). Homologous recombination catalyzed by human cell extracts. Mol. Cell. Biol. 5, 714–720.
- Kuilman, T., Michaloglou, C., Vredeveld, L.C.W., Douma, S., van Doorn, R., Desmet, C.J., Aarden, L.A., Mooi, W.J., and Peeper, D.S. (2008). Oncogene-Induced Senescence Relayed by an Interleukin-Dependent Inflammatory Network. Cell 133, 1019–1031.
- Kumar, A., Bhatkar, D., Jahagirdar, D., and Sharma, N.K. (2017). Non-homologous End Joining Inhibitor SCR-7 to Exacerbate Low-dose Doxorubicin Cytotoxicity in HeLa Cells. J. Cancer Prev. 22, 47–54.
- Kumar, T.S., Kari, V., Choudhary, B., Nambiar, M., Akila, T.S., and Raghavan, S.C. (2010). Anti-apoptotic Protein BCL2 Down-regulates DNA End Joining in Cancer Cells. J. Biol. Chem. 285, 32657–32670.
- Kunz, C., Saito, Y., and Schär, P. (2009). DNA Repair in mammalian cells: Mismatched repair: variations on a theme. Cell. Mol. Life Sci. CMLS 66, 1021–1038.
- Kurashige, T., Shimamura, M., and Nagayama, Y. (2016). Differences in quantification of DNA double-strand breaks assessed by 53BP1/γH2AX focus formation assays and the comet assay in mammalian cells treated with irradiation and N-acetyl-L-cysteine. J. Radiat. Res. (Tokyo) 57, 312–317.
- Kusakabe, M., Onishi, Y., Tada, H., Kurihara, F., Kusao, K., Furukawa, M., Iwai, S., Yokoi, M., Sakai, W., and Sugasawa, K. (2019). Mechanism and regulation of DNA damage recognition in nucleotide excision repair. Genes Environ. 41, 2.
- La, D.K., and Swenberg, J.A. (1996). DNA adducts: biological markers of exposure and potential applications to risk assessment. Mutat. Res. Genet. Toxicol. 365, 129–146.
- Labhart, P. (1999). Nonhomologous DNA end joining in cell-free systems. Eur. J. Biochem. 265, 849–861.
- Lacoste, S., Bhatia, S., Chen, Y., Bhatia, R., and O'Connor, T.R. (2017). Autologous hematopoietic stem cell transplantation in lymphoma patients is associated with a decrease in the double strand break repair capacity of peripheral blood lymphocytes. PLOS ONE 12, e0171473.
- Lafont, F., Ayadi, N., Charlier, C., Weigel, P., Nabiev, I., Benhelli-Mokrani, H., and Fleury, F. (2018). Assessment of DNA-PKcs kinase activity by quantum dot–based microarray. Sci. Rep. 8, 10968.
- Lam, I., and Keeney, S. (2015). Mechanism and Regulation of Meiotic Recombination Initiation. Cold Spring Harb. Perspect. Biol. 7, a016634.
- Lambin, P., van Stiphout, R.G.P.M., Starmans, M.H.W., Rios-Velazquez, E., Nalbantov, G., Aerts, H.J.W.L., Roelofs, E., van Elmpt, W., Boutros, P.C., Granone, P., et al. (2013). Predicting outcomes in radiation oncology—multifactorial decision support systems. Nat. Rev. Clin. Oncol. 10, 27–40.
- Laurini, E., Marson, D., Fermeglia, A., Aulic, S., Fermeglia, M., and Pricl, S. (2020). Role of Rad51 and DNA repair in cancer: A molecular perspective. Pharmacol. Ther. 208, 107492.
- Lavin, M.F., Delia, D., and Chessa, L. (2006). ATM and the DNA damage response. Workshop on ataxia-telangiectasia and related syndromes. EMBO Rep. 7, 154–160.
- Lavrik, O.I. (2020). PARPs' impact on base excision DNA repair. DNA Repair 93, 102911.
- Leatherbarrow, E.L., Harper, J.V., Cucinotta, F.A., and O'Neill, P. (2006). Induction and quantification of γ-H2AX foci following low and high LET-irradiation. Int. J. Radiat. Biol. 82, 111–118.
- Lebedeva, N.A., Rechkunova, N.I., Dezhurov, S.V., Khodyreva, S.N., Favre, A., Blanco, L., and Lavrik, O.I. (2005). Comparison of functional properties of mammalian DNA polymerase λ and DNA polymerase β in reactions of DNA synthesis related to DNA repair. Biochim. Biophys. Acta BBA - Proteins Proteomics 1751, 150–158.
- Lee, J.-H., and Paull, T.T. (2007). Activation and regulation of ATM kinase activity in response to DNA double-strand breaks. Oncogene 26, 7741–7748.

- Lee, Y., Wang, Q., Shuryak, I., Brenner, D.J., and Turner, H.C. (2019). Development of a high-throughput γ-H2AX assay based on imaging flow cytometry. Radiat. Oncol. 14.
- Lees-Miller, S.P., Godbout, R., Chan, D.W., Weinfeld, M., Day, R.S., Barron, G.M., and Allalunis-Turner, J. (1995). Absence of p350 subunit of DNA-activated protein kinase from a radiosensitive human cell line. Science 267, 1183–1185.
- Lehmann, A.R. (2011). DNA polymerases and repair synthesis in NER in human cells. DNA Repair 10, 730–733.
- Li, J., Liu, Z., Tan, C., Guo, X., Wang, L., Sancar, A., and Zhong, D. (2010). Dynamics and mechanism of repair of ultraviolet-induced (6–4) photoproduct by photolyase. Nature 466, 887–890.
- Li, J., Sun, H., Huang, Y., Wang, Y., Liu, Y., and Chen, X. (2019a). Pathways and assays for DNA double-strand break repair by homologous recombination. Acta Biochim. Biophys. Sin. 51, 879–889.
- Li, J., Sun, H., Huang, Y., Wang, Y., Liu, Y., and Chen, X. (2019b). Pathways and assays for DNA double-strand break repair by homologous recombination. Acta Biochim. Biophys. Sin. 51, 879–889.
- Li, W., Li, F., Huang, Q., Shen, J., Wolf, F., He, Y., Liu, X., Hu, Y.A., Bedford, J.S., and Li, C.-Y. (2011). Quantitative, Noninvasive Imaging of Radiation-Induced DNA Double-Strand Breaks In Vivo. Cancer Res. 71, 4130–4137.
- Li, Z., Pearlman, A.H., and Hsieh, P. (2016). DNA mismatch repair and the DNA damage response. DNA Repair 38, 94–101.
- Liang, L., Deng, L., Nguyen, S.C., Zhao, X., Maulion, C.D., Shao, C., and Tischfield, J.A. (2008). Human DNA ligases I and III, but not ligase IV, are required for microhomology-mediated end joining of DNA double-strand breaks. Nucleic Acids Res. 36, 3297–3310.
- Liang, M.-L., Hsieh, T.-H., Liu, Y.-R., Chen, Y.-W., Lee, Y.-Y., Chang, F.-C., Lin, S.-C., Huang, M.-C., Ho, D.M.-T., Wong, T.-T., et al. (2018). Significance of cyclin D1 overexpression in progression and radio-resistance of pediatric ependymomas. Oncotarget 9, 2527–2542.
- Liccardi, G., Hartley, J.A., and Hochhauser, D. (2011). EGFR Nuclear Translocation Modulates DNA Repair following Cisplatin and Ionizing Radiation Treatment. Cancer Res. 71, 1103–1114.
- Lin, J., Fallahi-Sichani, M., Chen, J., and Sorger, P.K. (2016). Cyclic Immunofluorescence (CycIF), A Highly Multiplexed Method for Single-cell Imaging. Curr. Protoc. Chem. Biol. 8, 251–264.
- Lindahl, T. (1982). DNA Repair Enzymes. Annu. Rev. Biochem. 51, 61–87.
- Liu, J., Doty, T., Gibson, B., and Heyer, W.-D. (2010). Human BRCA2 protein promotes RAD51 filament formation on RPA-covered single-stranded DNA. Nat. Struct. Mol. Biol. 17, 1260–1262.
- Liu, J., Sneeden, J., and Heyer, W.-D. (2011). In vitro assays for DNA pairing and recombination-associated DNA synthesis. In DNA Recombination, H. Tsubouchi, ed. (Totowa, NJ: Humana Press), pp. 363–383.
- Liu, J., Zhang, C., Hu, W., and Feng, Z. (2019). Tumor suppressor p53 and metabolism. J. Mol. Cell Biol. 11, 284–292.
- Liu, Y., Beard, W.A., Shock, D.D., Prasad, R., Hou, E.W., and Wilson, S.H. (2005). DNA Polymerase β and Flap Endonuclease 1 Enzymatic Specificities Sustain DNA Synthesis for Long Patch Base Excision Repair. J. Biol. Chem. 280, 3665–3674.
- Liu, Y., Zhang, L., Liu, Y., Sun, C., Zhang, H., Miao, G., Di, C.X., Zhou, X., Zhou, R., and Wang, Z. (2015). DNA-PKcs Deficiency Inhibits Glioblastoma Cell-Derived Angiogenesis After Ionizing Radiation: GLIOBLASTOMA CELL-DERIVED ANGIOGENESIS. J. Cell. Physiol. 230, 1094–1103.
- Liu, Y., Li, Y., and Lu, X. (2016). Regulators in the DNA damage response. Arch. Biochem. Biophys. 594, 18–25.
- Löbrich, M., Shibata, A., Beucher, A., Fisher, A., Ensminger, M., Goodarzi, A.A., Barton, O., and Jeggo, P.A. (2010). γH2AX foci analysis for monitoring DNA double-strand break repair: Strengths, limitations and optimization. Cell Cycle 9, 662–669.

- Lok, B.H., and Powell, S.N. (2012). Molecular pathways: understanding the role of Rad52 in homologous recombination for therapeutic advancement. Clin. Cancer Res. Off. J. Am. Assoc. Cancer Res. 18, 6400–6406.
- Lopez, B., Rousset, S., and Coppey, J. (1987). Homologous recombination intermediates between two duplex DNA catalysed by human cell extracts. Nucleic Acids Res. 15, 5643–5655.
- Lopez-Canovas, L., Martinez Benitez, M.B., Herrera Isidron, J.A., and Flores Soto, E. (2019). Pulsed Field Gel Electrophoresis: Past, present, and future. Anal. Biochem. 573, 17–29.
- Lopez-Martinez, D., Liang, C.-C., and Cohn, M.A. (2016). Cellular response to DNA interstrand crosslinks: the Fanconi anemia pathway. Cell. Mol. Life Sci. 73, 3097–3114.
- López-Saavedra, A., Gómez-Cabello, D., Domínguez-Sánchez, M.S., Mejías-Navarro, F., Fernández-Ávila, M.J., Dinant, C., Martínez-Macías, M.I., Bartek, J., and Huertas, P. (2016). A genome-wide screening uncovers the role of CCAR2 as an antagonist of DNA end resection. Nat. Commun. 7, 12364.
- Lord, C.J., and Ashworth, A. (2012). The DNA damage response and cancer therapy. Nature 481, 287–294.
- Lord, C.J., and Ashworth, A. (2017). PARP inhibitors: Synthetic lethality in the clinic. Science 355, 1152–1158.
- Lou, J., Priest, D.G., Solano, A., Kerjouan, A., and Hinde, E. (2020). Spatiotemporal dynamics of 53BP1 dimer recruitment to a DNA double strand break. Nat. Commun. 11, 5776.
- Lu, G., Duan, J., Shu, S., Wang, X., Gao, L., Guo, J., and Zhang, Y. (2016). Ligase I and ligase III mediate the DNA double-strand break ligation in alternative end-joining. Proc. Natl. Acad. Sci. 113, 1256–1260.
- Lu, H., Saha, J., Beckmann, P.J., Hendrickson, E.A., and Davis, A.J. (2019). DNA-PKcs promotes chromatin decondensation to facilitate initiation of the DNA damage response. Nucleic Acids Res. 47, 9467–9479.
- Lukas, C., Savic, V., Bekker-Jensen, S., Doil, C., Neumann, B., Sølvhøj Pedersen, R., Grøfte, M., Chan, K.L., Hickson, I.D., Bartek, J., et al. (2011a). 53BP1 nuclear bodies form around DNA lesions generated by mitotic transmission of chromosomes under replication stress. Nat. Cell Biol. 13, 243–253.
- Lukas, J., Lukas, C., and Bartek, J. (2011b). More than just a focus: The chromatin response to DNA damage and its role in genome integrity maintenance. Nat. Cell Biol. 13, 1161–1169.
- Ma, Y., and Lieber, M.R. (2006). In Vitro Nonhomologous DNA End Joining System. In Methods in Enzymology, (Elsevier), pp. 502–510.
- Ma, W., Halweg, C.J., Menendez, D., and Resnick, M.A. (2012). Differential effects of poly(ADP-ribose) polymerase inhibition on DNA break repair in human cells are revealed with Epstein-Barr virus. Proc. Natl. Acad. Sci. 109, 6590–6595.
- Ma, W., Westmoreland, J.W., and Resnick, M.A. (2013). Homologous recombination rescues ssDNA gaps generated by nucleotide excision repair and reduced translesion DNA synthesis in yeast G2 cells. Proc. Natl. Acad. Sci. U. S. A. 110, E2895-2904.
- Machida, Y.J., Machida, Y., Chen, Y., Gurtan, A.M., Kupfer, G.M., D'Andrea, A.D., and Dutta, A. (2006). UBE2T Is the E2 in the Fanconi Anemia Pathway and Undergoes Negative Autoregulation. Mol. Cell 23, 589–596.
- MacPhail, S.H., Banáth, J.P., Yu, Y., Chu, E., and Olive, P.L. (2003). Cell Cycle-Dependent Expression of Phosphorylated Histone H2AX: Reduced Expression in Unirradiated but not X-Irradiated G 1 -Phase Cells. Radiat. Res. 159, 759–767.
- Mah, L.-J., El-Osta, A., and Karagiannis, T.C. (2010). γH2AX: a sensitive molecular marker of DNA damage and repair. Leukemia 24, 679–686.
- Makarova, A.V., and Burgers, P.M. (2015). Eukaryotic DNA polymerase ζ. DNA Repair 29, 47–55.

- Makharashvili, N., Tubbs, A.T., Yang, S.-H., Wang, H., Barton, O., Zhou, Y., Deshpande, R.A., Lee, J.-H., Lobrich, M., Sleckman, B.P., et al. (2014). Catalytic and Noncatalytic Roles of the CtIP Endonuclease in Double-Strand Break End Resection. Mol. Cell 54, 1022–1033.
- Malinge, J.-M., Giraud-Panis, M.-J., and Leng, M. (1999). Interstrand cross-links of cisplatin induce striking distortions in DNA. J. Inorg. Biochem. 77, 23–29.
- Mamrak, N.E., Shimamura, A., and Howlett, N.G. (2017). Recent discoveries in the molecular pathogenesis of the inherited bone marrow failure syndrome Fanconi anemia. Blood Rev. 31, 93–99.
- Manié, E., Popova, T., Battistella, A., Tarabeux, J., Caux-Moncoutier, V., Golmard, L., Smith, N.K., Mueller, C.R., Mariani, O., Sigal-Zafrani, B., et al. (2016). Genomic hallmarks of homologous recombination deficiency in invasive breast carcinomas: Genomic hallmarks of homologous recombination defect. Int. J. Cancer 138, 891–900.
- Mansour, W.Y., Borgmann, K., Petersen, C., Dikomey, E., and Dahm-Daphi, J. (2013). The absence of Ku but not defects in classical non-homologous end-joining is required to trigger PARP1-dependent end-joining. DNA Repair 12, 1134–1142.
- Marnef, A., and Legube, G. (2017). Organizing DNA repair in the nucleus: DSBs hit the road. Curr. Opin. Cell Biol. 46, 1–8.
- Marrero, A., Lawrence, S., Wilsker, D., Voth, A.R., and Kinders, R.J. (2016). Translating pharmacodynamic biomarkers from bench to bedside: analytical validation and fit-for-purpose studies to qualify multiplex immunofluorescent assays for use on clinical core biopsy specimens. Semin. Oncol. 43, 453–463.
- Marteijn, J.A., Lans, H., Vermeulen, W., and Hoeijmakers, J.H.J. (2014). Understanding nucleotide excision repair and its roles in cancer and ageing. Nat. Rev. Mol. Cell Biol. 15, 465–481.
- Martin, S.A. (2016). The DNA mismatch repair pathway. In DNA Repair in Cancer Therapy, (Elsevier), pp. 151–177.
- Masters, J.R. (2002). HeLa cells 50 years on: the good, the bad and the ugly. Nat. Rev. Cancer 2, 315–319.
- Masutani, C., Kusumoto, R., Yamada, A., Dohmae, N., Yokoi, M., Yuasa, M., Araki, M., Iwai, S., Takio, K., and Hanaoka, F. (1999). The XPV (xeroderma pigmentosum variant) gene encodes human DNA polymerase η. Nature 399, 700–704.
- Mateos-Gomez, P.A., Gong, F., Nair, N., Miller, K.M., Lazzerini-Denchi, E., and Sfeir, A. (2015). Mammalian polymerase θ promotes alternative NHEJ and suppresses recombination. Nature 518, 254–257.
- Matsuoka, S., Ballif, B.A., Smogorzewska, A., McDonald, E.R., Hurov, K.E., Luo, J., Bakalarski, C.E., Zhao, Z., Solimini, N., Lerenthal, Y., et al. (2007). ATM and ATR Substrate Analysis Reveals Extensive Protein Networks Responsive to DNA Damage. Science 316, 1160–1166.
- Matsuzaki, K., Harada, A., Takeiri, A., Tanaka, K., and Mishima, M. (2010). Whole cell-ELISA to measure the γH2AX response of six aneugens and eight DNA-damaging chemicals. Mutat. Res. Toxicol. Environ. Mutagen. 700, 71–79.
- Mattiroli, F., Vissers, J.H.A., van Dijk, W.J., Ikpa, P., Citterio, E., Vermeulen, W., Marteijn, J.A., and Sixma, T.K. (2012). RNF168 Ubiquitinates K13-15 on H2A/H2AX to Drive DNA Damage Signaling. Cell 150, 1182–1195.
- Maya, R. (2001). ATM-dependent phosphorylation of Mdm2 on serine 395: role in p53 activation by DNA damage. Genes Dev. 15, 1067–1077.
- McCullough, A.K., Sanchez, A., Dodson, M.L., Marapaka, P., Taylor, J.S., and Lloyd, R.S. (2001). The reaction mechanism of DNA glycosylase/AP lyases at abasic sites. Biochemistry 40, 561–568.

- McKay, M.J., Craig, J., Kalitsis, P., Kozlov, S., Verschoor, S., Chen, P., Lobachevsky, P., Vasireddy, R., Yan, Y., Ryan, J., et al. (2019). A Roberts Syndrome Individual With Differential Genotoxin Sensitivity and a DNA Damage Response Defect. Int. J. Radiat. Oncol. 103, 1194–1202.
- McKinnon, P.J. (2012). ATM and the Molecular Pathogenesis of Ataxia Telangiectasia. Annu. Rev. Pathol. Mech. Dis. 7, 303–321.
- McKinnon, P.J., and Caldecott, K.W. (2007). DNA Strand Break Repair and Human Genetic Disease. Annu. Rev. Genomics Hum. Genet. 8, 37–55.
- McManus, K.J., and Hendzel, M.J. (2005). ATM-dependent DNA Damage-independent Mitotic Phosphorylation of H2AX in Normally Growing Mammalian Cells. Mol. Biol. Cell 16, 5013–5025.
- McNeill, D.R., Whitaker, A.M., Stark, W.J., Illuzzi, J.L., McKinnon, P.J., Freudenthal, B.D., and Wilson, D.M. (2020). Functions of the major abasic endonuclease (APE1) in cell viability and genotoxin resistance. Mutagenesis 35, 27–38.
- McVey, M., Khodaverdian, V.Y., Meyer, D., Cerqueira, P.G., and Heyer, W.-D. (2016). Eukaryotic DNA Polymerases in Homologous Recombination. Annu. Rev. Genet. 50, 393–421.
- Meaney-Delman, D., and Bellcross, C.A. (2013). Hereditary Breast/Ovarian Cancer Syndrome. Obstet. Gynecol. Clin. North Am. 40, 475–512.
- Mehta, A., and Haber, J.E. (2014). Sources of DNA Double-Strand Breaks and Models of Recombinational DNA Repair. Cold Spring Harb. Perspect. Biol. 6, a016428–a016428.
- Mehta, A., Awah, C.U., and Sonabend, A.M. (2018). Topoisomerase II Poisons for Glioblastoma; Existing Challenges and Opportunities to Personalize Therapy. Front. Neurol. 9, 459.
- Mehta, R., Wood, A.C., Yu, J., and Kim, R. (2021). Investigational PARP inhibitors for the treatment of biliary tract cancer: spotlight on preclinical and clinical studies. Expert Opin. Investig. Drugs 1–11.
- Melendez-Colon, V.J., Luch, A., Seidel, A., and Baird, W.M. (1999). Cancer initiation by polycyclic aromatic hydrocarbons results from formation of stable DNA adducts rather than apurinic sites. Carcinogenesis 20, 1885–1891.
- Meredith, A.-M., and Dass, C.R. (2016). Increasing role of the cancer chemotherapeutic doxorubicin in cellular metabolism. J. Pharm. Pharmacol. 68, 729–741.
- Meresse, P., Dechaux, E., Monneret, C., and Bertounesque, E. (2004). Etoposide: Discovery and Medicinal Chemistry. Curr. Med. Chem. 11, 2443–2466.
- Meryet-Figuière, M., Lambert, B., Gauduchon, P., Vigneron, N., Brotin, E., Poulain, L., and Denoyelle, C. (2016). An overview of long non-coding RNAs in ovarian cancers. Oncotarget 7, 44719–44734.
- Meuth, M. (2010). Chk1 suppressed cell death. Cell Div. 5, 21.
- Mijit, M., Caracciolo, V., Melillo, A., Amicarelli, F., and Giordano, A. (2020). Role of p53 in the Regulation of Cellular Senescence. Biomolecules 10, 420.
- Millau, J.-F. (2006). Test fonctionnel de mesure des activités enzymatiques de réparation de l'ADN par excision resynthèse sur support miniaturisé : mise au point et applications. Joseph Fourier Grenoble 1.
- Millau, J.-F., Raffin, A.-L., Caillat, S., Claudet, C., Arras, G., Ugolin, N., Douki, T., Ravanat, J.-L., Breton, J., Oddos, T., et al. (2008a). A microarray to measure repair of damaged plasmids by cell lysates. Lab. Chip 8, 1713.
- Millau, J.-F., Raffin, A.-L., Caillat, S., Claudet, C., Arras, G., Ugolin, N., Douki, T., Ravanat, J.-L., Breton, J., Oddos, T., et al. (2008b). A microarray to measure repair of damaged plasmids by cell lysates. Lab. Chip 8, 1713.
- Mimitou, E.P., and Symington, L.S. (2010). Ku prevents Exo1 and Sgs1-dependent resection of DNA ends in the absence of a functional MRX complex or Sae2. EMBO J. 29, 3358–3369.
- Mimitou, E.P., and Symington, L.S. (2011). DNA end resection—Unraveling the tail. DNA Repair 10, 344–348.

- Min, A., and Im, S.-A. (2020). PARP Inhibitors as Therapeutics: Beyond Modulation of PARylation. Cancers 12, 394.
- Miyaoka, Y., Berman, J.R., Cooper, S.B., Mayerl, S.J., Chan, A.H., Zhang, B., Karlin-Neumann, G.A., and Conklin, B.R. (2016). Systematic quantification of HDR and NHEJ reveals effects of locus, nuclease, and cell type on genome-editing. Sci. Rep. 6.
- Mizutani, H., Tada-Oikawa, S., Hiraku, Y., Kojima, M., and Kawanishi, S. (2005). Mechanism of apoptosis induced by doxorubicin through the generation of hydrogen peroxide. Life Sci. 76, 1439–1453.
- Mjelle, R., Hegre, S.A., Aas, P.A., Slupphaug, G., Drabløs, F., Sætrom, P., and Krokan, H.E. (2015). Cell cycle regulation of human DNA repair and chromatin remodeling genes. DNA Repair 30, 53–67.
- Mladenov, E., Magin, S., Soni, A., and Iliakis, G. (2016). DNA double-strand-break repair in higher eukaryotes and its role in genomic instability and cancer: Cell cycle and proliferation-dependent regulation. Semin. Cancer Biol. 37–38, 51–64.
- Mladenova, V., Mladenov, E., and Russev, G. (2009). Organization of Plasmid DNA into Nucleosome-Like Structures after Transfection in Eukaryotic Cells. Biotechnol. Biotechnol. Equip. 23, 1044–1047.
- Mohiuddin, I.S., and Kang, M.H. (2019). DNA-PK as an Emerging Therapeutic Target in Cancer. Front. Oncol. 9.
- Mohs, R.C., and Greig, N.H. (2017). Drug discovery and development: Role of basic biological research. Alzheimers Dement. Transl. Res. Clin. Interv. 3, 651–657.
- Moller, P. (2006). The Alkaline Comet Assay: Towards Validation in Biomonitoring of DNA Damaging Exposures. Basic Clin. Pharmacol. Toxicol. 98, 336–345.
- Møller, P., Azqueta, A., Boutet-Robinet, E., Koppen, G., Bonassi, S., Milić, M., Gajski, G., Costa, S., Teixeira, J.P., Costa Pereira, C., et al. (2020a). Minimum Information for Reporting on the Comet Assay (MIRCA): recommendations for describing comet assay procedures and results. Nat. Protoc.
- Møller, P., Azqueta, A., Boutet-Robinet, E., Koppen, G., Bonassi, S., Milić, M., Gajski, G., Costa, S., Teixeira, J.P., Costa Pereira, C., et al. (2020b). Minimum Information for Reporting on the Comet Assay (MIRCA): recommendations for describing comet assay procedures and results. Nat. Protoc. 15, 3817–3826.
- Morris, J.R., Boutell, C., Keppler, M., Densham, R., Weekes, D., Alamshah, A., Butler, L., Galanty, Y., Pangon, L., Kiuchi, T., et al. (2009). The SUMO modification pathway is involved in the BRCA1 response to genotoxic stress. Nature 462, 886–890.
- Moser, J., Kool, H., Giakzidis, I., Caldecott, K., Mullenders, L.H.F., and Fousteri, M.I. (2007). Sealing of Chromosomal DNA Nicks during Nucleotide Excision Repair Requires XRCC1 and DNA Ligase IIIα in a Cell-Cycle-Specific Manner. Mol. Cell 27, 311–323.
- Moynahan, M.E., and Jasin, M. (2010). Mitotic homologous recombination maintains genomic stability and suppresses tumorigenesis. Nat. Rev. Mol. Cell Biol. 11, 196–207.
- Moynahan, M.E., Cui, T.Y., and Jasin, M. (2001). Homology-directed dna repair, mitomycin-c resistance, and chromosome stability is restored with correction of a Brca1 mutation. Cancer Res. 61, 4842–4850.
- Muggiolu, G., Pomorski, M., Claverie, G., Berthet, G., Mer-Calfati, C., Saada, S., Devès, G., Simon, M., Seznec, H., and Barberet, P. (2017). Single α-particle irradiation permits real-time visualization of RNF8 accumulation at DNA damaged sites. Sci. Rep. 7, 41764.
- Mullins, E.A., Rodriguez, A.A., Bradley, N.P., and Eichman, B.F. (2019). Emerging Roles of DNA Glycosylases and the Base Excision Repair Pathway. Trends Biochem. Sci. 44, 765–781.
- Nagasawa, H., Lin, Y.-F., Kato, T.A., Brogan, J.R., Shih, H.-Y., Kurimasa, A., Bedford, J.S., Chen, B.P.C., and Little, J.B. (2017). Coordination of the Ser2056 and Thr2609 Clusters of DNA-PKcs in Regulating Gamma Rays and Extremely Low Fluencies of Alpha-Particle Irradiation to G0/G1 Phase Cells. Radiat. Res. 187, 259.

- Nagel, Z.D., Margulies, C.M., Chaim, I.A., McRee, S.K., Mazzucato, P., Ahmad, A., Abo, R.P., Butty, V.L., Forget, A.L., and Samson, L.D. (2014). Multiplexed DNA repair assays for multiple lesions and multiple doses via transcription inhibition and transcriptional mutagenesis. Proc. Natl. Acad. Sci. 111, E1823–E1832.
- Nagel, Z.D., Kitange, G.J., Gupta, S.K., Joughin, B.A., Chaim, I.A., Mazzucato, P., Lauffenburger, D.A., Sarkaria, J.N., and Samson, L.D. (2017). DNA Repair Capacity in Multiple Pathways Predicts Chemoresistance in Glioblastoma Multiforme. Cancer Res. 77, 198–206.
- Naipal, K.A.T., Verkaik, N.S., Ameziane, N., van Deurzen, C.H.M., ter Brugge, P., Meijers, M., Sieuwerts, A.M., Martens, J.W., O'Connor, M.J., Vrieling, H., et al. (2014). Functional Ex Vivo Assay to Select Homologous Recombination-Deficient Breast Tumors for PARP Inhibitor Treatment. Clin. Cancer Res. 20, 4816–4826.
- Nair, R.R., Bagheri, M., and Saini, D.K. (2015). Temporally distinct roles of ATM and ROS in genotoxic-stress-dependent induction and maintenance of cellular senescence. J. Cell Sci. 128, 342–353.
- Nakamura, A.J., Rao, V.A., Pommier, Y., and Bonner, W.M. (2010). The complexity of phosphorylated H2AX foci formation and DNA repair assembly at DNA double-strand breaks. Cell Cycle 9, 389–397.
- Neal, J.A., and Meek, K. (2019). Deciphering phenotypic variance in different models of DNA-PKcs deficiency. DNA Repair 73, 7–16.
- Neeley, W.L., and Essigmann, J.M. (2006). Mechanisms of Formation, Genotoxicity, and Mutation of Guanine Oxidation Products. Chem. Res. Toxicol. 19, 491–505.
- Nelson, B.C., Wright, C.W., Ibuki, Y., Moreno-Villanueva, M., Karlsson, H.L., Hendriks, G., Sims, C.M., Singh, N., and Doak, S.H. (2017). Emerging metrology for high-throughput nanomaterial genotoxicology. Mutagenesis 32, 215–232.
- Niedernhofer, L.J., Daniels, J.S., Rouzer, C.A., Greene, R.E., and Marnett, L.J. (2003). Malondialdehyde, a Product of Lipid Peroxidation, Is Mutagenic in Human Cells. J. Biol. Chem. 278, 31426–31433.
- Nikitaki, Z., Nikolov, V., Mavragani, I.V., Mladenov, E., Mangelis, A., Laskaratou, D.A., Fragkoulis, G.I., Hellweg, C.E., Martin, O.A., Emfietzoglou, D., et al. (2016). Measurement of complex DNA damage induction and repair in human cellular systems after exposure to ionizing radiations of varying linear energy transfer (LET). Free Radic. Res. 50, S64–S78.
- Nikoletopoulou, V., Markaki, M., Palikaras, K., and Tavernarakis, N. (2013). Crosstalk between apoptosis, necrosis and autophagy. Biochim. Biophys. Acta BBA - Mol. Cell Res. 1833, 3448–3459.
- Nikolova, T., Marini, F., and Kaina, B. (2017). Genotoxicity testing: Comparison of the γH2AX focus assay with the alkaline and neutral comet assays. Mutat. Res. Toxicol. Environ. Mutagen. 822, 10–18.
- Nilsen, H., and Krokan, H.E. (2001). Base excision repair in a network of defence and tolerance. Carcinogenesis 22, 987–998.
- Nimonkar, A.V., Genschel, J., Kinoshita, E., Polaczek, P., Campbell, J.L., Wyman, C., Modrich, P., and Kowalczykowski, S.C. (2011). BLM-DNA2-RPA-MRN and EXO1-BLM-RPA-MRN constitute two DNA end resection machineries for human DNA break repair. Genes Dev. 25, 350–362.
- Noël, G., Godon, C., Fernet, M., Giocanti, N., Mégnin-Chanet, F., and Favaudon, V. (2006). Radiosensitization by the poly(ADP-ribose) polymerase inhibitor 4-amino-1,8-naphthalimide is specific of the S phase of the cell cycle and involves arrest of DNA synthesis. Mol. Cancer Ther. 5, 564–574.
- Nomura, Y., Adachi, N., and Koyama, H. (2007). Human Mus81 and FANCB independently contribute to repair of DNA damage during replication. Genes Cells Devoted Mol. Cell. Mech. 12, 1111–1122.
- Noon, A.T., and Goodarzi, A.A. (2011). 53BP1-mediated DNA double strand break repair: Insert bad pun here. DNA Repair 10, 1071–1076.

- Noon, A.T., Shibata, A., Rief, N., Löbrich, M., Stewart, G.S., Jeggo, P.A., and Goodarzi, A.A. (2010). 53BP1-dependent robust localized KAP-1 phosphorylation is essential for heterochromatic DNA double-strand break repair. Nat. Cell Biol. 12, 177–184.
- Nurgali, K., Jagoe, R.T., and Abalo, R. (2018). Editorial: Adverse Effects of Cancer Chemotherapy: Anything New to Improve Tolerance and Reduce Sequelae? Front. Pharmacol. 9, 245.
- Nutley, B.P., Smith, N.F., Hayes, A., Kelland, L.R., Brunton, L., Golding, B.T., Smith, G.C.M., Martin, N.M.B., Workman, P., and Raynaud, F.I. (2005). Preclinical pharmacokinetics and metabolism of a novel prototype DNA-PK inhibitor NU7026. Br. J. Cancer 93, 1011–1018.
- Oberle, C., and Blattner, C. (2010). Regulation of the DNA Damage Response to DSBs by Post-Translational Modifications. Curr. Genomics 11, 184–198.
- O'Driscoll, M. (2012). Diseases Associated with Defective Responses to DNA Damage. Cold Spring Harb. Perspect. Biol. 4, a012773–a012773.
- Ogi, T., Limsirichaikul, S., Overmeer, R.M., Volker, M., Takenaka, K., Cloney, R., Nakazawa, Y., Niimi, A., Miki, Y., Jaspers, N.G., et al. (2010). Three DNA Polymerases, Recruited by Different Mechanisms, Carry Out NER Repair Synthesis in Human Cells. Mol. Cell 37, 714–727.
- Ohgaki, H., and Kleihues, P. (2005). Epidemiology and etiology of gliomas. Acta Neuropathol. (Berl.) 109, 93–108.
- Okazawa, S., Furusawa, Y., Kariya, A., Hassan, M.A., Arai, M., Hayashi, R., Tabuchi, Y., Kondo, T., and Tobe, K. (2013). Inactivation of DNA-dependent protein kinase promotes heat-induced apoptosis independently of heat-shock protein induction in human cancer cell lines. PloS One 8, e58325.
- Olaussen, K.A., Adam, J., Vanhecke, E., Vielh, P., Pirker, R., Friboulet, L., Popper, H., Robin, A., Commo, F., Thomale, J., et al. (2013). PARP1 impact on DNA repair of platinum adducts: Preclinical and clinical read-outs. Lung Cancer 80, 216–222.
- Olive, P. (2009). Impact of the comet assay in radiobiology. Mutat. Res. Mutat. Res. 681, 13–23.
- Olive, P.L., and Banáth, J.P. (2006). The comet assay: a method to measure DNA damage in individual cells. Nat. Protoc. 1, 23–29.
- Olive, P.L., Wlodek, D., and Banáth, J.P. (1991). DNA double-strand breaks measured in individual cells subjected to gel electrophoresis. Cancer Res. 51, 4671–4676.
- Olive, P.L., Banáth, J.P., and Keyes, M. (2008). Residual γH2AX after irradiation of human lymphocytes and monocytes in vitro and its relation to late effects after prostate brachytherapy. Radiother. Oncol. 86, 336–346.
- van Oorschot, B., Hovingh, S., Dekker, A., Stalpers, L.J., and Franken, N.A.P. (2016). Predicting Radiosensitivity with Gamma-H2AX Foci Assay after Single High-Dose-Rate and Pulsed Dose-Rate Ionizing Irradiation. Radiat. Res. 185, 190.
- Orta, M.L., Höglund, A., Calderón-Montaño, J.M., Domínguez, I., Burgos-Morón, E., Visnes, T., Pastor, N., Ström, C., López-lázaro, M., and Helleday, T. (2014). The PARP inhibitor Olaparib disrupts base excision repair of 5-aza-2′-deoxycytidine lesions. Nucleic Acids Res. 42, 9108–9120.
- Ostling, O., and Johanson, K.J. (1984). Microelectrophoretic study of radiation-induced DNA damages in individual mammalian cells. Biochem. Biophys. Res. Commun. 123, 291–298.
- Oza, P., Jaspersen, S.L., Miele, A., Dekker, J., and Peterson, C.L. (2009). Mechanisms that regulate localization of a DNA double-strand break to the nuclear periphery. Genes Dev. 23, 912–927.
- Pacher, P., Liaudet, L., Bai, P., Virag, L., Mabley, J.G., Haskó, G., and Szabó, C. (2002). Activation of Poly(ADP-Ribose) Polymerase Contributes to Development of Doxorubicin-Induced Heart Failure. J. Pharmacol. Exp. Ther. 300, 862–867.
- Paddock, M.N., Bauman, A.T., Higdon, R., Kolker, E., Takeda, S., and Scharenberg, A.M. (2011). Competition between PARP-1 and Ku70 control the decision between high-fidelity and mutagenic DNA repair. DNA Repair 10, 338–343.

- Paiva, C.N., and Bozza, M.T. (2014). Are Reactive Oxygen Species Always Detrimental to Pathogens? Antioxid. Redox Signal. 20, 1000–1037.
- Panier, S., and Boulton, S.J. (2014). Double-strand break repair: 53BP1 comes into focus. Nat. Rev. Mol. Cell Biol. 15, 7–18.
- Pannunzio, N.R., Watanabe, G., and Lieber, M.R. (2017). Nonhomologous DNA End Joining for Repair of DNA Double-Strand Breaks. J. Biol. Chem. jbc.TM117.000374.
- Park, H.J., Bae, J.S., Kim, K.M., Moon, Y.J., Park, S.-H., Ha, S.H., Hussein, U.K., Zhang, Z., Park, H.S., Park, B.-H., et al. (2018). The PARP inhibitor olaparib potentiates the effect of the DNA damaging agent doxorubicin in osteosarcoma. J. Exp. Clin. Cancer Res. 37, 107.
- Parris, C.N., Adam Zahir, S., Al-Ali, H., Bourton, E.C., Plowman, C., and Plowman, P.N. (2015). Enhanced γ-H2AX DNA damage foci detection using multimagnification and extended depth of field in imaging flow cytometry: Enhanced DNA Damage Foci Detection Using Imagestream. Cytometry A 87, 717–723.
- Pascal, J.M. (2018). The comings and goings of PARP-1 in response to DNA damage. DNA Repair 71, 177–182.
- Pastwa, E., Neumann, R.D., Mezhevaya, K., and Winters, T.A. (2003). Repair of Radiation-Induced DNA Double-Strand Breaks is Dependent upon Radiation Quality and the Structural Complexity of Double-Strand Breaks. Radiat. Res. 159, 251–261.
- Pastwa, E., Somiari, R.I., Malinowski, M., Somiari, S.B., and Winters, T.A. (2009). In vitro non-homologous DNA end joining assays—The 20th anniversary. Int. J. Biochem. Cell Biol. 41, 1254–1260.
- Patel, A.G., Sarkaria, J.N., and Kaufmann, S.H. (2011). Nonhomologous end joining drives poly(ADP-ribose) polymerase (PARP) inhibitor lethality in homologous recombination-deficient cells. Proc. Natl. Acad. Sci. 108, 3406–3411.
- Patne, K., Rakesh, R., Arya, V., Chanana, U.B., Sethy, R., Swer, P.B., and Muthuswami, R. (2017). BRG1 and SMARCAL1 transcriptionally co-regulate DROSHA, DGCR8 and DICER in response to doxorubicin-induced DNA damage. Biochim. Biophys. Acta BBA - Gene Regul. Mech. 1860, 936–951.
- Paudyal, S.C., Li, S., Yan, H., Hunter, T., and You, Z. (2017). Dna2 initiates resection at clean DNA double-strand breaks. Nucleic Acids Res. 45, 11766–11781.
- Paul, K., Wang, M., Mladenov, E., Bencsik-Theilen, A., Bednar, T., Wu, W., Arakawa, H., and Iliakis, G. (2013). DNA Ligases I and III Cooperate in Alternative Non-Homologous End-Joining in Vertebrates. PLoS ONE 8, e59505.
- Pauty, J., Côté, M.-F., Rodrigue, A., Velic, D., Masson, J.-Y., and Fortin, S. (2016). Investigation of the DNA damage response to SFOM-0046, a new small-molecule drug inducing DNA double-strand breaks. Sci. Rep. 6, 23302.
- Peña-Diaz, J., Bregenhorn, S., Ghodgaonkar, M., Follonier, C., Artola-Borán, M., Castor, D., Lopes, M., Sartori, A.A., and Jiricny, J. (2012). Noncanonical Mismatch Repair as a Source of Genomic Instability in Human Cells. Mol. Cell 47, 669–680.
- Pendleton, M., Lindsey, R.H., Felix, C.A., Grimwade, D., and Osheroff, N. (2014). Topoisomerase II and leukemia: Topoisomerase II and leukemia. Ann. N. Y. Acad. Sci. 1310, 98–110.
- Peng, G., Chun-Jen Lin, C., Mo, W., Dai, H., Park, Y.-Y., Kim, S.M., Peng, Y., Mo, Q., Siwko, S., Hu, R., et al. (2014). Genome-wide transcriptome profiling of homologous recombination DNA repair. Nat. Commun. 5, 3361.
- Peng, Y., Woods, R.G., Beamish, H., Ye, R., Lees-Miller, S.P., Lavin, M.F., and Bedford, J.S. (2005). Deficiency in the catalytic subunit of DNA-dependent protein kinase causes down-regulation of ATM. Cancer Res. 65, 1670–1677.

- Pereira, S., Bodgi, L., Duclos, M., Canet, A., Ferlazzo, M.L., Devic, C., Granzotto, A., Deneuve, S., Vogin, G., and Foray, N. (2018). Fast and Binary Assay for Predicting Radiosensitivity Based on the Theory of ATM Nucleo-Shuttling: Development, Validation, and Performance. Int. J. Radiat. Oncol. 100, 353–360.
- Perez, M., García-Heredia, J.M., Felipe-Abrio, B., Muñoz-Galván, S., Martín-Broto, J., and Carnero, A. (2020). Sarcoma stratification by combined pH2AX and MAP17 (PDZK1IP1) levels for a better outcome on doxorubicin plus olaparib treatment. Signal Transduct. Target. Ther. 5, 195.
- Perrault, R., Wang, H., Wang, M., Rosidi, B., and Iliakis, G. (2004). Backup pathways of NHEJ are suppressed by DNA-PK. J. Cell. Biochem. 92, 781–794.
- Pfeiffer, P., Odersky, A., Goedecke, W., and Kuhfittig-Kulle, S. (2014). Analysis of Double-Strand Break Repair by Nonhomologous DNA End Joining in Cell-Free Extracts from Mammalian Cells. In Molecular Toxicology Protocols, P. Keohavong, and S.G. Grant, eds. (Totowa, NJ: Humana Press), pp. 565–585.
- Pierce, A.J., Johnson, R.D., Thompson, L.H., and Jasin, M. (1999). XRCC3 promotes homology-directed repair of DNA damage in mammalian cells. Genes Dev. 13, 2633–2638.
- Pischel, D., Buchbinder, J.H., Sundmacher, K., Lavrik, I.N., and Flassig, R.J. (2018). A guide to automated apoptosis detection: How to make sense of imaging flow cytometry data. PLOS ONE 13, e0197208.
- Pogozelski, W.K., and Tullius, T.D. (1998). Oxidative Strand Scission of Nucleic Acids: Routes Initiated by Hydrogen Abstraction from the Sugar Moiety. Chem. Rev. 98, 1089–1108.
- Polo, S.E., and Jackson, S.P. (2011). Dynamics of DNA damage response proteins at DNA breaks: a focus on protein modifications. Genes Dev. 25, 409–433.
- Popp, H.D., Brendel, S., Hofmann, W.-K., and Fabarius, A. (2017). Immunofluorescence Microscopy of γH2AX and 53BP1 for Analyzing the Formation and Repair of DNA Double-strand Breaks. J. Vis. Exp.
- Pouliliou, S.E., Lialiaris, T.S., Dimitriou, T., Giatromanolaki, A., Papazoglou, D., Pappa, A., Pistevou, K., Kalamida, D., and Koukourakis, M.I. (2015). Survival Fraction at 2 Gy and γH2AX Expression Kinetics in Peripheral Blood Lymphocytes From Cancer Patients: Relationship With Acute Radiation-Induced Toxicities. Int. J. Radiat. Oncol. 92, 667–674.
- Pouliot, J.J., Yao, K.C., Robertson, C.A., and Nash, H.A. (1999). Yeast Gene for a Tyr-DNA Phosphodiesterase that Repairs Topoisomerase I Complexes. Science 286, 552–555.
- Powers, K.T., and Washington, M.T. (2018). Eukaryotic translesion synthesis: Choosing the right tool for the job. DNA Repair 71, 127–134.
- Powley, I.R., Kondrashov, A., Young, L.A., Dobbyn, H.C., Hill, K., Cannell, I.G., Stoneley, M., Kong, Y.-W., Cotes, J.A., Smith, G.C.M., et al. (2009). Translational reprogramming following UVB irradiation is mediated by DNA-PKcs and allows selective recruitment to the polysomes of mRNAs encoding DNA repair enzymes. Genes Dev. 23, 1207–1220.
- Prigent, C., Satoh, M.S., Daly, G., Barnes, D.E., and Lindahl, T. (1994). Aberrant DNA repair and DNA replication due to an inherited enzymatic defect in human DNA ligase I. Mol. Cell. Biol. 14, 310–317.
- Rahal, E.A., Henricksen, L.A., Li, Y., Williams, R.S., Tainer, J.A., and Dixon, K. (2010). ATM regulates Mre11-dependent DNA end-degradation and microhomology-mediated end joining. Cell Cycle 9, 2938–2949.
- Rass, E., Grabarz, A., Plo, I., Gautier, J., Bertrand, P., and Lopez, B.S. (2009). Role of Mre11 in chromosomal nonhomologous end joining in mammalian cells. Nat. Struct. Mol. Biol. 16, 819–824.
- Ray, U., Raul, S.K., Gopinatha, V.K., Ghosh, D., Rangappa, K.S., Mantelingu, K., and Raghavan, S.C. (2020). Identification and characterization of novel SCR7-based small-molecule inhibitor of DNA end-joining, SCR130 and its relevance in cancer therapeutics. Mol. Carcinog. 59, 618–628.

- Ray Chaudhuri, A., and Nussenzweig, A. (2017). The multifaceted roles of PARP1 in DNA repair and chromatin remodelling. Nat. Rev. Mol. Cell Biol. 18, 610–621.
- Redon, C.E., Nakamura, A.J., Zhang, Y.-W., Ji, J., Bonner, W.M., Kinders, R.J., Parchment, R.E., Doroshow, J.H., and Pommier, Y. (2010). Histone H2AX and Poly(ADP-Ribose) as Clinical Pharmacodynamic Biomarkers. Clin. Cancer Res. 16, 4532–4542.
- Redon, C.E., Nakamura, A.J., Sordet, O., Dickey, J.S., Gouliaeva, K., Tabb, B., Lawrence, S., Kinders, R.J., Bonner, W.M., and Sedelnikova, O.A. (2011). γ-H2AX Detection in Peripheral Blood Lymphocytes, Splenocytes, Bone Marrow, Xenografts, and Skin. In DNA Damage Detection In Situ, Ex Vivo, and In Vivo, V.V. Didenko, ed. (Totowa, NJ: Humana Press), pp. 249–270.
- Reed, E. (1998). Platinum-DNA adduct, nucleotide excision repair and platinum based anti-cancer chemotherapy. Cancer Treat. Rev. 24, 331–344.
- Reindl, J., Girst, S., Walsh, D.W.M., Greubel, C., Schwarz, B., Siebenwirth, C., Drexler, G.A., Friedl, A.A., and Dollinger, G. (2017). Chromatin organization revealed by nanostructure of irradiation induced γH2AX, 53BP1 and Rad51 foci. Sci. Rep. 7, 40616.
- Reynolds, P., Cooper, S., Lomax, M., and O'Neill, P. (2015). Disruption of PARP1 function inhibits base excision repair of a sub-set of DNA lesions. Nucleic Acids Res. 43, 4028–4038.
- Riabinska, A., Daheim, M., Herter-Sprie, G.S., Winkler, J., Fritz, C., Hallek, M., Thomas, R.K., Kreuzer, K.-A., Frenzel, L.P., Monfared, P., et al. (2013). Therapeutic Targeting of a Robust Non-Oncogene Addiction to PRKDC in ATM-Defective Tumors. Sci. Transl. Med. 5, 189ra78-189ra78.
- Richard, D.J., Bolderson, E., Cubeddu, L., Wadsworth, R.I.M., Savage, K., Sharma, G.G., Nicolette, M.L., Tsvetanov, S., McIlwraith, M.J., Pandita, R.K., et al. (2008). Single-stranded DNA-binding protein hSSB1 is critical for genomic stability. Nature 453, 677–681.
- Ricoul, M., Gnana Sekaran, T.S., Brochard, P., Herate, C., and Sabatier, L. (2019). γ-H2AX Foci Persistence at Chromosome Break Suggests Slow and Faithful Repair Phases Restoring Chromosome Integrity. Cancers 11, 1397.
- Ridley, A.J., Whiteside, J.R., McMillan, T.J., and Allinson, S.L. (2009). Cellular and sub-cellular responses to UVA in relation to carcinogenesis. Int. J. Radiat. Biol. 85, 177–195.
- Robertson, A.B., Klungland, A., Rognes, T., and Leiros, I. (2009). DNA Repair in Mammalian Cells: Base excision repair: the long and short of it. Cell. Mol. Life Sci. 66, 981–993.
- Robu, M., Shah, R.G., Petitclerc, N., Brind'Amour, J., Kandan-Kulangara, F., and Shah, G.M. (2013). Role of poly(ADP-ribose) polymerase-1 in the removal of UV-induced DNA lesions by nucleotide excision repair. Proc. Natl. Acad. Sci. 110, 1658–1663.
- Rocha, C., Silva, M., Quinet, A., Cabral-Neto, J., and Menck, C. (2018). DNA repair pathways and cisplatin resistance: an intimate relationship. Clinics 73.
- Rogakou, E.P., Pilch, D.R., Orr, A.H., Ivanova, V.S., and Bonner, W.M. (1998). DNA Double-stranded Breaks Induce Histone H2AX Phosphorylation on Serine 139. J. Biol. Chem. 273, 5858–5868.
- Rogakou, E.P., Boon, C., Redon, C., and Bonner, W.M. (1999). Megabase Chromatin Domains Involved in DNA Double-Strand Breaks in Vivo. J. Cell Biol. 146, 905–916.
- Roidos, P., Sungalee, S., Benfatto, S., Serçin, Ö., Stütz, A.M., Abdollahi, A., Mauer, J., Zenke, F.T., Korbel, J.O., and Mardin, B.R. (2020). A scalable CRISPR/Cas9-based fluorescent reporter assay to study DNA double-strand break repair choice. Nat. Commun. 11, 4077.
- Rojas, E., Lorenzo, Y., Haug, K., Nicolaissen, B., and Valverde, M. (2014). Epithelial cells as alternative human biomatrices for comet assay. Front. Genet. 5.
- Ronson, G.E., Piberger, A.L., Higgs, M.R., Olsen, A.L., Stewart, G.S., McHugh, P.J., Petermann, E., and Lakin, N.D. (2018). PARP1 and PARP2 stabilise replication forks at base excision repair intermediates through Fbh1-dependent Rad51 regulation. Nat. Commun. 9, 746.
- Rooney, S.M., and Moore, P.D. (1995). Antiparallel, intramolecular triplex DNA stimulates homologous recombination in human cells. Proc. Natl. Acad. Sci. U. S. A. 92, 2141–2144.

- Roos, W.P., and Kaina, B. (2013). DNA damage-induced cell death: From specific DNA lesions to the DNA damage response and apoptosis. Cancer Lett. 332, 237–248.
- Roots, R., Kraft, G., and Gosschalk, E. (1985). The formation of radiation-induced dna breaks: The ratio of double-strand breaks to single-strand breaks. Int. J. Radiat. Oncol. 11, 259–265.
- Rossner, P., Binkova, B., Rossnerova, A., and Sram, R.J. (2015). Molecular Epidemiology and Air Pollution. In Current Air Quality Issues, F. Nejadkoorki, ed. (InTech), p.
- Rothkamm, K., and Lobrich, M. (2003). Evidence for a lack of DNA double-strand break repair in human cells exposed to very low x-ray doses. Proc. Natl. Acad. Sci. 100, 5057–5062.
- Rothkamm, K., Barnard, S., Moquet, J., Ellender, M., Rana, Z., and Burdak-Rothkamm, S. (2015). DNA damage foci : meaning and significance. Environ. Mol. Mutagen. 56, 491–504.
- Roy, U., and Schärer, O.D. (2016). Involvement of translesion synthesis DNA polymerases in DNA interstrand crosslink repair. DNA Repair 44, 33–41.
- Rübe, C.E., Dong, X., Kühne, M., Fricke, A., Kaestner, L., Lipp, P., and Rübe, C. (2008). DNA Double-Strand Break Rejoining in Complex Normal Tissues. Int. J. Radiat. Oncol. 72, 1180–1187.
- Sachadyn, P. (2010). Conservation and diversity of MutS proteins. Mutat. Res. Mol. Mech. Mutagen. 694, 20–30.
- Saha, T., Smulson, M., and Rosen, E.M. (2010). BRCA1 regulation of base excision repair pathway. Cell Cycle Georget. Tex 9, 2471–2472.
- Sak, A., and Stuschke, M. (2010). Use of γH2AX and Other Biomarkers of Double-Strand Breaks During Radiotherapy. Semin. Radiat. Oncol. 20, 223–231.
- Sakai, W., Swisher, E.M., Karlan, B.Y., Agarwal, M.K., Higgins, J., Friedman, C., Villegas, E., Jacquemont, C., Farrugia, D.J., Couch, F.J., et al. (2008). Secondary mutations as a mechanism of cisplatin resistance in BRCA2-mutated cancers. Nature 451, 1116–1120.
- Sakata, K., Someya, M., Matsumoto, Y., and Hareyama, M. (2007). Ability to repair DNA double-strand breaks related to cancer susceptibility and radiosensitivity. Radiat. Med. 25, 433–438.
- Saldivar, J.C., Cortez, D., and Cimprich, K.A. (2017). The essential kinase ATR: ensuring faithful duplication of a challenging genome. Nat. Rev. Mol. Cell Biol. 18, 622–636.
- Sartori, A.A., Lukas, C., Coates, J., Mistrik, M., Fu, S., Bartek, J., Baer, R., Lukas, J., and Jackson, S.P. (2007). Human CtIP promotes DNA end resection. Nature 450, 509–514.
- Sassa, A., Tada, H., Takeishi, A., Harada, K., Suzuki, M., Tsuda, M., Sasanuma, H., Takeda, S., Sugasawa, K., Yasui, M., et al. (2019). Processing of a single ribonucleotide embedded into DNA by human nucleotide excision repair and DNA polymerase η. Sci. Rep. 9, 13910.
- Sauvaigo, S., Serres, C., Signorini, N., Emonet, N., Richard, M.-J., and Cadet, J. (1998). Use of the Single-Cell Gel Electrophoresis Assay for the Immunofluorescent Detection of Specific DNA Damage. Anal. Biochem. 259, 1–7.
- Sauvaigo, S., Sarrazy, F., Batal, M., Caillat, S., Pitiot, B., Mouret, S., Cléry-Barraud, C., Boudry, I., and Douki, T. (2016). Impact of topical application of sulfur mustard on mice skin and distant organs DNA repair enzyme signature. Toxicol. Lett. 241, 71–81.
- Savic, V., Yin, B., Maas, N.L., Bredemeyer, A.L., Carpenter, A.C., Helmink, B.A., Yang-Iott, K.S., Sleckman, B.P., and Bassing, C.H. (2009). Formation of Dynamic γ-H2AX Domains along Broken DNA Strands Is Distinctly Regulated by ATM and MDC1 and Dependent upon H2AX Densities in Chromatin. Mol. Cell 34, 298–310.
- Schaeffer, L., Roy, R., Humbert, S., Moncollin, V., Vermeulen, W., Hoeijmakers, J., Chambon, P., and Egly, J. (1993). DNA repair helicase: a component of BTF2 (TFIIH) basic transcription factor. Science 260, 58–63.

- Schaeffer, L., Moncollin, V., Roy, R., Staub, A., Mezzina, M., Sarasin, A., Weeda, G., Hoeijmakers, J.H., and Egly, J.M. (1994). The ERCC2/DNA repair protein is associated with the class II BTF2/TFIIH transcription factor. EMBO J. 13, 2388–2392.
- Schärer, O.D. (2013). Nucleotide excision repair in eukaryotes. Cold Spring Harb. Perspect. Biol. 5, a012609.
- Scheffner, M., Werness, B.A., Huibregtse, J.M., Levine, A.J., and Howley, P.M. (1990). The E6 oncoprotein encoded by human papillomavirus types 16 and 18 promotes the degradation of p53. Cell 63, 1129–1136.
- Schrank, B.R., Aparicio, T., Li, Y., Chang, W., Chait, B.T., Gundersen, G.G., Gottesman, M.E., and Gautier, J. (2018). Nuclear ARP2/3 drives DNA break clustering for homology-directed repair. Nature 559, 61–66.
- Schreier, W.J., Schrader, T.E., Koller, F.O., Gilch, P., Crespo-Hernandez, C.E., Swaminathan, V.N., Carell, T., Zinth, W., and Kohler, B. (2007). Thymine Dimerization in DNA Is an Ultrafast Photoreaction. Science 315, 625–629.
- Schwartz, D.C., Saffran, W., Welsh, J., Haas, R., Goldenberg, M., and Cantor, C.R. (1983). New Techniques for Purifying Large DNAs and Studying Their Properties and Packaging. Cold Spring Harb. Symp. Quant. Biol. 47, 189–195.
- Schwertman, P., Lagarou, A., Dekkers, D.H.W., Raams, A., van der Hoek, A.C., Laffeber, C., Hoeijmakers, J.H.J., Demmers, J.A.A., Fousteri, M., Vermeulen, W., et al. (2012). UV-sensitive syndrome protein UVSSA recruits USP7 to regulate transcription-coupled repair. Nat. Genet. 44, 598–602.
- Scully, R., Ganesan, S., Vlasakova, K., Chen, J., Socolovsky, M., and Livingston, D.M. (1999). Genetic Analysis of BRCA1 Function in a Defined Tumor Cell Line. Mol. Cell 4, 1093–1099.
- Scully, R., Panday, A., Elango, R., and Willis, N.A. (2019). DNA double-strand break repair-pathway choice in somatic mammalian cells. Nat. Rev. Mol. Cell Biol. 20, 698–714.
- Sears, C.R., and Turchi, J.J. (2012). Complex Cisplatin-Double Strand Break (DSB) Lesions Directly Impair Cellular Non-Homologous End-Joining (NHEJ) Independent of Downstream Damage Response (DDR) Pathways. J. Biol. Chem. 287, 24263–24272.
- Sebesta, M., and Krejci, L. (2016). Mechanism of Homologous Recombination. In DNA Replication, Recombination, and Repair, F. Hanaoka, and K. Sugasawa, eds. (Tokyo: Springer Japan), pp. 73–109.
- Sedelnikova, O.A., Rogakou, E.P., Panyutin, I.G., and Bonner, W.M. (2002). Quantitative Detection of 125 IdU-Induced DNA Double-Strand Breaks with γ-H2AX Antibody. Radiat. Res. 158, 486–492.
- Seol, J.-H., Shim, E.Y., and Lee, S.E. (2018). Microhomology-mediated end joining: Good, bad and ugly. Mutat. Res. Mol. Mech. Mutagen. 809, 81–87.
- Sfeir, A., and Symington, L.S. (2015). Microhomology-Mediated End Joining: A Back-up Survival Mechanism or Dedicated Pathway? Trends Biochem. Sci. 40, 701–714.
- Shabalala, S., Muller, C.J.F., Louw, J., and Johnson, R. (2017). Polyphenols, autophagy and doxorubicin-induced cardiotoxicity. Life Sci. 180, 160–170.
- Shah, K., Boghozian, R.A., Kartsonaki, C., Shah, K.A., and Vallis, K.A. (2016). γH2AX expression in cytological specimens as a biomarker of response to radiotherapy in solid malignancies. Diagn. Cytopathol. 44, 141–146.
- Sharma, S., and Raghavan, S.C. (2010). Nonhomologous DNA End Joining in Cell-Free Extracts. J. Nucleic Acids 2010, 1–11.
- Sharma, Javadekar, Pandey, Srivastava, Kumari, and Raghavan (2015a). Homology and enzymatic requirements of microhomology-dependent alternative end joining. Cell Death Dis. 6, e1697–e1697.
- Sharma, A., Singh, K., and Almasan, A. (2012). Histone H2AX Phosphorylation: A Marker for DNA Damage. In DNA Repair Protocols, L. Bjergbæk, ed. (Totowa, NJ: Humana Press), pp. 613–626.

- Sharma, P.M., Ponnaiya, B., Taveras, M., Shuryak, I., Turner, H., and Brenner, D.J. (2015b). High Throughput Measurement of γH2AX DSB Repair Kinetics in a Healthy Human Population. PLOS ONE 10, e0121083.
- Sharma-Kuinkel, B.K., Rude, T.H., and Fowler, V.G. (2014). Pulse Field Gel Electrophoresis. In The Genetic Manipulation of Staphylococci, J.L. Bose, ed. (New York, NY: Springer New York), pp. 117–130.
- Shen, H., Schultz, M., Kruh, G.D., and Tew, K.D. (1998). Increased expression of DNA-dependent protein kinase confers resistance to adriamycin. Biochim. Biophys. Acta 1381, 131–138.
- Shilkin, E.S., Boldinova, E.O., Stolyarenko, A.D., Goncharova, R.I., Chuprov-Netochin, R.N., Khairullin, R.F., Smal, M.P., and Makarova, A.V. (2020). Translesion DNA Synthesis and Carcinogenesis. Biochem. Mosc. 85, 425–435.
- Shiloh, Y., and Ziv, Y. (2013). The ATM protein kinase: regulating the cellular response to genotoxic stress, and more. Nat. Rev. Mol. Cell Biol. 14, 197–210.
- Shin, H.-J., Kwon, H.-K., Lee, J.-H., Gui, X., Achek, A., Kim, J.-H., and Choi, S. (2015). Doxorubicin-induced necrosis is mediated by poly-(ADP-ribose) polymerase 1 (PARP1) but is independent of p53. Sci. Rep. 5, 15798.
- Shinozaki, T., Nota, A., Taya, Y., and Okamoto, K. (2003). Functional role of Mdm2 phosphorylation by ATR in attenuation of p53 nuclear export. Oncogene 22, 8870–8880.
- Siddiqui, M.S., François, M., Fenech, M.F., and Leifert, W.R. (2015). Persistent γH2AX: A promising molecular marker of DNA damage and aging. Mutat. Res. Mutat. Res. 766, 1–19.
- Sigurdsson, S., Van Komen, S., Petukhova, G., and Sung, P. (2002). Homologous DNA Pairing by Human Recombination Factors Rad51 and Rad54. J. Biol. Chem. 277, 42790–42794.
- Singh, A., Compe, E., Le May, N., and Egly, J.-M. (2015). TFIIH Subunit Alterations Causing Xeroderma Pigmentosum and Trichothiodystrophy Specifically Disturb Several Steps during Transcription. Am. J. Hum. Genet. 96, 194–207.
- Slebos, R.J.C., and Taylor, J.A. (2001). A Novel Host Cell Reactivation Assay to Assess Homologous Recombination Capacity in Human Cancer Cell Lines. Biochem. Biophys. Res. Commun. 281, 212–219.
- Smirnov, A., Fishman, V., Yunusova, A., Korablev, A., Serova, I., Skryabin, B.V., Rozhdestvensky, T.S., and Battulin, N. (2019). DNA barcoding reveals that injected transgenes are predominantly processed by homologous recombination in mouse zygote. Nucleic Acids Res. gkz1085.
- Smith, J., Mun Tho, L., Xu, N., and A. Gillespie, D. (2010). The ATM–Chk2 and ATR–Chk1 Pathways in DNA Damage Signaling and Cancer. In Advances in Cancer Research, (Elsevier), pp. 73–112.
- Smith-Ravin, J., and Jeggo, P.A. (1989). Use of Damaged Plasmid to Study DNA Repair in X-ray Sensitive (Xrs) Strains of Chinese Hamster Ovary (CHO) Cells. Int. J. Radiat. Biol. 56, 951–961.
- So, A., Le Guen, T., Lopez, B.S., and Guirouilh-Barbat, J. (2017). Genomic rearrangements induced by unscheduled DNA double strand breaks in somatic mammalian cells. FEBS J. 284, 2324–2344.
- So, A., Muhammad, A., Chailleux, C., Sanz, L.S., Ragu, S., Le Cam, E., Canitrot, Y., Masson, J.Y., Dupaigne, P., Lopez, B.S., et al. (2019). Mammalian RAD51 prevents non-conservative alternative end-joining and single strand annealing through non-catalytic mechanisms (Molecular Biology).
- So, S., Adachi, N., Lieber, M.R., and Koyama, H. (2004). Genetic Interactions between BLM and DNA Ligase IV in Human Cells. J. Biol. Chem. 279, 55433–55442.
- Soldani, C., and Scovassi, A.I. (2002). Poly(ADP-ribose) polymerase-1 cleavage duringapoptosis: An update. APOPTOSIS 7, 321–328.
- Soll, J.M., Sobol, R.W., and Mosammaparast, N. (2017). Regulation of DNA Alkylation Damage Repair: Lessons and Therapeutic Opportunities. Trends Biochem. Sci. 42, 206–218.

- Sollier, J., and Cimprich, K.A. (2015). Breaking bad: R-loops and genome integrity. Trends Cell Biol. 25, 514–522.
- Solovjeva, L., Firsanov, D., Pleskach, N., and Svetlova, M. (2017). Immunofluorescence Analysis of γ-H2AX Foci in Mammalian Fibroblasts at Different Phases of the Cell Cycle. In Fast Detection of DNA Damage, V.V. Didenko, ed. (New York, NY: Springer New York), pp. 187–194.
- Song, J., Kemp, M.G., and Choi, J.-H. (2017). Detection of the Excised, Damage-containing Oligonucleotide Products of Nucleotide Excision Repair in Human Cells. Photochem. Photobiol. 93, 192–198.
- Soussain, C., Ricard, D., Fike, J.R., Mazeron, J.-J., Psimaras, D., and Delattre, J.-Y. (2009). CNS complications of radiotherapy and chemotherapy. The Lancet 374, 1639–1651.
- Soutoglou, E., and Misteli, T. (2008). Activation of the Cellular DNA Damage Response in the Absence of DNA Lesions. Science 320, 1507–1510.
- Sowd, G.A., Mody, D., Eggold, J., Cortez, D., Friedman, K.L., and Fanning, E. (2014). SV40 Utilizes ATM Kinase Activity to Prevent Non-homologous End Joining of Broken Viral DNA Replication Products. PLoS Pathog. 10, e1004536.
- Speit, G., and Rothfuss, A. (2012). The Comet Assay: A Sensitive Genotoxicity Test for the Detection of DNA Damage and Repair. In DNA Repair Protocols, L. Bjergbæk, ed. (Totowa, NJ: Humana Press), pp. 79–90.
- Spencer, D.M.S., Bilardi, R.A., Koch, T.H., Post, G.C., Nafie, J.W., Kimura, K.-I., Cutts, S.M., and Phillips, D.R. (2008). DNA repair in response to anthracycline–DNA adducts: A role for both homologous recombination and nucleotide excision repair. Mutat. Res. Mol. Mech. Mutagen. 638, 110–121.
- Spies, J., Lukas, C., Somyajit, K., Rask, M.-B., Lukas, J., and Neelsen, K.J. (2019). 53BP1 nuclear bodies enforce replication timing at under-replicated DNA to limit heritable DNA damage. Nat. Cell Biol. 21, 487–497.
- Spivak, G. (2015). Nucleotide excision repair in humans. DNA Repair 36, 13–18.
- Srivastava, M., and Raghavan, S.C. (2015). DNA Double-Strand Break Repair Inhibitors as Cancer Therapeutics. Chem. Biol. 22, 17–29.
- Staaf, J., Glodzik, D., Bosch, A., Vallon-Christersson, J., Reuterswärd, C., Häkkinen, J., Degasperi, A., Amarante, T.D., Saal, L.H., Hegardt, C., et al. (2019). Whole-genome sequencing of triple-negative breast cancers in a population-based clinical study. Nat. Med. 25, 1526–1533.
- Staresincic, L., Fagbemi, A.F., Enzlin, J.H., Gourdin, A.M., Wijgers, N., Dunand-Sauthier, I., Giglia-Mari, G., Clarkson, S.G., Vermeulen, W., and Schärer, O.D. (2009). Coordination of dual incision and repair synthesis in human nucleotide excision repair. EMBO J. 28, 1111–1120.
- Stark, J.M., Pierce, A.J., Oh, J., Pastink, A., and Jasin, M. (2004). Genetic steps of mammalian homologous repair with distinct mutagenic consequences. Mol. Cell. Biol. 24, 9305–9316.
- Stiff, T., O'Driscoll, M., Rief, N., Iwabuchi, K., Löbrich, M., and Jeggo, P.A. (2004). ATM and DNA-PK Function Redundantly to Phosphorylate H2AX after Exposure to Ionizing Radiation. Cancer Res. 64, 2390–2396.
- Strom, C.E., Johansson, F., Uhlen, M., Szigyarto, C.A.-K., Erixon, K., and Helleday, T. (2011). Poly (ADP-ribose) polymerase (PARP) is not involved in base excision repair but PARP inhibition traps a single-strand intermediate. Nucleic Acids Res. 39, 3166–3175.
- Sukup-Jackson, M.R., Kiraly, O., Kay, J.E., Na, L., Rowland, E.A., Winther, K.E., Chow, D.N., Kimoto, T., Matsuguchi, T., Jonnalagadda, V.S., et al. (2014). Rosa26-GFP Direct Repeat (RaDR-GFP) Mice Reveal Tissue- and Age-Dependence of Homologous Recombination in Mammals In Vivo. PLoS Genet. 10, e1004299.
- Sun, G., Yang, L., Dong, C., Ma, B., Shan, M., and Ma, B. (2017). PRKDC regulates chemosensitivity and is a potential prognostic and predictive marker of response to adjuvant chemotherapy in breast cancer patients. Oncol. Rep. 37, 3536–3542.

- Sung, P., Krejci, L., Van Komen, S., and Sehorn, M.G. (2003). Rad51 Recombinase and Recombination Mediators. J. Biol. Chem. 278, 42729–42732.
- Surovtseva, Y.V., Jairam, V., Salem, A.F., Sundaram, R.K., Bindra, R.S., and Herzon, S.B. (2016). Characterization of Cardiac Glycoside Natural Products as Potent Inhibitors of DNA Double-Strand Break Repair by a Whole-Cell Double Immunofluorescence Assay. J. Am. Chem. Soc. 138, 3844–3855.
- Suzuki, R., and Shimodaira, H. (2006). Pvclust: an R package for assessing the uncertainty in hierarchical clustering. Bioinforma. Oxf. Engl. 22, 1540–1542.
- Swenberg, J.A., Lu, K., Moeller, B.C., Gao, L., Upton, P.B., Nakamura, J., and Starr, T.B. (2011). Endogenous versus Exogenous DNA Adducts: Their Role in Carcinogenesis, Epidemiology, and Risk Assessment. Toxicol. Sci. 120, S130–S145.
- Symington, L.S. (2014). End Resection at Double-Strand Breaks: Mechanism and Regulation. Cold Spring Harb. Perspect. Biol. 6, a016436–a016436.
- Tacar, O., Sriamornsak, P., and Dass, C.R. (2013). Doxorubicin: an update on anticancer molecular action, toxicity and novel drug delivery systems: Doxorubicin cell and molecular biological activity. J. Pharm. Pharmacol. 65, 157–170.
- Tatin, X., Muggiolu, G., Sauvaigo, S., and Breton, J. Evaluation of DNA double-strand break repair capacity in human cells: critical overview of current functional methods.
- Tavecchio, M., Munck, J.M., Cano, C., Newell, D.R., and Curtin, N.J. (2012). Further characterisation of the cellular activity of the DNA-PK inhibitor, NU7441, reveals potential cross-talk with homologous recombination. Cancer Chemother. Pharmacol. 69, 155–164.
- Tay, I.J., Park, J.J.H., Price, A.L., Engelward, B.P., and Floyd, S.R. (2020). HTS-Compatible CometChip Enables Genetic Screening for Modulators of Apoptosis and DNA Double-Strand Break Repair. SLAS Discov. Adv. Sci. Drug Discov. 25, 906–922.
- Tembe, V., and Henderson, B.R. (2007). Protein trafficking in response to DNA damage. Cell. Signal. 19, 1113–1120.
- Thompson, L.H. (2012). Recognition, signaling, and repair of DNA double-strand breaks produced by ionizing radiation in mammalian cells: The molecular choreography. Mutat. Res. Mutat. Res. 751, 158–246.
- Thompson, L.H., and Schild, D. (2002). Recombinational DNA repair and human disease. Mutat. Res. Mol. Mech. Mutagen. 509, 49–78.
- Tice, R.R., and Setlow, R.B. (1985). DNA repair and replication in aging organisms and cells. Handb. Biol. Aging Ed. CE Finch EL Schneider Assist. Assoc. Ed. RC Adelman GM Martin EJ Masoro.
- Tichy, A., Durisova, K., Salovska, B., Pejchal, J., Zarybnicka, L., Vavrova, J., Dye, N.A., and Sinkorova, Z. (2014). Radio-sensitization of human leukaemic MOLT-4 cells by DNA-dependent protein kinase inhibitor, NU7441. Radiat. Environ. Biophys. 53, 83–92.
- Timme, C.R., Rath, B.H., O'Neill, J.W., Camphausen, K., and Tofilon, P.J. (2018). The DNA-PK Inhibitor VX-984 Enhances the Radiosensitivity of Glioblastoma Cells Grown In Vitro and as Orthotopic Xenografts. Mol. Cancer Ther. 17, 1207–1216.
- Tornaletti, S., Reines, D., and Hanawalt, P.C. (1999). Structural characterization of RNA polymerase II complexes arrested by a cyclobutane pyrimidine dimer in the transcribed strand of template DNA. J. Biol. Chem. 274, 24124–24130.
- Torudd, J., Protopopova, M., Sarimov, R., Nygren, J., Eriksson, S., Marková, E., Chovanec, M., Selivanova, G., and Belyaev, I. (2005). Dose-response for radiation-induced apoptosis, residual 53BP1 foci and DNA-loop relaxation in human lymphocytes. Int. J. Radiat. Biol. 81, 125–138.
- Toulany, M. (2019). Targeting DNA Double-Strand Break Repair Pathways to Improve Radiotherapy Response. Genes 10, 25.

- Tremblay, S., and Wagner, J.R. (2007). Dehydration, deamination and enzymatic repair of cytosine glycols from oxidized poly(dG-dC) and poly(dI-dC). Nucleic Acids Res. 36, 284–293.
- Tremblay, S., Douki, T., Cadet, J., and Wagner, J.R. (1999). 2'-Deoxycytidine glycols, a missing link in the free radical-mediated oxidation of DNA. J. Biol. Chem. 274, 20833–20838.
- Trenner, A., and Sartori, A.A. (2019). Harnessing DNA Double-Strand Break Repair for Cancer Treatment. Front. Oncol. 9, 1388.
- Truong, L.N., Li, Y., Shi, L.Z., Hwang, P.Y.-H., He, J., Wang, H., Razavian, N., Berns, M.W., and Wu, X. (2013). Microhomology-mediated End Joining and Homologous Recombination share the initial end resection step to repair DNA double-strand breaks in mammalian cells. Proc. Natl. Acad. Sci. 110, 7720–7725.
- Trzeciak, A.R., Barnes, J., and Evans, M.K. (2008). A Modified Alkaline Comet Assay for Measuring DNA Repair Capacity in Human Populations. Radiat. Res. 169, 110–121.
- Tu, W.-Z., Li, B., Huang, B., Wang, Y., Liu, X.-D., Guan, H., Zhang, S.-M., Tang, Y., Rang, W.-Q., and Zhou, P.-K. (2013a). γH2AX foci formation in the absence of DNA damage: Mitotic H2AX phosphorylation is mediated by the DNA-PKcs/CHK2 pathway. FEBS Lett. 587, 3437–3443.
- Tu, W.-Z., Li, B., Huang, B., Wang, Y., Liu, X.-D., Guan, H., Zhang, S.-M., Tang, Y., Rang, W.-Q., and Zhou, P.-K. (2013b). γH2AX foci formation in the absence of DNA damage: Mitotic H2AX phosphorylation is mediated by the DNA-PKcs/CHK2 pathway. FEBS Lett. 587, 3437–3443.
- Tudek, B., Zdżalik-Bielecka, D., Tudek, A., Kosicki, K., Fabisiewicz, A., and Speina, E. (2017). Lipid peroxidation in face of DNA damage, DNA repair and other cellular processes. Free Radic. Biol. Med. 107, 77–89.
- Turner, H.C., Brenner, D.J., Chen, Y., Bertucci, A., Zhang, J., Wang, H., Lyulko, O.V., Xu, Y., Shuryak, I., Schaefer, J., et al. (2011). Adapting the γ-H2AX Assay for Automated Processing in Human Lymphocytes. 1. Technological Aspects. Radiat. Res. 175, 282–290.
- Valdiglesias, V., Pásaro, E., Méndez, J., and Laffon, B. (2011). Assays to Determine DNA Repair Ability. J. Toxicol. Environ. Health A 74, 1094–1109.
- Valdiglesias, V., Giunta, S., Fenech, M., Neri, M., and Bonassi, S. (2013). γH2AX as a marker of DNA double strand breaks and genomic instability in human population studies. Mutat. Res. Mutat. Res. 753, 24–40.
- Varon, R., Demuth, I., and Chrzanowska, K.H. (1993). Nijmegen Breakage Syndrome. In GeneReviews®, M.P. Adam, H.H. Ardinger, R.A. Pagon, S.E. Wallace, L.J. Bean, G. Mirzaa, and A. Amemiya, eds. (Seattle (WA): University of Washington, Seattle), p.
- Veuger, S.J., Curtin, N.J., Richardson, C.J., Smith, G.C.M., and Durkacz, B.W. (2003). Radiosensitization and DNA Repair Inhibition by the Combined Use of Novel Inhibitors of DNA-dependent Protein Kinase and Poly(ADP-Ribose) Polymerase-1. Cancer Res. 63, 6008.
- Vignard, J., Mirey, G., and Salles, B. (2013). Ionizing-radiation induced DNA double-strand breaks: A direct and indirect lighting up. Radiother. Oncol. 108, 362–369.
- Vigneron, N., Vernon, M., Meryet-Figuière, M., Lambert, B., Briand, M., Louis, M.-H., Krieger, S., Joly, F., Lheureux, S., Blanc-Fournier, C., et al. (2020). Predictive Relevance of Circulating miR-622 in Patients with Newly Diagnosed and Recurrent High-Grade Serous Ovarian Carcinoma. Clin. Chem. 66, 352–362.
- Vilenchik, M.M., and Knudson, A.G. (2003). Endogenous DNA double-strand breaks: Production, fidelity of repair, and induction of cancer. Proc. Natl. Acad. Sci. 100, 12871–12876.
- Vogin, G., Bastogne, T., Bodgi, L., Gillet-Daubin, J., Canet, A., Pereira, S., and Foray, N. (2018). The Phosphorylated ATM Immunofluorescence Assay: A High-performance Radiosensitivity Assay to Predict Postradiation Therapy Overreactions. Int. J. Radiat. Oncol. 101, 690–693.
- Vyas, S., Matic, I., Uchima, L., Rood, J., Zaja, R., Hay, R.T., Ahel, I., and Chang, P. (2014). Family-wide analysis of poly(ADP-ribose) polymerase activity. Nat. Commun. 5, 4426.

- Wang, J. (2001). DNA damage and apoptosis. Cell Death Differ. 8, 1047–1048.
- Wang, J.C. (2002). Cellular roles of DNA topoisomerases: a molecular perspective. Nat. Rev. Mol. Cell Biol. 3, 430–440.
- Wang, B., Matsuoka, S., Carpenter, P.B., and Elledge, S.J. (2002). 53BP1, a mediator of the DNA damage checkpoint. Science 298, 1435–1438.
- Wang, D., Kreutzer, D.A., and Essigmann, J.M. (1998). Mutagenicity and repair of oxidative DNA damage: insights from studies using defined lesions. Mutat. Res. Mol. Mech. Mutagen. 400, 99–115.
- Wang, H., Lu, C., Li, Q., Xie, J., Chen, T., Tan, Y., Wu, C., and Jiang, J. (2014). The role of Kif4A in doxorubicin-induced apoptosis in breast cancer cells. Mol. Cells 37, 812–818.
- Wang, J., Hyun, W., Lamborn, K., and Deen, D.F. (1996). Measurement of Radiation-induced Damage in Human Glioma Cells with Flow Cytometry. Cancer Res. 56, 154.
- Wang, M., Wu, W., Wu, W., Rosidi, B., Zhang, L., Wang, H., and Iliakis, G. (2006). PARP-1 and Ku compete for repair of DNA double strand breaks by distinct NHEJ pathways. Nucleic Acids Res. 34, 6170–6182.
- Wang, M., Chu, H., Zhang, Z., and Wei, Q. (2013). Molecular epidemiology of DNA repair gene polymorphisms and head and neck cancer. J. Biomed. Res. 27, 179–192.
- Wang, Q.-L., Sun, S.-C., Han, J., Kwak, Y.-C., Kim, N.-H., and Cui, X.-S. (2012). Doxorubicin induces early embryo apoptosis by inhibiting poly(ADP ribose) polymerase. Vivo Athens Greece 26, 827–834.
- Wang, Y., Luo, W., and Wang, Y. (2019). PARP-1 and its associated nucleases in DNA damage response. DNA Repair 81, 102651.
- Ward, I.M., and Chen, J. (2001). Histone H2AX Is Phosphorylated in an ATR-dependent Manner in Response to Replicational Stress. J. Biol. Chem. 276, 47759–47762.
- Ward, A., Dong, L., Harris, J.M., Khanna, K.K., Al-Ejeh, F., Fairlie, D.P., Wiegmans, A.P., and Liu, L. (2017). Quinazolinone derivatives as inhibitors of homologous recombinase RAD51. Bioorg. Med. Chem. Lett. 27, 3096–3100.
- Waters, L.S., Minesinger, B.K., Wiltrout, M.E., D'Souza, S., Woodruff, R.V., and Walker, G.C. (2009). Eukaryotic Translesion Polymerases and Their Roles and Regulation in DNA Damage Tolerance. Microbiol. Mol. Biol. Rev. 73, 134–154.
- Weingeist, D.M., Ge, J., Wood, D.K., Mutamba, J.T., Huang, Q., Rowland, E.A., Yaffe, M.B., Floyd, S., and Engelward, B.P. (2013). Single-cell microarray enables high-throughput evaluation of DNA double-strand breaks and DNA repair inhibitors. Cell Cycle 12, 907–915.
- Werbrouck (2009). Prediction of late normal tissue complications in RT treated gynaecological cancer patients: Potential of the γ-H2AX foci assay and association with chromosomal radiosensitivity. Oncol. Rep. 23.
- Werbrouck, J., Duprez, F., De neve, W., and Thierens, H. (2011). Lack of a correlation between γH2AX foci kinetics in lymphocytes and the severity of acute normal tissue reactions during IMRT treatment for head and neck cancer. Int. J. Radiat. Biol. 87, 46–56.
- West, S.C., and Howard-Flanders, P. (1984). Duplex-duplex interactions catalyzed by RecA protein allow strand exchanges to pass double-strand breaks in DNA. Cell 37, 683–691.
- Wildenberg, J., and Meselson, M. (1975). Mismatch repair in heteroduplex DNA. Proc. Natl. Acad. Sci. U. S. A. 72, 2202–2206.
- Willers, H., Gheorghiu, L., Liu, Q., Efstathiou, J.A., Wirth, L.J., Krause, M., and von Neubeck, C. (2015). DNA Damage Response Assessments in Human Tumor Samples Provide Functional Biomarkers of Radiosensitivity. Semin. Radiat. Oncol. 25, 237–250.

- Williams, G.J., Lees-Miller, S.P., and Tainer, J.A. (2010). Mre11–Rad50–Nbs1 conformations and the control of sensing, signaling, and effector responses at DNA double-strand breaks. DNA Repair 9, 1299–1306.
- Williams, H.L., Gottesman, M.E., and Gautier, J. (2013). The differences between ICL repair during and outside of S phase. Trends Biochem. Sci. 38, 386–393.
- Willmore, E., de Caux, S., Sunter, N.J., Tilby, M.J., Jackson, G.H., Austin, C.A., and Durkacz, B.W. (2004). A novel DNA-dependent protein kinase inhibitor, NU7026, potentiates the cytotoxicity of topoisomerase II poisons used in the treatment of leukemia. Blood 103, 4659–4665.
- Willoughby, C.E., Jiang, Y., Thomas, H.D., Willmore, E., Kyle, S., Wittner, A., Phillips, N., Zhao, Y., Tudhope, S.J., Prendergast, L., et al. (2019). Selective DNA-PKcs inhibition extends the therapeutic index of localized radiotherapy and chemotherapy. J. Clin. Invest. 130, 258–271.
- Wilson, D.M., and Barsky, D. (2001). The major human abasic endonuclease: formation, consequences and repair of abasic lesions in DNA. Mutat. Res. 485, 283–307.
- Winczura, A., Zdżalik, D., and Tudek, B. (2012). Damage of DNA and proteins by major lipid peroxidation products in genome stability. Free Radic. Res. 46, 442–459.
- Windhofer, F., Wu, W., Wang, M., Singh, S.K., Saha, J., Rosidi, B., and Iliakis, G. (2007). Marked Dependence on Growth State of Backup Pathways of NHEJ. Int. J. Radiat. Oncol. 68, 1462–1470.
- Winters, T.A., Weinfeld, M., and Jorgensen, T.J. (1992). Human HeLa cell enzymes that remove phosphoglycolate 3′-end groups from DNA. Nucleic Acids Res. 20, 2573–2580.
- Woodhouse, B.C., and Dianov, G.L. (2008). Poly ADP-ribose polymerase-1: An international molecule of mystery. DNA Repair 7, 1077–1086.
- Wozniak, M., Szulawska-Mroczek, A., Hartman, M.L., Nejc, D., and Czyz, M. (2013). Parthenolide complements the cell death-inducing activity of doxorubicin in melanoma cells. Anticancer Res. 33, 3205–3212.
- Wright, W.D., Shah, S.S., and Heyer, W.-D. (2018). Homologous recombination and the repair of DNA double-strand breaks. J. Biol. Chem. 293, 10524–10535.
- Wurster, S., Hennes, F., Parplys, A.C., Seelbach, J.I., Mansour, W.Y., Zielinski, A., Petersen, C., Clauditz, T.S., Münscher, A., Friedl, A.A., et al. (2016). PARP1 inhibition radiosensitizes HNSCC cells deficient in homologous recombination by disabling the DNA replication fork elongation response. Oncotarget 7, 9732–9741.
- Xiong, X., Du, Z., Wang, Y., Feng, Z., Fan, P., Yan, C., Willers, H., and Zhang, J. (2015). 53BP1 promotes microhomology-mediated end-joining in G1-phase cells. Nucleic Acids Res. 43, 1659–1670.
- Xu, Y., Chen, K., Cai, Y., Cheng, C., Zhang, Z., and Xu, G. (2019). Overexpression of Rad51 predicts poor prognosis and silencing of Rad51 increases chemo-sensitivity to doxorubicin in neuroblastoma. Am. J. Transl. Res. 11, 5788–5799.
- Yan, Z., Delannoy, M., Ling, C., Daee, D., Osman, F., Muniandy, P.A., Shen, X., Oostra, A.B., Du, H., Steltenpool, J., et al. (2010). A Histone-Fold Complex and FANCM Form a Conserved DNA-Remodeling Complex to Maintain Genome Stability. Mol. Cell 37, 865–878.
- Yang, S., and Wang, X.Q. (2017). XLF-mediated NHEJ activity in hepatocellular carcinoma therapy resistance. BMC Cancer 17, 344.
- Yang, C., Wang, Q., Liu, X., Cheng, X., Jiang, X., Zhang, Y., Feng, Z., and Zhou, P. (2016). NU7441 Enhances the Radiosensitivity of Liver Cancer Cells. Cell. Physiol. Biochem. 38, 1897–1905.
- Yang, F., Teves, S.S., Kemp, C.J., and Henikoff, S. (2014). Doxorubicin, DNA torsion, and chromatin dynamics. Biochim. Biophys. Acta 1845, 84–89.
- Yao, Y., and Wei, D. (2014). Genomic Instability and Cancer. J. Carcinog. Mutagen. 05.
- Yi, C., and He, C. (2013). DNA Repair by Reversal of DNA Damage. Cold Spring Harb. Perspect. Biol. 5, a012575–a012575.

- Yosef, R., Pilpel, N., Papismadov, N., Gal, H., Ovadya, Y., Vadai, E., Miller, S., Porat, Z., Ben-Dor, S., and Krizhanovsky, V. (2017). p21 maintains senescent cell viability under persistent DNA damage response by restraining JNK and caspase signaling. EMBO J. 36, 2280–2295.
- You, Z., and Bailis, J.M. (2010). DNA damage and decisions: CtIP coordinates DNA repair and cell cycle checkpoints. Trends Cell Biol. 20, 402–409.
- You, Y.-H., Lee, D.-H., Yoon, J.-H., Nakajima, S., Yasui, A., and Pfeifer, G.P. (2001). Cyclobutane Pyrimidine Dimers Are Responsible for the Vast Majority of Mutations Induced by UVB Irradiation in Mammalian Cells. J. Biol. Chem. 276, 44688–44694.
- You, Z., Shi, L.Z., Zhu, Q., Wu, P., Zhang, Y.-W., Basilio, A., Tonnu, N., Verma, I.M., Berns, M.W., and Hunter, T. (2009). CtIP Links DNA Double-Strand Break Sensing to Resection. Mol. Cell 36, 954–969.
- Yu, A.M., and McVey, M. (2010). Synthesis-dependent microhomology-mediated end joining accounts for multiple types of repair junctions. Nucleic Acids Res. 38, 5706–5717.
- Yu, X., and Chen, J. (2004). DNA Damage-Induced Cell Cycle Checkpoint Control Requires CtIP, a Phosphorylation-Dependent Binding Partner of BRCA1 C-Terminal Domains. Mol. Cell. Biol. 24, 9478–9486.
- Yu, C., Liu, Y., Ma, T., Liu, K., Xu, S., Zhang, Y., Liu, H., La Russa, M., Xie, M., Ding, S., et al. (2015). Small Molecules Enhance CRISPR Genome Editing in Pluripotent Stem Cells. Cell Stem Cell 16, 142–147.
- Yu, X., Fu, S., Lai, M., Baer, R., and Chen, J. (2006). BRCA1 ubiquitinates its phosphorylation-dependent binding partner CtIP. Genes Dev. 20, 1721–1726.
- Zhang, Y., and Hunter, T. (2014). Roles of Chk1 in cell biology and cancer therapy. Int. J. Cancer 134, 1013–1023.
- Zhang, J., Jing, L., Tan, S., Zeng, E.-M., Lin, Y., He, L., Hu, Z., Liu, J., and Guo, Z. (2020). Inhibition of miR-1193 leads to synthetic lethality in glioblastoma multiforme cells deficient of DNA-PKcs. Cell Death Dis. 11, 602.
- Zhang, R., Zhu, L., Zhang, L., Xu, A., Li, Z., Xu, Y., He, P., Wu, M., Wei, F., and Wang, C. (2016). PTEN enhances G2/M arrest in etoposide-treated MCF-7 cells through activation of the ATM pathway. Oncol. Rep. 35, 2707–2714.
- Zhang, X., Horibata, K., Saijo, M., Ishigami, C., Ukai, A., Kanno, S., Tahara, H., Neilan, E.G., Honma, M., Nohmi, T., et al. (2012). Mutations in UVSSA cause UV-sensitive syndrome and destabilize ERCC6 in transcription-coupled DNA repair. Nat. Genet. 44, 593–597.
- Zhang, X., Xu, R., Zhang, C., Xu, Y., Han, M., Huang, B., Chen, A., Qiu, C., Thorsen, F., Prestegarden, L., et al. (2017). Trifluoperazine, a novel autophagy inhibitor, increases radiosensitivity in glioblastoma by impairing homologous recombination. J. Exp. Clin. Cancer Res. 36.
- Zhao, H., Halicka, H.D., Li, J., Biela, E., Berniak, K., Dobrucki, J., and Darzynkiewicz, Z. (2013). DNA damage signaling, impairment of cell cycle progression, and apoptosis triggered by 5-ethynyl-2′-deoxyuridine incorporated into DNA: DNA Damage Signaling, Impairment of Cell Cycle Progression, and Apoptosis Triggered by EdU. Cytometry A 83, 979–988.
- Zhao, H., Halicka, H.D., Garcia, J., Li, J., and Darzynkiewicz, Z. (2017). ATM Activation and H2AX Phosphorylation Induced by Genotoxic Agents Assessed by Flow- and Laser Scanning Cytometry. In ATM Kinase, S.V. Kozlov, ed. (New York, NY: Springer New York), pp. 183–196.
- Zheng, H., Wang, X., Warren, A.J., Legerski, R.J., Nairn, R.S., Hamilton, J.W., and Li, L. (2003). Nucleotide Excision Repair- and Polymerase η-Mediated Error-Prone Removal of Mitomycin C Interstrand Cross-Links. Mol. Cell. Biol. 23, 754–761.
- Zhou, B.-B.S., and Elledge, S.J. (2000). The DNA damage response: putting checkpoints in perspective. Nature 408, 433–439.
- Zhou, J., Gelot, C., Pantelidou, C., Li, A., Yücel, H., Davis, R.E., Farkkila, A., Kochupurakkal, B., Syed, A., Shapiro, G.I., et al. (2020). Polymerase Theta Inhibition Kills Homologous Recombination Deficient Tumors (Cancer Biology).

- Zhu, H., Sarkar, S., Scott, L., Danelisen, I., Trush, M.A., Jia, Z., and Li, Y.R. (2016). Doxorubicin Redox Biology: Redox Cycling, Topoisomerase Inhibition, and Oxidative Stress. React. Oxyg. Species Apex NC 1, 189–198.
- Ziv, Y., Bielopolski, D., Galanty, Y., Lukas, C., Taya, Y., Schultz, D.C., Lukas, J., Bekker-Jensen, S., Bartek, J., and Shiloh, Y. (2006). Chromatin relaxation in response to DNA double-strand breaks is modulated by a novel ATM- and KAP-1 dependent pathway. Nat. Cell Biol. 8, 870–876.

APPENDIXES

LIST OF APPENDIXES

APPENDIX FIGURES

APPENDIX TABLES

1. Chapter I appendixes – Bibliographic context

Appendix 1. Other repair mechanisms

Direct reversal

As opposed to most DNA repair pathways, direct reversal repair (DR) does not rely on base or nucleotide excision. As indicated by its name, this pathway directly processes single base lesions without removing the associated nucleobase. The latter is merely flipped outside the DNA double helix and repaired (Yi and He, 2013). Human DR processes a relatively small number of DNA lesions, mainly alkylated bases; it mobilizes two enzyme families:

- O^6-alkylguanine-DNA alkyltransferases (AGTs) like MGMT, which reverse a subset of O-alkylation events
- Dioxygenases of the AlkB family, that N-alkylated base adducts and some ethenobases.

These enzymes possess conserved zinc finger structures and domains with high affinity toward specific substrates, which allow the recognition and cleavage of the alkyl group (Ahmad *et al.*, 2015; Yi and He, 2013). Appendix figure 1 illustrates the reversion process of these enzymes on two different substrates.

DR is a very simple process that does not rely on numerous repair factors. The absence of repair intermediates also make DR a very fast process, with kinetics of about 10^{-8} s (Li *et al.*, 2010). Finally, it is an essentially error-free mechanism.

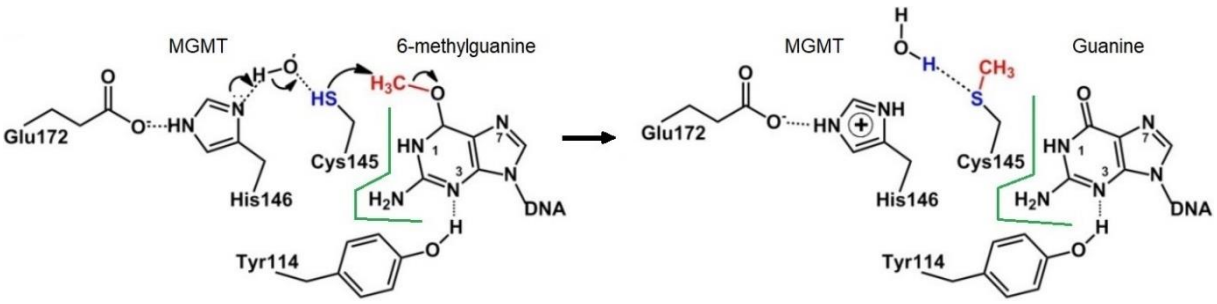

Appendix figure 1. Direct reversal of 6-methyl guanine into guanine by MGMT. Adapted from Ahmad et al. (Ahmad et al., 2015).

Mismatch repair

DNA replication can generate occasional errors such as mispaired bases, as described in chapter I, section 1.1. Such errors sometimes escape proof-reading mechanisms and can result in permanent mutations if left unrepaired. Mismatched bases as well as IDLs are processed through mismatch repair (Martin, 2016). MMR is associated with DNA replication and is thus mainly active in S-phase, but some studies describe examples of "noncanonical" MMR occurring outside S-phase (Peña-Diaz *et al.*, 2012).

In humans, MMR is initiated by two heterodimers, the MutS homologs (MSH) (appendix figure 2). The MutSα complex (MSH2/MSH6) recognizes mispaired bases and short IDLs (1-2 nucleotides), while the MutS β heterodimer (MSH2/MSH3) detects larger IDLs (Sachadyn, 2010). According to the classical MMR model, mismatch-bound MutS recruits another heterodimer, MutLα, and undergoes an ATP-consuming conformational switch, allowing it to translocate along the DNA molecule. However, more recent studies found that MutS could also be trapped MutL at the mismatched site (Chatterjee and Walker, 2017).

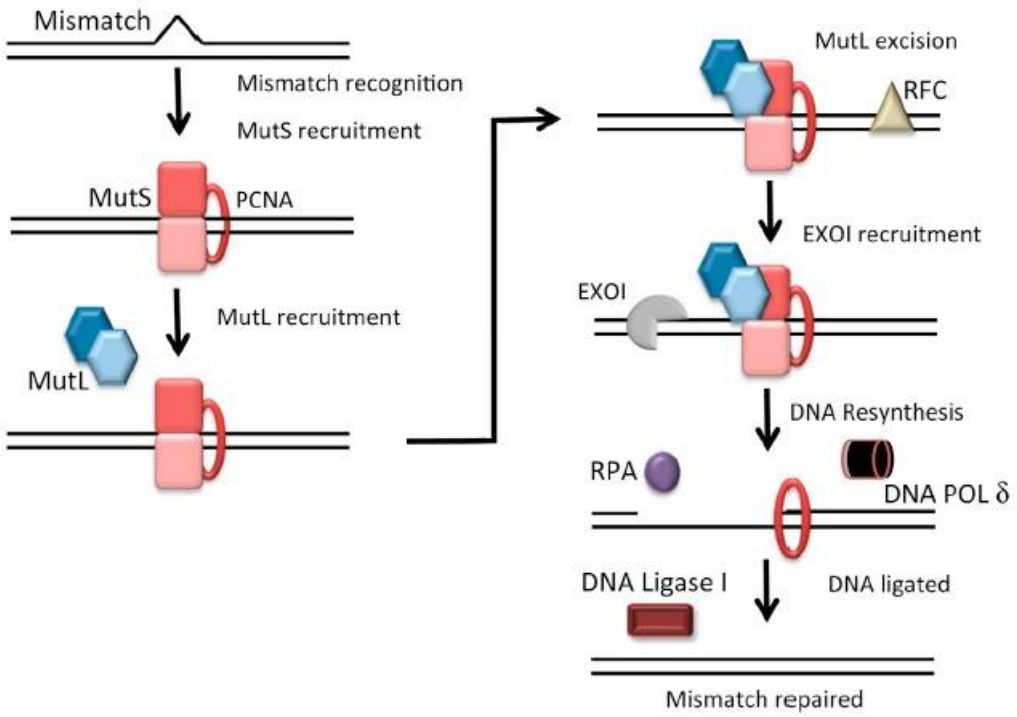

Appendix figure 2. Detail of the mismatch repair mechanism. Adapted from S.A. Martin (Martin, 2016).

MutLα acts as an endonuclease when bound to MutS and it participates in the differentiation between the lagging strand and the leading strand (Martin, 2016). The interaction between both dimers results in the recruitment of exonuclease 1 (EXO1), in a process that requires the proliferating cell nuclear antigen (PCNA) and replication factor C (RFC). EXO1 carries out the cleavage of the newly synthesized strand and the subsequent ssDNA gap is covered by RPA. High mobility group box 1 protein (HMGB1) RFC, Pol δ and LIG1 then displace RPA, synthesize new DNA and ligate the ends of the DNA strand back together. MMR termination is also though (Jiricny, 2006; Li *et al.*, 2016; Martin, 2016).

MMR is in close interaction with DSBR, in which it may participate (Bhargava *et al.*, 2016). Proteins such as PARP1 are also thought to play a role in the regulation of these mechanisms (Pascal, 2018).

2. Chapter II appendixes – Material & methods

Appendix 2. Competitive ATP inhibition

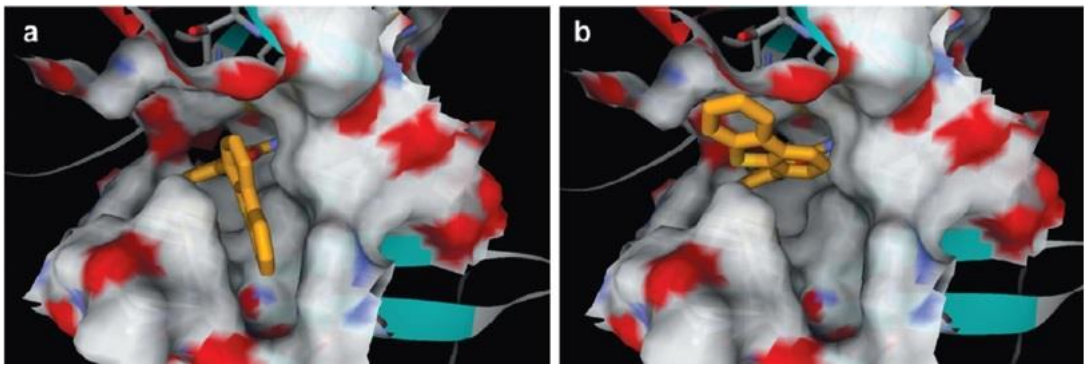

Appendix figure 3. Model of DNA-PKcs inhibition based on the insertion of NU7441 in the ATP-binding site, in an orthogonal (a) or plane (b) fashion (Clapham et al.*, 2012).*

NU7441 is a derivative of NU7026 with a similar mode of action (Davis *et al.*, 2013; Hollick *et al.*, 2007).

Appendix 3. Additional cell lines

HCC1937 and MCF-7 cells (appendix table 1) were also planned for the project but their use was limited to preliminary tests.

HCC1937 breast cells were isolated in 1995 from a TNM stage IIB (grade 3) primary ductal carcinoma in a 23-year-old female patient. This cell line has a *BRCA1* insertion mutation (C at nucleotide 5382) resulting in a deregulated HR proficiency (Scully *et al.*, 1999), although without a complete deficiency of the pathway (Peng *et al.*, 2014). MCF-7 cells were considered for comparative purposes due to their absence of mutations directly targeting DSB repair actors. This cell line originates from a pleural effusion in a 69 years-old patient affected with a metastatic breast adenocarcinoma. The MCF-7 cell line is a common research model that is described by easily available literature.

Appendix table 1. Main characteristics of additional cellular models. Source: Catalogue Of Somatic Mutations In Cancer, https://cancer.sanger.ac.uk

CELL LINE	ORIGIN	CANCER	TYPE	MUTATION OF INTEREST	CONSEQUENCES	OTHER MUTATIONS
HCC1937	Breast	Adenocarcinoma	Epithelial	***BRCA1*** **5382C**	**HR deregulation**	TP53, TP63, MAPK13 MAP3K13, WNT7B, PALB2, PIK3CA
MCF-7	Breast	Adenocarcinoma	Epithelial	-	-	

HCC1937 (CRL-2336™) and MCF-7 (HTB-22™) cells were purchased from the ATCC and cultured in RPMI-1640 medium (21875-034, Gibco, USA) completed with 10% heat-inactivated FBS, 1% non-essential amino acids solution and 1% penicillin-streptomycin solution. Cells were passaged twice a week by a

ratio of 1/4th or one half. After rinsing with D-PBS, cells were detached in 0.05% Trypsin-EDTA for 5 minutes at 37°C under 5% CO_2 and diluted to the required subculture ratio in complete medium after centrifugation (5 minutes, 1,500 g). Flasks were incubated at 37°C under 5% CO_2. As previously mentioned, few experiments were conducted on these cell lines due to several delays in the course of the project.

Appendix 4. Proliferation rate of the different models

Appendix table 2. Population doubling time of the cellular models.

CELL LINE	DOUBLING TIME (H)
HeLa	22
M059J	46
M059K	40
HCC1937	72
MCF-7	45

Appendix 5. Whole cell extracts

Preliminary tests were conducted in order to compare the influence of the type of extracts on the cellular response. To extract total proteins, cells were thawed and quickly transferred in Eppendorf® tubes before centrifugation (500 g, 5 minutes at 4°C). Unless otherwise stated, all further processing steps were conducted at 4°C with cold reagents. Samples were rinsed with 1X PBS and suspended in buffer A (see Appendix table 3) to lyse cell membranes. This step was completed by three rounds of freezing/thawing cycles in liquid nitrogen for 30 seconds and 4°C for 2 minutes. Buffer B was then directly added on the cells (see Appendix table 3) before another freezing/thawing cycle. After a final centrifugation at 16,000 g for 10 minutes, proteins isolated in the supernatant were aliquoted, snap-frozen into liquid nitrogen and stored at -80°C. Debris contained in the pellets were discarded.

Appendix table 3. Composition of lysis buffers for whole cell protein extraction. Solvent: Milli-Q®-purified H_2O.

BUFFER A		BUFFER B	
Cytoplasmic membrane lysis		Nuclear membrane lysis	
Reagent	Concentration	Reagent	Concentration
HEPES-KOH	83 mM	HEPES-KOH	45 mM
EDTA-NaOH	1.8 mM	EDTA-NaOH	0.25 mM
Glycerol	18%	Glycerol	2%
DTT	0.9 mM	DTT	1 mM
KCl	580 mM	PMSF	103 µM
Triton X-100	0.9%	Antiproteases	0.7X
28.5 µl per million cells		16.5 µl per million cells	

3. Chapter III appendixes – Results

Appendix 6. 53BP1 foci in M059J and M059K cells

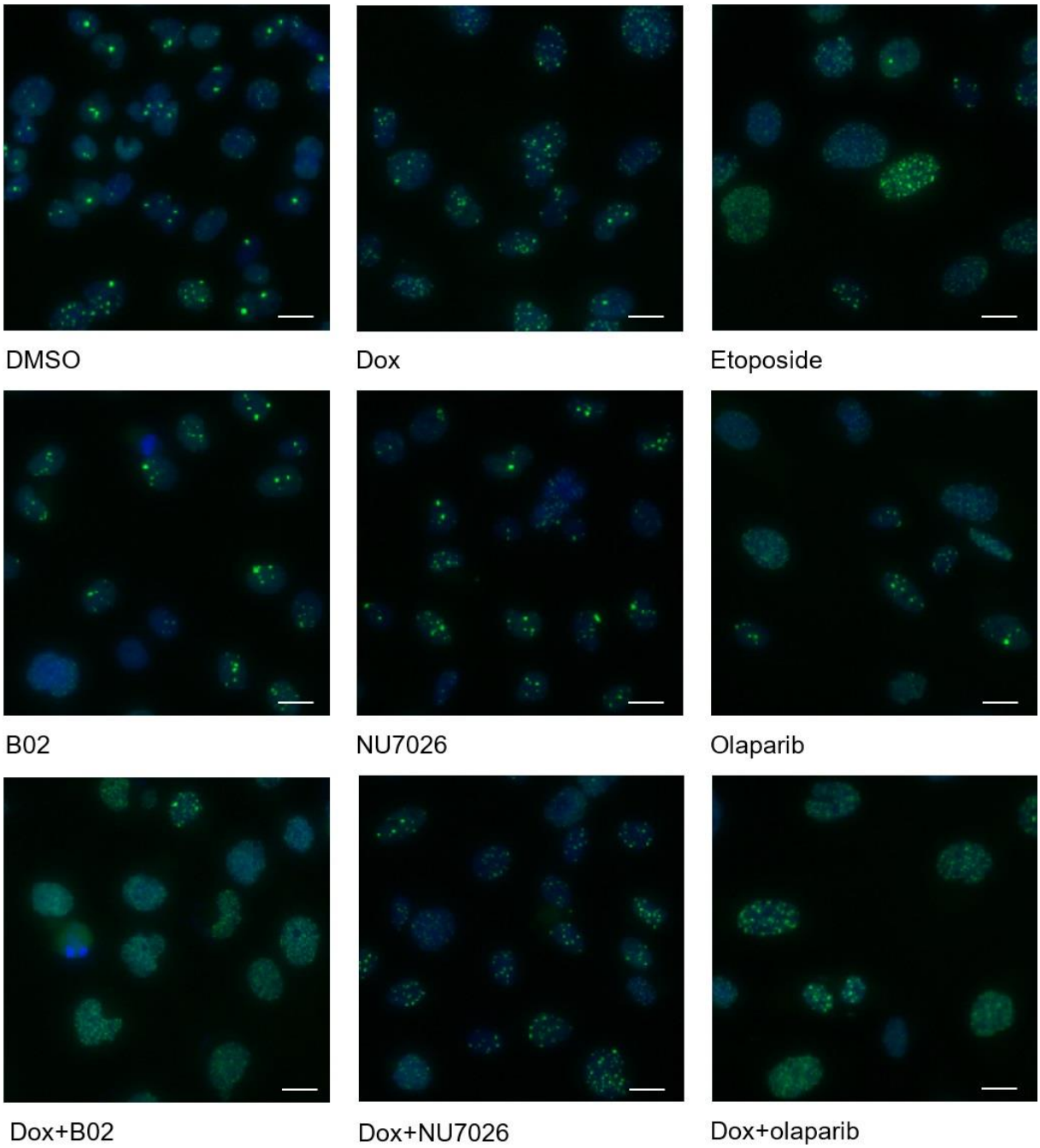

Appendix figure 4. 53BP1 foci in HeLa cells after exposure to doxorubicin and/or DSB repair inhibitors B02, NU7026 and olaparib for 48h.
Positive control: etoposide 0.5 µM. Scale bar: 15 µm.

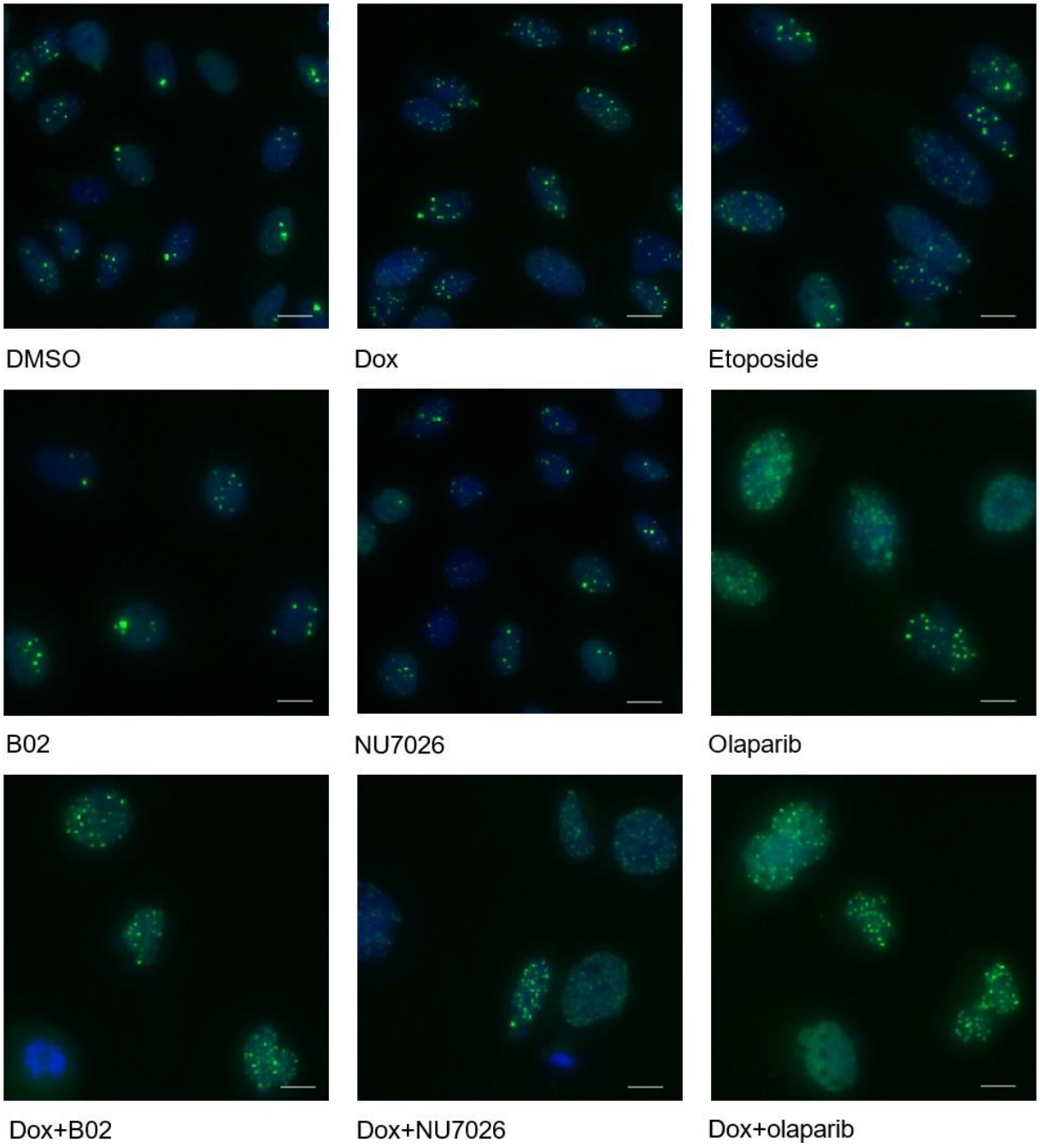

Appendix figure 5. 53BP1 foci in M059K cells after exposure to doxorubicin and/or DSB repair inhibitors B02, NU7026 and olaparib for 48h.
Positive control: etoposide 0.5 µM. Scale bar: 15 µm.

Appendix 7. p-values for pairwise comparisons of 53BP1 foci numbers

Appendix table 4. Pairwise comparisons using Wilcoxon rank sum test with Bonferroni P-value adjustment method.

HeLa	DMSO	Dox	B02	B02_Dox	NU7026	NU7026_Dox	Olap	Olap_Dox
Dox	0.00039	-	-	-	-	-	-	-
B02	1.80E-07	0.00274	-	-	-	-	-	-
B02_Dox	1.80E-07	0.00034	0.00382	-	-	-	-	-
NU7026	1.80E-07	0.05066	0.02014	1.20E-05	-	-	-	-
NU7026_Dox	1.80E-07	2.10E-06	5.90E-05	0.3253	1.20E-05	-	-	-
Olap	1.80E-07	0.00034	1.20E-05	1.90E-05	1.20E-05	2.20E-05	-	-
Olap_Dox	1.80E-07	0.00034	1.20E-05	1.40E-05	1.20E-05	1.20E-05	1	-
Etoposide	1.80E-07	2.10E-06	1.20E-05	1.20E-05	1.20E-05	7.90E-09	0.51122	1
M059K	DMSO	Dox	B02	B02_Dox	NU7026	NU7026_Dox	Olap	Olap_Dox
Dox	1.00E-06	-	-	-	-	-	-	-
B02	5.70E-05	1	-	-	-	-	-	-
B02_Dox	1.00E-06	0.16655	0.00855	-	-	-	-	-
NU7026	0.114	0.0003	0.25195	6.90E-05	-	-	-	-
NU7026_Dox	1	0.02911	0.61027	7.60E-05	1	-	-	-
Olap	1.00E-06	0.28268	0.00583	1	0.00017	4.10E-05	-	-
Olap_Dox	5.80E-06	1	1	0.37477	0.00587	0.10115	0.2301	-
Etoposide	1.00E-06	1	1	0.05339	0.0010	0.06493	0.08984	1
M059J	DMSO	Dox	B02	B02_Dox	NU7026	NU7026_Dox	Olap	Olap_Dox
Dox	1.00E-06	-	-	-	-	-	-	-
B02	6.50E-06	6.90E-05	-	-	-	-	-	-
B02_Dox	1.00E-06	7.60E-05	0.00313	-	-	-	-	-
NU7026	0.0484	6.90E-05	0.04082	6.90E-05	-	-	-	-
NU7026_Dox	1.00E-06	8.40E-05	6.90E-05	1	6.90E-05	-	-	-
Olap	1.30E-06	6.00E-07	0.0043	1	0.00039	1	-	-
Olap_Dox	1.00E-06	0.00134	0.00015	1	6.90E-05	1	1	-
Etoposide	1.00E-06	1	8.40E-05	0.00478	6.90E-05	0.00682	0.00024	0.04096

Appendix 8. Loading control in Western blotting

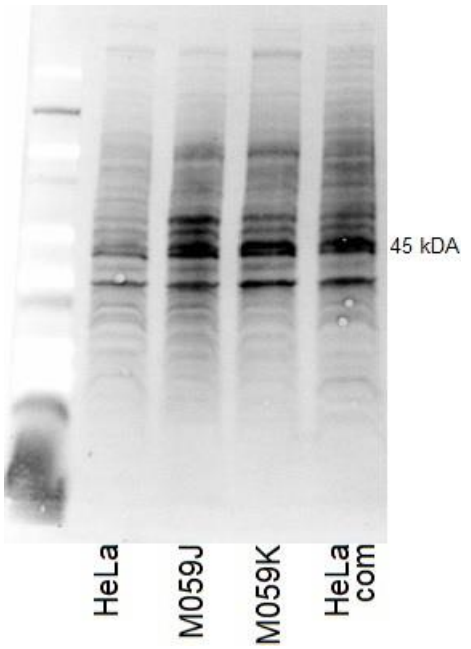

Appendix figure 6. Uncropped membrane used for the quantification of total proteins in nuclear extracts for the different cell lines, before of staining of phosphoS2056-DNA-PKcs and total DNA-PKcs.
The reference of protein loading in each lane was calculated as the sum of the signals from all individual bands. Raw levels of proteins of interest were adjusted accordingly. The bands around 45 kDa served as a visual illustration of total protein content.

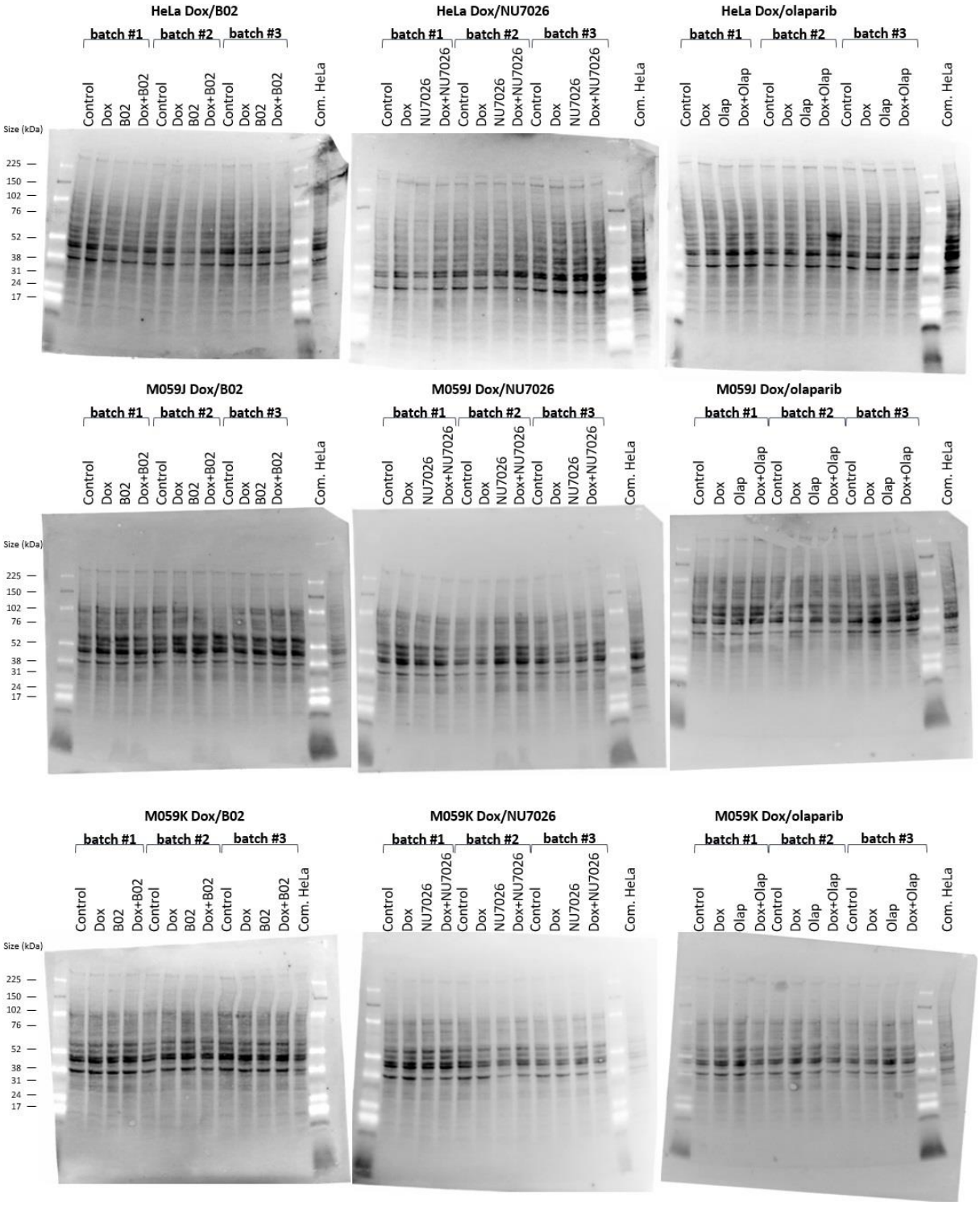

Appendix figure 7. Total protein signals used for the quantification of loaded content in western blot experiments. *The reference of protein loading in each lane was calculated as the sum of the signals from all individual bands. Raw levels of proteins of interest were adjusted accordingly. The bands around 45 kDa served as a visual illustration of total protein content.*

Appendix 9. Excision-resynthesis activities on the CisP lesion

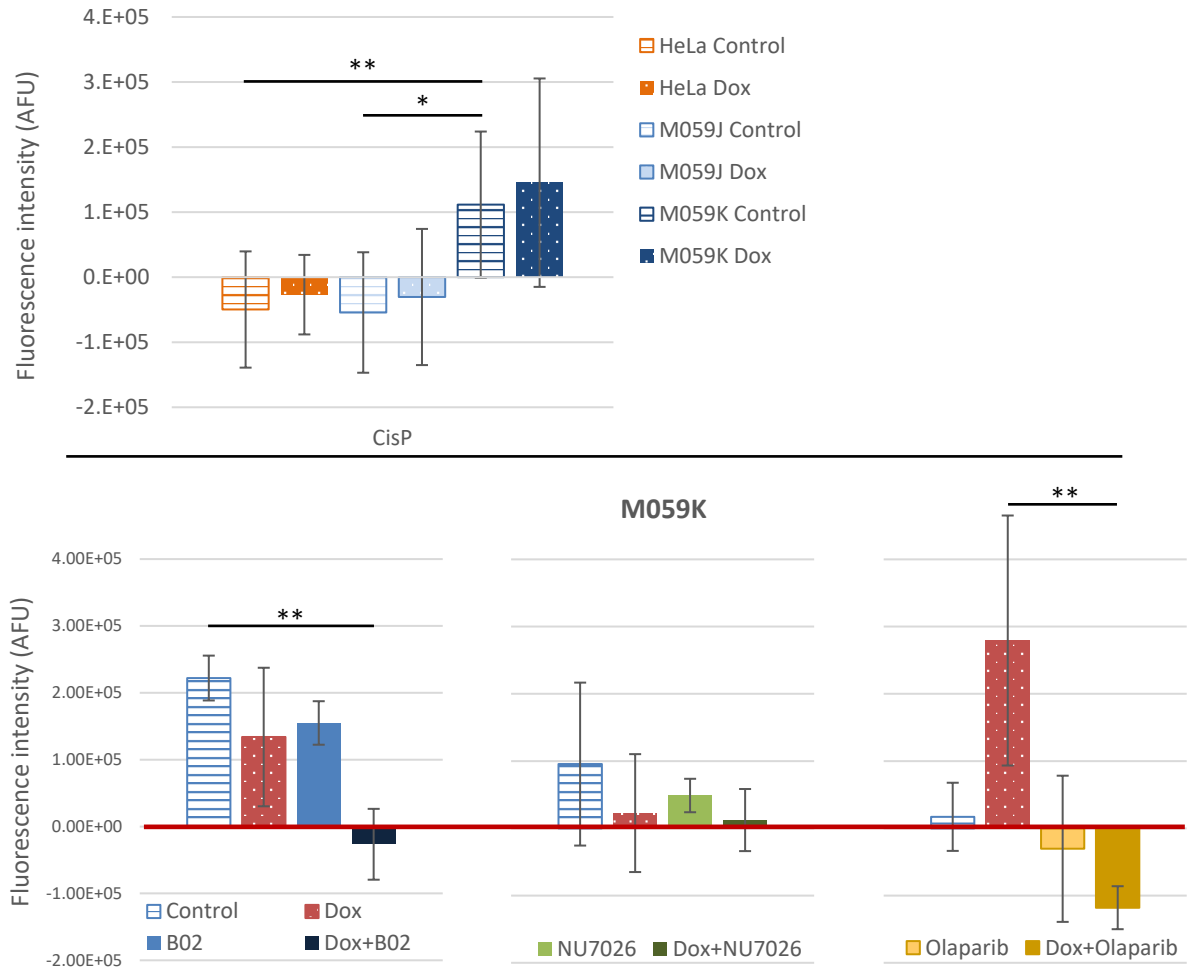

Appendix figure 8. Repair activities on the CisP lesion, measured by the ExSy-SPOT assay at the basal level and in nuclear extracts from M059K cells treated with doxorubicin and/or repair inhibitors.
*Data is normalized to the undamaged plasmid (see "Material and methods") but not to the untreated control condition due to negative values. At least three independent experiments were performed (n=3); * p<α/2, ** p<0.01 (non-parametric Dunn test). Error bars: standard deviation.*

Negative values observed for the CisP lesion result from polymerase blockage in the presence of DNA crosslinks, causing low repair intensities to appear on the CisP lesion compared to the lesion-free plasmid (which is also cleaved and targeted by nuclear proteins in the cell extracts). Hence, negative values appeared after subtracting the control's FI from the signal obtained on the CisP plasmid; this experimental artefact does not impact our conclusions.

Consequently, this lesion was not normalized relative to the untreated control cells treated with DMSO only and it was analyzed separately. As shown in standard deviation size and in the variation in repair

levels between the controls (DMSO and doxorubicin only) from one batch of treatment to another, inter-experimental variability in CisP response was high.

Only the repair of CisP adducts was inhibited in M059K exposed to the combination of B02 and doxorubicin, but this was not observed in the other models. These adducts are mostly repaired by NER (Reed, 1998) and can also mobilize HR factors, especially in S-phase (Laurini *et al.*, 2020).

PARP inhibition also produced a clear effect, in a doxorubicin-dependent manner. This suggests the activation of NER or ICLR by doxorubicin as well as an inhibitory effect of olaparib on these mechanisms.

No such effects were seen in HeLa and M059J (data not shown), which remains unexplained.

Appendix 10. Unsupervised hierarchical clustering of ExSy-SPOT data

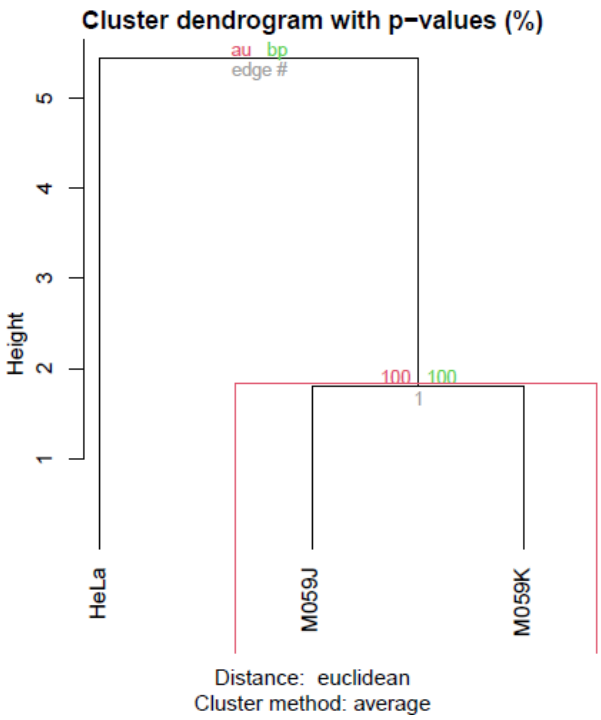

Appendix figure 9. Identified clusters of cell lines from unsupervised hierarchical clustering on ExSy-SPOT data (Euclidean distance).
Plotted data corresponds to log_2(treated/control) values across treatments. Significant clusters (approximately unbiased p-value > 0.95) are indicated by red rectangles.

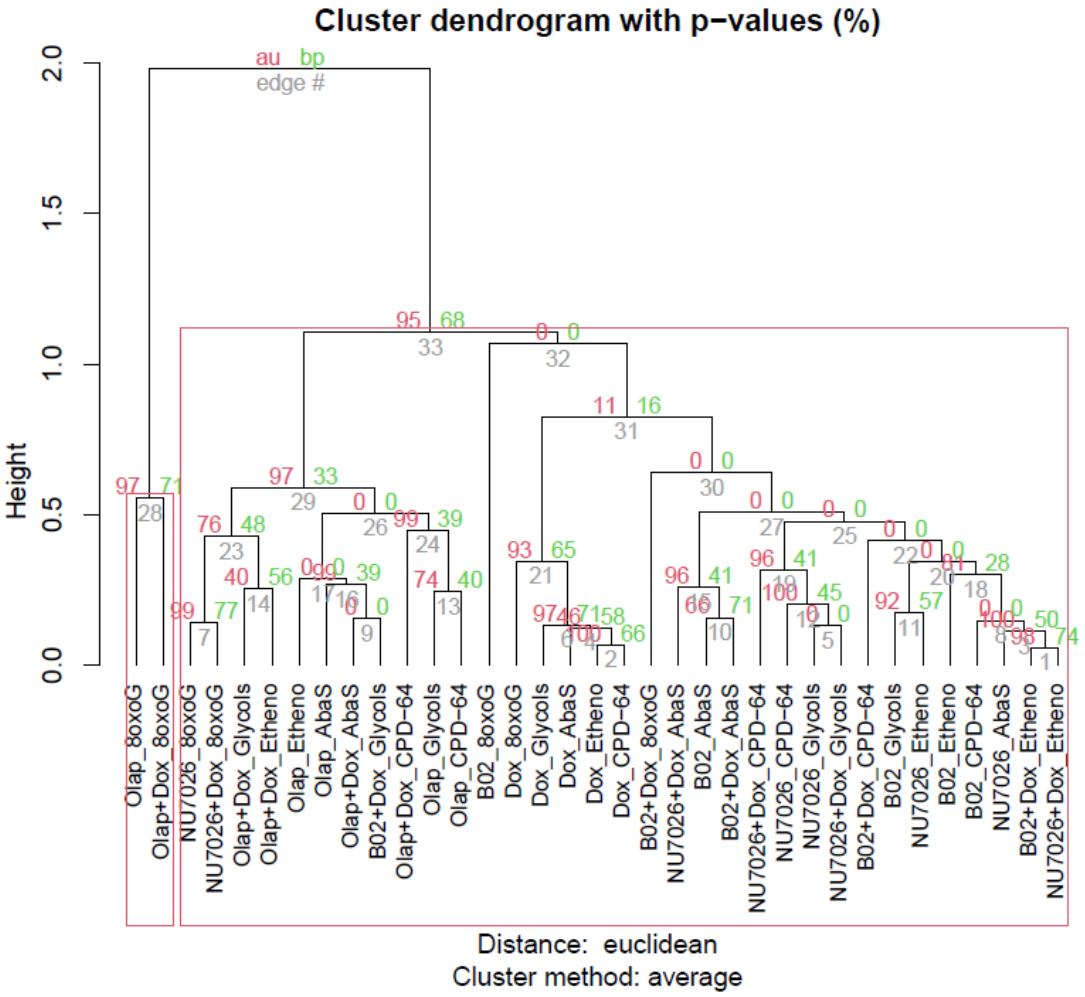

Appendix figure 10. Identified clusters of treatments from unsupervised hierarchical clustering on ExSy-SPOT data (Euclidean distance).

Plotted data corresponds to log_2(treated/control) values in the three cellular models. Significant clusters (approximately unbiased p-value > 0.95) are indicated by red rectangles.

Appendix 11. Electrophoretic tests with Cy5 staining

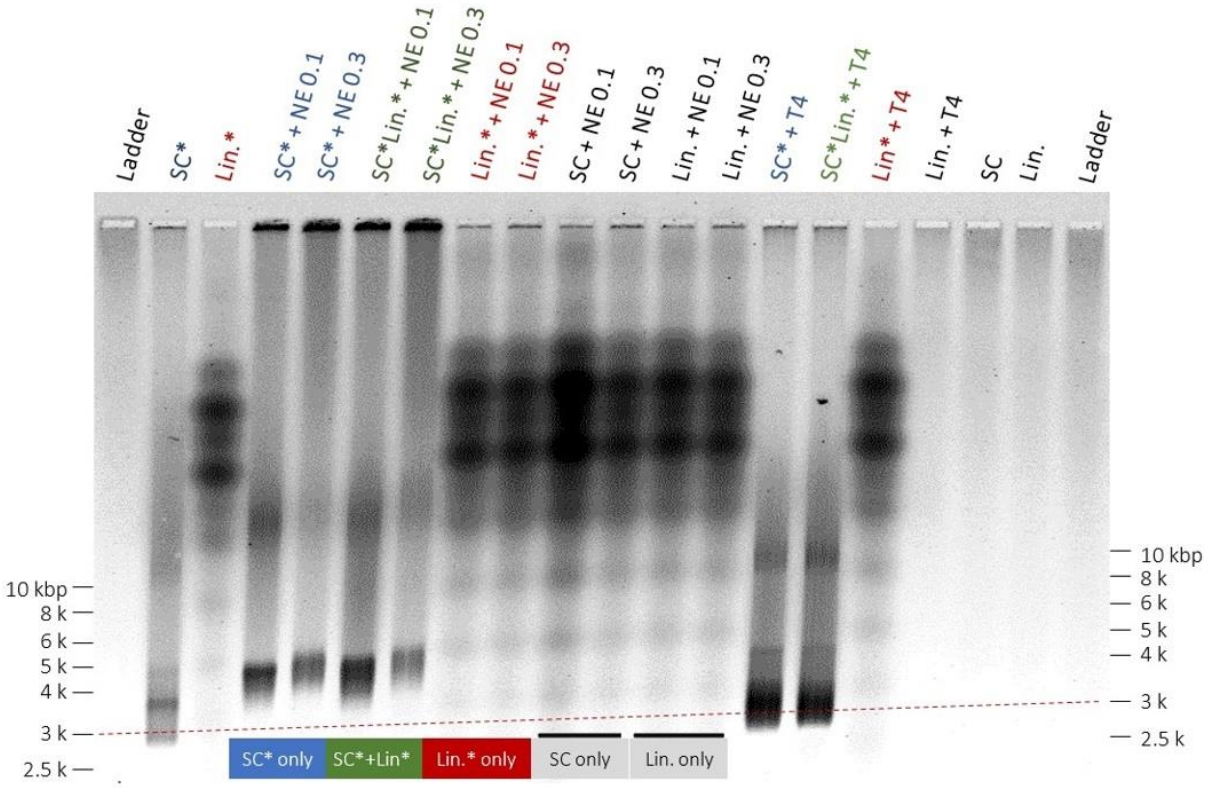

Appendix figure 11. Cy5 readout of an electrophoretic NHEJ assay exposing a supercoiled (SC) and/or linear (Lin) pBlueScript plasmid to HeLa nuclear extracts (0.1 or 0.3 mg protein/ml).

Ligation products were not precipitated and were incubated with 0.5 mg/ml proteinase K. Asterisks indicate biotin-bound SC or cy3-labelled Lin, either alone (2x 2.5 ng/µl; blue and red, respectively) or mixed together (2.5 ng/µl each, green). A biotin-bound supercoiled plasmid was stained with streptavidin-Cy5. Control: T4 ligase. Red line: 3 kbp marker.

Appendix 12. Dose-response curves from the electrophoretic NHEJ assay

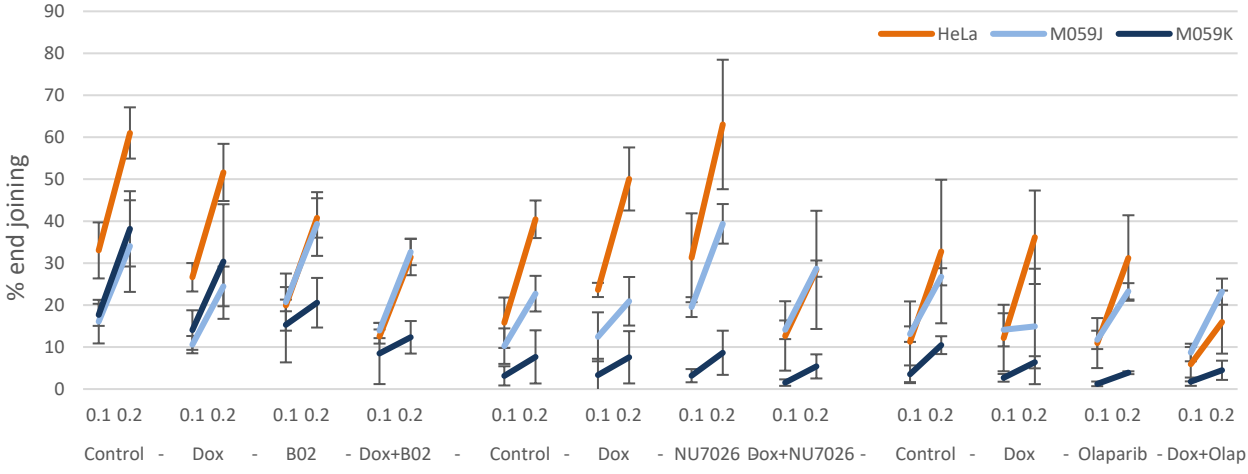

Appendix figure 12. Dose-response curves obtained in nuclear extracts from treated cells.

Nuclear protein extracts were introduced at a final concentration of 0.1 or 0.2 mg/ml. Mean ± SD of at least 3 biological replicates.

Appendix 13. Example of electrophoretic results

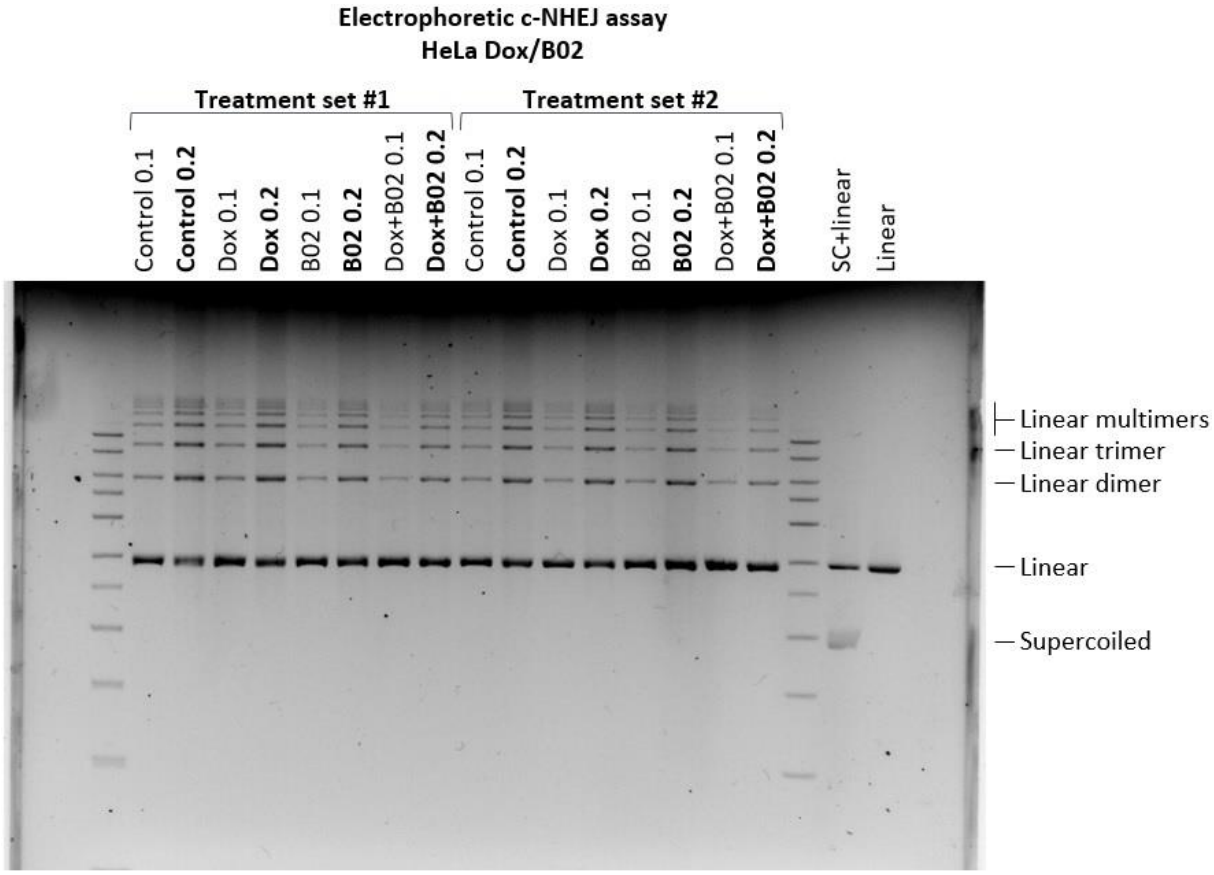

Appendix figure 13. Linear plasmid religation in nuclear extracts (0.1 or 0.2 mg protein/ml) from HeLa cells exposed to doxorubicin and/or RAD51 inhibitor B02.

Appendix 14. Optimization of the Next-SPOT assay

Results were more robust after switching to a different supplier (SCHOTT Nexterion AG, Germany), which also enabled printed slides to be used within 24 hours instead of two weeks due with the previous material.

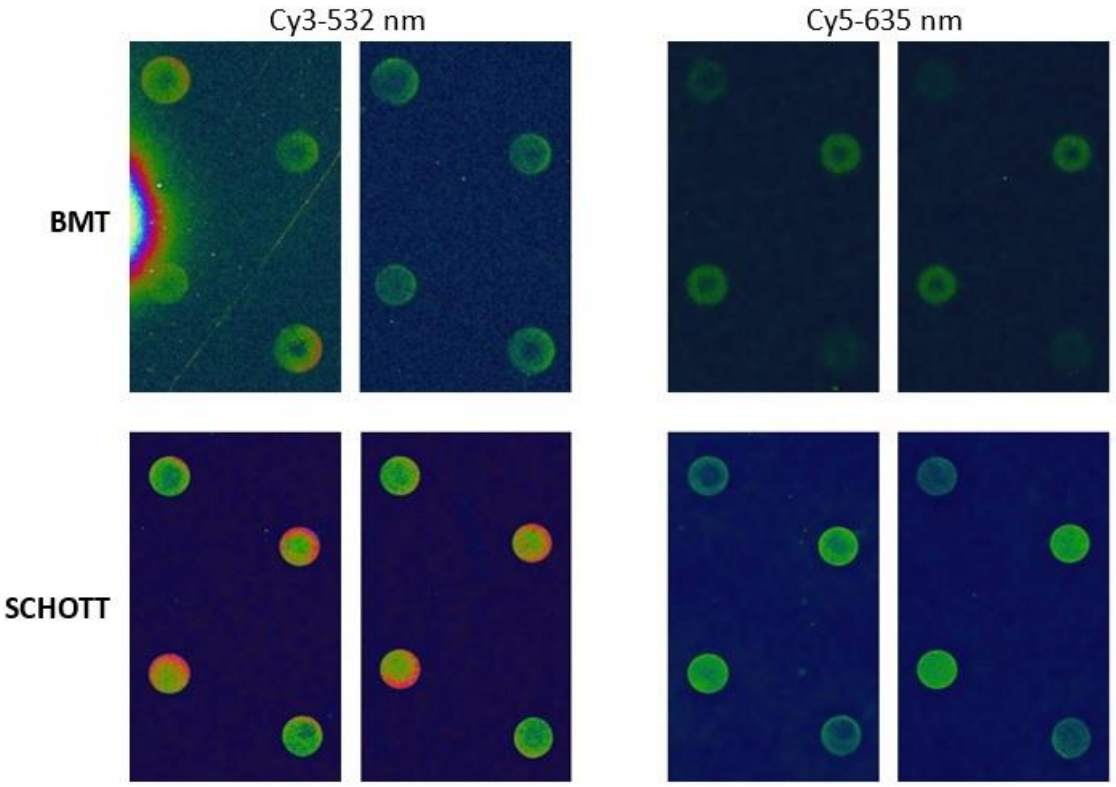

Appendix figure 14. Improvement of the fluorescent signal in Schott slides at both wavelengths read in the Next-SPOT assay.
On average, plasmids spots were more blurred on BTM slides, with which abnormal signal (top right) was observed more often. An indirect staining with dCTPs-biotin and streptavidin-Cy5 was used.

The assay was further optimized by removing the initial proteinase K bath (0.1 mg/ml, 30 min at 30°C), which increased the length of the assay without providing noticeable benefits on SCHOTT® slides (data not shown). The initial assay also used T4 ligase (NEB, USA) as an internal control, but it required a specific reaction mix to be prepared, thereby preventing the identification of experimental variations in the samples mix. Hence, T4 ligase was replaced by commercial HeLa extracts in subsequent experiments.

Appendix 15. Statistical tests performed for Next-SPOT results in cells treated with doxorubicin and/or olaparib

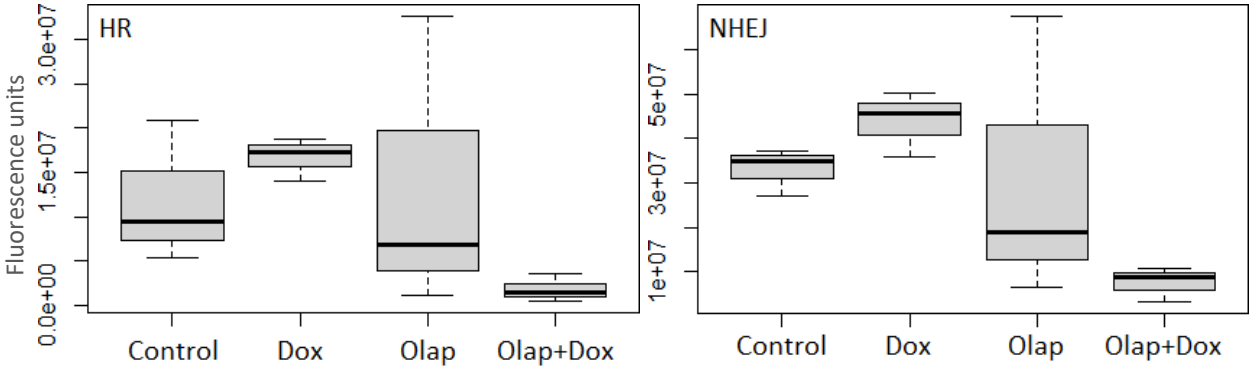

Appendix figure 15. Boxplot of raw fluorescence levels obtained with Next-SPOT for HR and NHEJ in nuclear extracts from HeLa cells treated with doxorubicin and/ or PARP inhibitor olaparib.

Only the "doxorubicin only" and "olaparib + doxorubicin" were compared for the **HR** signal. For **NHEJ**, a high outlier value was removed from the set of "olaparib only" measures; this condition was thus tested in duplicate only (n=2). p-values are summarized in appendix table 5..

Appendix table 5. Statistical tests on the selected values.

HR	**Kruskal-Wallis test** p-value 0.04953			**NHEJ**	**Kruskal-Wallis test** p-value 0.03987		
Dunn test	Control	Dox	Olap	**Dunn test**	Control	Dox	Olap
Dox	X			Dox	0.1944		
Olap	X	0.0248*		Olap	0.1027	0.0208*	
Dox+Olap	X	X	X	Dox+Olap	0.0424	0.0049*	0.3916

alpha = 0.05

Reject H_0 if p <= alpha/2

A similar correction was applied for on relative pathway contributions on the alt-NHEJ pathway (appendix figure 16 and appendix table 6).

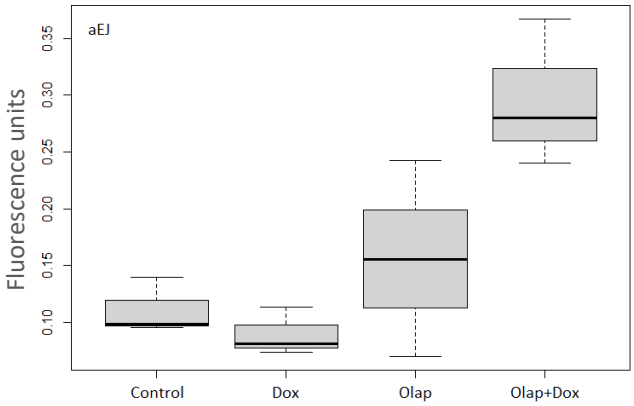

Appendix figure 16. Raw contribution of aEJ in Next-SPOT data obtained in nuclear extracts from HeLa cells treated with doxorubicin and/ or PARP inhibitor olaparib.

Appendix table 6. Statistical tests on the selected values.

aEJ	**Kruskal-Wallis test** p-value 0.0484		
Dunn test	Control	Dox	Olap
Dox	0.4092		
Olap	0.1254	0.1791	
Dox+Olap	0.0058*	0.0108*	0.0841

alpha = 0.05

Reject H_0 if p <= alpha/2

In M059K, raw fluorescence values on the "olaparib + doxorubicin" condition were removed from analysis.

Appendix 16. Cluster significance from unsupervised hierarchical clustering

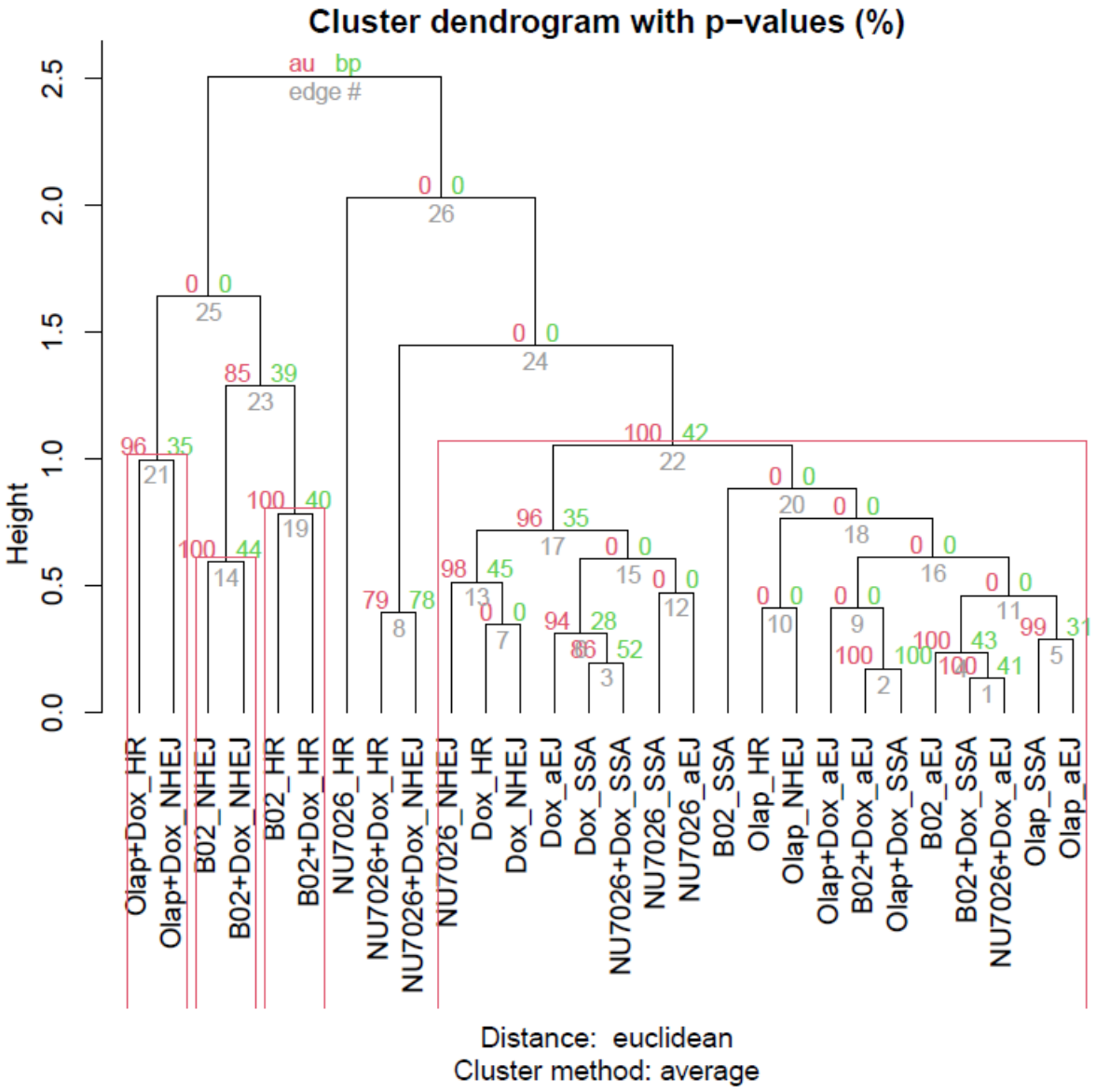

Appendix figure 17. Identified clusters of treatments from unsupervised hierarchical clustering on Next-SPOT data (Euclidean distance).
Plotted data corresponds to log_2(treated/control) values. Significant clusters (approximately unbiased p-value > 0.95) are indicated by red rectangles.

Appendix 17. Unsupervised hierarchical clustering using correlation dissimilarity measure (Next-SPOT assay)

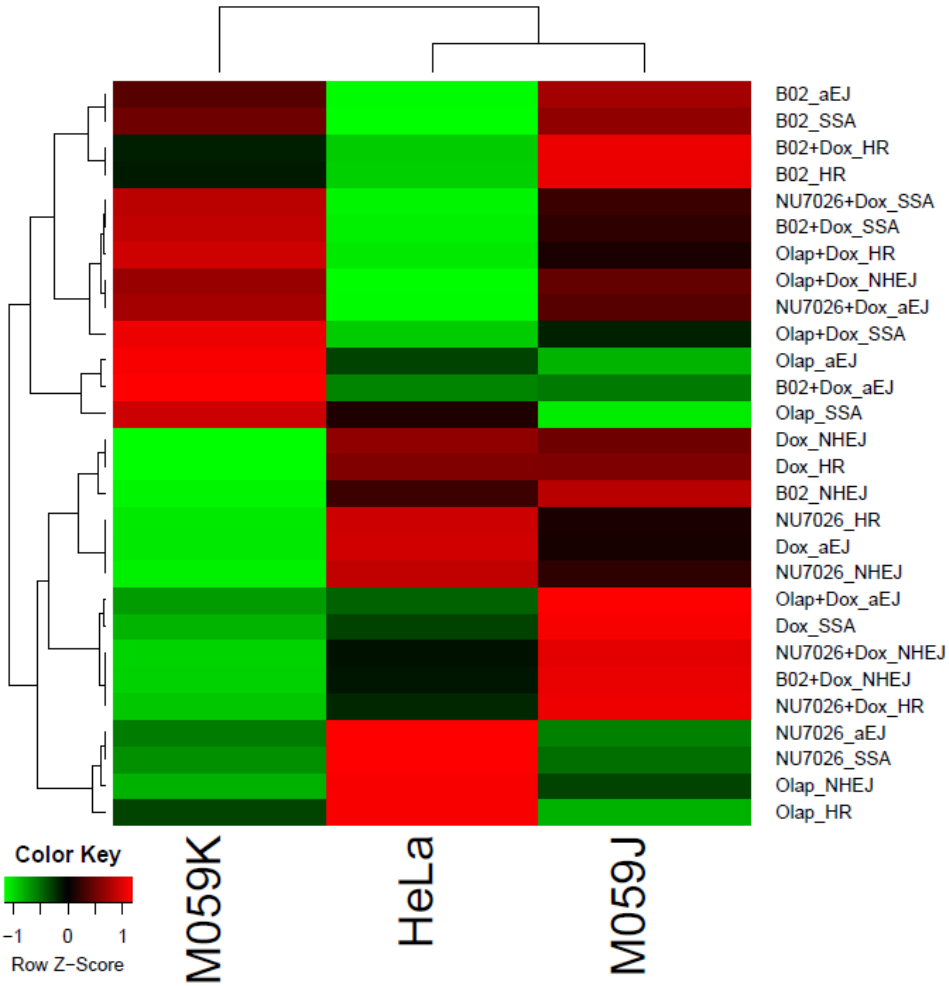

Appendix figure 18. Analysis of the DNA repair response in the cellular models across treatments and repair pathways. No significant distinction was seen across cell lines or treatments (approximately unbiased p-value < 0.95).

Heatmap based on the log2-transformed ratios of the fluorescence intensity obtained on each Next-SPOT condition between treated and non-treated cell lines (log2(T/NT)). Hierarchical clustering algorithm with correlation dissimilarity measure was used. In the first dimension, cell lines were clustered by similarity of the covariation of their DSBR response profile across treatments. In the second dimension, treatments were clustered by similarity of their response across the cell lines. Colors reflect the positive (red) or negative (green) correlation score across cell lines.

Appendix 18. Elaboration of the *in vitro* Next-SPOT protocol

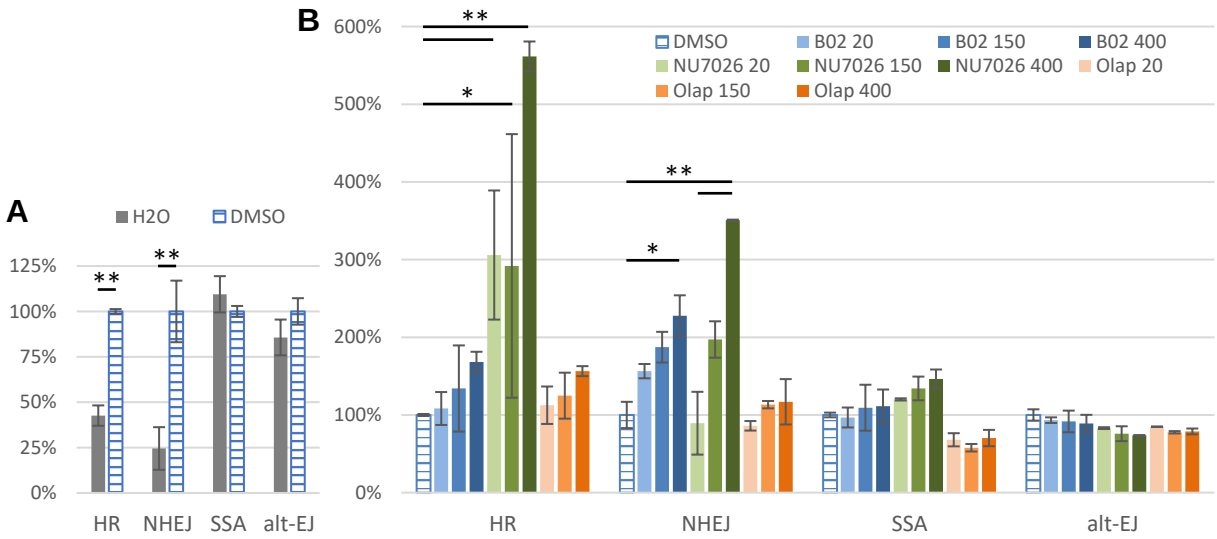

Appendix figure 19. Setup experiment for in vitro treatments in HeLa cells.
A. *Effect of 3% DMSO in the reaction mix.* ***B.*** *Impact of various doses of repair inhibitors, 3% DMSO. Extracts were incubated with repair inhibitors diluted to a final concentration of 20 to 400 µM in 3% DMSO. Results are normalized to the basal DMSO condition based on two experimental replicates (n=2). * p<α/2, ** p<0.01 (non-parametric Dunn test).*

An increase in fluorescence is seen at 532 nm (HR and NHEJ) compared to a classical reaction mix without DMSO. No effect was found at 635 nm. In comparison, DMSO did not impact fluorescence in preliminary Next-SPOT experiments based on cellular treatments with 0.3% DMSO, or in other assays used by LXRepair (George, 2017). Low doses of inhibitors only produced limited effects.

Appendix 19. Ratio between NHEJ and HR upon DNA-PKcs inhibition

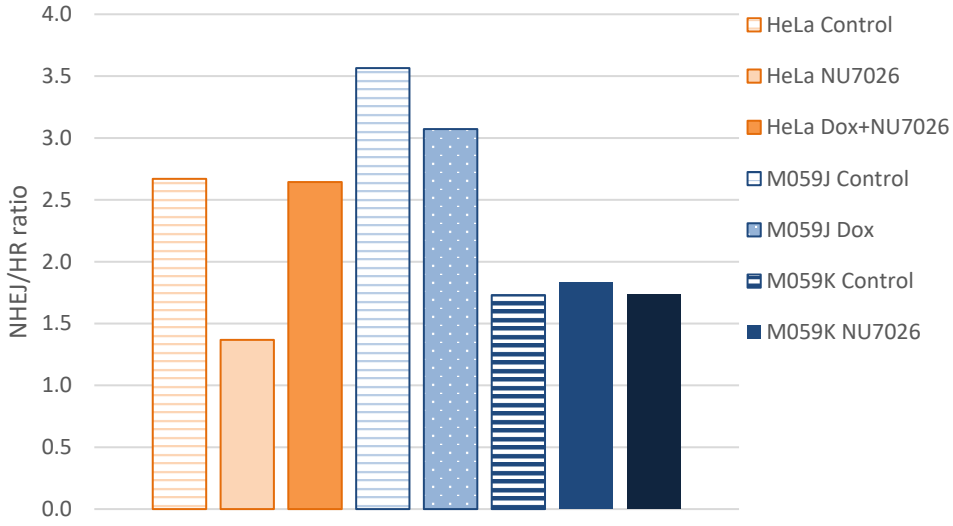

Appendix figure 20. Ratio between NHEJ and HR signals obtained using the Next-SPOT assay.
Raw fluorescence data was compiled from presented experiments using 0.2 mg/ml nuclear extracts. Ratio of the mean fluorescence values from at least 3 independent experiments.

Appendix 20. Relative pathway contributions following *in vitro* addition of repair inhibitors (Next-SPOT assay)

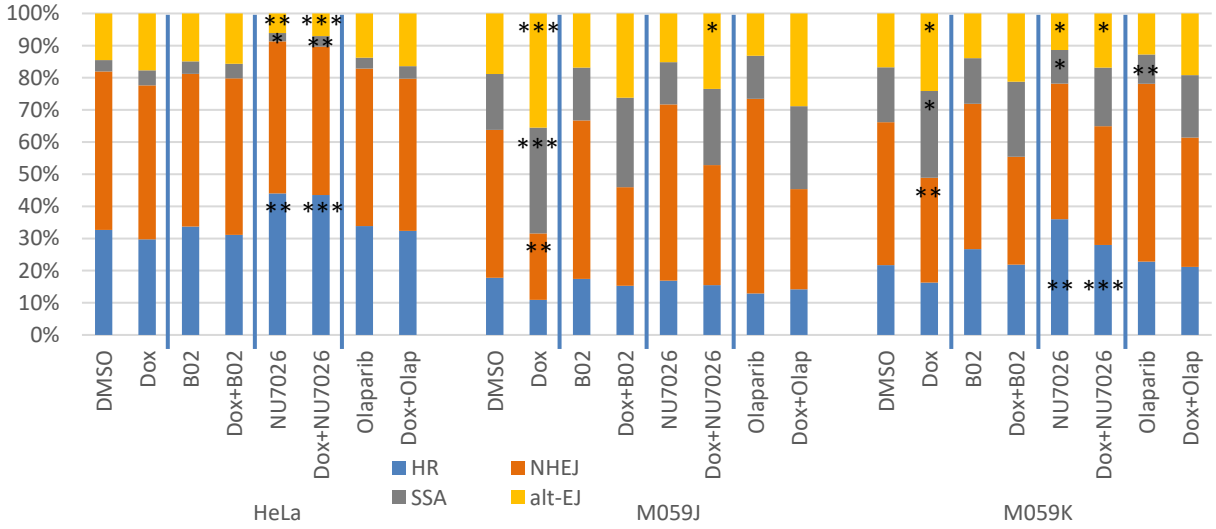

Appendix figure 21. Relative pathway contribution obtained with Next-SPOT following treatment of the nuclear extracts (“in vitro” treatments)
*Three independent experiments were performed (n=3); * p<α/2, ** p<0.01 (non-parametric Dunn test).*

Appendix 21. Comparison of DNA-PKcs deficiency and inhibition using the "*in vitro*" Next-SPOT assay

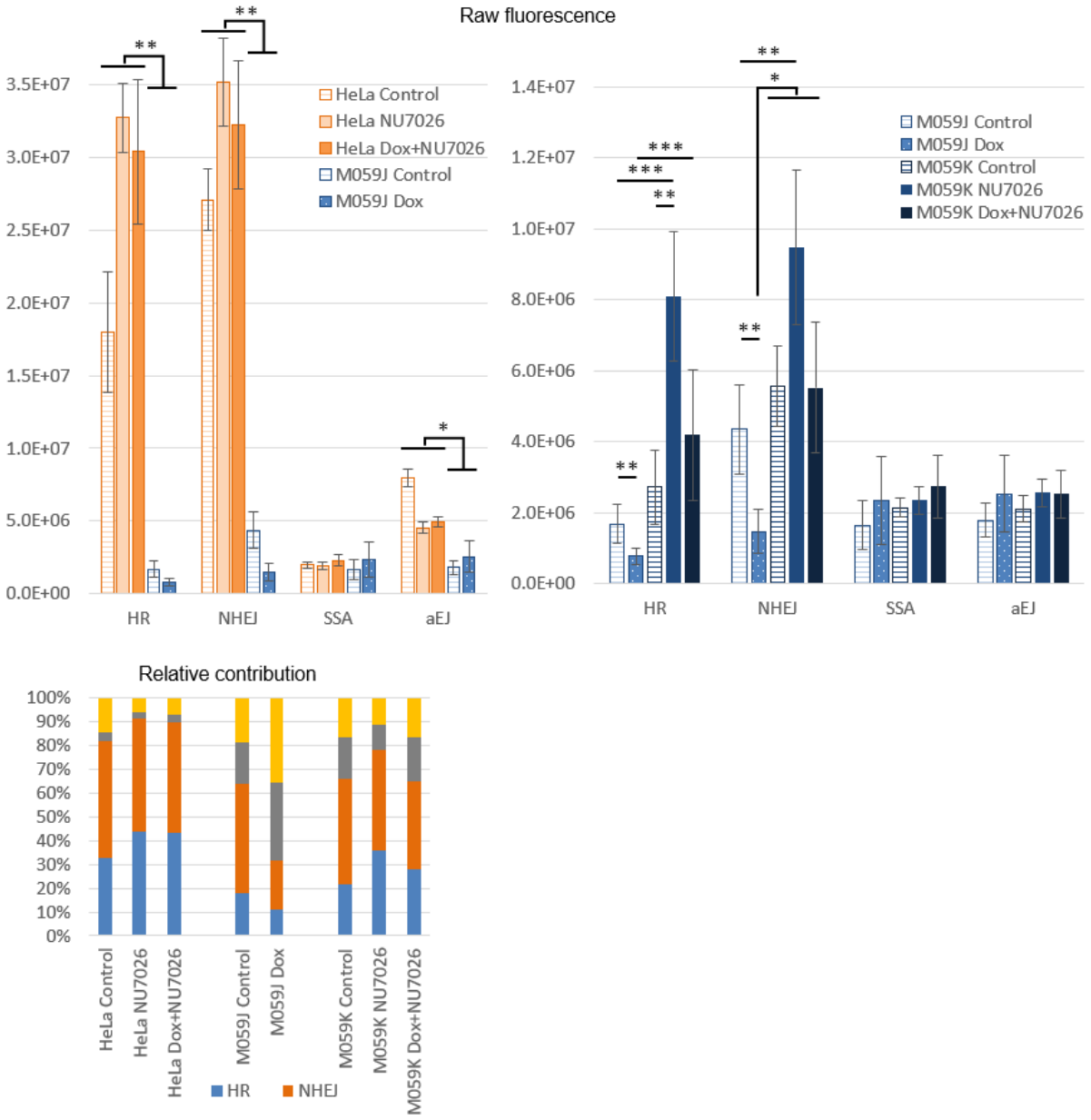

Appendix figure 22. Raw fluorescence and relative pathway contributions in M059J cells (untreated or exposed to doxorubicin) and HeLa or M059K cells additionally exposed to DNA-PKcs inhibitor NU7026.

Treatment of HeLa extracts with NU7026 did not provide the same DSBR signals as for M059J. No clear difference is seen between extracts from i) control M059J, ii) control M059K and iii) M059K exposed to doxorubicin and treated *in vitro* with NU7026. NU7026 added *in vitro* in extracts from control M059K has either no effect or increases the difference to the response obtained in M059J. Hence, it cannot be concluded that the treatments provide an M059J-like profile to M059K.

Summary

Human cells are under constant threat from DNA-damaging agents. Double-strand breaks (DSBs) are highly deleterious DNA lesions that can induce chromosomal translocations, increase mutation rate and participate in malignant transformation. DSBs are also induced by standard anticancer treatments, in order to trigger cell death mechanisms in cancerous cells. In humans, DSBs are processed by complex repair systems that operate with different speed and fidelity. The last two decades saw the emergence of several repair inhibitors that target major repair pathways and reduce repair capacity in tumor cells. A better understanding of DSB repair processes would improve the identification of tumors that could respond to repair inhibitors. In addition, it may also allow the identification of specific repair profiles associated with an increased risk of treatment-induced adverse effects. Thus, functional approaches allowing the characterization of DSB repair profiles could complement current genotyping methods.

In this intent, LXRepair developed a multiplexed assay on biochip that allows the analysis of several DSB repair activities. Repair profiles have been characterized in three human cancer cell lines as part of technical and biological assay validations. Repair activities were studied both at the basal level and following exposure to DSB-inducing chemical doxorubicin, combined or not with various repair inhibitors. In collaboration with the CIBEST team, results were compared to a reference assay based on agarose gel electrophoresis. In addition, 53BP1 foci and repair protein levels or activity were investigated, together with the activity of repair pathways that process lesions other than DSBs, allowing further characterizations of the cellular response to the treatments. This study highlighted the interest of the biochip approach compared to the chosen reference method, both from the technical and biological perspective. The assay reduced experimental workload while providing information on several repair pathways simultaneously. However, this work also reflects the complexity of the regulation of DNA repair systems and raises a set of questions that call for further investigation. Overall, the results obtained within the course of this project highlight the potential of the biochip method for various applications in oncology, fundamental research or biomolecular screening.

Keywords: double-strand break, DNA repair, biochip, repair inhibitor, doxorubicin, enzymatic assay.

Résumé

Les cellules humaines sont constamment exposées à des facteurs divers qui endommagent leur ADN. Les cassures double-brin (CDB) comptent parmi les lésions de l'ADN les plus délétères ; elles peuvent induire des translocations chromosomiques, augmentent le risque de mutation et participent à la transformation en cellules cancéreuses. Des CDB sont d'autre part induites par les agents anticancéreux les plus courants, qui visent à déclencher la mort cellulaire dans les cellules tumorales. Chez l'Homme, ces lésions sont prises en charge par des mécanismes complexes de réparation qui opèrent de manière plus ou moins rapide et fidèle. Le développement d'inhibiteurs de réparation a permis de bloquer des mécanismes-clé et de diminuer la capacité de réparation des cellules tumorales. Une compréhension plus complète des mécanismes de réparation des CDB permettrait d'une part de mieux identifier les tumeurs susceptibles de répondre à des inhibiteurs de réparation et pourrait d'autre part permettre d'associer des profils de réparation spécifiques à une susceptibilité accrue de développer des effets indésirables liés aux traitements. Des méthodes fonctionnelles permettant de caractériser des profils de réparation pourraient ainsi compléter les techniques actuelles de génotypage.

Dans cette optique, l'entreprise LXRepair a développé une méthode multiplexée sur biopuce permettant d'étudier la réparation des CDB via différentes voies. Dans le cadre de l'optimisation technique et biologique de ce test, les profils de réparation de plusieurs lignées cancéreuses humaines ont été comparés en l'absence de traitements et suite à une exposition à un composé génotoxique, la doxorubicine, combiné ou non à des inhibiteurs de réparation. En collaboration avec l'équipe CIBEST, les résultats obtenus ont été comparés à une approche de référence fondée sur l'électrophorèse sur gel d'agarose. En parallèle, la quantification de foci 53BP1, la mesure de l'abondance et de l'activité de protéines de réparation des CDB ainsi que l'étude de l'activité de voies de réparation d'autres lésions à l'ADN ont permis de mieux caractériser la réponse des modèles cellulaires aux différents traitements. Cette étude a mis en évidence l'intérêt de l'approche sur biopuce par rapport à la méthode de référence, aussi bien sur des aspects techniques (réduction du temps d'analyse par échantillon) que biologiques (caractérisation de plusieurs mécanismes de réparation simultanément). Cependant, les profils de réparation obtenus soulignent la complexité de la régulation de la réparation de l'ADN, ce qui soulève de nouvelles pistes de recherches. Dans l'ensemble, les résultats obtenus au cours de ce projet mettent en évidence l'intérêt la méthode sur biopuce, qui trouve des applications directes en oncologie, en recherche fondamentale ou en criblage biomoléculaire.

Mots-clés : cassure double-brin, réparation de l'ADN, biopuce, inhibiteur de réparation, doxorubicine, test enzymatique.